Heparin and heparin-like molecules inhibit the Alzheimer's β-secretase (BACE1): considerations for biological assay and future therapeutic development

Thesis submitted in accordance with the requirements of Keele University for the degree of Doctor in Philosophy

By

Lynsay Claire Hadfield

June 2018

Abstract

The biologically and medically important heparan sulphate and heparin polysaccharides have previously been shown to modulate the activity of an aspartyl protease, β-secretase (BACE1), implicated in the aetiology of Alzheimer's disease. Research groups investigating the activity of heparin with BACE1 have demonstrated both inhibitory and stimulatory effects of this glycosaminoglycan, and other analogues. In an attempt to understand this relationship, a review of the available recombinant BACE1 products was conducted to determine if protein purification tag had an effect on the heparin/heparan sulphate interaction with BACE1. FLAG-tagged BACE1 was identified as a suitable proxy for native, untagged BACE1 for activity studies.

In this study, the common purification tag, IgG Fc region, has been shown to interact with heparin and other glycosaminoglycans at acid pH (pH 4.0 and pH 5.0) with heparin affinity of > 800 mM. Further investigation, first of whole immunoglobulin (IgG & IgM) and then with Fab and F(ab')2 antibody fragments, identified heparin binding at acid pH in all fragments tested. Thermal stability studies were conducted to identify heparin/HS structural requirements for this novel interaction, which suggest sulphate is necessary but not sufficient for activity.

Finally, a library of chemically sulphated non-heparin polysaccharides were utilised to identify 'hit' BACE1 inhibitors with beneficial BACE1 therapeutic attributes such as low molecular weight, minimal charge and attenuated off-target effects, such as anti-coagulant activity. Differential scanning fluorimetry was identified as a potential high-throughput screening assay to replace fluorescence resonant energy transfer, during the initial non-heparin polysaccharide library BACE1 inhibitor screening.

Table of contents

Acknowledgements

I would like to thank my supervisors Dr. Mark Skidmore, Dr. Edwin Yates, and Prof. Steven Allin for their time, guidance and counsel.

Thanks must also go to the MRC, Charnwood Molecular, and Keele University for their financial support. Thank you to the University of Liverpool for the use of equipment throughout the project.

In addition I would like to thank Ms. Patricia Proctor, Prof. Jeremy Turnbull, Dr Scott Guimond, Dr. Marissa Maciej-Hulme, Mr. Anthony Devlin, Miss. Courtney Mycroft-West, and Dr. Joseph Holman for their support and assistance throughout this study.

Finally, I would like to thank my wonderful husband and family; it has been a long journey and I am truly grateful for the company.

List of figures

List of tables

Glossary of terms

2FDG	2-fluorodeoxy-D-glucose
5-HT	5-hydroxytryptamine
6-mer	6 monosaccharides
AD	Alzheimer's disease
ADAM-10	A disintegrin and metalloproteinase domain-containing protein 10
adp-1	Antibody raised to BACE1
AICD	APP intracellular domain
APH-1	Anterior pharynx-defective 1 protein identified in Notch signalling
APLP-1	Amyloid like protein-1
APLP-2	Amyloid like protein-2
Apo-E4	Apolipoprotein E4
APP	Amyloid precursor protein
APP_{SW}	Amyloid precursor protein, Swedish mutation
aPTT	Activated partial thromboplastin time
Aβ	β-amyloid
BACE1	β-secretase APP cleaving enzyme 1
BACE2	β-secretase APP cleaving enzyme 2
BaF	murine interleukin dependent pro-B cell line
BBB	Blood brain barrier
BLH	Boving lung heparin
BSE	Boving spongiform encephalopathy
C4/C5/C6	Carbon 4/5/6
CD	Circular dichroism
CD4	Cluster of differentiation 4
CDR	Complementarity-determining regions
CJD	Creutzfeldt-Jakob disease
CMH	Chemically modified heparin
CMP	Cytidine monophosphate
CNS	Central nervous system
CSA	Chondroitin sulphate A

CSC	Chondroitin sulphate C
CSF	Cerebrospinal fluid
d.p.	Degrees of polymerisation
DNP	2,4-Dinitrophenol
DS	Dermatan sulphate
DSF	Differential scanning fluorimetry
EC_{50}	Half maximal effective concentration
ECM2	Extracellular matrix protein 2
ECMX	Extracellular matrix protein X
EDTA	Ethylenediaminetetraacetic acid
eIF2α	Eukaryotic Initiation Factor 2
ELISA	Enzyme-linked immunosorbent assay
Ext1	Exostosin-1 gene
F(ab')2	Fragment antigen binding 2
Fab	Fragment antigen binding
Fc	Fragment crystabizable
FcRn	Neonatal Fc receptor
FDA	USA Food and Drug Administration
FGF	Fibroblast growth factor
FGFR	Fibroblast growth factor receptor
FRET	Fluorescent resonant energy transfer
FTIR	Fourier transform infra-red
GAG	Glycosaminoglycan
GalN	Galactosamine
GalNAc	N-acetyl galactosamine
GF	Growth factor
GlcA	Glucuronic acid
GlcN	Glucosamine
GlcNAc	N-acetyl-D-glucosamine
GlcNS	N-sulpho-D-glucosamine
GST	Glutathione *S*-transferase
HA	Hyaluronic acid/hyaluronan
HB-EGF	Heparin-binding EGF-like growth factor

HDO	Heparin derived oligosaccharide
HEA	Hydroxyethylamine
HEK	Human embryonic kidney cells
HGF/SF	Hepatocyte growth factor or scatter factor
HIT	Heparin induced thrombocytopenia
HIV	Human immunodeficiency virus
HPLC	High performance liquid chromatography
HS	Heparan sulphate
HSPG	Heparan sulphate proteoglycan
IC_{50}	The concentration of an inhibitor where the response (or binding) is reduced by half
ICAM-1	Intercellular Adhesion Molecule 1 (CD54)
IdoA	Iduronic acid
Ig	Immunoglobulin
IgG	Immunoglobulin G
IgM	Immunoglobulin M
IMAC	Immobilised metal affinity chromatography
INF-ϒ	Interferon ϒ
IVIG	Intravenous immunoglobulin
Ki	Equlibrium constant
KS	Keratan sulphate
LMWH	Low molecular weight heparin
LRP	Lipoprotein receptor-related proteins
MALDI-TOF MS	Matrix-assisted laser desorption/ionization mass spectroscopy
MCA	7-methoxycoumarin
miRNA	Micro RNA
mMC-CPA	Mouse mast cell carboxypeptidase A
mMCP	Mouse mast cell protease
Mn	Number molecular weight
mRNA	messenger RNA
Mw	Weight average molecular weight
MWCO	Molecular weight cut-off
NDST	N-deacetylase/N-sulfotransferase enzyme

NFT	Neurofibrillary tangle
NG2	Neural/glial antigen 2
NICE	The National Institute for Health and Care Excellence
NK cells	Natural killer cells
NMDA	N-methyl-D-aspartate receptor
NMR	Nuclear magnetic resonance spectroscopy
NRG1	Neuregulin-1
NRG3	Neuregulin-3
PBS	Phosphate buffered saline
PC1	Principle component 1
PC2	Principle component 2
PCA	Principle component analysis
PD	Parkinson's disease
PDI	Polydispersity index
PEN-2	Presenilin enhancer 2
PET	Positron emission tomography
PF-4	Platelet factor 4
PfCTRP	*Plasmodium falciparum* micronemal protein
PfWARP	*Plasmodium falciparum* von Willebrand factor A domain-related protein
PG	Proteoglycan
PHF	Paired helical filament
pI	Isoelectric point
PMH	Porcine mucosal heparin
PMIH	Porcine musical intestinal heparin
PRELP	Proline And Arginine Rich End Leucine Rich Repeat Protein
PSLG-1	P-selectin glycoprotein ligand 1
PT	Prothrombin time
PVS	Polyvinyl sulphonate
RA	Rheumatoid arthritis
RAGE	Receptor for advanced glycation end-products
RT-PCR	Real time Polymerase chain reaction
SANS	Small-angle neutron scattering

SAXS	Small-angle X-ray scattering
SEC	Size exclusion chromatography
Ser-Gly	Serine-glycine
SHH	Sonic hedgehog gene
shRNA	Short hairpin RNA
SKNSH-SY5Y	Sub clone of human neuroblastoma cell line
SLRPS	Small leucine-rich proteoglycans
SRCD	Synchrotron radiation dircular dichroism
ST6Gal1	ST6 β-galactoside alpha-2,6-Sialyltransferase 1
TCA	Tricyclic antidepressants
Tm	Melting temperature
TNF-α	Tumour necrosis factor-α
UA	Uronic acid
UNLB	Unlabelled
UV	Ultra-violet
VEGF	Vascular endothelial growth factor
VH	Variable heavy chain
VL	Variable light chain
WHO	World Health Organisation
Xyl	Xylose

Chapter 1: Introduction

1.1 Proteoglycans

Proteoglycans (PGs) are a family of biomolecules comprised of a core protein with projecting glycosaminoglycan (GAG) chains (Esko JD, 2009; Ey, Prowse, & Jenkin, 1978). GAGs are a structurally complex class of carbohydrate polymers, composed of disaccharides with alternating monosaccharide residues; they are polyanionic and linear in structure (*idem*). A wide variety of different protein cores exist and this, combined with the polydisperse nature of the covalently bound glycosaminoglycans (GAGs), creates a ubiquitous group of molecules with wide ranging actions (*idem*).

The GAG family includes chondroitin sulphate (CS), dermatan sulphate (DS), keratan sulphate (KS), hyaluronan (HA), heparan sulphate (HS) and heparin (*idem*). The disaccharide building blocks of GAGs are composed of a (N-acetylated, N-sulphated or unsubstituted) hexosamine and a uronic acid residue (glucuronic acid or the C5 epimer, iduronic acid) (Backstrom et al., 1979; Bjorck & Kronvall, 1984; Hagner-McWhirter, Li, Oscarson, & Lindahl, 2004; Jacobsson et al., 1984).

A high level of structural variability is conferred through modifications to saccharide unit position, chain length, and the arrangement of sulphated modifications, which is specific to the biosynthetic cell origin and environment (Akerstrom & Bjorck, 1986; Gallagher & Walker, 1985). This diversity enables the formation of binding sites for a multitude of different ligands, encompassing growth, development and maintenance (e.g vascular endothelial growth factor (VEGF) (Ashikari- Hada, Habuchi, Kariya, & Kimata, 2005; Park, Keller, & Ferrara, 1993), hepatocyte growth factor/scatter factor (HGF/SF) (Ashikari, Habuchi, & Kimata, 1995), hepatocyte growth factor receptor (HGFR) (Jonquieres, Pizarro-Cerda, & Cossart, 2001), heparin binding-epidermal growth factor (HB-EGF) (Cook, Ashton, Karkaria, Siess, & Shipley, 1995), fibroblast growth factor (FGF) (Yates, Guimond, & Turnbull, 2004; Yayon, Klagsbrun, Esko, Leder, & Ornitz, 1991),

fibroblast growth factor receptors (FGFRs) (Esko & Lindahl, 2001), Wnt signaling pathway, sonic hedgehog protein (SHH) and stem cells), inflammation (e.g chemokines (Kuschert et al., 1999)), inhibition of lectin and selectin (Koenig, Norgard-Sumnicht, Linhardt, & Varki, 1998), coagulation (Damus, Hicks, & Rosenber.Rd, 1973), interferon- ϒ (INF-ϒ) (Sasaki et al., 2001) and tumor necrosis factor-α (TNF-α) (Kenig, Gaberc-Porekar, Fonda, & Menart, 2008)), neurodegenerative disease (e.g Alzheimer's disease (Snow & Wight, 1989), Parkinson's disease (Cohlberg, Li, Uversky, & Fink, 2002), prion disease (Bovine spongiform encephalopathy, Creutzfeldt-Jakob disease (Snow et al., 1990)), infectious disease (e.g malaria (Barragan et al., 2000), African sleeping sickness (Nishimura, Shima, Asakura, Ohnishi, & Yamasaki, 2005), leishmaniasis (Love, Esko, & Mosser, 1993), Human immunodeficiency virus (HIV) (Vives, Imberty, Sattentau, & Lortat-Jacob, 2005) and herpes simplex virus (Tiwari et al., 2006)) and other disease states such as cancer (Park et al., 1993).

Members of the GAG family have a varied phenotype, with CD, DS, KS, HS and HA expressed in multiple cell types and locations. Chondroitin sulphate, the most abundant GAG in the body (Buddecke, 2009), is present in PGs on the cell membranes in NG2 (nerve/glial antigen 2) (Price et al., 2011) and phosphacan (Maurel, Rauch, Flad, Margolis, & Margolis, 1994), secreted pericellularly in type XV collagen along with HS (Rehn, Hintikka, & Pihlajaniemi, 1994), extracellularly as aggrecan along with KS (Heinegard, 2009) and in versican (Shinomura, Nishida, Ito, & Kimata, 1993; Zimmermann & Ruoslahti, 1989) (Table 1).

Heparan sulphate is ubiquitously expressed on the cell membranes in syndecan (Bernfield et al., 1999) and in glycosylphosphatidylinositol–anchored proteoglycans, glypicans (Filmus & Selleck, 2001). HS can also be secreted in pericellular proteoglycans such as agrin, perlican and type XVIII collagen (Table 1) (Rehn et al., 1994).

Table 1: Four families of proteoglycans based on cellular location, and both gene and protein homology, adapted from (Iozzo & Schaefer, 2015).

Name	Predominant GAG	Location	Classification
Serglycin	Heparin	Intracellular	Secretory granules
Syndecan 1-4	HS	Cell surface	Transmembrane
NG2	CS	Cell surface	Transmembrane
Betaglycan	CS/HS	Cell surface	Transmembrane
Phosphacan	CS	Cell surface	Transmembrane
Glypican, 1-6	HS	Cell surface	GPI-anchored
Perlecan	HS	Pericellular	Basement membrane
Agrin	HS	Pericellular	Basement membrane
Collagen XVIII	HS	Pericellular	Basement membrane
Collagen XV	CS/HS	Pericellular	Basement membrane
Aggrecan	CS/KS	Extracellular	Hyalectan/lectican
Versican	CS	Extracellular	Hyalectan/lectican
Neurocan	CS	Extracellular	Hyalectan/lectican
Brevican	CS	Extracellular	Hyalectan/lectican
Biglycan	CS	Extracellular	SLRPS- C1 Canonical
Decorin	DS	Extracellular	SLRPS- C1 Canonical
Asporin	None	Extracellular	SLRPS- C1 Canonical
ECM2	None	Extracellular	SLRPS- C1 Canonical
ECMX	None	Extracellular	SLRPS- C1 Canonical
Fibromodulin	KS	Extracellular	SLRPS- CII Canonical
Lumican	KS	Extracellular	SLRPS- CII Canonical
PRELP	polylactosamine	Extracellular	SLRPS- CII Canonical
Keratocan	KS	Extracellular	SLRPS- CII Canonical
Osteoadherin	KS	Extracellular	SLRPS- CII Canonical
Epiphycan	DS/CS	Extracellular	SLRPS- CIII Canonical
Opticin	None	Extracellular	SLRPS- CIII Canonical
Osteoglycin	KS	Extracellular	SLRPS- CIII Canonical
Chondroadherin	KS	Extracellular	SLRPS- CIV Non-canonical
Nyctalopin	None	Extracellular	SLRPS- CIV Non-canonical
Tsukushi	None	Extracellular	SLRPS- CIV Non-canonical
Podocan	None	Extracellular	SLRPS- CV Non-canonical
Podocan-like I	None	Extracellular	SLRPS- CV Non-canonical
Testican, 1-3	HS	Extracellular	SPOCK

Keratan sulphate is also found extracellularly, in small leucine-rich PG (SLRPS) (Iozzo, 1997), fibromodulin (Heinegard et al., 1986) and lumican (Svensson, Narlid, & Oldberg, 2000). Dermatan sulphate is found in the SLRPS decorin (Krumdieck, Hook, Rosenberg, & Volanakis, 1992) and epiphycan (H. J. Johnson et al., 1997) as shown in Table 1. Prolargin (PRELP) does not have GAG branching but binds HS through collagen and

perlecan binding in the basement membrane. Similarly, asporin does not have the serine-glycine repeats required for GAG modification but maintains structural homology with the other CII canonical SLRPS (Table 1) (Henry et al., 2001).

Heparin is expressed solely in mast cell and basophil secretory granules through attachment to a serine-glycine rich protein core serglycin (Metcalfe et al., 1979). Serglycin utilises electrostatic forces to bind proteases, inflammatory mediators, chemokines, cytokines and growth factors into granular storage (Douaiher et al., 2014).

Proteoglycans are involved with many physiological processes, including skin and tendon strength, viscoelasticity of blood vessels, cartilage structure and as an essential component of the extracellular matrix (Buddecke, 2009), with a GAG constituents playing the primary role in these functions.

1.2 Glycosaminoglycans

The disaccharide chains of GAGs are composed of repeating residues comprising of a uronic acid, typically glucuronic acid (GlcA), or its C-5 epimer iduronic acid (IdoA), and a hexosamine (Backstrom et al., 1979; Hagner-McWhirter et al., 2004; Jacobsson et al., 1984), usually glucosamine (GlcN) or galactosamine (GalN) (Turnbull, Powell, & Guimond, 2001) forming a linear polysaccharide. Covalent modification to the disaccharide chain allow GAGs specific to tissue and cell type to be manufactured through a process of incomplete enzymatic modifications (Buddecke, 2009). The uronic acid residues can be 2-O-sulphated (IdoA2S or more rarely GlcA2S) (Rong, Habuchi, Kimata, Lindahl, & Kusche-Gullberg, 2001) or remain unsulphated, while the glucosamine residues can be N-sulphated (GlcNS)(Lindahl, Feingold, & Roden, 1986) and/or O-sulphated, N-acetylated (GlcNAc) (Habuchi, Habuchi, & Kimata, 1995; Liu, Shworak, Fritze, Edelberg, & Rosenberg, 1996) or remain unsulphated as the free amine (GlcN) (Born, Jann, Assmann, Lindahl, & Berden, 1996). Galactosamine (GalNAc) containing GAGs (CS, DS and KS) can be O-sulphated but

not N-sulphated (*idem*). Hyaluronic acid contains no sulphate moieties and it is not covalently attached to a core protein, but instead interacts with proteoglycans via a HA binding motif (Laurent & Fraser, 1992). O-linked and N-linked glycans (typically 10-14 residues) still populate the core protein structure, but these glycans are dwarfed in size by the significantly larger GAG chains (40-10,000 kDa) (Casu, 2005).

Heparin, HS, DS and CS have a common tetrasaccharide linkage region consisting of uronic acid (β1-3)Gal(β1-3)Gal(β1-3)Xyl(β1-0)-Ser containing sulphation at both position C4 and C6 in the galactose residues (Sugahara, Ohi, Harada, Dewaard, & Vliegenthart, 1992; L. J. Zhang & Esko, 1994) and phosphorylation at C2 of the xylose (Moses, Oldberg, Cheng, & Fransson, 1997). Preferential synthesis of HS occurs over CS when the linkage region contains three closely spaced Ser-Gly repeats in the core protein, with the amino acid environment containing a hydrophobic residue and a group of acidic residues (L. J. Zhang & Esko, 1994).

1.3 Heparin and heparan sulphate

1.3.1 Structure

Heparan sulphate and the more highly sulphated homogenous analogue heparin have been shown to contain the most structural diversity of any of the molecules expressed in multicellular organisms (Casu & Lindahl, 2001). Both heparin and HS have β1-4 glycosidic linkages and share a common biosynthetic pathway (Rabenstein, 2002) originating from the unsulphated precursor N-acetyl heparosan (Casu & Lindahl, 2001).

HS has a domain-like secondary structure, with regions of high sulphation levels (NS domains), intermediate domains comprising of sulphated and non-sulphated (N-acetylated) disaccharides (NA/NS domains) and low/unsulphated sulphate regions (NA domains)(Figure 1) (Esko & Lindahl, 2001).

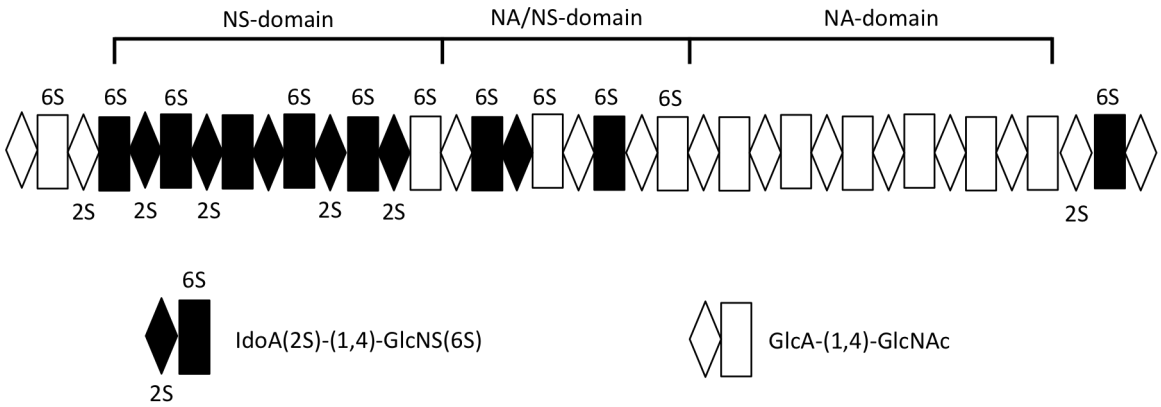

Figure 1: Schematic illustrating the domain organisation of heparan sulphate. Tri-sulphated disaccharide, IdoA(2S)-GlcNS(6S) most predominantly in the NS-domain, while unsulphated disaccharide GlcA-GlcNAc appears most predominantly in the NA-domain. Adapted from (Rabenstein, 2002)

The monosaccharide content is much more varied in HS than heparin. Uronic acid residues, β-D-glucuronic acid and α-L-iduronic acid can be 2-O-sulphated (IdoA(2S) or more rarely GlcA(2S)) and found in the NS domain, or unsulphated in the NA/NS domains (Casu, 2005). The α-D-N-acetylglucosamine can be N-sulphated (GlcNS), N-acetylated (GlcNAc), 6-O-sulphated (GlcNS(6S) or GlcNAc(6S)) or more rarely, unsubstituted (GlcN)(Figure 2) (Esko & Lindahl, 2001). Rarely, the GlcNS and GlcNS(6S) can also be 3-O-sulphated (GlcNS(3S) and GlcNS(3,6S)) (Rabenstein, 2002). The ratio of GlcNS to GlcNAc is approximately 1:1 in HS, due to GlcNAc predominantly in the NA domains (*idem*).

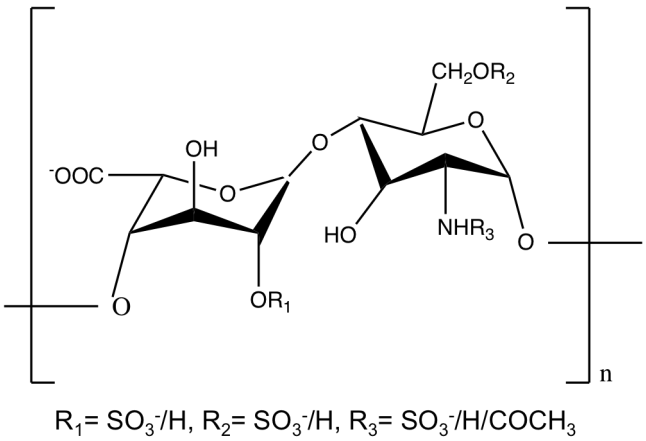

Figure 2: Schematic of the heparan sulphate disaccharide repeat unit, demonstrating the structural diversity of this glycopolymer. Adapted from (Patey, Edwards, Yates, & Turnbull, 2006).

Heparin exists as a linear glycopolymer comprised of pyranose rings adopting a variety of structures dependent on the ring substitutions and neighboring ring modifications, usually in energetically favorable conformations (B. Mulloy, Forster, Jones, & Davies, 1993). Glucuronic acid and glucosamine adopt the $^{4}C_{1}$ chair conformation in which all functional groups apart from the anomeric hydroxyl group of glucosamine are equatorial (Ferro et al., 1986). The more flexible IdoA adopts either the $^{1}C_{4}$ chair or $^{2}S_{0}$ boat conformations, with unsubstituted IdoA most commonly occupying the $^{1}C_{4}$ conformation (Yates et al., 1996).

Heparin may be thought of as more highly sulphated, homogenous version of HS, representing the NS domain; although it does include regions of lower sulphation interspersed throughout the molecule (Rabenstein, 2002). The GlcNS to GlcNAc ratio is 4:1 representing the absence of the NA unsulphated region present in HS (*idem*). The most common disaccharide in heparin is α-L-iduronic acid(2S)-(1-4)-α-D-N-sulphoglucosamine (6S), accounting for ≈ 90 % of bovine lung heparin (BLH) and ≈ 70 % of porcine mucosal heparin (PMH) (*idem*). Heparin is more highly sulphated than HS, largely due to the more restricted enzymatic action of the endosulphatases, thereby reducing O-sulphate levels that are most prominent at position 6 of the glucosamine residue (Casu, 2005). Dynamic biosynthesis of HS creates variable regions of sulphation depending on cell and tissue type and degree of cell differentiation. This complexity is thought to be responsible for the enormous variation in biological functions (Turnbull et al., 2001).

Since 1935, heparin has been extracted and purified from animals and utilised pharmaceutically as an anticoagulant. This is due to the ability of heparin to bind the plasma serine protease inhibitor, antithrombin III (AT). The discovery of a pentasaccharide AT binding sequence was the first evidence that a specific structural modification in the GAGs enabled this interaction (Casu et al., 1981). The pentasaccharide sequence GlcNAc/NS(6S)-GlcA-GlcNS(3,6S)-IdoA(2S)-GlcNS(6S) includes a rare 3-O-sulphate

modification on GlcNS(6S) (Casu et al., 1981; Riesenfeld, Thunberg, Hook, & Lindahl, 1981). Only one third of all heparin chains confer anticoagulant activity in this AT binding pentasaccharide (*idem*).

1.3.2 Biosynthesis

Heparin biosynthesis begins from a serglycin protein core through a tetrasaccharide linker comprising of xylose, galactose (two) and glucuronic acid residues in the form of the β-GlcA-(1-3)- β-Gal-(1-3)- β-Gal-(1-4)- β-Xyl- motif attached to random serine residues within serglycin (Lindahl, 1989). Polymerisation of the glycan chain occurs from this GlcA residue with sequential addition of the monosaccharides GlcNAc and GlcA $[GlcA\text{-}(1,4)\text{-}GlcNAc]_n$ (Figure 3) (*idem*).

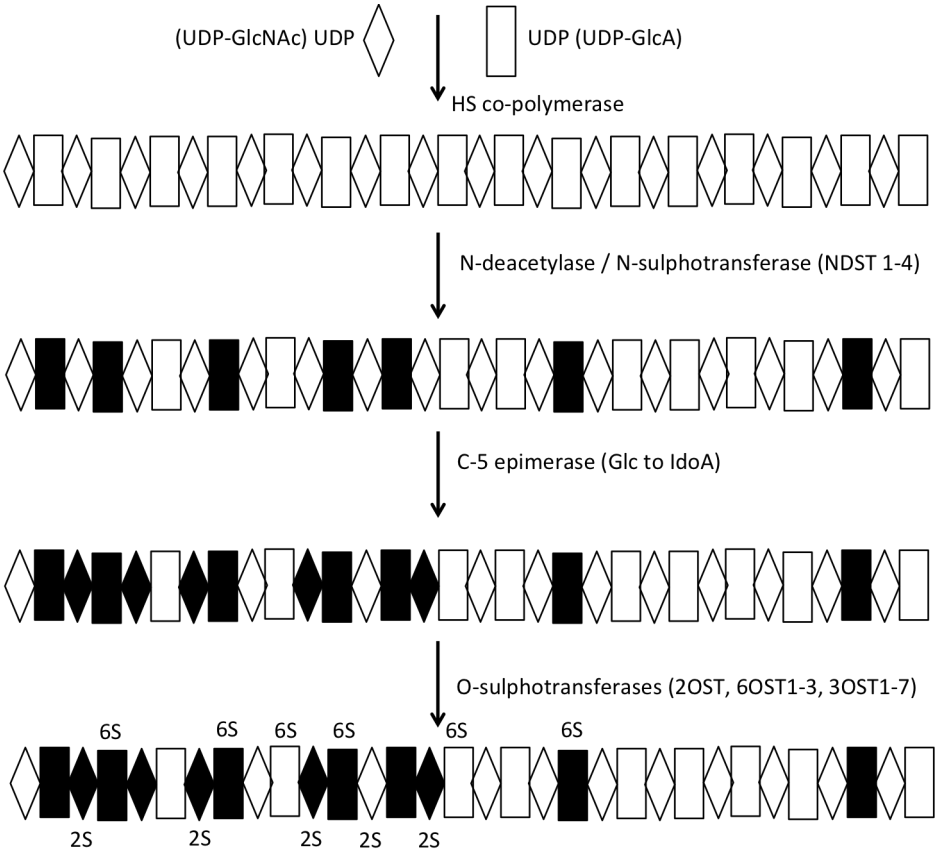

Figure 3: Schematic of the enzymes responsible for heparan sulphate polymerisation of UDP-GlcNAc and UDP-GlcA, and the covalent modification of the residues. Figure modified from (Bernfield et al., 1999)

Enzymes may modify the polymer chain although this does not necessarily occur to completion. N-deacetylase/N-sulphotransferase (NDST) may partially convert GlcNAc to GlcNS; NDST proceeds along the heparin chain until reaching an intractable GlcNAc residue, leading to the incomplete N-sulphation of the heparin chain (Kjellen & Lindahl, 1991). The action of N-deacetylase/N-sulphotransferase restricts further chain modification, as the subsequent enzymatic modifications rely on the presence of GlcNS residues (Rabenstein, 2002). C5-epimerase catalyses GlcA to IdoA and is specific only to GlcA residues at the reducing end of GlcNS in the GAG chain (Hagner-McWhirter, Lindahl, & Li, 2000). IdoA can be modified with 2-O-sulphotransferase, but if attached to C-1 of GlcNS(6S) is not a viable substrate (Rabenstein, 2002). GlcNS can be modified with a 6-O-sulphotransferase, however the disaccharide IdoA(2S)-GlcNS(6S) is abundant in heparin indicating the 2-O-sulphation occurs before the 6-O-sulphation (*idem*).

Less frequently, modifications are seen that require 2-O-sulphation of GlcA (GlcA(2S)), 6-O-sulphation can occur in the GlcNAc adjacent to a disaccharide containing a GlcNS and GlcNS(6S) can be 3-O-suphated as seen in the AT binding pentasaccharide (Lindahl, Backstrom, Thunberg, & Leder, 1980).

In HS, chain formation, polymerisation and modification occur similarly, but with an organised domain structure, therefore containing fewer O-sulphate modifications (Rabenstein, 2002). The domain regions are split into a structurally modified region (NS domain), which includes a higher proportion of epimerised IdoA, an intermediate region of modification (NA/NS domain) and a region of low enzymatic modification (NA domain) (Sugahara & Kitagawa, 2000).

In the final phase of biosynthesis, desulphation by an endosulphatase produces HS whereas depolymerisation through selective cleavage of GlcA by an endo-β-D-glucuronidase results in a polydisperse mixture of heparin chains (Robinson, Horner, Hook, Ogren, & Lindahl, 1978).

1.3.3 Bioactivity

Heparin and heparan sulphate interact with a multitude of extracellular proteins that regulate and modulate bioactivity. The more flexible pyranose ring in IdoA, compared to GlcA and GlcN monosaccharide units, is thought to explain the ability of heparin and HS in binding to a wide range proteins; this is believed to be due to the anionic groups interacting with cationic amino groups present on the target proteins (Rabenstein, 2002). Non-ionic hydrogen bonding and hydrophobic interactions may also contribute to protein binding (Noti & Seeberger, 2005). Utilising conformationally locked synthetic carbohydrates; Das *et al*. were able to show that the $^{2}S_{0}$ skew-boat IdoA conformation regulates the exogenous anti-thrombotic activity of heparin (Das et al., 2001).

Studies utilising gene disruption of N-deacetylase/N-sulphotransferase-2 in transgenic mice produced a low-sulphated version of heparin (Humphries et al. 1999). The mast cells located in transgenic murine skeletal muscle lacked metachromatic granules and failed in storing mouse mast-cell proteases (mMCP)-4, (mMCP)-5 and carboxypeptidase (mMC-CPA) (Humphries et al., 1999). The study conducted by Humphries *et al.* illustrated the action of heparin during post-translational modification of the proteases, showing control in levels of specific positively charged proteases inside mast cells (*idem*). These proteases have a variety of roles *in vivo*: inflammatory and anti-inflammatory, protective and deleterious, in allergy, tissue homeostasis and innate immunity (Caughey, 2011). Research done to reduce the pro-inflammatory mediator histamine in the transgenic mice indicated a stabilising relationship between deprotonated histamine (pH 5.2-6.0) (Humphries et al., 1999) (R. G. Johnson, Carty, Fingerhood, & Scarpa, 1980) and highly negatively charged heparin through electrostatic interactions (Rabenstein, 2002).

Heparan sulphate proteoglycans (HSPGs) have many wide-ranging activities with modifications to the GAG sequence and protein core permitting a plethora of different HSPGs. Examples of HSPGs include:

- HSPGs in basement membrane such as perlecan, agrin and type XVIII collagen (Rehn et al., 1994) that work in conjunction with components of the extracellular matrix to form basement membranes

- HSPG scaffolds that bind cytokines, chemokines, growth factors (GF) and morphogens providing a region for accumulation and interaction including morphogen gradient formation, essential for cell specification and development. One example includes morphogen gradients utilised in leukocyte recruitment and homing during an immune response (D. Yan & Lin, 2009)

-HSPGs act as protease receptors, maintaining spatial distribution and activity (Casu et al., 1981)

-HSPGs in cell membranes act to facilitate extracellular matrix-cell attachment, cell-cell attachment and motility with integrins and other factors

-HSPGs in cell membranes co-operate as receptors for growth factors such as tyrosine kinase (Cohen et al., 1995) and fibroblast (Yayon et al., 1991) GF receptors

-HSPGs in membranes act as endocytic receptors for clearance of ligands such as lipoprotein lipase in the liver (Sarrazin, Lamanna, & Esko, 2011).

1.3.4 Coagulation

Heparin binds the serpin AT at residues Lys114, Lys 125, Arg 129, Asn45, Arg46, Arg47, Lys11, Arg13 and Glu113 (Schedin-Weiss, Arocas, Bock, Olson, & Bjork, 2002) (Huntington, 2005). The heparin:AT pair then go on to form complexes when thrombin (factor IIa), factor IXa, Xa, XIa, and XIIa serine proteases (Lever & Page, 2002) attack the Arg 393-Ser394 bond (Olson & Bjork, 1994) in the carboxyl terminal region of AT, inducing a conformational change and inhibiting the serine protease (Fu, Liu, Frost, & Lemere, 2010). Optimal levels of heparin accelerate the natural anticoagulant action of AT by up to 2000-fold (*idem*). The heparin pentasaccharide binds AT altering the conformation of the

serpin creating a more effective binding site for the serine proteases; factors IXa, Xa, XIa and XIIa (Racke et al., 2005); AT acts as a suicide substrate (Huntington, 2005).

Heparin also includes a polysaccharide sequence (≥ 18 saccharides long) utilised as a scaffold, bringing the proteinase thrombin and the serpin AT into close proximity therefore increasing the AT inhibition of thrombin (Bjork & Lindahl, 1982). These longer polysaccharides in unfractionated (UF) heparin also stimulate the release of platelet factor 4 (PF-4) from platelets and can form complexes that become auto-reactive in heparin-induced thrombocytopenia type 2 (HIT) (Deitcher & Carman, 2001).

1.3.5 Clinical use

Low molecular weigh heparins (LMWHs) have been developed by chemical depolymerisation (cleavage by β-elimination of benzyl ester, nitrous acid depolymerisation and peroxyl radical cleavage) (Hirsh et al., 1998) (Quader, Stump, & Sumpio, 1998) to form ardeparin, dalteparin, enoxoparin and reviparin, through enzymatic methods (β-elimination by heparinase 3) to form tinzaparin or by size fractionation of unmodified heparin (Linhardt & Gunay, 1999). These LMWH have reduced content of the 18-saccharide scaffold contained in full-length heparin preparations and therefore reduce thrombin interactions, leading to an improved therapeutic index, while retaining the specific AT binding pentasaccharide (Lindhardt and Sibel-Gunay 1999). The factor IIa:factor Xa binding ratio of these LMWHs ranges from 1.6 in tinzaparin to 4.2 in reviparin (Gray, Mulloy, & Barrowcliffel, 2008).

1.3.6 Research into other applications of heparin as a potential therapeutic

Heparin has been researched as a possible treatment for many HSPG binding protein related diseases with success in many varied pathologies including but not limited to the following examples.

Heparin has been identified as a molecule capable of blocking parasite invasion of host cells by competing with exogenous HS; in *P.falciparum* malaria, heparin is thought to bind the viral TRAP (thrombospondin-related anonymous protein) sporozoite surface receptor (Akhouri, Bhattacharyya, Pattnaik, Malhotra, & Sharma, 2004). Heparin also reduces cytoadherance (Xiao, Yang, Patterson, Udhayakumar, & Lal, 1996) and rosetting (Carlson et al., 1992) of *P. falciparum* infected erythrocytes helping to reduce the burden of the disease on the sufferer.

Heparin can also block viral cell invasion through competition with host cell HS surface receptors. Diseases such as herpes (Nahmias & Kibrick, 1964), influenza (Skidmore et al., 2015), dengue fever (Y. L. Lin et al., 2002), yellow fever (Germi et al., 2002), varicella zoster (responsible for chicken pox/shingles), hepatitis B (Schulze, Gripon, & Urban, 2007) and C (Basu et al., 2007), HIV (M. Ito et al., 1987), coxsackie virus (Frizelle, Schwarz, Huber, & Leslie, 1992) and Zika virus (Ghezzi et al., 2017) all show heparin inhibition.

Aberrant protein aggregation diseases such as type II diabetes (Jaikaran & Clark, 2001), neurodegenerative diseases bovine spongiform encephalopathy (BSE), Creutzfeldt-Jakob disease (CJD) (Vieira, Cordeiro, Caughey, & Silva, 2014), Parkinson's disease (PD) (Cohlberg et al., 2002), and Alzheimer's disease (AD) (Bergamaschini, Rossi, Vergani, & De Simoni, 2009) all include HSPGs in aggregates.

Heparan sulphate proteoglycans are thought to act as a nucleation point for aberrant fibril formation, rich in β-sheet structure; fibrils are the main component of amyloid plaques. Extracellular prion-like conversion to fibrillar protein progresses through the neurons via cell membrane HSPG binding (B. B. Holmes et al., 2013). Cellular uptake of fibrillar protein and therefore propagation of seed fibril proteins was halted by heparin, chlorate, heparinase and knockdown of HSPG biosynthetic enzyme, Ext1 (exostosin glycosyltransferase 1) (*idem*).

1.4 Dementia

Dementia is commonly defined as a chronic or progressive syndrome of a diseased brain, which manifests as disturbances in higher functioning including memory, language, comprehension, learning capacity, and judgement with no changes seen in consciousness (WHO, 2012). These chronic disturbances are usually preceded by changes in mood, emotional control or motivation (*idem*). Neurological changes can be expressed in different behavioural and psychological symptoms that are commonly seen in dementia sufferers including aggression, anxiety, disinhibition, euphoria, irritability, depression, and hallucinations (Hughes, 2011).

The most common form of dementia is AD, which represents approximately 60% of all dementia cases (Boltz, 2011). Other forms of dementia include vascular dementia, dementia with Lewy bodies, fronto-temporal dementia and even more rarely Creutzfeldt-Jakob disease (*idem*). Vascular dementia is caused by the loss of brain tissue through impaired cerebral blood supply, strokes, sclerotic lesions in cerebral vessels, high blood pressure, high cholesterol, and diabetes (*idem*). Dementia with Lewy bodies has characteristics seen commonly in both AD and PD, caused by α-synuclein protein deposits (Lewy bodies) in neuronal cytoplasm, found throughout the brain (Lee, Goedert, & Trojanowski, 2001). Fronto-temporal dementias are a range of conditions describing morphological changes to the frontal lobe and/or temporal lobes of the brain (*idem*). Approximately half of these cases are due to aggregation of microtubule stabilising tau protein into tangles or 'Pick bodies', while the other half are due to a protein that stains for ubiquitin called transactive response DNA binding protein (TDP-43) (Hughes, 2011).

In April 2012, the World Health Organisation (WHO) announced via press release that 'dementia cases set to triple by 2050, but still largely ignored' (WHO, 2012). The statistics released with this report highlight 35.6 million people are currently living with dementia, with this figure estimated to rise to 115.4 million people by 2050 (*idem*). The

report highlights problems in early diagnosis, with progress in this area allowing medical intervention to control symptoms, affording few more years to ailing individuals. The report also notes medical intervention currently treats some of the symptoms of dementia, but goes no way to address the causes of the condition (*idem*).

1.5 Alzheimer's disease

There are 2 main sites of anomalous protein deposits in AD; plaques formed by β-amyloid (Aβ) protein and neurofibrillary tangles formed by hyperphosphorylated tau proteins (microtubule associated protein τ) (Lee et al., 2001). The amyloid hypothesis of AD was first suggested by Dennis Selkoe in 1991 and has become a central theme in the aetiology of AD (Selkoe, 1991). Alongside this protein misfolding, oxidative and inflammatory damage result in neuronal energy failure, synaptic dysfunction and cell death (Querfurth & LaFerla, 2010).

Tau is a low molecular weight (55 – 70 kDa) microtubule associated protein (MAP) expressed predominantly in CNS axons, encoded by a single 16 exon gene at chromosome 17q21 (Neve, Harris, Kosik, Kurnit, & Donlon, 1986). Tau modulates the assembly of microtubules into bundled forms, which provide strength and stability to axons during morphogenesis and provide tracks for vesicular transport (Drechsel, Hyman, Cobb, & Kirschner, 1992). Tau isoforms differ developmentally, with only the smallest isoform present in the foetal human brain and 6 isoforms present in adults (Goedert, Spillantini, Jakes, Rutherford, & Crowther, 1989).

The microtubule binding motifs occur at the carboxy-terminal of tau, with phosphorylation sites located flanking these binding regions; increasing phosphorylation at these sites negatively regulates microtubule binding (Drechsel et al., 1992). Hyperphosphorylation of tau excludes microtubule binding and leads to self-association to form paired helical filaments (PHF) of tau either consisting of a pair of proteins twisted

round a third (Crowther & Wischik, 1985), or straight filaments lacking this helical structure (Crowther, 1991). Aggregates of PHF form neuronal and glial cell inclusions called neurofibrillary tangles (NFT), which are thought to play a role in cellular degeneration through disruption to axon cytoskeleton, vesicle transport and synaptic dysfunction (Lee et al., 2001). The exact aetiology of tau in AD has yet to be fully elucidated, with NFT formation also thought to have a neuroprotective role as a neuronal response to oxidative damage (Medina & Avila, 2014).

For information regarding other hypotheses for AD pathogenesis, including the role of tau cytoskeletal microtubule associated protein, the reader is referred to the review by Kaj Blennow *et al.* (Blennow, de Leon, & Zetterberg, 2006).

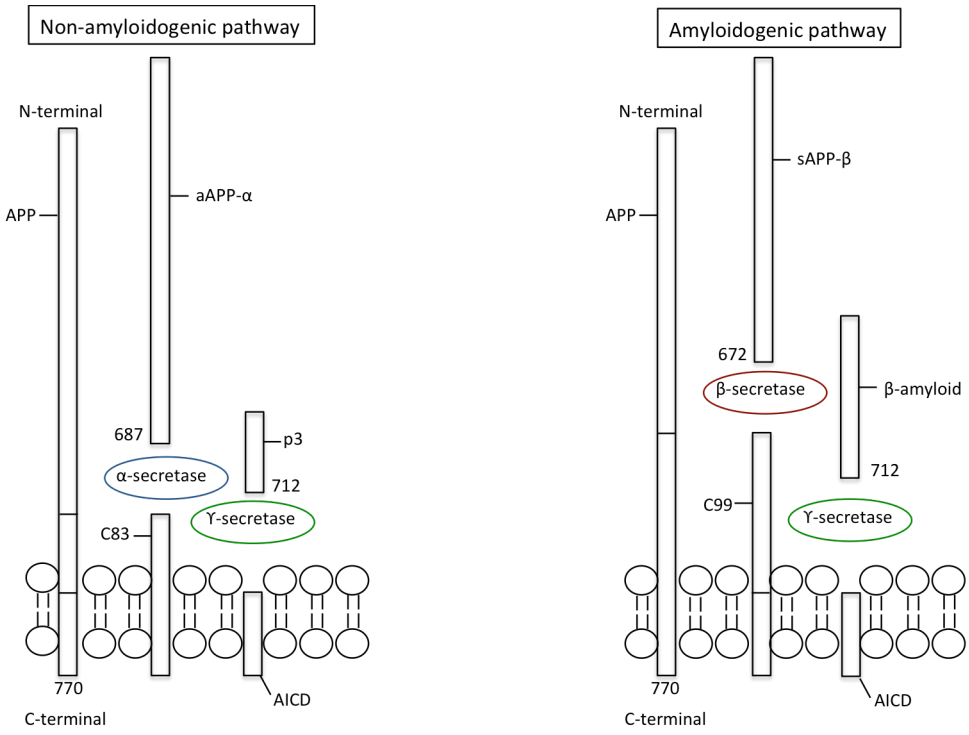

Figure 4: Schematic of non-amyloidogenic and amyloidogenic metabolism of the 770 amino acid transmembrane APP. Modified from (Stanga et al., 2010).

Aβ is a 36-43 residue peptide produced in normal metabolism through the sequential processing of amyloid precursor protein (APP) (largest isoform 770 residues in length); a single trans-membrane protein expressed mainly in neuronal synapses (Figure 4) (Ballard et al., 2011). In the amyloidogenic pathway, implicated in Alzheimer's disease,

APP is cleaved by a β-secretase known as BACE1 (β-site APP cleaving enzyme) or memapsin-2; a class I transmembrane aspartyl protease (Selkoe, 1991). APP cleavage by BACE1 liberates soluble APP-β peptide with the remaining C99 peptide membrane anchored (*idem*). BACE1 processing is followed by γ-secretase (multi-unit enzyme) cleavage of the membrane anchored C99 peptide. γ-secretase is a multi-subunit protease consisting of a presenilin (catalytic subunit), nicastrin, APH-1 and PEN-2 (Kimberly et al., 2003). γ-secretase proteolysis of C99 results in the formation of an amyloidogenic Aβ fragment, which is released into the cerebral intracellular space, and the APP intracellular cytoplasmic domain (AICD) (Selkoe, 1991), targeted to the nucleus signalling transcription activation (Querfurth & LaFerla, 2010).

In the non-amyloidogenic pathway, APP is first cleaved by α-secretase, a disintegrin and metalloproteinase domain-containing protein 10 (ADAM-10) consisting of a disintegrin and a metalloprotease domain that liberates sAPP-α peptide and a membrane bound C83 peptide (Querfurth & LaFerla, 2010). This is then further modified by the same γ-secretase cleavage to release p3 fragment, leaving the APP intracellular domain (AICD) (*idem*).

Following APP cleavage by BACE1, $A\beta_{40}$ is a much more prevalent species than pro-aggregating $A\beta_{42}$ species, with 90-95% $A\beta_{40}$ and only 5-10% $A\beta_{42}$ (Iwatsubo, Saido, Mann, Lee, & Trojanowski, 1996). One explanation of AD pathogenesis suggests imbalance between production and clearance of these $A\beta_{42}$ peptides allowing them to coalesce, aggregate and deposit (Querfurth & LaFerla, 2010). This imbalance was suggested from the study of early-onset dementia that occurs frequently in trisomy 21 (Down's syndrome) sufferers, as the APP gene is located on the long arm of chromosome 21 at position 21.3 (Mrak & Griffin, 2004). This extra gene increases transcription levels of APP mRNA, leading to an increase in $A\beta_{42}$ when compared to that of healthy controls; Mrak and Griffin believe this to be a contributing factor to Down's early onset AD (Mrak & Griffin, 2004).

Investigations by Ehehalt *et al*. postulate the processing pathway of APP depends on the cholesterol and sphingolipid rich lipid raft formations present in the cell membranes (Ehehalt, Keller, Haass, Thiele, & Simons, 2003). The apolipoprotein E4 allele has been shown to be a major risk factor for AD (Corder et al., 1993), with low-density lipoprotein (LDL) cholesterol levels in mid-life correlating with increased AD risk (Kivipelto et al., 2001). The removal of lipid rafts inhibited the production of Aβ in mouse neuroblastoma N2a cells (Ehehalt et al., 2003). Amyloid precursor protein present in raft formations was cleaved by BACE1, while APP found outside these formations was processed non-amyloidogenically (*idem*).

Aβ spontaneously coalesces into multiple different protein conformations, beginning as oligomeric forms consisting of 2 to 6 peptides (Kayed et al., 2003). These accretions then collect into intermediate formations before forming insoluble fibrils with complex β-pleated sheet formations called senile plaques (Kayed et al., 2003). Neurotoxic oligomers and plaques disrupt critical neuronal metabolic processes, cell-to-cell transport and communications, illicit immune response network causing inflammatory damage and oxidative damage (Lesne et al., 2006). In both transgenic mouse models and human AD brains, a mixture of Aβ species is present, from monomers to mature plaques (Haass & Selkoe, 2007). The hypothesis that soluble oligomers of Aβ cause the biochemical, and electrophysiological effects (e.g through the inhibition of hippocampal long term potentiation) seen in the brain is supported by other related neurodegenerative diseases, such as Parkinson's and Huntington's (*idem*). It is hypothesised large plaque formations represent reservoirs in equilibrium with the soluble Aβ species (*idem*).

Synapses in the hippocampus begin to decline in the early stages of AD, referred to as mild cognitive impairment (MCI) with an increasing loss of synapses (Querfurth & LaFerla, 2010). Aggregation of Aβ causes neuronal dysfunction at the synapses, a reduction

in dendritic spines (reducing communication with other axons) and reduced synaptic transmission (Querfurth & LaFerla, 2010).

The pathway of neuronal degeneration begins in the entorhinal cortex, through the hippocampus, into the posterior temporal and parietal neocortex into the surrounding cerebral cortex in late stage AD (Vemuri & Jack, 2010). The progression of AD causes initial generalised atrophy in the mild AD brain with increased ventricle size moving to severe cortical shrinkage and enlarged ventricles in the severely affected patient (Vemuri & Jack, 2010).

The typical symptom of memory loss, seen in AD patients, is due to hippocampal and cortical acetylcholine transferase level insufficiencies and loss of cholinergic projections into the basal forebrain (Selkoe, 1991). Neuronal loss leads to a reduction in the release of neurotransmitter and the number of receptors available in the acetylcholine, dopamine and N-methyl-D-aspartate (NMDA) pathways (*idem*). Memantine, an NMDA receptor agonist, aids regulation of glutamate as a neuroprotectant against excesses associated with neuron loss (NICE, 2011). Cholinesterase inhibitors like donepezil, galantamine and rivastigmine block the normal breakdown of acetylcholine, increasing intrinsic efficacy (*idem*). These treatments help remaining functional neurons retain their limited capacity, however the action of these drugs diminishes with reducing neuron number, therefore a treatment plateau occurs when this limit is met; the currently available pharmaceuticals do not treat the causes of AD, which progresses typically.

BACE1 catalyses the initial and rate limiting cleavage of APP as a precursor to the production of $A\beta_{42}$ and is therefore seen as a superior drug target for the therapy of AD (Sinha et al., 1999).

1.6 β-Site APP cleaving enzyme 1 (BACE1)

BACE1 (β-site APP cleaving enzyme 1) is a type-1 transmembrane aspartyl protease ubiquitously expressed in the brain and pancreas (Sathya et al., 2012). High enzymatic activity is only found in the brain due to alternative splice variants of BACE1 (Mowrer & Wolfe, 2008). The BACE1 gene is located on the long arm of chromosome 11 at position 23.2 (Sathya et al., 2012), spans approximately 30 kilobases and includes 9 exons (Cole & Vassar, 2007). Maturation of pro-BACE1 to BACE1 occurs after endoplasmic reticulum processing and involves the removal of both the pro-peptide domain region and N-terminal signal sequence, and the N-glycosylation of 4 asparagine residues (Haniu et al., 2000). Mature BACE1 is sulphated at N-glycosylated moieties and three C-terminal cysteine residues are palmitoylated (Benjannet et al., 2001). N-glycosylation is required for enzymatic function while palmitoylation is utilised for cellular trafficking and localisation (*idem*).

The 501 amino acid splice variant with β-secretase activity is found almost exclusively in the neuronal endosome, Golgi apparatus and the trans-Golgi network (Vassar et al., 1999). BACE1 present in the human pancreas is expressed in high levels but has low levels of β-secretase activity; this splice variant is missing a large majority of exon 3 (Ehehalt et al., 2002)

BACE1 has optimum enzymatic activity at pH ≈ 4.5, due to the primary action in acidified endosomes (Willem, Lammich, & Haass, 2009). BACE1 forms homodimers when localised in cell membrane, but does not when released as a soluble form (Westmeyer et al., 2004). The dimerisation occurs before pro-BACE1 processing to mature BACE1 and improves the affinity and turnover of APP processing (*idem*).

BACE1 is transported to the axonal membrane (predominantly the pre-synaptic membrane) and can be released from the axon terminal (Lazarov, Lee, Peterson, & Sisodia, 2002). BACE1 and APP are internalised together from the neuronal cell membrane to the

early endosomes; this is where APP processing occurs, ultimately generating Aβ (Koo & Squazzo, 1994). BACE1 is subsequently recycled into the trans-Golgi network (*idem*). BACE1 proteolysis of APP and the production of Aβ is dependant on endocytosis, with α-secretase cleavage showing no change in activity when endocytosis is inhibited (Ehehalt et al., 2003).

The production of $A\beta_{42}$ species, through cleavage of APP by BACE1, is increased in most familial AD (FAD) mutations (X. D. Cai, Golde, & Younkin, 1993). Such modification in regions that enhance the substrate binding to BACE1, for example in the Swedish APP_{670NL} mutation, lysine-methionine is replaced with asparagine-leucine at position 670 becoming an improved substrate of BACE1 therefore generating greater turnover of all products including $A\beta_{42}$ (X. D. Cai et al., 1993; Haass et al., 1995).

1.6.1 Structure

BACE1 peptide forms a compact globular arrangement with enzyme activity conferred through the typical motif for eukaryotic aspartyl protease; two aspartic acid residues at positions 93 and 289 (Hong et al., 2002). As a result of gene duplication, aspartyl proteases have a double domain structure, each presenting an aspartyl residue in the enzyme active site (Holm, Ollo, Panthier, & Rougeon, 1984). Aspartyl proteases were historically called acid proteinases due to their optimal activities at pH 1.5 – 5.0 (Polgar, 1987). When crystallised, BACE1 was found to share 30-37% amino acid homology (Haniu et al., 2000) with other mammalian and fungal aspartyl proteases, for example renin, cathepsin D, pepsin, pencillopepsin and rhisopus pepsin (Venugopal, Demos, Rao, Pappolla, & Sambamurti, 2008).

The action of aspartyl proteases is widely accepted to occur through an acid-base mechanism. The deprotonated α-carboxylic acid in the aspartate residue forms a hydrogen bond with a water molecule, which completes a nucleophilic attack of the carbonyl carbon

in the scissile bond, creating a tetrahedral oxyanion intermediate (Suguna, Padlan, Smith, Carlson, & Davies, 1987) (Brik & Wong, 2003). Protonation of the amide nitrogen caused by

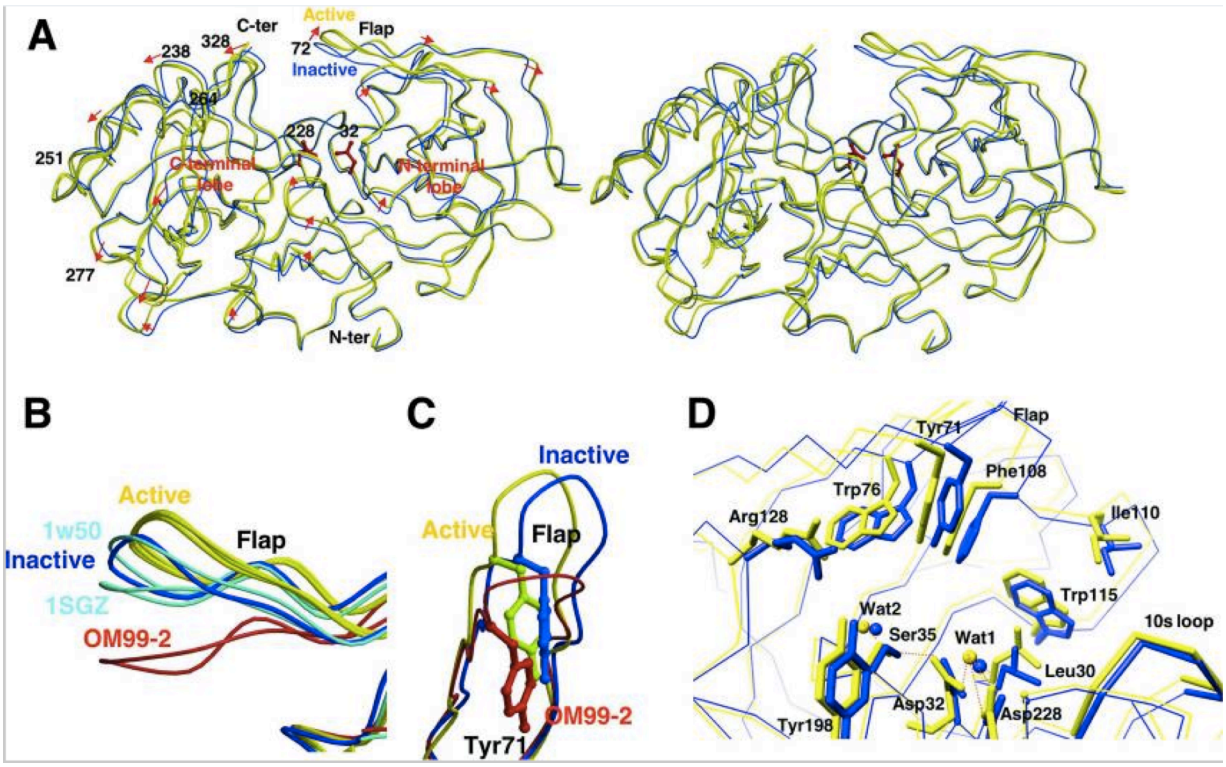

Figure 5: Structure of BACE1. A) Inactive structure pH 7.0 dark blue, active structure pH 4.0, 4.5 & 5.0 (–) Catalytic aspartic acids represented in (–). B) Close up of flap conformation (–): active, inactive: (–). Immature structure: (–), complexed with OM99-2 inhibitor: (–). C) Front view. D) Differences in residue conformation in active form (–) and active form (–). Image reproduced with permission from the rights holder, American Society of Biology (Shimizu et al., 2008).

the intermediate rearrangement leads to the separation of the peptide (*idem*).

Six ectodomain cysteine residues are involved in the formation of the enzyme active site structure through the formation of three disulphide bonds (Haniu et al., 2000). In comparison to other aspartyl proteases, BACE1 contains an extra loop region forming 3 subsites that seem to increase the ligand recognition cleft creating a requirement for an increased substrate size (Figure 5) (Turner, Hong, Koelsch, Ghosh, & Tang, 2005). Structural studies by Hong *et al.* (2002) with the BACE1 inhibitor OM00-3 (Glu-Leu-Asp-Leu-Ala-Val-Glu-Phe, K(i) = 0.3 nM) identified four hydrogen bonds within the catalytic aspartic acids and ten other hydrogen bonds, involved with OM00-3 inhibitor binding (Hong et al., 2000). The BACE1 active site is also less hydrophobic than that of other

aspartyl proteases (*idem*). The two domains of BACE1 contain a flexible β-hairpin loop forming a 'flap', which both blocks or manoeuvres substrates depending on conditions and is thought to aid removal of reaction products (Shimizu et al., 2008).

Shimizu *et al.* (2008) crystallised BACE1 with a peptidomimetic inhibitor OM99-2 at different pH (pH 4.0, 4.5, 5.0 and 7.0) (Figure 5) and found the main structural modifications occur between the inactive and active forms of the enzyme and not between active conformations, with the most obvious change occurring at positions 67 to 77 residues which form the flap region (Shimizu et al., 2008). This flap region is created by the hairpin loop of the N-terminal lobe and acts to partially cover the cleft region formed between the two lobes (Hong & Tang, 2004). Various conformations of the flap have been identified in the quest for a BACE1 inhibitor. BACE1 in complex with a peptide or peptide-like inhibitor, showed the flap moving closer to the catalytic aspartic acids, whereas complexing with non-peptide inhibitors awards much greater variation in flap conformation, with modifications of the Tyr71 residue leading to self-inhibition (Gorfe & Caflisch, 2005). To date, around 180 structural elucidations of BACE1 are recorded in the Protein Data Bank, either crystallised with a ligand or in its immature form (Cosconati et al., 2012).

1.6.2 Normal action

The action of BACE1 is not limited to the proteolytic processing of APP (Vassar, Kovacs, Yan, & Wong, 2009); BACE1 substrates include Golgi-localised membrane-bound α-2,6 sialytransferase (ST6Gal1) (Kitazume et al., 2001), P-selectin glycoprotein ligand 1 (PSLG-1) (Lichtenthaler et al., 2003), APP homologs APLP-1 and APLP-2 (Eggert et al., 2004), low-density lipoprotein receptor-related protein (LRP) (von Arnim et al., 2005), voltage gated sodium channel β-subunit 2 ($Na_v\ \beta_2$) (D. Y. Kim, Ingano, Carey, Pettingell, &

Kovacs, 2005), neuregulin-1 (NRG1) (Willem et al., 2006) and neuregulin-3 (NRG3) (Hu et al., 2006).

Golgi-localised membrane-bound α-2,6 sialytransferase (ST6Gal1) catalyses sialic acid transfer from CMP-sialic acid to galactose containing substrates involved in cell-differentiation antigen formation (Kitazume et al., 2001). ST6Gal1 is secreted from the Golgi following BACE1 cleavage, with ST6Gal1 expression increased with BACE1 overexpression (*idem*).

P-selectin glycoprotein ligand 1 (PSLG-1) moderates leukocyte adhesion in inflammation as a counter-receptor for cell adhesion molecules P-, E- and L-selectin, expressed in T-lymphocytes and myeloid cells, adhering leukocytes to activated platelets and endothelium (Lichtenthaler et al., 2003).

Low-density lipoprotein receptor-related protein (LRP) is a type I transmembrane receptor and is involved in the endocytosis of AD ligands such as APP, apolipoprotein E and is involved in trafficking and degradation of Aβ (von Arnim et al., 2005).

Voltage gated sodium channel β-subunit 2 (Na_v β_2) expression is not required for channel action but is required for full voltage-gated sodium channel functionality and cellular localisation (D. Y. Kim et al., 2005). Na_v β_2 is cleaved by both BACE1 and γ-secretase with the resulting protein fragments involved in a feedback mechanism utilised to moderate Na^+ current and alterations in membrane excitability (*idem*). Another physiological action of BACE1 is with neuregulin-1 (NRG1). NRG1 is a known regulator of peripheral nervous system myelination, halting BACE1 cleavage of NRG1 causes a reduction in myelin sheath thickness in both peripheral, sciatic, and optic nerves (Willem et al., 2006).

The identification of all the BACE1 substrates is essential in evaluating the effects of toxicity associated with BACE1 inhibitors (Vassar et al., 2009). Soluble BACE1 has no

proteolytic activity, suggesting a transmembrane site for proteolytic cleavage, as BACE1 substrates are all present as transmembrane species (Hu et al., 2006).

1.6.3 BACE1 homology

BACE2, the BACE1 homolog has 64% sequence similarity, sharing common attributes such as aspartyl protease and C-terminal active site domains; however the cellular localisation of BACE2 in astrocytes differs from BACE1 (neurons and microglia) (Basi et al., 2003). BACE2 has been seen to function similarly to α-secretase, acting antagonistically with BACE1, but does not compensate for the amyloidogenic action under BACE1 inhibition (Y. Luo et al., 2001). The active site binding residues in BACE1 and BACE2 are extremely similar but this structural homology does not preclude the formulation of inhibitors with high specificity exclusively for each protease (Turner et al., 2002). Ghosh *et al.* (2016) have identified a BACE2 inhibitor with > 170000 fold selectivity over BACE1 with a K_i of 0.03 nM (Ghosh et al., 2016). Ghosh *et al.* (2012) identified multiple inhibitors of BACE1 with very high selectivity over BACE2, for example, K_i of 17.0 pM in BACE1 inhibition and > 7000 fold selectivity over BACE2 (Ghosh et al., 2012). Other physiologically relevant aspartyl proteases include renin, pepsin, pepsinogen and cathepsin D and E. Ghosh *et al.* (2008) outline the importance of off target effects in these enzymes when identifying BACE1 inhibitors (Ghosh et al., 2008).

Pepsin and pepsinogen are present only in their zymogen form until exposed to gastric juices and denature upon entering the intestines (*idem*). These proteases are not adversely affected by off-target aspartyl protease inhibitors (*idem*). Renin, an important enzyme involved in blood pressure homeostasis, has an extremely high specificity, with Ghosh *et al.* commenting it is unlikely to be inhibited by a off-target BACE1 inhibitor; however this test is relatively cheap and would allow a conclusive evidence of any interaction (*idem*). Cathepsin D is found ubiquitously in the cell lysosome and is involved

with protein degradation and precursor activation. The phenotype of double cathepsin D knockout mice is seizures and blindness around post-natal day 26 (Koike et al., 2000) and therefore must be assayed for off-target effects of BACE1 inhibitors; cathepsin structural homology is so high, only one can be tested (*idem*). The off-target inhibition of any of the aforementioned aspartyl proteases could cause major systemic damage; therefore the BACE1 inhibitor must have high selectivity for BACE1 with little or no action at other related aspartyl proteases, in order to be a potential drug candidate.

1.6.4 Consequences of BACE1 inhibition

In 2001, three different teams furthered understanding of the action of BACE1 (H. B. Cai et al., 2001; Y. Luo et al., 2001; Roberds et al., 2001). Cai *et al.* (2001) brief communication utilised homologous recombination of murine embryonic stem cells to create a population of $BACE1^{-/-}$ mice, removing cortical neurons for immunoprecipitation-mass spectrometry analysis (H. B. Cai et al., 2001). Double knockout mice expressed no APP cleavage to form $A\beta_{42}$ and no compensatory cleavage by BACE2; suggesting this enzyme is not significantly involved in APP processing in the neurons (*idem*). Experiments with human APP cDNA designed with the Swedish APP mutation were completed in cell culture; $BACE1^{+/+}$ cells produced high levels of both $A\beta_{40}$ and $A\beta_{42}$ whereas $BACE^{-/-}$ cells produced no detectable levels (*idem*). Cai and team then went on to find whether APP processing through the α-secretase increases if the BACE1 pathway is non-functional (idem). This showed an approximately 2-fold increased flux across the α-secretase pathway suggesting that BACE1 processing is in direct competition with α-secretase processing of APP; therefore when BACE1 is inhibited, APP is processed through the non-amyloidogenic pathway (*idem*). These investigations revealed 100% BACE1 inhibition in mice abolishes the production of amyloidogenic Aβ species, with no alternative route for Aβ production; this result was mirrored in human APP producing neuronal cultures (wild-

type and Swedish mutation) (*idem*). The non-amyloidogenic α-secretase pathway increased the rate of APP processing due to the increase in substrate APP, displaying a compensatory mechanism for the processing of APP.

Luo *et al.* (2001) investigated the effects of this genotype on mouse phenotype with anatomy and histology, fertility, haematology, chemistry and general health screening (Y. Luo et al., 2001). Compared to wild type and heterozygous littermates, the $BACE^{-/-}$ mice showed no variations in pathology under microscopic brain analysis, no modifications to clinical chemistry metabolites and no alterations to blood cells (Y. Luo et al., 2001). The mice appeared healthy, fertile and behaved normally, however the mice were not challenged by any conditions of stress therefore the effects this may have on the homozygous mice is unknown (Y. Luo et al., 2001). Stress resulting in increased hypothalamic-pituitary-adrenal (HPA) axis activation, endocrine up-regulation, increasing blood brain barrier (BBB) permeability, immune system activation, neuroplasticity and decline in long-term potentiation (Olfe, Domanska, Schuett, & Kiank, 2010), along with the $BACE^{-/-}$ genotype could negatively impact the resulting mouse phenotype.

Roberds *et al.* (2001) found no abnormalities between genotypes according to SHIRPA (Smith Kline Beecham, Harwell, Imperial College, Royal London Hospital, phenotype assessment) to test phenotypic abnormalities, with no adverse effects on mouse behaviour (Roberds et al., 2001). Harrison *et al.* (2003) used two differing mouse models to demonstrate BACE1 modifications do have an effect on mouse behaviour, without changing typical factors such as morbidity and mortality (Harrison et al., 2003). Mice designed to over express BACE1 had increased 5-hydroxytryptamine (5-HT or serotonin, a monoamine neurotransmitter) turnover that caused the mice to be energetic and exploratory (SHIRPA behaviour screening); this was expected as low 5-HT turnover leads to anxiety (*idem*). BACE1 knockout mice in this study exhibited more anxious and less

exploratory behaviour, possibly revealing a link between BACE1 incidence and the serotonin pathway (*idem*).

Positive effects of BACE1 inhibition, following a measurable reduction in amyloidogenic Aβ to recordable reductions in AD-linked behaviour, were not characterised until the paper published by Ohno *et al.* (Ohno et al., 2004). This study created a $BACE1^{-/-}$ mouse that overexpressed human APP ($Tg2576^{+}$) (*idem*). This model produced dramatically reduced levels of $A\beta_{40}$ and $A\beta_{42}$ with none of the cognitive and electrophysical abnormalities seen in the single mutation $Tg2576^{+}$ (APP over-expression) model (*idem*). In tests for social recognition memory, $BACE1^{-/-}$/ $Tg2576^{+}$ mice outperformed $Tg2576^{+}$ mice and were equivalent to wild-type littermates in a maze task, again showing significant differences between the two groups (*idem*). The study concludes that inhibition of BACE1 to reduce Aβ levels works to correct hippocampal cholinergic dysfunctions in these mouse models (*idem*). BACE1 null mice exhibit minor behavioural changes over wild type mice, suggesting partial inhibition sought through BACE1 therapeutics should not have detrimental effects to the patient, however human studies are required to confirm this expectation.

Investigations by Edbauer *et al.* (Edbauer et al., 2003) and Kimberly *et al*. (Kimberly & Wolfe, 2003), into the effects of γ-secretase knockouts was undertaken to determine whether this second phase of the APP processing pathway could be targeted with inhibitors, to produce a clinically relevant reduction in Aβ (*idem*). Presenilin-1, nicastrin, anterior pharynx-defective 1 (APH-1) and presenilin enhancer 2 (PEN-2) forming the γ-secretase complex were assessed as possible AD therapeutic targets. In a presenilin-1 knockout mouse, the result is embryonic lethal phenotype (Shen et al., 1997). The resultant null mutation progeny has severe deformities and suffered from central nervous system haemorrhage suggesting a whole-body role for presenillin-1, highlighting the γ-secretase complex as an non-viable target for inhibition to treat AD (*idem*).

Willem *et al.* (2006) noted the highest levels of BACE1 found in the post-natal mouse brain were found during periods in development involving peripheral nerve myelination, with levels falling until adulthood where expression is low (Willem et al., 2006). Peripheral nerve cell myelination by Schwann cells is dependent on the presence of (type III) epidermal growth factor (EGF)-like factor neuregulin-1 (NRG1), which is thought to require endoproteolysis for its signalling activity (*idem*). NRG1 (type III) activates receptor-tyrosine kinase ErbB2 and ErbB3 receptors on the surface of Schwann cells triggering activation; NRG1 (type III) and ErbB knockouts cause peripheral nerve hypomyelination, whereas over expression of NRG1 (type III) leads to hypermyelination (Hu et al., 2006) (Willem et al., 2006). Garratt *et al*. (2000) showed BACE1 may process NRG-1 (type III), activating this ligand, allowing binding to ErbB2 and ErbB3 receptors, leading to myelination and peripheral bundling of axons by activated Schwann cells (Garratt, Britsch, & Birchmeier, 2000). Sankaranarayanan *et al.* (2008) tested the effects of BACE1 inhibition on NRG-1 processing and showed inhibition; although lowering Aβ levels in aged mice, BACE1 inhibition did not significantly lower NRG-1 processing (Sankaranarayanan et al., 2008).

BACE1 null mice synthesise no $A\beta_{42}$ amyloidogenic species, with no compensation seen from BACE2 (H. B. Cai et al., 2001). The non-amyloidogenic pathway processes APP, removing the possibility of APP cellular toxicity (*idem*). No phenotypic changes are seen in BACE-1 null mice, both behavioural (Harrison et al., 2003) and biochemical (Y. Luo et al., 2001), but hypomyelination is observed (Willem et al., 2006). As this myelination phase occurs post-natal, the effect of BACE-1 inhibition in aged patients suffering with Alzheimer's disease is unlikely to be applicable (Sankaranarayanan et al., 2008).

Levels of BACE1 protein and proteolytic activity are significantly increased in AD brains, as identified by Fukumoto *et al.* (2002) in dissections of brains donated through the Massachusetts Alzheimer's Disease Research Centre brain bank (Fukumoto, Cheung,

Hyman, & Irizarry, 2002). This research determined BACE1 enzyme activity was increased by 63% in the temporal neocortex of sufferers, a 13% increase in the frontal neocortex but no increase in the cerebellar cortex (*idem*). BACE1 protein level was increased in the frontal cortex by 14%, with 15% increase in temporal cortex and no difference in the cerebellar cortex (*idem*). The amount of BACE1 activity in the temporal neocortex was seen to increase with AD duration, but did not correlate with measures of insoluble Aβ levels; the neurotoxic soluble Aβ levels were not tested (*idem*). The increase in BACE1 expression and activity could be a causative factor in the development of AD, suggesting the inhibition of this target could improve disease outcomes.

Genetic analysis of the BACE1 open reading frame in sporadic AD patients found no mutations in a study conducted by Li *et al.* suggesting the increase in BACE1 levels and activity are not due to a gene mutation in this group of AD sufferers (R. Li et al., 2004). BACE1 mRNA expression was found to be elevated in the same regions of increased BACE1 protein activity; the authors postulate the stability of BACE1 mRNA could be a cause of the increased BACE1 activity, however this had not been explored further (*idem*). Faghihi *et al.* (2008) demonstrated the BACE1 noncoding antisense transcript improves BACE1 stability *in vitro* with levels increased alongside BACE1 in AD *in vivo* (Faghihi et al., 2008).

BACE1 levels of translation also increase alongside amplified cellular stressors such as oxidative damage, hypoxia, ischemia, neighbouring apoptosis and trauma (Vassar et al., 2009). A reduced capacity for efficient glucose metabolism is characteristic of an AD brain and is thought to be due to the reduction or loss of axonal transport and cytoskeletal function caused by increased tau and Aβ levels (Braak, Braak, Bohl, & Reintjes, 1996). Neurons affected in the early stages of AD, in the medial temporal lobe and hippocampus, have high metabolic rates and therefore glucose requirements (*idem*). The reduced neuronal activity and eventual neuronal loss seen initially these areas, is thought to be due to ineffective glucose metabolism (*idem*). Reduced glucose metabolism can be used in

diagnostic positron emission tomography (PET) scanning with 2-fluorodeoxy-D-glucose (2FDG) (Velliquette, O'Connor, & Vassar, 2005).

Mimicking the disruption in glucose metabolism in mouse models, causes a two-fold elevation in BACE1 levels, imitating the effects seen in AD patients (Fukumoto et al., 2002; Velliquette et al., 2005). O'Connor *et al*. (2008) determined this rise was due to increased translation of BACE1 mRNA, attributable to phosphorylation of the translation initiation factor eIF2α (O'Connor et al., 2008). Mouse models given inhibitors of energy metabolism produced an increased amount of phosphorylated eIF2α, BACE1, Aβ and amyloid plaques; with the increase in phosphorylated eIF2α positively correlated with Aβ levels in post-mortem brains of people with AD (*idem*).

1.7 BACE1 inhibitors

1.7.1 Early peptidomimetic inhibitors

The active site of BACE1 poses problems with inhibitor design due to the extended cleft region along with the flexibility of the enzyme structure and the requirements for blood brain barrier access (McGaughey & Holloway, 2007). The design of small molecule inhibitors for BACE1 was first published in 2000, through work done by Arun Ghosh *et al*. (Ghosh et al., 2000). Peptide-based inhibitors have low toxicity metabolites *in vivo*, but the intact delivery to the brain and the low passive diffusion across the BBB create a problem for their action as potential therapeutics (Egleton & Davis, 1997).

Early inhibitor designs were based around the Swedish mutation of APP (APP_{SW}), which converted APP from a poor substrate (k_{cat}/K_m= $40s^{-1}$ M^{-1}) to an excellent target (k_{cat}/K_m= $2450s^{-1}$ M^{-1}) (SEVKM/DAEFR to SEVNL/DAEFR) (Ghosh et al., 2000). Aspartic acid (D) was substituted with alanine (A) increasing lipophilicity and reducing polarity (*idem*); both modifications that ultimately improve blood brain barrier penetration (Kearney & Aweeka, 1999).

The scissile bond in APPsw was replaced with a hydroxyethylene transition-state isostere (Figure 6) that acts to mimic the intermediate state of the APP cleavage, and therefore blocks the action of the enzyme through competitive inhibition (Wangsell et al., 2010). OM99-1 has the sequence Val-Asn-Leu*Ala-Ala-Glu-Phe, where the asterisk represents the position of the transition state isostere, whereas OM99-2 has the sequence Glu-Val-Asn-Leu*Ala-Ala-Glu-Phe (Ghosh et al., 2000).

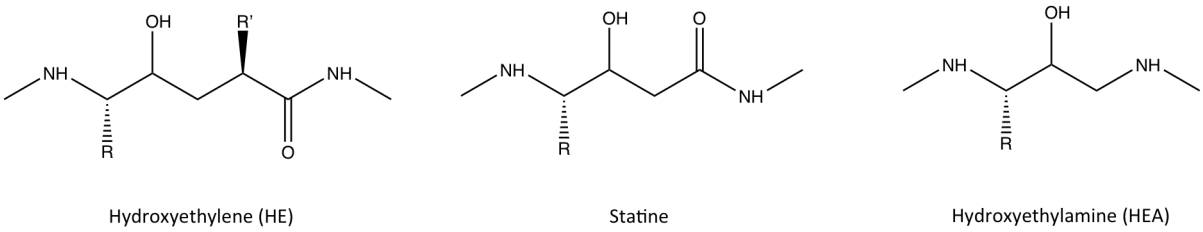

Figure 6: Examples of hydroxyethylene, statine and hydroxyethylamine transition-state isostere structures. The peptide bond is replaced with a stable hydroxyl group. Modified from (Wangsell et al., 2010).

The therapeutic possibilities of OM99-1 and OM99-2 are limited, due to the high molecular weight (1.1 kDa) and peptidic nature if these inhibitors, reducing the BBB penetration (Hong et al., 2002). Improvements to the lipophilicity of these inhibitors, through increasing the number of lipophilic groups or reducing the hydrogen binding potential, were investigated to improve BBB passive diffusion (Egleton & Davis, 1997). Enhancements to OM99-2 have lead to OM00-3, consisting of Glu-Leu-Asp-Leu*Ala-Val-Glu-Phe with a K_i of 0.3 nM; the replacement of the second alanine with valine stabilises the Glu-Phe binding (Hong et al., 2002). Although these compounds have excellent BACE1 inhibitory activity, OM99 and OM00 compounds have low brain retention *in vivo* due to high efflux through P-glycoprotein transport (Hunt & Turner, 2009).

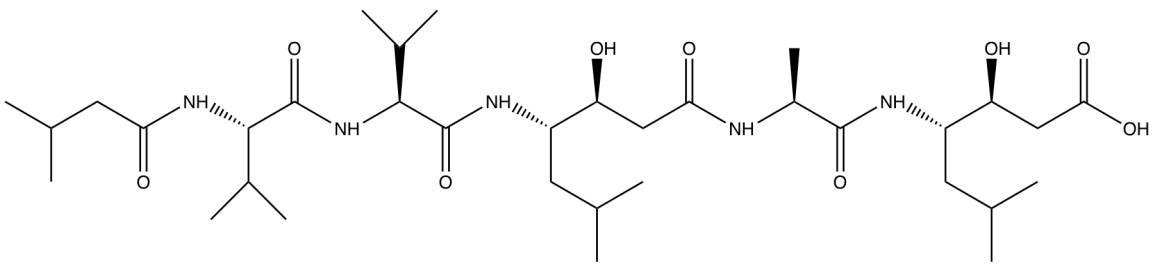

Figure 7: The structure of pepstatin, a hexapeptide containing the statine residue. Adapted from (Rich, Sun, & Ulm, 1980).

Other studies focused on pepstatin, discovered by Umezawa *et al.* (1970), a known aspartic protease inhibitor, which contains the γ amino acid (amine attached to γ-carbon) statine; (3S,4S)-4-amino-3-hydroxy-6-methylheptanoic acid (Figure 7) (Umezawa et al., 1970). With a poor K_i of 300 μM, APP_{SW} residues were added to give the inhibitor a specificity and potency not seen in the generic statine (X. L. Lin et al., 2000). This cell permeable P_{10}-P_4' (Schechte.I & Berger, 1967) (Thr662-Phe674), P_1(S)-statine-substituted amino acid inhibited BACE1 dose dependently, with half maximal inhibitory concentration (IC_{50}) of approximately 40 μM (Sinha et al., 1999). Through the modification of single residues, the highest potency BACE1 inhibitor was obtained through substitution of valine for aspartic acid at position P_1' (P_{10}-P_4'StatVal) ($IC_{50} \approx 30$ nM) (*idem*). As these APP-statine based inhibitors are highly peptidic in nature, they have little or no capacity for brain penetration; they will not lower the neurotoxic Aβ found in the CNS of AD sufferers (Probst & Xu, 2012).

The first generations of statine-based inhibitors were replaced with a hydroxyethylene (HE) (Figure 8) pentapeptide, with the example in Figure 8 exhibiting enhanced potency (IC_{50} of 20 nM) compared to the statine relatives (Ghosh et al., 2005). The lipophilic modifications, along with increasing potency in both BACE1 inhibition and cell activity assays, ensured cell permeability (*idem*).

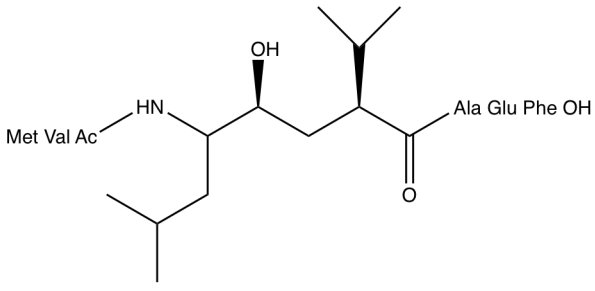

Figure 8: HE based inhibitor '14', which has a BACE1 inhibition IC_{50} of 20 nM. Modified from (Ghosh, Kumaragurubaran, & Tang, 2005).

The work of Eli Lilly & Company on structure-activity relationship studies of Phe-Ala hydroxyethylene (HE) isostere pentapeptide inhibitors revealed potent molecules,

including BACE1 inhibitory IC_{50} and cellular activity IC_{50} results (Ghosh et al., 2005). Merck have similarly researched HE isosteres reporting Phe-Ala HE based inhibitors with reduced molecular weights (< 600 Da), through modifications at the P_1' position (Brady et al., 2004).

Hydroxyethylamines (HEA) (Figure 6) have been one of the most investigated templates in BACE1 inhibitor studies (Probst & Xu, 2012). HEA based inhibitors have opposite stereochemistry to the statine-based inhibitors and are less peptidic in nature (Probst & Xu, 2012). These modifications allow this class of inhibitors greater opportunity for penetration into the CNS and capacity for lowering of CNS Aβ (Probst & Xu, 2012).

In vivo studies in guinea pigs reported that the HEA compound (Figure 9) lowered total Aβ in the brain by 28% and in the CSF by 32% (5 doses 30mg/kg in 2.5 days, results taken 6 hours post final dose) (Probst & Xu, 2012). During the testing for off-target effects of this compound, it was found to also inhibit the non-target, aspartic protease, cathepsin D (IC_{50} = 490 nM) (*idem*).

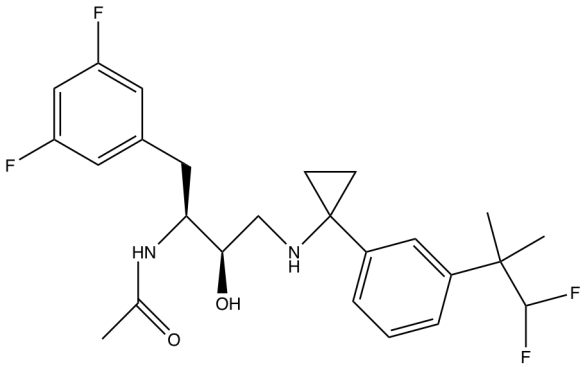

Figure 9: HEA based BACE1 inhibitor with potent off-target effects, with inhibition seen in other aspartyl proteases. Modified from (Probst & Xu, 2012).

BACE1 inhibitor IV is a hydroxyethylamine containing inhibitor with an IC_{50} of 15 nM in human BACE1 (Stachel et al., 2004). However, this compound displays poor membrane permeability and low aqueous solubility (*idem*).

Despite the number of BACE1 inhibitors identified to date, there have been more failures than successes. Unsuccessful trials include the compounds tramiprosate, R-

flurbiprofen and semagacestat (Selkoe, 2011). At the time writing, two small molecule BACE1 inhibitors are in late stage trials; AstraZeneca and Eli Lilly co-development inhibitor AZD3293 trials are due to end in May 2019 and Merck are testing MK-8931 (Verubecestat) in mixed phase II/III trials estimated to end in July 2019.

For further information in regard to the history and success of BACE1 inhibitors, the reader is directed to the review article by Probst and Xu (2012) (Probst & Xu, 2012).

1.7.2 Carrier peptide

Investigations by Chang *et al.* (2004) produced BACE1 inhibitors bound to a carrier protein that allowed efficient delivery of relatively large inhibitors across the BBB (Chang et al., 2004). Inhibitors OM99-2 and OM00-3, containing a FITC reporter and a 9 or 12 residue carrier peptide sequence entered HEK293 cells at a concentration of 4 - 400 nM (*idem*). These bound inhibitors were not uniformly distributed within the HEK293 cells, suggesting the accumulation or organisation into specific cell areas (*idem*). The conjugated inhibitor Fs-[OM00-3]$_D$R$_9$ (D-arginine) halted the formation of both C99 and Aβ through inhibition of intracellular BACE1 in Tg2576 mice (*idem*). The standard inhibitor OM00-3 (unconjugated) demonstrated no inhibition with the same delivery method (intra-peritoneal) (*idem*). The modification from a limited chemical inhibitor to a cell penetrant inhibitor, allowed CoMentis and Chang *et al.* to produce CTS-21166, which has undergone extensive clinical trials (Ghosh et al., 2008). In phase I clinical trials, CTS-21166 IV injection between 7.5 mg and 225 mg demonstrated a dose dependant reduction in plasma Aβ, with 80% reduction of plasma Aβ at the maximal concentration of 225 mg (IC_{50} = 1.2 - 3.6 nM depending on cell line) (X. Y. Luo & Yan, 2010).

1.7.3 Alternative treatments aimed at β-Amyloid

There are many avenues of investigations being conducted into AD pathology and treatments, including β-amyloid and tau targeted treatments, immune stimulation, gene

therapy, and pharmaceuticals to target inflammation of the brain. Alternative treatments being researched that target β-amyloid and the production of β-amyloid in the AD brain include immune therapy, gene therapy, and inhibitors of receptors for advanced glycation end-products (RAGE).

1.7.4 Immunisation

β-amyloid immunotherapy is currently an active area of AD research. Antibodies that penetrate the BBB and bind to Aβ, to aid the processing by microglia/macrophage or with complement activation, are being investigated as therapeutics for AD (van Marum, 2008). The reduction of plasma Aβ through antibody binding and immune destruction may create a 'peripheral sink' to draw out cerebral Aβ (DeMattos et al., 2001). *In vivo* studies of AD mouse models with solanezumab (humanised monoclonal IgG1, Eli Lilly Ltd), a soluble Aβ recognising monoclonal antibody, demonstrated reduced Aβ in the periphery (Siemers et al., 2016). This antibody also reduced cerebral Aβ and lead to improvements in murine cognitive functions (DeMattos et al., 2001; Dodart et al., 2002). Further investigations of solanezumab have indicated that action may not be to clear the Aβ through immune routes, but to stabilise the non-toxic monomeric structures of Aβ, limiting the formation of more toxic oligomers (Yamada et al., 2009). Mechanism aside, the use of this monoclonal antibody was not associated with the commonly seen cerebral vessel microhaemorrhage (thought to be due to activated T-cells) that has troubled the progression of other promising monoclonal antibodies (Fu et al., 2010; Racke et al., 2005). However, the results from phase III double-blind clinical trials by Eli Lilly showed no improvement to cognition or functional stability in mild to moderate AD sufferers (Doody et al., 2014).

The more essential target of these antibodies however, could be seen as the already *in situ* plaques, which potentially contribute to tau aggregation, altered synaptic transmission and neuronal death, causing the symptoms associated with AD. Elimination of

these existing plaques has also been a target for antibody research. The formulation of these antibodies involves immunisation with pre-aggregated or soluble $A\beta_{42}$ with an adjuvant to illicit an immune response, create antibody titre, and propagate an anti-$A\beta_{42}$ assault (Morgan, 2011). The antibody AN1792 (Janssen, Pfizer) was a version of this treatment taken to clinical trials (Elan/Wyeth 2000). The trials were terminated in 2002 due to 6% of immunised patients suffering from sub-acute aseptic meningioencephalitis, with white matter abnormalities and neurological effects (Orgogozo et al., 2003). Subjects were continually monitored; the drug appeared not to have any impact in the prognosis, with each patient continuing into severe dementia and death (*idem*). AD progression continued despite the clearance of Aβ plaque and the expression of anti-Aβ antibodies; patients with near complete removal of Aβ plaques shown at autopsy, still progressed into severe dementia (Haas, 2012). This suggests the removal of plaques does not contribute to the improvement of the patient and may not be therapeutically viable and lends credence to the neurotoxic Aβ form being soluble (C. Holmes et al., 2008).

Passive immunisation using pooled intravenous immunoglobulin (IVIG) or monoclonal antibodies raised to different regions of Aβ peptide, reduces the number of adverse events and increases the number of subjects generating significant antibody responses (van Marum, 2008). In December 2012, Baxter Healthcare Corp completed a phase III trial on IVIG in mild to moderate AD patients (NCT00818662).

Monoclonal antibody AAB-001 (bapineuzumab) had varied results in clinical trials with positive results being seen in non-ApoE4 carriers, showing significant cognitive improvement, possibly due to differences in microvasculature in the basement membrane of subjects (with adverse effects occurring most often in Apo-E4 carriers) (Salloway et al., 2002; Salloway et al., 2009). Bapineuzumab is undergoing multiple phase III trials currently; however some have been halted due to findings of 'no clinical benefit' to patients

(NCT00676143). Studies are finished in non-ApoE4 carrying patients but results (as of September 2017) are yet to be released (NCT00575055).

1.7.5 Gene therapy

Although the complete removal of APP transcript and protein have been shown to have negative effects in cell function including in axonal transport and transmission, dendritic length, neuronal cell survival and long-term cell health; APP knockout mice do not exhibit a damaged phenotype (Haas, 2012). This knockout therapy could be beneficial to patients suffering from familial forms of AD. Viral delivery of micro RNA (miRNA), targeting the 3' untranslated region of APP mRNA transcripts causes a reduction of protein levels by 2-3 times (Patel et al., 2008). Short interfering RNA (shRNA) is also being designed to target specific gene mutations associated with familial AD, which binds to the mutated gene blocking transcription with the wild-type gene being the only template then available (Rodriguez-Lebron, Gouvion, Moore, Davidson, & Paulson, 2009). In mouse models used within this study, neural injection of shRNA resulted in significant improvement in the cognitive performance equalling the performance by the wild-type (unaffected) control group (*idem*). This would suggest that therapeutic use of shRNA have the potential as an AD treatment.

1.7.6 RAGE Inhibitors

Receptors for advanced glycation end-products (RAGE) are associated with the aberrant formation of intracellular plaques through Aβ binding on both the cell surface and the BBB (V. Srikanth et al., 2011). For furthur information in regard to RAGE in AD, the reader is directed to Ramasamy *et al*. (2005) (Ramasamy et al., 2005). The RAGE inhibitor PF-04494700 (TransTech Pharma LLP) has now reached phase III study (V. Srikanth et al., 2011) with results due in 2018.

1.8 Heparin and heparan sulphate in Alzheimer's disease

1.8.1 Heparan sulphate proteoglycans and Alzheimer's plaques

HSPGs have been linked with Aβ in AD through co-localisation in plaques (Brunden, Richtercook, Chaturvedi, & Frederickson, 1993; Perlmutter, Chui, Saperia, & Athanikar, 1990) catalysing the polymerisation of Aβ into plaques *in vitro* (Castillo, Ngo, Cummings, Wight, & Snow, 1997), and have been demonstrated to protect plaques from proteolysis, halting degradation and removal (Bame, Danda, Hassall, & Tumova, 1997). *In vivo* there are a number of molecules that are associated with the Aβ plaque architecture along with HSPGs including apolipoprotein E (ε2, ε3, ε4), compliment factors C1q, C3c, C4d, C5b-9, compliment inhibition factor clusterin, acute phase proteins such as α1-antichymotrypsin and ICAM-1 (Verbeek, Otte-Holler, Veerhuis, Ruiter, & De Waal, 1998). Snow *et al.* (1994) found HSPGs present in diffuse plaques in the hippocampus, amygdala, neocortex and the cerebellum; locations usually plagued by plaque formation in AD (Snow, Sekiguchi, Nochlin, Kalaria, & Kimata, 1994). The presence of the HSPG, perlecan, was thought to either potentiate the formation of plaques (seeding) or to allow plaque formation to persist, resisting deconstruction (*idem*). HS was demonstrated to co-localise with Aβ in immature amyloid plaque formations in subjects with Down's syndrome and AD, further adding to the evidence that HS is important in plaque formation (*idem*).

A HSPG derived from a marine sponge (*Microciona prolifera* aggregation factor-MAF) induced structural modifications in aggregates of $A\beta_{40}$ and $A\beta_{42}$ from random formations to β-structures, seen in circular dichroism spectroscopy, that inhibit proteolysis, perpetuate further formation and allow for improved stability (McLaurin, Franklin, Kuhns, & Fraser, 1999).

Investigations by Watson *et al.* (1997) found heparin binds to fibrillar but not non-fibrillar Aβ *in vitro*, indicating this interaction occurs with the aggregated state Aβ rather

than the primary sequence of the Aβ protein (Watson, Lander, & Selkoe, 1997). This research also found human amylin (found in pancreatic deposits associated with type II diabetes) binds heparin while non-amyloidogenic and non-toxic rat amylin does not; indicating that the ability to bind HSPG may be the general progressing factor from non-amyloidogenic to amyloidogenic proteins (*idem*).

A molecule with the ability to pass through the blood brain barrier (BBB) to compete with HS may reduce HS/Aβ binding and therefore the preliminary stages of plaque formation in AD (Leveugle et al., 1998). Low molecular weight anionic sulphate or sulphonate compounds were tested for this capacity in a study done by Kisilevsky *et al.* (1995) on splenic amyloid formations in animal models (Kisilevsky et al., 1995). Kisilevsky *et al.* (1995) research into acute amyloidogenesis found anionic polyvinyl sulphonate (PVS) inhibited formation of virtually all deposited amyloid as compared to control mice (*idem*). Sodium 1,2-ethanesulphonate and sodium 1,3-propanesulphonate were more effective inhibitors than other mono-sulphonates or their related sodium 1,4-, 1,5- and 1,6-disuphonates (butane, pentane and hexane) (*idem*). Sodium 1,3-propanediol disulphate inhibited the formation of Aβ plaques and exhibited ability to disassemble fibrils (*idem*).

The ability of low molecular weight heparin (LMWH) to pass through the BBB was initially investigated by Leveugle *et al.* (1998) (Leveugle et al., 1998). This research utilised a BBB model formed using a co-culture of bovine brain capillary endothelial cells and rat astrocytes (*idem*). Heparin and pentosan polysulphate (used due to its similarities to heparin in both blood anti-coagulation, high molecular mass and sulphation levels) could not pass through the BBB model, except for passive diffusion expected of every molecule at very low levels (after 2.5 hours incubation) (*idem*). However, all the depolymerised heparins, including disaccharides, tetrasaccharides and a mixture of different sized oligosaccharides were efficiently transported across the monolayer of the BBB model (*idem*). Heparin fractions passing through the BBB model with increasing order of

efficiency were heparin hexa- and octosaccharides < 3 kDa heparin (10 - 18 saccharides) < heparin disaccharides < heparin tetrasaccharides, with analysis showing the fractions were not metabolised throughout the passage as they remained identical on the luminal side of the monolayer (*idem*).

The heparin derived oligosaccharide (HDO), C3, a mixture of low molecular weight HDO with fewer sulphate groups and an average molecular weight of 2 kDa, was demonstrated to cross the BBB by Ma et al. (2002); however the mechanism of transport was not determined (Ma et al., 2002).

Using step gradient affinity chromatography on a Aβ column, heparin was found to bind with high affinity to Aβ peptide while depolymerised fragments bound with low affinity showing they do not directly bind to the Aβ to cause plaques, unlike heparin (Leveugle et al., 1998). This suggests multivalency and the size of GAG chain are the key factors for this interaction (*idem*). Using affinity chromatography, the high affinity binding of heparin to Aβ was inhibited by LMWHs dose dependently with disaccharides; hexasaccharides and octasaccharides being particularly successful (*idem*).

Small *et al*. (1994) identified APP as a HSPG binding protein and identified at least two distinct heparin-binding regions, one low affinity site between $APP_{96\text{-}110}$ (Small et al., 1994) and a higher affinity site between $APP_{316\text{-}337}$ (Multhaup, 1994). The HSPG binding domains of APP were further elucidated in crystallisation studies where APP residues 96-110 were found to form a highly charged basic region suitable for GAG binding (Rossjohn et al., 1999). The residues involved in forming the basic patch suitable for GAG binding are Arg 40, Lys 60, Lys 99, Arg 100, Arg 102, Lys 103 and Lys 106 with 2 histidines, His 108 and His 110 creating a region suitable for an octasaccharide heparin fragment (*idem*). The basic region between residues 96 and 110 is part of a β-hairpin loop structure, which is the most mobile of regions on the APP protein (*idem*).

1.8.2 Heparin and heparan sulphate associations with BACE1

Matsumoto *et al.* (1996) found HSPGs bound to BACE1 sourced from human brain cortex samples (2 AD patients and 2 aged controls) using 2D electrophoresis and antibody adp-2 to BACE1 and 10E4 raised to HS, suggesting HSPG may be involved with amyloidogenesis and therefore the toxicity of Aβ (Matsumoto, Matsumoto, Enomoto, & Baba, 1996).

In 1997, a seminal paper published by Leveugle *et al.* found heparin caused a five fold increase in the transcription of APP, increased APP secretion into cell media up to a plateau of 10 μg/ml heparin concentration causing a four fold increase and promoted the production of sAPPβ in human neuroblastoma SKNSH-SY5Y cells (Leveugle et al., 1997). GAG size was shown to be important in increasing sAPPβ production, with full length heparin providing the most effect, and reducing saccharide size lowering the production of sAPPβ; dextran, CS and HA had no effect (*idem*). Leveugle *et al*. (1997) postulated a ternary structure requirement for APP processing, which includes heparin/HS, BACE1 and APP, but the interaction between BACE1 and GAGs could not be verified, possibly due to the choice of cell line used in validatory experiments (*idem*).

Scholefield *et al*. (2003) further investigated the action of HS and heparin in BACE1 activity (Scholefield et al., 2003). Heparin and HS were both found to inhibit the proteolytic action of BACE1, with a maximum level of ~50-60% with bovine lung heparin (BLH) (IC_{50} ~ 1-2 μg/ml or 100 nM) (*idem*). The possibility of HS enhancing BACE1 activity at low concentrations was investigated and apart from a slight increase in BACE1 activity at 10-100 ng/ml (~ 5-10%), no enhancement was seen under these conditions (*idem*). Using APP substrate, *in vitro* experiments into the action of BLH and PMH found inhibition of BACE1 cleavage action by ~90-100% (BLH IC_{50}~ 1-2 μg/ml 100 nM and PMH IC_{50}~ 5 μg/ml 200 nM) (Figure 10) (*idem*).

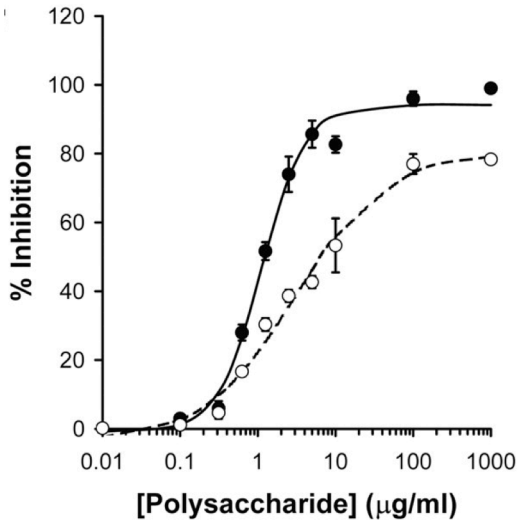

Figure 10: Dose response curve for percentage inhibition of BACE1 with BLH and PMH using FRET APP fluorescent substrate in 100 mM sodium acetate buffer, pH 4.5. PMH (empty circle) BLH (solid circle) Original figure from (Scholefield et al., 2003), Image reproduced with permission from the rights holder.

HS and the sulphated analogue heparin are effective in inhibiting both *in vivo* and *in vitro* BACE1 with the most effective heparin form in the SY-SY5Y cell model being full length heparin, with chemically modified, N-acetylated heparin the second most potent (Scholefield et al., 2003). Scholefield *et al.* suggest the binding of heparin may occur in a region close to or in the active site, blocking access to other ligands by completive means (*idem*). These experiments have determined the successful inhibition of BACE1 does not occur through charge density of the molecule GAG, but results from specificity in the structure of the binding glycan (*idem*). Experimental evidence for this binding specificity was presented through modifications to the glycans including the removal of the N-sulphates and replacement with N-acetyl groups (*idem*). This modification increases inhibition, possibly through a reduction of charged groups causing an 'enhanced interaction' at the active site (*idem*). Removal of the iduronate-2-O-sulphate or glucosamine 6-O-sulphate caused a reduced inhibitory capacity at BACE1 (*idem*). The covalent modification of the disaccharide sugar units leads to adjustment of the iduronic acid ring and glycosidic linkage conformation, which in turn changes the substrate-enzyme specificity (Yates et al., 2000).

Immunofluorescence microscopy in SH-SY5H APP_{SW} and HEK-BACE cells was utilised to determine cellular localisation of both BACE1 and HS, with co-localisation occurring in both the cell membrane and in the Golgi complex (Scholefield et al., 2003). This paper notes only a fraction of the cellular HSPG were associated with BACE1, and the HSPGs preferentially associated with the protease were smaller in size ranging from 70-100 kDa; inclusion of a competitive inhibitor to HSPG binding, heparin, eliminated BACE1 mediated immunoprecipitation (*idem*).

Beckman *et al.* (2006) published a paper to further investigate the relationship between heparin and BACE1 and found the relationship to be more complex, with low concentrations of heparin (1 μg/ml) exhibiting stimulated rBACE1 activity, while higher concentrations (10 or 100 μg/ml) displaying inhibitory activities (Beckman, Holsinger, & Small, 2006). Heparin affinity chromatography was utilised to understand the binding affinity between BACE1 and heparin and found semi-active zymogen, pro-BACE1 could bind heparin with high affinity (1.2 M NaCl fraction) (*idem*). This fraction was strongly activated by low concentrations of heparin (1 μg/ml) and the authors suggest this is due to the pro-domain including 5 positively charged residues, (4 of which are arginines) forming a high affinity heparin-binding region, absent in mature BACE1 (*idem*). Removal of the BACE1 pro-domain abolished the stimulatory effect caused by heparin (1 μg/ml), suggesting activation of BACE1 by heparin relies on the presence of pro-BACE1 zymogen in *in vitro* assays (*idem*). The stimulatory effect was investigated using matrix assisted laser desorption ionisation time-of-flight (MALDI-TOF) mass spectrometry (MS) to determine whether heparin was triggering autocatalytic cleavage of the pro-region, and subsequent efficacious BACE1 activity; heparin was shown at 1 μg/ml to have no autocatalytic activity (*idem*).

Patey *et al.* (2006) expanded on the work done by Scholefield *et al.,* exploring a wider range of structurally modified heparins (Patey et al., 2006). The chemically modified

heparin (CMH) compounds shown in Figure 11 were tested for *in vitro* BACE1 inhibitory activity and screened for undesirable off target effects with anti-factor Xa, cathepsin D and renin (*idem*). Attenuation of these off target effects while exhibiting potent BACE1 activity was possible, with the most promising therapeutic ratio (BACE1 inhibition/ Xa activity) achieved by de-N-sulphated re-N-acetylated porcine mucosal intestinal heparin (PMIH) (Figure 11) (*idem*). The inhibition of BACE1 measured by fluorescent resonant energy transfer (FRET) *in vitro* assay, with full length PMIH yielding a half maximal inhibitory concentration (IC_{50}) of 28 ng/ml with de-N-sulphated re-N-acetylated PMIH yielding a very similar IC_{50} of 31 ng/ml (*idem*). Figure 11 outlines the structural modifications of PMIH and the IC_{50} inhibition of BACE1 (*idem*).

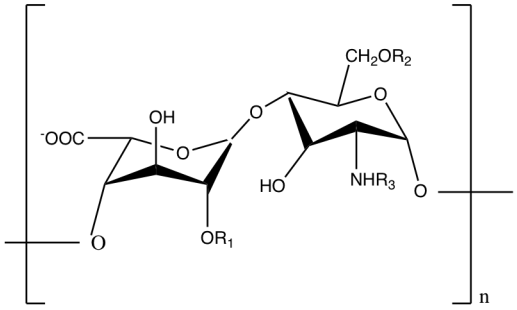

R_1= SO_3^-/H, R_2= SO_3^-/H, R_3= SO_3^-/H/$COCH_3$

CMH	Compound	R1	R2	R3	BACE1 IC_{50} (ng/ml)	R^2 of IC_{50}	Anti-coagulant activity relative to PMIH	Therapeutic ratio (BACE1 inhibition/anti-Xa)
1	PMIH	SO_3^-	SO_3^-	SO_3^-	28	0.998	100%	1
2	N-acetyl	SO_3-	SO_3^-	$COCH_3$	31	0.995	0.03%	3136
3	UA-2-OH	H	SO_3^-	SO_3^-	53	0.995	0.40%	147
4	UA-2-OH, N-acetyl	H	SO_3^-	$COCH_3$	91	0.999	0.03%	1092
5	GlcN-6-OH	SO_3^-	H	SO_3^-	100	0.996	0.50%	61
6	GlcN-6-OH, N-acetyl	SO_3^-	H	$COCH_3$	410	0.995	0.03%	237
7	UA-2-OH, GlcN-6-OH	H	H	SO_3^-	786	0.994	0.03%	123
8	UA-2-OH, GlcN-6-OH, N-acetyl	H	H	$COCH_3$	>100000	n/a	0.03%	1
9	Per-sulphated	SO_3^-	SO_3^-	SO_3^-	53	0.998	35.00%	2

Figure 11: Chemically modified heparin (CMH) structural information displayed in a schematic with BACE1 inhibitory activity as determined by FRET activity assay, and anti-coagulant activity of each chemical modification. Adapted from (Patey et al., 2006).

Specific structural modifications show neither the N-sulphate nor 2-O-sulphate are specifically required to maintain an inhibitory capacity similar to PMIH when also supplemented with 6-O-sulphation (Patey et al., 2006). This is evidenced by the fully desulphated CMH8 maintaining none of the BACE1 inhibitory capacity (*idem*). Per-sulphated CMH9 is additionally sulphated at position 3 of the uronate residue and displays similar BACE1 potency to PMIH, CMH2 and CMH3 (*idem*). The effect of these CMH on the coagulation cascade was measured through anti-factor Xa activity, which was attenuated by >3000 fold with de-N-sulphated heparin as shown in compounds CMH2, CMH4, CMH6, and CMH8 (*idem*).

There are 2 GlcNS residues present in the antithrombin III (AT) pentasaccharide binding sequence of heparin; the chemical modification of GlcNS to GlcNAc in compound 2 interrupts the anticoagulant activity, with the small effect seen due to an incomplete de-N-sulphation reaction permitting minor activity (*idem*). A 200-fold reduction in anti-coagulation capacity occurs with the removal of 2-O or 6-O-sulphate groups (*idem*). The pentasaccharide sequence includes 6-O-sulphate in the three glucosamine residues with one including the additional and rare 3-O-sulphate modification essential for anticoagulant activity and a 2-O-sulphate on iduronate; removal of either/or the 6-O-sulphate and 2-O-sulphate has similarly adverse effects (*idem*).

Utilising the systematically modified heparin library in Figure 11, Patey *et al.* found heparin-based compounds with high potency in BACE1 inhibition assays and desirable diminished anti-coagulant capabilities (Patey et al., 2006). The off-target effects of the four best BACE1 inhibitors (PMH, CHM2, CMH3 and CMH4) were tested with FRET cleavage assays with related aspartyl proteases cathepsin D, pepsin and renin (*idem*). The study found PMIH had some inhibitory effects with pepsin (IC_{50} of 0.23 μg/ml) and cathepsin D (IC_{50} of 0.1 μg/ml), but this effect was reduced by 14 fold in N-acetylated heparin and had no activity in 2-O-desulphated, N-acetylated heparin (*idem*). N-acetylated heparin and 2-O-

desulphated heparin inhibited cathepsin D, but to a lesser degree than PMIH (IC_{50} of 0.27 μg/ml and IC_{50} of 0.77 μg/ml respectively) and all compounds showed no inhibition in the aspartyl protease, renin (*idem*). Hit compounds CMH2, CMH3, and CMH4 showed less inhibition potency in renin, pepsin and cathepsin D, than did the currently administered PMIH (*idem*).

Finally, size fractionation of the chemically modified heparins was completed to identify the minimum size requirements for the BACE1 inhibition activities; a ten-fold increase in BACE1 inhibition activity was seen between deca- and octa- saccharides signifying a minimum saccharide size for potent activity (Patey et al., 2006). Furthermore, the activity of an 18-mer is equivalent to full length PMIH (*idem*). Leveugle *et al.* (1998) used a BBB model to demonstrate the passage of saccharides of 3 kDa (≈ 10-18 mer) occurs through this endothelial BBB model, with disaccharide analysis confirming no changes to the saccharide structure (Leveugle et al., 1998). The potent BACE1 inhibitory activity of the 18-mer PMIH, chemical modifications retaining BACE1 activity while attenuating anti-factor Xa activity and the BBB model success with heparin saccharides suggest chemically modified heparins as promising compounds for further study.

Patey *et al.* (2008) subsequently modified the PMIH further, retaining 2-O-sulphtion and 6-O-sulphation while modifying the N-sulphate with increasingly non-polar groups to improve BACE1 activity and BBB permeability (Patey et al., 2008).

The addition of an increasing length carbon chain in the form of N-propanoyl heparin (CMH 11) N-butanoyl heparin (CMH 12) and only very slightly reduced the inhibitory capacity of BACE1 (Patey et al., 2008). The free amine heparin was a less potent inhibitor, demonstrating a negative or neutral charge is required at the amino moiety in the glucosamine residue and/or the modification of ring conformation under this condition allows for more tolerant binding (*idem*). The nitrogen in the N-sulpho-aziridine heparin bonds to both C2 and C3 and the iduronic acid is 3-sulphated; these modifications endow

N-sulpho-aziridine heparin with a BACE1 inhibitory potency akin to unmodified PMIH (*idem*). Interestingly, the parent compound of N-sulpho-aziridine (Figure 12) heparin is persulphated PMIH, and shows improved potency than this more highly sulphated parent (persulphated heparin includes 3-sulphate on the iduronic acid and 3-O-sulphate on the glucosamine), suggesting lower levels of sulphation can exhibit BACE1 inhibitory activity (Table 2) (*idem*). The activity of free amine heparin was reduced relative to N-acetyl heparin and compared to N-propanoyl and N-butanoyl heparins, demonstrating a carbon containing functional group at this position is required for potent activity (*idem*).

Table 2: Further chemical modifications to heparin with modifications at the N-sulphate to improve BACE1 inhibitory activity (IC_{50}) and BBB permeability. Modified from (Patey et al., 2008).

CMH	Compound	R1	R2	R3	BACE1 IC_{50} (ng/ml)	R^2 of IC_{50}
10	NH_2PMH	SO_3-	SO_3-	H	159	0.997
11	N-propanoyl	SO_3-	SO_3-	$COCH_2CH_3$	53	0.997
12	N-butanoyl	SO_3-	SO_3-	$COCH_2CH2CH_3$	55	0.995
13	50% N-sulphate 50% N-acetyl	SO_3-	SO_3-	$SO_3/COCH_3$	147	0.981
14	Aziridine	SO_3-	SO_3-	N-Sulpho-aziridine ring	31	0.999

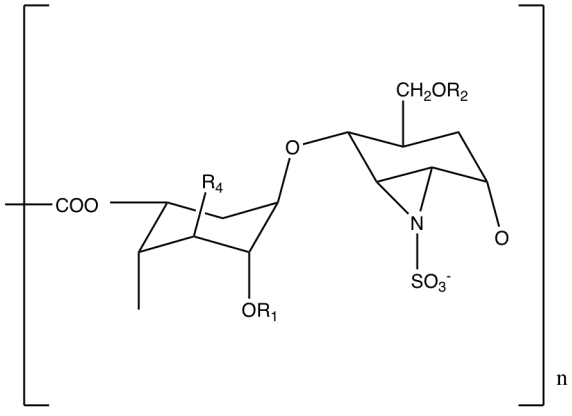

$R_1 = SO_3^-/H$ $R_2 = SO_3^-/H$ $R_3 = SO_3^-/H/COCH_3$ $R_4 = OH/SO_3^-$

Figure 12: Schematic of N-sulpho-aziridine heparin, demonstrating the four modifiable group positions. Figure modified from (Patey, Edwards, Yates, & Turnbull, 2008).

Klaver *et al*. (2010) expanded the work done by Beckman *et al.* (2006) by investigating the structural requirements for the interaction between heparin and pro-

BACE1 during enzyme activation (Klaver et al., 2010). The activation of pro-BACE1 required specific structural requirements met by BLH, PMH, and kidney HS (KHS). BLH, PMH and KHS activated pro-BACE1 more effectively than other GAGs but CS also exhibited significant stimulatory activity (*idem*). Highly sulphated analogues such as polysialic acid and poly-D-glutamic acid were also tested and had little effect, suggesting charge alone is not sufficient to promote the activity of pro-BACE1 (*idem*). More highly sulphated BLH at 1 μg/ml increased activity by 1600% while PMH and KHS increased activity by 900% suggesting the extent of GAG sulphation is important for this effect (*idem*). GAG chain length was also investigated, with 5 kDa chain length stimulating pro-BACE1 to a similar level to PMH; decreasing chain length reduced the ability of PMH to stimulate the enzyme, with a tetrasaccharide able to stimulate only 25% the amount of unfractionated PMH (PMH >1000% activity tetrasaccharide ≈250%), and a disaccharide unable to stimulate the enzyme (*idem*). Interestingly, although the disaccharide did not inhibit pro-BACE1, the addition along side PMH reduced the activation of the enzyme, suggesting a competitive action between the GAGs (*idem*).

Structural analysis of pro-BACE1 found a possible heparin-binding region of positive electrostatic potential adjacent to the BACE1 active site that includes the prodomain (Klaver et al., 2010). The results also suggested flap constructed by the loop region would be in the open position to accommodate a GAG chain; the team modelled the enzyme without this loop region and found a significantly larger positive electrostatic region (*idem*). This indicated heparin binding could require the loop region to be in the full open position, away from the active site with multiple GAG binding orientations possible in the large positively charged region (*idem*).

The paradox of both the inhibitive and promotive activities of heparin with BACE1 may be explained by the binding orientation of the heparin chains (Klaver et al., 2010). Some heparin binding positions in the BACE1 enzyme affording higher affinity binding

occurring at relatively low concentrations, and lower affinity binding occurring at relatively high heparin concentrations (*idem*). The high binding affinity regions therefore, have the capacity to modify the structure of the enzyme to stimulate ligand proteolysis, while lower affinity binding positions occupied at high heparin concentrations modify the structure alternatively, causing inhibition in proteolysis of APP ligand (*idem*). The specific structural requirements for heparin inhibition including 2-O-sulphation of the iduronic acid and N-acetylation of the glucosamine may contribute to the binding in the lower affinity regions, inhibiting the action of BACE1 (Patey et al., 2006).

Both Klaver *et al*. and Scholefield *et al.* postulate a model for BACE1 activity, with HS co-localised with pro-BACE1 in the Golgi, and after the removal of the pro-domain by a furin-like pro-protein convertase, further co-localised into the ER, endosomes and the cell membrane (Klaver et al., 2010; Scholefield et al., 2003). The heparin-binding domain on APP between residues 96-110 is a mobile region formed by a β-hairpin loop structure that may afford flexibility in spatial orientation (*idem*). HS may act to modulate the enzyme and orientate the APP ligand for proteolysis by BACE1 (*idem*).

Recent development into HS based BACE1 inhibitors has utilised disaccharide building blocks to formulate a library of 16 compounds, yielding high potency octa- deca- and dodecasaccharides (IC_{50} of 1-5 nM) (Schworer, Zubkova, Turnbull, & Tyler, 2013). Patey *et al.* (2006) previously found saccharides smaller than decasaccharides had a 10-fold reduction in BACE1 inhibitory activity; some modified octasaccharides in the Schworer library showed activity similar to decasaccharides in the previous work (Schworer et al., 2013). The most potent octasaccharide tested had the structure GlcNAc6S-[IdoA2S-GlcNAc6S]$_3$-IdoA2S with an IC_{50} of 3.9 nM (*idem*).

1.8.3 Challenges of heparin-based therapeutics for Alzheimer's disease

Unfractionated heparin has been utilised as an anti-coagulant for over 90 years and has become one of the most widely prescribed drugs, credited for the survival of millions of people (Wardrop & Keeling, 2008). There are many factors that preclude this polydisperse mixture of GAGs as being a useful drug for treating anything other than haemostatic problems. Heparin induced thrombocytopaenia (HIT) is a decrease in the platelet count of a heparinised patient caused by an autoimmune reaction to complexes of antibodies raised to heparin bound to platelet factor 4 (PF4) (Visentin, Ford, Scott, & Aster, 1994). Heparin:PF4:IgG complexes activate platelet FcϒIIa receptors through the IgG Fc region, with activated platelet aggregates causing clotting and thrombocytopaenia (*idem*).

Low molecular weight heparins still originate in porcine and bovine mucosa and have to be vigilantly purified before chemical or enzymatic digestion to produce derivatives of smaller molecular weights. These preparations have attenuated anti-coagulant activity, with a reduced capability for platelet factor 4 binding and in bone density reductions (which can lead to osteoporosis in the elderly in treatment is prolonged) (Boneu & de Moerloose, 2001). Elderly patients suffering from renal insufficiency associated with advancing age must be monitored closely through the biochemical testing of anti-factor Xa, to ensure the drugs are not causing renal damage; insufficient metabolism of the drug could cause toxicity (i.e increased from approximately 1.5 hours to approximately 4.5 hours half-life for Enoxaparin in patients who are renally impaired)(*idem*).

The therapeutic use of heparin is limited due to poor oral availability (Hirsh & Fuster, 1994). Intra-venous infusion is the preferred method for therapy, with the use of subcutaneous injection reducing the bioavailability (Hull et al., 1986). The use of subcutaneous heparin administration, allowing for more flexible treatment, has to ensure the initial dosage is higher to negate the reduction in bioavailability afforded by this

method (*idem*). The anticoagulant effect of a subcutaneous injection is delayed for 2-3 hours due to the bioavailability, therefore requiring an IV bolus for immediate anti-coagulant action (Hirsh & Fuster, 1994).

Upon administration, highly polyanionic heparin binds many plasma proteins including heparin-binding proteins, endothelial cells and macrophages, reducing the plasma concentration (Hirsh & Fuster, 1994). The non-specific binding of heparin *in vivo* causes variability in patient response, thromboembolic variation, and heparin resistance (Young, Prins, Levine, & Hirsh, 1992).

Metabolism and clearance of heparin occurs in two main pathways depending on the concentration. Initial quick clearance occurs with the binding of heparin to macrophages and endothelial cells; upon internalisation of heparin from the circulation, heparin is depolymerised (Dawes & Pepper, 1979). This is a rapid and saturable mechanism due to the number of available heparin binding receptors present on these circulating cells and is patient specific (*idem*). At higher heparin concentrations, above saturation of the cell-based metabolism, a slower hepatic metabolism and renal clearance of heparin occurs in a dose dependant manner (Olsson, Lagergren, & Ek, 1963).

The complexity regarding the bioavailability of heparin and heparin derivatives, limiting the therapy in an oral form, would limit the potential as an accessible, worldwide AD therapy. The challenges of a heparin-based AD drug include identifying a BACE1 inhibitor with the ability to permeate the BBB and target to neurons to reach BACE1. This inhibitor would be tractable and unambiguous in source or design. The identification of such compounds with low or no off-target effects and a specific binding pathway would allow the further development of administration methods. These could target the oral route to make the therapy feasible for widespread use and would require pharmacokinetics and dynamics studies prior to clinical trials.

Chapter 2: Materials and methods

2. 1 Materials

8-Anilino-1-naphthalenesulfonic acid, Sigma, UK. Catalogue No. A1028

Acetic acid, 99.5%. Fisher, Sweden. Catalogue No. 10230753

Acetic acid, glacial, 99.7%. Fisher, Sweden. Catalogue No. A/0400/PB17

Acetone. Fisher, Sweden. Catalogue No. 10225900

Ammonium chloride, ≥99.5%. Sigma, UK. Catalogue No. 9434

Ammonium sulphate 99.5%, Acros Belgium. Catalogue No. 10731424

Antithrombin. Hyphen Biomed, UK. Catalogue No. PP004C

L(+)-Ascorbic acid, 99%. Acros, Belgium. Catalogue No. 105021000

BACE1, human, Fc tag. Acro Biosystems, USA. Catalogue No. BA1-H5261

BACE1, human, FLAG tag. Sigma, UK. Catalogue No. S4195

BACE1, human, tag free. Acro Biosystems, USA. Catalogue No. BA1-H5213

Barium chloride. Sigma, UK. Catalogue No. 342920

Barium sulphate extra pure, Acros Belgium. Catalogue No. 10442031

β-Secretase inhibitor I. AnaSpec, USA. Catalogue No.AS-23958

β-Secretase inhibitor IV. Merck Millipore, UK. Catalogue No. 565788

Bovine lung heparin, sodium salt (149 IU.mg-1). Calbiochem, UK. Catalogue No. 375093

Bovine serum albumin (fraction V). Sigma, UK. Catalogue No. 05470

Calcium chloride, anhydrous. Sigma, UK. Catalogue No. 1023780500

Calcium sulphate 99%, Acros Belgium. Catalogue No. 10308310

Copper sulphate pentahydrate 99+%, Acros Belgium. Catalogue No. 10604902

D-(+)-10-camphorsulfonic acid. Fisher, Sweden. Catalogue No. 10030610

Chlorosulphonic acid, 99%. Sigma, UK. Catalogue No. 571024

Citric acid, monohydrate. Fisher, Sweden. Catalogue No. C/6200/53

Deuterium oxide 99.9 atom % D. Aldrich, UK. Catalogue No. 151882

Dextran sulphate, Mr ≈ 500 kDa. Fluka, UK. Catalogue No. 43097

Dimethylsulfoxide, anhydrous, ≥99.9%. Sigma, UK. Catalogue No. 276855

Ethanol, absolute. Fisher, Sweden. Catalogue No. E/0650DF/17

Ethylenediamine tetraacetic acid, disodium salt dihydrate, 99+%. Acros, Belgium. Catalogue No. 409971000

Factor Xa. Innovative research, USA. Catalogue No. IBFXa-18496

Factor Xa substrate. Biophen, USA. Catalogue No. CS-11(22)

HCl, 5M. Fisher, Sweden. Catalogue No. J/4310/15

HPLC (analytical) grade H_2O. Fisher, Sweden. Catalogue No. W/0106/17

Human alpha-thrombin. Innovative Research, USA. Catalogue No. IHaT

IgG UNLB, Mouse. Southern Biotech, USA. Catalogue No. 0107-01

IgG1k anti-green fluorescent protein, Human. BioRad, UK. Catalogue No. HCA192

IgG2k anti-green fluorescent protein, Human. BioRad, UK. Catalogue No. HCA193

IgM anti-desipramine, Mouse. Fitzgerald Industries, USA. Catalogue No. 10C-CR2068M2

IgM anti-GFP, Human. BioRad, UK. Catalogue No. HCA191S

Iron (II) sulphate extra pure, Fisher Sweden. Catalogue No. 10060010

Iron (III) sulphate, Fisher Sweden. Catalogue No. 10050210

Lithium sulphate 99% extra pure, Acros Belgium. Catalogue No. 10184650

Magnesium sulphate 99%, Acros Belgium. Catalogue No. 12198721

Manganese (II) sulphate 99+%, Acros Belgium. Catalogue No. 10701234

MCA-SEVNLDAEFRK(Dnp)RR-NH_2 Fluorogenic Peptide Substrate. R and D Systems, USA. Catalogue No. ES004

Normal citrated human plasma. Technoclone, Austria. Catalogue No. 3016137-004

OM99-2 BACE1 inhibitor (H-Glu-Val-Asn-[(2R,4S,5S)-5-amino-4-hydroxy-2,7-dimethyl-octanoyl]-Ala-Glu-Phe-OH Trifluoroacetate salt). Bachem, Sweden. Catalogue No. H-5108

Pathromtin SL. Siemens, UK. Catalogue No. 10484200

Phosphate buffered saline. HyClone, USA. Catalogue No. SH30258.02

Polyethylene glycol. Fisher, Sweden. Catalogue No. 25322-68-3

Porcine mucosal heparin sodium salt (201 IU.mg-1). Celsus, USA. Catalogue No. PH-03004

Potassium sulphate ≥ 99%, Fisher Sweden. Catalogue No. 10214590

Purified human IgG F(ab')2/k. Bethyl Laboratories, USA. Catalogue No. P80-130

Purified human IgG Fab. Bethyl Laboratories, USA. Catalogue No. P80-115

Purified human IgG Fc, Bethyl Laboratories, USA. Catalogue No. P80-104

Pyridine anhydrous, 99.8%. Sigma, UK. Catalogue No. 270970

Rhodizonic acid, disodium salt, 98%. Acros, Belgium. Catalogue No. 132340050

Silver sulphate 99%, Acros Belgium. Catalogue No. 10174930

Sodium acetate anhydrous ≥99.0%. Sigma, UK. Catalogue No. S8750

Sodium acetate trihydrate ≥99.0%. Sigma, UK. Catalogue No. S7670

Sodium bicarbonate. Fisher, Sweden. Catalogue No. 10244683

Sodium chloride 99.5%. Fisher, Sweden. Catalogue No. S/3160/53

Sodium chloride HPLC grade. Fisher, Sweden. Catalogue No. 10274392

Sodium citrate dihydrate ≥99.0%. Sigma, UK. Catalogue No. W302600

Sodium hydroxide 50% wt solution. Acros, Belgium. Catalogue No. 259860010

Sodium sulphate anhydrous, 99+% extra pure, Fisher Sweden. Catalogue No. 10606082

Sypro® Orange Protein Gel Stain. Sigma, UK. Catalogue No. S5692

Thrombin substrate. Hyphen Biomed, USA. Catalogue No. Biophen CS-01(38)

Thromborel S. Siemens, UK. Catalogue No. 10484202

Tris(hydroxymethyl) methylamine. Fisher, Sweden. Catalogue No. T/P630/60

Vanadyl sulphate hydrate extra pure, Fisher Sweden. Catalogue No. 10142450

Zinc sulphate heptahydrate 99%, Acros Belgium. Catalogue No. 10267273

2.2 Equipment

400 MHz NMR spectrometer, Bruker, USA.

1.6 x 70 cm HPLC Column. GE Life Sciences, USA. Catalogue No. 19-5103-01

Black, non-sterile, flat-bottom, 96-well reaction plate 350 µl, Sterilin. Fisher, Sweden. Catalogue No. 611F96BK

Clear, non-sterile, flat-bottom, 96-well reaction plate, 350 µl. Fisher, Sweden. Catalogue No. 11349163

Coagulation analyser, Thrombotrack. Axis Shield, UK.

Coagulation cuvettes & ball bearings. Behnk Elektronik, Germany. Catalogue No. 050-220

Dialysis tubing, 3500 Da MWCO cellulose acetate. Fisher, Sweden. Catalogue No. 11552541

Dowex Marathon ion exchange resin. Acros, Belgium. Catalogue No. 428787

Eppendorf MiniSpin centrifuge. Eppendorf, Germany. Catalogue No. 022620100

FT-IR Nicolet iS5 Spectrometer. Thermo Scientific, UK.

HiTrap heparin affinity column 1ml. GE Healthcare Sciences, USA. Catalogue No. 17-0406-01

HPLC Cecil 1100, with CE1200 wavelength monitor. Cecil, UK. Catalogue No. 1100

Jasco J1500 CD Machine. Jasco, UK. Catalogue No. J-1500

Lyophiliser, ModulyoD. Edwards Modulyo, UK.

MicroAmp® optical 96-well reaction plate. Fisher, Sweden, Catalogue No. 10411785

MicroAmp™ optical adhesive film. Fisher, Sweden. Catalogue No. 10567414

OMNIC series software. Thermo Scientific, UK. Catalogue No. INQSOF018

PD10 desalting HPLC column. GE Life Sciences, USA. Catalogue No. 17-0851-01

Sephacryl® 100-HR, MW range 1000-100,000 Da (globular proteins). GE Life sciences, USA. Catalogue No. S100-HR

Sephacryl® 500-HR, MW range 40-20,000 KDa (globular proteins). GE Life sciences, USA. Catalogue No. S500-HR

Step One Plus RT-PCR machine. Fisher, Sweden.

Tecan Infinite M200 Multiwell plate reader. Tecan, Switzerland. Catalogue No. M200

2.3 Methods

2.3.1 Far-ultraviolet (UV) circular dichroism

Delivered antibodies and fragments were removed from their stabilizing buffers using either 10 kDa or 50 kDa Corning spin filters at 12100 g in a Eppendorf® MiniSpin centrifuge for 10 minutes, washing with water three times before the protein was reconstituted with desired buffer solution.

The J-1500 Jasco circular dichrosim spectrometer was calibrated with D-(+)-10-camphorsulfonic acid at a concentration of 1 mg/ml (aq.), with peaks observed at λ = 290.5 nm and λ = 192.5 nm.

Human antibody fragments, whole antibodies and BACE1 (3 μM) were assayed on a J-1500 Jasco circular dichroism spectrometer in P/L 0.2 mm glass cuvette in 50 mM sodium acetate pH 4.0 or PBS pH 7.4 to a final volume of 32 μl. Variables include addition of 3 μM PMH (17 kDa mean molecular weight) or chemically modified heparin. Chemically modified heparin molecular weight ratios are as follows: IdoA(2S)-GlcNS(6S) 1, CMH2 1.1, CMH3 1.18, CMH4 1.32, CMH5 1.18, CMH6 1.32, CMH7 1.44, CMH8 1.66, CMH9 0.81. Data collection was completed by Spectral Manager II and data analysis was done in Prism 6 with second order polynomial smoothed to 10 neighbors. BeStSel analysis was completed on the unsmoothed data.

2.3.2 Differential scanning fluorimetry (DSF)

Differential scanning fluorimetry was completed with a method by Niesen *et al.* 2007 and Uniewicz *et al* 2014 with modifications for microplate use (Niesen et al., 2007) (Uniewicz, Ori, Ahmed, Yates, & Fernig, 2014).

Antibodies and antibody fragments were purified from their stabilising buffers using either 10 kDa or 50 kDa Corning spin filters at 12100 g in a Eppendorf® MiniSpin centrifuge for 10 minutes, replacing the buffer with water three times before the protein was reconstituted with desired buffer solution.

IgG1k (Mw 146 kDa), IgG2k (146 kDa), and IgM (950 kDa) were assayed at 1 µM in 96 well PCR plates along with 20x Sypro orange in 50mM sodium acetate pH 4.0 to a final well volume of 40 µl. Human antibody fragments Fc (32 kDa), Fab (50 kDa), and F(ab')2 (110 kDa) and BACE1 were assayed at 3 µM in PCR plates along with 20x Sypro orange in 50 mM sodium acetate pH 4.0 to a final well volume of 40 µl. PMH or chemically modified heparins were added to the reaction at a maximum concentration of 6 µM.

Modifications to the buffer system include ionic strength changes from 20-100 mM sodium acetate, pH changes between 4.0, 4.5 and 5.0 and phosphate buffered saline pH 4.0 to 7.4.

Differential scanning fluorimetry assays were conducted on a StepOne plus RT-PCR machine with TAMRA filter with an initial incubation phase of 2 minutes at 25°C, increasing 0.5°C increments every 30 seconds up to a final temperature of 99°C. Data analysis was completed in Prism 6 with first derivative plots smoothed to 4 neighbors fitting a second order polynomial.

2.3.3 Synthesis of cation heparin library

Dowex marathon ion exchange resin beads were washed in HPLC H_2O, the supernatant discarded, and immersed in 1 M HCl and mixed thoroughly. The beads were then washed in HPLC H_2O until neutralised. Celsus PMH (150 mg/ml) was incubated with prepared beans (1 hr) and removed with syringe filter; supernatant retained. 10 mM

cation salt was incubated with supernatant, prior to overnight dialysis in HPLC water with 1kDa PlusOne Mini Dialysis kits and further PD10 desalting.

2.3.4 Heparin affinity chromatography

Heparin affinity chromatography used a Cecil Instruments Q-ADEPT Q-2, Binary HPLC system. Antibodies and antibody fragments were loaded on to a 1 ml HPLC HiTrap Heparin column (GE Healthcare). Runs were completed either in 50 mM sodium acetate pH 4.0, or in PBS at varying pH levels (pH 4.0 – 7.0). Unbound material was isocratically eluted 1 ml/min with 0 – 2 minutes 100% buffer, then bound material was eluted with a linear 2 – 17 minutes 0 – 100% buffer + 2M NaCl. Run method then allowed for column clearing and stabilising with 17 – 19 minutes 100% buffer + 2M NaCl, then 19 – 24 minutes 100 % buffer. 40 µg protein was loaded and detected with UV/vis detector λ_{abs}= 210 nm (PBS) and λ_{abs}= 280 nm ($C_2H_3NaO_2$). Standard antibody preservative NaN_3 (sodium azide) was determined not to bind to the column. Data was collected in PowerStream CE4900 and processed in Prism 6.

2.3.5 Fluorescence (Förster) resonance energy transfer (FRET)

To determine the chemically sulphated polysaccharides BACE1 inhibition activity, FRET was employed to detect loss of fluorescence at λ_{em}= 405 nm. In a black 96 well flat bottomed microplate, 10 Sigma units of BACE1 (C-terminal FLAG-tag Sigma) were added alongside aqueous test compound of varying concentrations or water only and 10 µM MCA-SEVNLDAEFRK(DNP)RR-NH_2 fluorogenic peptide substrate in 50 mM sodium acetate pH 4.0. Upon addition of fluorescent substrate, the plates were measured at 37 °C immediately and subsequently every 5 minutes for 1 hour at λ_{ex}= 320 nm λ_{em}= 405 nm on a Tecan Infinite® 200 Pro microplate reader. The change in fluorescence over 1 hour was calculated and was compared to a no-inhibitor control and substrate only

control representing both a full reaction and no fluorescence respectively to demonstrate percentage inhibition of the BACE1 activity. Prism 6 was used for data analysis after calculation of normalised percentage inhibition (NPI):

$$NPI = \frac{\bar{c}_+ - x_i}{\bar{c}_+ - \bar{c}_-}$$

Where x_i is the raw measurement on the ith compound $\bar{c}_+$ and $\bar{c}_-$ are means of the positive and negative controls in an antagonist assay (Malo, Hanley, Cerquozzi, Pelletier, & Nadon, 2006).

2.3.6 Chemical sulphation of polysaccharides

Chemical sulphation of polysaccharides was achieved as per the method of Yoshida et al., 1995 modified as below (Yoshida et al., 1988). Polysaccharide (0.5 g) was added to 80 ml anhydrous pyridine on ice. Chlorosulfonic acid (10 ml) was added dropwise, with caution. The solution was heated to 95 °C for 1 hour, before cooling and precipitation with 50% w/v NaOH on ice. The neutralised solution was further precipitated by addition of ice-cold ethanol saturated with sodium acetate. The precipitate was recovered and washed in ice-cold ethanol saturated with sodium acetate. The precipitate was dissolved in water and dialysed (>3.5 kDa) over three days against running water; a final dialysis against HPLC grade water was performed. Dowex marathon beads were prepared by first incubating with 1 M HCl for 1 hour, with occasional vortexing. Acid was then removed with Corning spin filters and a bench top centrifuge. Marathon beads were washed with HPLC grade water removed using the spin filters and repeated until the resulting solution was neutralised.

The sulphated polysaccharide solution was incubated for 1 hour with H^+ Dowex Marathon ion exchange resin pre-prepared in the acid form. Beads were removed with a

spin filer and the resulting solution was neutralised dropwise by the addition of saturated sodium hydrogen carbonate. The resulting polysaccharide solution was desalted utilising a PD10 column as per manufacturers instructions. Polysaccharides were then frozen (-80 °C), lyophilised, and weighed to calculate yield of each chemical sulphation of polysaccharide.

2.3.7 Activated partial thromboplastin time (aPTT)

A cuvette, ball bearing, 50 mM calcium chloride and test sample (or water) were pre-warmed to 37°C on coagulation analyser. 50 µl normal human citrated plasma, 25 µl aqueous test sample or HPLC grade water and 50 µl Pathromtin SL reagent were incubated in a cuvette for 2 minutes at 37 °C. Time for clot formation was read immediately following the addition of 25 µl 50mM calcium chloride solution, time for clot recorded to a maximum of 2 minutes.

2.3.8 Prothrombin time (PT)

Cuvettes, ball bearing, Thromborel S reagent and test sample (or controls) were pre-warmed to 37°C on coagulation analyser. In a cuvette, 50 µl normal human citrated plasma was added and incubated for 1 minute at 37 °C. Aqueous test sample or HPLC grade water (50 µl) was then added followed by 50 µl Thromborel S reagent, with time for clot formation measured immediately following addition of Thromborel S, time for clot recorded to a maximum of 2 minutes.

2.3.9 Factor Xa inhibition

Anti-thrombin, factor Xa and factor Xa substrate were all diluted into experiment buffer 50 mM tris, 175 mM NaCl, 7.5mM EDTA, 0.1% PEG to pH 8.4. PMH calibration curve was completed at 0, 0.25, 0.50, 0.75, and 1.0 IU/ml.

On a clear 96 microwell plate incubated at 37°C, 28 mIU anti-thrombin (30 µl) was added to 30 µl test polysaccharide or water, this was mixed and incubated for 2 minutes at 37°C. To this, 0.21 nkats (30 µl) of preincubated factor Xa was added and the microwell plate was mixed and incubated at 37°C for exactly 2 minutes. Preincubated factor Xa substrate was then added at 1 mg/ml (30 µl) and the microwell plate was mixed and incubated at 37°C for exactly 2 minute. The reaction was stopped upon addition of 20 mg/ml citric acid (60 µl) and the plate was read at λ_{abs} = 405 nm.

2.3.10 Factor IIa inhibition

Anti-thrombin, thrombin and thrombin substrate were all diluted into experiment buffer 50 mM tris, 175 mM NaCl, 7.5 mM EDTA, 0.2% BSA to pH 8.4. PMH calibration curve was completed at 0, 0.25, 0.50, 0.75, and 1.0 IU/ml.

To a clear 96 microwell plate incubated at 37°C, 7.5 µIU anti-thrombin (30 µl) was added to 30 µl test polysaccharide or water, this was mixed and incubated for 2 minutes at 37°C. To this, 0.720 NIH U (30µl) thrombin was added and the microwell plate was mixed and incubated at 37°C for exactly 2 minutes. Preincubated thrombin substrate was then added at 1 mg/ml (30 µl) and the microwell plate was mixed and incubated at 37°C for exactly 1 minute. The reaction was stopped upon addition of 20 mg/ml citric acid (60 µl) and the plate was read at λ_{abs} = 405 nm.

2.3.11 Colourimetric determination of sulphate level

Sulphate level determination was achieved as per the method of Terho and Hartiala 1971 modified as below (Terho & Hartiala, 1971).

Test polysaccharides were hydrolysed at 1 mg/ml in solution with 1 M HCl at 100°C for 2 hours and subsequently lyophilised and reconstituted in HPLC water at 1 mg/ml. Dextran sulphate control was similarly hydrolysed, lyophilised and reconstituted at 25

mg/ml. A dilution series of each polysaccharide and dextran sulphate control was assayed to allow for linear range analysis.

Equal volumes of hydrolysed polysaccharide and ethanol (30µl) were added to a 96 well microwell plate, along with barium chloride buffer consisting of 100 mM acetic acid, 50 µM $BaCl_2$, 800 µM $NaHCO_3$ in ethanol, to a final well volume of 120 µl. Finally, rhodizonate detection solution was added to a final concentration of 0.14 mM rhodizonic acid and 3.4 mM L(+)-ascorbic acid in ethanol. The plate was shaken during colour development and allowed to stand in the dark for 10 minutes to develop. The microwell plate was read at λ_{abs} = 520 nm.

2.3.12 Gel permeation chromatography (GPC)

Gel permeation chromatography (GPC) was completed on hit compounds using a Cecil 1100 HPLC with 2 linked 1.6 x 70 cm columns, the first packed with Sephacryl S100 matrix, and the second with Sephacryl S500, reported to separate $1 \times 10^3 - 1 \times 10^5$ Da (peptides and small proteins) and $4 \times 10^4 - 2 \times 10^7$ Da (Dextrans) respectively. An isocratic 250 mM ammonium chloride was used to separate at 0.5 ml/min with a sampling rate of 2.63 Hz using Analogue devices AD 7194 data collection software at λ_{abs} = 210 nm on a Cecil CE1200 wavelength monitor with a run time of 9.38 hours. Void volume was determined with dextran blue (λ_{abs} = 380 nm) before calibration with gamma globulin (158 kDa), ribonuclease A (13.7 kDa), ovalbumin (44 kDa) and vitamin B12 (1350 Da) at 0.5 ml/min at λ_{abs} = 280 nm.

2.3.14 Fourier transform infra-red spectroscopy (FTIR)

FTIR spectra were recorded using a Nicolet iS5 IR-TF (Thermo Fisher) spectrometer scanning in the 4000–400 cm^{-1} region, with a spectral resolution of 2 cm^{-1} over 128 scans. A background air spectrum was obtained and subtracted from all spectra. In

order to further improve the comparison between samples, the mean of 5 FTIR spectra per sample was normalized to % transmittance. All spectra were processed using ThermoFisher Omnics software.

2.3.14 Nuclear magnetic resonance spectroscopy (NMR)

Chemically sulphated polysaccharide and unmodified polysaccharides were dissolved in deuterium oxide. ^{1}H NMR was measured with a Bruker 400 MHz spectrometer, ns = 128 d = 2 sec, with water suppression. Spectra collected with Topspin and analysed with iNMR.

2.3.16 Correlation analysis

Pearson product-moment correlation coefficient (or Pearson correlation coefficient, r) measures the strength of a linear relationship between two variables. A two-tailed correlation matrix of r is computed for each variable within a dataset (CI 95%). Analysis completed with Prism 6.

2.3.17 Principle component analysis (PCA)

Principle component analysis was completed with Minitab, inputting data from the 1^{St} derivative melt curves of DSF. Each concentration of CMH was inputted into a correlation matrix, where multivariate analysis was completed with PCA to elucidate the eigenvalues and principle component values. Eigenvalues accounting for ≥ 85% of the variance were plotted, with principle component values for each CMH concentration or test polysaccharide, which for this data formed a PC1 v PC2 plot.

CHAPTER 3: The effect of biochemical tags on BACE1 structure

3.1 Introduction

Initial investigations were conducted to identify the suitability of BACE1 enzyme available for use in the fluorescent resonance energy transfer (FRET) assay that is commonly used to identify BACE1 inhibitors. Recombinant human BACE1 was obtained in various forms, containing biochemical tags and in the untagged, native form. Four types of BACE1 were investigated in order to determine the effect of heparin on the binding and any structural changes seen during protein-heparin binding. Identification of the most suitable form of BACE1 for further areas of this study, including structural and enzyme activity experiments, was completed. The typically employed buffer system of BACE1 *in vitro*, acetate buffer and acidic pH of pH 4.0 – 4.5, closely represents the physiological environment experienced by BACE1 in the endosome.

Ideally, native (untagged) BACE1 would be used throughout the activity and structural experiments to ensure there are no adverse changes or artifacts arising from the presence of the included tag, but native BACE1 is ≈ 160 % more expensive than tagged BACE1. This increase in price is due to the more complex and time-consuming extraction and purification required for tag-free protein.

Three commercially available protein tags were investigated; 10-His tag, Fc tag, and FLAG tag alongside the native un-tagged BACE1.

3.1.1 Histidine tag

The poly-histidine tag usually comprises of between 6 and 14 histidine residues and is most commonly utilised as a fast and convenient method for protein purification in concert with immobilised metal affinity chromatography (IMAC) (Porath, Carlsson, Olsson, & Belfrage, 1975). IMAC employs metal ions e.g nickel (Ni^{2+}) and colbalt (Co^{2+}) coated beaded agarose resin, which enable high affinity metal ion co-ordination with the

poly-histidine tag region of the protein, and ensures separation of the labelled protein away from cell culture supernatant (*idem*).

The position, structure and sequence length of the histidine tag influences protein purification, through modifications to the expression rate, accessibility to the metal cation during IMAC, protein structure, and crystal formation; this affects ultimately protein solubility and bioactivity (Block et al., 2009).

Variations in the poly-histidine tag size allows for purification under a range of conditions. Soluble protein purification may require a hexahistidine tag (H_6), whereas purification of a membrane protein under conditions containing detergent, may require a longer histidine tag (H_{10}/H_{14}) or a linker region (Block et al., 2009). Furthermore, detergent micelles may encapsulate some of the tag during purification, reducing metal cation binding (*idem*). A 10-histidine tag is currently used conjugated to the BACE1 C-terminus due to the membrane spanning nature of the enzyme.

3.1.2 IgG Fc region tag

The immunoglobulin Fc region has been utilised in biomedical research since the CD4-Fc fusion agonists developed by Capon *et al.* (1989) (Capon et al., 1989). The fusion of the IgG Fc peptide confers improved plasma retention *in vivo* due to the FcRn salvage interaction (Akilesh, Christianson, Roopenian, & Shaw, 2007). IgG Fc improves the solubility of fusion proteins both *in vivo* and *in vitro*, through improvements to stability (Kontermann, 2011). The addition of IgG Fc to recombinant protein also increases the circulating time of fusion proteins through attenuated renal clearance (*idem*), and allows cost-effective purification in protein A/G sepharose affinity chromatography (Carter, 2011). The IgG Fc region is additionally employed in the production of fusion-dimers and more complex polymer structures due to propensity of the Fc region to dimerise

(*idem*) and permits the binding of fusion molecules to a variety of Fc receptors, including immune cell receptors; acting as a delivery molecule (Jazayeri & Carroll, 2008; Nimmerjahn & Ravetch, 2008).

Currently used protein-based therapeutics (≈ 70 kDa and smaller) are eliminated with a typical half-life of from a few minutes to a hours; the addition of an Fc region enables neonatal Fc receptor (FcRn) recirculation, resisting renal elimination. The serum half-life increases to days and weeks, therefore producing more efficacious therapies (Carter, 2011).

Protein expression with an Fc tag allows for the simple and cost effective purification of Fc-fusion protein through protein A or protein G beaded agarose affinity chromatography (Table 3). Protein A is a 42 kDa, high affinity immunoglobulin binding protein found on the *Staphylococcus aureus* cell wall (Ey et al., 1978; Langone, 1978). This protein specifically binds IgG Fc and the VH3 of Fab regions (Nilsson, Abrahmsen, & Uhlen, 1985; Uhlen et al., 1983). Protein G is expressed as a 58 kDa to 68 kDa protein in group G Streptococcus (Akerstrom, Brodin, Reis, & Bjorck, 1985; Bjorck & Kronvall, 1984).

Table 3: The affinity of protein A and protein G for the antibody fragments and whole immunoglobulin. Strong binding between the immunoglobulin and purification protein allows purification of the immunoglobulin through sepharose affinity chromatography (Langone, 1978).

Antibody class	Protein A	Protein G
κ light chain 1,3,4	None	None
λ light chain	None	None
Heavy chain	Strong	Strong
IgG1	Strong	Strong
IgG2	Strong	Strong
IgG3	Weak	Strong
IgG4	Strong	Strong
IgA	Weak	Weak
IgM	Weak	Weak
IgE	Weak	Weak
IgD	None	None

Fc-fusion proteins can be utilised to both increase and decrease effector functions of immune cells e.g NK cells through the interaction with the Fc receptor FcϒRIIIA promoting antibody dependent cellular toxicity (ADCC) in cancer cells (Congy-Jolivetab, Probst, Watier, & Thibaulta, 2007), and mast cell downregulation through the activation of inhibitory Fc receptor, FcϒRIIB (Daeron, Malbec, Latour, Arock, & Fridman, 1995).

Clinical Fc-fusion proteins have been available since 1998, with the introduction of Etanercept ('Enbrel' by Amgen/Pfizer), a tumor necrosis factor receptor (TNFR)-IgG1 Fc fusion protein used in the treatment of rheumatoid arthritis (RA). Treatments for psoriasis (Alefacept), transplant rejection (Alefacept and Betatacept), RA (Etanercept and Abatacept), thrombocytopaenia (Romiplostim), cryopyrin-associated periodic syndromes (genetic autoimmune disease) (Rilonacept), and age related macular degeneration (Aflibercept) have all been developed utilising the Fc-fusion mechanism (Czajkowsky, Hu, Shao, & Pleass, 2012). In 2012, Fc fusion therapeutics represented 20% of the USA Food and Drug Administration (FDA) approved antibody-based medicines (*idem*).

The fusion partner of Fc is commonly attached at the hinge region below the constant heavy chain immunoglobulin domain CH2, through a modified hinge, with the Fc regions dimerising, as would native immunoglobulin (Czajkowsky et al., 2012). Single ligand specificity in bivalent fusion constructs such as the fibroblast growth factor I (FGF1) Fc-fusion protein, function effectively with FGFR1 on T-cells (Dikov, Reich, Dworkin, Thomas, & Miller, 1998), therapeutic examples that mimic this interaction include Abatacept and Alefacept (Czajkowsky et al., 2012).

Cytokine traps are examples of monovalent fusion constructs with multiligand specificity such as Aflibercept, a vascular endothelial growth factor receptor

(VEGFR1/VEGFR2) Fc-fusion protein, designed to treat macular degeneration (Czajkowsky et al., 2012). Multi-ligand binding domains co-operate to form a single binding region capable of trapping a single ligand (Economides et al., 2003).

Multivalent fusion proteins with single-ligand specificity, are constructed from multiple copies of binding regions separated by flexible linkers to form a large region, possible for ligand interaction (Cines, Yasothan, & Kirkpatrick, 2008). The Fc-fusion protein Romiplostim is utilized in thrombocytopenia, to regulate platelet production by mimicking the action of the endogenous protein analogue thrombopoietin (*idem*).

Single ligand specificity in multivalent fusion constructs bind large single proteins between the dimer creating a stable scaffold for ligand binding. The extracellular domain of the TNFα-receptor II is bound to the Fc dimer forming the antagonist therapy, Etanercept as a treatment for RA (Scallon et al., 2002).

Non-clinical applications of Fc-fusion include the use of this tag in flow cytometry, immunohistochemistry and ELISA, and in protein microarray technologies (Flanagan, Arias, Hu, Khawli, & Epstein, 2007). The BACE1 selected is conjugated to a C-terminal Fc tag.

3.1.3 FLAG-tag

The FLAG-tag is constructed of the hydrophilic amino acid sequence DYKDDDDK, N- to C- terminus, which is designed to ensure the tag remains on the surface of recombinant protein due to the hydrophilic nature of the tag (Terpe, 2003). Protein purification using FLAG-tag employs calcium dependant monoclonal (M1) antibody epitope recognition for the 8 amino acid tag, with the antibody conjugated to agarose beads enabling immunoprecipitation of the conjugated protein (*idem*). Purification conditions are non-denaturing so they can accommodate active fusion proteins, with the

antibody:FLAG epitope complex dissociated with decreasing pH or metal chelating agents such as EDTA (*idem*).

3.1.4 Other commonly used protein tags

The polyarginine tag (Arg-tag) consists of 5 or 6 basic arginine residues (Sassenfeld & Brewer, 1984) and is purified with cation exchange sulfopropyl (SP) resin and is eluted with NaCl at alkaline pH (Terpe, 2003). However, inclusion of the Arg-tag may modify tertiary structure in protein with a hydrophobic C-terminal such as BACE1, which contains a single transmembrane domain near its C-terminus (455-480) (Cole & Vassar, 2007).

The c-myc tag consists of 11 residues EQKLISEEDL recognised by the monoclonal antibody, 9E10 (Evan, Lewis, Ramsay, & Bishop, 1985). Purification of recombinant protein with a c-myc tag is conducted with divinyl sulphone-activated agarose at physiological pH, followed by elution in acidic conditions. This elution step can have a denaturing effect on protein activity (Terpe, 2003); hence why this tag is not commonly used for purification processes.

Polyarginine or c-myc tagged BACE1 is currently not available commercially, therefore was not screened in this study.

Recombinant addition of a glutathione S-transferase tag produces a fusion of glutathione S-transferase (GST), which can be purified from media using high affinity binding between GST and reduced glutathione (GSH), whereby the bound fusion protein can be eluted with 10 mM GSH (Terpe, 2003). A GST tag can be removed from the protein with a site-specific protease such as thrombin or factor Xa and GSH-agarose affinity chromatography (*idem*).

3.1.5 Native BACE1

BACE1 without a purification tag would be the ideal protein for both activity and structural studies, but the increased cost of this form of protein causes us to look elsewhere for a suitable replacement.

The native BACE1 used in this study is expressed with a tag, which is removed by specific proteolysis by an enteropeptidase. The gene sequence includes the C-terminal DDDDK acting as a recognition site for the enteropeptidase proteolysis, the full sequence for recombinant native BACE1 can be found in Appendix.

3.1.6 Method information

3.1.6.1 Differential scanning fluorimetry

Differential scanning fluorimetry (DSF) and far-UV circular dichroism (CD) were both employed in this chapter to study the changes in BACE1 thermal stability and secondary structure respectively, upon interaction with UF PMH.

In DSF, the hydrophobic dye Sypro Orange binds to regions of hydrophobicity within the study protein. Sypro Orange is a merocyanine containing a quaternary ammonium electron acceptor and a tertiary amino electron donor. The use of Sypro Orange is preferred to 1-anilino-naphthalene-8-sulfonate (1,8-ANS) with which the technique was initially engineered, as conventional quantitative real time polymerase chain reaction (RT-PCR) machines utilise the dye TAMRA (tetramethylrhodamine), which has excitation and emission wavelengths in the required range for Sypro exploitation (λ_{ex}= 560 nm λ_{em}= 582 nm) (Semisotnov et al., 1991; Uniewicz et al., 2010). The precision of the peltier heating and ramping time in a RT-PCR machine are of benefit in the real-time monitoring of protein unfolding (Niesen et al., 2007). Increasing the temperature causes the protein to unfold and denature, increasing the exposure of

hitherto unexposed hydrophobic regions within the protein (Figure 13). Sypro Orange binds to these exposed regions, and fluoresces under hydrophobic conditions. This fluorescence emission is detected in the similar range to the commonly used RT-PCR fluorophore TAMRA, with λ_{exc}= 542 nm and λ_{em}= 568 nm.

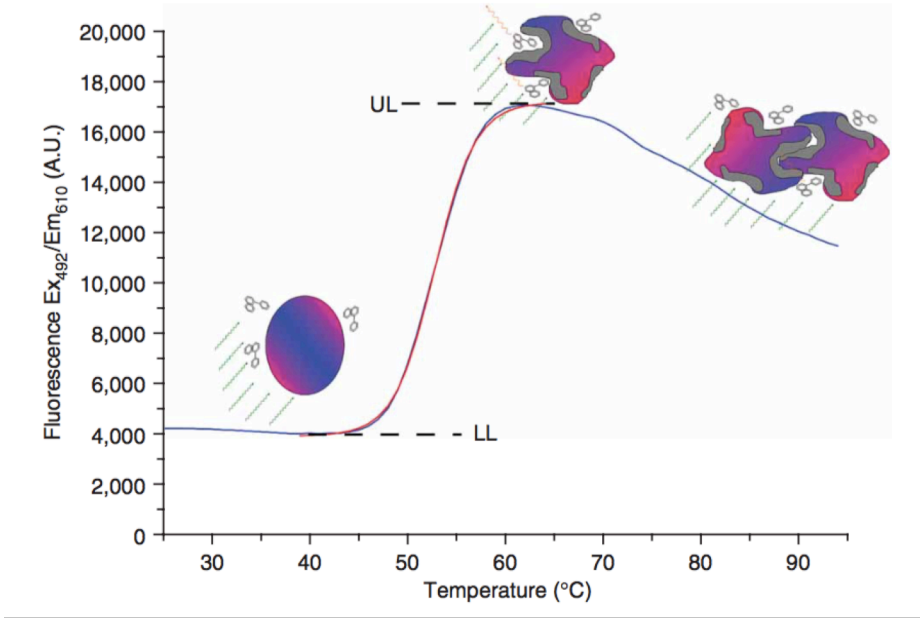

Figure 13: Differential scanning fluorimetry of the unfolding of citrate synthase example protein with Sypro orange. Increasing the temperature causes protein unfolding from a globular structure at position LL, exposing hydrophobic regions. These hydrophobic regions bind Sypro orange dye and fluoresce at the emission wavelength, shown here at λ_{em}= 610 nm. Lower level (LL) and upper level (UL) fluorescence intensity is shown (Niesen, Berglund, & Vedadi, 2007). Image reproduced with permission from the rights holder

Differential scanning fluorimetry measures changes to protein thermal stability, to determine any structural change conferred in BACE1, which may suggest the binding of GAG chain/s. Protein stability is related to the temperature dependant on Gibbs free energy of unfolding ΔG_u, with increasing temperature reducing the ΔG_u, until this measure reaches zero (Niesen et al., 2007). At zero ΔG_u, equilibrium between folded and denatured protein occurs and is characterised as the melting point (Tm) (*idem*). Most commonly, the binding of a ligand is thermodynamically advantageous, conferring an increase in ΔG_u, a more stable protein, and therefore a higher Tm (*idem*). Investigations

by Matulis *et al.* (2005) and Vedadi *et al.* (2006) demonstrate the increase in Tm due to protein stabilisation is proportional to the ligand concentration, and binding affinity (Matulis, Kranz, Salemme, & Todd, 2005; Vedadi et al., 2006). However, thermodynamic elucidations must be limited, as the magnitude of the Tm shift is not unique to a particular binding affinity (Niesen et al., 2007). This is because either the entropic and enthalpic components may give rise to the same Tm shift, or competing components could mask actual protein changes (*idem*). The comparison of Tm within a group of ligands can be made when the group has similar physicochemical properties (*idem*). This ensures in the later chapters, the GAG family, chemically modified heparin library studies, and degree of polymerization (d.p.) studies in DSF give Tm results that can be compared within these discrete data sets. The presence or absence of a ligand may alter the melting point (Tm) through changes to the protein structure and therefore thermal stability. Other factors that influence protein structure such as buffer strength, salts, and detergents may also have an affect on Tm in DSF (*idem*).

3.1.6.2 Far-UV circular dichroism

Circular dichroism spectroscopy is one of the most widley used methods for characterising protein and peptide conformation in solution. This comparatively low-resolution (when compared to NMR and XRAY crystallography) spectroscopic method is non-destructive, robust and simple to both use and interpret (Greenfield, Davidson, & Fasman, 1967). The principle utilises the chromophore present in optically active molecules to absorb left and right circularly polarised light to differing degrees; therefore producing an absorption spectra specific to the test molecule in solution (*idem*). Amino acids are especially suited to this form of spectroscopy due to the enantiomeric nature of the amino acid (aside from glycine) and also the peptide bond in

peptides and proteins. In far-UV CD spectroscopy (λ_{abs} = 180 nm - 240 nm) this peptide bond produces two bands, an intense band at 190 nm and weak band at 210 nm (*idem*). Addition of a ligand leading to backbone conformational changes in the protein modify the relative absorbance of light at these wavelengths, causing changes to the CD spectra. High concentrations of protein (≈ 10 mg/ml) are required for appreciable spectra in CD therefore the technique can be financially prohibitive.

Circular dichroism (CD) provides low-resolution protein conformational data, allowing for the characterization of protein structure in solution and upon the addition of potential ligands. Far-UV circular dichroism was utilised to determine the secondary structural changes in BACE1 with the addition of UF PMH. Far-UV circular dichrosim operates between λ = 240 nm and λ = 180 nm, and was employed to monitor the secondary structural changes, such as α-helix and β-sheet conformations, through the peptide bond absorption (W. C. Johnson, 1988). Near-UV range (λ = 320 nm – 260 nm) monitors changes to the environments of aromatic amino acids, tryptophan (λ = 280 nm – 300 nm), phenylalanine (λ = 250 nm - 270 nm) and tyrosine (λ = 270 nm - 290 nm) (*idem*). Signal strength in the near-UV range is much lower than far-UV CD spectroscopy and therefore requires higher concentrations of sample; due to the expense of this and the problems with protein aggregation, far-UV was chosen for this work (*idem*).

Heparin does not absorb light in the visible and near-UV range (Barbara Mulloy, 2012). Heparin has far-UV absorption spectra with a weak band at λ = 234 nm corresponding to the unsaturated uronic acid present from β-elimination at the new non-reducing end (*idem*). Chemically sulphated polysaccharides were screened for CD spectra and appropriate controls were conducted to ensure demonstration of protein only structural changes.

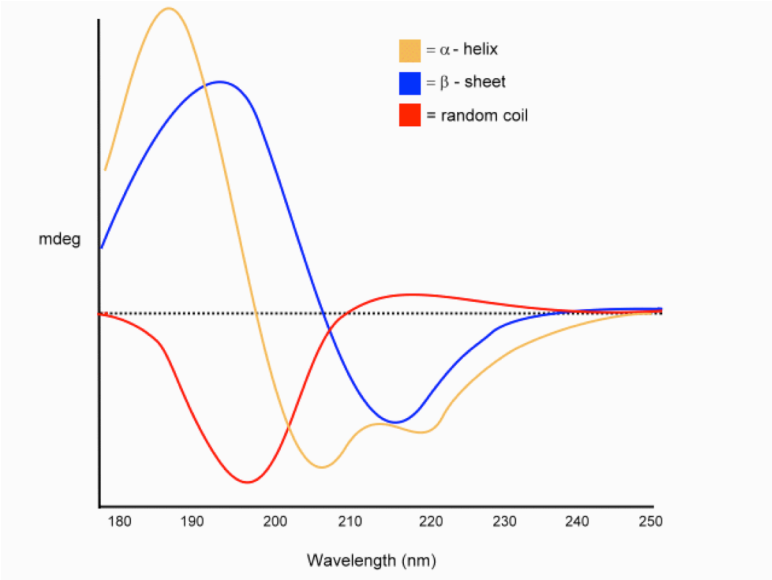

Figure 14: Characteristic far-UV circular dichroism spectra of α-helix, β-sheet, and random coil secondary protein structures. The approximate fraction of the structural motifs present in the protein under study can be determined by deconvolution of the resulting CD spectra with analysis software such as BeStSel. Protein mutation, ligand binding, and solution effects can be studied by the resulting change in structural characteristics.

Circular dichroism analysis software such as BeStSel (Micsonai et al., 2015) uses an idealised library of proteins with known structural motifs to determine the secondary structure of the protein under study. The structural characteristics are described as proportions of the common motifs, α-helix, β-sheet, and random coil, quantifying the protein secondary structure (Figure 14).

3.1.7 Experimental aims

As heparin and other GAGs are highly negatively charged glycopolymers, their influence on the structure and therefore function of BACE1, with and without biochemical tags, will be assessed to determine whether a proxy for native BACE1 can be identified for use in further experiments. This investigation will be conducted employing far-UV circular dichroism (far-UV CD) and differential scanning fluorimetry (DSF). Far-UV CD will illustrate changes to the protein secondary structure upon addition of heparin. DSF will demonstrate changes in the protein stability upon

interaction with heparin, measured by the change in melting temperature of the protein. All protein chosen for structural studies has been obtained from manufacturers with quoted batch enzymic activity to ensure the BACE1 enzyme is in an active form.

The use of native, untagged BACE1 is expensive due to the cost of production for an untagged protein and the comparatively large amount of protein required for structural experiments. DSF and far-UV CD have been employed to identify structural changes associated with the addition of the purification tags FLAG-tag, 10-His tag, Fc tag alongside native untagged BACE1 for comparison. The aim of this study was to identify which BACE1 type may be used for further BACE1 structural studies with a library of chemically modified heparins, other GAG compounds and to aid in the identification of 'hit' chemically sulphated GAG analogues as potential BACE1 inhibitors.

The second aim of this chapter was to demonstrate changes in BACE1 structure and stability, to gain an understanding as to how PMH studied by Scholefield et al. (2003) and Patey *et al.* (2006, 2008), inhibit BACE1 activity *in vitro* (Patey et al., 2006, 2008; Scholefield et al., 2003).

3.2 Results

3.2.1 Far-UV circular dichroism analysis of BACE1 and the effect of heparin

The far-UV spectra of native BACE1, 10-His tagged BACE1, FLAG-tagged BACE1, and Fc-BACE, are shown in Figures 15 and 16, in addition to the spectra obtained for each BACE1 type with UF PMH, in a 1:1 molar concentration ratio. The minor spectral contribution of UF PMH has been subtracted from the relevant BACE1 spectra, to ensure accurate comparison of the change in BACE1 secondary structure in sodium acetate at pH 4.0. The physiological action of BACE1 occurs in the endosome and the enzyme has been shown to be most active at pH 4.0, representative of this environment. The flap region covering the active site of BACE1 is open at this acidic pH, also signifying the enzyme is in the active state.

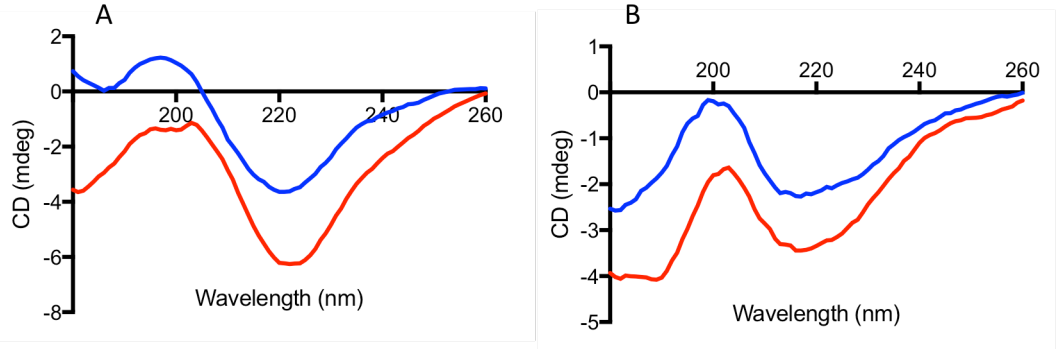

Figure 15: Far-UV circular dichroism spectra of native untagged BACE1 and FLAG-BACE1 ± UF PMH in 50 mM sodium acetate pH 4.0. **A**) (–) Native BACE1, (–) native BACE1 with UF PMH. B) (–) FLAG-BACE1, (–) FLAG-BACE1 with UF PMH.

Figure 15A shows the spectra of native BACE1 with no purification tag present (i.e native). The native BACE1 spectrum has a trough at a λ = 221 nm and a peak at λ = 199 nm. When UF PMH is included, the spectra is shifted into a more negative ellipticity, with peaks at λ = 222 nm and λ = 197 nm, displaying a subtle wavelength shift.

Figure 15B is the spectra of FLAG-tagged BACE1 in the 50 mM sodium acetate buffer at pH 4.0. FLAG-BACE1 has two spectral peaks, occurring at λ = 217 nm and 202 nm; the spectra have similar features, with a low peak at λ = 202 nm and a peak high at λ = 217 nm.

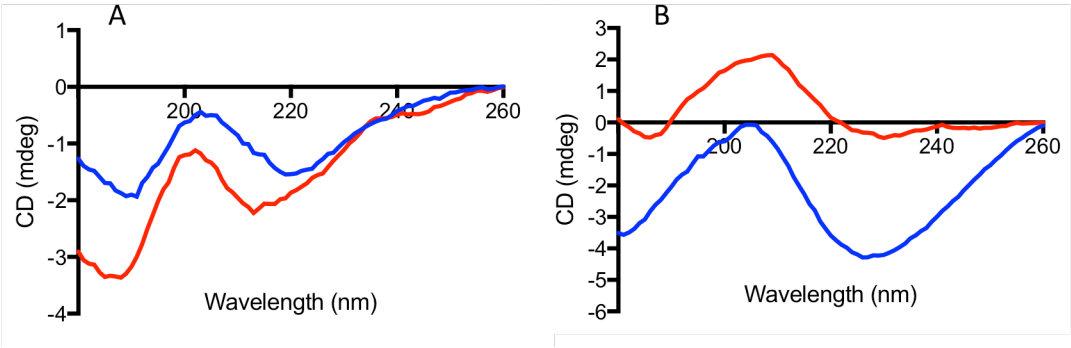

Figure 16: Far-UV circular dichroism spectra of 10-His BACE1 and Fc-BACE1 ± UF PMH in 50 mM sodium acetate pH 4.0. **A**) (–) 10-His BACE1, (–) 10-His BACE1 with UF PMH. **B**) (–) Fc-BACE1, (–) Fc-BACE1 with UF PMH.

BACE1 with a 10-His tag has spectral troughs at λ = 219 nm and λ = 190 nm, with a high peak of λ = 201 nm (Figure 16A). With the addition of UF PMH the wavelength of these peaks shifts to 213 nm and 188 nm for the troughs, and 202 nm for the peak. The shift from 219 nm to 213 nm is the largest peak transition with the addition of heparin in the four BACE1 types tested. The CD spectrum of Fc-BACE1 (Figure 16B) has a trough with λ = 227 nm, with a peak at λ = 208 nm. With the addition of UF PMH, the low peak shifts to λ = 230 nm, but looses the clear peak maxima, flattening the spectra at this wavelength. The 208 nm peak shifts to 205 nm with the addition of UF PMH.

BeStSel structural analysis of the CD spectra was conducted to quantify changes to the BACE1 secondary structure due to the tag present and the addition of UF PMH (Table 4). Native BACE1 comprised of 35% antiparallel β-sheets, and 20% turn regions. This proportion changed with the addition of UF PMH, to 31% antiparallel β-sheets and 21% turn regions. The proportion of structure identified as 'other' increased with

heparin addition, suggesting a move from ordered structure to a more disordered assembly.

Table 4: Far-UV circular dichroism spectra analysed by BeStSel software, quantification of antiparallel β-sheets and turn regions in BACE1 secondary structure ± UF PMH.

BACE type	Antiparallel β-sheets	Turn regions
Native	35%	20%
Native with UF PMH	31%	21%
Fc-BACE1	28%	23%
Fc-BACE1 with UF PMH	35%	20%
FLAG-BACE1	32%	20%
FLAG-BACE1 with UF PMH	28%	20%
10-His BACE1	34%	20%
10-His BACE1 with UF PMH	33%	20%

Fc-BACE1 comprised of 28% antiparallel β-sheets and 23% turn regions, which translated to 35% antiparallel β-sheets and 20% turn regions with the addition of UF PMH. The proportion of 'other' regions, of undetermined secondary structure was reduced in Fc-BACE1 with the addition of heparin, suggesting a novel action to the glycosaminoglycan interaction, which is not present in the native, untagged BACE1 protein binding to heparin.

FLAG-BACE1 contains 32% antiparallel β-sheets and 20% turn regions, with the addition of UF PMH reducing the proportion of antiparallel β-sheets to 28%. The addition of heparin does not change the levels of turn region, but does increase the disordered protein structure labelled 'other' by 2%.

10-His tagged BACE1 has antiparallel β-sheet, which constitutes 34% of the protein structure and 20% turn regions. The inclusion of heparin into this CD experiment causes a change in antiparallel β-sheet proportion to 33%, and a increase in 'other' regions but no change to the proportion of turn regions.

Native BACE1 and FLAG-BACE1 show similar secondary structural changes with the addition of UF PMH, displaying a 4% reduction in antiparallel β-sheets, negligable

change to the turn region component and a increase in the undefinable secondary structure characteristics identified as 'other' in BeSeSel analysis.

Interestingly, the action of UF PMH on the Fc tagged BACE1 increases the proportion of antiparallel β-sheet, which does not occur in the other BACE1 types tested. This increase is due to the increase in right-twisted antiparallel β-sheet from 9% to 17% with heparin present. As this change is not seen in the other BACE1 types, it may be caused by the presence of the relatively large Fc purification tag; this is investigated in Chapter 4.

3.2.2 Differential scanning fluorimetry of BACE1 types and the effect of heparin

Differential scanning fluorimetry (DSF) is a method for the analysing the stability of a protein (with or without a ligand) under defined conditions using thermal degradation to obtain the protein melting point (Tm). Here, DSF was used to determine whether the Tm, and therefore a measure of thermal stability of the BACE1 protein, changed upon inclusion of the known BACE1 modulator, heparin. The known hydroxyethylamine containing inhibitor IV (Figure 17) was used to demonstrate the effect of potent inhibitor binding on secondary structure of BACE1.

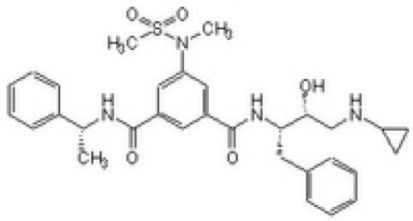

Figure 17: Chemical structure of hydroxyethylamine containing BACE1 inhibitor IV.

Figure 18A shows the first derivative of native, untagged human BACE1 in 50 mM sodium acetate at pH 4.0 in order to demonstrate the Tm as the peak maxima. The Tm of native BACE1 with no ligand present in the pH 4.0 conditions is 45.80 °C, and with the addition of 3.0 μM of inhibitor IV, the protein experiences no change in Tm. At this

inhibitor IV concentration BACE1 is inhibited (Stachel et al., 2004), therefore the concentration chosen for these experiments is indicative of the structural change upon inhibitor binding and action. The addition of heparin at the same concentration of 3.0 µM caused the reduction in the Tm of BACE1 to 38.78 °C, suggesting a stability change that causes an increase in BACE1 sensitivity to thermal denaturation.

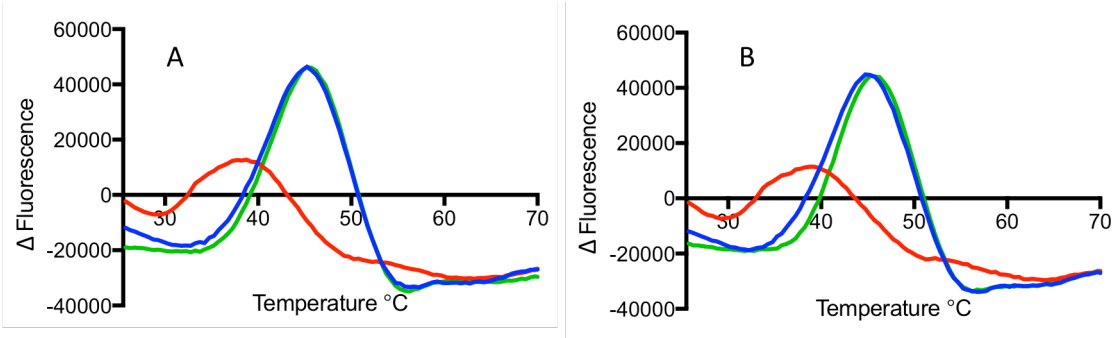

Figure 18: First derivative melt curve of differential scanning fluorimetry data of native BACE1 ± UF PMH and inhibitor IV in 50 mM sodium acetate pH 4.0. **A**) (–) Native BACE1 (–) native BACE1 with inhibitor IV, (–) native BACE1 with UF PMH. **B**) (–) FLAG-BACE1 (–) FLAG-BACE1 with inhibitor IV, (–) FLAG-BACE1 with UF PMH.

The thermal denaturation of FLAG-BACE1 is similar to the native BACE1, with a Tm of 45.38 °C, but is slightly increased with the addition of inhibitor IV to 46.14 °C (Figure 18B). The process of measuring the fluorescence of the hydrophobic region binding fluorophore occurs at temperature increments of 0.5 °C, with the temperature error of the RT-PCR machine of ± 0.19 °C. Therefore, Tm changes greater than 0.5 °C are deemed meaningful. The addition of UF PMH causes the Tm of FLAG-BACE1 to be reduced, as with native BACE1, to 39.95 °C, similarly suggesting reduction in thermal stability.

10-His tagged BACE1 has a reduced Tm than native and FLAG-tagged BACE1. The Tm of this BACE1 form is 43.69 °C (Figure 19B). The inclusion of inhibitor IV does not modify the Tm of 10-His BACE1 but UF PMH addition causes the reduction of Tm to 40.52 °C. This suggests the addition of 10-His enables BACE1 to resist the structural

change caused by the addition of heparin seen with both native and FLAG-BACE1 seen above.

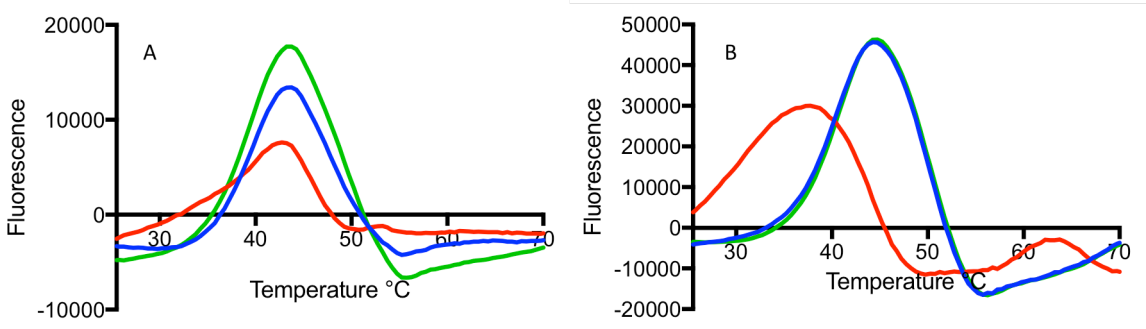

Figure 19: First derivative melt curve of differential scanning fluorimetry data of 10-His BACE1 and Fc-BACE1 ± UF PMH and inhibitor IV in 50 mM sodium acetate pH 4.0. **A**) (–) 10-His BACE1. (–) 10-His BACE1 with inhibitor IV, (–) 10-His BACE1 with UF PMH. **B**) (–) Fc-BACE1. (–) Fc-BACE1 with inhibitor IV, (–) Fc-BACE1 with UF PMH.

Fc-tagged BACE1 has a Tm of 44.24 °C, which does not change with the addition of ligand inhibitor IV (Figure 19B). However, the addition of UF PMH causes the Tm of Fc-BACE1 to drop to 35.35 °C. This 8.9 °C temperature reduction is the largest seen in the four types of BACE1 tested, suggesting an interaction caused by the Fc region, Fc specifically bound to BACE1 or a combination of these.

3.3 Discussion

The far-UV spectra of native BACE1 is most similar to that of FLAG-tagged BACE1. The peak positioned at λ = 221 nm in native BACE1 shifts by λ = 1 nm with the addition of UF PMH, and the trough by λ = 2 nm. Of the three purification tagged BACE1 proteins, FLAG-BACE1 has more similar spectra to native, with no change occurring at the trough and a λ = 2 nm change at the peak. Analysis of the secondary structural characteristics of the CD spectra for both types of BACE1 enzyme shows similar structural changes with the addition of UF PMH. Heparin causes the reduction in antiparallel β-sheets by 4% in both protein types, and a similar increase of turn regions. The level of unordered or indefinable disordered protein regions increases in both native and FLAG-tagged BACE1 types.

Cimmperman *et al*. (2008) demonstrates ligand binding to most protein causes an increase in thermal stability (Tm) when detected by thermal calorimetry (Cimmperman et al., 2008). This increase in Tm is due to ligand-binding stabilising the protein structure (*idem*). One of the main methods of drug candidate screening is thermal shift assay (ThermoFluor) which enables high throughput screening of candidate libraries (Pantoliano et al., 2001). This method identifies high affinity stabilising ligands, which increase the Tm of the target protein, as most ligands stabilise protein when bound (*idem*).

Ligand binding causes protein unfolding or binds preferentially to the unfolded state of a protein and causing a reduction in thermal stability (Tm) (Cimmperman et al., 2008). Ligand binding was revealed to contribute to the destabilisation of target protein (*idem*). Heparin binding to native BACE1 demonstrated a large Tm shift to lower temperatures, suggesting either heparin bound the unfolded protein preferentially,

causing a destabilisation or heparin bound to the unfolded state, halting normal protein folding equlibria. Hayley *et al.* (2009) demonstrated BACE1 in the inactive form at pH 7.4 was structurally more stable than the active form at pH 4.8 (Hayley, Perspicace, Schulthess, & Seelig, 2009). BACE1 is less-stable at low pH, signifying structural equilibrium of the protein is shifted toward the unfolded state at this pH (Robertson & Murphy, 1997). Therefore, this interaction could be described by heparin binding preferentially to BACE1 in an more unfolded state, causing destabilisation and a reduction in Tm.

GAG interactions with other proteases, such as the cathepsin family, have been shown to occur through destabilisation of the pro-domain, but in these cases the destabilisation causes a stimulation of enzyme activity (Caglic, Pungercar, Pejler, Turk, & Turk, 2007). Beckman *et al.* (2006) also demonstrated a heparin-binding site in the pro-domain of BACE1 (Beckman et al., 2006) with the same group investigating the GAG structural requirements for this interaction (Klaver et al., 2010). However, this group found heparin has stimulating effect on BACE1 at low concentrations (1 μg/ml), with inhibition occurring only at the high concentrations tested (100 μg/ml). Scholefield *et al.* (2003) and Patey *et al*. (2006) only identify heparin/ HS and modified heparin as inhibitors of BACE1 (Patey et al., 2006; Scholefield et al., 2003).

DSF demonstrates a similar melting temperature for the native and FLAG-tagged BACE1 proteins. The addition of UF PMH causes a large shift in Tm to a lower Tm of 38.78 °C in native BACE1 and 39.95 °C in FLAG-BACE1. The action of the hydroxyethylene containing inhibitor IV is also similar with both proteins, with Tm of ≈ 46 °C in both FLAG-tagged and native BACE1. This suggests the small size of the FLAG tag, being 8 amino acids in length and hydrophilic in nature, does not alter the structure of BACE1 sufficiently, or display an interaction with the UF PMH added, to cause a

change in both secondary structure and resulting melting temperature. The similarity between native BACE1 melt curves, with and without the added ligands suggests the FLAG-BACE1 can be used as a more economical native BACE1 proxy, when conducting studies including heparin and heparin derivatives. Therefore, in the activity studies required to detect new glycosaminoglycan-like inhibitors of BACE1, FLAG-tagged BACE1 will be used for the large library screening required to identify hit inhibitor compounds in Chapter 8.

The 10-His tagged BACE1 displays a resistance to the destabilising effect of UF PMH in these thermal stability experiments. A change is seen in the far-UV CD spectra of 10-His BACE1 when challenged with UF PMH, suggesting heparin binding still occurs causing a secondary structural change to the protein conformation. This may suggest the inclusion of this type of positively charged tag affords the protein resistance to the destabilisation caused by heparin binding to the unfolded state at pH 4.0. This could be caused by the interaction with the positively charged 10-His tag and negatively charged heparin, rather than the BACE1-heparin interaction, seen with other types of BACE1. Beckman *et al.* (2006) showed the BACE1 stimulation activity of heparin did not occur due to the presence of the 10-His tag on BACE1, and used this form for FRET activity assays (Beckman et al., 2006), but this does not conclude whether a structural or destabilisation event occurs with 10-His tag.

Fc-BACE1 demonstrated the greatest change in thermal destabilisation and in secondary structure with the addition of UF PMH. Uniewicz *et al.* (2014) used IgG Fc as a scaffold to dimerise the membrane protein neuropilin-1, to characterise the heparin binding interactions of this protein (Uniewicz et al., 2014). Heparin binding regions of the IgG Fc region of the recombinant protein were seen, however, the optical biosensor and DSF experimentation did not highlight any heparin interaction between the IgG Fc

and heparin in pH 7.4 PBS (*idem*). The weak heparin binding was thought to be due to the neuropilin-1 acting as a scaffold to form weak heparin binding sites on IgG Fc and the other b1-b2 domain outside of the neuropilin-1 moiety (*idem*). West *et al.* (2005) also worked with an Fc-fusion neuropilin-1 and determined no binding was observed between IgG Fc and heparin in a resonant mirror biosensor (IAsys) experiment (West et al., 2005). However, the DSF data shown here demonstrates a thermal destabilisation event stronger in Fc-BACE1 than in native BACE1, suggesting some aspect of the fusion protein causes a greater reduction in the Tm. The far-UV CD spectrum of Fc-BACE1 shows an increase in antiparallel β-sheets and a reduction in 'other' non-specific regions as identified in BeStSel CD analysis software.

Investigation into the role of the Fc part of this fusion BACE1 protein will be made in the next chapter to determine if heparin has a direct effect on the IgG Fc region in the conditions required for BACE1 enzyme activity analysis (Chapter 4). Later, the specific structural requirements for the heparin/HS interaction with native BACE1 will be identified (Chapter 7) and the activity of PMH and BLH will be demonstrated, to accept or refute the action of heparin as an inhibitor or stimulator of BACE1 activity at different concentrations, using FLAG-BACE1 (Chapter 8).

Chapter 4: Investigations into the interaction between IgG Fc and glycosaminoglycans

4.1 Introduction

4.1.1 Humoral immunity and the antibody

The mammalian immune system can be broadly characterised into 2 pathways, encompassing the initial response to pathogens through innate immunity, and the more specific and enduring, adaptive immunity. Innate immunity utilises phagocytes, examples of which are neutrophils and macrophages, to remove pathogens, alongside soluble molecules with pattern recognition capabilities, e.g INF and complement. Antigen stimulated B-lymphocytes proliferate and differentiate into plasma cells and memory cells. Antibodies produced by plasma cells mediate adaptive immunity, also known as humoral immunity, with memory cells retained ready for future immune events. Each antibody is highly specific for an antigen, with antibodies produced for each possible antigen encountered throughout the lifetime of an individual. The number of specific antibodies is thought to reach 10^9 (limited by B-lymphocyte number); this library of immunoglobulins produced is generally refered to as the antibody repertoire (Parham, 2015). Each B-lymphocyte displays a specific membrane bound antibody, upon clonal selection with the corresponding antigen, the B-cell proliferates and differentiates into antibody producing plasma cells and memory cells (Nossal & Lederberg, 1958). The antibody is commonly presented to by helper T_{FH} lymphocytes in the lymph nodes or spleen (*idem*).

4.1.2 Antibody structure

The antibody molecule is composed of four polypeptide chains; two identical heavy chains (H) of approximately 55 kDa (≈ 450 residues) or more and two identical light chains (L) of approximately 22 kDa (≈ 220 residues) (Ionescu, Vlasak, Price, &

Kirchmeier, 2008). These chains fold into domains of ≈ 110 residues each forming a distinct β-sheet fold known as the immunoglobulin domain (Ig domain) with light chains being bound to heavy chains through salt bridges, hydrogen bonding, and hydrophobic interactions (Brown, Newcomb, & Ishizaka, 1970). Heavy chains are bound through disulphide bonding, creating a 'dimer of dimers' (*idem*). Each antibody domain structure comprising of seven to nine anti-parallel β-strands in a pleated sheet structure, that form an overall β-sandwich structure (Bork, Holm, & Sander, 1994). The tertiary structure of the antibody is generated from the β-sheet forming globular domains. The heavy and light chain globular regions interact at the tertiary level, which allows both simultaneous antigen binding and effector function.

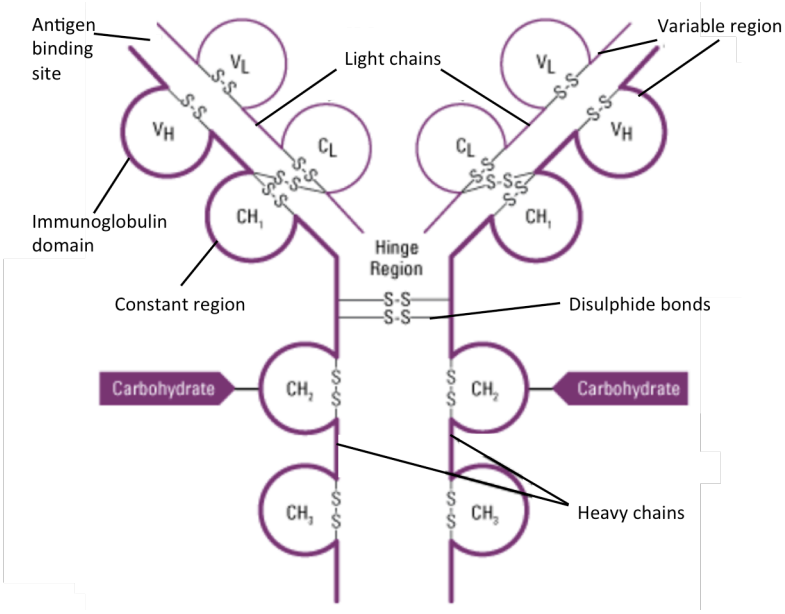

Figure 20: Schematic of an IgG antibody, with the V_H/V_L and the CH1/CL regions cleaved removing the hinge region constitutes the Fab. V_H/V_L and the CH1/CL regions cleaved including the hinge region constitutes the F(ab')2. CH2 and CH3 region cleaved including the hinge region constitutes the Fc. Figure modified from (Goldsby.R.A, 2000).

The initial 110 amino acid residues at the N-terminal of both the heavy and light chains contribute to the variable (V) region of the antibody (V_L and V_H) (Figure 20). This variable region functions as the antigen recognition and binding site and is known as the complementarity-determining region (CDR) (Ionescu et al., 2008). The second region

forms the last Ig domain of the Fab region, with the first constant (C) domain of the light chain (CL) and the first constant domain of the heavy chain (CH1) (*idem*). Light chains in humans exist in 2 forms, κ and λ, with ≈ 60% of light chains being κ, whereas in mice ≈ 95% of the chains are κ (Parham, 2015). Each antibody contains soley κ or λ light chain (*idem*). Subtypes of λ, characterised by subtle changes in sequence are subdivided into λ1, λ2, λ3 and λ4 (*idem*).

Upon papain digestion the antibody molecule is cleaved at the hinge region to yield the fragment antigen binding (Fab) region (45 kDa) and fragment crystalizable (Fc) region (50 kDa) (Parham, 2015). In humans, the Fc region is formed by a dimer of identical constant regions CH2 and CH3. ϒ, δ, α heavy chains contain different amino acid sequences forming CH2 and CH3, with an additional heavy chain region, CH4, in μ and ε heavy chains (*idem*). The type of heavy chain present denotes antibody isotype; IgD contains δ, IgA contains α, IgG contains ϒ, IgM contains μ, and IgE contains ε heavy chains (*idem*). There are 2 subtypes of IgA α1 and α2 (IgA1 and IgA2), four subtypes of ϒ1, ϒ2, ϒ3 and ϒ4 (IgG1, IgG2, IgG3 and IgG4) (*idem*).

The CH2 contains a N-linked glycan at an asparagine residue. This N-glycan is predominantly a diantennary complex-type N-glycan, comprised of a α-1,6-fucose, 0- to 2- galactose residues, 1 or 2 α-2,6-sialic acids with small amounts of branching GlcNAc (Stadlmann, Pabst, Kolarich, Kunert, & Altmann, 2008). Recombinantly produced antibodies yield simpler N-glycan structures, often omitting fucosylated residues and branching GlcNAc (*idem*). Human glycosylation patterns require a group of complex enzymes not present in cells such as murine cell lines NS0 and Sp2/0, utilised in recombinant anibody production (Hossler, Khattak, & Li, 2009). The position of the N-glycan leads to a distended globular structure at the CH2 regions, which allows access for complement and other antibody binding molecules (Stadlmann et al., 2008).

Digestion with pepsin liberates an alternate active fragment, F(ab')2, with the remaining fragment digested to smaller peptides (Parham, 2015).

4.1.3 The role of Fc in complement activation

The complement system is an enzyme cascade of plasma proteins that causes opsonisation of pathogens and inflammation (Janeway C.A 2001). A small number of activated complement enzymes proteolytically cleave the zymogen targets, which themselves become active complement enzymes (with a different zymogen target), in a cascade arrangement (*idem*). Each enzyme activation amplifies the original activation, rapidly triggering a large-scale immune response (*idem*). There are three mechanisms by which complement can be activated: the classical pathway, mannan-binding lectin pathway, and the alternative pathway (*idem*).

The classical pathway of complement can be activated through the direct binding of protein complex C1q, to a bacterial surface, or through more specific forms of immunoglobulin binding (Karsten & Kohl, 2012). The initial immune effector molecules, IgM, along with IgG3, are highly effective at activating the major innate mechanism for effector cell recruitment (*idem*). Activation of the complement cascade occurs through the binding of globular heads of C1q to the antigen activated IgM pentamer, at the CH2 domain of the Fc regions of each antibody (Duncan & Winter, 1988). C1q binds to the CH2 residues at Glu318, Lys320 and Lys322, with these residues highly conserved in IgG subclasses (Duncan & Winter, 1988). The relative potency of C1q activation by the IgG subclasses is thought to be due to the differing hinge region lengths between Fc and Fab regions. IgG1 and IgG3, the most potent of IgG complement activators, have longer hinge regions allowing greater Fab/Fc region flexibility and therefore accessibility for C1q globular heads (Karsten & Kohl, 2012). However, a modified IgG3 with the shorter and

more rigid hinge region of IgG4 displays high potency in complement activation (Norderhaug et al., 1991) and modified IgG4 with the longer more flexible hinge region from IgG3 possesses no detectable activation of complement (Tan, Shopes, Oi, & Morrison, 1990) (Karsten & Kohl, 2012). Reduction of the disulphide bridge between the Fc region dimer also negated complement activation (Schur & Christian, 1964).

Variation of the amino acid sequence of CH2 domain in IgG4 to an IgG1 CH2 domain created a mutant nearly as functional as IgG1 (Greenwood, Clark, & Waldmann, 1993). Other amino acid modifications have been assessed for contributions to the subclass variation displayed, the study by Tao *et al.* 1993 suggests other residues than positions 318, 320 and 322 can modify the potency of complement response to IgG (Tao, Smith, & Morrison, 1993). Furthermore, a functional and dimerised CH3 domain of IgG is required for optimal complement activation, irrespective of the non-binding nature of this immunoglobulin region (Utsumi, Okada, Udaka, & Amano, 1985). These varied amino acid sequence modifications suggest neither the orientation of CH domains nor the functional orientation of the C1q binding site alone are the sole reason for the variation in subclass complement potency (Karsten & Kohl, 2012).

Residues on the corresponding heavy chain region in IgM, CH3, that are required for C1q binding are Asp432, Pro434, Pro436, Asp356 and Asp417 (Arya et al., 1994), which demonstrates that the binding site for C1q is not identical in IgG and IgM (Karsten & Kohl, 2012). Karsten and Köhl (2012) state that several features in the C1q binding regions of IgG and IgM promote the successful activation of complement through the common pathway (*idem*), suggesting the modification to the Fc structure, through disulphide reduction, hinge region modification or CH residue changes will alter the ability of the immunoglobulin to activate complement effectively.

C1q binding has 10,000-fold lower affinity to monomeric IgG than the binding of immune complexed IgG (Burton & Woof, 1992). Upon activation, a conformational change in the C1q bound C1r2:C1s2 proenzyme complex causes autolysis of C1r; this continues the further downstream activations (Karsten & Kohl, 2012). Ultimately, the coating of the pathogen with C3b stimulates either neutrophil or macrophage phagocytosis through the CR1 receptor, or further complement progress to membrane attack complex formation and cell membrane rupture (Parham, 2015). The activation of complement in this manner is an example of adaptive immunity lending specificity, with innate immunity contributing strength to the host response to an invading pathogen (*idem*).

4.1.4 Fc receptors

The Fc receptors are a group of surface membrane molecules that recognise homologous or heterologous immunoglobulin through the Fc region, mediating biological function (Unkeless, Scigliano, & Freedman, 1988). Fc receptors (FcR) are involved in a wide range of critical activities, including receptor mediated endocytosis of antigen:antibody complexes, antibody dependent cell-mediated cytotoxicity and ligand-triggered transmission across plasma membranes (Ravetch & Kinet, 1991). Fc receptors are found on the surface of immune cells e.g macrophages and neutrophils (Dickler, 1976), on cells e.g hepatocytes and brain parenchyma (Nyland & Nilsen, 1982), and in cells that do not express FcR e.g fibroblasts post viral infection (Para, Baucke, & Spear, 1980). The wide variety of cellular responses caused by antibody/immune complex binding can be attributed to FcR structural heterogeneity (Ravetch & Kinet, 1991). The Fc region binding domains of these FcR have minimal structural heterogeneity, but

differ in the transmembrane and intracellular domain structures, eliciting a variety of distinct cellular responses.

FcR mediated endocytosis of antibody or antibody complex occurs through pinocytosis of soluble complexes or phagocytosis of larger particles by natural killer (NK) cells and macrophages (Ravetch & Kinet, 1991). IgG1 and IgG3 opsonized antigen complexes are phagocytosed by macrophages through interaction with the high affinity FcγRI (CD64) on the cell surface, which deliver the complexes to endosome and ultimately lysosomal compartments (Ravetch & Kinet, 1991). This IgG:FcγRI binding occurs at the lower hinge region of CH2 in the Fc region of IgG (Parham, 2015). FcγRI:IgG binding is unique among the FcR as it can occur in the absence of antigen; macrophages, dendritic cells and neutrophils utilise this receptor binding to trap antigenic molecules acting as antigen presenting cells (*idem*). Two lower affinity FcγR, FcγRII (CD32) and FcγRIII (CD16) contain two Ig-like domains, rather than three in FcγRI (*idem*). These lower affinity receptors require multiple cross-linked IgG binding to antigen prior to activation. This enables the more specific antibody response to antigen, which triggers opsonization, and stops non-specific IgG blocking (*idem*).

FcγRIII is the only receptor present on the cell surface of NK cells and is utilised in the detection of IgG1 and IgG3 antibodies specific for cell surface antigens. FcγRIII:IgG binding on NK cells triggers antibody dependant cell-mediated cytotoxicity through the release of lytic granuals from the NK cell, causing apoptosis of the IgG-opsonized cell (*idem*).

IgE is found bound to FcεRI on mast cells, basophils and activated eosinophils. Upon binding to the antigen, the IgE:FcεRI complex activates a transmembrane signalling event to release the contents of inflammatory granules, which include

histamine, cytokines, proteolytic enzymes, and reactive oxygen species, to defend parasite invasion.

The IgG receptor FcRn is thought to be involved with maintaining the high concentration of IgG in extracellular space through the high affinity binding of two FcRn on the surface of epithelial cells to one IgG molecule in the serum, transcytosis releases the IgG on the basolateral cell surface, increasing IgG concentration. FcRn acts to protect circulating IgG from normal plasma protein degradation, explaining the increased half-life of this antibody isotype (Pyzik, Rath, Lencer, Baker, & Blumberg, 2015). FcRn are involved in transport of maternal IgG through the human placental membranes, providing neonatal immunity, prior to birth.

Fifteen highly conserved residues are involved in the binding of IgG subtypes and FcRn at the CH2-CH3 IgG domain interface; Ile253 and His310 being key residues (J. K. Kim, Tsen, Ghetie, & Ward, 1994; Medesan, Radu, Kim, Ghetie, & Ward, 1996). Utilising human-mouse chimeric IgGs, regions distal to the CH2-CH3 domain interface have been identified as required for the binding to FcRn (Zuckier, Chang, Scharff, & Morrison, 1998). CH domain shuffling between IgG subtypes found the IgG:FcRn coupling could be effected by residues other than the required fifteen identified, with these modifications occurring in proximal β-strand regions, but distal in the amino acid sequence (Ghetie & Ward, 2000). The removal of the Fc hinge region results in a shorter serum half-life through the inability to bind protective FcRn (J. K. Kim, Tsen, Ghetie, & Ward, 1995). The FcRn does not interact directly with the Fc hinge region, rather the hinge acts to orientate the CH2-CH3 domain interface for optimal FcRn binding (J. K. Kim et al., 1995). FcR binding is highly conformationally dependent, as seen with classical complement activation through IgG and IgM interactions with C1q (Ghetie & Ward, 2000).

Transcytosis of IgG across membranes using FcRn requires a net pH difference between the luminal (pH 6.0 – 6.5) and basolateral epithelial surfaces (pH 7.4) (Raghavan, Bonagura, Morrison, & Bjorkman, 1995). IgG binds FcRn in acidic environments, is transported as a complex in acidic clathrin-coated pits, and dissociates upon encountering pH 7.4 (Rodewald & Kraehenbuhl, 1984). The FcRn:IgG affinity is reduced by two orders of magnitude across from luminal to basolateral surfaces, triggering dissociation of the complex (Raghavan et al., 1995). The pH dependence of this interaction is caused by the imidazole side chains of histidine residues (His310 and His 433) present in the CH2-CH3 domain interface of Fc being deprotonated over the pH 6.0 to pH 7.0 range (*idem*). Two histidine residues (His250 and His251), present within the FcRn heavy chain, also become deprotonated over this pH range, adding to the dissociative effect (*idem*).

4.1.5 The effect of temperature on IgG Fc stability

With a pI of 7.2, the human IgG1 Fc region has a net positive charge at lower pH (< 7.2) (Zhang-van Enk et al., 2013). The Linderstrom-Lang model of thermal stability of proteins suggests the maximal stability and therefore Tm will be highest at the isoelectric point (pI) of a protein. The Tm of IgG Fc being higher at pH 7.2 than the Tm at pH 4.8 evidences this (Zhang-van Enk et al., 2013). Buffer constituents for example pH, salt and ion concentration are also important for the stability of the Fc region (Tischenko, Abramov, & Zav'yalov, 1998). The CH2 region of the Fc fragment has a lower melting temperature than the CH3 region, suggesting that it may unfold first during thermal denaturation (*idem*); denaturation was shown to be irreversible after the CH3 domain unfolded (Zhang-van Enk et al., 2013)

Tischenko et al. (1998) demonstrated the Fc region from rabbit IgG has four cooperative transitions upon thermal denaturation, with the most stable being the CH3 interaction at the C-terminal, when tested between pH 2.5 and 5.5 in MES and glycine buffers (Tischenko et al., 1998). This thermal denaturation represents two unequal stages that cannot be characterised by melting of the homodimer (*idem*). Tischenko *et al*. (1998) postulated this unequal thermal denaturation might be due to the CH3 domain containing two non-identical subdomains, which are bound to the opposite domain in the diamer in a non-symmetric manner (*idem*).

The melting temperature of CH2 is lower than that of CH3, but follows the same pattern of unequal stage thermal denaturation, which is attributed to the presence of sub-domain structure within the CH2 domain; binding in the dimer with the opposite subdomain creating a heterodimer of sorts (Tischenko et al., 1998). This two transition melting is seen in thermal denaturation data between pH 4.2 and 8.0 (10mM glycine, 10mM acetate and 10mM phosphate buffers) (Tischenko et al., 1998). CH2 domains are glycosylated at Asp297 with the N-glycans held between the heavy chain regions, thereby blocking the binding between these domains, a distinction from the other domains (Janeway C.A 2001). This reduced association explains the CH2 domain structure decrease in thermal stability. At pH 8, the more stable CH3 domain lends stability to the CH2 domain through *cis* interactions (reducing CH3 Δ G) (*idem*). At pH 3.8, dimerisation of the CH3 domains have been shown to strongly stabilize the dimer but CH2 domains no longer gain stability from the CH3 domain (*idem*). While structural changes of the F(ab) region are most sensitive to heat treatment, the structure of the Fc region is most sensitive to the lowering of pH (Vermeer & Norde, 2000).

4.1.6 The effect of anions on the stability of the IgG Fc region

Zhang-van Enk *et al.* (2013) investigated the effects of Hofmeister anions on the thermal degredation of human IgG1 Fc region (Zhang-van Enk et al., 2013). The Hofmeister series is commonly used to predict the stabilising effect of a buffer salt at high concentrations (*idem*). Hofmeister anions can confer stability, improve solubility, and can reduce denaturation of proteins (*idem*). Low concentrations of a given salt can have stabilising or destabilizing effects according to the specific protein (*idem*). Low concentrations of counterions bind the surface of proteins causing neutralization in net charge, reducing the repulsive electrostatic effects and therefore promoting destabilisation and/or aggregation (*idem*). Hofmeister anions can confer a stabilising effect through the organisation of water molecules; this reduces the fluidity of the solution and improves protein stability (Zhao, 2016).

4.1.7 Low molecular weight heparins

Low molecular weight heparins are defined as heparins between 1000 and 10,000 Da in size and are a class of anti-coagulants that have a more specific activity in the coagulation cascade than that of UF PMH. Five types of LMWH are employed in this work to act as LMW proxies of heparin. Dalteparin (Fragmin) is prepared by nitrous acid depolymerisation of UF PMH, followed by a reduction to form an anhydromannitol ring at the reducing end (Bisio et al., 2017), with a mean molecular weight of 4-6 kDa. Tinzaparin (Innohep) is prepared through enzymatic depolymerisation of UF PMH yielding an average molecular weight of 5.5 to 7.5 kDa. Enoxaparin (Lovenox/Clexane) is produced through β-elimination of the benzyl ester of UF PMH with a mean molecular weight of 4 - 4.5 kDa. Reviparin (Clivarine) is produced by nitrous acid digestion of UFPMH with an average molecular weight of 3.9 kDa. Fondaparinux (arixtra) is a

synthetic pentasaccharide representing the binding region required for factor Xa inhibition, with no binding region for interaction with thrombin. The reduction of the 18-saccharide binding region negates the possibility of heparin-induced thrombocytopenia. The molecular weight is 1,727 Da.

4.1.8 Method information

Three biochemical assays were utilised to investigate the interaction between IgG Fc region and GAGs e.g heparin. These were differential scanning fluorimetry and far-UV circular dichroism used in the previous chapter and heparin affinity HPLC.

4.1.8.1 Heparin affinity HPLC

Heparin affinity HPLC utilises heparin covalently attached to a beaded agarose matrix produced by the N-hydroxysuccinamide coupling of beaded agarose media to N-unsubstituted glucosamines of heparin (Iverius, 1971). The N-hydroxysuccinamide containing cross-linking agent includes a spacer (i.e five carbon or eight carbon) on which N-unsubstituted amine groups of heparin attach under mildly basic conditions (Hage.D.S, 2005). HiTrap heparin HPLC is deployed commonly for the purification of heparin binding proteins (e.g. coagulation factors and lipoproteins), with elution usually performed with a linear or stepwise NaCl gradient. In these experiments, the human IgG Fc region is eluted with a linear 0 - 2 M NaCl gradient. The two buffer systems employed in this study were sodium acetate buffer and PBS (containing 137 mM NaCl).

4.1.9 Experimental aims

Building on the stability experiments of biochemically tagged BACE1 in Chapter 3, the immunoglobulin fragment, Fc region, has been investigated for interactions with heparin and chemically modified heparins. This work was conducted to further

understand the relative stability changes seen in DSF with BACE-1 Fc fusion protein. Detailed DSF experiments using a chemically modified heparin library and size fractionated heparin have been employed to inform the structural requirements for the interactions observed with IgG Fc.

BACE-1 experiments have been conducted at an acidic pH, as the aspartyl-protease demonstrates highest activity in subcellular compartments of the Golgi, trans-Golgi network and the endosomes, which maintain an acidic enviroment. Destabilisation effects were seen in the BACE-1-Fc thermal stability assays when challenged with heparin in a concentration dependant manner. However, this action could not be attributed to the interaction between BACE-1 and the GAG, as the positively charged Fc tag at pH 4 could also be binding the negatively charged GAG molecules.

Initial investigations have been conducted to determine the Fc-heparin binding affinity and whether the counterion and salt concentration present in the chosen buffer solution affected the nature of the Fc-heparin interaction.

Next, titrations of heparin, chemically modified heparin derivatives, and size defined heparin fragments (d.p.2 – d.p.20) were employed to elucidate specific structural requirements and minimum size requirements for any Fc-heparin interaction.

Finally, a library of defined cation forms of heparin was used with DSF to identify differences between thermal stability of IgG Fc with distinct cation forms of heparin.

4.2 Results

Investigation into the action of heparin with the Fc-fusion protein, BACE1-Fc, exhibited different structural stability results when compared to native BACE1 alone and in the presence of BACE1 inhibitor OM99-2 in solution (Figure 21). The melting point (Tm) of BACE1-Fc and BACE1-Fc with 1 mM OM99-2 in 50 mM sodium acetate buffer pH 4.5 was 45°C, while addition of 50 mM PMH to BACE1-Fc in the same buffer reduced the Tm to 36°C (Figure 21). This nine degree reduction in Tm of BACE1-Fc in this buffer system could be caused by PMH binding impacting the stability of the enzyme or binding to the Fc tag, alongside BACE1 binding, modifying the thermal denaturation rate of the enzyme. In order to understand the difference between these two protein stabilities, examination of the ineraction between heparin and human IgG Fc fragment was undertaken to aid understanding of this effect. Fc-fusion proteins are used commonly to aid purification and to promote native dimerization and stabilisation.

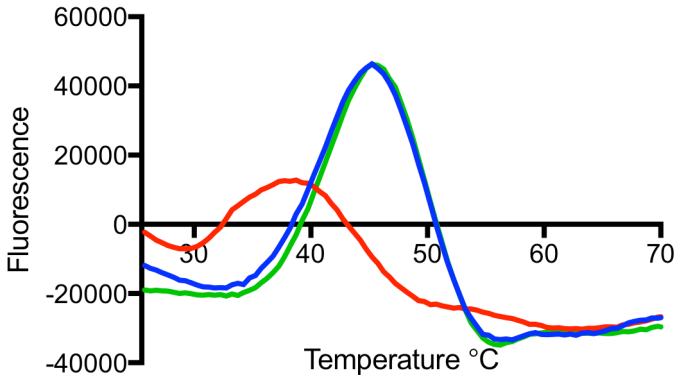

Figure 21: DSF melt curve (1st derivative) of Native BACE1 ± UF PMH and inhibitor IV (–) Native BACE1, (–) native BACE1 with inhibitor IV, and (–) native BACE1 with UF PMH, in 50 mM sodium acetate pH 4.0.

The following investigations into the effect of PMH on the protein tag IgG Fc were completed to determine whether PMH binds human IgG Fc region and causes the lower Tm exhibited during the thermal denaturation of BACE1-Fc fusion protein.

4.2.1 Human IgG Fc region binds to heparin in acidic conditions

Heparin HiTrap High Performance Liquid Chromatography (HPLC) is commonly utilised to purify heparin-binding proteins from solution, including lipoproteins, coagulation factors and protein synthesis factors. Heparin sepharose HiTrap HPLC has also been utilised in the identification and elucidation of binding affinity in previously unknown heparin binding proteins.

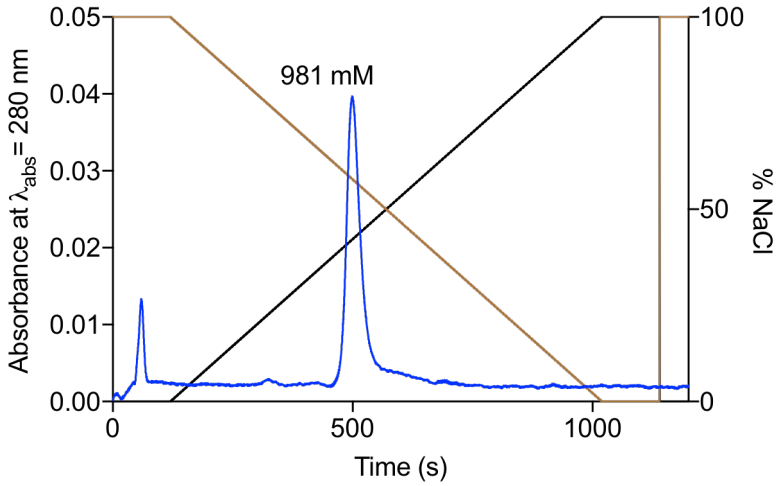

Figure 22: Heparin Hi-Trap affinity HPLC of Human IgG Fc region, in 50 mM sodium acetate at pH 4.0 with a linear gradient of 2 M NaCl.

Human IgG Fc region (purified polyclonal IgG from human plasma) was utilised in heparin HiTrap HPLC to determine if this heavy chain antibody fragment bound to heparin-sepharose under the same buffer conditions as BACE1 proteolytic cleavage of APP is measured. Heparin HiTrap HPLC (over 24 minutes with elution with a linear gradient of 2M NaCl) demonstrates IgG Fc binding to heparin sepharose matrix with an affinity of 981 mM NaCl, in the presence of 50 mM sodium acetate at pH 4.0 (Figure 22). Acetate ions absorb strongly at the prefered absorbance wavelength for peptide bonds of λ_{abs} = 215 nm. The absorbance therefore was read at λ_{abs} = 280 nm to detect the aromatic rings of amino acids such as Phe, Tyr and Trp. The antibody fragment

preservative, sodium azide, was also accounted for in the blank runs and did not bind to the column; this ensured the remaining peaks were Fc fragment only (data not shown).

To determine if the binding of human IgG Fc region was dependent on the presence of BACE1 buffer sodium acetate, the heparin HiTrap HPLC was run in phosphate buffered saline (PBS) at a range of pHs, to determine a relationship between buffer constituents and pH. HPLC absorbance was detected at λ_{abs} = 215 nm to recognise the peptide bond.

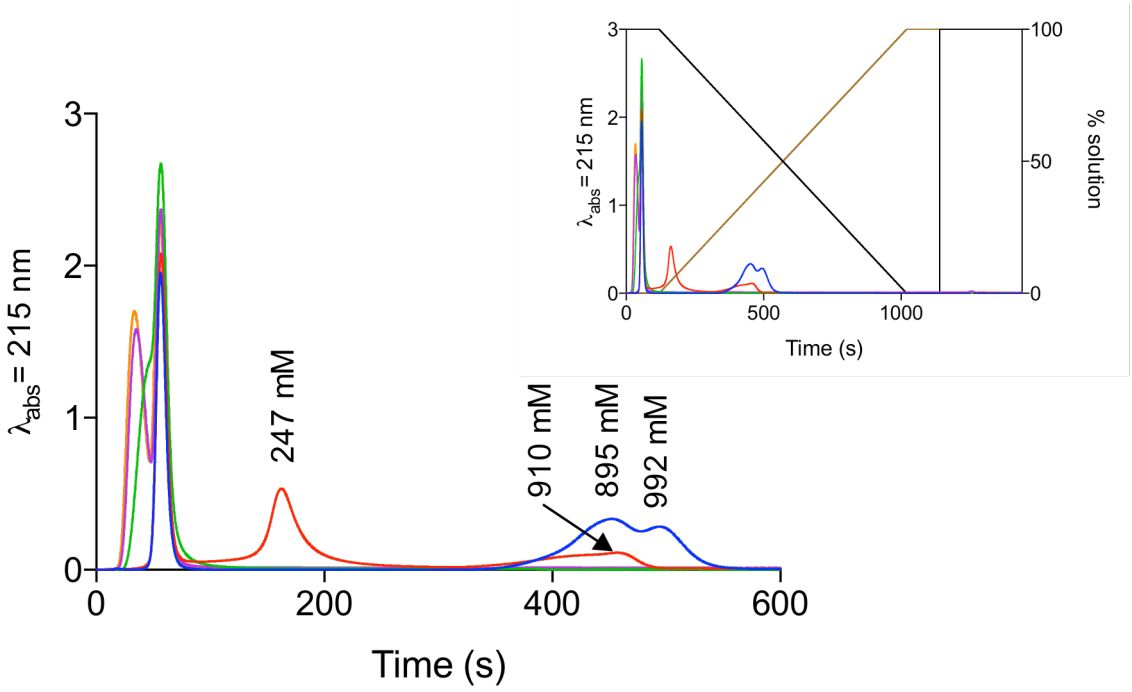

Figure 23: Human IgG Fc region in heparin HiTrap affinity HPLC. PBS buffer at differing pH and elution with 2M NaCl linear gradient. (–) PBS pH 4, (–) PBS pH 5.0, (–) PBS pH 6.0, (–) PBS pH 7.0, (–) PBS pH 7.4.

The dimer of heavy chain regions constructing the Fc fragment of human IgG1, made by cleavage with papain, was tested in heparin HiTrap HPLC in PBS at varying pHs with elution by a linear gradient of 2M NaCl (Figure 23). At each pH tested, a proportion of the protein did not bind the heparin column. At pH 4.0, the IgG Fc region bound to the column, released as a rounded double peak with 895 mM and 992 mM NaCl. Increasing

the pH to 5.0, shifts the Fc region elution to 247 mM NaCl, with a small hump at the greater concentration of 910 mM NaCl, as shown in Figure 23.

Another source of human IgG Fc region was obtained from Southern Biotech to corroborate the Fc-heparin binding interaction demonstrated in Figures 22 and 23. This purified human polyclonal IgG fragment was run in heparin HiTrap HPLC in PBS at a variety of pH, with elution by a linear gradient of 2 M NaCl. At pH 6 - 7.4, the protein did not bind the heparin column. At pH 4.0, the IgG Fc region bound to the column, released as a rounded double peak with 810 mM and 977 mM NaCl with a similar peak shape to the IgG Fc region from Bethyl Labs. Increasing the pH to 5.0 shifts Fc region elution to the lower affinity, 390 mM NaCl, with a small amount protein not binding to the column and eluting prior to the NaCl gradient, shown in Figure 24.

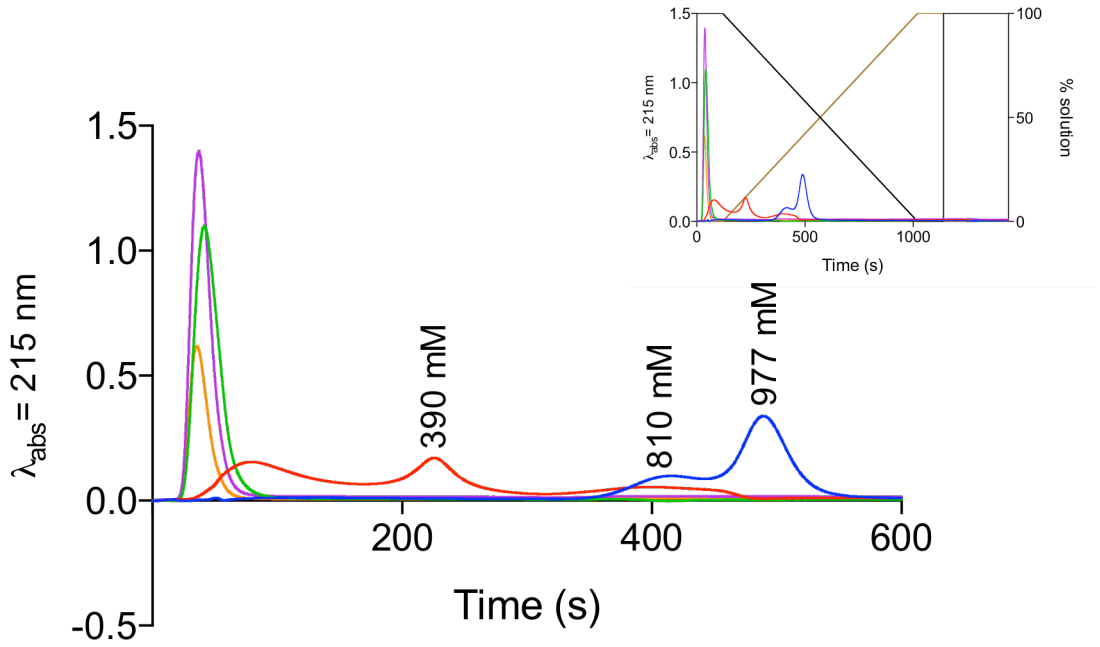

Figure 24: Human IgG Fc region in heparin HiTrap affinity HPLC in PBS buffer at differing pH and elution with linear gradient of 2M NaCl. (–) PBS pH 4, (–) PBS pH 5.0, (–) PBS pH 6.0, (–) PBS pH 7.0, (–) PBS pH 7.4.

Human IgG Fc region binds heparin sepharose in HiTrap HPLC in both 50 mM sodium acetate at pH 4.5 and in PBS more strongly at pH 4.0 than 5.0 but does not bind at pH > 5.0.

Investigations into the stability of the Fc region of human IgG led to the use of DSF as a method to determine the melting temperature (Tm) and changes in stability that can occur upon addition of a ligand.

Initially experiments were conducted in PBS with different pH levels. The average melting point (Tm) change of human IgG Fc with addition of 6.0 μM UF PMH was 1.5°C lower than the IgG Fc region alone. A greater change of Tm is seen in the secondary peak than the primary peak, but this secondary peak is not present at pH ≥ 7.0 (Figure 23). The two peaks may represent two stages of protein denaturation at the lower pH values tested, with the single peak in the pH 7.0 experiments having higher fluorescence intensity. This may suggest full IgG Fc region denaturation occurs at 65°C with no secondary stage of denaturation or secondary protein population, even with the addition of heparin.

When human IgG Fc region in pH 4.0 50 mM sodium acetate was assayed in DSF, the addition of heparin destabilised the protein, shifting the Tm of the Fc region from 45.54°C with a secondary peak at 70.70°C, to 34.66°C with a secondary peak at 66.67°C upon addition of 6.0 µM UF PMH. At a higher pH of 5.0, IgG Fc region has a Tm of 56.82°C, with a secondary peak at 81.72°C. With the addition of 6.0 µM UF PMH, the Tm is reduced to similar Tm as with pH 4.0 sodium acetate buffer (35.10°C and 68.48°C)(Figure 25). The binding of UF PMH occluding the exposed hydrophobic regions of the Fc region could cause this reduction in fluorescence of Sypro orange. UF PMH binding excess Sypro orange, reducing the amount of free dye available for protein binding could also explain this reduction.

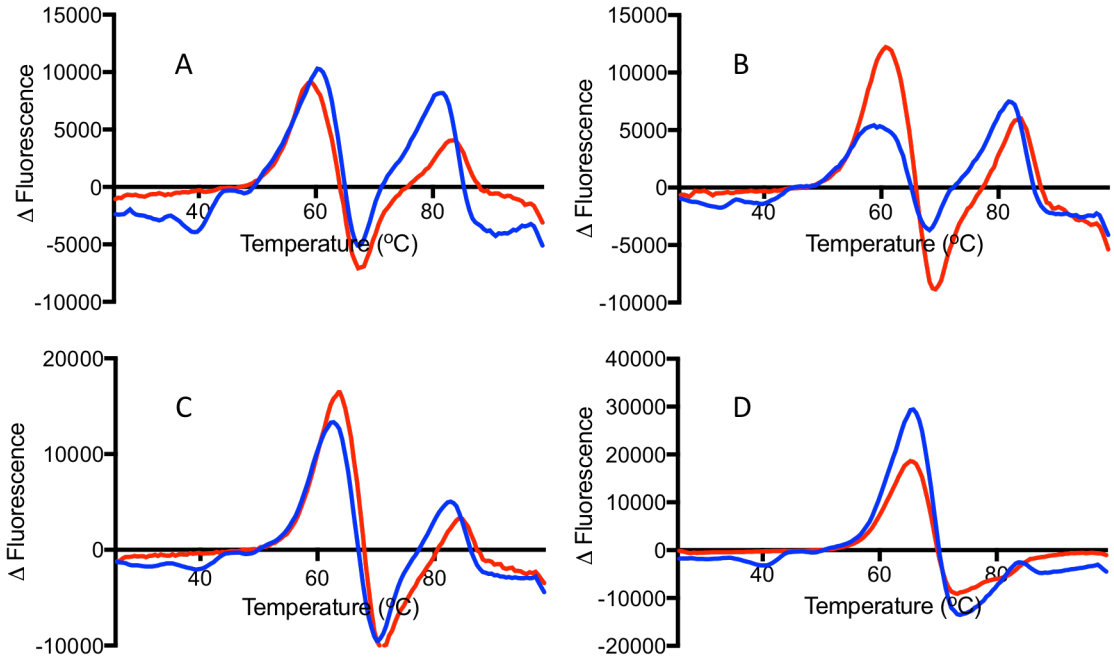

Figure 25: Differential scanning fluorimetry in PBS pH 4.0-7.0 with 3 µM human IgG Fc region. **A**= PBS pH 4.0, **B**= PBS pH 5.0 **C**= PBS pH 6.0 **D**= PBS pH 7.0. (–) IgG Fc region in PBS, (–) IgG Fc region with 3 µM UF PMH

An investigation into the stability of human IgG Fc in sodium acetate buffer was conducted at pH 4.0 and 5.0 to elucidate structural changes occurring at different pH values.

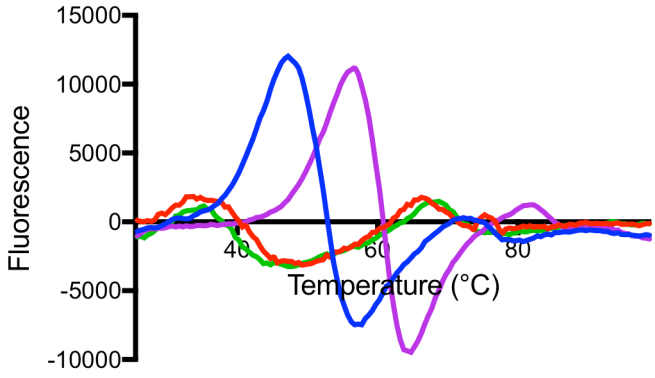

Figure 26: Differential scanning fluorimetry of human IgG Fc region 3 µM in 50 mM acetate buffer pH 4.0 and 5.0 ± UF PMH (–) 50 mM sodium acetate buffer pH 4.0 and (–) 50 mM sodium acetate buffer pH 5.0, (–) 50 mM sodium acetate buffer pH 4.0 with 6 µM UF PMH and (–) 50 mM sodium acetate buffer pH 5.0 with 6 µM UF PMH.

IgG Fc region is more stable at pH 5.0 in sodium acetate buffer (Figure 26), with this increase in stability echoed in PBS DSF experiments in Figure 25, displaying increasing protein stability with increasing pH up to a most stable conformation around pH 7. In 50 mM sodium acetate at pH 4.0, IgG Fc has a Tm of 47.30°C, which is increased to 56.56°C at pH 5.0. With the addition of 6 µM UF PMH these Tm are reduced to 34.12°C at pH 4.0 and 35.19°C at pH 5.0. The secondary peaks also show a reduction in Tm with the addition of UF PMH, going from 72.65°C (pH 4.0) and 81.44°C (pH 5.0) to lower temperatures of 66.10°C (pH 4.0) and 68.22°C (pH 5.0). The peak shapes and Tm are similar with the addition of UF PMH and do not show a pH variation as seen with IgG Fc region.

To determine whether the dramatic reduction in Tm of IgG Fc with the addition of heparin is caused by the denaturation of the protein prior to denaturation temperatures, circular dichrosim (CD) was used to identify protein structural changes with the addition of PMH in these buffers.

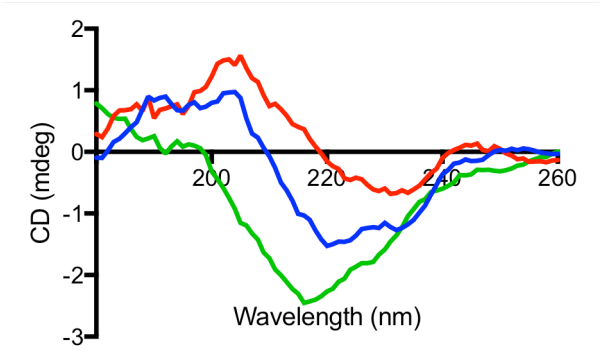

Figure 27: Far-UV circular dichroism spectra of human IgG Fc region ± UF PMH and IdoA-GlcNAc, calibrated with D-(+)-10-camphorsulfonic acid. Reaction buffer 50 mM sodium acetate pH 4.0. (–) 3 μM IgG Fc region, (–) 3 μM IgG Fc region with 30 μM UF PMH. (–) 3 μM IgG Fc region with 30 μM IdoA-GlcNAc

The CD spectra of IgG Fc in 50mM sodium acetate pH 4.0 smoothed and normalised to λ = 260 nm demonstrates a change upon addition of 30 μM UF PMH and IdoA-GlcNAc at the same molar concentration (Figure 27). Completely desulphated heparin was used to determine if the addition of disaccharide alone was required to stimulate a structural shift that indicated heparin binding, or whether the presence of a sulphate functional group was required.

The circular dichroism spectrum of human IgG Fc region in 50 mM sodium acetate buffer pH 4.0 has a structure representing a protein secondary structure rich in β-sheet structure, which is the main structural component of the immunoglobulin domain (Figure 27). The addition of UF PMH (30 μM) causes the spectra to shift from a peak at λ = 220 nm to λ = 230 nm. This may suggest a shift toward more random coil formation due to the progress of the peak back toward zero elipticity at these wavelengths. The addition of IdoA-GlcNAc heparin produces a peak at λ = 215 nm, a shift of λ = 5 nm in the opposite direction, with greater elipticity (Figure 27). IgG Fc region alone has a peak maxima at λ = 203 nm, which is present also with UF PMH but absent with IdoA-GlcNAc; at λ > 240 nm, all three spectra have similar characteristics.

Both the addition of UF PMH and IdoA-GlcNAc cause a structrural change in human IgG Fc in 50 mM sodium acetate buffer pH 4.0, but this structural change is distinct for both GAGs tested. There are no similar spectral changes seen in IgG Fc in the presence of UF PMH in the physiological buffer PBS as seen in Figure 28.

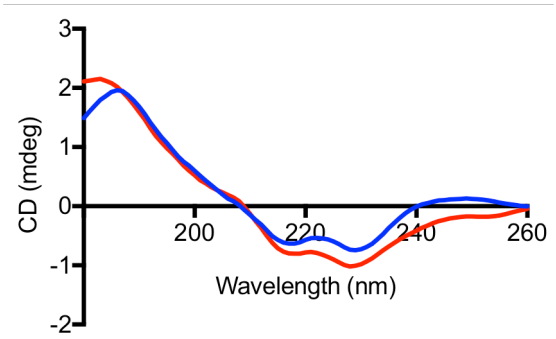

Figure 28: Far-UV circular dichroism spectra of IgG Fc region ± UF PMH in PBS, calibrated with D-(+)-10-camphorsulfonic acid. Reaction buffer PBS pH 7.4. (–) 3 µM IgG Fc region, (–) 3 µM IgG Fc region with 3 µM UF PMH.

To try to identify the structural requirements for heparin binding to IgG Fc region, a library of chemically distinct heparin chains were employed. The discrete structural characteristics of these compounds may elucidate specific functional group features required for the binding of heparin.

4.2.2 Structural requirements for the binding of heparin to the IgG Fc region

Human IgG Fc was screened in DSF with a library of chemically modified heparins, representing the most common structural features of HS/heparin. This library is constructed of heparin derivatives refered to as CMH 1-9 as shown in Figure 29 alongside the chemical structure of these glycopolymers.

The most common chemical modifications in heterogeneous UF PMH are CMH1 and CMH6. Nine chemically modified heparins, including a per-sulphated heparin CMH9, were used in DSF to probe structural requirements for the binding of heparin to the IgG

Fc region, with the structural modifications to the constituent disaccharides taken in to account when calculating the molecular weight of each heparin modification. The binding between heparin and protein is represented by a change in melting temperature. An investigation into the concentration dependency of this interaction using a concentration gradient of chemically modified heparin indicated the strength of heparin binding responsible for structural changes.

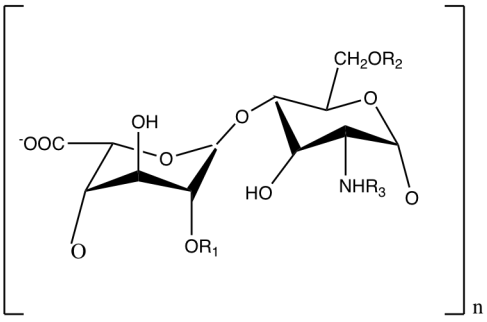

$R_1 = SO^{3-}/H, R_2 = SO^{3-}/H, R_3 = SO^{3-}/H/COCH^3$

Chemically modified heparin	Disaccharide unit	R1	R2	R3
1	IdoA(2S)-GlcNS(6S)	SO_3^-	SO_3^-	SO_3^-
2	IdoA(2S)-GlcNAc(6S)	SO_3^-	SO_3^-	$COCH_3$
3	IdoA-GlcNS(6S)	$COCH_3$	SO_3^-	SO_3^-
4	IdoA-GlcNAc(6S)	$COCH_3$	SO_3^-	$COCH_3$
5	IdoA(2S)-GlcNS	SO_3^-	$COCH_3$	SO_3^-
6	IdoA(2S)-GlcNAc	SO_3^-	$COCH_3$	$COCH_3$
7	IdoA-GlcNS	$COCH_3$	$COCH_3$	SO_3^-
8	IdoA-GlcNAc	$COCH_3$	$COCH_3$	$COCH_3$
9	IdoA(2S,3S)-GlcNS(3S,6S)	SO_3^-	SO_3^-	SO_3^-

Figure 29: Chemically modified heparin reference structures for CMH1 to CMH9 including a schematic for the heparin disaccharide.

The Fc region alone in DSF gives a peak Tm at 45.54°C, with a secondary peak at a higher temperature of 70.70°C (Figure 30A). The reduction in Tm from the major Fc region peak with 6.0 μM CMH1 included is 15.73°C (Figure 30A). At concentrations of 3.0 μM to 0.75 μM the curve follows the same structure as 6.0 μM with both curves shifted to lower temperatures compared to 6.0 μM. At 3.0 μM the intensity of the peak at 29.8°C is increased to 4000 ΔFU and at 0.75 μM the secondary peak shifts to a Tm of 60.53°C with an intensity of 600 ΔFU. At 0.38 μM the curve has a Tm of 33.51°C and

60.53°C. The concentration of CMH1 at 0.19 µM has a more intermediate shape with a shouldered initial peak with the main Tm of 46.8°C and a shoulder at a lower temperature mirroring the more concentration CMH1 peaks at 34.72°C. The secondary, high temperature peak exists as 70.69°C, in the same region as the lower concentration CMH1 curves and the protein only Fc peak. The intensity of the shouldered peak of 0.19 µM CMH1 is 4400 ΔFU with a shoulder of 1300 ΔFU, with the secondary peak intensity at 800 ΔFU. Lower concentrations of CMH1 (0.09 µM and 0.05 µM) have the same shape as the Fc only curve, with Tm of 46.3°C and 45.69°C respectively and secondary peaks at 70.7°C. The Δ fluorescence intensity of the two lowest concentrations of CMH1 increases up to the value of Fc region alone.

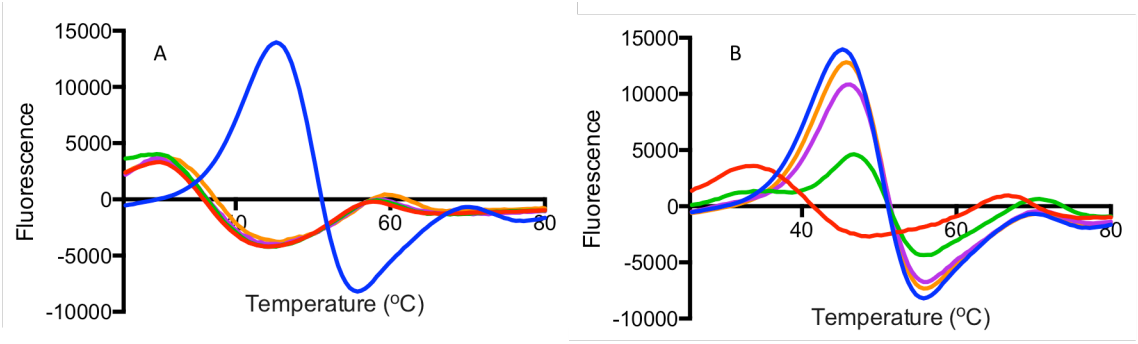

Figure 30: Differential scanning fluorimetry of human IgG Fc region with CMH1 in 50 mM sodium acetate buffer pH 4.0, **A**= (–) 3 µM IgG Fc region with (–) 6.0 µM CMH1, (–) 3.0 µM CMH1, 1.5 µM CMH1, (–) 0.75 µM CMH1. **B**= (–) 3 µM IgG Fc region with (–) 0.38 µM CMH1, (–) 0.19 µM CMH1, (–) 0.09 µM CMH1, (–) 0.05 µM CMH1.

Principle component analysis (PCA) of the first derivative DSF melt curve of human IgG Fc with CMH1 is shown in Figure 31. Correlation analysis of the variance within CMH1 concentration dataset demonstrates the first two principle components from the data in Figure 30. Fc alone is grouped with 0.05 µM and 0.09 µM CMH1, with 0.19 µM more similar to this group in the PC1, but shows variation in the PC2. 0.19 µM and 0.38 µM have similar PC2 values but demonstrate variance in the PC1. The second grouping is constructed of the higher concentrations of CMH1.

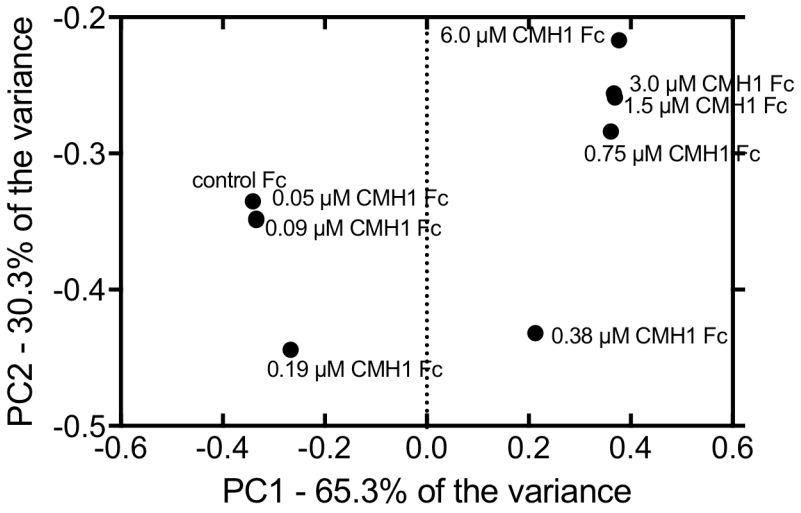

Figure 31: PCA of human IgG Fc region with different concentrations of CMH1 from DSF (1st derivative data) in 50 mM sodium acetate pH 4.0.

The IgG Fc region with CMH2 follows a similar change as CMH1 with the reduction of Tm upon addition of 6.0 µM CMH2 of 15.02°C, seen in Figure 32A. The intensity of the initial peak is 4600 ΔFU and the higher temperature peak is lower at 2300 ΔFU. Figure 32A indicates 3.0 µM CMH2 follows the same pattern but has a slight reduction in intensity at the lower Tm (4100 ΔFU). The 1.5 µM concentration of CMH2 has an increased Tm with initial shift at 33.05°C and a secondary Tm at 61.06°C. The primary peak of CMH2 at 0.75 µM 8.8 nM has a Tm if 34.9°C and intensity 3770 units, and a secondary peak at 63.59°C with intensity of 2800 ΔFU.

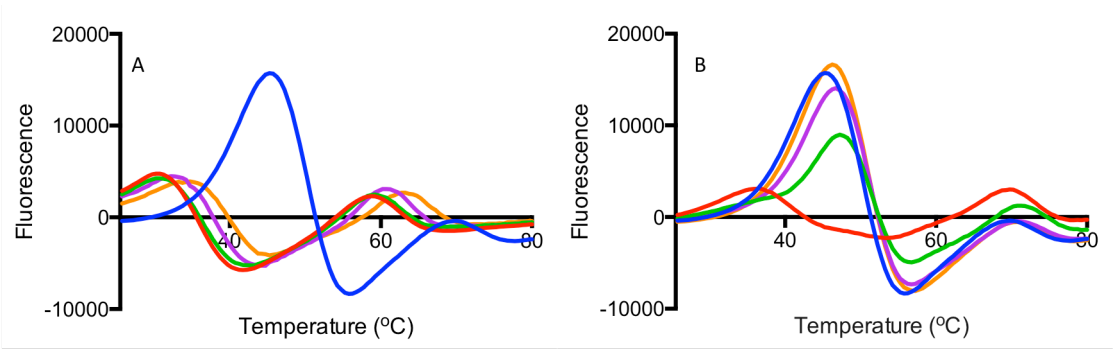

Figure 32: Differential scanning fluorimetry of human IgG Fc region with CMH2 in 50 mM sodium acetate buffer pH 4.0. **A**= (–) 3 µM IgG Fc region with (–) 6.0 µM CMH2, (–) 3.0 µM CMH2, (–) 1.5 µM CMH2, (–) 0.75 µM CMH2. **B**= (–) 3 µM IgG Fc region with (–) 0.38 µM CMH2, (–) 0.19 µM CMH2, (–) 0.09 µM CMH2, (–) 0.05 µM CMH2.

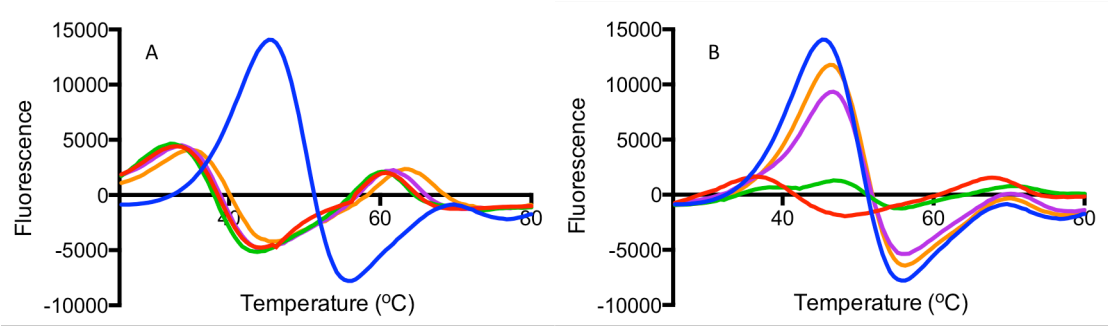

Figure 33: Differential scanning fluorimetry of human IgG Fc region with CMH3 in 50 mM sodium acetate buffer pH 4.0, **A**= (–) 3 µM IgG Fc region with (–) 6.0 µM CMH3, (–) 3.0 µM CMH3, (–) 1.5 µM CMH3, (–) 0.75 µM CMH3. **B**= (–) 3 µM IgG Fc region with (–) 0.38 µM CMH3, (–) 0.19 µM CMH3, (–) 0.09 µM CMH3, (–) 0.05 µM CMH3.

The difference between IgG Fc alone and 6.0 µM CMH3 is a Tm change of 12.8°C between the initial peaks of both concentrations (Figure 33A). Each concentration tested has two peaks, with the immunoglobulin fragment initial peak at 45.69°C with an intensity of 14200 ΔFU and a secondary peak at 69.44°C. CMH3 at 6.0 µM shifts both peaks to 32.89°C with a lower intensity of 4300 ΔFU and the secondary peak to 60.68°C with a higher intensity than Fc only at 2150 ΔFU. Intensity and curve shape changes with 0.38 µM CMH3, with the initial Tm at 36.91°C with a reduced intensity of 1680 ΔFU and a secondary peal at 68.59 °C, which mimics the Ig only secondary peak but with higher intensity of 1600 ΔFU. At 0.19 µM CMH3, the curve further flattens into an intermediate shape with three peaks visible; at Tm 38.06°C, 47.43°C and 69.02°C. The concentrations of 0.09 µM and 0.05 µM have initial Tm that are slightly increased compared to the Tm of IgG Fc alone.

Addition of 6.0 µM CMH4 to IgG Fc changes the Tm from 45.54°C to a lower Tm of 30.06°C, a difference of 15.48°C (Figure 34A). The intensity change between these two peaks is 11300 ΔFU. The secondary peaks also displays a difference in Tm of 13.0°C, with Fc Tm of 71.15°C and 6.0 µM Tm of 58.13°C. At 3.0 µM, the Tm of the initial peak is 30.04°C with a secondary peak at 58.52°C, with intensities mirroring that of the higher concentration 6.0 µM CMH4. At 0.38 µM, the Tm shifts at 35.0°C and 66.61°C with the

secondary peak in a more intermediate location between peaks of higher concentration CMH4 and their more dilute counterparts.

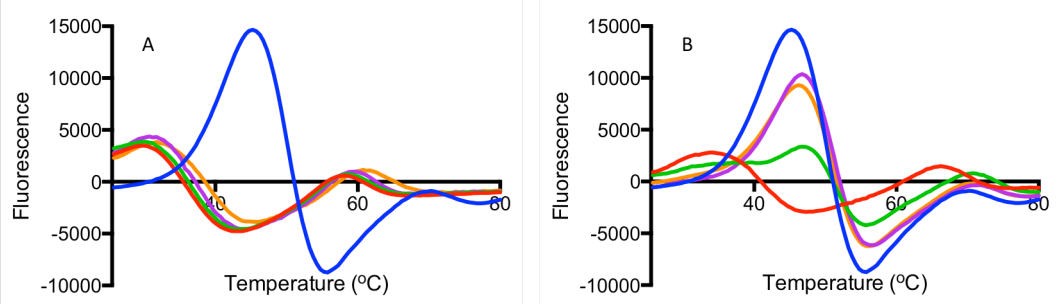

Figure 34: Differential scanning fluorimetry of human IgG Fc region with CMH4 in 50 mM sodium acetate buffer pH 4.0, **A**= (–) 3 µM IgG Fc region with (–) 6.0 µM CMH4, (–) 3.0 µM CMH4, (–) 1.5 µM CMH4, (–) 0.75 µM CMH4. **B**= (–) 3 µM IgG Fc region with (–) 0.38 µM CMH4, (–) 0.19 µM CMH4, (–) 0.09 µM CMH4, (–) 0.05 µM CMH4.

The drop in Tm seen upon addition of 6.0 µM CMH5 is 14.48°C to 32.07°C, with a secondary peak also at the lower melting temperature of 61.93°C (Figure 35A). Concentrations of CMH5 tested down to 0.38 µM have the same peak shape with approximately equal peak intensities, but the Tm of both peak one and peak two increase with decreasing CMH5 concentration, with the exception of 0.38 µM, with intensity of peak one reduced to 2300 ΔFU. At 0.19 µM CMH5, the peak shifts to 48.09°C (7500 ΔFU) and has a small hump at lower temperatures (1700 ΔFU). Peak 2 at this concentration occurs at similar Tm as Fc only (71.28°C), with intensity higher than Fc only (850 ΔFU). CMH5 concentrations of 0.09 µM and 0.05 µM show the same characteristics as in the other chemically modified heparins tested.

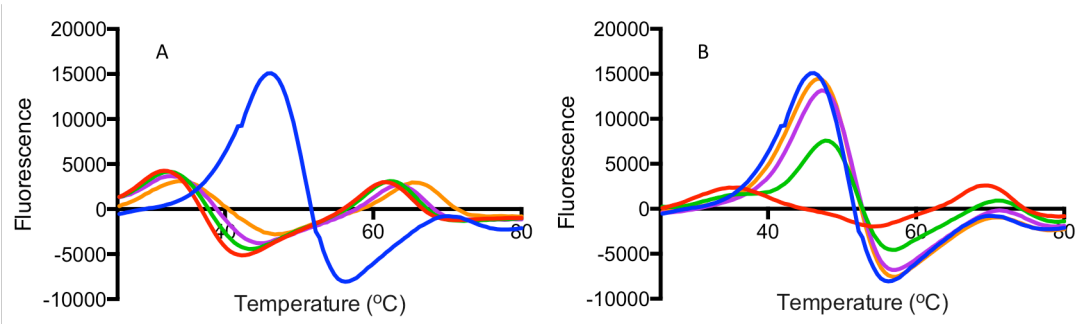

Figure 35: Differential scanning fluorimetry of human IgG Fc region with CMH5 in 50 mM sodium acetate buffer pH 4.0, **A**= (–) 3 µM IgG Fc region with (–) 6.0 µM CMH5, (–) 3.0 µM CMH5, (–) 1.5 µM CMH5, (–) 0.75 µM CMH5. **B**= (–) 3 µM IgG Fc region with (–) 0.38 µM CMH5, (–) IgG 0.19 µM CMH5, (–) 0.09 µM CMH5, (–) 0.05 µM CMH5.

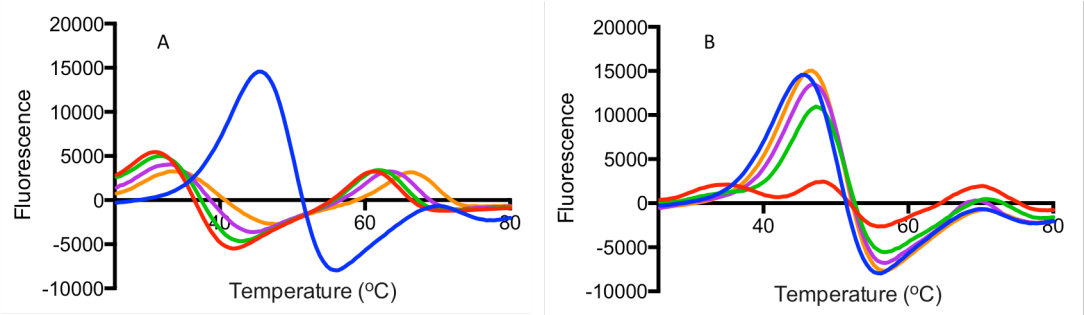

Figure 36: Differential scanning fluorimetry of human IgG Fc region with CMH6 in 50 mM sodium acetate buffer pH 4.0, **A**= (–) 3 µM IgG Fc region with (–) 6.0 µM CMH6, (–) 3.0 µM CMH6, (–) 1.5 µM CMH6, (–) 0.75 µM CMH6**. B**= (–) 3 µM IgG Fc region with (–) 0.38 µM CMH6, (–) 0.19 µM CMH6, (–) 0.09 µM CMH6, (–) 0.05 µM CMH6.

IgG Fc with 6.0 µM CMH6 has a Tm of 30.98°C with a second peak at 61.2°C. The Tm of the first peak at 1.5 µM CMH6 drops to 32.98°C and a secondary Tm of 63.74 °C. An intermediate concentration of 0.38 µM CMH6 yields 3 peaks with Tm of 34.6 °C, 48.38 °C and 69.36 °C; each peak at this concentration has an intensity of approximatley 2000 ΔFU. The first peak mirrors higher concentrations of CMH6, the centre peak mimics the Fc region only peak and the final peak Tm mimics the Fc region only secondary peak, but retains the intensity seen in secondary peaks at higher concentrations of CMH6. At concentrations of CMH6 lower than this intermediate peak, ≤ 0.19 µM, CMH6 the curves have initial peak Tm above Fc only, with secondary Tm the same as IgG Fc only; in a similar way to the lower concentrations seen in other IgG Fc graphs.

The reduction in Tm seen upon addition of 6.0 µM CMH7 on the secondary peak is 11.84°C but in this case an increase in intensity is seen (3100 ΔFU). Decreasing concentrations of CMH7 increase the Tm of IgG Fc moving to a initial Tm of 35.41°C and secondary Tm of 64.69°C at 0.38 µM. At these concentrations the intensity of the peaks remains similar to 6.0 µM CMH7. The peak shape at 0.19 µM is different from the higher concentrations of CMH7 as the peaks are shifted to a higher melting temperature more

significantly in both the primary and secondary regions (37.11°C and 69.9°C). The position of the secondary peak at this concentration has the same Tm as IgG Fc alone, and remains at this temperature with decreasing concentrations of CMH7. At lower concentrations of CMH7 (0.09 µM and 0.05 µM), the curves follow the same pattern as above with the initial Tm slightly higher than Ig alone.

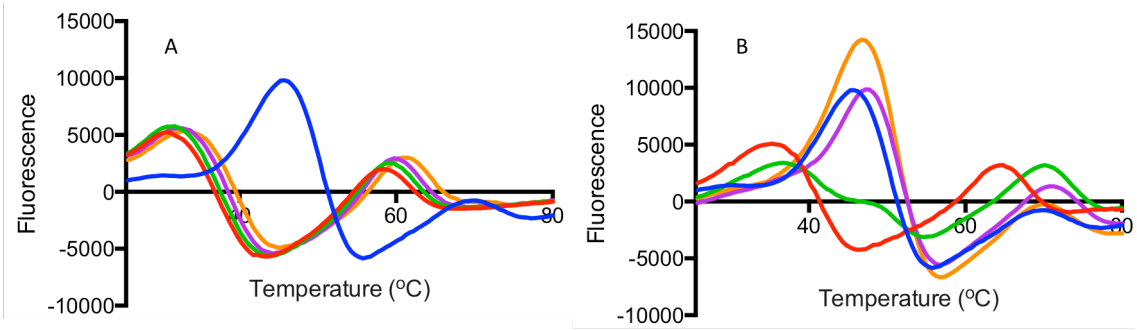

Figure 37: Differential scanning fluorimetry of human IgG Fc region with CMH7 in 50 mM sodium acetate buffer pH 4.0, **A**= (–) 3 µM IgG Fc region with (–) 6.0 µM CMH7, (–) 3.0 µM CMH7, (–) 1.5 µM CMH7, (–) 0.75 µM CMH7. **B**= (–) 3 µM IgG Fc region with (–) 0.38 µM CMH7, (–) 0.19 µM CMH7, (–) 0.09 µM CMH7, (–) 0.05 µM CMH7.

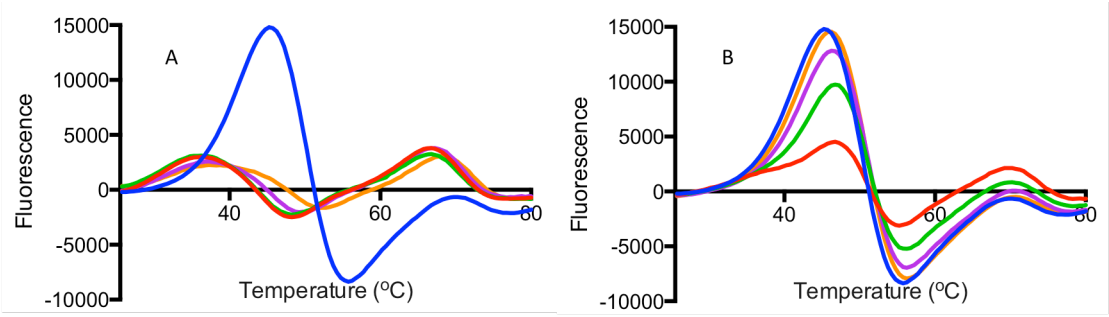

Figure 38: Differential scanning fluorimetry of human IgG Fc region with CMH8 in 50 mM sodium acetate buffer pH 4.0, **A**= (–) 3 µM IgG Fc region with (–) 6.0 µM CMH8, (–) 3.0 µM CMH8, (–) 1.5 µM CMH8, (–) 0.75 µM CMH8. **B**= (–) 3 µM IgG Fc region with (–) 0.38 µM CMH8, (–) 0.19 µM CMH8, (–) 0.09 µM CMH8, (–) 0.05 µM CMH8.

The smallest change on addition of 6.0 µM the chemically modified heparin library is seen in CMH8, with a change in Tm of 9.2°C (Figure 38A). The Tm at 6.0 µM CMH8 is 36.2°C (2900 ΔFU), with a larger secondary peak at 67.02°C (3700 ΔFU). The peaks remain similar for concentrations to 0.75 µM, with approximately the same intensity. At 0.38 µM CMH8, the initial peak shifts too a higher melting point of 46.76°C

and a secondary peak at 70.25°C. These Tm are then the same the lower concentrations (0.19 µM, 0.09 µM and 0.05 µM) tested, with the initial Tm slightly increased compared to IgG Fc alone.

The difference between the no CMH9 and 6.0 µM CMH9 with human IgG Fc is 14.54°C in this experiment (Figure 39A). At concentrations tested 0.75 µM to 6.0 µM the curve shape is different from other IgG Fc graphs, with an initial flattened hump with no further peak structure at higher temperatures. CMH9 at 0.38 µM the intensity of the initial peak increases to 2400 ΔFU with a Tm of 32.24°C, and a flattened secondary hump at 68.96 °C. At 0.19 µM CMH9 and below, the peaks resemble the IgG Fc only peak and the lower concentrations seen in the other chemically modified heparins. The initial Tm of ≤ 0.19 µM CMH9 are all slightly higher than IgG Fc alone.

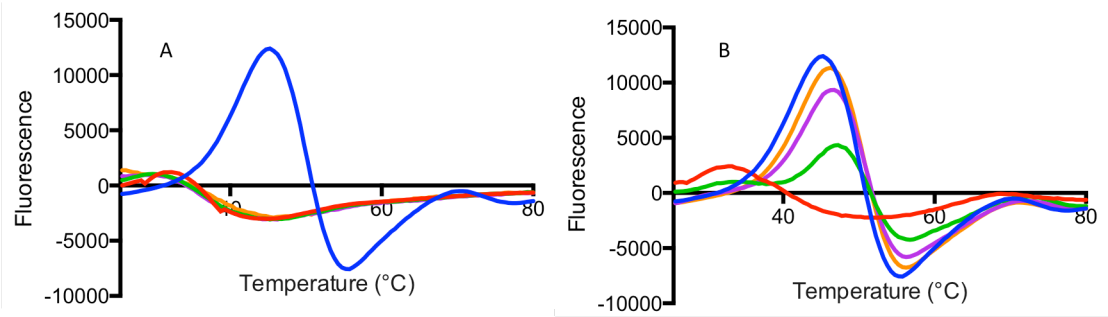

Figure 39: Differential scanning fluorimetry of human IgG Fc region with CMH9 in 50 mM sodium acetate buffer pH 4.0, **A**= (–) 3 µM IgG Fc region with (–) 6.0 µM CMH9, (–) 3.0 µM CMH9, (–) 1.5 µM CMH9, (–) 0.75 µM CMH9, **B**= (–) 3 µM IgG Fc region with (–) 0.38 µM CMH9, (–) 0.19 µM CMH9, (–) 0.09 µM CMH9, (–) 0.05 µM CMH9.

The largest reduction in Tm and therefore destabilisation of IgG Fc was seen with the addition of 6.0 µM of CMH1 at 15.73 °C, followed by 6.0 µM CMH4 at 15.48 °C.

Principle component analysis of the DSF data (1st derivative) demonstrate a similarity between the resulting thermal stability IgG Fc with CMH1 (Figure 40), CMH2, CMH4, CMH5, CMH7 and CMH9 (Figure 40). The PCA analysis of CMH6 and CMH8 exhibit similar groupings. The concentrations of CMH3 tested, when analysed with PCA

have a different grouping pattern, but still maintains the grouping separation of high vs low CMH concentration, demonstrated with the whole CMH library with IgG Fc.

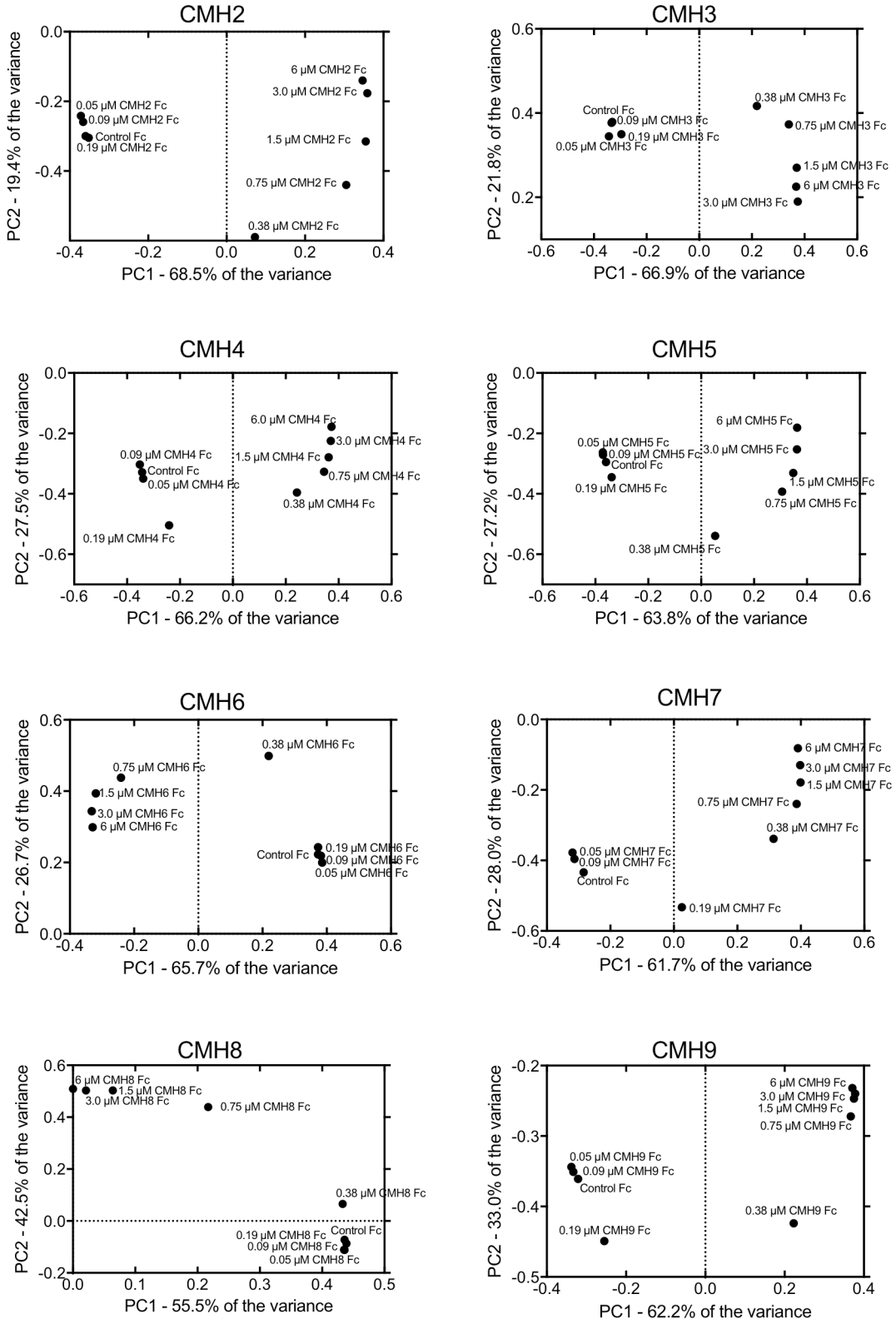

Figure 40: PCA analysis of 1st derivative DSF thermal stability data of IgG Fc region with CMH2-CMH9. Scree plots indicated PC1 and PC2 represent >85% of the data variance (data not shown).

4.2.3 Circular dichroism of the Fc region and chemically modified heparin

Far-UV circular dichroism was employed to determine the secondary structural change in IgG Fc region with the addition of each chemically modified heparin. Even the least modified heparin, CMH8 has an effect on the stability if human IgG Fc in 50 mM sodium acetate pH 4.0. However this modification shows the least change in Tm when compared to the other chemically modified heparins tested. CMH6 (Figure 42B) has a similar Tm to that of CMH8 (Figure 42D) at 3.0 µM, with Tm mimicking that of no heparin; this suggests at 3.0 µM these two heparins do not affect the structural stability of IgG Fc unlike the other heparins at this concentration. Both CMH6 and CMH8 include an unmodified GlcNAc, which is unique in this library.

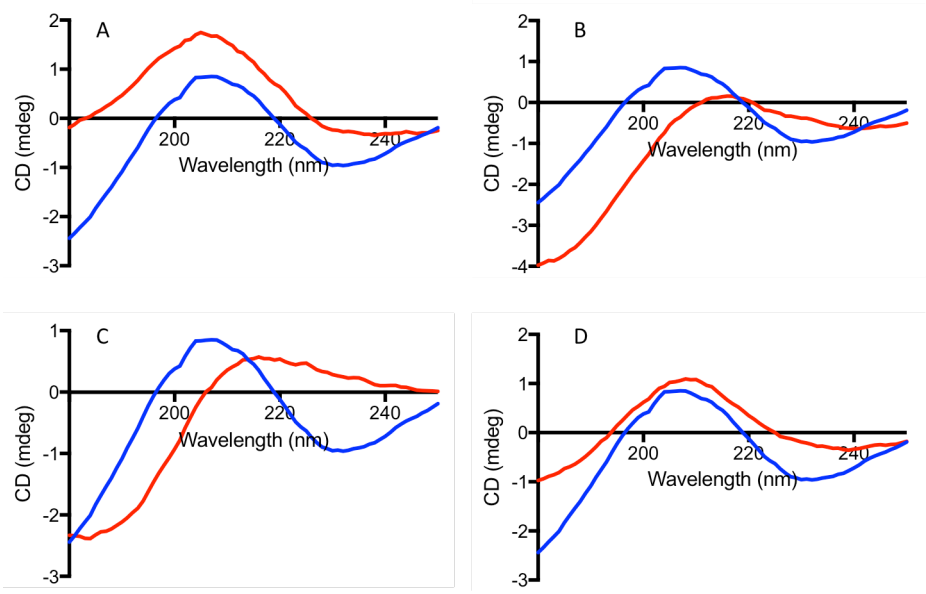

Figure 41: Far-UV circular dichroism spectra of human IgG Fc region with CMH 1-4, calibrated with D-(+)-10-camphorsulfonic acid, reaction buffer 50 mM sodium acetate pH 4.0. **A**)(–) 3 µM IgG Fc region with (–) 3 µM CMH1, **B**)(–) IgG Fc region with (–) 3 µM CMH2, **C**)(–) IgG Fc region with (–) 3 µM CMH3 **D**)(–) IgG Fc region with (–) 3 µM CMH4.

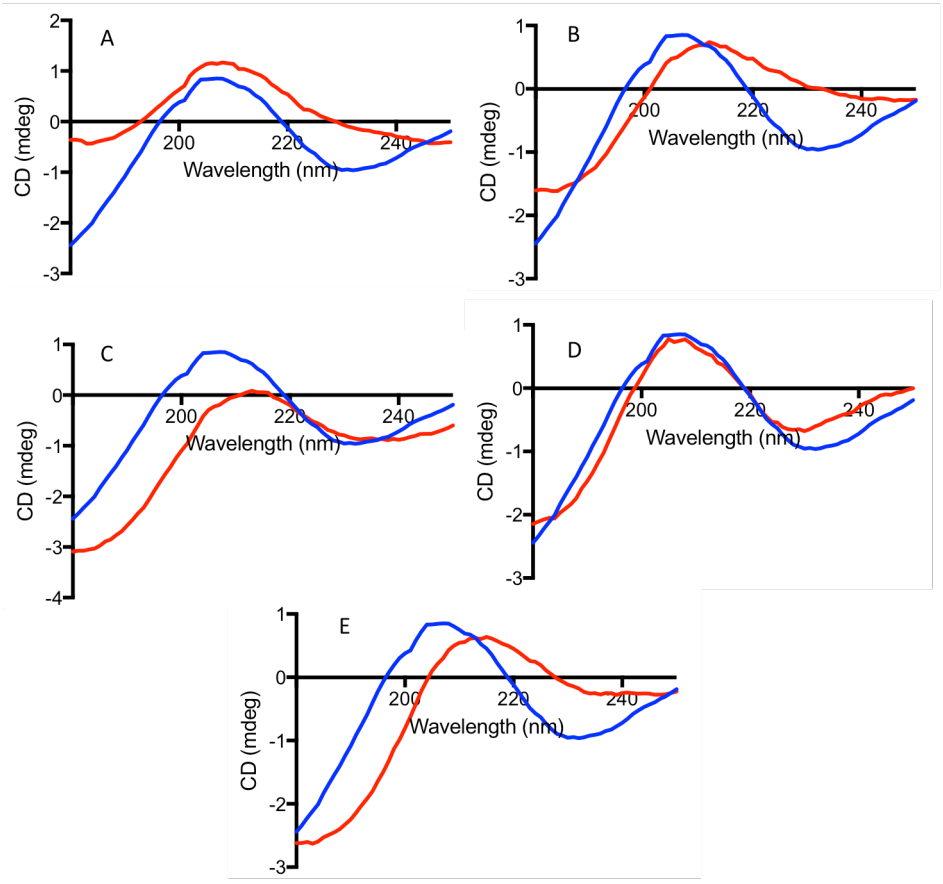

Figure 42: Far-UV circular dichroism spectra of human IgG Fc region with CMH 5-9, calibrated with D-(+)-10-camphorsulfonic acid. Reaction buffer 50 mM sodium acetate pH 4.0 **A**)(–) 3 µM IgG Fc region with (–) 3 µM CMH5, **B**)(–) IgG Fc region with (–) 3 µM CMH6, **C**)(–) IgG Fc region with (–) 3 µM CMH7 **D**)(–) IgG Fc region with (–) 3 µM CMH8, **E**)(–) IgG Fc region with (–) 3 µM CMH9.

4.2.4 The effect of other glycosaminoglycan and sulphated compounds on the Fc region

In order to identify if the change in structure of human IgG Fc was due to the addition of sulphate alone, DSF with an equivalent molar concentration of sulphate in the form of sodium sulphate was completed (representing the highest concentration of PMH tested). This experiment showed no change in structure with the addition of sodium sulphate; suggesting the inclusion of these anions is not solely the cause of structural changes (Figure 43). Na_2SO_4 does not modify the Tm of IgG Fc region.

The trisulphated HS/heparin disaccharide UA(2S)-GlcNS(6S) shifts the Tm of IgG Fc to a lower temperature by 2.6°C (Figure 43), suggesting some interaction between the protein and disaccharide. Disaccharide standard UA(2S)-GlcNS(6S) reduces the Tm by 2.56°C to 42.38°C with intensity of 9800 ΔFU with the second peak Tm at 68.66°C.

Heparan sulphate was used at 2x concentration to represent the presence of a similar level of sulphate as the PMH experiment, with the structure and functional group positioning remaining similar to the polymer structure of heparin. HS and PMH destabilised the IgG Fc region, reducing the Tm by 14°C (Figure 43).

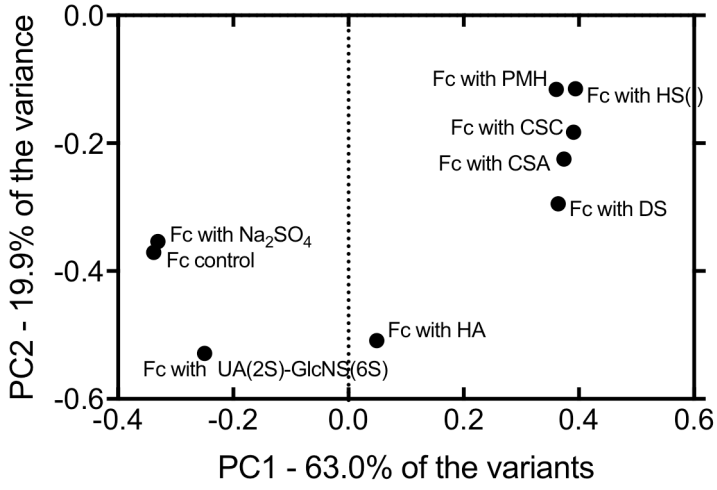

Figure 43: PCA of first derivative DSF of human IgG Fc region with glycosaminoglycans (PMH, HS, CSC, CSA, DS, HA) and sulphate controls.

The effect of these other GAG compounds on the Tm of IgG Fc region in DSF from greatest to least structural change in Tm is PMH/HS>CSC>CSA>DS>HA>UA(2S)-GlcNS(6S)>Na_2SO_4 as demonstrated by the PCA analysis of first derivative DSF data in Figure 43. PMH at 6.0 μM causes a reduction in stability equivalent to a decrease in Tm of 14.72°C with Fc region Tm at an average of 44.96°C ± 0.115 °C and the PMH Tm at 30.24 °C with intensity of 3720 ΔFU.

The Tm change seen with HS and the IgG Fc region has the same initial curve shape as PMH, with Tm of 30.28°C but the second peak is more defined than with PMH,

with a increased Tm of 59.22°C. The initial peak of chondroitin sulphate C (CSC) has a Tm with Fc region occuring at 31.55°C, which is 14.41°C less than the IgG Fc region alone (Figure 44). The shift seen of the secondary peak is larger with dermatan sulphate (DS) (8.18°C) than with CSC.

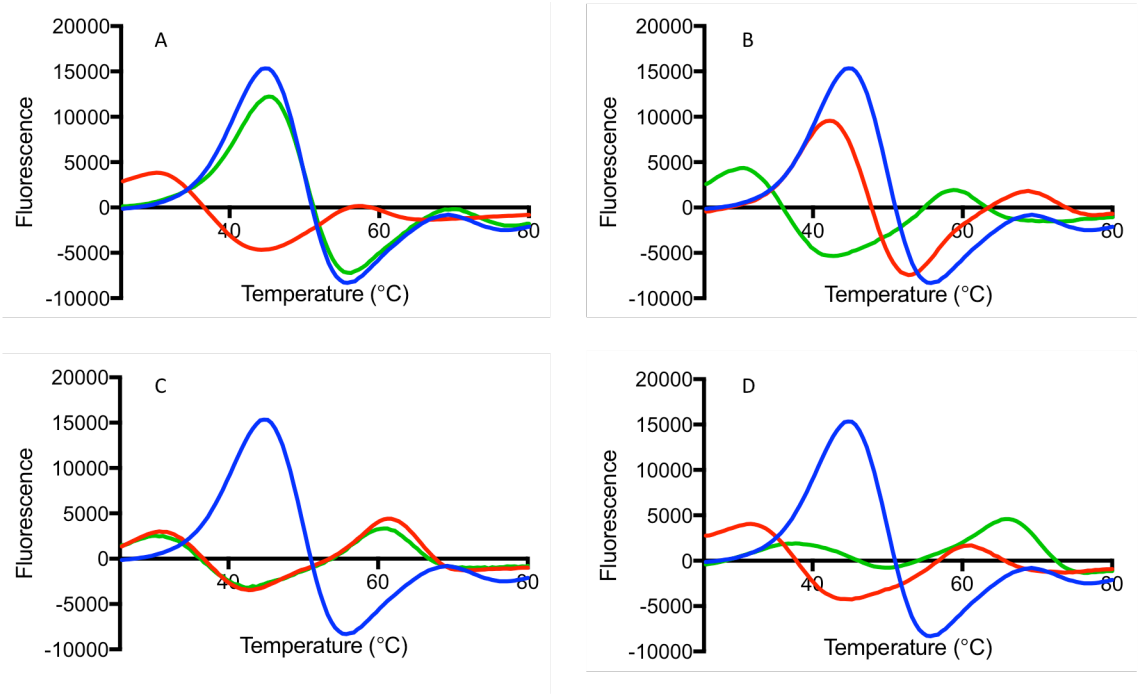

Figure 44: Differential scanning fluorimetry with human IgG Fc region with GAGs and sulphate controls in 50 mM sodium acetate buffer pH 4.0. **A**) (–) 3 µM human IgG Fc region with (–) 6.0 µM UF PMH, (–) 500 nM sodium sulphate, **B**) (–) 3 µM human IgG Fc region (–) 6.0 µM UA(2S)-GlcNS(6S) (–) 12.0 µM HS, **C**) (–) 3 µM human IgG Fc region with (–) 6.0 µM CSA, (–) 6.0 µM CSC, **D**) (–) 3 µM human IgG Fc region with (–) 6.0 µM DS, (–) 6.0 µM HA.

Chondroitin sulphate A (CSA) addition causes a reduction in Tm of 13.9°C, to a Tm of 31.06 °C for the first peak. The second peak shift is 7.07°C to 62.13°C. DS with Fc region has a similar shaped curve to HS, including a higher intensity secondary peak. The Tm of the initial peak is at 31.57°C (4220 ΔFU). The Tm shift seen in the initial peak from Fc alone is 13.39°C with DS, and the secondary peak shift is 8.18°C. This similar effect to HS and UF PMH could be due to all having iduronic acid present in the glycopolymer. Adding hyaluronic acid (HA) produces an intermediate initial peak with

Tm of 37.70°C (Tm **Δ** 7.26°C), which is flattened compared to the other GAGs at 2100 ΔFU.

4.2.5 The size requirements for heparin/HS:IgG Fc region binding

A library of size fractionated heparin oligosaccharides ranging from a disaccharide (d.p.2) to eicosaccharide (d.p.20) was utilised in DSF to identify any minimum size requirement for heparin binding to human IgG Fc region. A change in Tm is indicative of an effect of oligosaccharide binding.

Table 5: The DSF Tm of each PMH polymerization (d.p.) fragment with IgG Fc region in 50 mM sodium acetate buffer pH 4.0.

d.p. of PMH	Peak 1 Tm (°C)	Peak 2 Tm (°C)	Peak 3 Tm (°C)
Protein only control	44.98	69.14	
2	45.43	69.82	
4	38.54	68.39	
6	33.90	64.92	
8	33.64	63.21	
10	34.23	62.37	
12	32.44	61.26	
14	32.05	60.47	
16	31.62	59.60	
18	31.04	59.50	
20	30.81	59.72	81.35
UF PMH	29.85	57.80	

IgG Fc region with (molar equivalent to UF PMH) d.p.2 has the same curve shape with similar Tm and intensity. A d.p.4 reduces the Tm of the first peak to 38.54°C with intensity of 6650 ΔFU and the secondary peak to a lesser extent with Tm of 68.39 °C but increased intensity of 2770 ΔFU. The Tm of the initial population peak reduces with increasing saccharide length to a minimum of 30.81°C with the d.p.20, with the Tm of UF PMH, 29.85°C. The secondary peak population Tm also decreases with increasing saccharide size, with the d.p.18 with Tm most like that of UF PMH. A Tm reduction between d.p.4 and d.p.6 of 4.6°C is the greatest change upon addition of a disaccharide; further reductions in Tm with increasing oligosaccharide size are gradual. This suggests

a minimum hexasaccharide requirement for a notable change in Tm, and therefore interaction with IgG Fc region. The PCA analysis of this data in Figure 45 demonstrates a d.p.4 has an intermediate effect, with hexasaccharide grouped with the larger PMH fragments.

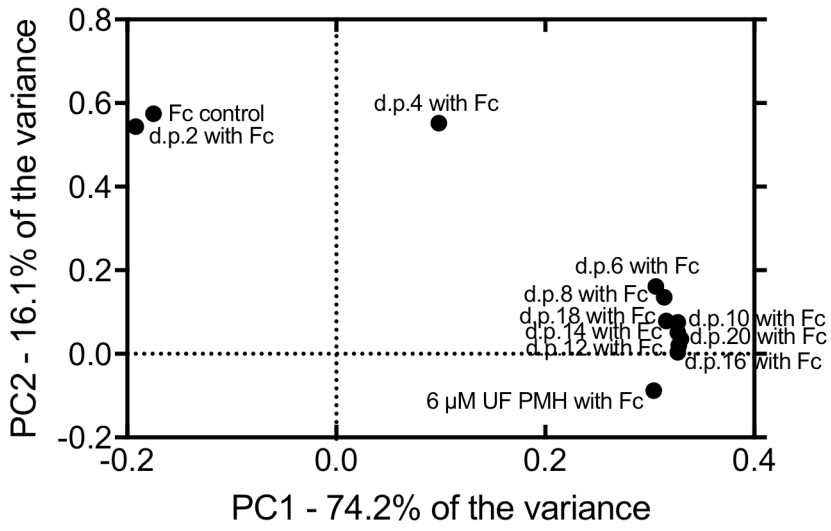

Figure 45: PCA analysis of the heparin size requirement for human IgG Fc thermal destabilisation as measured in DSF.

4.2.6 The effect of other heparin based anti-coagulants on the IgG Fc region

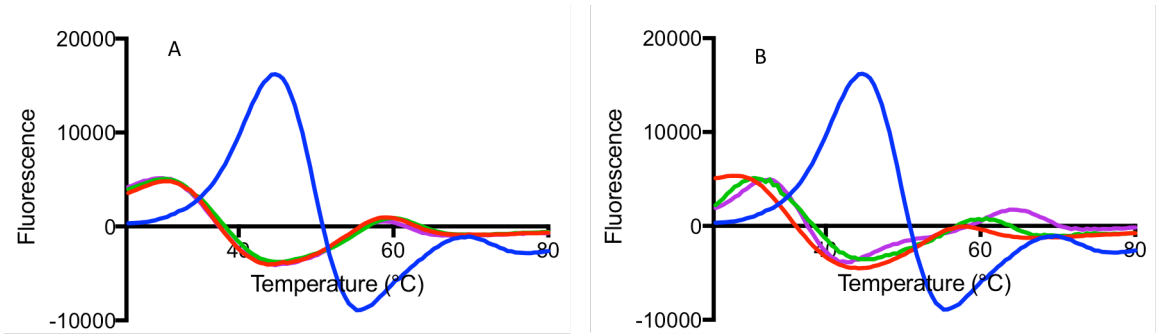

Figure 46: Differential scanning fluorimetry of human IgG Fc region with LMWHs in 50 mM sodium acetate buffer pH 4.0. **A**= (–) 3 µM IgG Fc region with (–) 6.0 µM dalteparin (–) 6.0 µM enoxaparin, (–) 6.0 µM tinzaparin. **B**= (–) 3 µM IgG Fc region with (–) 6.0 µM UF PMH (–) 6.0 µM reviparin, (–) 6.0 µM fondaparinux.

Low molecular weight heparins (dalteparin, enoxaparin, tinzaparin and reviparin) and a synthetic heparin (fondaparinux), were assayed to determine whether

low molecular weight heparins also bind to change the stability of human IgG Fc region in DSF.

Dalteparin, enoxaparin, tinzaparin and reviparin the same molar concentration as PMH have similar Tm at 30.50°C and 58.90°C. Fondaparinux has Tm at 32.97°C and 64.79°C. LMWH/synthetic heparins were assayed 6.0 μM and dalteparin, enoxaparin, tinzaparin and reviparin each reduce IgG Fc region stability to the same Tm as UF PMH. The minimum requirements for GAG binding to IgG Fc are met in these LMWHs, suggesting a similar manner of action to PMH; this is demonstrated in Figure 47 with PCA analysis.

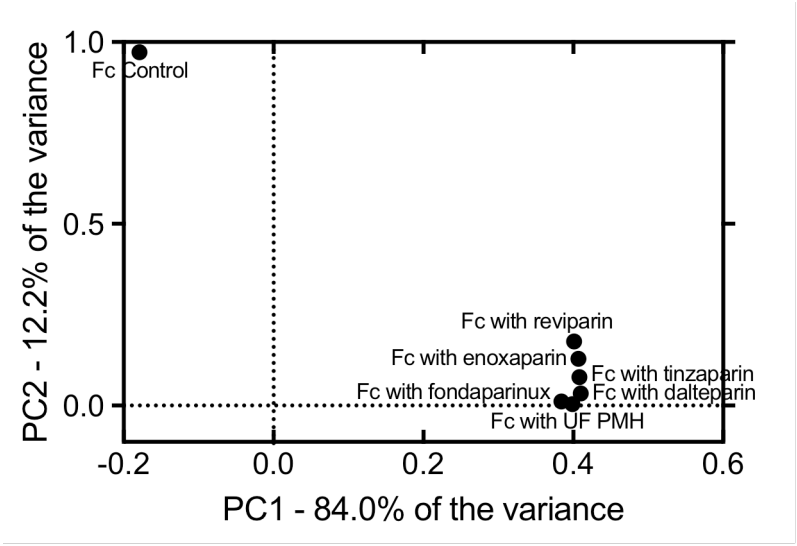

Figure 47: PCA analysis of the first derivative DSF melt curve of IgG Fc region with LMWHs.

4.2.7 Sodium acetate buffer concentration experiments with BACE1

The effect of increasing buffer strength on the stability of the human IgG Fc region was investigated, with the addition of UF PMH to identify any requirement for binding.

Table 6: Differential scanning fluorimetry of human IgG Fc region (3 μM) in 20 mm – 100 mM buffer strength and pH 4.0 – 5.0 sodium acetate, ± 6.0 μM UFPMH. The Tm from the first derivative graphs of each melt curve is found below.

	20 mM Sodium acetate buffer			
	No UFPMH		100 μg/ml UFPMH	
	Tm	Tm	Tm	Tm
pH 4.0	48.30	73.59	34.14	65.26
pH 4.5	54.95	80.19	38.68	73.91
pH 5.0	55.81	81.41	32.37	64.18

	30 mM Sodium acetate buffer			
	No UFPMH		100 μg/ml UFPMH	
	Tm	Tm	Tm	Tm
pH 4.0	47.20	73.10	33.99	63.37
pH 4.5	53.43	79.17	37.60	71.15
pH 5.0	56.21	81.24	33.74	66.09

	40 mM Sodium acetate buffer			
	No UFPMH		100 μg/ml UFPMH	
	Tm	Tm	Tm	Tm
pH 4.0	47.14	72.51	34.67	66.10
pH 4.5	53.05	78.99	36.59	70.96
pH 5.0	56.23	81.71	35.02	68.10

	50 mM Sodium acetate buffer			
	No UFPMH		100 μg/ml UFPMH	
	Tm	Tm	Tm	Tm
pH 4.0	46.28	72.81	31.68	
pH 4.5	52.97	78.59	37.97	72.35
pH 5.0	56.83	82.13	35.12	69.01

	60 mM Sodium acetate buffer			
	No UFPMH		100 μg/ml UFPMH	
	Tm	Tm	Tm	Tm
pH 4.0	44.88	71.11	34.19	64.02
pH 4.5	52.88	78.50	37.69	72.08
pH 5.0	56.61	82.15	35.56	70.29

	80 mM Sodium acetate buffer			
	No UFPMH		100 μg/ml UFPMH	
	Tm	Tm	Tm	Tm
pH 4.0	45.20	70.27	35.27	65.38
pH 4.5	51.90	78.18	38.15 / 52.80 / 73.34	
pH 5.0	56.81	82.20	37.14	72.61

	100 mM Sodium acetate buffer			
	No UFPMH		100 μg/ml UFPMH	
	Tm	Tm	Tm	Tm
pH 4.0	34.42	64.65	35.59	65.93
pH 4.5	39.37	73.51	38.49	72.51
pH 5.0	56.70	81.88	38.48	73.61

This buffer screen was completed for sodium acetate at varying buffer strengths at pH 4.0, 4.5 and 5.0, with and without 6.0 μM UF PMH. The Fc region is most stable in the concentrations of acetate buffer tested, at 50 mM acetate buffer at pH 5.0 and least stable at 100 mM acetate buffer pH 4.0. The shape of the first derivative melt curve along with the Tm with the addition of UF PMH at all sodium acetate concentrations tested mimic the effect seen with 100 mM sodium acetate without UF PMH; this suggests a similar degree of structural change in both instances. Increasing the pH from 4.0 to 5.0 leads to an increase in Tm in the Fc region when tested without UF PMH indicating a more stable conformation, as expected, as physiological pH is 7.4. The peak Tm range increases at each pH value tested, with increasing acetate concentration. PCA analysis of the first derivative melt curves determined by DSF are shown in Figure 48.

Increasing the acetate concentration (including the acetic acid required to pH solution) increases the Tm difference at the three pH tested, in both the main peak and secondary smaller peak.

The addition of 6.0 μM UF PMH to the IgG Fc region with acetate buffer at different concentrations and pH levels, does not show a similar relationship. Peak 1 variation in Tm seen at each concentration across the three pH tested is lower with PMH added, with no pattern to the range of Tm from pH change seen in 20 mM to 100 mM acetate buffer. The most stable pH acetate buffer is pH 4.5 across all concentrations tested. The lowest Tm with PMH varies with the two lowest concentrations at 20 mM and 30 mM being pH 5.0, and higher concentrations ≥ 40 mM least stable at pH 4.0 as shown in Table 6.

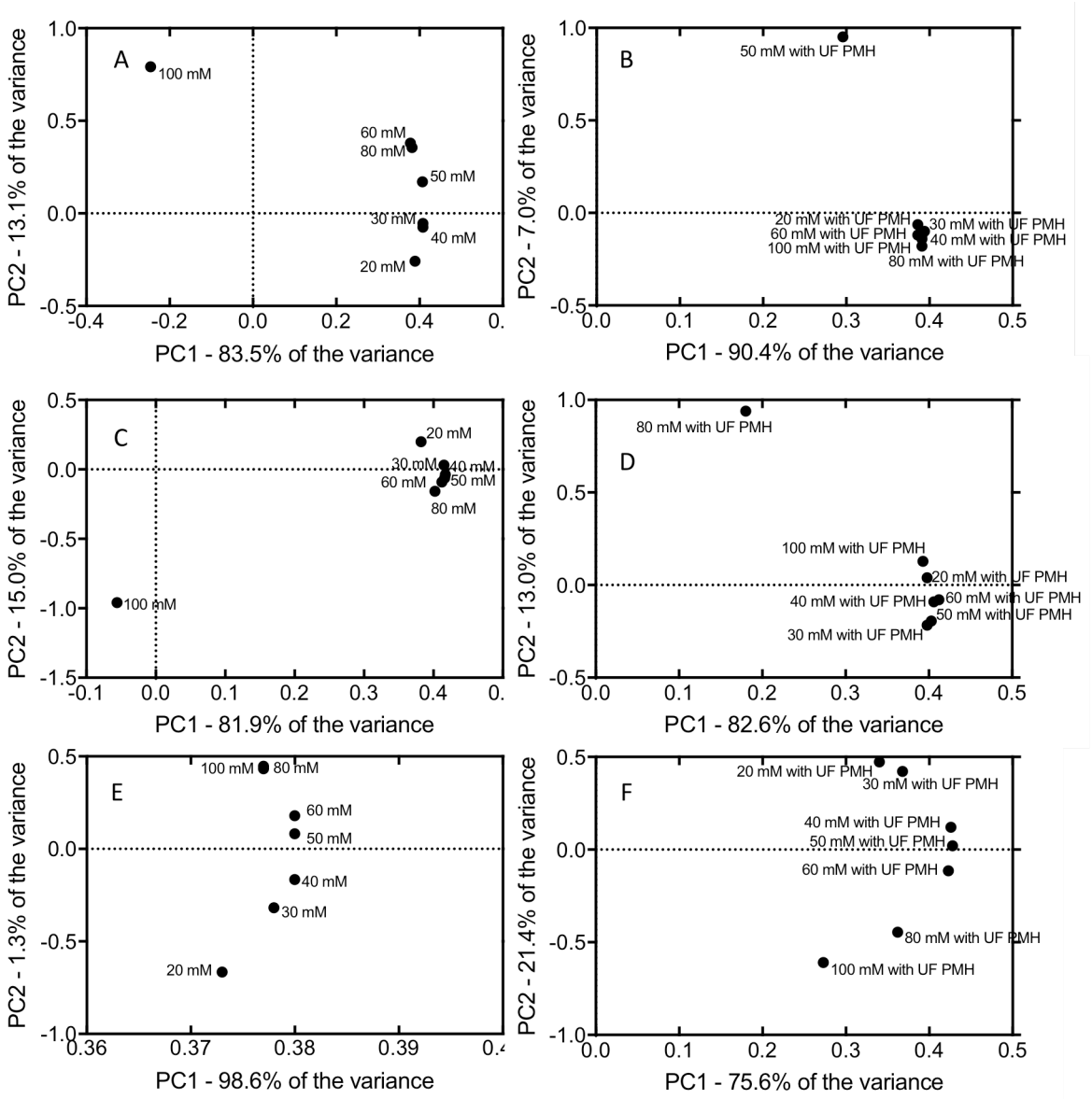

Figure 48: PCA from 1st derivative DSF of IgG Fc region buffer experiments ± UF PMH, Tm stated in Table 6. 50 mM Sodium acetate buffer **A**) pH 4.0, **B**) pH 4.0 with UF PMH, **C**) pH 4.5, **D**) pH 4.5 with UF PMH, **E**) pH 5.0 **F**) pH 5.0 with UF PMH.

4.2.8 IgG Fc region studies with cation forms of heparin

Highly polyanionic heparin chains are associated with positively charged ions in solution. Data published shows the presence and modification of these bound cations can have an effect on the heparin function. It is not known whether the resulting change

in properties are due to the change in charge distrubution or an altered polymer chain conformation (Meneghetti et al., 2015).

Fourteen cation heparins were prepared and tested in DSF with human IgG Fc region to identify any modifications to the protein melting temperature, implying alterations to protein binding and stability. Table 7 includes the Tm of the first peak taken from the first derivative of the melt curve for human IgG Fc region. The data at the lower concentrations tested exhibited most variation between cation forms.

At 0.75 μM each prepared cation PMH tested caused accelerated thermal denaturation of IgG Fc region to a similar degree (35°C -37°C) (Table 7).

Table 7: DSF of human IgG Fc with defined cation forms of heparin in 50 mM sodium acetate buffer pH 4.0. Cation heparin concentrations ranging from 0.75 μM to 0.09 μM.

Concentration of heparin	0.75 μM	0.38 μM	0.19 μM	0.09 μM	none: Fc only
	Tm (°C)	Tm (°C)	Tm (°C)	Tm (°C)	Tm (°C)
Celsus UF PMH	31.25	32.87	35.44	47.88	45.37
Sodium heparin	35.50	36.64	49.06	47.71	45.34
Potassium heparin	37.22	48.82	48.62	47.91	46.61
Lithium heparin	36.48	38.04	48.85	46.84	46.07
Ammonium heparin	35.32	47.77	49.19	47.94	44.95
Magnesium heparin	37.07	38.25	48.20	46.95	45.98
Calcium heparin	36.69	48.81	48.45	47.67	47.09
Barium heparin	35.77	35.93	48.66	48.83	44.94
Zinc heparin	36.66	48.61	48.68	48.08	46.67
Iron (II) heparin	37.13	38.21	49.14	48.04	47.15
Copper heparin	36.85	37.05	48.79	47.90	47.13
Iron (III) heparin	36.72	37.60	47.98	46.89	44.55
Silver heparin	36.60	48.84	47.60	46.50	45.00
Vanadium heparin	37.79	48.45	47.73	46.51	44.77
Manganese heparin	36.21	36.85	47.92	47.08	44.56

Unmodified Celsus PMH in the sodium form causes the greatest shift in melting temperature than any prepared cation heparin at all concentrations tested, apart from the smallest concentration 0.09 μM. The greater the concentration of Celsus heparin tested, the greater the difference Celsus heparin and the cation heparins tested. The

sodium form of heparin tested in DSF displays the most dramatic difference from unmodified Celsus PMH (sodium form) at 0.19 μM, with unmodified PMH exhibiting a

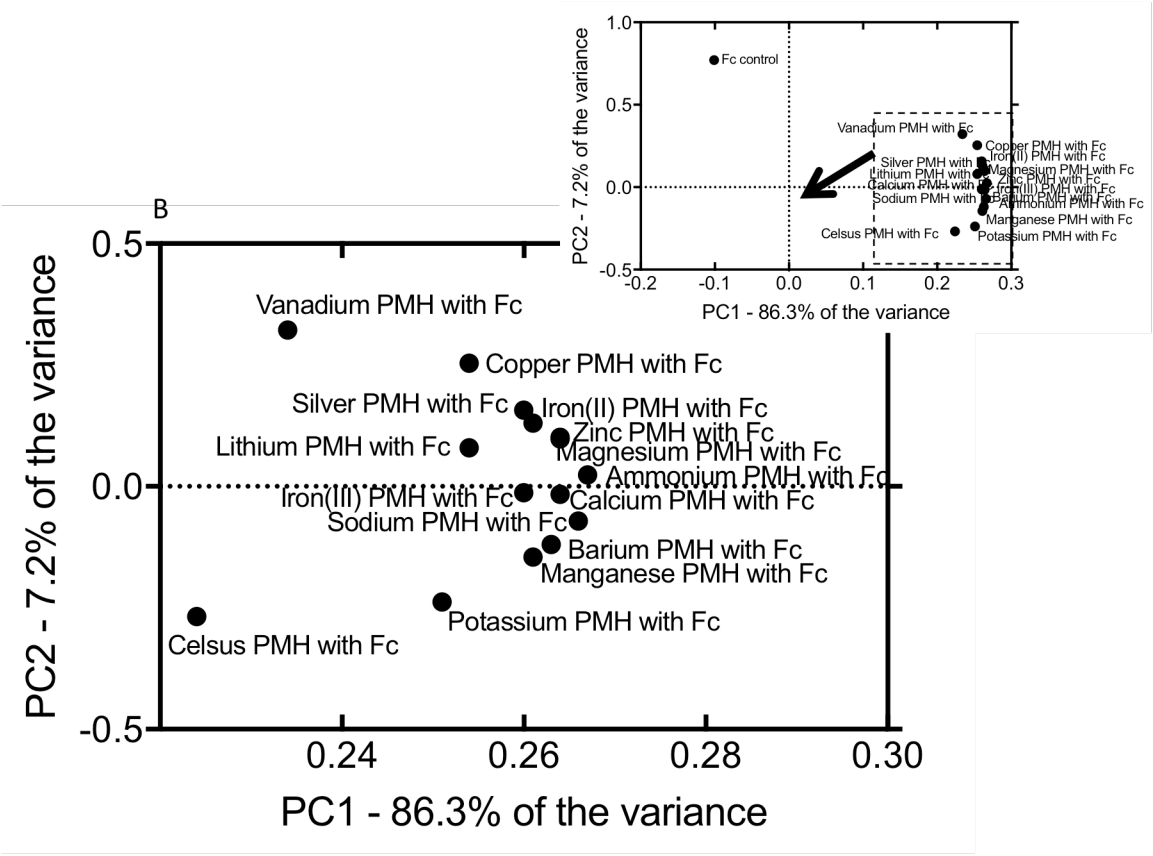

Figure 49: PCA analysis of 1st derivative DSF data of IgG Fc region with 6 μM defined cation form of PMH.

Tm of 35.44°C and sodium PMH a Tm of 49.06°C; a melt temperature higher than that of the IgG Fc region with no heparin present (45.34°C).

The trend of increased resistance to temperature denaturation is also present in the lowest concentration of sodium PMH tested (0.09 μM). At 0.09 μM only, Celsus PMH also shows increased resistance to temperature denaturation. All other cation forms of PMH enhance the stability of IgG Fc region in this DSF experiment, at different concentrations and to different degrees. Potassium, ammonium, calcium, zinc, silver and vanadium forms of PMH at 0.38 μM increase the Tm of IgG Fc region, and improve the resistance to thermal denaturation. At 0.38 μM, sodium, lithium, magnesium, barium,

iron (II) and iron (III), copper and manganese PMH each destabilise IgG Fc region, leading to a reduction in melting temperature and promotion of thermal denaturation.

At 0.19 μM and 0.09 μM each cation heparin improves the stability of IgG Fc region, as shown through an increased Tm when compared with the protein alone. Of these two concentrations, the stabilising effect is more prominent at 0.19 μM than 0.09 μM.

PCA of the highest concentration of each defined cation heparin type from the 1st derivative DSF data of IgG Fc (Figure 49) shows potassium heparin is the most similar to Celsus PMH in both principle components (PC) 1 and 2, however, vanadium PMH is most similar to Celsus PMH in the PC1 alone, and the most different of the cation forms in PC2. Zinc and magnesium, both divalent cations, have the same effect in the variance of the data.

4.3 Discussion

Initial investigations into the change in stability of BACE1 with a IgG Fc tag in the presence of PMH indicated that in FRET conditions of 50 mM sodium acetate pH 4.0, PMH reduced the melting temperature of BACE1-Fc by 9 °C, a change in the conformation of the protein caused by the action of UF PMH. To measure the strength of binding affinity between the IgG Fc region and PMH, HiTrap heparin affinity chromatography was completed in the same buffer system. This indicated a 981 mM binding affinity between IgG Fc region and the heparin-sepharose column in 50 mM sodium acetate pH 4.0. Binding of PMH in 50 mM sodium acetate at pH 4.0 to the Fc region could be occurring through the positively charged amino acids present in the domain structure such as Lys248 and Lys338 exposed in the CH2 α-helices which form the CH3-CH2 domain interface (Latypov, Hogan, Lau, Gadgil, & Liu, 2012). Positively charged imidazole ions of histidine and guanidinium ions of arginine are equally likely to have a role in heparin binding at this pH (Zhang-van Enk et al., 2013). The highly sulphated nature of PMH may allow sulphate ions to act as chaotrophes through the disordering of hydrogen bonding. This change in covelent bonding structure in the CH2-CH3 domain structure of IgG Fc due to the presence of highly charged PMH could be the cause of the reduction in melting temperature seen in the DSF experiments with BACE1-Fc fusion.

Ejima *et al.* (2007) showed during the purification process for monoclonal antibodies and Fc-fusion proteins, immunoglobulins are exposed to low pH conditions in affinity resin elution and to inactivate viral particles (Ejima et al., 2007). In pH 2.7 - 3.9, 0.1 M citrate buffer, humanised IgG4 and mouse monoclonal antibodies tested by Ejima *et al.* (2007) displayed only limited conformation modifications and did not reach the

'molton globule structure' associated with acid treatment of multi-domain protein (*idem*). The IgG remaned stable and in monomeric form, but had a reduced Tm when compared to antibodies at pH 6 (*idem*).

Hari *et al.* (2010) investigated the unfolding and aggregation kinetics of IgG Fc region under acidic conditions (Hari, Lau, Razinkov, Chen, & Latypov, 2010). At 25 °C in pH 3.5 acetate buffer, IgG1 was resistant to aggregation but IgG2 aggregated in the presence of 0.5 M sodium chloride (*idem*). At the same pH, acetate and citrate buffer systems had differing effects on IgG aggregation, with thermal stability of antibodies higher in equivalent citrate buffer than acetate (*idem*).

At pH 5.5, Vlasov *et al.* (1996) demonstrated the CH2 domain of rabbit IgG displayed significant reductions in co-operation and lower levels of interaction with the surrounding domains, in a transition independent to the whole IgG molecule (Vlasov, Kravchuk, & Martsev, 1996). At pH 3.0, the CH2 domain undergoes tertiary unfolding, with the rest of the IgG retaining native secondary and tertiary structure (*idem*). The increase of pH > 3.0 leads to a conformer with reduced domain interaction between the CH2 and CH3 Fc regions, resulting in contrary modifications to effector functions; improved C1q binding and reduced affinity for protein A (*idem*).

DSF experiments in PBS rather than sodium acetate indicate only a small change in structure at low pH upon addition of PMH, suggesting the sodium acetate buffer system promotes the destabilising action of PMH. HiTrap heparin affinity chromatography of IgG Fc in PBS across a pH range between 4.0 and 7.4 shows binding at a similar affinity to sodium acetate at pH 4.0 (977 mM NaCl) and lower affinity binding at pH 5.0, with a similar lack of binding at more neutral pH. With the physiological buffer system PBS prompting only a negligable structural change in the presence of PMH, the binding of IgG Fc at pH 4.0 and 5.0 may suggest a possibility of

physiological action in regions of localised acidic pH (e.g inflammation or trauma) or in specific regions of favourable conditions (e.g endosomes, lysosomes, and secretory granules).

The melting temperature of IgG Fc is more variable between pH 4.0 and 5.0 in sodium acetate than in PBS, by the addition of PMH to these conditions produces the same structural change to result in a significant reduction of Tm.

Sulphate groups present throughout PMH may more readily bind to the Fc region through electrostatic interactions in pH 4.0 and 5.0 sodium acetate buffers. Zhang-van Enk *et al*. (2013) noted the addition of sulphate ions to IgG Fc contradict the standard kosmotrophic action of sulphate ions, with sulphate acting more potently than SCN^- as a strongly destabilising chaotrope (Zhang-van Enk et al., 2013). Zhang-van Enk *et al*. (2013) postulated the cause of this destabilisation could be due to the interaction of the divalent anion and positively charged side chains, causing solubilisation of hydrophobic regions and disruption of intra-protein covelent bonding, triggering a net change in CH2 domain structure (*idem*) and a reduction in melting point. The IgG Fc region has net negative charge at pH lower than 7.2, and the CH2 domain has a lower melting point than CH3 with the denaturation of the Fc fragment irreversible after CH3 unfolding (idem).

Hofmeister anions have conflicting actions with different proteins, as demonstrated with SO_4^{2-} with human IgG1 Fc region (Zhang-van Enk et al., 2013). Sulphate ions typically exhibit protein-stabilising (kosmotropic) activities; reduce the solubility of proteins, reduce the denaturation rate and increase protein stability (*idem*). At pH 4.8, the protonated CH2 domain of IgG Fc region was destabilised by the addition of SO_4^{2-}, more potent than the strongly destabilising chaotrope SCN^- (*idem*).

Zhang-van Enk *et al.* (2013) suggested at pH 4.8, the anions tested follow the order SO_4^{2-} > SCN^- > Cl^- > F^- in the ability of the anion to reduce the Tm of IgG Fc region at salt concentrations below 50 mM; with KF^- increasing the Tm at this pH (Zhang-van Enk et al., 2013). At pH 7.2, the destabilizing effect on IgG Fc region was attenuated, with concentrations below 100 mM showing a slightly different effect on the Tm; $SCN^- \cong SO_4^{2-}$ > Cl^- > F^- (*idem*).

Heparin is a polymer containing multiple anionic groups, with sulphates accounting for 70% of charged groups present on the polysaccharide (Diakun, Edwards, Wedlock, Allen, & Phillips, 1978). Protein binding to heparin causes some portion of heparin neutralisation through the liberation of charged moities such as sulphate groups (Mascotti & Lohman, 1995). Replacing SO_4^{2-} from sodium sulphate (Zhang-van Enk et al., 2013) with the sulphated glycosaminoglycan heparin, the change in structural stability witnessed upon addition of the hofmeister anion SO_4^{2-} in IgG Fc region has been demonstrated.

Circular dichroism demonstrates the secondary structure of IgG Fc is different with the addition of PMH and un-sulphated CMH8. This may suggest the presence of CMH8 has an effect on the secondary structure of IgG Fc in a different way to the highly polyanionic PMH.

Utilising a library of heparin derivatives displaying a range of structural characteristics found commonly in heparan sulphate, investigations into the effect of specific chemical modifications in IgG Fc binding was completed. DSF was utilised to indicate the change in IgG Fc associated with the binding of polysaccharide.

Each of the nine chemically modified heparins tested at high concentration, reduced the melting point of IgG Fc, suggesting a reduction in stability of the protein. The smallest effect was seen in the addition of unsulphated CMH8, with a maximum

reduction in Tm of 9.2 °C. Conversley the greatest change in Tm and therefore destabilisation effect was seen with high concentrations of CMH1. The addition of 6.0 μM of CMH1 at 15.73 °C displays the highest level of IgG Fc destabilisation followed by the 6.0 μM CMH4 at 15.48 °C. The number of sulphates per disaccharide does not completely correspond to the stability of the Fc region, with persulphated heparin CMH9 not having a more marked Tm reducing destabilisation effect than CMH1. Both CMH3 and CMH7 act to destabilise IgG Fc at 0.09 μM, whereas all other heparins tested had little to no action at this concentration, suggesting more effective binding or more potent destabilisation at this concentration. Both CMH3 and CMH7 have unsubstituted iduronic acid residues and N-sulpho-glucosamine residues present, which is unique in this library. This may suggest a role of unsubstituted IdoA bound to a GlcNS as a binding requirement.

Principle component analysis of the CMH library with IgG Fc region indicated two groupings of CMH with similar principle components; one group containing CMH1, CMH2, CMH4, CMH5, CMH7 and CMH9, another group containing CMH6 and CMH8. CMH3 demonstrates a different layout of the PCA data. Interestingly, CMH6 and CMH8 are the only library members to both contain an unsulphated GlcNAc residue, which may suggest this modification produces a change in the effect of Fc destabilisation therefore an altered effect on the variance of the 1st derivative.

The effect of the sulphate anions alone on the stability of IgG Fc region, without the presence of the glycosaminoglycan scaffold structure allowed clarification of the role of these moieties. At sulphate concentrations equivalent to the most perturbing chemically modified disaccharide CMH1, Na_2SO_4 did not destabilise IgG Fc structure, indicating a important role for the GAG structure alongside the presence of sulphate anion alone.

The presence of more discrete domain structure was investigated with the use of heparan sulphate in DSF with IgG Fc region. HS was used at double the molar concentration of PMH in order to replicate the sulphate levels associated with PMH. The structural changes, therefore, could be attributed to structural differences between the GAGs, and not soley the sulphate levels. The effect of HS was the same as PMH in DSF with IgG Fc, indicating these GAGs have a similar effect on the stability of the Fc region. This may be due to the presence of sulphate moieties presented in a similar way in both heparin and HS to modify hydrogen bonding and therefore structure of IgG Fc when bound.

The effect of other GAGs on the stability of IgG Fc was investigated to identify structural requirements for the interaction. The action of each GAG in DSF was determined from most to least change in Tm as PMH/HS>CSC>CSA>DS>HA> IdoA(2S)-GlcNS(6S) >Na_2SO_4. The GAGs CSC, CSA and DS all display similar changes to the melting point of IgG Fc, with the Tm of these GAGs separated by only 0.5 °C, this may be due to the similarities in the level of sulphation. The addition of HA has a smaller effect on the stability of IgG Fc but still shows perturbation of Fc melting, demonstrating the absence of sulphate in this GAG still allows for destabilisation of the protein. The reduced structural effect of HA in DSF of Fc shows a role of an unsulphated GAG in destabilisation of the immunoglobulin fragment that was shown with CMH8, and alluded to with HS, but not fully shown. These results suggest the presence of sulphate anions for the full reduction in Tm seen with the other saccharides. The intermediate nature of the Tm change could be a result of diminished GAG binding to the Fc region therefore disrupting less of the hydrogen bonding and therefore retaining more of the stable CH2-CH3 domain structure.

Investigation into the size requirement of the HS oligosaccharide required for reduction of IgG Fc melting point and therefore indication of GAG binding and destabilisation was made. The presence of a HS disaccharide did not markedly change in the melting point of IgG Fc, an intermediate change in Tm was produced with the presence of a d.p.4, with a greater change seen upon addition of d.p.6. This reduction in Tm was produced with the greatest change seen with d.p.20. The addition of d.p.20 was most similar to the effects seen with PMH. The disaccharide tested showed no change in stability indicating binding, with the tetrasaccharide showing an intermediate level of destabilisation indicating some effect, but the increase from a 4mer to hexasaccharide showed the greatest change in melting point. As a pentasaccharide was not tested, the minimum size requirement of heparin oligosaccharide in IgG Fc binding has been shown to require a 6mer, this could also have the same effect with a 5mer. This sized oligosaccharide was screened in the form of the synthetic LMWH pentasaccharide, fondaparinux.

Low molecular weight heparins were tested in DSF with IgG Fc and acetate buffer to determine if depolymerised heparins dalteparin, enoxaparin, tinzaparin and reviparin and the synthetic pentasaccharide fondaparinux showed any binding activity of IgG Fc. The derived LMWHs dalteparin, enoxaparin, tinzaparin and reviparin, at the same molar concentration as PMH, displayed similar destabilisation of the IgG fragment than PMH. This may suggest at 6.0 μM these LMWH mimic the binding and destabilisation of PMH, and with a d.p.6 only required to show a large destabilisation effect in DSF, the sulphation level and GAG size of these derivatives is sufficient to mimic PMH. Fondaparinux however, is a synthetic d.p.5 representing only the pentasaccharide sequence sufficient for antithrombin III binding. This synthetic GAG did not destabilise

IgG Fc to the same extent as the derived LMWH tested suggesting it does not bind as effectively to the immunoglobulin fragment.

Investigations were made in to the effects of increasing acetate concentration in IgG Fc DSF at pH 4.0. In acetate buffer at all strengths tested (20 mM to 100 mM) IgG Fc is destabilised. This destabilisation caused by sodium acetate increases with increasing acetate concentration until 80 mM. However, a significant structural destabilisation occurred between 80 mM sodium acetate and 100 mM sodium acetate, reducing the Tm by a further 10.67°C. At this acetate concentration, buffer ions may act more strongly on the protein structure through electrostatic interactions to destabilise the IgG Fc fragment.

In DSF with the same concentration gradient of acetate buffer with the addition of 6.0 μM PMH, IgG Fc stability curves have the same appearance as 100 mM sodium acetate without PMH. This suggests the degree of destabilisation of 100 mM sodium acetate on this Ig fragment is similar to the destabilisation seen with the binding of PMH and the other GAG fragments tested. This destabilisation could be due to weakening of the hydrophobic effect, solubilisation of hydrophobic regions and disruption of internal non-covelent bonding, triggering a net change in protein folding. The 100 mM sodium acetate with PMH experiments does not further decrease the Tm, signifying no cumulative effect with these two factors.

The conformation of IgG Fc region was investigated with NMR ^{1}H-^{15}N HSQC analysis between pH 2.5 and 4.7 (Latypov et al., 2012). At pH 4.7, amide peaks (117 assigned resonances) were highly dispersed indicating a folded conformation, at pH 3.5 a similar degree of dispersity was seen (116 assigned resonances) but a number of peaks had reduced intensity and new peaks were seen not present at pH 4.7 (*idem*). These structural changes are indicative of protonation of acidic side-chains such as

Glu380 and Glu430, which form salt bridges with Lys248 and Lys388 in the native Fc region (*idem*). At pH 3.1, some peaks present at higher pH disappeared (46 assigned resonances) and were replaced with peaks seen at pH 3.5, suggesting a more disordered protein conformation (*idem*). At pH 2.5 the remaining native peaks disappeared (*idem*). The most prominent changes in chemical shift between pH 4.7 and 3.5 occurred between residues 250-255 and 310-315, both regions of interface between the CH2 and CH3 Fc domains (*idem*). This interface region formed by CH2 α-helices is the region containing the corresponding Lys248 and Lys338 residues involved in salt bridge formation with protonated glutamic acid residues at pH 3.5 (*idem*). The peaks indicating the presence of CH2 domain structure were not present at pH 3.1 suggesting unfolding of this immunoglobulin fold structure (*idem*).

An investigation into the effects of concentration and pH of sodium acetate buffer was expanded to cover 20 mM to 100 mM at pH 4.0, 4.5 and 5.0. The melting point of IgG Fc region was determined by DSF. This determined the Ig Fc fragment was more stable at pH 5.0 than pH 4.0 as expected as binding to FcRn on luminal surfaces occurs at around pH 6.0 when His310 and His433 are protonated and dissociates at pH 7.4 on the basolateral surfaces due to deprotonation (Raghavan et al., 1995). The working pH of this Ig fragment therefore occurs over pH range of 6.0 to 7.4 and therefore is required to maintain structural stability in this range, however in sodium acetate buffer this pH may differ. With the addition of 6 μM PMH, the most stable pH of IgG Fc is reduced to pH 4.5.

Due to the highly polyanionic nature of heparin, the HS and heparin are present physiologically with bound cations which act to neutralise the highly charged GAG chains. Heparin pharmaceutical preparations are available in the sodium, calcium and lithium forms. The effect of the bound cations has been investigated in biological systems where heparin and HS are utilised, such as in the FGF/FGFR signalling

pathways. Rudd *et al.* (2007) utilised Synchrotron Radiation Circular Dichroism (SRCD) to illustrate sodium, potassium, magnesium, calcium, manganese (II), copper and iron (III) PMH each had unique spectra and the binding of these cations subtly modified PMH conformation and flexibility when measured by NMR. The conversion between cation states, for example from potassium form into copper form, changed the bioactivity of PMH in fibroblast growth factor 2 (FGF2):FGFR1c signalling from an inactive state to active (Rudd et al., 2007).

Unmodified Celsus heparin had the most destabilising effect on IgG Fc region at the three highest concentrations tested (18.8 nM, 9.4 nM and 4.7 nM). A stabilising effect was seen at the 0.09 μM cation-PMH concentration which increased the Tm of the Fc fragment when compared to the melting temperature of the fragment alone in sodium acetate buffer.

A stabilising effect is seen with 0.19 μM and 0.09 μM of all of the cation forms of heparin tested. This suggests either the process of preparing cation forms of heparin reduces the magnitude of destabilising effect of heparin in this assay, or unmodified Celsus heparin includes unknown factors that enhance the action in DSF with Fc region. This unknown factor could be attributed to the mixture of cations bound to the heparin chain, the unmodified chain structure retaining a asset removed in the cation formulation process, or some other undefined effect.

The effect of cation on the stability of IgG Fc region at 0.38 μM can be identified as either promoting or protecting from thermal denaturation, when compared to the IgG Fc protein alone. One group of cation heparin including potassium, ammonium, calcium, zinc, silver and vanadium PMH increased the Tm and therefore IgG Fc region stability at a concentration of 0.38 μM. Another group containing sodium, lithium, magnesium, barium, iron (II), iron (III), copper and manganese PMH decreased the Tm of IgG Fc

region in DSF and therefore the fragment stability at this concentration. The two groups of cation forms do not ascribe to simple explanations such as separation by valency or similar atomic radii; with a range of valencies and radii included in each group. Chevalier *et al.* (2002) indentified the presence of Ca^{2+} binding sites on the heparin/HS chain, which acted to stiffen the molecule through specific binding regions between iduronate and glucosamine residues; similar specific binding sites for other divalent cations were not identified (Chevalier, Angulo, Lucas, Nieto, & Martin-Lomas, 2002). The action of divalent cations in both increasing and decreasing the Tm of Fc region suggests this possible 'stiffening' of the PMH chain upon cation binding is not solely the cause of the change in Fc region binding and variations in stability.

The increase of Tm seen at 0.19 μM and 0.09 μM in 3 μM IgG Fc with the cation PMH suggests the presence of low concentrations of single cation heparin binds IgG Fc region and promotes stability of the protein; at these concentrations the differentiation of cation is not relevant.

Previous work done by Rudd *et al.* (2007) on the FGF/FGFR signalling pathway grouped the cation forms of PMH tested using principle component analysis of the SRCD data; iron (III), manganese, potassium and sodium into one group, calcium and magnesium into another group and copper as the sole member of the third group (*idem*). This group structure is not reflected in the cation PMH forms tested in this work, with potassium and calcium improving Fc stability at the low concentrations tested, while sodium, magnesium, iron (III), copper and manganese PMH forms promoting thermal degredation.

Chapter 5: Investigations of glycosaminoglycan interactions with whole immunoglobulin

5.1 Introduction

To determine whether the interaction between the glycosaminoglycans and IgG Fc region at pH 4.0 – 5.0 seen in Chapter 4 was a product of the formation of IgG Fc region from a whole IgG or a property endowed by the immuloglobulin Fc region in the physiological molecule, in this chapter, work was done to evaluate the effect of heparin, and the library of screening glycosaminoglycans employed in the previous chapter, on a wider range of immunoglobulins to further understand this interaction.

5.1.1 Antibody action

In humans, approximately 80% of expressed antibodies are IgG class, with the subclass expression of IgG1 to IgG4, named according to physiologic abundance. 5-10% of immuglobulin is IgM, which is expressed in a pentameric form from plasma cells, but as a monomer when membrane bound on B-lymphocytes. IgM is utilised in the initial stage of a humoural immune response but has a short half-life, therefore the presence of these antibodies suggests an acute or recent infection. Pentameric IgM has 10 antigen binding sites making it practical as an agglutinin and in complement activation.

This study focuses on the IgG and IgM antibody as the most abundantly expressed antibody classes and due to time constraints, IgE, IgA and IgD were not investigated.

5.1.2 IgG structure

IgG hinge region size, number of disulphide bonds, and position of disulphide bonds, differentiate the four subclasses of IgG present in humans (Schroeder & Cavacini, 2010). These subclass variations are caused by amino acid sequence differences and allow for the variation in IgG biological activity (*idem*). IgG1, 3, and 4 can cross the

placenta, while IgG1, 2, and 3 can activate compliment. Fc receptors bind IgG subclasses with varying affinity; with IgG1 and 3 demonstrating the highest binding affinity (*idem*).

To complete this study, three types of IgG antibody will be challenged with heparin in various forms, to identify if the IgG Fc binding seen in Chapter 4 exists when in the complete immunoglobulin protein form.

If an antibody is chosen that has been raised to a possible heparin/HS/GAG binding domain, there may be a possibility that addition of heparin to this antigen binding site will cause antibody binding; this will mask the evidence of heparin binding to the non-antigen binding antibody regions. Therefore, antibodies were chosen in a manner to ensure no possible GAG/heparin/HS recognition. Green fluorescent protein (GFP) is a 234-residue protein from *Aequorea victoria* jellyfish, but is commonly used as a gene expression reporter (Tsien, 1998). No heparin binding interactions have so far been reported with this protein. Human IgG1k and IgG2k raised to GFP were used in these experiments to determine heparin binding and specific structural changes associated with the binding interaction.

5.1.3 IgM structure

IgM has an additional heavy chain immunoglobulin domain CH4, increasing the size of the Fc region (Schroeder & Cavacini, 2010). The pentamer of IgM is constructed by additional disulphate bridges between this extra CH4 domain of the 5 monomers, alongside the J-chain or joining chain (*idem*). The J-chain is a 137 amino acid cysteine rich polypeptide present in both IgM and IgA to allow for polymerisation (*idem*). The J-chain in IgM allows for the secretion of pentameric IgM to mucosal surfaces alongside IgA (*idem*).

Desipramine (Norpramin, Pertofane) is a tricyclic (selective nor-adrenaline/ serotonin re-uptake inhibitor) anti-depressant (TCA). The anti-desipramine monoclonal IgM antibody is used to detect the presence of this pharmaceutical in patient blood samples to assess patient therapeutic regime and to identify potential overdose. In this chapter, anti-desipramine IgM will be used to determine heparin binding.

5.2 Results

Initial experimentation using thermal stability assay DSF was employed to study the stability of whole immunoglobulin with structurally defined heparins.

5.2.1 IgG1k stability in the presence of chemically modified heparins

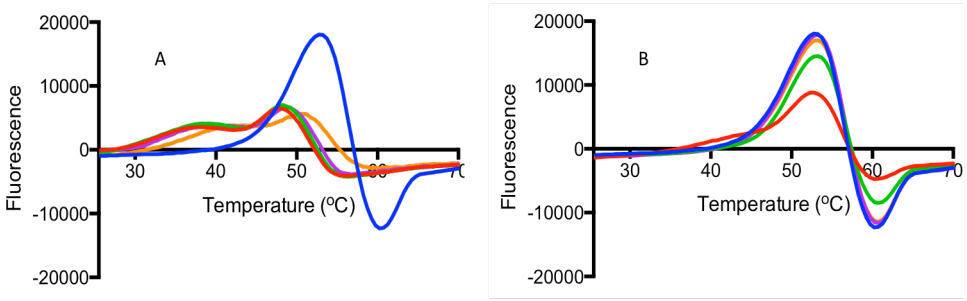

Figure 50: DSF of human IgG1k with CMH1 in 50 mM sodium acetate buffer pH 4.0 **A**= (–) 1 µM human IgG1k with (–) 6.0 µM CMH1, (–) 3.0 µM CMH1, (–) 1.5 µM CMH1, (–) 0.75 µM CMH1. **B**= (–) 1 µM human IgG1k with (–) 0.38 µM CMH1, (–) 0.19 µM CMH1, (–) 0.09 µM CMH1, (–) 0.05 µM CMH1.

IgG1k 1st derivative melt curve demonstrated a peak at a temperature of 53.3°C. The difference between the Tm of 6 µM CMH1 and IgG1k alone is 14.86°C. CMH1 at 6 µM to 1.5 µM moves the first derivative peak to a lower temperature, with a shoulder on the curve at 38.4°C and a lower intensity, suggesting the population of the protein only peak has been spread representing more of a range of conformations or stabilities, with different Tm with CMH1 present to 1.5 µM concentration. The higher intensity peak at these CMH1 concentrations is shifted to a lower Tm also compared to the IgG1k peak, shifting from Tm 53.3°C to Tm 48.7°C. At 0.75 µM CMH1 concentration, the flattened, more spread peak moves to a main peak at 42.0°C with a shoulder at a lower temperature of 51.0°C. At 0.38 µM, the main peak is present at the same Tm as IgG1k only, and with decreasing concentrations of CMH1, stays at this Tm. The curve at 0.38 µM is different from subsequent lower CMH1 concentrations by the slight shoulder

present at 44.5°C, mirroring the shape seen in higher CMH1 concentrations, but without the defined peak. The intensity of the fluorescence increases in inverse proportion to CMH1 concentration, with highest peak intensity seen in IgG1k alone. The full range of CMH1 dilutions are assayed with Sypro Orange without protein to ensure no change in fluorescence was seen (data not shown).

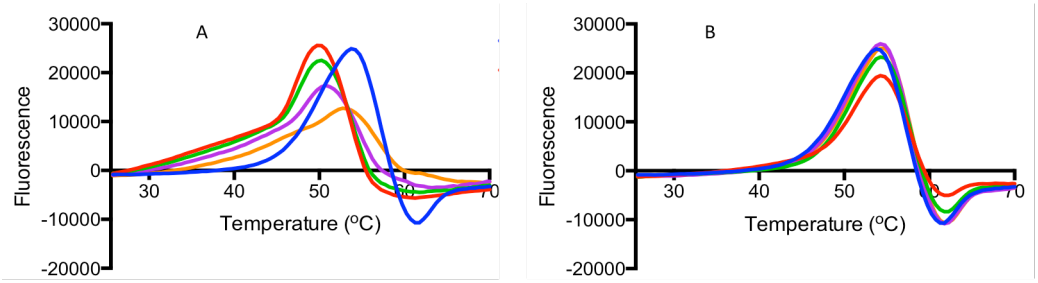

Figure 51: DSF of human IgG1k with CMH2 in 50 mM sodium acetate buffer pH 4.0 **A**= (–) 1 µM human IgG1k with (–) 6.0 µM CMH2, (–) 3.0 µM CMH2, (–) 1.5 µM CMH2, (–) 0.75 µM CMH2. **B**= (–) 1 µM human IgG1k with (–) 0.38 µM CMH2, (–) 0.19 µM CMH2, (–) 0.09 µM CMH2, (–) 0.05 µM CMH2.

The difference between the Tm of the most concentrated CMH2 (6.0 µM) and IgG1k only Tm is 4.34°C. The Tm of 6.0 µM and 3.0 µM CMH2 is 50.53°C, compared to the IgG1k only peak at 54.69°C. The peaks of 6.0 µM and 3.0 µM CMH2 have a sloping shoulder, unlike the more clear shoulder on IgG1k with CMH1.

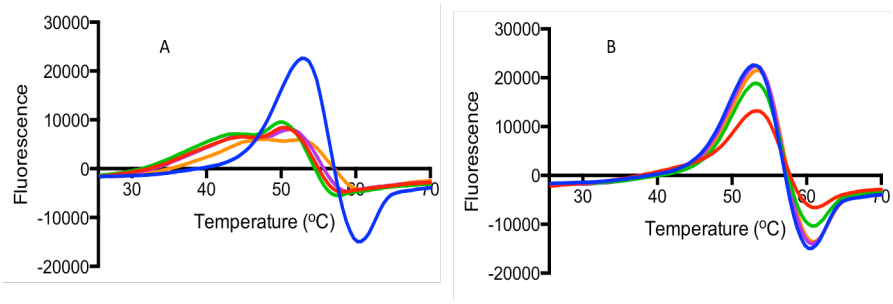

Figure 52: DSF of human IgG1k with CMH3 in 50 mM sodium acetate buffer pH 4.0 **A**= (–) 1 µM human IgG1k with (–) 6.0 µM CMH3, (–) 3.0 µM CMH3, (–) 1.5 µM CMH3, (–) 0.75 µM CMH3. **B**= (–) 1 µM human IgG1k with (–) 0.38 µM CMH3, (–) 0.19 µM CMH3, (–) 0.09 µM CMH3, (–) 0.05 µM CMH3.

The change in Tm between 6.0 µM CMH3 (highest concentration tested) and the IgG1k only control is 9.95°C. The CMH3 concentrations of 6.0, 3.0, and 1.5 µM have a

shoulder step at ≈ 43°C, moving into peaks at 51.8°C to 46.9°C. CMH3 at 0.75 µM gives a curve with only a discernable shoulder at 46.96 °C, with the peak of this flat region at 54.0°C. The intensity of the peaks then increases with decreasing CMH3 concentration.

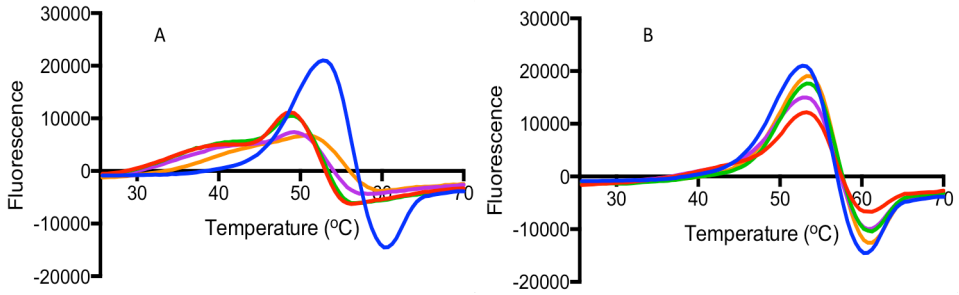

Figure 53: DSF of human IgG1k with CMH4 in 50 mM sodium acetate buffer pH 4.0 **A**= (–) 1 µM human IgG1k with (–) 6.0 µM CMH4, (–) 3.0 µM CMH4, (–) 1.5 µM CMH4, (–) 0.75 µM CMH4. **B**= (–) 1 µM human IgG1k with (–) 0.38 µM CMH4, (–) 0.19 µM CMH4, (–) 0.09 µM CMH4, (–) 0.05 µM CMH4.

The highest concentration of CMH4 tested (6.0 µM) tested compared with the IgG1k control gives a Δ Tm of 12.7°C. 6.0 µM and 3.0 µM CMH4 exhibit melt curves with a shoulder at 40.24°C and 41.67°C respectively, with a major peak at 49.50°C. CMH4 at 1.5 µM gives a long stretched out peak with a shoulder at a temperature of 43.25°C, leading in to a peak at 50.29°C. At 0.75 µM the curve no longer has a typical 'peak' with a long flattened curve with maximal height at 51.78°C. Subsequent concentrations show slight but not significant increases in Tm compared to the IgG1k only.

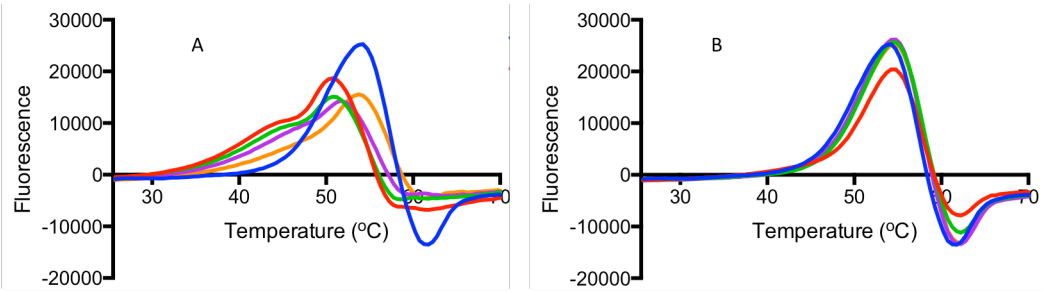

Figure 54: DSF of human IgG1k with CMH5 in 50 mM sodium acetate buffer pH 4.0 **A**= (–) 1 µM human IgG1k with (–) 6.0 µM CMH5, (–) 3.0 µM CMH5, (–) 1.5 µM CMH5, (–) 0.75 µM CMH5. **B**= (–) 1 µM human IgG1k with (–) 0.38 µM CMH5, (–) 0.19 µM CMH5, (–) 0.09 µM CMH5, (–) 0.05 µM CMH5.

The difference in Tm between the highest concentration of CMH5 and the IgG1k control is 9.09°C. The peak of CMH5 with 6.0 µM has a shoulder at Tm 45.36°C, with a

maxima at 51.89°C. This peak shape is mirrored by 3.0 µM with IgG1k, with a shoulder at 45.99°C and a main peak at 51.68°C. The peak at 0.75 µM is a more traditional shape with Tm at 54.43°C, with a higher peak intensity than that of 1.5 µM. Successive decreasing concentrations retain approximately the same Tm.

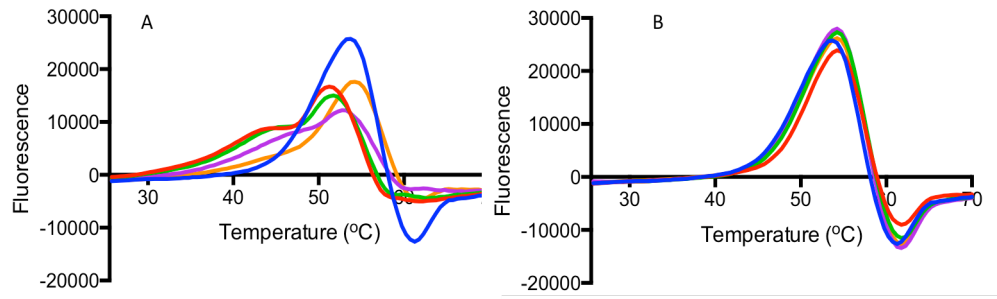

Figure 55: DSF of human IgG1k with CMH6 in 50 mM sodium acetate buffer pH 4.0 **A**= (–) 1 µM human IgG1k with (–) 6.0 µM CMH6, (–) 3.0 µM CMH6, (–) 1.5 µM CMH6, (–) 0.75 µM CMH6. **B**= (–) 1 µM human IgG1k with (–) 0.38 µM CMH6, (–) 0.19 µM CMH6, (–) 0.09 µM CMH6, (–) 0.05 µM CMH6.

Comparing the highest concentration of CMH6 tested against the IgG1k control has a difference in Tm of 8.93°C. The IgG1k with 6.0 µM peak has a Tm of 51.99°C, with a shoulder of lower Tm at 45.01°C. At 1.5 µM, the peak is more flat, not giving the defined shoulder of the more concentrated peaks, with a graduated peak stopping at a Tm of 54.24°C. The Tm of 0.38 µM with IgG1k is 54.38°C with decreasing concentrations of CMH6 remaining with the same Tm of 54.37°C.

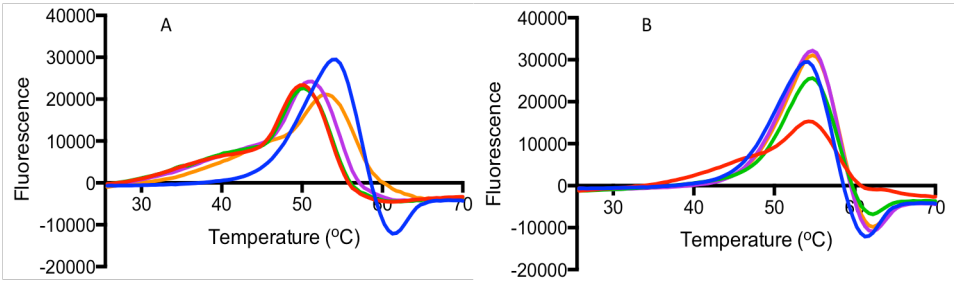

Figure 56: DSF with human IgG1k with CMH7 in 50 mM sodium acetate buffer pH 4.0 **A**= (–) 1 µM human IgG1k with (–) 6.0 µM CMH7, (–) 3.0 µM CMH7, (–) 1.5 µM CMH7, (–) 0.75 µM CMH7. **B**= (–) 1 µM human IgG1k with (–) 0.38 µM CMH7, (–) 0.19 µM CMH7, (–) 0.09 µM CMH7, (–) 0.05 µM CMH7.

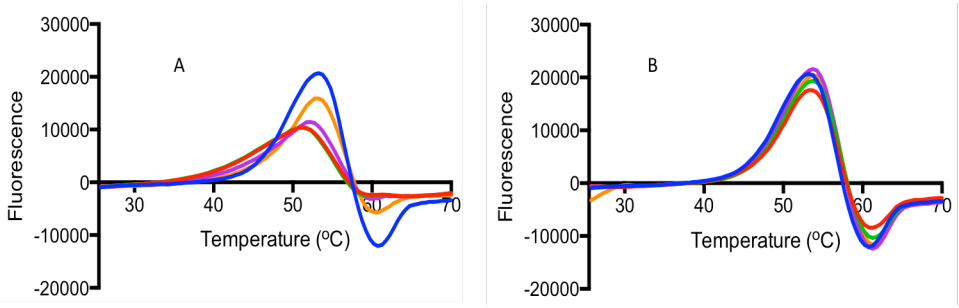

Figure 57: DSF with human IgG1k with CMH8 in 50 mM sodium acetate buffer pH 4.0. **A**= (–) 1 µM human IgG1k with (–) 6.0 µM CMH8, (–) 3.0 µM CMH8, (–) 1.5 µM CMH8, (–) 0.75 µM CMH8. **B**= (–) 1 µM human IgG1k with (–) 0.38 µM CMH8, (–) 0.19 µM CMH8, (–) 0.09 µM CMH8, (–) 0.05 µM CMH8.

The difference between 6.0 µM CMH7 and protein only in this IgG1k DSF is 4.04°C. The 6.0, 3.0, and 1.5 µM concentrations of CMH7 have Tm curves with a sloping shoulder but with no discernable peak at the lower Tm. The Tm peaks for 6.0 and 3.0 µM are 50.34 and 50.43°C, with the peak of 1.5 µM at 51.56°C. The shape of the peak remains for 0.75 µM concentration of CMH7, but shifted toward the higher temperatures, with the peak at 53.50°C. Both 0.09 and 0.05 µM have a slightly increased Tm compared to IgG1k only, 55.1°C and 55.71°C respectively, with IgG1k only Tm 54.38°C.

The highest concentration of CMH8 with IgG1k gives a Tm of 51.51°C compared to IgG1k only Tm of 53.1°C. This gives a difference in Tm of 1.59°C, the smallest difference seen in this group of chemically modified heparins. At 3.0 µM the Tm is the same as 6.0 µM, with 1.5 µM giving a Tm of 52.67°C. The Tm of the subsequent CMH8 concentrations gives Tm slightly higher than that of IgG1k only.

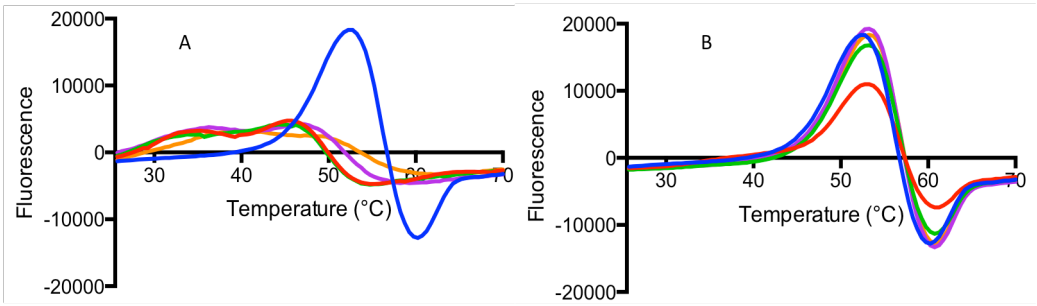

Figure 58: DSF of human IgG1k with CMH9 in 50 mM sodium acetate buffer pH 4.0 **A**= (–) 1 µM human IgG1k with (–) 6.0 µM CMH9, (–) 3.0 µM CMH9, (–) 1.5 µM CMH9, (–) 0.75 µM CMH9. **B**= (–) 1 µM human IgG1k with (–) 0.38 µM CMH9, (–) 0.19 µM CMH9, (–) 0.09 µM CMH9, (–) 0.05 µM CMH9.

Of all the chemically modified heparins tested with IgG1k, CMH9 displays the most disruption to the protein in DSF as seen in the flattening of the melt curves at concentrations > 0.38 µM CMH9. The difference in Tm between the highest concentration of CMH9 tested (6.0 µM) and the protein only control is 17.39°C. However, the curves for the 6.0 - 0.75 µM experiments do not give a defined initial shoulder but they do show a broad peak beginning at ≈ 35°C. The curve for 6.0 µM shows a broad peak with initial maxima at 34.97°C, with a more defined peak at 45.97°C. This shape is mimicked by 3.0 µM CMH9, with 1.5 µM showing a shift in the shoulder to a Tm of 35.45°C with a peak at 47.2 °C. The 0.75 µM concentration of CMH9 curve is wider, with less defined peak regions across the whole of the curve. At lower concentrations of CMH9, the 1st derivative melt curves follow a more traditional curve structure. The last 4 concentrations studied showing a slight stabilisation versus IgG1k control.

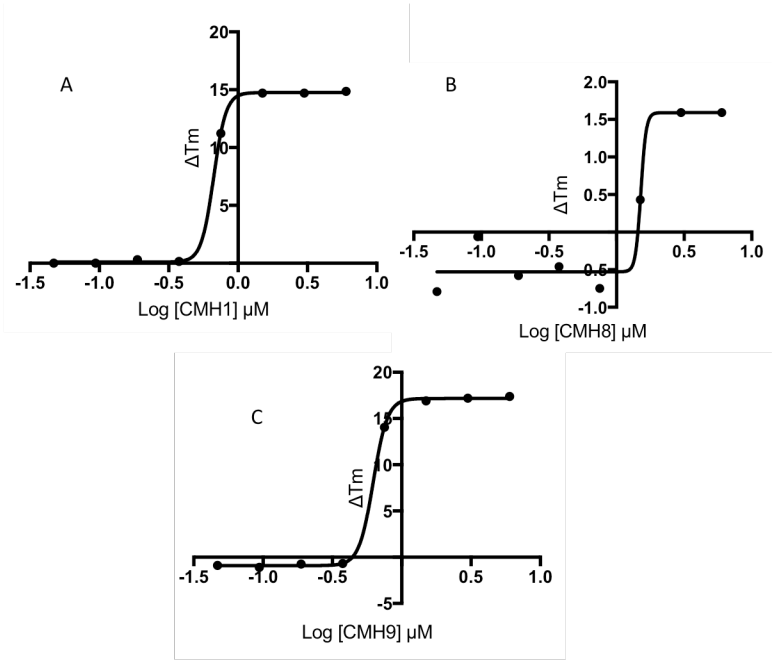

Figure 59: Differential scanning fluorimetry of IgG1k with CMH in 50 mM sodium acetate buffer pH 4.0 Δ Tm from DSF plotted as a function of CMH concentration (compared to IgG1k alone). IgG1k with **A**) 6 µM CMH1 EC_{50} = 0.667 µM **B**) 6 µM CMH8 EC_{50} = 1.513 µM **C**) 6 µM CMH9 EC_{50} = 0.623 µM.

Plotting the change in Tm observed by the addition of increasing concentrations of chemically modified heparin, produces a simple graphical representation of the DSF data. Figure 59 shows the greatest change is seen with the addition of persulphated CMH9 heparin, with CMH1 following closely behind. Unsulphated CMH8 has the highest number of concentrations with no change in Tm, and at the highest CMH8 concentrations tested this Tm change remains the lowest of the library tested.

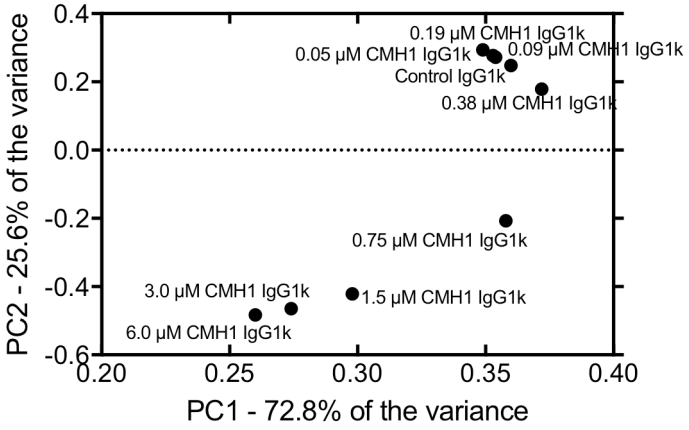

Figure 60: PCA of the 1st derivative DSF melt curve of human IgG1k with CMH1 at varying concentrations.

PCA of CMH1 with IgG1k demonstrates a relationship between 0.75 µM CMH1 and the protein only control in principle component 1, but a difference between 0.75 µM CMH1 and the protein only control in the principle component 2. The concentrations of CMH1 < 0.19 µM are grouped with the IgG1k protein only control. PCA analysis of CMH 2-9 is shown in Figure 61. CMH2-9 with IgG1k in Figure 61 exhibit analogous PCA spectra to CMH1, with PC1 increasing with decreasing CMH1 concentration to the IgG protein only control value, before switching and decreasing again with the low concentrations of CMH1 shown to have a stabilising effect in the 1st derivative DSF data (Figures 61). This suggests both the destabilising and stabilising effects of CMH1 represent +/- structural transitions, which pass through the same intermediate.

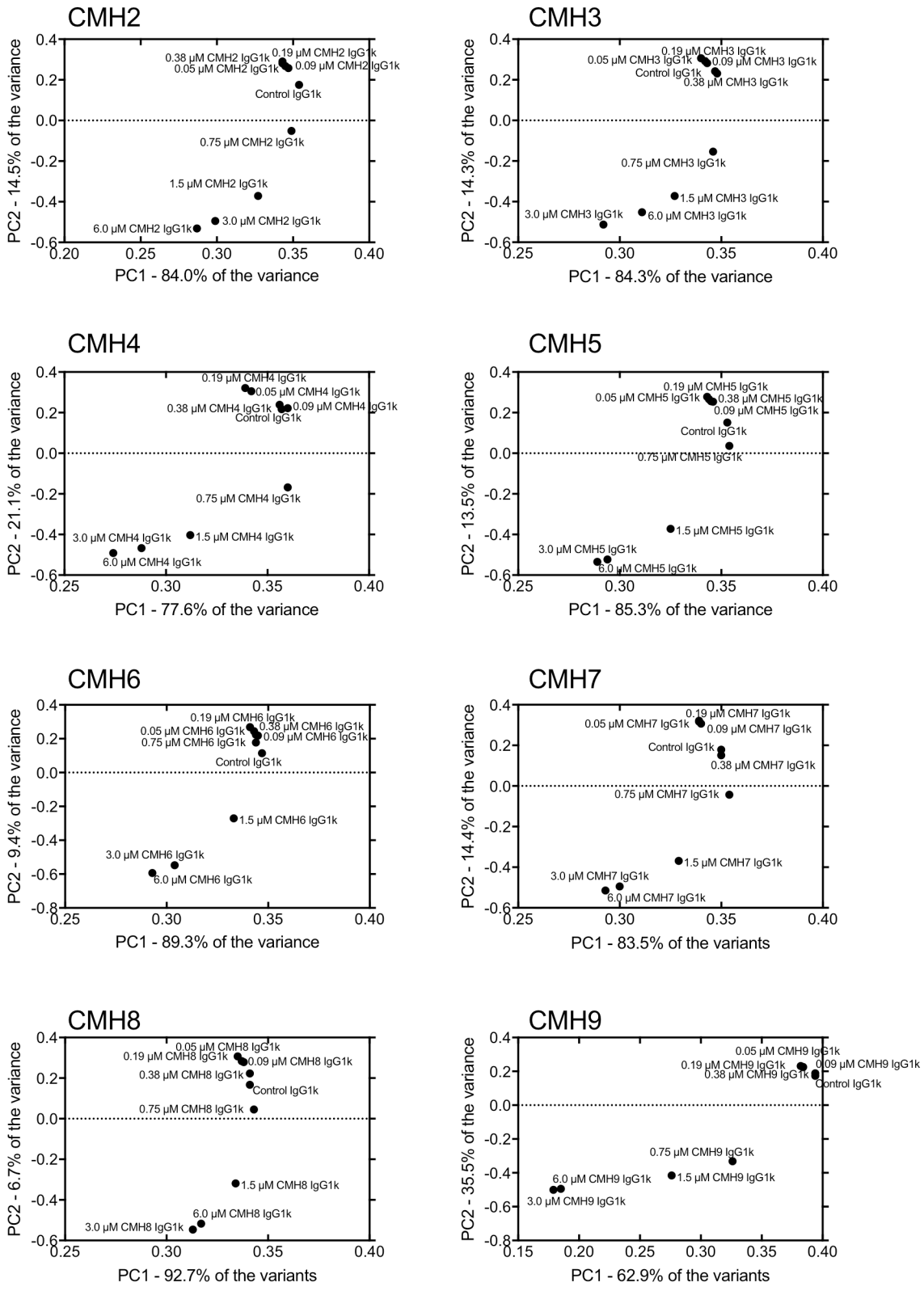

Figure 61: PCA of the 1st derivative DSF data of IgG1k with varying concentrations of CMH 2-9.

Table 8: DSF of human IgG1k with CMH in 50 mM sodium acetate buffer pH 4.0, Δ Tm compared to IgG1k alone.

CMH	Δ Tm (°C)
CMH1	15.38
CMH2	14.05
CMH3	12.21
CMH4	13.56
CMH5	4.10
CMH6	3.97
CMH7	14.24
CMH8	0.50
CMH9	17.89

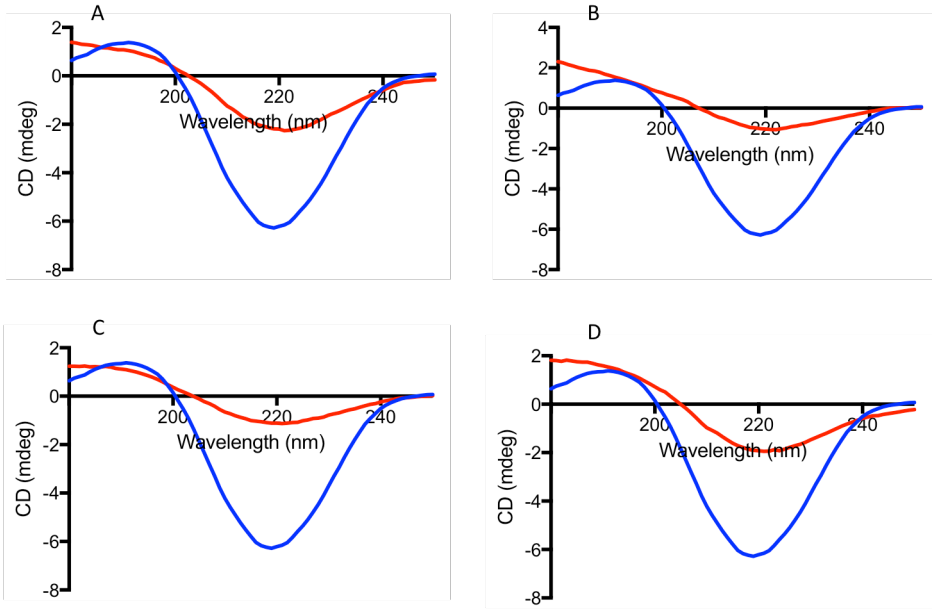

Figure 62: Far-UV circular dichroism spectra of mouse IgG with CMH1-4. Reaction buffer 50 mM sodium acetate pH 4.0. (–) 3 µM mouse IgG with **A**) (–) 3 µM CMH1, **B**) (–) 3 µM CMH2, **C**) (–) 3 µM CMH3, **D**) (–) 3 µM CMH4.

In order to complete a full screen on the chemical modifications and their ability to modify the CD spectra of IgG1k, a mouse IgG isotype control antibody was selected for further circular dichroism experiments because of the amount of material needed, and the cost of this.

The addition of each form of chemically modified heparin removes the peak intensity around λ = 219 nm to differing degrees, with peak shift approximately λ = 2 nm

to the right in all cases (Figure 62). Both IgG with CMH2 (Figure 62B) and CMH3 (Figure 62C) have a similar spectral shapes.

Figure 63 below shows the peak at λ = 219 nm is removed completely with the addition of CMH6 (Figure 63B), and is only very slightly discernable with the addition of CMH5 (Figure 63A) and the persulphated modification, CMH9 (Figure 63E). Mouse IgG with unsulphated CMH8 displays the least change to secondary structure with a spectral shift occurring of 2 nm to λ = 220 nm with a CD intensity most similar to that of the IgG only control spectra (Figure 63D).

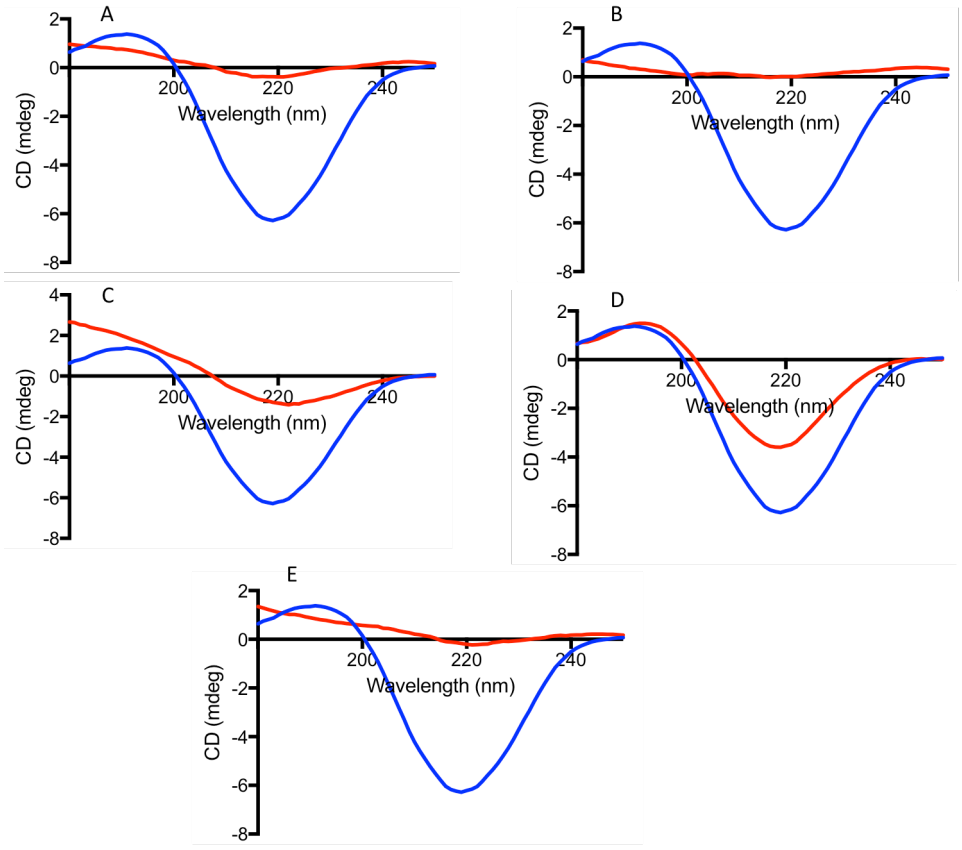

Figure 63: Far-UV circular dichroism spectra of mouse IgG with CMH5-9. Reaction buffer 50 mM sodium acetate pH 4.0. (–) 3 µM mouse IgG with **A**) (–) 3 µM CMH5, **B**) (–) 3 µM CMH6, **C**) (–) 3 µM CMH7, **D**) (–) 3 µM CMH8, **E**) (–) 3 µM CMH9.

This CD data show chemically modified heparin forms, analogues to the varied regions seen in heparan sulphate and heparin, change the secondary structure of the

immunoglobulin, IgG. This structural change shows no simple correlation between spectral features and the arrangement of sulphate groups on both the uronic acid and glucosamine residues.

However, two modified heparins CMH5 and CMH6 show the most perturbation in CD spectra, apart from the per-sulphated heparin. This anomaly is repeated in the DSF data, with the least change in Tm with the addition of 6 µM seen in the same two compounds, apart from unsulphated CMH8 (Table 8). This shows the change in secondary structure identified in CD does not always lead to a change in protein thermal destabilisation and vice versa.

5.2.2 IgG1k stability in the presence of low molecular weight heparins

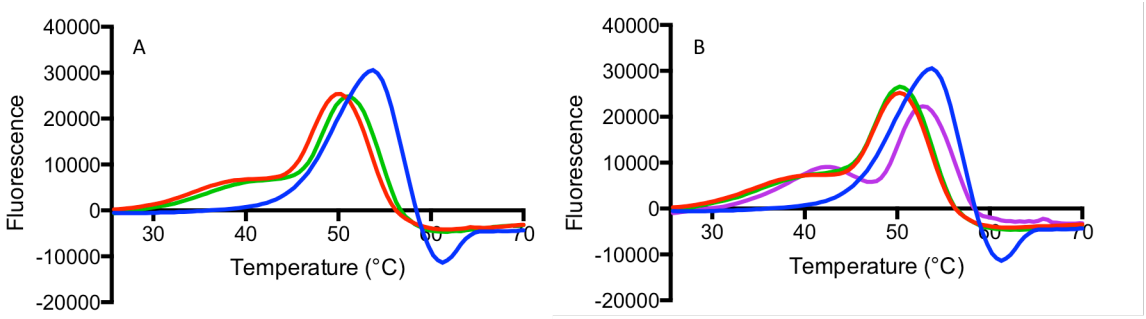

Figure 64: DSF of human IgG1k with LMWH in 50 mM sodium acetate buffer pH 4.0. **A**) (–) 1 µM human IgG1k with (–) 6.0 µM dalteparin, (–) 6.0 µM enoxaparin **B**) (–) 1 µM human IgG1k (–) 6.0 µM tinzaparin, (–) 6.0 µM reviparin, (–) 6.0 µM fondaparinux.

A library of low molecular weight heparins (LMWH) were utilised in DSF to represent modified structures from depolymerisation and synthesis, with known structural features. Tm of human IgG1k alone is 53.46°C with a wide peak (Figure 64). With the addition of 6.0 µM CMH1, the peak Tm shifts to a shouldered peak with Tm of 38.04°C and 49.78°C with the highest intensity peak at 49.78°C. Addition of dalteparin at 6.0 µM gives a similar shouldered peak at Tm of 38.79°C and 50.23°C with the highest intensity at 50.23°C. Enoxaparin at the same molar concentration gives a peak Tm with IgG1k at 40.47°C and 51.38 °C, with the 51.38°C peak the same intensity as dalteparin.

The tinzaparin peak is the same shape as dalteparin and enoxaparin and the Tm of the peak and shoulder is between these two LMWH, at a temperature of 39.62°C and 50.61°C. Reviparin at the same molar concentration has a peak with a less defined shoulder, with the Tm at 50.66°C. Fondaparinux with IgG1k gives a double peak with Tm of 42.62°C and 53.17°C. The main peak of fondaparinux mirrors the high intensity peak of IgG1k protein control.

The synthetic pentasaccharide fondaparinux has a limited effect on the thermal stability if human IgG1k, with the PCA demonstrating grouping with IgG1k protein only control, compared to the distribution of the other LMWH tested. Dalteparin is the most similar to UF PMH in the PCA, which is corroborated in the 1st derivative DSF spectra. Dalteparin, reviparin and tinzaparin are grouped together with enoxaparin occupying a intermediate position between the LMWH group and fondaparinux with IgG1k (Figure 65).

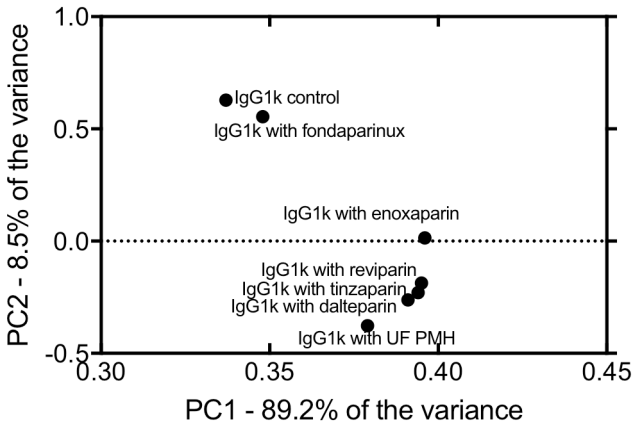

Figure 65: PCA of 1st derivative DSF of human IgG1k with LMWH in 50 mM sodium acetate buffer pH 4.0.

5.2.3 IgG1k stability in the presence of GAGs and heparin controls

Other GAGs were then assessed for their ability to perturb the Tm of IgG1k (Figure 66). Alongside these GAGs, a Na_2SO_4 control was also conducted to identify any action due to sulphate moieties alone, and the disaccharide standard 6 (UA(2S)–GlcNS(6S)) was used as a depolymerised heparin control.

The greatest change in Tm seen with all that GAGs, disaccharides and Na_2SO_4 tested is seen on the addition of 6.0 µM UF PMH; a Tm change of 14.26°C. The Tm shift between IgG1k alone and the highest intensity peak at 6.0 µM UF PMH is 3.80°C. The Na_2SO_4 control does not appreciably change the Tm of IgG1k (Figure 66A) suggesting the incidence of sulphate functional groups on the glycopolymer are not the sole cause of protein thermal destabilisation. Addition of 12.0 µM HS exhibits a main peak with a shoulder with Tm 43.97°C and a peak Tm of 51.22°C. The reduction in Tm from IgG1k alone to 12.0 µM HS to the shoulder Tm gives a 9.06°C change in Tm.

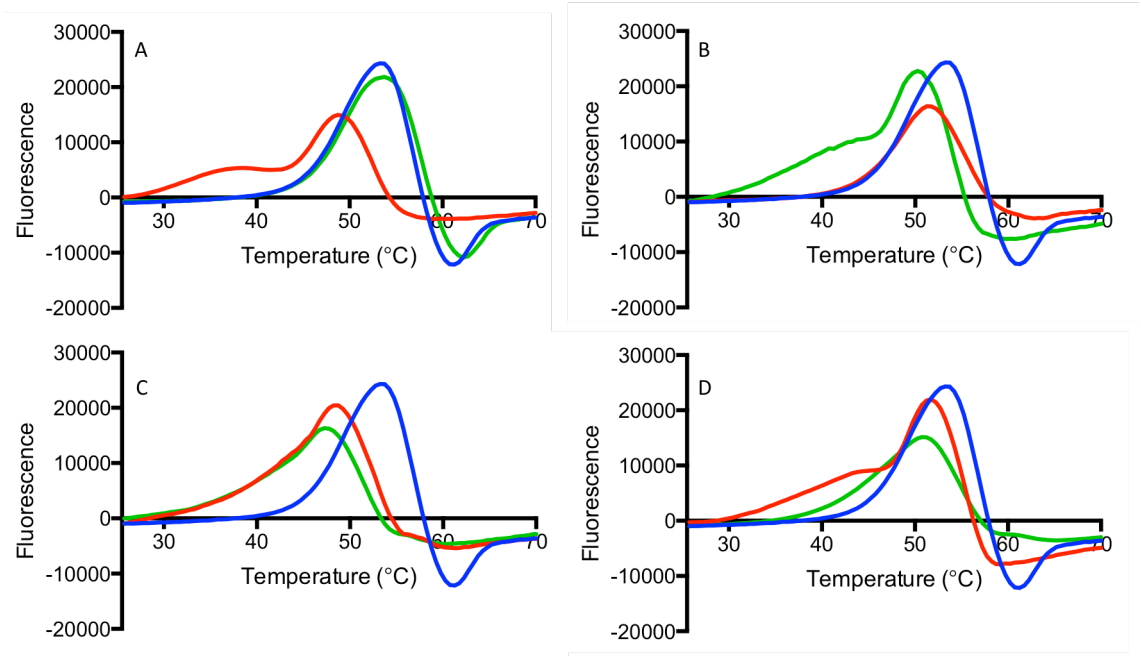

Figure 66: Differential scanning fluorimetry of human IgG1k with GAGs and sulphate controls in 50 mM sodium acetate buffer pH 4.0 (–) 1 µM human IgG1k **A**) (–) 6.0 µM UF PMH, (–) 500 nM sodium sulphate, **B**) (–) 6.0 µM UA(2S)-GlcNS(6S) disaccharide (–) 12.0 µM HS, **C**) (–) 6.0 µM CSA, (–) 6.0 µM CSC, **D** (–) 6.0 µM DS, (–) 6.0 µM HA.

In DS the peak shape also includes a shoulder peak at Tm 45.72°C, with the larger fluorescence peak Tm of 52.62°C. The change in Tm seen with DS is 7.31°C if the shoulder Tm is compared to IgG1k alone. The next largest shift in Tm is seen with CSC, with the reduction in Tm on addition of 6.0 μM CSC of 4.61°C, which is a greater change than comparing the highest intensity peak of UF PMH and IgG1k. The Tm of CSC is 48.42°C, with a long sloping curve up to the peak maxima. CSA then follows, with 6.0 μM CSA with IgG1k causing a Tm reduction of 3.15°C to a Tm of 49.88°C. HA and UA(2S)-GlcNS(6S) (DS6) both have the same Tm with IgG1k, with Tm of 52.05°C with a negligible change in Tm compared to IgG1k only of 0.98°C.

The PCA analysis of the DSF data from Figure 67 indicates a similarity in the principle components of CSA and UF PMH in the thermal denaturation spectra of IgG1k. CSC and CSA demonstrate differences in principle component 1 suggesting the carbon-4 vs carbon-6 sulphation shows a distinction in the thermal denaturation of IgG1k.

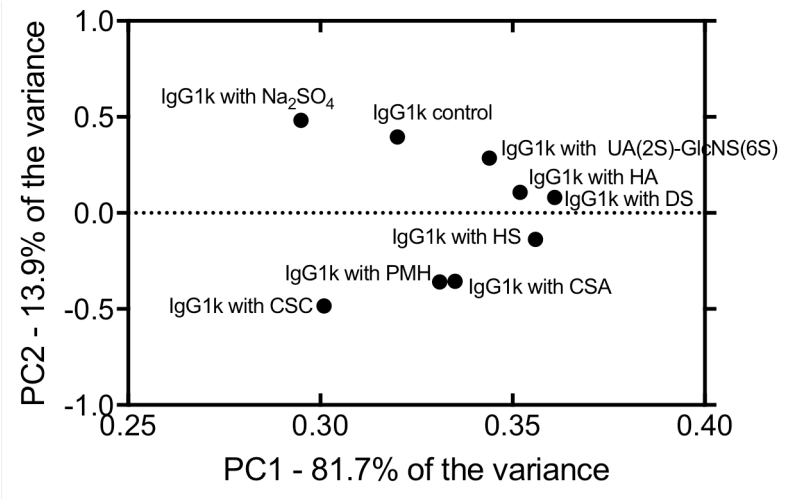

Figure 67: PCA from DSF 1st derivative data of human IgG1k with GAGs and sulphate controls.

5.2.4 IgG1k stability in the presence of size defined heparin fractions

The addition of d.p.2 has the same melt curve shape as IgG1k alone, with a small increase in Tm increase of 1.03°C. IgG1k with d.p.4 changes the curve shape to a two-peak structure with the Tm of 50.30°C and 57.89°C. Addition of d.p.6 modifies the curve shape again to a smaller initial peak with larger main peak, with Tm of 45.61°C and 54.96°C respectively. Increasing the heparin size with d.p.8 produces a peak with shoulder at lower temperatures with the Tm being 44.87°C and 53.58°C for the main peak. The d.p.12 fraction demonstrates shoulder peak Tm at 44.82°C with the main peak at 51.88°C. Each subsequent increasing d.p. has similar curve shape to d.p.12, with progressive reduction in the Tm. Only d.p.14 with IgG1k does not have a clear peak shoulder. The size fragment with the Tm closest to that of UF PMH is d.p.18. The fraction to d.p.20 has a higher main peak Tm at 52.35°C and is comparable with the Tm of d.p.10.

Table 9: DSF Tm of PMH polymerization (d.p.) fragment with human IgG1k in 50 mM sodium acetate buffer pH 4.0.

d.p.	Tm 1 (°C)	Tm 2 (°C)
IgG1k control		53.37
2		54.40
4	50.30	57.89
6	45.61	54.96
8	44.87	53.58
10	44.84	52.76
12	44.82	51.88
14		51.25
16	39.98	50.44
18	39.65	50.39
20	39.68	52.35
UF PMH	38.74	49.58

5.2.5 IgG1k stability changes at differing buffer concentrations and pH

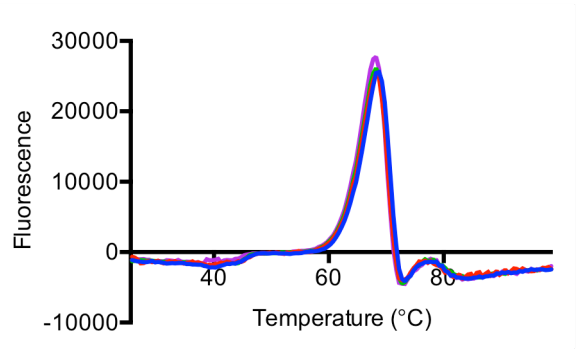

Figure 68: DSF of human IgG1k with UF PMH in PBS buffer pH 7.4 ± UF PMH **A**) (–) 1 µM human IgG1k region with (–) 6.0 µM UF PMH, (–) 137 mM NaCl.

In order to determine the buffer concentration and pH dependence of the interaction between IgG1k and UF PMH, structural stability changes of IgG1k with DSF were determined.

DSF with human IgG1k in PBS buffer was conducted to resolve if the heparin destabilisation of IgG1k occurred at pH 7.4 in physiological buffer (Figure 68). This DSF experiment showed no structural stability change (Tm of 68°C) with the addition of UF PMH in PBS buffer pH 7.4.

The binding affinity between IgG1k and heparin has been determined using affinity Hi-Trap HPLC with sodium acetate and PBS buffer tested under a range of pH.

Figure 69 is the heparin affinity chromatogram of human IgG1k in heparin Hi-Trap HPLC, demonstrating heparin binding with both pH 4.0 and pH 5.0 PBS, but indicates no heparin binding at pH 6.0. At pH 5.0 IgG1k binds heparin with an affinity of 928 mM, with the affinity for heparin increasing to 1.08 M at the lower pH 4.0 (Figure 69). The DSF in Figure 68 suggests changes in thermal stability signify no interaction between the human IgG1k and UF PMH in PBS at pH 7.4, and the heparin binding affinity at this pH reflects this (Figure 69). Heparin binding affinity of human IgG1k in the original buffer of 50 mM sodium acetate pH 4.0 is given as 849 mM as shown in Figure

70. Across two different buffers at pH 4.0, both mouse and human IgG tested bind to heparin as shown through heparin hi-trap affinity chromatography, with elution by 2M NaCl.

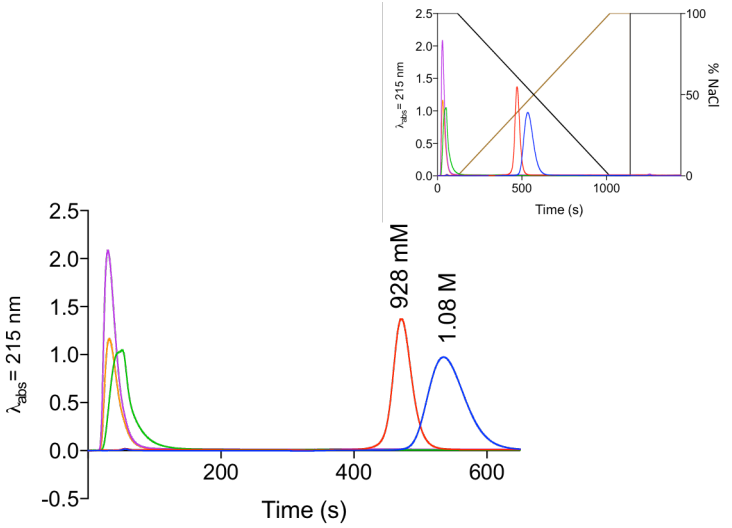

Figure 69: Human IgG1k in heparin HiTrap affinity HPLC in PBS at differing pH (4.0 – 7.4) and elution with linear gradient of 2M NaCl. (–) PBS pH 4, (–) PBS pH 5.0, (–) PBS pH 6.0, (–) PBS pH 7.0, (–) PBS pH 7.4.

The mouse isotype control IgG (Figure 71) used as a cheaper IgG proxy in far-UV CD demonstrated heparin binding in PBS, between pH 4.0 and 6.0. At pH 6.0, the IgG1k affinity for heparin is 704 mM, increasing to 933 mM at pH 5.0, and further increasing to 1.05 M affinity at pH 4.0. At a pH closer to physiological (pH ≥ 7.0) mouse IgG1k does not bind the heparin column.

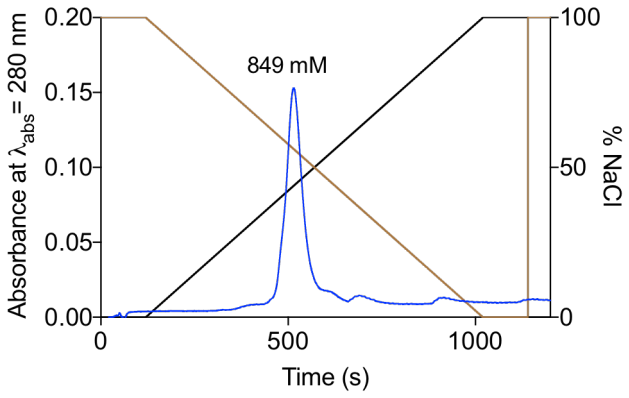

Figure 70: Human IgG1k in heparin HiTrap affinity HPLC in 50 mM sodium acetate pH 4.0 with 2M NaCl elution

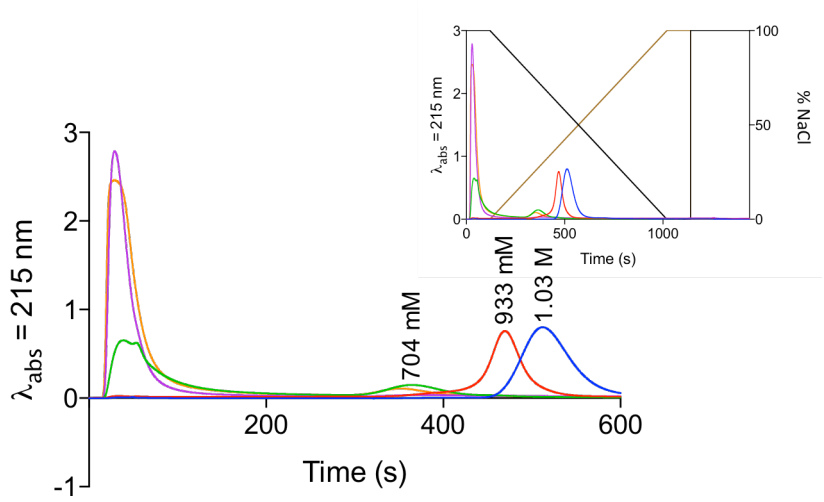

Figure 71: Mouse IgG isotype control in heparin HiTrap affinity HPLC in PBS at differing pH and elution with 2M NaCl. (–) PBS pH 4, (–) PBS pH 5.0, (–) PBS pH 6.0, (–) PBS pH 7.0, (–) PBS pH 7.4.

5.2.6 IgG2k stability in the presence of chemically modified heparins

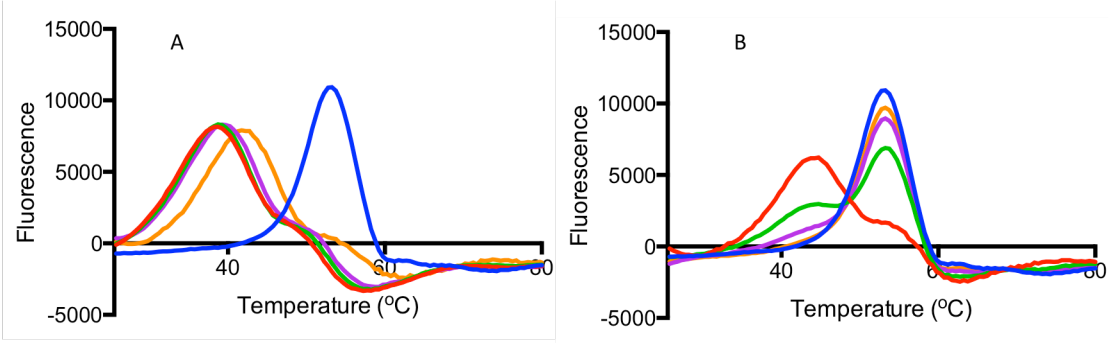

Figure 72: DSF of human IgG2k with CMH1 in 50 mM sodium acetate buffer pH 4.0 **A**= (–) 1 µM human IgG2k with (–) 6.0 µM CMH1, (–) 3.0 µM CMH1, (–) 1.5 µM CMH1, (–) 0.75 µM CMH1. **B**= (–) 1 µM human IgG2k with (–) 0.38 µM CMH1, (–) 0.19 µM CMH1, (–) 0.09 µM CMH1, (–) 0.05 µM CMH1.

The IgG2k 1st derivative melt peak has a Tm of 54.12°C and the difference between the highest concentration of CMH1 tested (6.0 µM) and IgG2k alone is 15.38°C. CMH1 at 6.0 µM with IgG2k has a peak Tm at 38.74°C, however this peak is more broad than the protein only peak. Concentrations of 3.0 µM and 1.5 µM CMH1 mirror the shape

of 6.0 µM CMH1 with IgG2k. The Tm of CMH1 at 0.75 µM is shifted to a higher temperature compared to the first 3 concentrations tested with a Tm of 42.33°C. The peak of CMH1 at 0.75 µM is wide toward the higher temperature end, but does not feature a shoulder or peak at higher temperatures like the higher CMH1 concentrations. The peak shape then changes with decreasing concentration of CMH1, with the 0.19 µM concentration curve containing a small shoulder peak to mirror the main peak of the higher concentrations (at 44.17°C) but the major peak at this concentration being at 54.09°C, approximately the same concentration of the shoulder at concentration 0.38 µM.

The difference between the IgG2k peak and the highest concentration of CMH2 tested is 14.05°C. The CMH2 and IgG2k peak at 6.0 µM has a double peak with the first peak Tm at 40.27°C and the second at 49.59°C. CMH2 at 3.0 µM and 1.5 µM also have this double peak structure, with the Tm of peaks at 3.0 µM 41.44°C and 50.42°C. The curve of 0.75 µM CMH2 seems to hold an intermediate position between the two peak concentrations and more standard single peak at concentrations of 0.38 µM CMH2 and lower. At 0.75 µM the peak shape is a wide peak with Tm of 53.91°C and concentrations of 0.38 µM and below have approximately the same Tm of around 54°C.

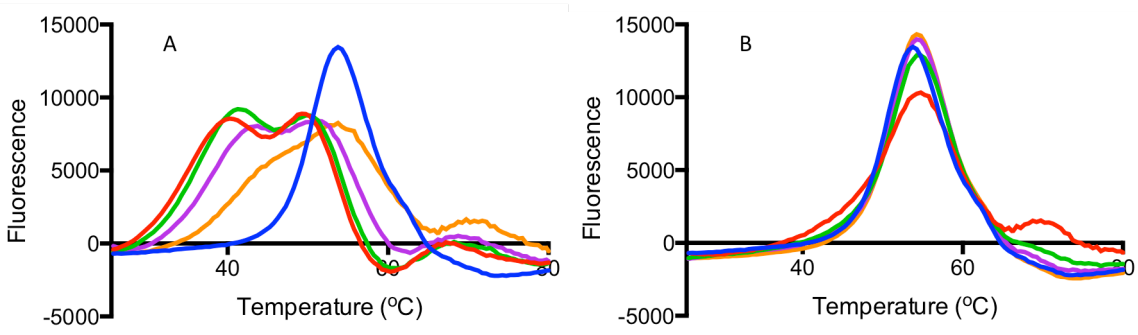

Figure 73: DSF of IgG2k with CMH2 in 50 mM sodium acetate buffer pH 4.0 **A**= (–) 1 µM human IgG2k with (–) 6.0 µM CMH2, (–) 3.0 µM CMH2, (–) 1.5 µM CMH2, (–) 0.75 µM CMH2. **B**= (–) 1 µM human IgG2k with (–) 0.38 µM CMH2, (–) 0.19 µM CMH2, (–) 0.09 µM CMH2, (–) 0.05 µM CMH2.

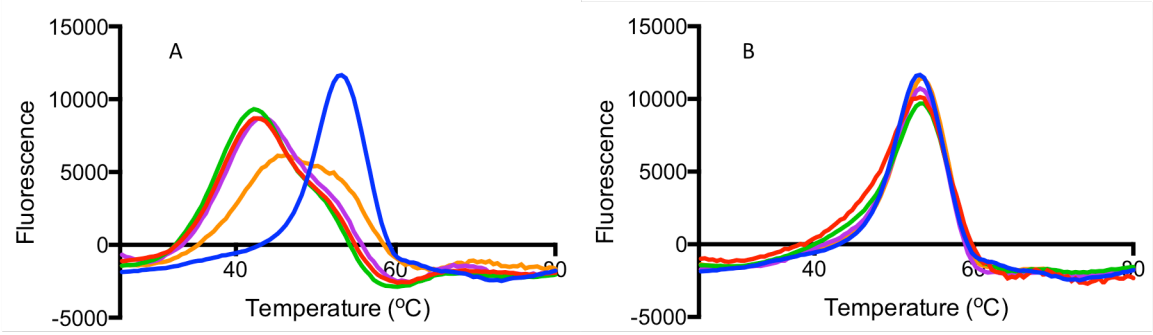

Figure 74: DSF of IgG2k with CMH3 in 50 mM sodium acetate buffer pH 4.0. **A**= (–) 1 µM human IgG2k with (–) 6.0 µM CMH3, (–) 3.0 µM CMH3, (–) 1.5 µM CMH3, (–) 0.75 µM CMH3. **B**= (–) 1 µM human IgG2k with (–) 0.38 µM CMH3, (–) 0.19 µM CMH3, (–) 0.09 µM CMH3, (–) 0.05 µM CMH3.

The change in Tm between no CMH3 and the 6.0 µM CMH3 is 12.21°C. With 6.0 µM, the Tm of IgG2k shifts to a lower temperature of 41.72°C, with a small shoulder at approximately 50 °C. CMH3 at 3.0 µM gives a higher intensity peak at its Tm of 43.60°C, however the shoulder at 50°C is less pronounced. At 1.5 µM the Tm with IgG2k is 43.74°C with the same intensity as 6.0 µM CMH3, including a similar shaped shoulder at 50°C. The intermediate concentration between the two families of peaks is 0.75 µM, with this curve more broad and flattened, demonstrating a Tm of 46.77°C, mirroring the shape of the shoulder on the peaks at higher concentrations of CMH3. The subsequent lower concentration peaks mimic the shape of the IgG2k only peak with the Tm for the peaks the same at 53.54°C.

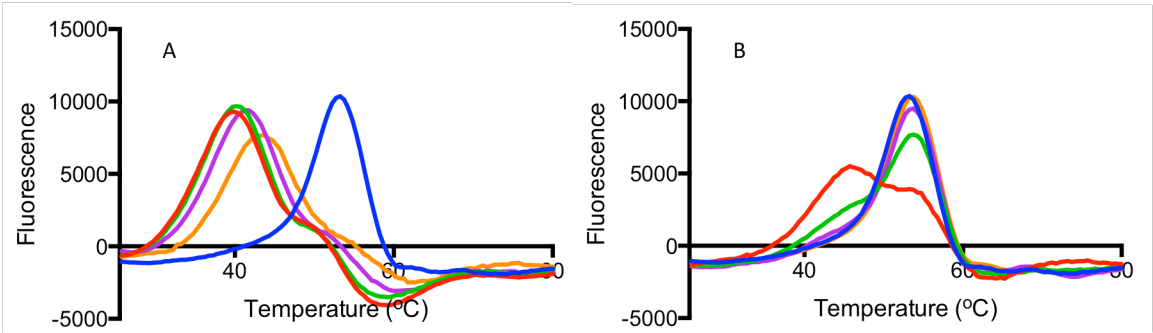

Figure 75: DSF of IgG2k with CMH4 in 50 mM sodium acetate buffer pH 4.0 **A**= (–) 1 µM human IgG2k with (–) 6.0 µM CMH4, (–) 3.0 µM CMH4, (–) 1.5 µM CMH4, (–) 0.75 µM CMH4. **B**= (–) 1 µM human IgG2k with (–) 0.38 µM CMH4, (–) 0.19 µM CMH4, (–) 0.09 µM CMH4, (–) 0.05 µM CMH4.

The Tm shift seen when measuring the fluorescence with 6 µM of CMH4 versus IgG2k alone is 13.56°C. Melting temperature of the protein alone in this assay was 53.8°C. The Tm shift with addition of 6.0 µM CMH4 moves to a main peak at 40.24°C, with a smaller shoulder peak at 49.02°C. This peak shape is similar at 3.0 µM CMH4, with Tm at this concentration being 40.97°C and shoulder at 49.34°C. Tm at 0.75 µM CMH4 is 43.58°C. At lower concentrations, the peaks change shape to resemble the protein only peak with 0.19 µM CMH4 Tm at 54.33°C, and a sloping shoulder at lower temperature (Tm of 46.80°C) similar to the major peaks seen at higher concentrations. The further 2 lower concentrations tested of 0.09 µM and 0.05 µM have Tm of 54.20°C and 53.89°C respectively.

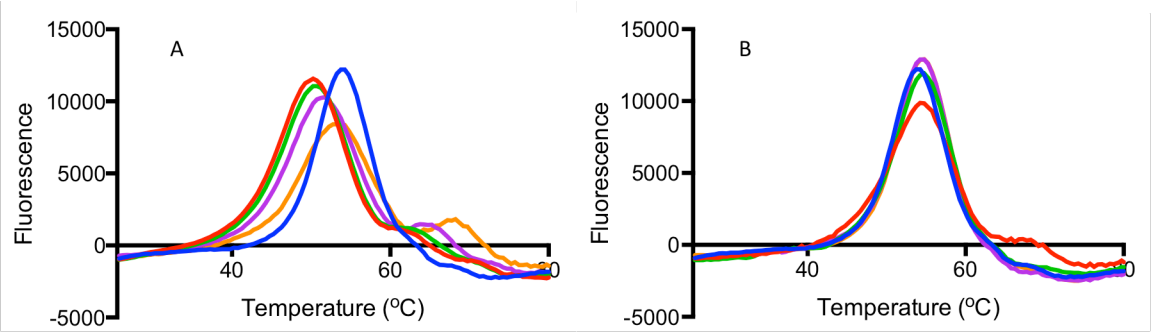

Figure 76: DSF of IgG2k with CMH5 in 50 mM sodium acetate buffer pH 4.0 **A**= (–) 1 µM human IgG2k with (–) 6.0 µM CMH5, (–) 3.0 µM CMH5, (–) 1.5 µM CMH5, (–) 0.75 µM CMH5. **B**= (–) 1 µM human IgG2k with (–) 0.38 µM CMH5, (–) 0.19 µM CMH5, (–) 0.09 µM CMH5, (–) 0.05 µM CMH5.

The shift in Tm seen upon addition of 6.0 µM of CMH5 with IgG2k is 4.1°C, with IgG1k alone Tm of 54.46°C. CMH5 at 6.0 µM also has a secondary shoulder at 62.63°C. The 3.0 µM CMH5 concentration has a Tm of 50.75°C and a shoulder at 62.97 °C. The Tm then shifts with 1.5 µM to 51.87°C, with a more pronounced shoulder peak at 65.02°C. CMH5 at 0.75 µM again acts as an intermediate peak at lower intensity with Tm of 53.16°C and shoulder at 68.06°C. CMH5 at 0.38 µM has a Tm of 54.9°C with a shoulder at 67.86°C.

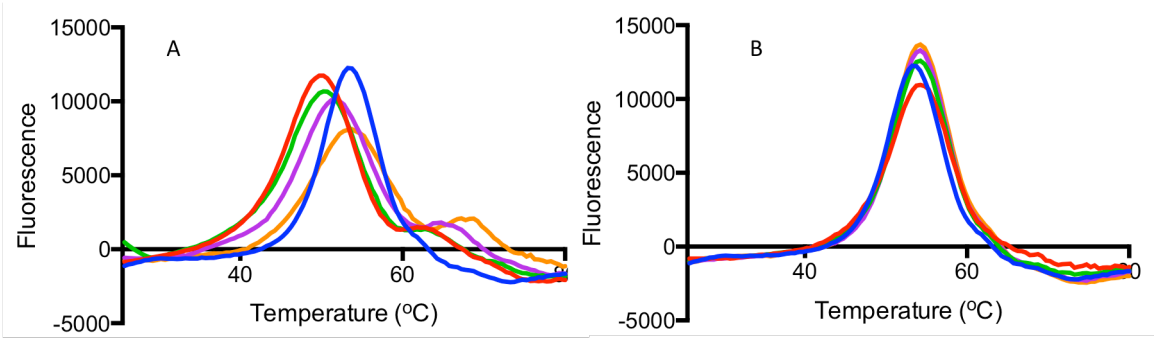

Figure 77: DSF of IgG2k with CMH6 in 50 mM sodium acetate buffer pH 4.0. **A**= (–) 1 µM human IgG2k with (–) 6.0 µM CMH6, (–) 3.0 µM CMH6, (–) 1.5 µM CMH6, (–) 0.75 µM CMH6. **B**= (–) 1 µM human IgG2k with (–) 0.38 µM CMH6, (–) 0.19 µM CMH6, (–) 0.09 µM CMH6, (–) 0.05 µM CMH6.

The IgG2k peak is shifted to a lower Tm upon addition of 6.0 µM CMH6, with a Tm change of 3.97°C. The 6.0 µM CMH6 peak has a Tm of 49.91°C, and a shoulder at 51.99 °C. Decreasing concentrations of CMH6 increase the Tm of IgG2k with 3.0 µM Tm of 45.51°C with a shoulder at 52.49°C. At 1.5 µM, the peak increases to 54.24°C with a shoulder peak at 65.39°C. The intensity drops to its lowest in 0.75 µM CMH6 with IgG2k, with the Tm 65.67°C, with the shoulder the highest with a Tm of 67.90°C. A concentration of 0.38 µM CMH6 gives a Tm of 54.38°C with increased intensity versus 0.75 µM, with no shoulder.

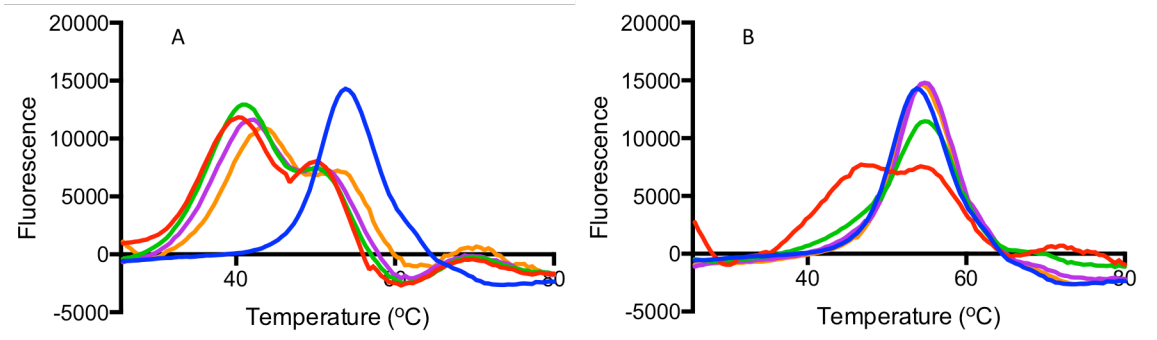

Figure 78: DSF of IgG2k with CMH7 in 50 mM sodium acetate buffer pH 4.0 **A**= (–) 1 µM human IgG2k with (–) 6.0 µM CMH7, (–) 3.0 µM CMH7, (–) 1.5 µM CMH7, (–) 0.75 µM CMH7. B= (–) 1 µM human IgG2k with (–) 0.38 µM CMH7, (–) 0.19 µM CMH7, (–) 0.09 µM CMH7, (–) 0.05 µM CMH7.

The IgG2k peak, with addition of 6.0 µM CMH7, causes the Tm to drop to 40.01°C, a reduction in Tm of 14.24°C. The shape of the 6.0 µM to 0.75 µM peaks is that of a major

peak with a large shoulder peak at a higher temperature, and a shoulder region at ≈ 69°C. The largest peak of 6.0 µM occurs with a Tm of 40.01°C, the second occurs at 51.07 °C with a third flattened hump at 68.45°C. This pattern is the same in 3.0 µM with the Tm of these three regions at 40.76°C, 50.38°C and 69.66°C. The intermediate peak occurs at 0.38 µM with a wide curve with Tm of 46.91°C and 55.06°C and a smaller shoulder at 69.90°C. At concentrations of 0.19 µM, the CMH7 and IgG2k peak resembles the protein only peak, with a Tm of 55.25°C and no discernable shoulder peak.

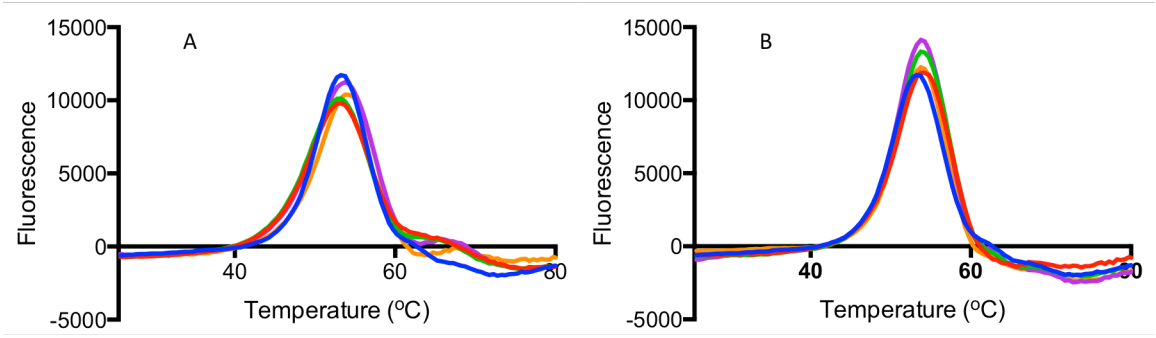

Figure 79: DSF of IgG2k with CMH8 in 50 mM sodium acetate buffer pH 4.0 **A**= (–) 1 µM human IgG2k with (–) 6.0 µM CMH8, (–) 3.0 µM CMH8, (–) 1.5 µM CMH8, (–) 0.75 µM CMH8. **B**= (–) 1 µM human IgG2k with (–) 0.38 µM CMH8, (–) 0.19 µM CMH8, (–) 0.09 µM CMH8, (–) 0.05 µM CMH8.

The IgG2k 1st derivative DSF peaks from CMH8 show the least change in thermal stability upon addition of a member of the chemically modified heparin library, with the reduction in Tm seen on addition of 6.0 µM CMH8 only 0.5°C.

The difference between the Tm of IgG2k with 6.0 µM CMH9 is the largest shift in Tm seen with this immunoglobulin is 17.89°C. At 6.0 µM the peak is shifted to a wide shape with Tm of 34.97°C. This shape is also seen in concentrations up to 0.75 µM, with Tm of 35.02°C (3.0 µM), 35.9°C (1.5 µM) and 37.46°C (0.75 µM). There are two intermediate peaks at 0.38 µM and 0.19 µM CMH9. At 0.38 µM, the major peak Tm is 38.94°C, and a second peak at 54.14°C, which mimics the Tm the lower concentrations.

At 0.19 µM the major peak is shifted to the higher temperature of 54.06°C, but a minor peak remains at the lower Tm of 38.95°C.

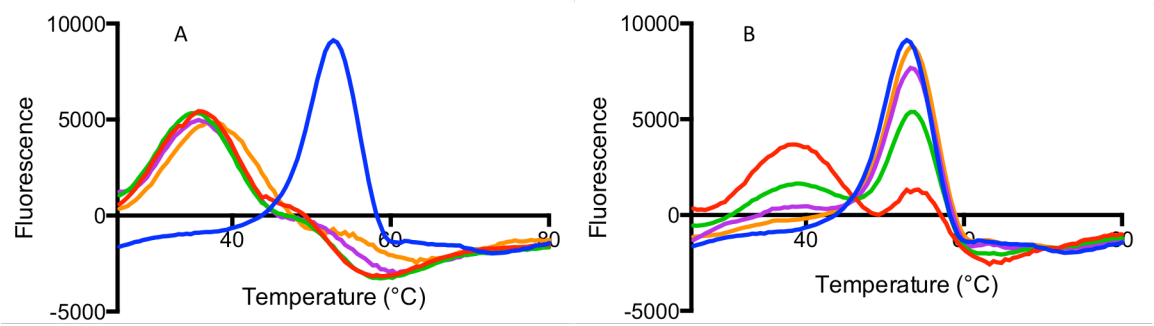

Figure 80: DSF of IgG2k with CMH9 in 50 mM sodium acetate buffer pH 4.0. **A**= (–) 1 µM human IgG2k with (–) 6.0 µM CMH9, (–) 3.0 µM CMH9, (–) 1.5 µM CMH9, (–) 0.75 µM CMH9. **B**= (–) 1 µM human IgG2k with (–) 0.38 µM CMH9, (–) 0.19 µM CMH9, (–) 0.09 µM CMH9, (–) 0.05 µM CMH9.

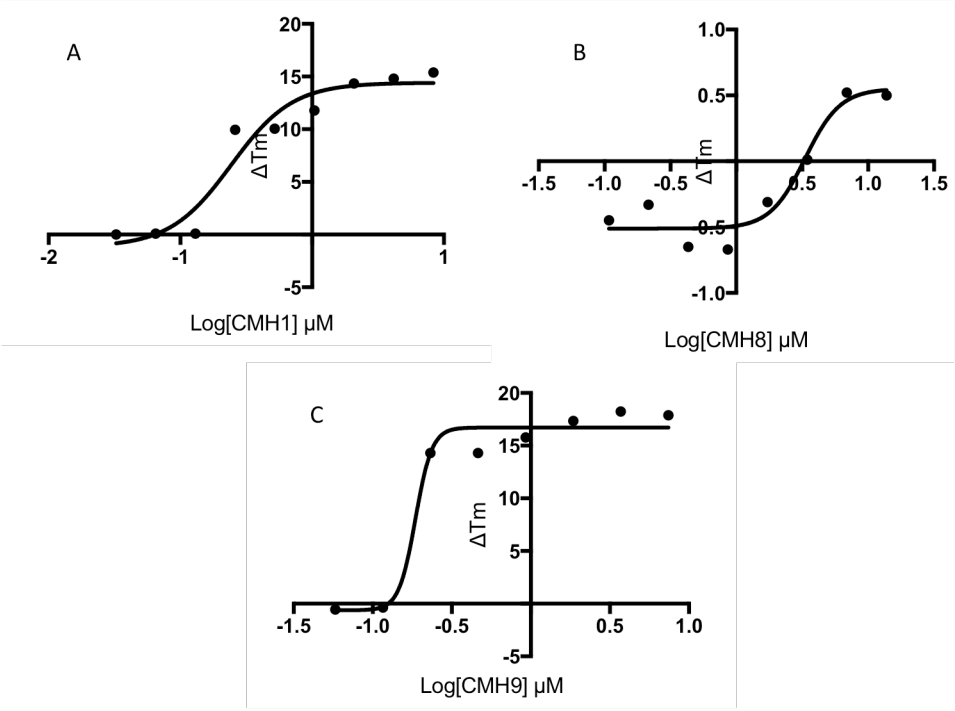

Figure 81: DSF Tm taken from 1st derivative data of IgG2k with CMH in 50 mM sodium acetate buffer pH 4.0. Δ Tm (compared to IgG2k control). IgG2k with **A**) 6 µM CMH1 EC_{50} = 0.243 µM **B**) 6 µM CMH8 EC_{50} = 3.327 µM **C**) 6 µM CMH9 EC_{50} = 0.1863 µM

Plotting the change in Tm observed by the addition of differing concentrations of chemically modified heparin produces a simple graphical representation of the DSF data. Figure 81 demonstrates the greatest change is seen with the addition of

persulphated CMH9 heparin. Unsulphated CMH8 has the highest number of concentrations with no change in Tm, and at the highest CMH8 concentrations tested this Tm change is the smallest of the chemically modified heparin library.

PCA of the CMH with IgG2k demonstrated the similarities in variance between each concentration of CMH explored in the thermal denaturation DSF experiments. CMH1 PCA is shown in Figure 82 with the full CMH library with IgG2k in Figures 72. CMH 1, 4 and 9 display similar relationships in the PC2, and CMH 2, 3, 5, 6 and 7 have similar distrubutions. CMH8 has no variation in PC1, with spread occuring only in the second principle component.

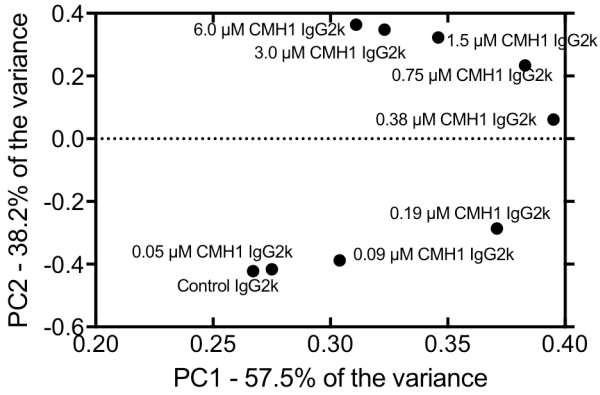

Figure 82: PCA from the 1st derivative DSF data of CMH1 with human IgG2k.

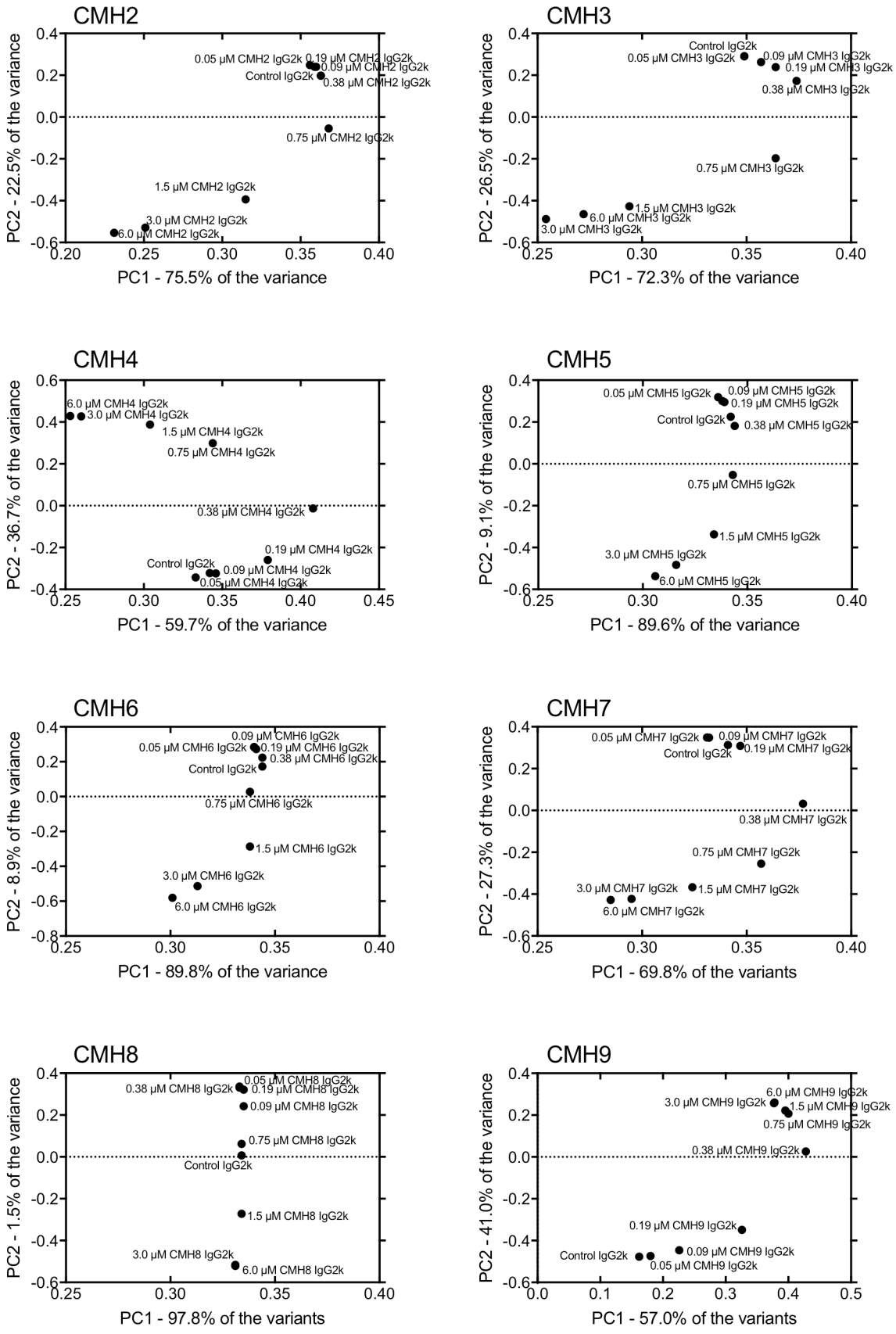

Figure 83: PCA of 1st derivative DSF data of CMH2-9 with human IgG2k.

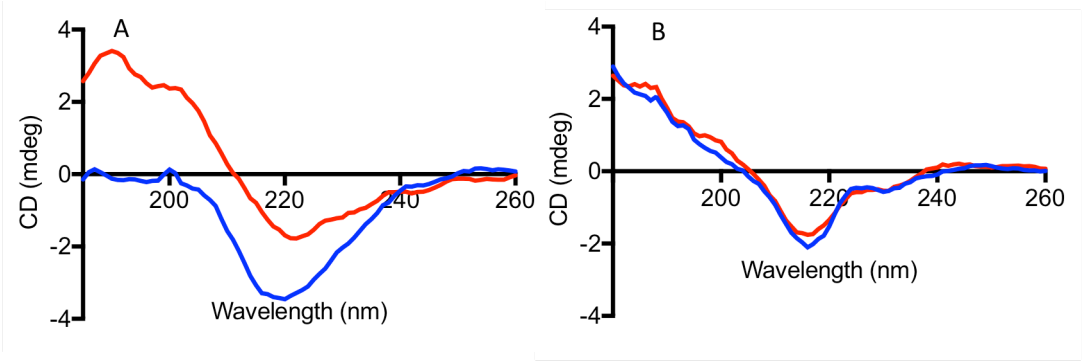

Figure 84: Far-UV CD spectra of human IgG2k ± UF PMH in acetate buffer and PBS **A**) 50 mM sodium acetate buffer pH 4.0 with (–) 3 µM human IgG2k with (–) 3 µM UF PMH **B**) PBS buffer pH 7.4 with (–) 3 µM human IgG2k with (–) 3 µM UF PMH.

The far-UV CD spectra of IgG2k in 50 mM sodium acetate buffer is shown in Figure 84, with the addition of UF PMH shifting the λ = 219 nm signal for β-sheet to λ = 222 nm. IgG2k alone in this buffer does not have a positive ellipticity reading, but with CMH1, the spectra are shifted toward the positive. IgG2k in pH 7.4 PBS the spectrum has similar features, suggesting no heparin interaction causing secondary structure changes.

5.2.7 IgG2k stability in the presence of low molecular weight heparins

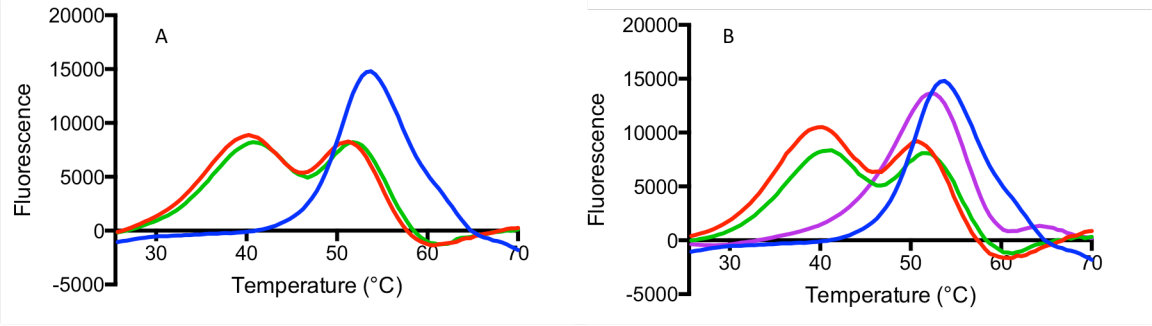

Figure 85: DSF of IgG2k with LMWH in 50 mM sodium acetate buffer pH 4.0 **A**) (–) 1 µM human IgG2k with (–) 6.0 µM dalteparin, (–) 6.0 µM enoxaparin **B**) (–) 1 µM human IgG2k with (–) 6.0 µM tinzaparin, (–) 6.0 µM reviparin, (–) 6.0 µM fondaparinux.

A library of low molecular weight heparins (LMWH) are utilised to represent more complex heparin structure. The IgG2k peak gives a Tm of 53.66°C with a small shoulder at 59.23 °C (Figure 85). Dalteparin, enoxaparin, tinzaparin and reviparin follow

the same peak structure with a double peak with Tm of ≈ 40.0°C and 51.5°C. Dalteparin, enoxaparin, reviparin and tinzaparin have a small hump at approximatley 71°. Fondaparinux at 6.0 μM with IgG2k has a peak at Tm of 52.39°C with a small secondary peak at 64.52°C.

5.2.8 IgG2k stability in the presence of GAGs and heparin controls

The largest reduction in the Tm of IgG2k is seen on with the inclusion of 6.0 μM UF PMH with a Tm of 38.46 °C with a shoulder at Tm of 59.50 °C (Figure 86). The change in Tm with 6.0 μM UF PMH is 15.09°C. As with IgG1k, the second largest Tm shift is seen with 12.0 μM HS, with the Tm of 40.35°C, a reduction of 13.20°C. This curve has double peaks with second Tm at 48.54°C. An 11.68°C Tm reduction is seen on addition of DS, with this curve also displaying a double linked peak shape, but with a more flattened appearance than that of HS. The Tm of the double peaks are 41.87°C and 50.03°C.

As with IgG1k, CSC is the more destabilising of the two CS, with a Tm reduction of 4.49°C compared to IgG2k alone. The curve has a shoulder peak at melting temperatures higher than that of IgG1k, at 62.72°C.

The Tm does not change with the inclusion of HA, with only the fluorescence intensity of the melting peak increasing. No change is seen in Tm with the addition of UA(2S)-GlcNS(6S) disaccharide and Na_2SO_4. The peak shape includes a small shoulder in IgG2k with Na_2SO_4, but this feature is not present in the UA(2S)-GlcNS(6S) disaccharide peak with IgG2k.

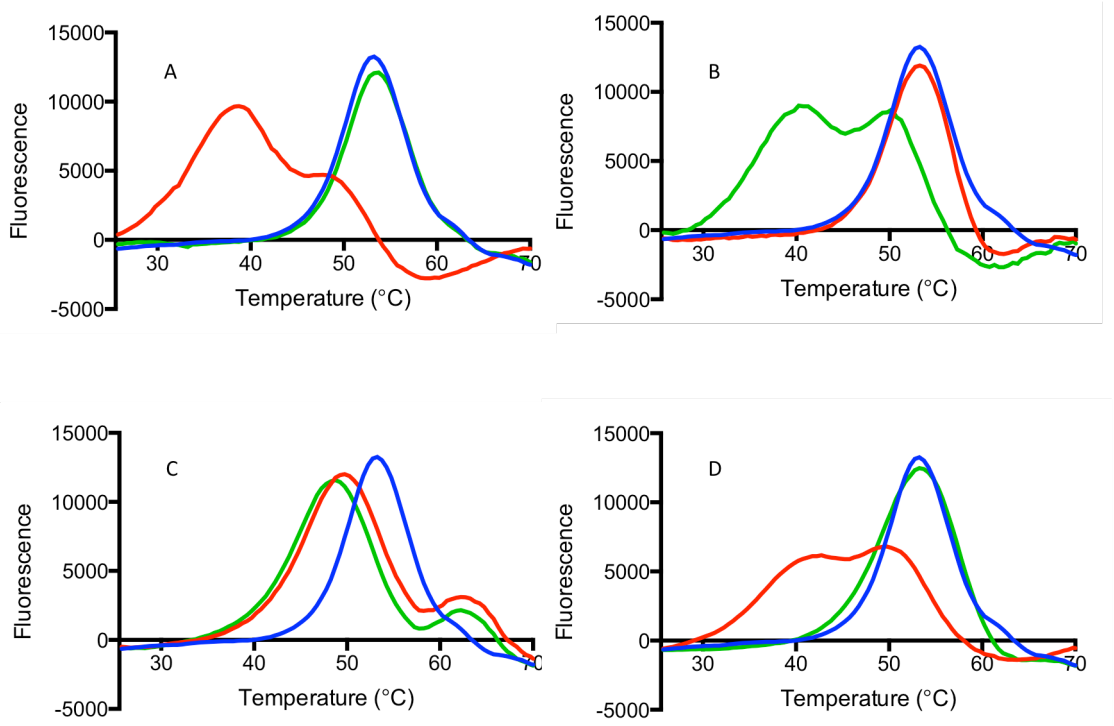

Figure 86: DSF of IgG2k with GAGs and sulphated controls in 50 mM sodium acetate buffer pH 4.0 (–) 1 µM human IgG2k with **A**) (–) 6.0 µM UF PMH, (–) 500 nM sodium sulphate, **B**) (–) 6.0 µM UA(2S)-GlcNS(6S) (–) 12.0 µM HS, **C**) (–) 6.0 µM CSA, (–) 6.0 µM CSC, **D**) (–) 6.0 µM DS, (–) 6.0 µM HA.

5.2.9 IgG2k stability in the presence of size defined heparin fractions

The d.p.2 heparin fragment stabilises the IgG2k to a Tm of 54.37°C with a small shoulder at ≈ 60°C which is mirrored in IgG2k alone. Addition of d.p.4 destabilises the IgG2k to a Tm of 52.94°C. With d.p.6, the main peak Tm is 53.44°C, but a secondary peak occurs at 67.57°C. With d.p.8, the peak shape changes to a 3 peak structure, with the initial peak at 42.44°C, the largest peak at 53.34°C and the minor peak at 66.55°C. This three peak structure is modified with d.p.10, with the first 2 peaks occurring in the same region of the first peak of d.p.8 and no peak occurring > 54°C. With d.p.>10, two peaks with similar intensity occur below 54°C. The occurrence of the higher fluorescence intensity peak at a Tm of ≈ 38°C mimics the UF PMH at 6.0 µM in IgG2k but the population at the higher Tm of ≈ 50°C is still present at these d.p. PMH fragments.

Table 10: DSF Tm of human IgG2k with each PMH polymerization (d.p.) fragment in 50 mM sodium acetate buffer pH 4.0.

d.p.	Tm 1 (°C)	Tm 2 (°C)	Tm 3 (°C)
None		53.71	
2		54.37	
4		52.94	
6		53.44	67.57
8	42.44	53.34	66.55
10	40.94	45.41	53.25
12	39.80	52.27	
14	39.84	51.61	
16	39.19	50.67	
18	38.85	50.37	
20	40.42	52.11	
UF PMH	38.33		

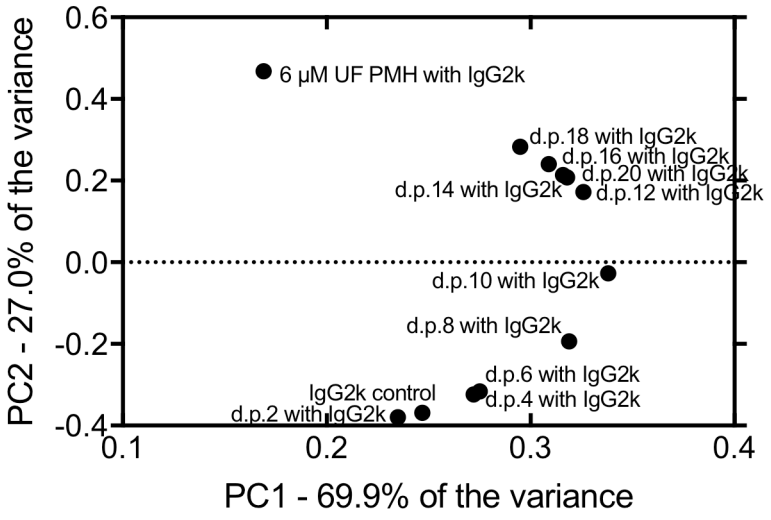

Figure 87: PCA of 1st derivative DSF data of IgG2k with d.p. heparin fractions.

PCA analysis of the d.p. heparin fractions suggests d.p.4 and d.p.6 have the same eigenvalues in both PC1 and PC2 and d.p.18 has the an effect on IgG2k most similar to that of UF PMH, but larger d.p. fragments would require testing to identify polymer size identical to that of UF PMH.

5.2.10 IgG2k binding at differing buffer concentrations and pH

Heparin affinity Hitrap HPLC experiments demonstrate IgG2k binds to heparin at pH 4.0 and pH 5.0 in PBS buffer. At pH 4.0 two small peaks at 1.01 M and 1.48 M suggest

two populations of protein with different binding affinities. At pH 5.0, binding affinity of the small peak is 937 mM. The IgG2k binds more strongly to heparin at a more acidic pH.

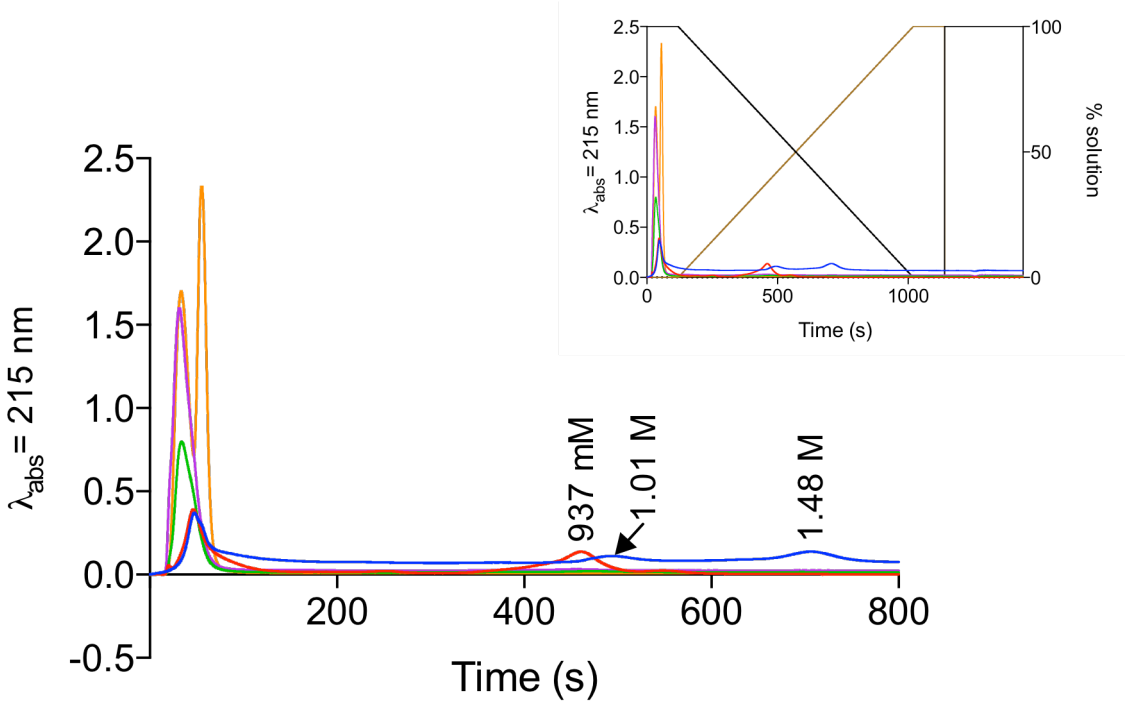

Figure 88: Human IgG2k in heparin HiTrap affinity HPLC in PBS at differing pH (4.0 – 7.4) and elution with 2M NaCl. (–) PBS pH 4, (–) PBS pH 5.0, (–) PBS pH 6.0, (–) PBS pH 7.0, (–) PBS pH 7.4.

5.2.11 IgM stability in the presence of chemically modified heparins

The reduction in Tm seen upon addition of 6.0 µM CMH1 to human anti-GFP IgM is 16.98°C, with the IgM only Tm of 53.27°C and 6.0 µM CMH1 with IgM is 37.45°C, with a further double peak at the higher temperatures of 63.51°C and 68.87°C. At 3.0 µM CMH1, the curve remains in the same position for the lower Tm at 37.45°, but the second peak is a single feature with the Tm 622.82 °C. CMH1 at 1.5 µM to 0.38 µM have the same structure, with the first Tm at 37.45°C (1.5 µM), 38.62°C (0.75 µM) and 41.44°C (0.38 µM). At 0.19 µM CMH1, the curve moves to a flattened shape, with less well defined peak structures with Tm of 43.75°C and 53.74°C. The largest peak at 0.09 µM has a shape similar to the IgM only peak, with a Tm of 54.3°C, but has a secondary peak which

mimics the shape of the second of the double peaks seen at the concentration 6.0 µM CMH1.

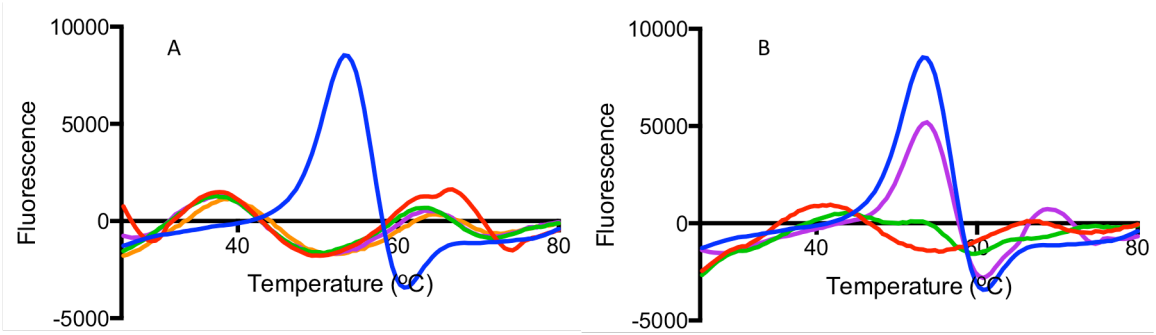

Figure 89: DSF of IgM with CMH1 in 50 mM sodium acetate buffer pH 4.0. **A**= (–) 1 µM IgM with (–) 6.0 µM CMH1, (–) 3.0 µM CMH1, (–) 1.5 µM CMH1, (–) 0.75 µM CMH1. **B**= (–) 1 µM IgM with (–) 0.38 µM CMH1, (–) 0.19 µM CMH1, (–) 0.09 µM CMH1, (–) 0.05 µM CMH1.

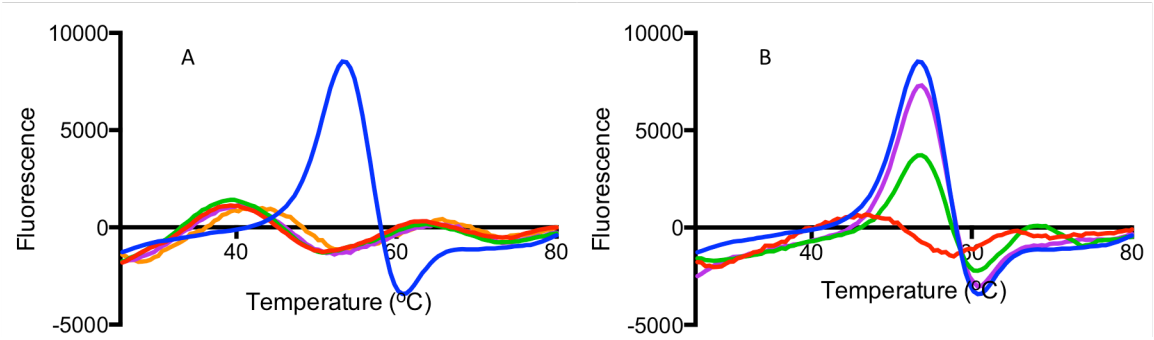

Figure 90: DSF of IgM with CMH2 in 50 mM sodium acetate buffer pH 4.0. **A**= (–) 1 µM IgM with (–) 6.0 µM CMH2, (–) 3.0 µM CMH2, (–) 1.5 µM CMH2, (–) 0.75 µM CMH2. **B**= (–) 1 µM IgM with (–) 0.38 µM CMH2, (–) 0.19 µM CMH2, (–) 0.09 µM CMH2, (–) 0.05 µM CMH2.

The Tm change between IgM only and 6 µM CMH2 is 15.30°C, with the Tm of IgM only 54.30°C and 6 µM CMH2 with IgM of 39.0°C. The peak of CMH2 at 6.0 µM has a second Tm at 62.84°C. Peaks of CMH2 at 3.0 µM and 1.5 µM and 0.75 µM have the same structure of 6 µM, with Tm of 39.94 °C, 40.52 °C and 41.84 °C. The Tm of the secondary peak at these concentrations varies between 63.19°C and 64.84°C. The initial peak shifts further at 0.38 µM, with a Tm of 54.01°C and 69.21°C. The two further lower concentrations (0.19 µM and 0.09 µM) have more regular peak structure, with only 0.19

μM exhibiting a secondary peak at higher Tm. CMH2 at 0.19 μM has a Tm of 54.01°C and 69.21°C; which is the highest Tm seen with this chemically modified heparin. At CMH2 concentration of 0.09 μM, the peak shape mirrors that of IgM only, with a Tm of 54.29°C.

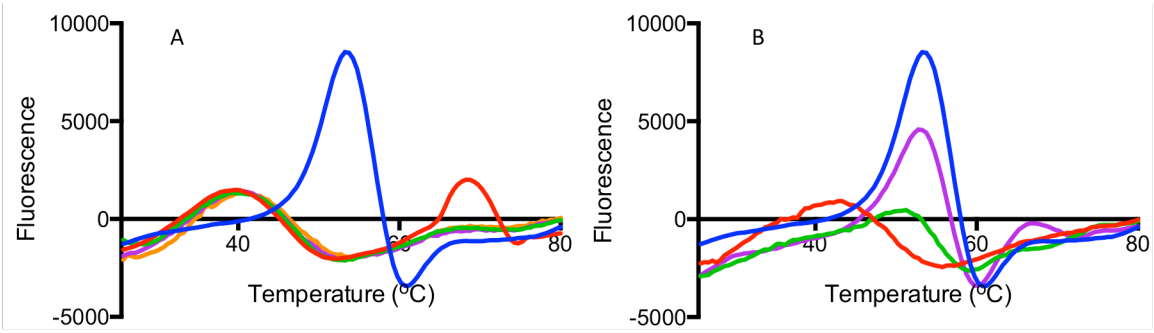

Figure 91: DSF of IgM with CMH3 in 50 mM sodium acetate buffer pH 4.0 **A**= (–) 1 μM IgM with (–) 6.0 μM CMH3, (–) 3.0 μM CMH3, (–) 1.5 μM CMH1, (–) 0.75 μM CMH3. **B**= (–) 1 μM IgM with (–) 0.38 μM CMH3, (–) 0.19 μM CMH3, (–) 0.09 μM CMH3, (–) 0.05 μM CMH3.

Tm change upon addition of 6.0 μM CMH3 is 12.21°C, with Tm of the initial peak at 6.0 μM CMH3 at 38.94°C, and a secondary peak at the same position as the secondary peak of CMH1 at 6.0 μM, at 69.33°C. CMH3 concentrations between 0.75 μM and 3.0 μM show similar curve shape, with Tm of 39.44°C (3.0 μM), 40.12°C (1.5 μM) and 42.37°C (0.75 μM). The peak shifts to an increased Tm at 0.19 μM with a Tm of 53.76°C.

The reduction in Tm after the addition of the highest concentration of CMH4 is 16.48°C, with a decrease in melting temperature from 54.21°C to 37.73°C with 6.0 μM CMH4. A second peak at this concentration occurs at 64.42°C. Tm at 3.0 μM is 38.65°C,

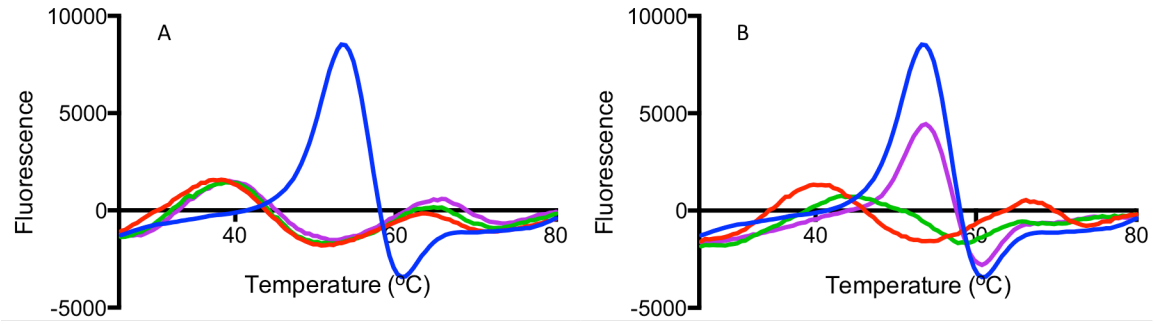

Figure 92: DSF of IgM with CMH4 in 50 mM sodium acetate buffer pH 4.0. **A**= (–) 1 μM IgM with (–) 6.0 μM CMH4, (–) 3.0 μM CMH4, (–) 1.5 μM CMH4 (–) 0.75 μM CMH4. **B**= (–) 1 μM IgM with (–) 0.38 μM CMH4, (–) 0.19 μM CMH4, (–) 0.09 μM CMH4, (–) 0.05 μM CMH4.

with a second Tm at 65.24°C. The CMH4 concentration of 0.75 µM with IgM has an initial Tm at 39.0°C with a secondary peak at 64.01°C with an intensity between that of 6.0 µM and 3.0 µM CMH4. CMH4 at 0.75 µM and 0.38 µM have first peak Tm at 38.92°C and 40.0 °C respectively and secondary peaks at 65.02°C and 66.31°C. The Tm of 0.09 µM CMH4 with IgM is the same as IgM alone at 53.89°C.

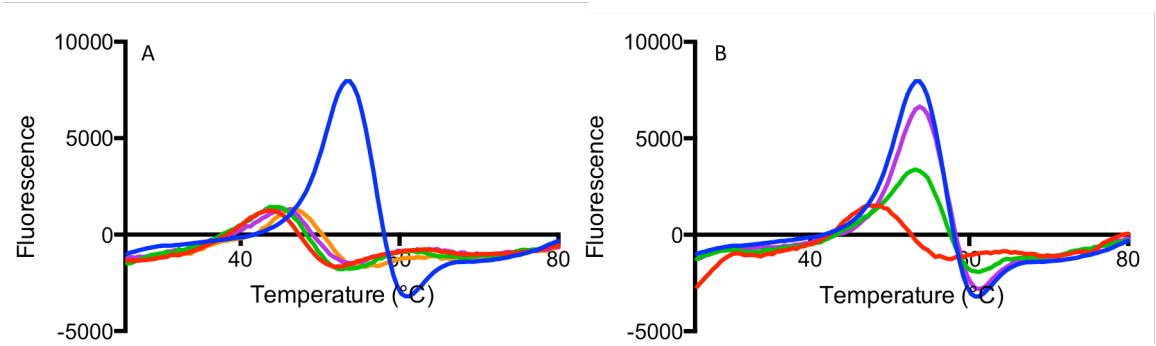

Figure 93: DSF of IgM with CMH5 in 50 mM sodium acetate buffer pH 4.0 **A**= (–) 1 µM IgM with (–) 6.0 µM CMH5, (–) 3.0 µM CMH5, (–) 1.5 µM CMH5, (–) 0.75 µM CMH5. **B**= (–) 1 µM IgM with (–) 0.38 µM CMH5, (–) 0.19 µM CMH5, (–) 0.09 µM CMH5, (–) 0.05 µM CMH5.

The change in Tm seen in IgM with the highest concentration of CMH5 tested (6.0 µM) is 10.39°C. At 6.0 µM CMH5 the Tm of IgM is 43.72°C. This Tm gradual increased with decreasing concentration of CMH5, with 3.0 µM giving a Tm of 44.5°C, 1.5 µM Tm of 44.96°C, 0.75 µM Tm of 46.61°C and 0.38 µM Tm of 47.6°C. The peak then shifts to mirror the IgM only peak, giving a Tm of 53.92 °C. At the lowest concentration of CMH5 tested (0.09 µM) the Tm is 54.09°C.

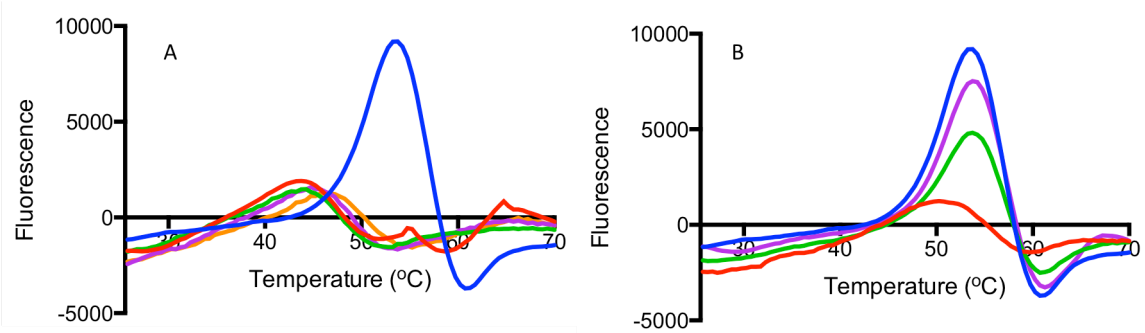

Figure 94: DSF of IgM with CMH6 in 50 mM sodium acetate buffer pH 4.0. **A**= (–) 1 µM IgM with (–) 6.0 µM CMH6, (–) 3.0 µM CMH6, (–) 1.5 µM CMH6, (–) 0.75 µM CMH6. **B**= (–) 1 µM IgM with (–) 0.38 µM CMH6, (–) 0.19 µM CMH6, (–) 0.09 µM CMH6, (–) 0.05 µM CMH6.

The Tm shift with 6.0 µM CMH6 (Tm of 43.53°C) is 10.39°C compared to IgM only with a Tm of 53.92°C. Concentrations of 3.0 µM and 1.5 µM have similar shaped curves with Tm of 43.48°C and 44.86°C. At 0.75 µM the Tm increases to 46.22°C. The intermediate peak at 0.38 µM has a Tm of 49.95°C and at 0.19 µM the curve resembles the shape seen in IgM only, with a Tm of 54.11°C. At the lowest concentration of CMH6 tested (0.09 µM), the Tm is 54.55°C, which suggests an increase in protein stability.

The difference between IgM only Tm and the Tm with 6.0 µM CMH7 is 15.75°C, with 6.0 µM Tm shifting to a lower temperature of 38.24°C, with a shoulder at a higher temperature than the Tm of IgM only, at 64.21°C. Reducing concentrations of CMH7 to 0.38 µM follow the same peak shape as the 6.0 µM CMH7. At 0.19 µM CMH7 shifts the Tm to 43.72°C with no discernable secondary peak at Tm > 60°C. At the lowest concentration of CMH7 tested (0.09 µM) the peak has a Tm of 53.61°C, however the secondary peak returns with a Tm of 68.42°C, mimicking the peak seen at this temperature with 0.75 µM CMH7.

CMH8 shows the least disruption to the Tm of IgM, with the difference between 6.0 µM CMH8 and IgM only being 5.95°C. The Tm increases with decreasing concentration of CMH8 up to 0.19 µM where the Tm is the same as IgM alone.

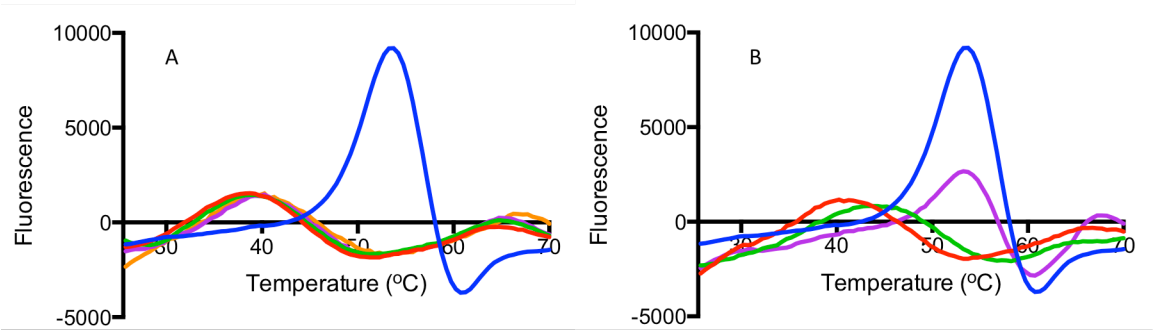

Figure 95: DSF of IgM with CMH7 in 50 mM sodium acetate buffer pH 4.0 **A**= (–) 1 µM IgM with (–) 6.0 µM CMH7, (–) 3.0 µM CMH7, (–) 1.5 µM CMH7, (–) 0.75 µM CMH7. **B**= (–) 1 µM IgM with (–) 0.38 µM CMH7, (–) 0.19 µM CMH7, (–) 0.09 µM CMH7, (–) 0.05 µM CMH7.

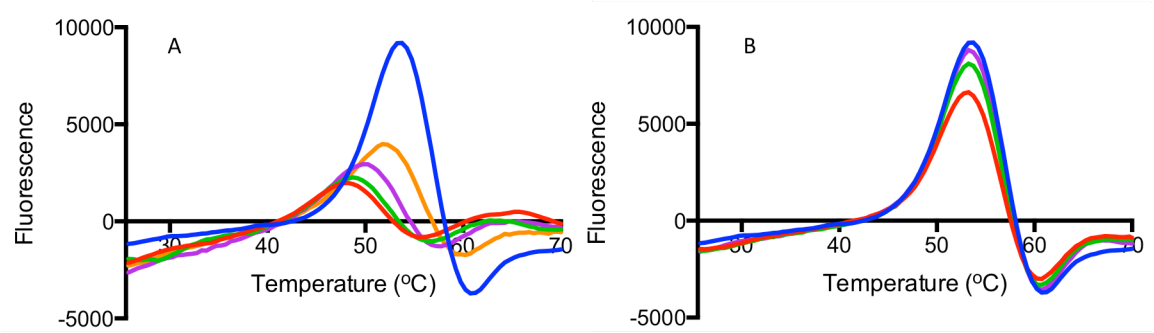

Figure 96: DSF of IgM with CMH8 in 50 mM sodium acetate buffer pH 4.0 **A**= (–) 1 µM IgM with (–) 6.0 µM CMH8, (–) 3.0 µM CMH8, (–) 1.5 µM CMH8, (–) 0.75 µM CMH8 **B**= (–) 1 µM IgM with (–) 0.38 µM CMH8, (–) 0.19 µM CMH8, (–) 0.09 µM CMH8, (–) 0.05 µM CMH8.

The greatest change in Tm is seen upon addition of CMH9 at 6.0 µM decreasing to 33.93 °C. The concentrations of CMH9 decreasing to 0.75 µM follow the same peak shape with higher fluorescence peak occurring at ≈ 61°C. At 0.38 µM the secondary peak occurs at a higher temperature of 68.99°C. At 0.09 µM the peak at 54.38°C mimics the peak seen at 0.19 µM.

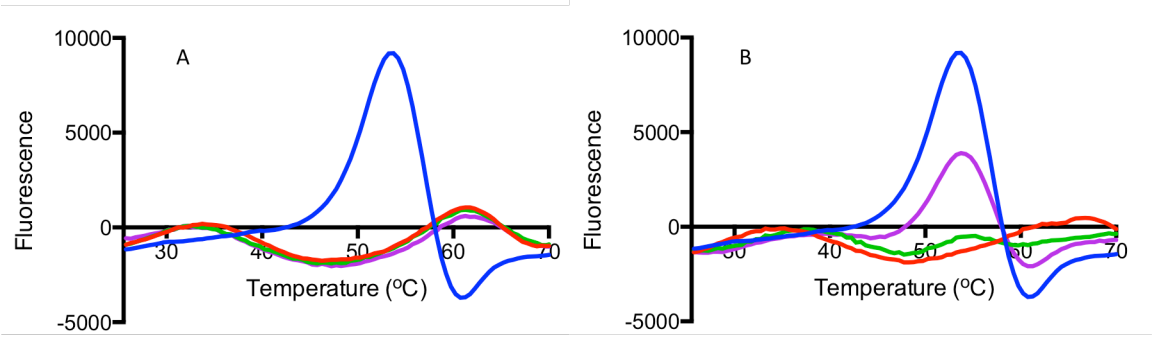

Figure 97: DSF of IgM with CMH9 in 50 mM sodium acetate buffer pH 4.0. **A**= (–) 1 µM IgM with (–) 6.0 µM CMH9, (–) 3.0 µM CMH9, (–) 1.5 µM CMH9, (–) 0.75 µM CMH9. **B**= (–) 1 µM IgM with (–) 0.38 µM CMH9, (–) 0.19 µM CMH9, (–) 0.09 µM CMH9, (–) 0.05 µM CMH9.

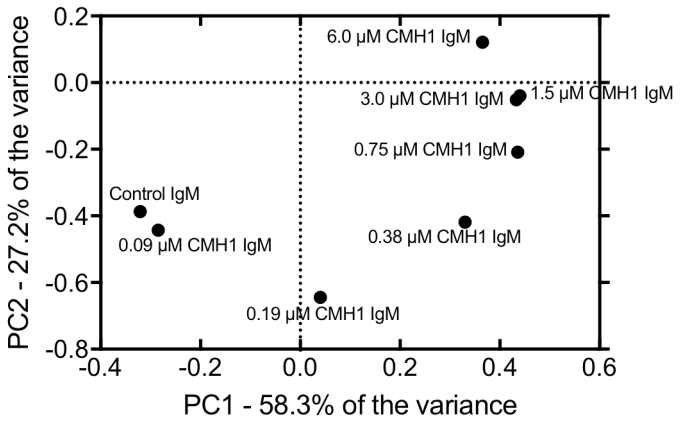

Figure 98: PCA of 1st derivative DSF data of IgM with CMH1.

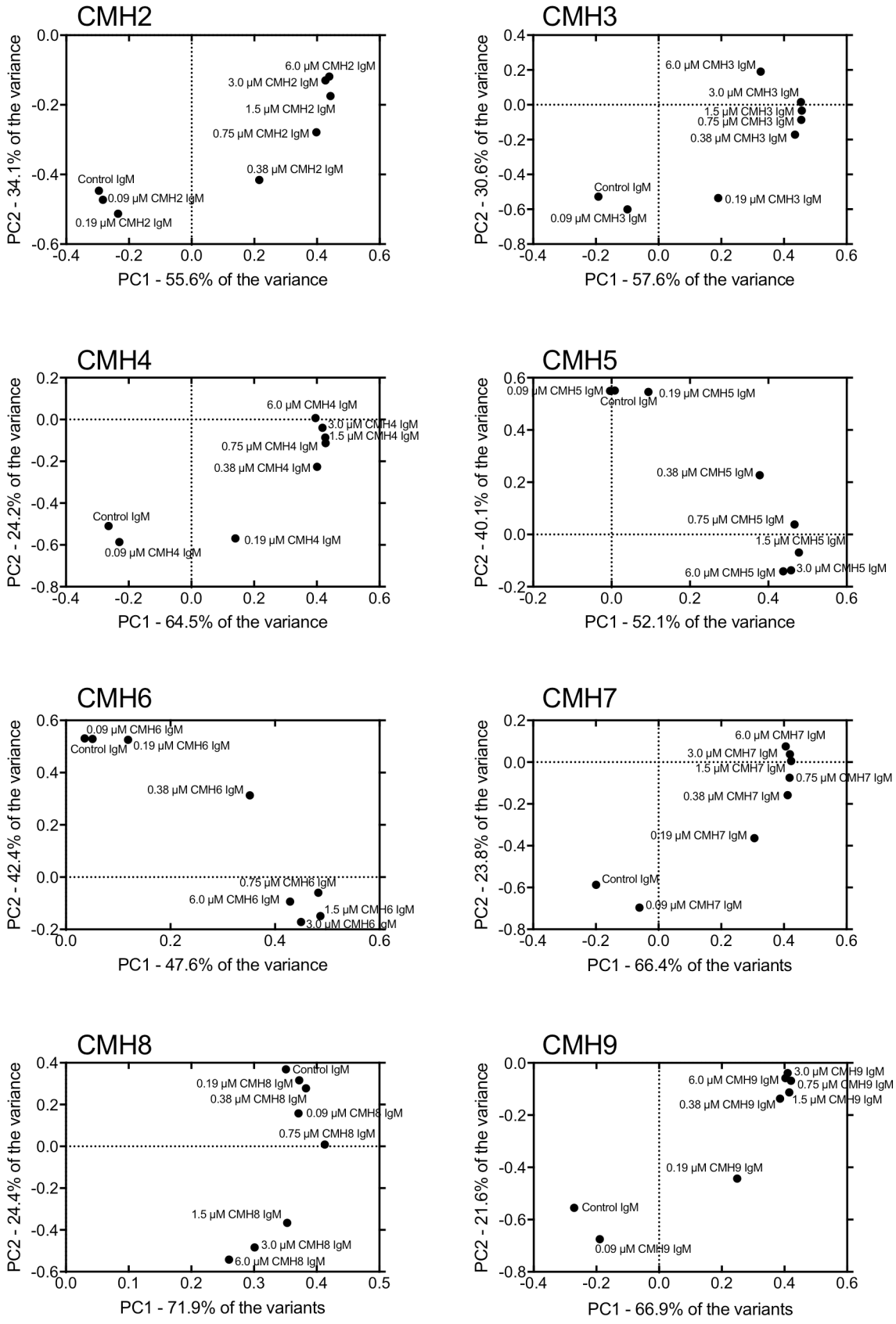

Figure 99: PCA of 1st derivative DSF data of IgM with CMH2-9.

CMH1 with IgM in PCA demonstrates no variance at the concentrations of 3.0 µM and 1.5 µM (Figure 98). The distribution of data points in the PCA of IgM with differing concentrations of CMH follows two distinct patterns; CMH1, 2, 3, 4, 7 and 9 can be grouped according to the PC1 v PC2 data arrangement, while CMH5, 6 and 8 can be classified as similar in distrubution (Figure 99). CMH5 and 6 both have an absence of 6-O-sulphate, and have 2-O-sulphate modifications, but CMH8 does not have this 2-O-sulphate. CMH5, 6 and 8 have 2, 1 and zero sulphate groups per disaccharide, suggesting no link to heparin disaccharide charge.

Plotting the change in Tm observed by the addition of differing concentrations of chemically modified heparin produces a simple graphical representation of the DSF data. Figure 100 shows the greatest change is seem with the addition of persulphated CMH9 heparin, with CMH1 following closely behind. This pattern follows both IgG1k and IgG2k in DSF with the chemically modified heparin library.

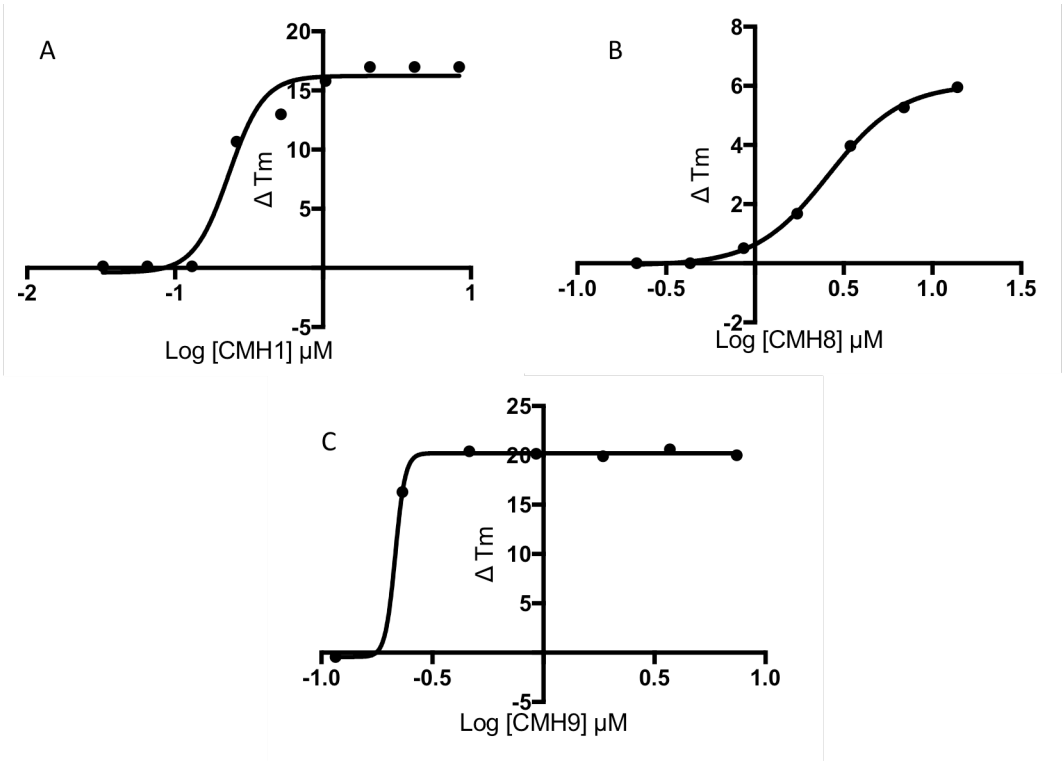

Figure 100: DSF 1st derivative of IgM with CMH1, CMH8 and CMH9 in 50 mM sodium acetate buffer pH 4.0, Δ Tm (compared to IgM alone) from DSF plotted as a function of chemically modified heparin concentration. IgM with **A**) 6 µM CMH1 EC_{50} = 0.231 µM, **B**) 6 µM CMH8 EC_{50} = 2.605 µM **C**) 6 µM CMH9 EC_{50} = 0.215 µM.

The far-UV CD spectra of a human IgM antibody, raised to green fluorescent protein, the same epitope as the IgG1 and IgG2 antibodies used in the earlier in this chapter. Human IgM anti-GFP in sodium acetate buffer (50 mM) pH 4.0 and PBS buffer in far-UV CD have a similar spectra at wavelengths between λ = 210nm – 260 nm (Figure 101). In acetate buffer, IgM has a trough at λ = 220 nm, with the addition of UF PMH shifting this peak to λ = 222 nm. The peak shape of IgM in this buffer however, both with and without PMH, has a similar spectral shape at all wavelengths, but at λ = > 220 nm the magnitude of ellipticity is increased in the IgM spectra including UF PMH (Figure 101A).

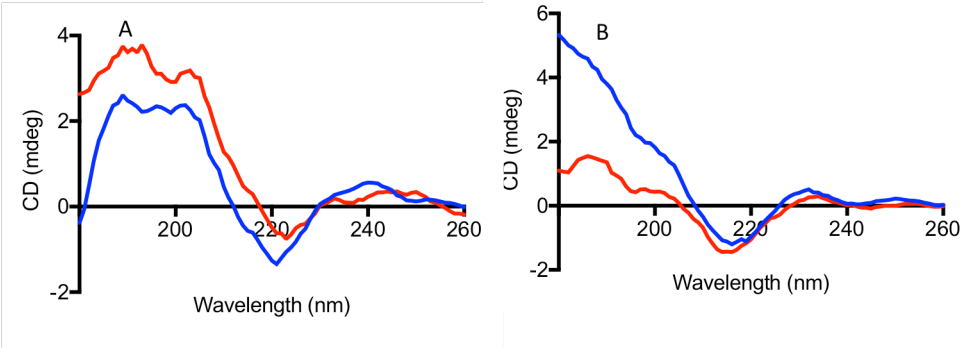

Figure 101: Far-UV CD spectra of IgM ± UF PMH in sodium acetate buffer and PBS **A**) 50 mM sodium acetate buffer pH 4.0 with (–) 3 μM IgM with (–) 3 μM UF PMH **B**) PBS buffer pH 7.4 with (–) 3 μM IgM with (–) 3 μM UF PMH.

In PBS pH 7.4 (Figure 101B), the CD spectrum if the human IgM has a negative peak at 218 nm, with the addition of UF PMH retaining a similar spectral shape, with the negative ellipticity peak occurring at 217 nm. At wavelengths lower than 210 nm, the spectra of human IgM in PBS and IgM with UF PMH in PBS diverge, with the heparin containing experiment causing an increase in absorbance in the region < 210 nm.

Table 11: BeStSel analysis of far-UV CD of IgM in sodium acetate and PBS buffer ± UF PMH, quantifying % secondary structure motif changes with the addition of UF PMH.

	50 mM sodium acetate buffer pH 4.0		PBS buffer	
Structural feature	IgM protein alone	with UF PMH	IgM protein alone	with UF PMH
Regular helix	2.7	4.2	1.5	0.0
Distorted helix	0.5	0.0	0.0	0.0
Antiparallel left twisted β-sheet	6.2	5.5	5.3	5.4
Antiparallel relaxed β-sheet	11.2	10.4	11.7	11.9
Antiparallel right twisted β-sheet	16.3	16.0	19.4	20.8
Parallel β-sheet	0.0	0.0	0.0	0.0
Turn	20.0	21.2	19.0	18.2
Other	43.2	42.6	43.1	43.6

Table 11 suggests a greater change in seconfary structural motifs with the addition of UF PMH in sodium acetate buffer pH 4.0 than PBS at pH 7.4. This change increases the proportion of α-helix and reduces the anti-parallel β-sheet proportion, which predominates the immunoglobulin fold.

5.2.12 IgM stability in the presence of low molecular weight heparins

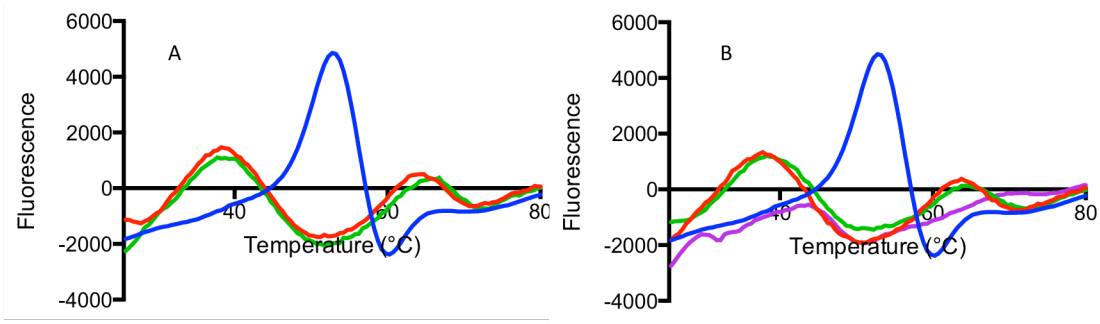

Figure 102: DSF of IgM with LMWH in 50 mM sodium acetate buffer pH 4.0. **A**) (–) 1 µM IgM with (–) 6.0 µM dalteparin, (–) 6.0 µM enoxaparin **B**) (–) 1 µM IgM with (–) 6.0 µM tinzaparin, (–) 6.0 µM reviparin, (–) 6.0 µM fondaparinux.

The library of low molecular weight heparins (LMWH) were utilised to represent more complex heparin structure with known structural features. The IgM Tm is 53.42 °C with fluorescence intensity of 5150 ΔFU (Figure 102). The addition of UF PMH at 6.0 µM shifts the Tm to the lower temperature of 37.45°C with further peaks in a double joined peak at Tm of 63.61°C and 69.02°C. The LMWH dalteparin, enoxaparin, tinzaparin and reviparin have similar curve shapes with IgM, with 2 wide peaks formed. The initial

peak occurs at Tm of 37.45°C with the secondary peaks occurring in the same area (dalteparin 64.16°C, enoxaparin 65.16°C, tinzaparin 63.67°C and reviparin 63.95°C). Fondaparinux at 6.0 μM has a single hump structure with a Tm of 43.63°C which occurs between the other LMWH/CMH1 and IgM protein only control.

The PCA of IgM with LMWH demonstrates a similar pattern of data distribution as IgG1k and IgG2k with LMWH; naturally derived LMWH group together, with the synthetic pentasaccharide fondaparinux more similar to the protein only control (Figure 103).

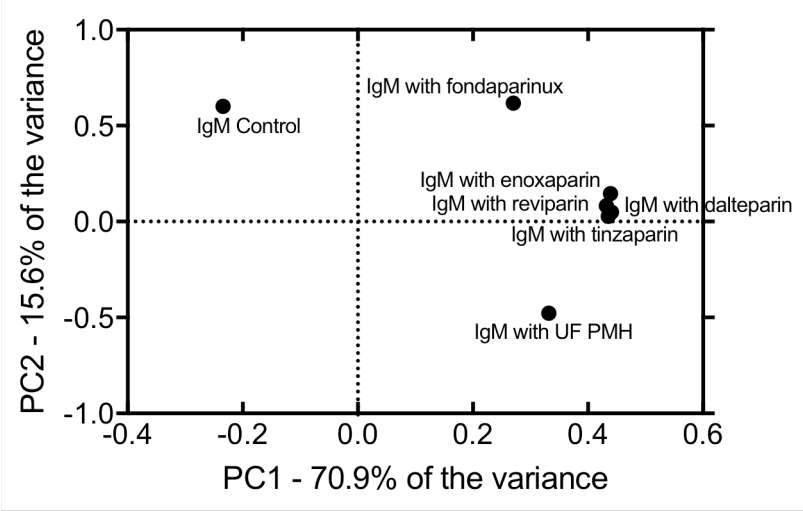

Figure 103: PCA of 1st derivative DSF data of LMWH with IgM.

5.2.13 IgM stability in the presence of GAGs and heparin controls

The addition of DS causes a destabilisation with IgM to reduce the Tm to 39.17°C (14.37°C change). The curve structure is similar to CMH1 with intensity of 1130 units and a secondary small shoulder at 62.84°C. HS at 12.0 μM mimics the curve shape seen with DS, and has a slightly increased Tm compared to DS at 39.26°C but a slightly reduced second Tm at 63.07°C. The change from IgM alone is 14.28°C with the addition of HS.

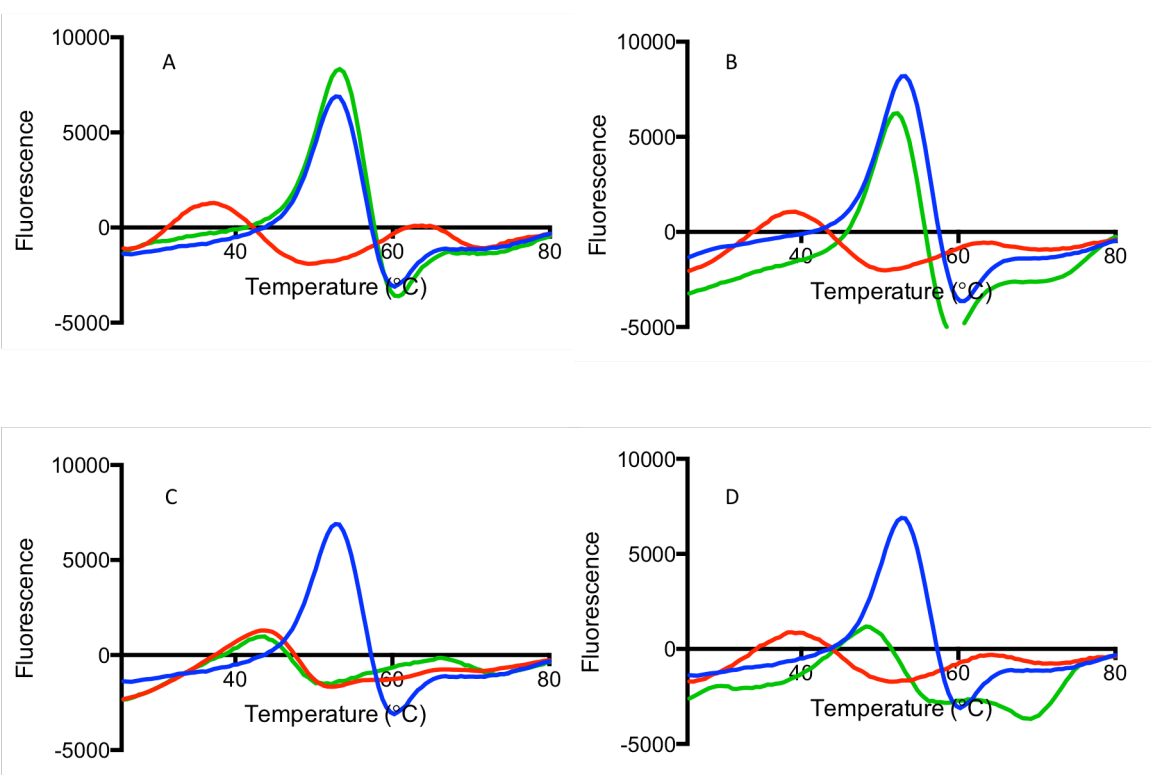

Figure 104: DSF of IgM with GAGs and sulphated controls in 50 mM sodium acetate buffer pH 4.0. (–) 1 µM IgM with **A**) (–) 6.0 µM UF PMH, (–) 500 nM sodium sulphate, **B**) (–) 6.0 µM UA(2S)-GlcNS(6S) (–) 12.0 µM HS, **C**) (–) 6.0 µM CSA, (–) 6.0 µM CSC, **D**) (–) 6.0 µM DS, (–)6.0 µM HA.

The difference between CSC and CSA is smaller with IgM, with CSC still displaying the larger reduction in Tm compared to IgM alone at 9.87°C whereas CSA change is 9.82°C.

The 6.0 µM UA(2S)-GlcNS(6S) disaccharide only reduces the Tm of IgM by 0.92°C. IgM alone and IgM with Na_2SO_4 have the same Tm, peak intensity and curve shape suggesting sulphate alone does not reduce IgM Tm and therefore protein stability.

5.2.14 IgM stability in the presence of size defined heparin fractions

The average Tm of IgM is 53.45°C in this data, with addition of 6.0 µM UF PMH change in Tm to the first peak at 37.40°C of 16.05°C. The peak shape with 6.0 µM UF PMH is one peak at low temperatures with a double peak at 63°C – 68°C with all three having similar peak fluorescence intensity.

Table 12: The Tm of each PMH polymerization (D.P) fragment with IgM from the DSF of IgM in 50 mM sodium acetate buffer pH 4.0.

d.p.	Tm 1 (°C)	Tm 2 (°C)
IgM control	53.45	
2	53.67	
4	50.37	63.55
6	45.68	
8	38.32	
10	37.95	68.83
12	37.39	
14	38.59	
16	37.99	
18	38.20	
20	37.14	
UF PMH	37.40	

Adding d.p.2 to IgM at the same concentration of UF PMH shows no change in Tm or intensity compared to IgM alone. IgM with d.p.4 reduces the Tm by 3.3°C to 50.37°C, with the occurrence of another peak at 63.55°C which mirrors the initial peak in the double structure seen with UF PMH addition. IgM with d.p.6 has no clear peak structure across the whole temperature spectrum with the only increase resembling peak structure at 45.68 °C. The curve of d.p 8 with IgM is similar to d.p 6 but with a wide, low fluorescence curve with maximum at Tm of 38.32°C.

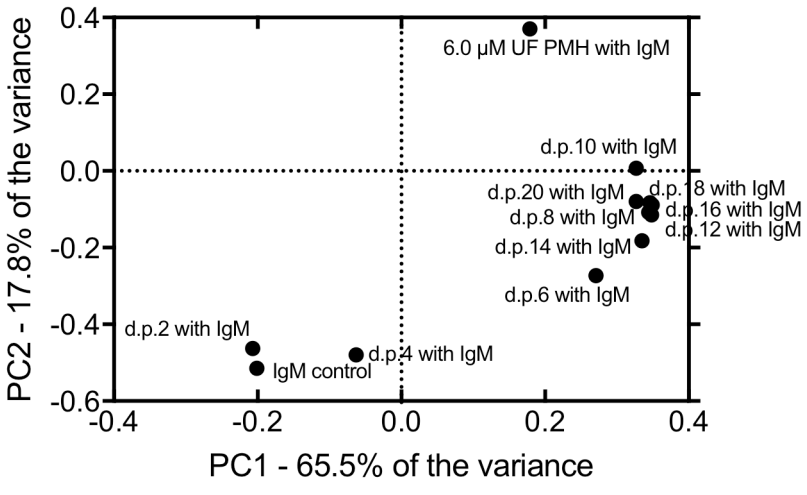

Figure 105: PCA of first derivative DSF data of IgM with heparin d.p. fragments

With heparin sizes greater than d.p.10, the Tm are similar, with a peak structure at very low intensity and only a simgle discernable peak at ≈ 37°C - 38°C. The heparin disaccharide size which has similar Tm to UF PMH is a decasaccharide, but this size does not have identical features to the UF PMH with IgM.

PCA of the heparin d.p. fragments show the minimum size requirement for a change in DSF spectra is a d.p.4, with increasing d.p. size > d.p.4 having a more pronounced effect. As with the Tm from the 1st derivative DSF data, d.p.10 is the most similar to UF PMH in PCA.

5.2.15 IgM stability changes at differing buffer concentrations and pH

Figure 106 demonstrates, as with IgG1k and IgG2k, IgM binds heparin in Hi-Trap affinity HPLC in PBS at pH 4.0 and 5.0, with binding also shown at pH 6.0 PBS. At pH 4.0, IgM has heparin binding affinity in PBS at 1.03 M, with increasing pH to 5.0 leading to binding affinity of 917 mM, and further increase to pH 6.0 PBS demonstrating 698 mM heparin binding affinity. Heparin binding affinity of the immunoglobulins decreases as pH increases.

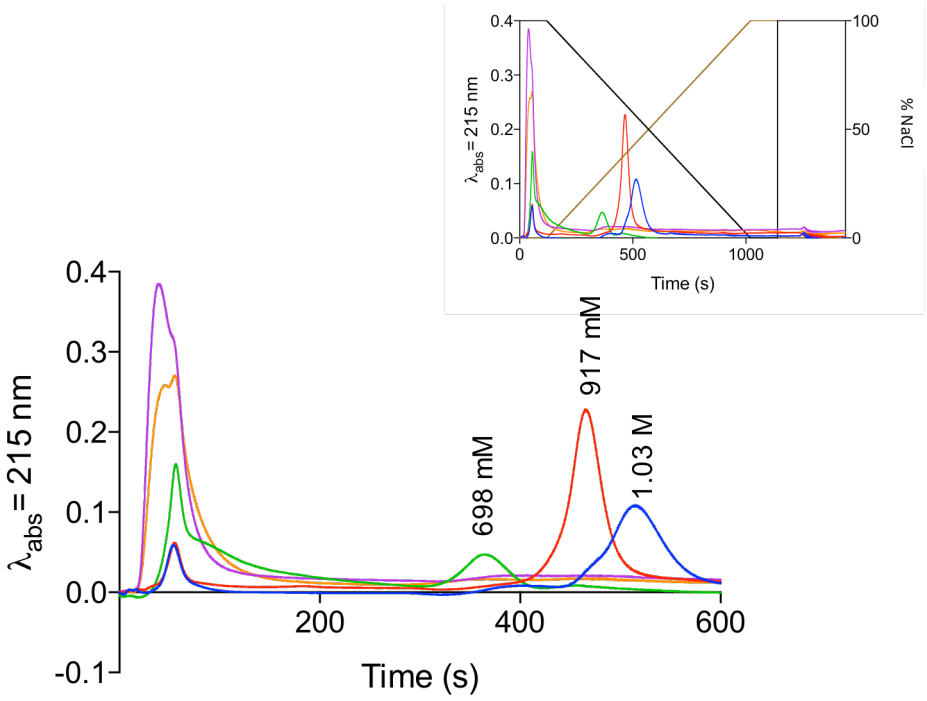

Figure 106: IgM in heparin HiTrap affinity HPLC in PBS at differing pH (4.0 – 7.4) and elution with 2M NaCl. (–) PBS pH 4, (–) PBS pH 5.0, (–) PBS pH 6.0, (–) PBS pH 7.0, (–) PBS pH 7.4.

5.3 Discussion

A library of chemically modified heparins represent 8 commonly found structures in the heparan sulphate polymer and per-sulphated heparin. The structure of the more homogenous glycopolymer, heparin, is constructed primarily (70-80% of IdoA(2S)-GlcNS(6S) (CMH1). In the presence of IgG1k and IgG2k the effects of this library of heparins cause modifications to the melting temperature and secondary structure of the immunoglobulin. Variation in melting temperature and secondary structure of the immunoglobulin occur due to structural changes conferred by the differing functional groups position, functional group conformation, and linkage region conformation of the glycopolymer. IdoA-GlcNAc (CMH8) has dramatically less capacity to affect the protein stability indicators of Tm and secondary structure change as measured by far-UV CD. Per-sulphated CMH9 has a greater destabilising effect on the immunoglobulins. The data does not point to a select disaccharide composition nor functional group requirement for the resulting protein structure changes. Singularly sulphated heparins show equal ability to peturb the stability of Ig than do tri-sulphated heparins.

However, the structural complexity of the differing heparins related to the presence and position of the sulphate groups, both O-sulphate and N-sulphate, is unclear when trying to isolate patterns in this data. In addition to the functional groups, the conformation and size of the chemically modified heparins may effect the immunoglobulin interaction. The presence of iduronic acid in the sequence allows for levels of conformational flexibility to alter the spatial orientation of the sulphate groups (Shriver, Capila, Venkataraman, & Sasisekharan, 2012). The $^{1}C_{4}$ chair and $^{2}S_{0}$ skew boat conformations of IdoA exist in relative equilibrium in solution, and the rate of

interchange between these forms is sufficiently fast to produce exchange-average (blended) chemical shifts in ^{1}H and ^{13}C NMR spectra (Ferro et al., 1986).

Protein-ligand interactions, demonstrated in thermal degradation experiments such as DSF, illustrate protein stability improvements with the addition of the ligand; the Tm of the protein in DSF increases in the presence of the ligand. In common protein-ligand interactions, such as catalytic events, ligand interaction with protein induces an increase in thermostability due to the coupling of binding, with unfolding equilibrium (Celej, Montich, & Fidelio, 2003). Equlibrium binding ligands usually increase the thermal stability of protein in a concentration and affinity dependant manner (Cimmperman et al., 2008). The addition of the sulphated members of the heparin library causes a reduction in the melting temperature of the immunoglobulin at low pH, and therefore suggests an aspect of structural destabilisation to promote untimely melting.

Destabilisation occurs when tested in acidic conditions (pH 4) to each antibody type tested, IgG1k, IgG2k and IgM; raised to common antigen or isotype controls. A model created by Cimmperman *et al*., 2008, suggests ligand that acts to reduce the protein melting temperature in DSF binds to the unfolded denatured protein, destabilising it (Cimmperman et al., 2008). Ligand that binds to the native, folded protein stabilises the protein and therefore shows increased thermal stability (*idem*). However, several weakly binding ligands that have preferential affinity to a unfolded protein structure may have a cumulative effect to reduce the Tm in a similar way to a high affinity ligand to the fully denatured protein structure (idem). The ability of some chemically modified heparin to act as destabilisers at high concentrations tested, may suggest the low pH environment pH 4.0 denatures some immunoglobulin to allow for the binding of the heparin based ligand. This model by Cimmperman *et al.* 2008,

however, assumes a single unfolded protein structure rather than a range of semi-flexible conformational states.

Regions of cellular apoptosis, necrosis, inflammation, and injury have the potential to harbour an acidic environment due to the lysing of acidic organelles. The lysing of the lysosome, endosome, and secretory granules could cause local pH reduction to < pH 6. The heparin binding activity of the immunoglobulins demonstrated in this study have the potential to be physiologically and pathologically relevant in these conditions.

Low molecular weight heparins are also tested for the destabilising effect seen, as a preliminary screen for activity. The type of pharmaceutical heparin administered to patients is primarily low molecular weight, due to the negative effects of unfractionated heparin, such as heparin-induced thrombocytopenia (HIT) and unpredictable pharmacokinetics. The plasma concentration of these drugs will be higher upon administration than physiological heparin/HS. The preliminary screen for LMWH destabilisation of whole immunoglobulins suggests an interaction, which needs further investigation. This will ensure administration of LMWH do not have an adverse effect on the humoral immune system.

The synthetic pentasaccharide fondaparinux has the lowest molecular weight of the LMWH tested, and is constructed including the factor Xa binding region only. Fondaparinux had significantly less effect on the stability of the whole immunoglobulins tested, suggesting the size or biochemical structure were not conducive to immunoglobulin interaction.

Experiments with sodium sulphate as a crude sulphate-containing compound indicated that sulphate alone (or negatively charged functional groups in general) did not fulfil the role in immunoglobulin destabilisation. Naturally unsulphated hyaluronic

acid was also shown to have no effect in the destabilisation of the IgG tested, suggesting the glycopolymeric backbone was not the singularly essential factor.

Determining the size requirement for this interaction, a library of depolymerised heparin fractions was utilised. The results from these experiments suggest a difference in glycopolymer size requirements in each isotype or subclass. IgG1k required a minimal saccharide size of d.p.4 to begin to destabilise (reduce Tm), with d.p.18 displaying similar melting characteristics of full-length heparin. IgG2k demonstrated a reduced Tm with a d.p.8, but the Tm is similar to unfractionated heparin after d.p.12. IgM demonstrates a requirement for d.p.8 as a minimum saccharide size.

Heparin affinity chromatography was employed to define the heparin binding affinity of a range of immunoglobulins. As with the Fc region investigated in Chapter 4, the binding of these whole immunoglobulins to the heparin column occurred at most commonly pH 4 and 5.

IgG1k bound heparin in PBS pH 4 with an affinity of 1.03 M, at pH 5.0 with 933 mM affinity and at pH 6 with an affinity of 704 mM. IgG1k binds pH 4 with 1.08 M affinity and at pH 5.0 with 928 mM affinity. This is mirrored in sodium acetate buffer at pH 4.0 with binding affinity of 849 mM NaCl. IgG2k has a heparin binding affinity of 1.03 M in PBS at pH 4.0, the same as IgG1k, suggesting the changes in hinge region that differentiated these immunoglobulins does not have a effect on heparin binding. IgG2k binds at pH 6.0 PBS similarly to IgG1k (698 mM NaCl).

IgM binds heparin in PBS pH 4.0 and elutes with two peaks, at 989 mM and 755 mM. This may indicate a heterogenous mixture of pentameric IgM or the variation due to access to the heparin matrix. The IgM structure is more structurally inaccessible, apart from in the antigen recognition region. The two elution peaks could indicate

binding affinities of singular or numerous heparin-binding occurances across the pentamer.

Heparin binding affinity of antithrombin III in Hi-trap affinity chromatography in 0.25 M citrate buffer pH 7.4 is quoted as 0.8 M NaCl (Jin et al., 1997) suggesting heparin-immunoglobulin binding is not a 'weak' interaction under these specified conditions. Expansion of the buffer type and pH range is required to investigate further the parameters for this binding interaction; this requires completion in the future.

The reduction in binding affinity with decreasing PBS pH suggests charge based binding. González-Iglesias *et al.* (2002) showed that the heparin-prion protein interaction at acid pH values could be due to histidine imidazole protonation; this was termed the acid pH-stabilised form of the protein (Gonzalez-Iglesias et al., 2002). Chapter 4 discussed the action of PMH and other chemically modified heparins on the stability of the IgG Fc region as a possible interaction between positively charged residues such as Lys248 and Lys388 in the CH2 region of Fc (Latypov et al., 2012). The action of imidazole ions of histidine and guanidinium ions of arginine at acidic pH may also have heparin-binding effect (Zhang-van Enk et al., 2013). The IgM pentamer therefore, comprises of multiple regions for polyanionic binding to ionised positively charged residues, across the 5 IgG-like monomers.

To further the investigation into the effects of glycosaminoglycans with immunoglobulins, the antigen binding regions Fab/k and F(ab')2 will be investigated for heparin binding properties.

Chapter 6: Antigen binding immunoglobulin domains and their interactions with glycosaminoglycans

6.1 Introduction

6.1.1 Antigen binding domain

The antigen-binding fragment of an immunoglobulin is composed of a single variable domain and a single constant domain of both the light and heavy chains. The antigen-binding region is formed from three non-consecutive variable amino acid sequences on each chain, which when folded, correspond to the complementary determining regions (CDR).

CDR1 and CDR2 are located in the 'variable' (V) region of the gene, while CDR3 is located in across variable (V region), diversity (D region in heavy chain only) and joining (J) regions (Brack, Hirama, Lenhardschuller, & Tonegawa, 1978; Sakano, Huppi, Heinrich, & Tonegawa, 1979; Sakano, Maki, Kurosawa, Roeder, & Tonegawa, 1980). The heavy chain and two light chain genes are located in different chromosomes, heavy chain at chromosome 14, kappa light chain at chromosome 2 and lambda light chain at chromosome 22 (Janeway C.A 2001). Each gene locus contains the V(D)J regions required for recombination (*idem*). The process by which antibodies form in immature B-cells, creating unique CDR regions is called somatic recombination (Brack et al., 1978; Sakano et al., 1979; Sakano et al., 1980).

Papain digestion of the whole IgG antibody yields an Fc region and two Fab regions (fragment antigen binding) by cutting at the amino side of the disulphide bonds joining the CH2 heavy chain regions, whereas pepsin digestion of the immunoglobulin occurs at the carboxy-terminal side of the disulphide bonds (Janeway C.A 2001). This yields a larger F(ab')2 fragment which contains more of the hinge region and the two antigen binding arms, and yields an additional, smaller pFc' region (*idem*). Unlike the Fab fragment, the larger F(ab')2 fragment can elicit a serologic reaction.

6.1.2 The immunoglobulin fold

An IgG molecule contains 12 immunoglobulin domain structures, each domain contains sequence features that cause protein folding to form a immunoglobulin fold (Peterson, Berggard, Edelman, & Cunningham, 1972). The immunoglobulin fold is characterised by 2 β-sheets sandwiched together, constructed by 5-10 antiparallel β-strands (Williams & Barclay, 1988). The strands form what is termed a Greek key motif, where 4 neighboring antiparallel β-strands are linked; 3 by hairpin loops and the 4th linked adjacent to the first strand, by a longer chain region from strand 3 (*idem*). The sandwiched β-sheets surround a hydrophobic protein core and are connected by a disulphide bond, with this bond essential for immunoglobulin fold stability and therefore, activity of the protein (K. J. Zhang & Filbin, 1994). 65-75 residues separate this disulphide bond in primary sequence, in the variable domain of immunoglobulin. The disulphide bond in the constant domain has a shorter separation of 55-60 residues (Williams & Barclay, 1988). Some non-antibody immunoglobulin fold containing proteins have as few as 40 residues separating the inter-sheet disulphide bond (*idem*).

The three loops at the end of the β-strands contain the hypervariable regions containing CDRs, which form the antigen-binding surface on both antibodies and T-cell receptors (Capra, 1971). The N- and C- termini occupy opposing sides of the immunoglobulin fold, allowing subsequent addition of further immunoglobulin domains, as seen in the antibody heavy and light chains (Berg, 2002)

More than 750 genes encode proteins with a primary sequence immunoglobulin fold in multicellular organisms, this structural motif has not yet been characterised in yeast or plant species (Berg, 2002).

6.1.3 Experimental aims

This chapter will identify whether the effector binding (heavy chain Fc) regions of immunoglobulin only binds heparin and other GAGs, or if heparin and related GAGs bind the antigen binding, immunoglobulin fragments.

6.2 Results

6.2.1 Fab/k stability in the presence of chemically modified heparins

The Fab/k 1st derivative peak has a Tm of 60.21°C. On addition of 6.0 µM CMH1, this Tm is reduced by 7.78°C to 52.43°C. The concentrations of chemically modified heparon of 3.0 µM, 1.5 µM and 0.75 µM all demonstrate the same peak shape with Tm of 52.41°C, 52.63°C and 53.25°C respectively. At 0.38 µM the Tm is shifted to 55.32 °C. The peak shape at this concentration is wider with a shoulder at the higher temperature of approximately 64°C, which mirrors the peaks at lower concentrations of CMH1. The CMH1 concentration of 0.19 µM has an intermediate structure with a double joined peak shape; the Tm of these peaks is 55.30°C and 65.81°C. The peak at 0.09 µM of CMH1 occurs at 63.22°C, which is higher than the IgG Fab/k only peak, but has a shoulder at lower temperatures, mirroring the peaks at higher CMH1 concentrations. At the lowest concentration tested (0.05 µM), the curve has the Tm 60.52°C.

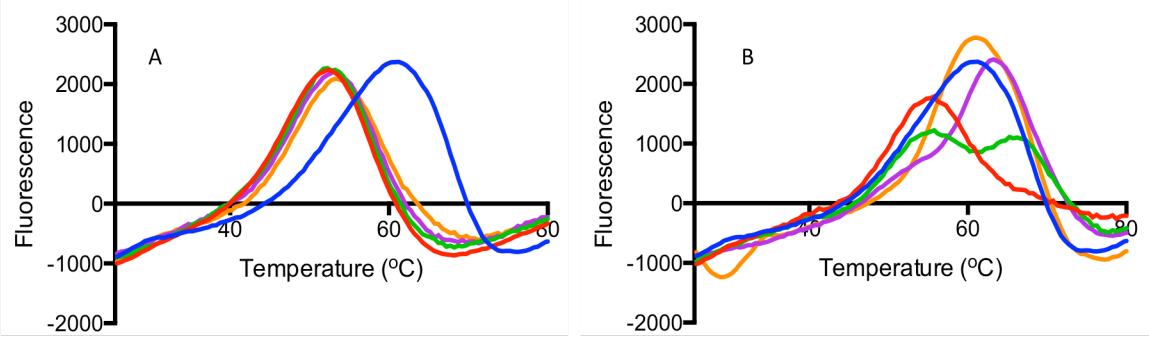

Figure 107: DSF of Fab/k with CMH1 in 50 mM sodium acetate buffer pH 4.0 **A**= (–) 3 µM IgG Fab/k region with (–) 6.0 µM CMH1, (–) 3.0 µM CMH1, (–) 1.5 µM CMH1, (–) 0.75 µM CMH1. **B**= (–) 3 µM IgG Fab/k region with (–) 0.38 µM CMH1, (–) 0.19 µM CMH1, (–) 0.09 µM CMH1, (–) 0.05 µM CMH1.

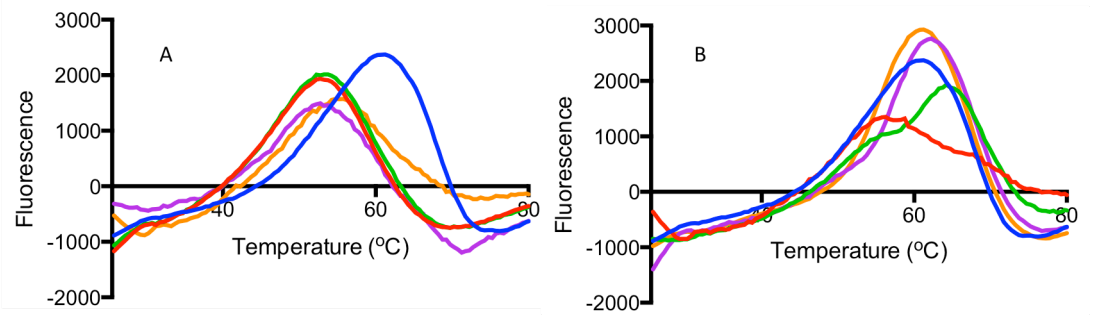

Figure 108: DSF of Fab/k with CMH2 in 50 mM sodium acetate buffer pH 4.0 **A**= (–) 3 µM IgG Fab/k region with (–) 6.0 µM CMH2, (–) 3.0 µM CMH2, (–) 1.5 µM CMH2, (–) 0.75 µM CMH2. **B**= (–) 3 µM IgG Fab/k region with (–) 0.38 µM CMH2, (–) 0.19 µM CMH2, (–) 0.09 µM CMH2, (–) 0.05 µM CMH2.

The change in Tm of Fab/k on addition of 6.0 µM CMH2 is 7.48°C, with the Tm of Fab/k at this concentration being 52.80°C. CMH2 at 3.0 µM has a peak shape, fluorescence intensity and Tm like that of 6.0 µM, with a Tm of 53.21°C. At 1.5 µM the Tm increases to 52.55 °C, with 0.75 µM CMH2 further increasing in Tm to 54.97°C. At 0.19 µM CMH2 the peak has a more intermediate shape containing a peak with a large shoulder. The peak occurs at Tm of 64.48°C with a shoulder at 56.14°C. The shape of peaks at 0.09 µM and 0.05 µM are similar; the Tm of these two peaks of 62.36°C (0.09 µM) and 60.94°C (0.05 µM).

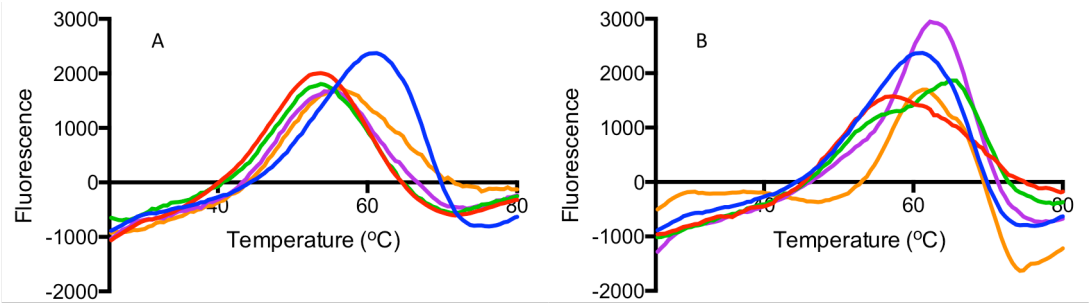

Figure 109: DSF of Fab/k with CMH3 in 50 mM sodium acetate buffer pH 4.0. **A**= (–) 3 µM IgG Fab/k region with (–) 6.0 µM CMH3, (–) 3.0 µM CMH3, (–) 1.5 µM CMH3, (–) 0.75 µM CMH3. **B**= (–) 3 µM IgG Fab/k region with (–) 0.38 µM CMH3, (–) 0.19 µM CMH3, (–) 0.09 µM CMH3, (–) 0.05 µM CMH3.

The reduction in Tm seen in IgG Fab/k with 6.0 µM CMH3 is 6.97°C, with the 6.0 µM CMH3 Tm of 53.29°C. The peaks of 1.5 µM and 0.75 µM have similar shapes, with the

Tm of these peaks at 55.10°C and 55.91°C respectively. At CMH3 concentration of 0.38 µM the peak is more broad, with a Tm of 58.03°C and moves to an intermediate peak at 0.19 µM (64.14°C), with a shoulder at 56.67°C. The highest fluorescence intensity peak in the data belongs to 0.09 µM CMH3 (Tm 62.60°C) with the 0.05 µM CMH3 peak occurring at a lower intensity (60.93°C).

The addition of 6.0 µM CMH4 reduces the IgG Fc Tm to 53.07°C. With addition of reducing concentrations of CMH4, the Tm increases up to 0.38 µM with a Tm of 56.26°C. At 0.19 µM CMH4 the peak splits into two joined peaks with Tm 56.84°C and 64.86°C respectively.

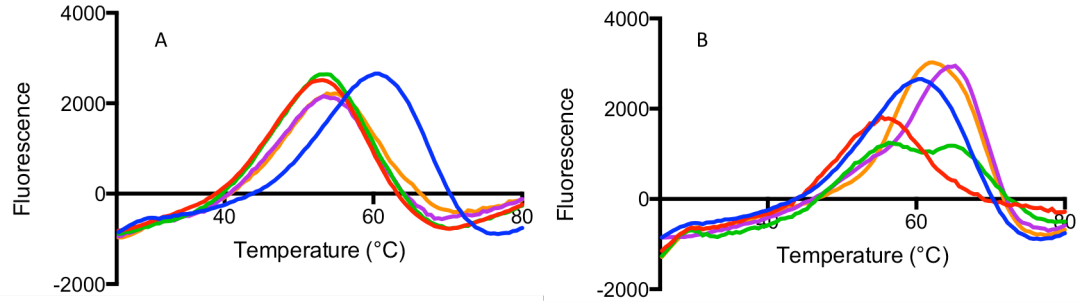

Figure 110: DSF of Fab/k with CMH4 in 50 mM sodium acetate buffer pH 4.0. **A**= (–) 3 µM IgG Fab/k region with (–) 6.0 µM CMH4, (–) 3.0 µM CMH4, (–) 1.5 µM CMH4, (–) 0.75 µM CMH4. **B**= (–) 3 µM IgG Fab/k region with (–) 0.38 µM CMH4, (–) 0.19 µM CMH4, (–) 0.09 µM CMH4, (–) 0.05 µM CMH4.

The addition of 6.0 µM CMH5 reduces the Tm of Fab/k to 55.97°C (Δ 4.11°C). This change however, is not the largest Tm shift in this data, with the difference between 6.0 µM and 0.19 µM CMH5 of 12.33°C. At 3.0 µM CMH5 displays the same peak shape as at 6.0 µM, with a Tm of 56.56°C. The CMH5 concentrations of 1.5 µM and 0.75 µM have with Tm of 57.15°C and 58.30°C. At 0.19 µM CMH5, the IgG Fab/k peak occurs at Tm of 64.55°C The peaks at 0.09 µM and 0.05 µM have both higher Tm than IgG Fab/k at 62.55°C and 61.45°C.

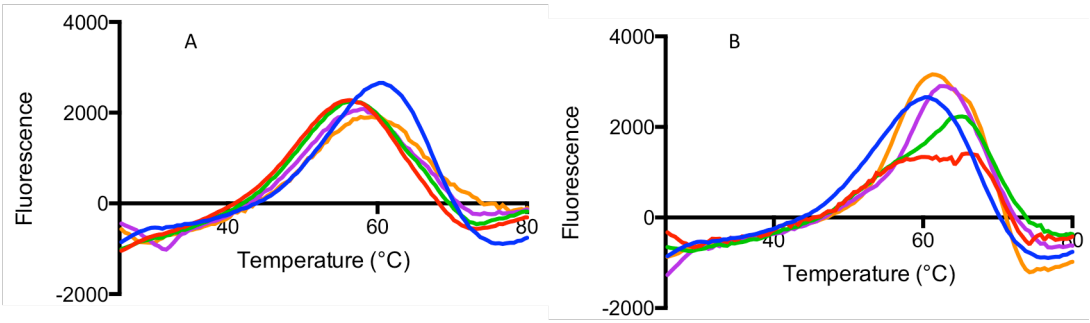

Figure 111: DSF of Fab/k with CMH5 in 50 mM sodium acetate buffer pH 4.0. **A**= (–) 3 µM IgG Fab/k region with (–) 6.0 µM CMH5, (–) 3.0 µM CMH5, (–) 1.5 µM CMH5, (–) 0.75 µM CMH5. **B**= (–) 3 µM IgG Fab/k region with (–) 0.38 µM CMH5, (–) 0.19 µM CMH5, (–) 0.09 µM CMH5, (–) 0.05 µM CMH5.

The largest shift in Tm seen with the addition of CMH6 is the difference between 6.0 µM CMH6 and 0.19 µM CMH5 of 7.48°C, also seen in CMH5 with IgG Fab/k. The Tm Tm shift seen from IgG Fab/k to the inclusion of 6.0 µM CMH6 is 3.94°C. The peaks of 6.0 µM, 3.0 µM, 1.5 µM and 0.75 µM increase in Tm from the 6.0 µM Tm of 56.14°C to 0.75 µM Tm at 57.17°C. The CMH6 concentration of 0.19 µM has a Tm of 63.62°C; greater than IgG Fab/k only.

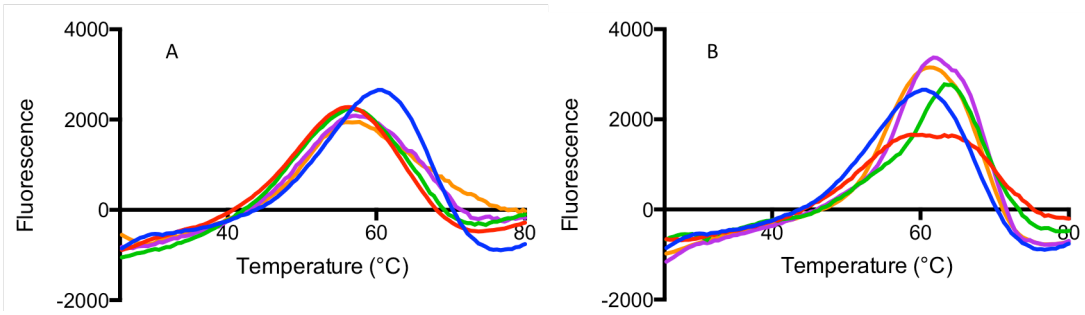

Figure 112: DSF of Fab/k with CMH6 in 50 mM sodium acetate buffer pH 4.0. **A**= (–) 3 µM IgG Fab/k region with (–) 6.0 µM CMH6, (–) 3.0 µM CMH6, (–) 1.5 µM CMH6, (–) 0.75 µM CMH6. **B**= (–) 3 µM IgG Fab/k region with (–) 0.38 µM CMH6, (–) 0.19 µM CMH6, (–) 0.09 µM CMH6, (–) 0.05 µM CMH6

The difference between the Tm between IgG Fab/k and 6.0 µM CMH7 follows the same trend of the other chemically modified heparins with this immunoglobulin fragment; the greatest difference in Tm seen is between 6.0 µM and 0.19 µM CMH7. The concentrations of 6.0 µM, 3.0 µM, and 1.5 µM CMH7 have the same Tm at approximately 53°C. The peak shape remains the same for 0.75 µM and 0.38 µM CMH7, but the Tm increases to 54.79°C and 55.53°C respectively.

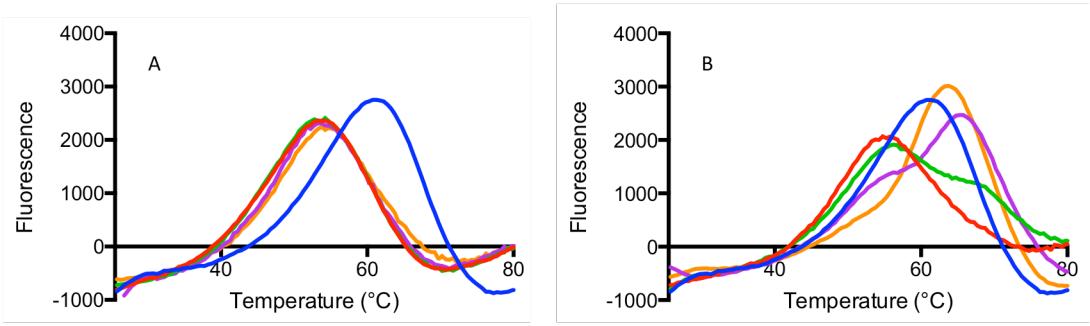

Figure 113: DSF of Fab/k with CMH7 in 50 mM sodium acetate buffer pH 4.0. **A**= (–) 3 µM IgG Fab/k region with (–) 6.0 µM CMH7, (–) 3.0 µM CMH7, (–) 1.5 µM CMH7, (–) 0.75 µM CMH7. **B**= (–) 3 µM IgG Fab/k region with (–) 0.38 µM CMH7, (–) 0.19 µM CMH7, (–) 0.09 µM CMH7, (–) 0.05 µM CMH7

All concentrations of CMH8 lead to an increased Tm compared to IgG Fab/k alone. The IgG Fab/k Tm is 60.60°C, with all CMH8 concentrations tested with IgG Fab/k Tm at 63.20°C.

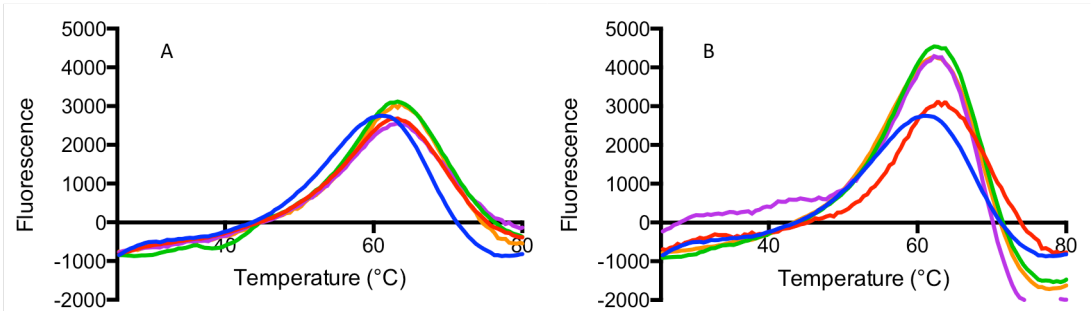

Figure 114: DSF of Fab/k with CMH8 in 50 mM sodium acetate buffer pH 4.0. **A**= (–) 3 µM IgG Fab/k region with (–) 6.0 µM CMH8, (–) 3.0 µM CMH8, (–) 1.5 µM CMH8, (–) 0.75 µM CMH8. **B**= (–) 3 µM IgG Fab/k region with (–) 0.38 µM CMH8, (–) 0.19 µM CMH8, (–) 0.09 µM CMH8, (–) 0.05 µM CMH8.

The greatest Tm shift seen with CMH9 is the difference in Tm between 6.0 µM and 0.75 µM CMH9 12.79°C. The 6.0 µM Tm peak occurs at 51.86°C. The 3.0 µM curve follows the same peak shape with similar Tm. CMH9 concentration of 1.5 µM and 0.75 µM have equivalent shaped curves with Tm 52.70°C. At 0.38 µM CMH9, the Tm shifts further to a higher melting temperature, at 53.64°C. CMH9 concentration 0.19 µM gives an intermediate peak with a double-peak structure at Tm of 55.55°C and 64.65°C with peak.

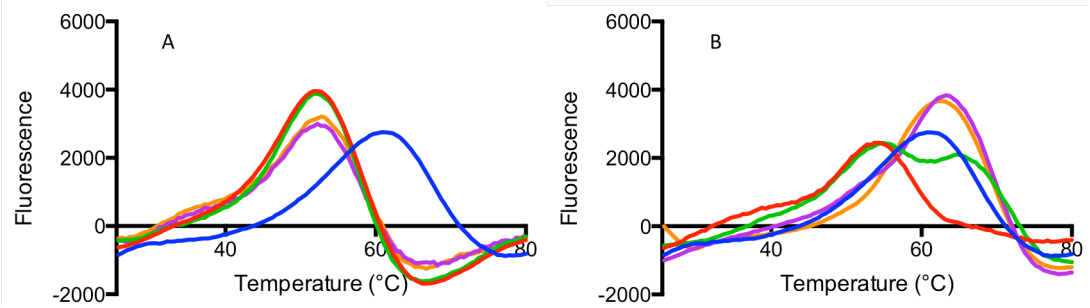

Figure 115: DSF of Fab/k with CMH9 in 50 mM sodium acetate buffer pH 4.0. **A**= (–) 3 µM IgG Fab/k region with (–) 6.0 µM CMH9 (–) 3.0 µM CMH9 (–) 1.5 µM CMH9 (–) 0.75 µM CMH9 **B**= (–) 3 µM IgG Fab/k region with (–) 0.38 µM CMH9 (–) 0.19 µM CMH9 (–) 0.09 µM CMH9 (–) 0.05 µM CMH9.

The PCA of Fab/k the 1st derivative DSF data with CMH 1-7 and CMH9 follow the same data distrubition of CMH1 in Figure 116 The protein only Fab/k control occurs as a mid-point within the concentrations of CMH tested. CMH8 however, the PC1 shows little variation and covers 93.3% of the variance of the data, suggesting all concentrations of CMH8 tested in DSF have a minimal effect on the thermal stability of Fab/k.

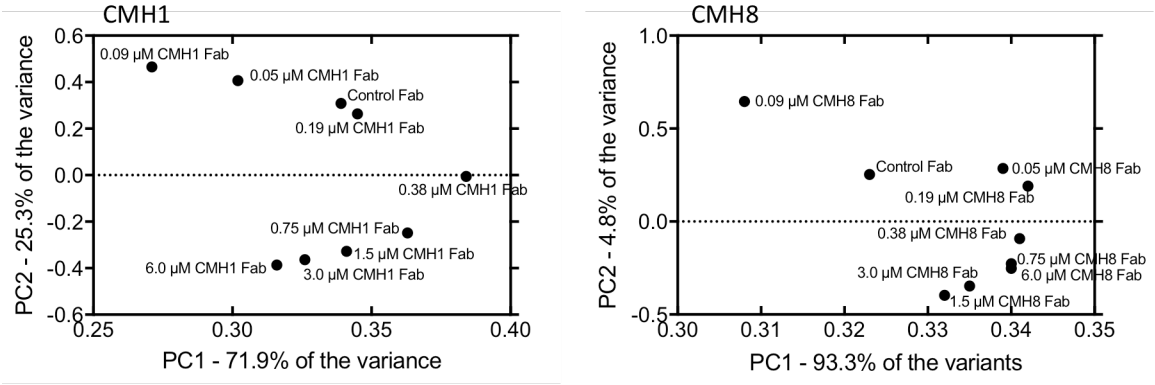

Figure 116: PCA of 1st derivative DSF melt curves of Fab/k with CMH1 and CMH8 in 50 mM sodium acetate pH 4.0.

6.2.2 Circular dichroism with IgG Fab/k region and chemically modified heparins

Far UV circular dichroism was utilised to show changes in Fab/k secondary structure upon addition of each member of the chemically modified heparin library.

Each chemically modified heparin modified the Fab/k spectra to different degrees. The positive ellipticity peak occurring at λ = 207 nm is altered to λ = 209 nm with CMH1, with the trough at λ = 228 nm in Fab/k alone shifted to λ = 231 nm with the CMH1 (Figure 117). The two-sulphated CMH2 shown in Figure 117B with Fab/k no longer retains the negative peak feature at λ = 228 nm, with a peak reading occurring at this wavelength. The positive λ = 207 nm peak is also shifted to a higher CD reading at λ = 210 nm. CMH3 contains a similar spectral feature to CMH2 in that the spectral trough is absent, and the positive mdeg peak occurs at λ = 211 nm (Figure 117C). The singularly sulphated CMH4 spectra incudes both the return of the trough at λ = 231 nm and the smaller shift of the positive peak at λ = 209 nm, like CMH1, (Figure 117D).

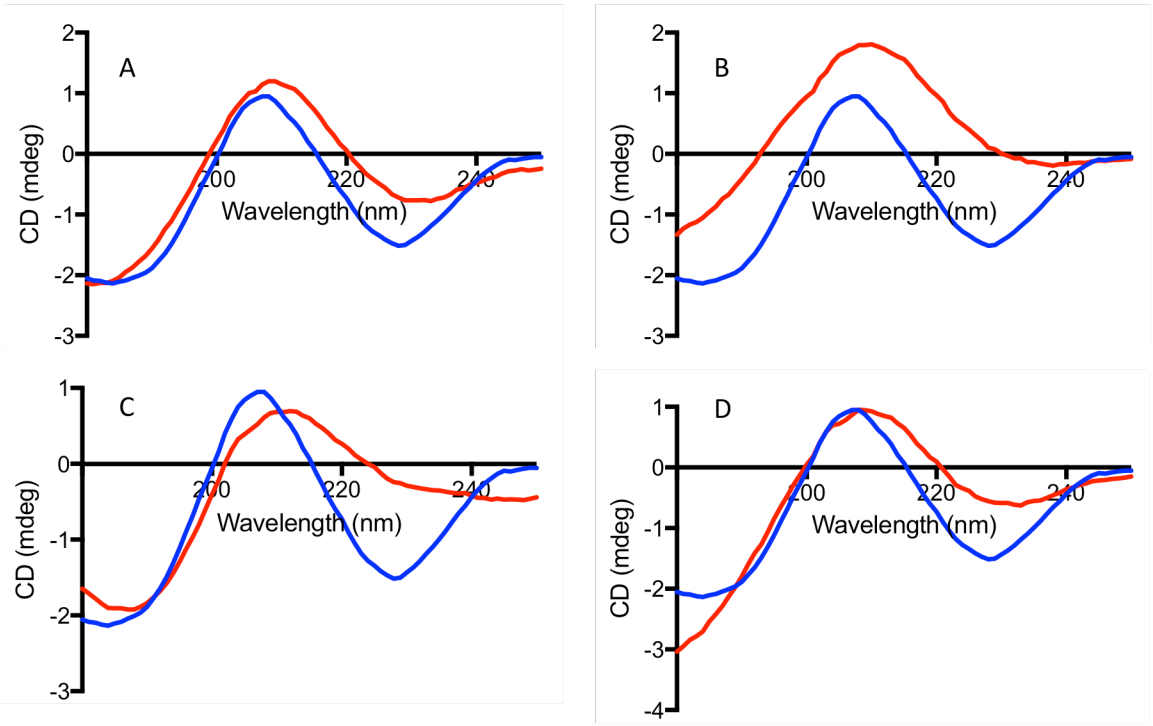

Figure 117: Far-UV CD spectra of Fab/k with CMH 1-4 in 50 mM sodium acetate pH 4.0. (–) 3 μM IgG Fab/k region with **A**) (–) 3 μM CMH1**, B**) (–) 3 μM CMH2, **C**) (–) 3 μM CMH3 **D**) (–) 3 μM CMH4.

Figure 118 continues these CD spectra of Fab/k including CMH5, which consists of a small trough at λ = 229 nm and a higher intensity peak at λ = 208 nm. While the wavelengths of the peaks do not differ largely from the Fab/k only spectra, the intensity of the CD spectra differs from the protein only spectra, showing that the two are not superimposable.

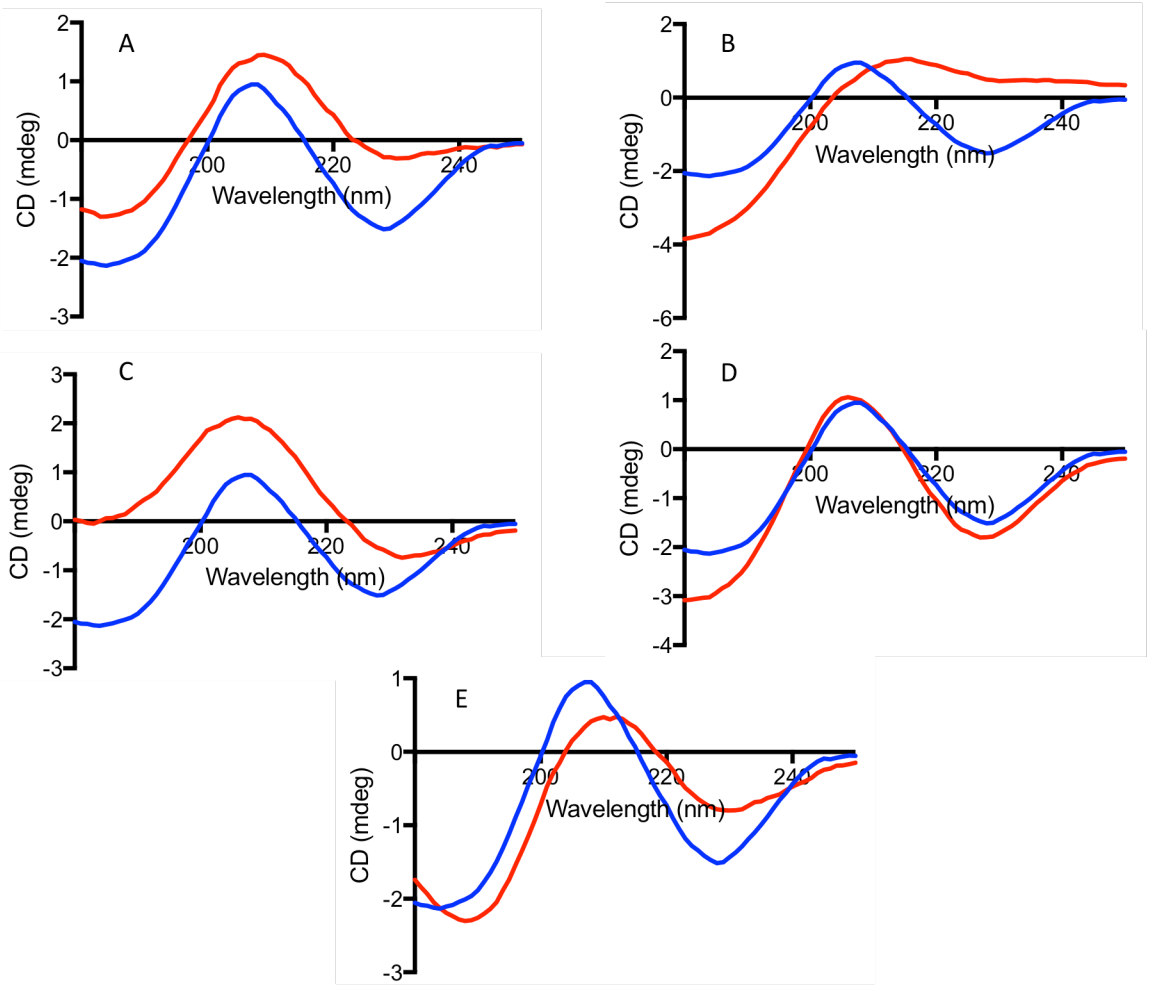

Figure 118: Far-UV circular dichroism spectra of Fab with CMH 5-9 in 50 mM sodium acetate pH 4.0. A)(–) 3 μM IgG Fab/k region (–) IgG Fab/k region with 3 μM CMH5, B)(–) IgG Fab/k region (–) IgG Fab/k region with 3 μM CMH6, C)(–) IgG Fab/k region (–) IgG Fab/k region with 3 μM CMH7 D)(–) IgG Fab/k region (–) IgG Fab/k region with 3 μM CMH8, E)(–) IgG Fab/k region (–) IgG Fab/k region with 3 μM CMH9.

The CMH6 spectra at wavelength greater than λ = 220 nm is all in the region, unlike each other chemically modified heparin tested (Figure 118A). The peak occurs at λ = 215 nm with a similar intensity as the Fab/k only peak at λ = 207 nm. CMH7 shifts

the trough to λ = 331 nm from the protein only λ = 228 nm (Figure 118C). The positive peak at λ = 207 nm the same as the protein only peak, but the intensity is greater. Unsulphated CMH8 shows no change to the Fab/k far-UV CD spectra. Unlike the other immunoglobulins tested thus far, per-sulphated CMH9 does not have the greatest structural change in Fab/k. The trough reaches λ = 230 nm, from the protein only peak of λ = 228 nm and the peak occurs at λ = 212 nm, from the protein only peak of λ = 207 nm (Figure 118E).

6.2.3 Fab/k stability in the presence of low molecular weight heparins

Five pharmaceutically relevant low molecular weight heparins were employed to determine the effect of these drugs on the stability of Fab/k fragment of immunoglobulin. In DSF the Fab/k only peak has a Tm of 60.86°C. Fondaparinux has a similar Tm to Fab only of 60.65°C. Addition of 6.0 µM of UF PMH reduces the Tm to 52.42°C; the remaining LMWH have Tm all of ≈ 53°C with peak shape similar to that of CMH1.

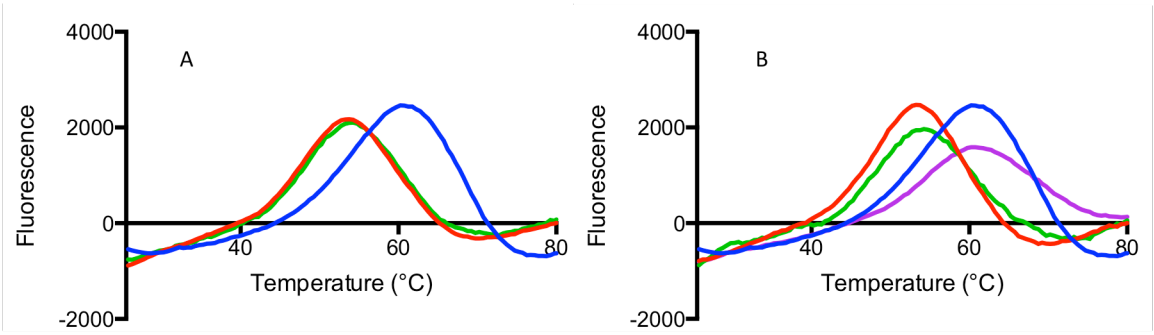

Figure 119: DSF of Fab/k with LMWH in 50 mM sodium acetate buffer pH 4.0 **A**= (–) 3 µM IgG Fc region (–) IgG Fc region with 6.0 µM dalteparin (–) IgG Fc region with 6.0 µM enoxaparin. **B**= (–) 3 µM IgG Fc region (–) IgG Fc region with 6.0 µM tinzaparin (–) IgG Fc region with 6.0 µM reviparin, (–) IgG Fc region with 6.0 µM fondaparinux.

6.2.4 Fab/k stability in the presence of GAGs and heparin controls

Sodium sulphate and UA(2S)-GlcNS(6S) (disaccharide standard 6) both do not alter the structural stability of Fab/k as shown in Figure 120 A&B. Heparan sulphate reduces the Tm of this protein similarly to CMH1 to 55.72°C. Chondroitin sulphate A and B do not change the Tm of Fab/k in DSF to the same degree as HS with a Tm of 59.13°C (Figure 120C).

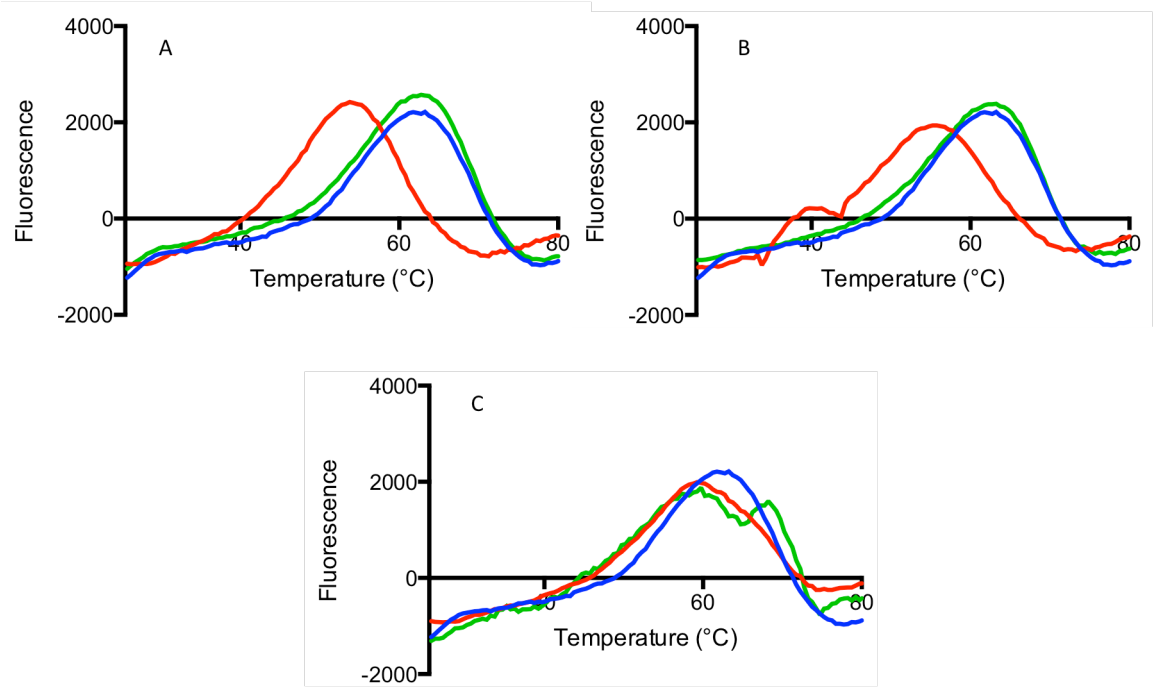

Figure 120: DSF of Fab/k with GAGs and sulphate controls in 50 mM sodium acetate buffer pH 4.0 (–) 3 µM human IgG Fab/k region with **A**) (–) 6.0 µM UF PMH, (–) 500 nM sodium sulphate, **B**) (–) 6.0 µM DS6 (–) 12.0 µM HS, **C**) (–) 6.0 µM CSA, (–) 6.0 µM CSC.

6.2.5 Fab/k stability in the presence of size defined heparin fractions

With the addition of 6.0 µM full length CMH1 to human IgG Fab/k fragment in 50 mM sodium acetate pH 4.0 in DSF, the Tm of the protein is reduced from 62.82°C to 54.39°C (Table 13).

The three smallest d.p. fragments increase the Tm of the Fab/k fragment alone, with d.p.2 Tm of 65.13°C. Saccharide of d.p.20 has a Tm of 54.32°C which is most similar

to UF PMH (0.07°C different) with Fab/k, with saccharides of d.p.12 and d.p.16 also have Tm similar to full length Fab (54.92°C and 54.81°C respectively). However, the d.p.14 has an increased Tm of 56.76°C which is 2.37°C above that of UF PMH.

Table 13: The Tm from DSF of Fab/k with each PMH polymerization (D.P) fragment in 50 mM sodium acetate buffer pH 4.0.

d.p.	Tm (°C)
None	62.82
2	65.13
4	63.73
6	63.33
8	60.63
10	60.10
12	54.92
14	56.76
16	54.81
18	55.81
20	54.32
UF PMH	54.39

6.2.6 Fab/k binds heparin in Hi-trap HPLC

Heparin affinity chromatography with IgG Fab/k in PBS at various pH determined heparin binding occurred at pH 4.0 and 5.0, however the majority of the protein was eluted prior to the 2M NaCl gradient suggesting no binding to the column (Figure 121). PBS at pH 5.0 gave a 247 mM heparin affinity, with pH 4 PBS allowing a stronger heparin binding at 755 mM and 989 mM.

Fab/k in heparin hi-trap affinity chromatography in 50 mM sodium acetate pH 4.0 has a 797 mM binding affinity; between the two binding affinities seen in pH 4 PBS (Figure 122). This data gives a clear peak when compared to the non-binding protein elution prior to salt gradient.

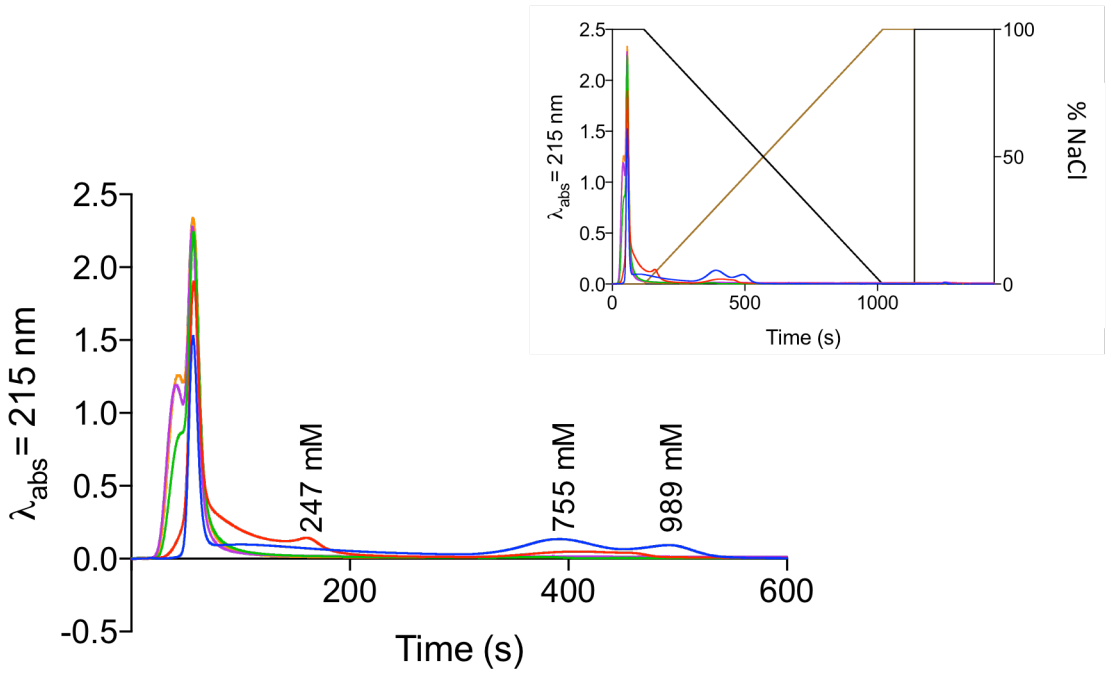

Figure 121: Human IgG Fab/k fragment in heparin HiTrap affinity HPLC in PBS at differing pH (4.0 – 7.4) and elution with 2M NaCl. (–) PBS pH 4, (–) PBS pH 5.0, (–) PBS pH 6.0, (–) PBS pH 7.0, (–) PBS pH 7.4.

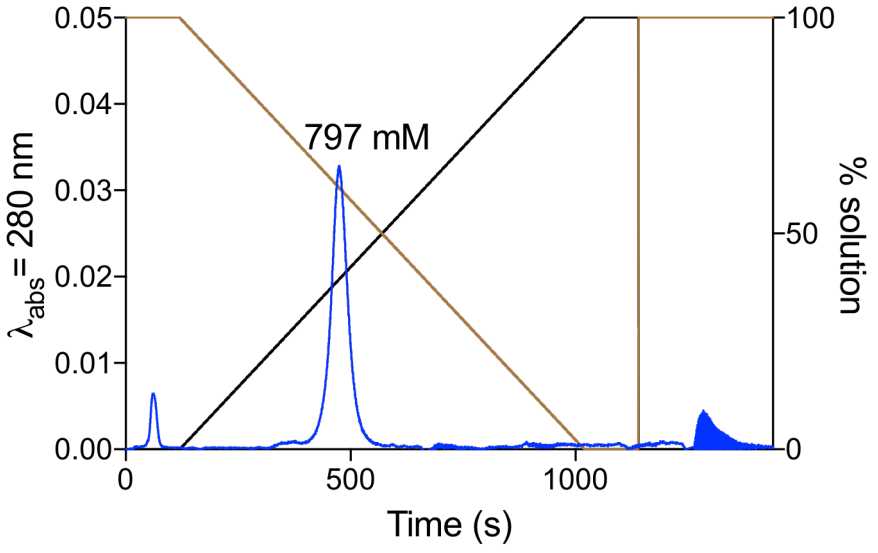

Figure 122: Human IgG Fab/k in heparin HiTrap affinity HPLC in 50 mM sodium acetate pH 4.0 with 2M NaCl elution.

6.2.7 F(ab')2 stability in the presence of chemically modified heparins

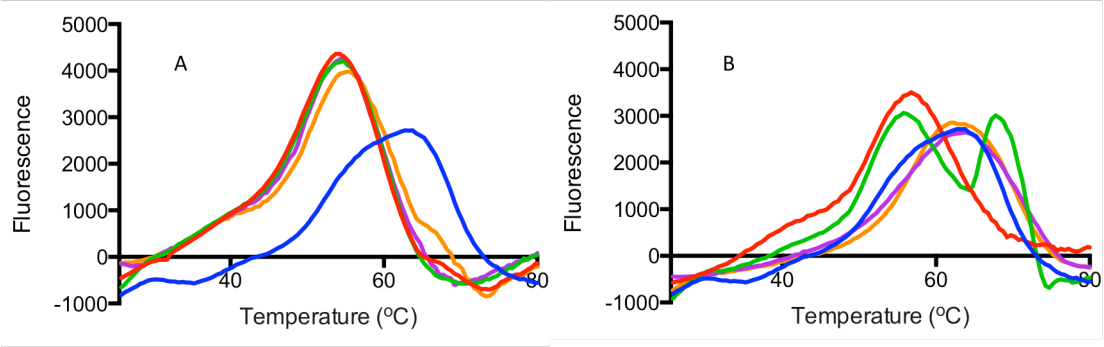

Figure 123: DSF of F(ab')2 with CMH1 in 50 mM sodium acetate buffer pH 4.0 **A**= (–) 3 µM IgG F(ab')2 region with (–) 6.0 µM CMH1, (–) 3.0 µM CMH1, (–) 1.5 µM CMH1, (–) 0.75 µM CMH1. **B**= (–) 3 µM IgG F(ab')2 region with (–) 0.38 µM CMH1, (–) 0.19 µM CMH1, (–) 0.09 µM CMH1, (–) 0.05 µM CMH1.

The IgG F(ab')2 alone has a Tm of 63.14°C. On addition of 6.0 µM CMH1, the Tm shifts 8.93°C, to a lower Tm of 54.21°C with a fluorescence intensity 4400 ΔFU. Addition of 3.0 µM and 1.5 µM CMH1 yields the same curve shape with Tm of 54.58°C and 54.38°C respectively. The CMH1 concentration of 0.38 µM with IgG F(ab')2 has a Tm of 57.10°C, with a slightly lower fluorescence intensity than that of the higher CMH1 concentrations (3400 ΔFU). The peak of 0.19 µM CMH1 has a Tm of 57.10°C with a secondary peak at Tm of 69.08°C.

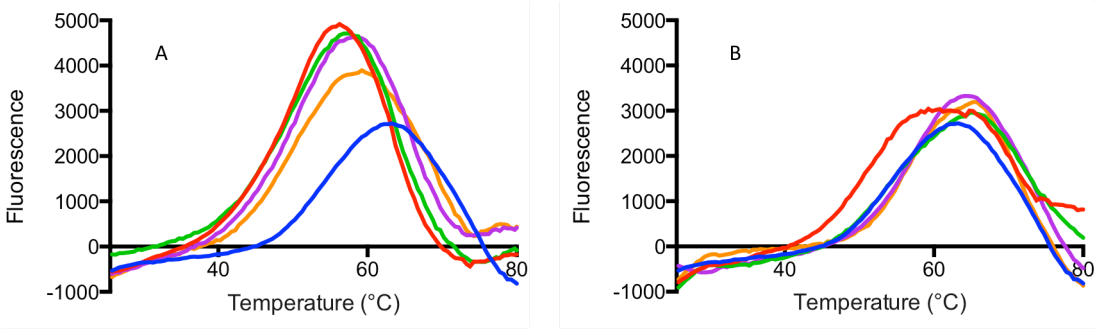

Figure 124: DSF of F(ab')2 with CMH2 in 50 mM sodium acetate buffer pH 4.0 **A**= (–) 3 µM IgG F(ab')2 region with (–) 6.0 µM CMH2, (–) 3.0 µM CMH2, (–) 1.5 µM CMH2, (–) 0.75 µM CMH2. **B**= (–) 3 µM IgG F(ab')2 region with (–)0.38 µM CMH2, (–) 0.19 µM CMH2, (–) 0.09 µM CMH2, (–) 0.05 µM CMH2.

The difference in Tm between IgG F(ab')2 alone and 6.0 µM CMH2 is larger than with CMH1 at 9.60°C. The addition of decreasing concentrations of CMH2 increases the Tm and reduces the fluorescence intensity of the peaks. The peak shape at 0.38 µM CMH2 is wider and flattened than that of higher concentrations of CMH2. At concentrations at 0.19 µM CMH2 has Tm above that of IgG F(ab')2 alone.

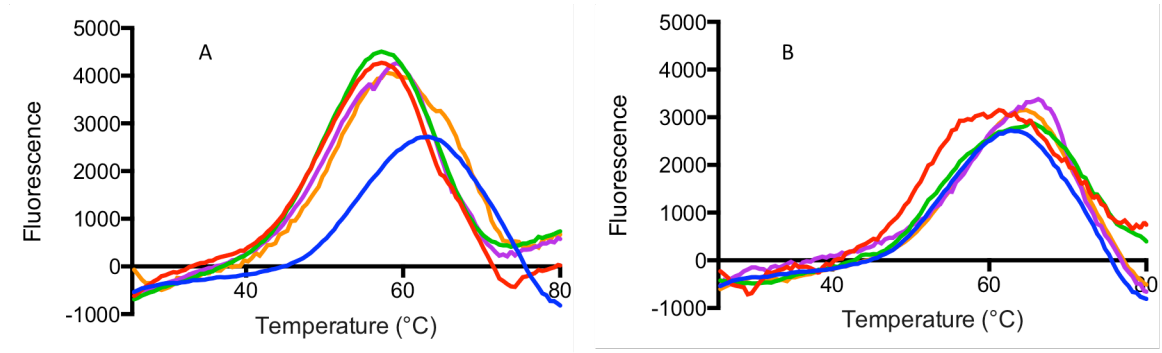

Figure 125: DSF of F(ab')2 with CMH3 in 50 mM sodium acetate buffer pH 4.0. **A**= (–) 3 µM IgG F(ab')2 region with (–) 6.0 µM CMH3, (–) 3.0 µM CMH3, (–) 1.5 µM CMH3, (–) 0.75 µM CMH3. **B**= (–) 3 µM IgG F(ab')2 region with (–) 0.38 µM CMH3, (–) 0.19 µM CMH3, (–) 0.09 µM CMH3, (–) 0.05 µM CMH3.

The greatest shift in Tm with CMH3 occurs with 6.0 µM compared to IgG F(ab')2 alone. This Tm change is 7.58°C, lower than both CMH1 and CMH2. The overall shape of the peak is similar to CMH2 with F(ab')2. At 6.0 µM the Tm is 56.97°C. Concentrations of 1.5 µM and 0.75 µM CMH3 have similar fluorescence intensity peaks (4070 ΔFU) with Tm of 58.88°C and 58.74°C respectively, however, 0.75 µM exhibits a possible air bubble due to a intensity spike at 60.59°C. CMH3 at 0.38 µM has a wider and flattened peak at 61.45°C with lower intensity of 3100 ΔFU. The curve at 0.19 µM mirrors the intensity and Tm of IgG F(ab')2 alone (Tm at 64.18°C). The concentrations of 0.09 µM and 0.05 µM have higher Tm than that of IgG F(ab')2 alone.

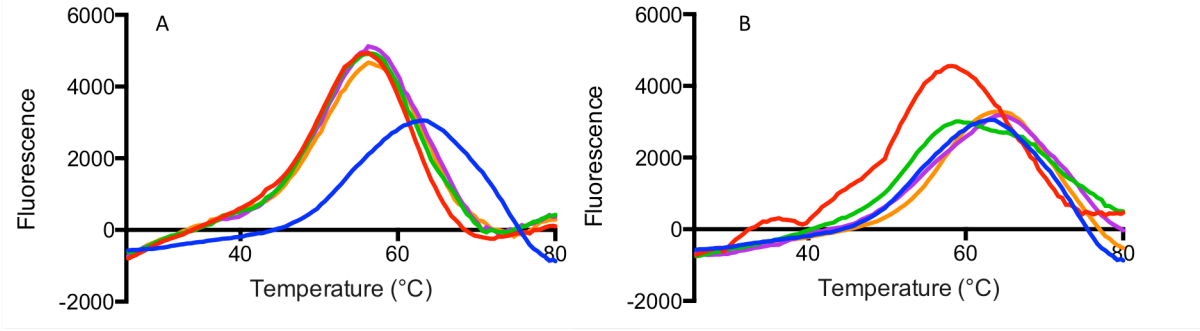

Figure 126: DSF of F(ab')2 with CMH4 in 50 mM sodium acetate buffer pH 4.0. **A**= (–) 3 µM IgG F(ab')2 region with (–) 6.0 µM CMH4, (–) 3.0 µM CMH4, (–) 1.5 µM CMH4, (–) 0.75 µM CMH4. **B**= (–) 3 µM IgG F(ab')2 region with (–) 0.38 µM CMH4, (–) 0.19 µM CMH4, (–) 0.09 µM CMH4, (–) 0.05 µM CMH4.

The reduction in Tm with the addition of 6.0 µM CMH4, compared to the F(ab')2 control only is 8.38°C, with the increase in fluorescence intensity seen in the other chemically modified heparins with this immunoglobulin fragment. The concentrations tested can be grouped into two, with the first higher intensity peaks belonging to CMH4 concentrations of 6.0 – 0.38 µM, with intensity at these concentrations 4500-5000 ΔFU. The 0.19 µM CMH4 concentration along with 0.09 µM and 0.05 µM belong in the second group which occur ≈ Tm of the IgG F(ab')2 control.

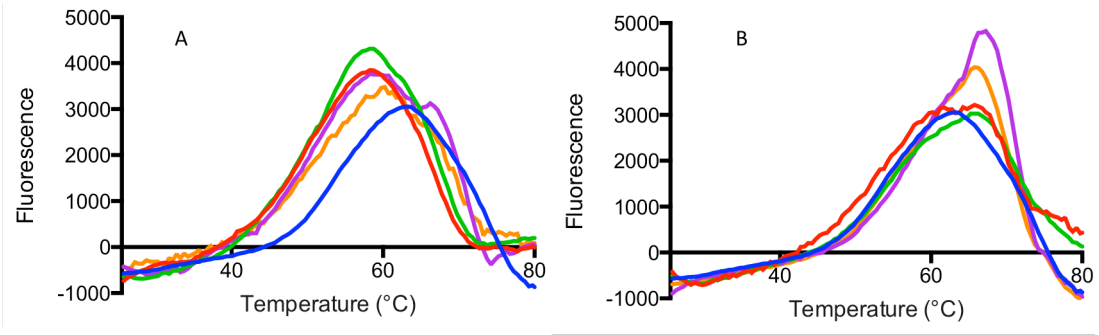

Figure 127: DSF of F(ab')2 with CMH5 in 50 mM sodium acetate buffer pH 4.0 **A**= (–) 3 µM IgG F(ab')2 region with (–) 6.0 µM CMH5, (–) 3.0 µM CMH5, (–) 1.5 µM CMH5, (–) 0.75 µM CMH5. **B**= (–) 3 µM IgG F(ab')2 region with (–) 0.38 µM CMH5, (–) 0.19 µM CMH5, (–) 0.09 µM CMH5, (–) 0.05 µM CMH5.

The reduction in Tm seen with 6.0 µM CMH5 addition is 6.13°C, with the Tm at this concentration at 58.18°C with an increased intensity of 3800 ΔFU. With 3.0 µM

CMH5 the Tm with IgG F(ab')2 reduces to 57.71°C with a higher fluorescence intensity. The CMH5 concentration of 1.5 µM has a similar fluorescence intensity peak as 6.0 µM with a Tm of 58.98°C, with the intensity falling with lowering CMH5 concentration but the peak has a secondary peak at 62.22°C which is mirrored in the 0.09 µM and 0.05 µM concentrations of CMH5 with this immunoglobulin fragment. CMH5 of 0.05 µM with F(ab')2 demonstrates the highest melting point with Tm of 67.18 °C.

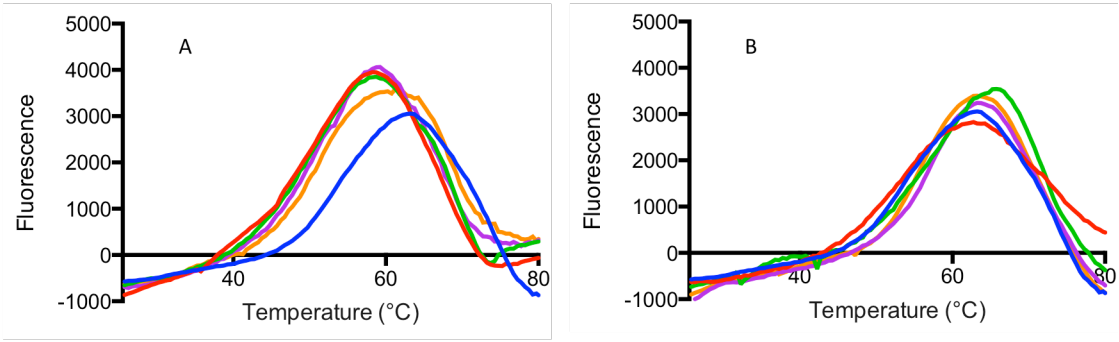

Figure 128: DSF of F(ab')2 with CMH6 in 50 mM sodium acetate buffer pH 4.0. **A**= (–) 3 µM IgG F(ab')2 region with (–) 6.0 µM CMH6, (–) 3.0 µM CMH6, (–) 1.5 µM CMH6, (–) 0.75 µM CMH6. **B**= (–) 3 µM IgG F(ab')2 region with (–) 0.38 µM CMH6, (–) 0.19 µM CMH6, (–) 0.09 µM CMH6, (–) 0.05 µM CMH6.

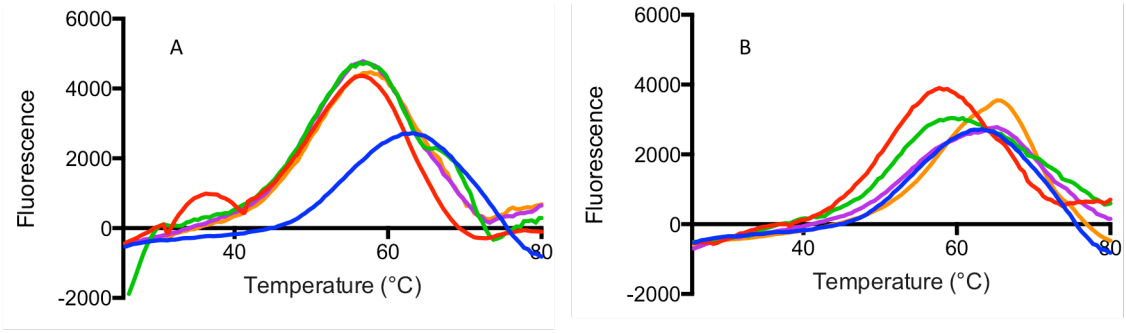

Figure 129: DSF with F(ab')2 and CMH7 in 50 mM sodium acetate buffer pH 4.0 **A**= (–) 3 µM IgG F(ab')2 region with (–) 6.0 µM CMH7, (–) 3.0 µM CMH7, (–) 1.5 µM CMH7, (–) 0.75 µM CMH7. **B**= (–) 3 µM IgG F(ab')2 region with (–) 0.38 µM CMH7, (–) 0.19 µM CMH7, (–) 0.09 µM CMH7, (–) 0.05 µM CMH7.

The Tm shift from IgG F(ab')2 alone to protein with 6.0 µM is 4.13°C, to a Tm of 58.59°C. The intensity of the 6.0 µM CMH6 with IgG F(ab')2 peak is 4000 ΔFU, with 3.0 µM and 1.5 µM CMH6 peaks with this Ig having the same peak shape and fluorescence

intensity. The Tm of 3.0 µM CMH6 is 58.34°C and at 1.5 µM the Tm is 58.28°C. The peak at 0.75 µM is more broad than the higher concentrations, with Tm of 60.52°C.

Melting temperature of IgG F(ab')2 decreases to 56.83°C with the addition of 6.0 µM CMH7; a reduction in Tm of 6.07°C. The fluorescence intensity with 6.0 µM CMH7 is increased from 2700 ΔFU (F(ab')2 control) to 4300 ΔFU. The concentrations 3.0 µM, 1.5 µM, and 0.75 µM CMH7 all have higher intensity peaks (3.0 µM highest at 5000 ΔFU) than 6.0 µM. CMH7 at 3.0 µM has a Tm of 56.84°C and a smaller sub-peak at 70.46°C. Concentrations of 1.5 µM and 0.75 µM CMH7 have a Tm of 56.99°C and 57.44°C respectively. At 0.38 µM CMH7, the intensity of the peak drops below that of 6.0 µM CMH7 to 3800 ΔFU, with a Tm of 58.61°C. The curve of 0.09 µM CMH7 with F(ab')2 mirrors the shape of the F(ab')2 alone peak but has a higher Tm of 63.69°C.

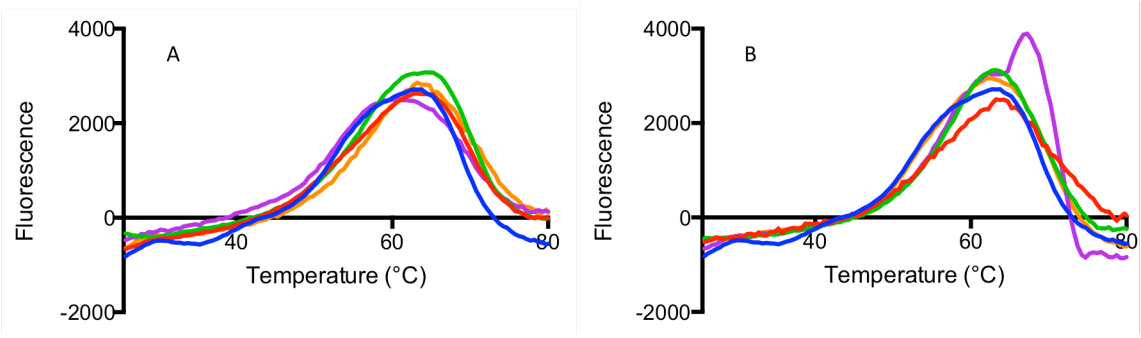

Figure 130: DSF of F(ab')2 with CMH8 in 50 mM sodium acetate buffer pH 4.0 with 3 µM human IgG F(ab')2 **A**= (–) 3 µM IgG F(ab')2 region with (–) 6.0 µM CMH8, (–) 3.0 µM CMH8, (–) 1.5 µM CMH8, (–) 0.75 µM CMH8. **B**= (–) 3 µM IgG F(ab')2 region with (–) 0.38 µM CMH8, (–) 0.19 µM CMH8, (–) 0.09 µM CMH8, (–) 0.05 µM CMH8.

Each concentration of CMH8 tested has ≈ Tm as IgG F(ab')2 alone (Tm of 62.50°C) apart from 1.5 µM CMH8 which has a Tm at 60.37°C. The concentration of 0.09 µM CMH8 has an anomalous spike at 68.87°C with a fluorescence intensity 4370 ΔFU.

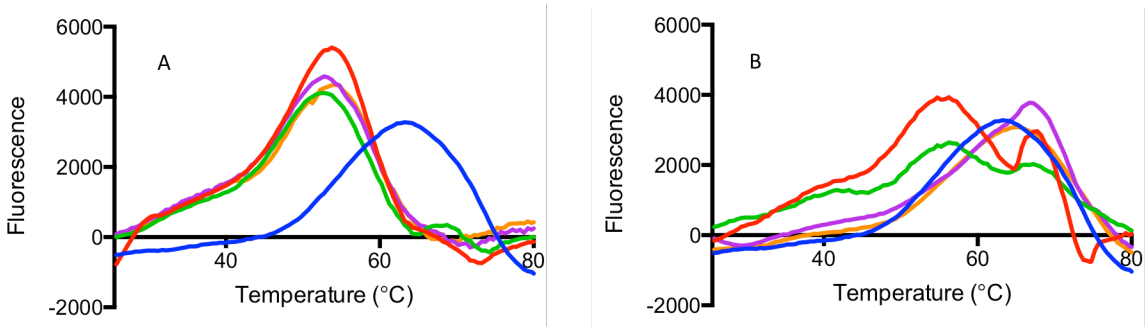

Figure 131: DSF of F(ab')2 with CMH9 in 50 mM sodium acetate buffer pH 4.0. **A**= (–) 3 µM IgG F(ab')2 region with (–) 6.0 µM CMH9, (–) 3.0 µM CMH9, (–) 1.5 µM CMH9, (–) 0.75 µM CMH9. **B**= (–) 3 µM IgG F(ab')2 region with (–) 0.38 µM CMH9, (–) 0.19 µM CMH9, (–) 0.09 µM CMH9, (–) 0.05 µM CMH9.

CMH9 with IgG F(ab')2 is the most complex of the dataset. A reduction in Tm of 9.97°C occurs on addition of 6.0 µM CMH9; the largest shift seen with this Ig. The difference in fluorescence intensity between these two peaks is an increase of 2100 ΔFU with the addition of CMH9 at 6.0 µM. The concentrations of 3.0 µM and 1.5 µM CMH9 have similar Tm to 6.0 µM CMH9 at 52.64°C and 52.13°C; these concentrations of CMH9 also have shoulder peaks at Tm of 67.78°C and 68.99°C. CMH9 at 0.38 µM has a joined peak with Tm of 55.38°C and 68.92 °C. At 0.19 µM CMH9 the curve is flattened across 30°C to 80°C. The highest point of this curve is Tm of 56.12°C with the second highest region with the Tm 67.77°C, the same Tm as the spiked peak at 0.38 µM CMH9. The CMH9 concentration of 0.09 µM has a Tm of 65.76°C. IgG F(ab')2 with 0.05 µM CMH9 has a peak which mimics the shape of IgG F(ab')2 only, with Tm of 64.66°C.

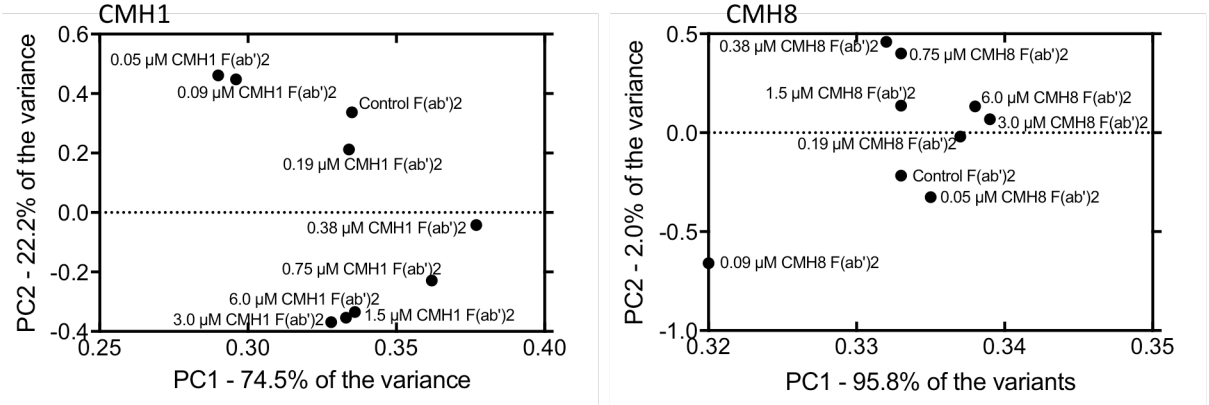

Figure 132: PCA of 1st derivative DSF data of F(ab')2 with CMH1 and CMH8.

The PCA of F(ab')2 and CMH demonstrates a similar relationship as Fab with the modified heparin library. CMH1-7 and CMH9 follow the same distribution pattern in both PC1 and PC2, with unsulphated CMH8 demonstrating limited variability in PC1.

6.2.8 Circular dichroism with F(ab')2 region and chemically modified heparins

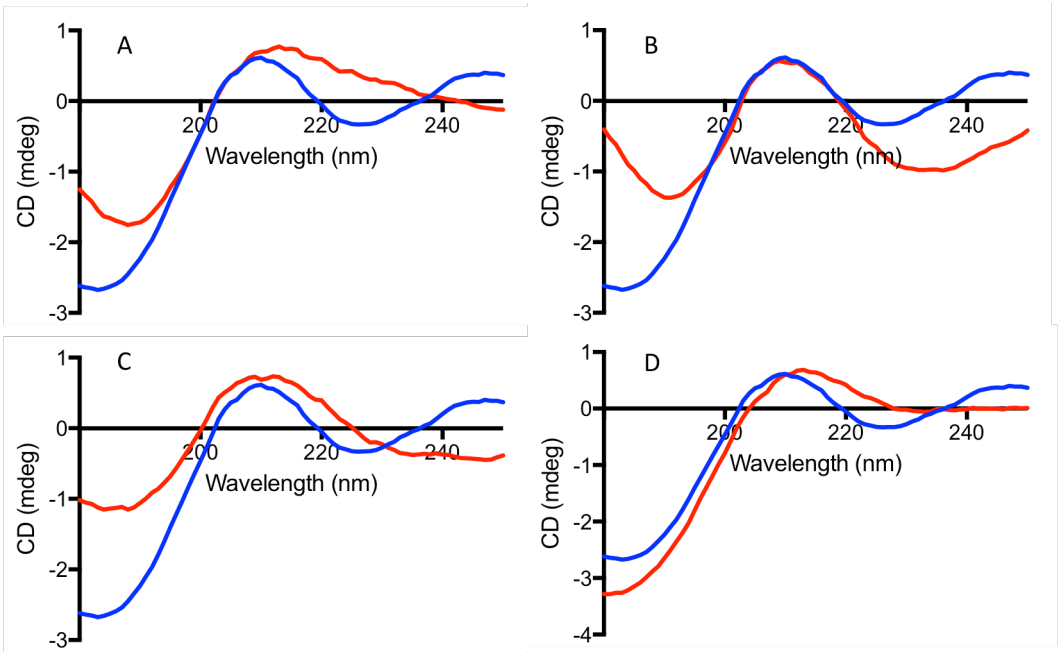

Figure 133: Far-UV CD spectra, of F(ab')2 with CMH 1-4 with 50 mM sodium acetate pH 4.0. (–) 3 µM IgG F(ab')2 region with **A**) (–) 3 µM CMH1, **B**) (–) 3 µM CMH2, **C**) (–) 3 µM CMH3 **D**) (–) 3 µM CMH4.

IgG F(ab')2 in far-UV circular dichroism, two regions of the spectrum will be compared to identify differences in the secondary structure with the addition of chemically modified heparin; the peak at λ = 209 nm and the trough at λ = 227 nm. CMH1 shifts the spectra to a peak at λ = 213 nm and flattens the peak in the higher wavelength region (Figure 133A). Both CMH2 and CMH3 with IgG F(ab')2 have a peak at λ = 209 nm, bit with CMH2 the trough is at λ = 234 nm (Figure 133B) and with CMH3 this peak region is flattened (Figure 133C). CMH4 shifts the peak to the higher wavelength of λ = 213 nm and flattens the ellipticity to 0 mdeg.

Both CMH5 (Figure 134A) and CMH9 (Figure 134E) retain the IgG F(ab')2 peak at λ = 209 nm but with CMH5, the trough is flattened to near 0, and with CMH9, this trough is shifted to the higher wavelength of λ = 231 nm. Interestingly, the effect of CMH9 does not display a large spectral change as seen in the other immunoglobulins tested. Unsulphated CMH8 causes a unique spectral shift to a lower wavelength from λ = 209 nm to λ = 205 nm (Figure 134D).

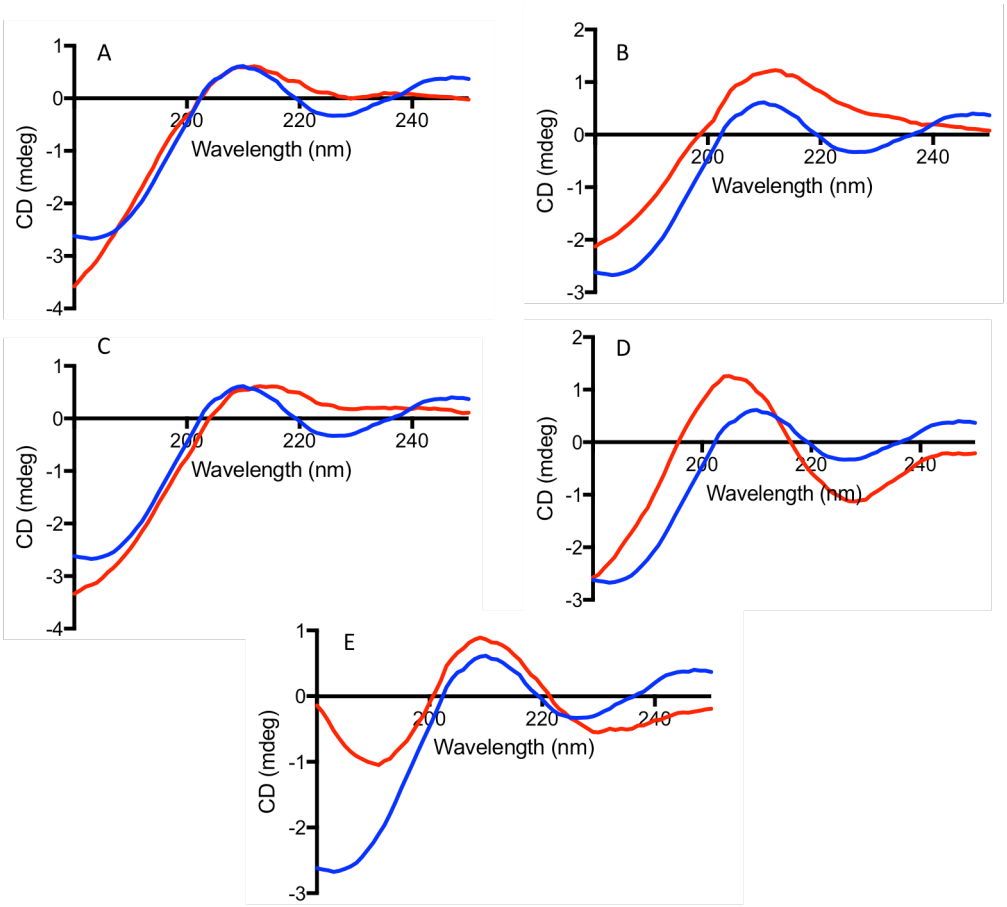

Figure 134: Far-UV CD, of F(ab')2 with CMH 5-9 in 50 mM sodium acetate pH 4.0. (–) 3 μM IgG F(ab')2 region with A) (–) 3 μM CMH5, **B**) (–) 3 μM CMH6, **C**) (–) 3 μM CMH7 **D**) (–) 3 μM CMH8, **E**) (–) 3 μM CMH9.

6.2.9 F(ab')2 stability in the presence of low molecular weight heparins

F(ab')2 region Tm is 60.13°C with an fluorescence intensity of 2000 ΔFU, with fondaparinux mimicking the same shape and Tm of 60.11°C. The other LMWH appear in the same region in two groups. UF PMH and tinzaparin have Tm of 53.80°C and 53.84°C

Dalteparin, enoxaparin, and reviparin have Tm of 53.87°C, 54.81°C and 54.84°C. This grouping is demonstrated in the PCA of 1st derivative DSF data (Figure 135).

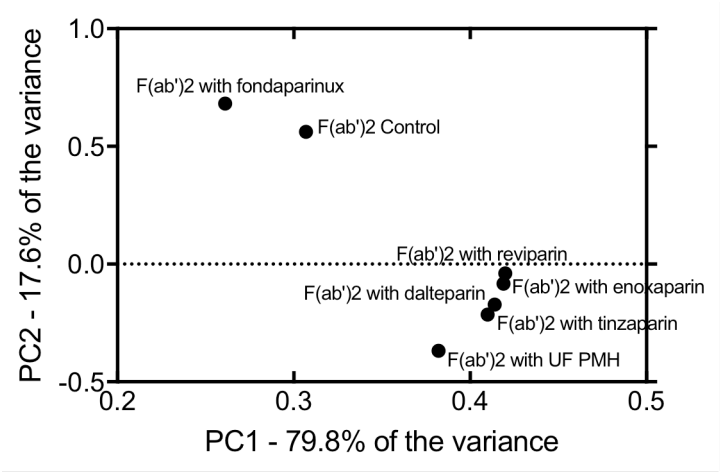

Figure 135: PCA of 1st derivative DSF data from F(ab')2 with LMWH and UF PMH.

6.2.10 F(ab')2 stability in the presence of GAGs and heparin controls

As shown previously, UF PMH reduces the Tm of F(ab')2 by 6.65°C, suggesting a reduction in structural stability of the immunoglobulin fragment (Figure 136A). The effects of the compounds tested varies with F(ab')2 compared to the other Ig tested so far. The destabilisation of F(ab')2 from most to least effect is CMH1 > DS > HS > CSC > CSA > Na_2SO_4 > DS6 > HA.

The Tm of DS with F(ab')2 is 54.57°C (Tm **Δ** 5.98°C) which is lower that that of HS but has a lower intensity peak compared to both CMH1 and HS at 2550 ΔFU and more resembles the CSC peak. HS peak shape is more similar to CMH1 in intensity (36700 ΔFU) but the Tm is higher at 55.56°C (Tm **Δ** 4.99°C)

The Tm of CSC is lower than that of CSA; 55.82°C and 57.45°C respectively. UA(2S)-GlcNS(6S) with F(ab')2 increases the Tm compared to F(ab')2 only by 1.14°C up to 61.69°C. The addition of Na_2SO_4 doesn't modify the Tm of the immunoglobulin fragment, but the fluorescence intensity of the curve is 50 units greater than F(ab')2 alone (2600 ΔFU). HA increases the Tm of F(ab')2 by 2.69°C to 63.24°C with no change in peak intensity.

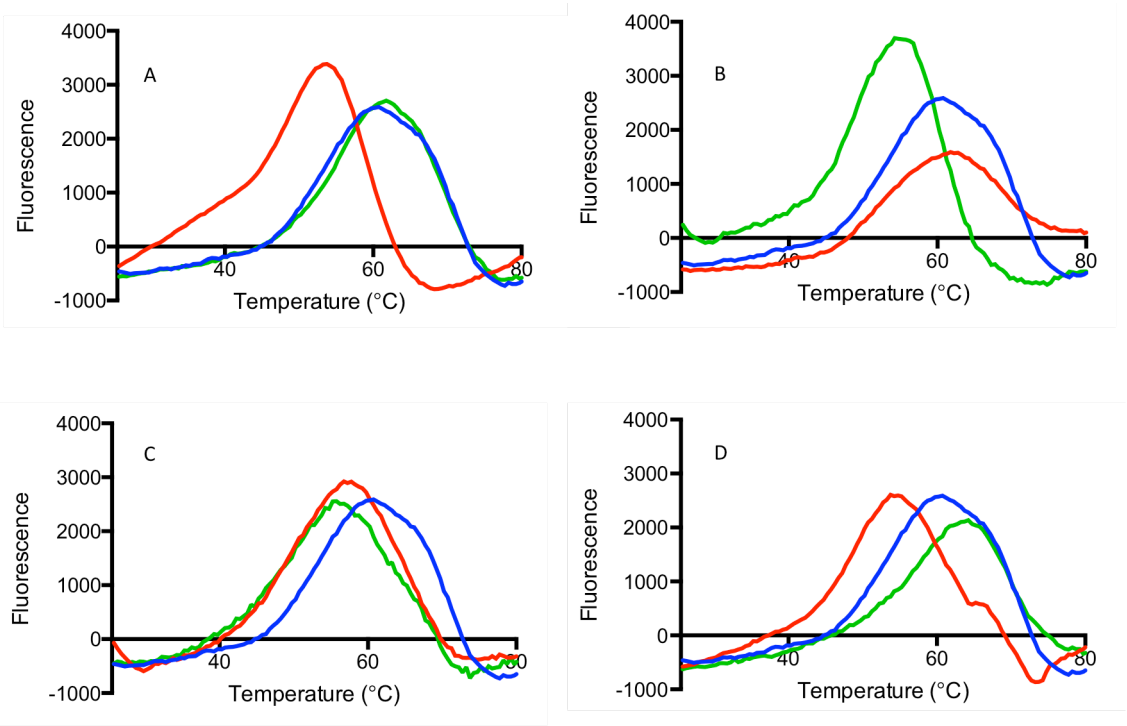

Figure 136: DSF of F(ab')2 with GAGs and sulphate controls in 50 mM sodium acetate buffer pH 4.0. (–) 3 µM F(ab')2 region with **A**) (–) 6.0 µM UF PMH, (–) 500 nM sodium sulphate, **B**) (–) 6.0 µM DS6 (–) 12.0 µM HS, **C**) (–) 6µM CSA, (–) 6.0 µM CSC, **D**) (–) 6.0 µM DS, (–) 6.0 µM HA.

6.2.10 F(ab')2 stability in the presence of size defined heparin fractions

. The d.p.2, 4 and 6 fragments with F(ab')2 have higher Tm that F(ab')2 alone, with the Tm from highest to lowest stability as d.p.4 > d.p.6 > d.p.2. From d.p.8 to d.p.16 the Tm decreased with increasing saccharide length, with d.p.8 having a Tm of 60.05°C and d.p.16 having a Tm of 53.61°C, the lowest Tm in this data and most similar to the UF PMH with F(ab')2. Heparin fragments of d.p.18 and d.p.20 have the Tm of 54.61°C and 54.17°C respectively. PCA of the d.p. fragments with F(ab')2 suggests similarity in the 1st derivative DSF spectra of UF PMH, d.p.16 and d.p.18, with d.p.20 and d.p.14 grouped separately.

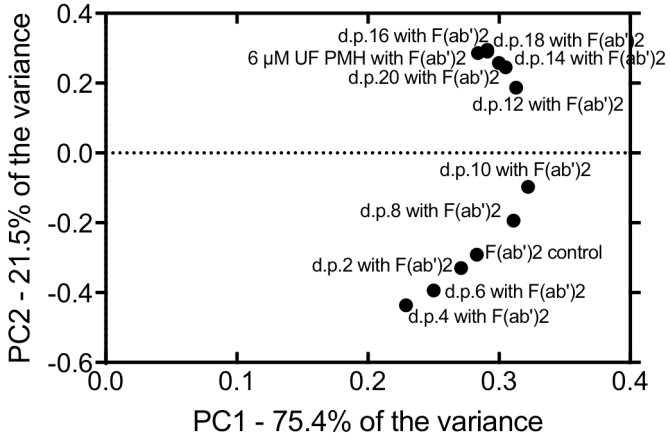

Figure 137: The PCA of 1st derivative DSF data of F(ab')2 with PMH polymerization (D.P) fragments in 50 mM sodium acetate buffer pH 4.0.

6.2.11 F(ab')2 binds heparin in Hi-trap HPLC

Heparin affinity chromatography with PBS tested at different pH and elution with 2 M NaCl demonstrated IgG F(ab')2 bound to the heparin column at pH 4.0 and 5.0, shown in Figure 138. Heparin binding affinity is 240 mM in pH 5.0 PBS, and at pH 4.0 PBS the binding affinity suggests a stronger interaction at 799 mM and 959 mM NaCl. As with the Fab/k region, at pH 4.0 PBS shows elution of two populations with different heparin affinities.

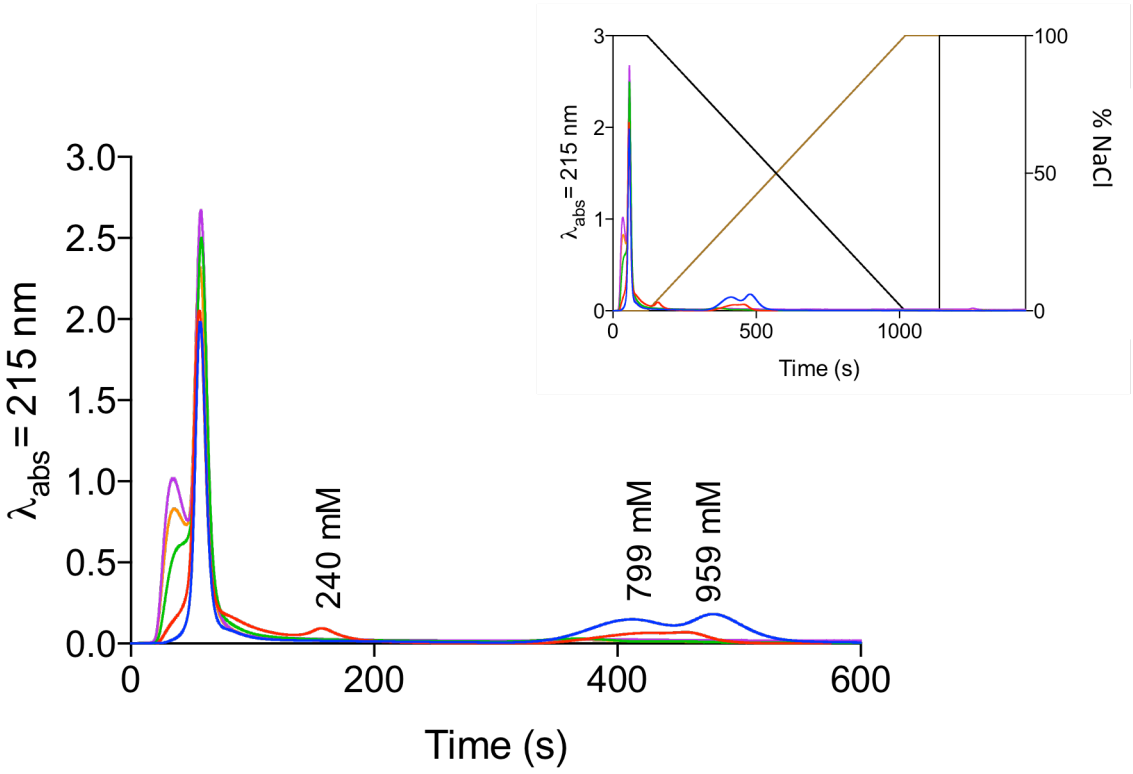

Figure 138: Human IgG F(ab')2 fragment in heparin HiTrap affinity HPLC in PBS at differing pH (4.0 – 7.4) and elution with 2M NaCl. (–) PBS pH 4, (–) PBS pH 5.0, (–) PBS pH 6.0, (–) PBS pH 7.0, (–) PBS pH 7.4.

The Hi-Trap affinity binding with 50 mM sodium acetate at pH 4.0, as with Fab/k, the resulting binding affinity occurs between the two populations eluted in pH 4.0 PBS; 814 mM NaCl (Figure 139).

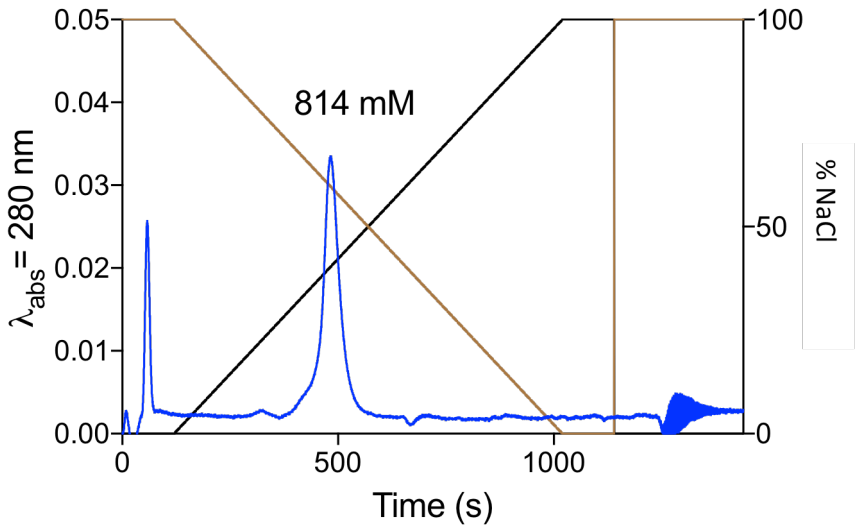

Figure 139: Human IgG F(ab')2 in heparin HiTrap affinity HPLC in 50 mM sodium acetate pH 4.0 with 2M NaCl elution.

6.3 Discussion

The melting point, an equilibrium between folded and denatured protein populations, differs by 3°C for Fab and F(ab')2 fragments of IgG. The Fab fragment has a Tm of 60°C, whereas the much larger, diamer F(ab')2 has a Tm of 63°C. This is a higher Tm than that of whole IgG (53°C) and Fc region (45°C) as measured in DSF. Tischenko *et al.* (1982) established the Fc and Fab fragments of IgG are thermodynamically independent species, even when separated from the whole immunoglobulin (Tischenko, Zavyalov, Medgyesi, Potekhin, & Privalov, 1982). The average of the Tm from both fragments (Fc and Fab) is similar to the Tm found for the whole IgG molecule in this data, as shown by Tischenko *et al.* (1982) (*idem*). The marginally increased Tm of the larger immunoglobulin fragment, F(ab')2 can be attributed to the retention of the hinge region and two disulphide bonds joining the CH2 domains. Disulphide bonds are present in both the folded (native) and unfolded protein states, so do not require additional energy to break during melting (*idem*). However the disulphide bonds contribute to the decrease in entropy of the denatured state (Zavodszky et al., 2001). By increasing the level of order in unfolded protein states, more energy is required to denature, indicated by an increase in Tm (*idem*).

Addition of the main disaccharide present in heparin, IdoA(2S)-GlcNS(6S) (CMH1) at the highest concentration tested (6 μM) caused a decrease in Tm in both Fab and F(ab')2 immunoglobulin fractions; Fab experienced a drop of Tm of 7.78°C, whereas F(ab')2 reduced by 8.93°C. This difference may be attributed to the increased initial Tm experienced by F(ab')2 alone, denaturation with heparin resulting in the same final unfolding.

The library of 9 chemically modified heparins caused differing effects on the stability of Fab and F(ab')2. CMH1 caused a reduction in Tm at concentrations greater

than 0.19 μM. At 0.19 μM, an intermediate state, demonstrated by a double peak, showed Tm values both lower (55.30°C) and higher (65.81°C) than that of Fab alone. Increased Tm of Fab with concentrations of CMH1 lower than 0.19 μM suggest a stabilisation effect with this concentration of chemically modified heparin.

This pattern of destabilisation at high concentrations tested, and a level of immunoglobulin stabilisation at low concentrations is mirrored with other chemically modified heparins. The same effect is seen at concentrations lower than 0.19 μM with CMH2, CMH3, and CMH4. With CMH5 and CMH6, an intermediate, double peak occurs with the addition of 0.38 μM CMH, with lower concentrations of this chemically modified heparin increasing the Tm, suggesting an increase in immunoglobulin stability. Desulphated CMH8 caused an increase in Tm of Fab, suggesting a stabilisation and increased resistance to thermal degradation at all concentrations tested. Persulphated CMH9 displayed the greatest reduction of Tm in IgG Fab. Addition of 6.0 μM of CMH9 caused a 12.79°C reduction in Tm; the highest destabilisation effect with Fab. However, a concentration of 0.19 μM displays an intermediate peak with two Tm, 55.55°C and 64.65°C. Concentrations below 0.19 μM have Fab stabilisation properties, even with the dramatic effects of this chemically modified heparin at higher concentrations.

F(ab')2 with the chemically modified heparin library displays a similar effect with the 0.19 μM concentration. CMH1 demonstrates an intermediate peak at this concentration, with one peak at 57.1°C and the other at 69.08°C. F(ab')2 appears better able to resist thermal degradation occuring with concentrations of CMH1 of 0.09 μM and 0.05 μM. This pattern of increasing F(ab')2 stability with 0.19 μM occurs with CMH2, CMH3, CMH4 and CMH6. With CMH5, this stabilising of F(ab')2 occuring at the higher concentration of 0.38 μM and with CMH7 stabilisation occurs at the lower concentration of 0.09 μM.

Unsulphated CMH8 has the least effect on F(ab')2 at all concentrations tested, but an anomalous peak occurs in the 0.09 μM experiment at Tm of 68.87°C, which is attributed to an air bubble. As in the Fab results, the effect of persulphated CMH9 on F(ab')2 is the most pronounced of the chemically modified heparins tested. The greatest reduction in Tm of F(ab')2 (9.97°C) occurs with the addition of 6.0 μM CMH9. A wide peak structure, with two discernable peaks occurs with 0.38 μM and 0.19 μM CMH9, one peak representing a less stable F(ab')2 form, one peak more stable than F(ab')2 alone.

Four compounds (CMH1, CMH2, CMH3 and CMH4) appear to affect the Tm of both Fab and F(ab')2 to a similar degree. These four compounds do not have the same number of sulphate moieties per disaccharide, therefore differing charges. This may be attributed to being no discernable structural differences caused by the binding of these four compounds to Fab or F(ab')2, or that the structural changes associated with the binding of these compounds may be different, but result is the same effect on thermal stability, as measured by DSF. Far-UV circular dichroism allows for elucidation of the secondary structure changes associated with the addition of these four chemically modified heparins with Fab and F(ab')2, which result in the similar effect on thermal stability.

CMH5 does not affect the Tm at high concentrations more predominantly than the other library members, but has a stabilising effect on the Tm of both Fab and F(ab')2 at a higher concentration (0.38 μM). This could suggest a less potent destabilisation effect on the immunoglobulin, and/or a more potent effect in increasing the resistance to thermal denaturation, with this concentration ratio of modified heparin to immunoglobulin fragment.

Unsulphated CMH8 has no effect on the stabilisation of Fab and F(ab')2. This may be due to the relatively uncharged nature of this modified heparin resulting in little or no charge dependent binding.

Persulphated heparin (CMH9) produces the greatest change in Fab and F(ab')2 thermal stability. The increased level of charge or the arrangement and conformation of the sulphated functional groups associated with this modified heparin, may account for the greatest change in thermal stability of both immunoglobulin fragments.

Far-UV CD of F(ab')2 with persulphated CMH9 and unsulphated CMH8 did not mimic the effects of the most and least expected structural change as seen in the change in melt profile from DSF. CMH1, CMH4 and CMH7 modify the spectra in the λ = 209 nm region in a similar way, with the peak seen in F(ab')2 alone in the λ = 227 nm region absent with in the presence of these chemically modified heparins. CMH8 causes a different spectral shift in F(ab')2 at λ = 209 nm, shifting this peak to λ = 205 nm unlike the other modified heparins, that cause a peak with an increased wavelength.

The greatest change in CD spectra with Fab was seen with CMH2 and CMH6. No change to the CD spectra occurs in the presence of unsulphated CMH8, unlike F(ab')2, however, like F(ab')2 persulphated CMH9 does not cause the greatest change in secondary structural characteristics as demonstrated by CD.

As with DSF, changes to the number and position of functional groups and conformation of the glycopolymer linkage regions of the chemically modified heparins, cause changes to the secondary structure of the Fab and F(ab')2 immunoglobulins in CD. The magnitude of spectral change however, does not represent the magnitude of change in the disaccharide composition. The biological and pharmacological activities of heparin and heparan sulphate have been attributed to a range of structural features, from high levels of sequence specificity to a sole dependence on high negative charge.

The synthetic pentsaccharide sequence, fondaparinux does not have a destabilising effect on either Fab or F(ab')2, as expected for such a specific structural formula and small molecular weight. Low molecular weight heparins dalteparin, enoxaparin, tinzaparin and reviparin have a similar effect as UF PMH and reduce the Tm of both Fab and F(ab')2.

The saccharide size requirement for the reduction in Tm, as shown by CMH1 for Fab is d.p 20, but a reduction in the Tm of Fab is seen with a d.p 16 heparin saccharide. In F(ab')2, the d.p 16 heparin saccharide demonstrates a reduction in Tm, but the d.p 18 has the same effect as full length heparin.

Hi-trap heparin binding HPLC with the Fab and F(ab')2 antibody fragments show heparin binding at the acidic pH tested. In pH 5.0 Fab bound with 247 mM NaCl affinity and F(ab')2 with 240 mM NaCl affinity. At pH 4.0, these binding affinities increased to 755 mM and 989 mM NaCl with Fab and 799 mM and 959 mM NaCl with F(ab')2. In 50 mM sodium acetate pH 4.0, heparin binding affinity of Fab is 797 mM NaCl, and F(ab')2 is 814 mM NaCl. In sodium acetate a single peak is eluted at pH 4.0, whereas at pH 4.0 in PBS the elution occurs over two peaks. The heparin affinity in sodium acetate occurs between the two quoted peaks present in pH 4.0 PBS HPLC.

The interaction between immunoglobulin fragment Fc region, whole immunoglobulins and the antigen binding regions Fab and F(ab')2 and the glycosaminoglycan heparin has been investigated. Fc bound BACE1 cannot be used under acidic conditions to demonstrate heparin-BACE1 interactions due to the heparin-Fc interaction. The use of glycosaminoglycans in experiments with immunoglobulins under acidic conditions requires further investigation to determine whether this relationship modifies the action or activity of the immunoglobulin.

Studies into the structural changes associated with heparin binding to BACE1 will be made using native, tag-free BACE1 to obtain a true representation of the BACE1-GAG interaction. This elucidation will aid the understanding of this regulating relationship, adding knowledge to the design of a GAG based BACE1 inhibitor.

Further to this research, in Chapter 8, chemically sulphated GAG analogues will be screened and developed for BACE1 inhibition.

Chapter 7: BACE1 structural changes induced by chemically modified heparins

7.1 Introduction

The binding and sequestration of cations to the carboxylate, N- and O-sulphate groups of heparin and HS is thought to be the evolutionary function of these complex polyanions (Heidarieh et al., 2013). The binding of cations to heparin is heterogenous, with both high and low affinity binding sites present across the heparin polymer (Landt, Hortin, Smith, McClellan, & Scott, 1994). Structural studies indicate long-range binding interactions that occur at low pH between the carboxylate groups and sodium, magnesium and calcium, with the sodium and magnesium binding occurring at a higher pH (Meneghetti et al., 2015).

The activity of heparin and HS can be dramatically varied in the presence of physiological concentrations of cations (*idem*). Cations such as potassium and sodium both intra- and extracellularly, and levels of rarer cations such as copper, increased during tumourigenesis and angiogenesis (*idem*).

7.2 Results

7.2.1 The effect of chemically modified heparins on BACE1 thermal stability

The melting point of native, tag-free human BACE1, in 50 mM sodium acetate pH 4.0 is 42.99 ± 0.087°C. As expected from the results with native BACE1 and heparin in Chapter 3, The addition of CMH1 at the highest GAG concentration tested (6.0 μM) reduced the native BACE1 Tm by 7°C to 35.96°C (Figure 140A). Decreasing concentrations of CMH1 (3.0 μM, 1.5 μM and 0.75 μM) result in less of a reduction in the Tm of native BACE1 to near the protein only Tm, at 41.96°C. At a CMH1 concentration of 0.38 μM, the Tm of native BACE1 increases dramatically, to a temperature higher than the native protein alone, 46.53°C (Figure 140B). From this high Tm, the subsequent reduction in the concentration of CMH1 to 0.19 μM and 0.09 μM have Tm of 45.93°C and

43.13°C respectivley. The lowest concentration of this chemically modified heparin returning the native BACE1 protein back to approximately the native Tm.

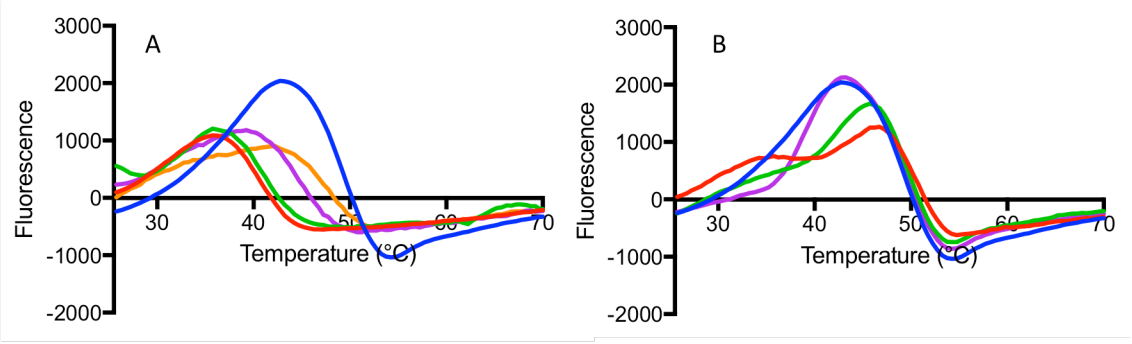

Figure 140: DSF of BACE1 with CMH1 in 50 mM sodium acetate buffer pH 4.0 **A**= (–) 3 µM native BACE1 with (–) 6.0 µM CMH1, (–) 3.0 µM CMH1, (–) 1.5 µM CMH1, (–) 0.75 µM CMH1. **B**= (–) 3 µM native BACE1 with (–) 0.38 µM CMH1, (–) 0.19 µM CMH1, (–) 0.09 µM CMH1, (–) 0.05 µM CMH1.

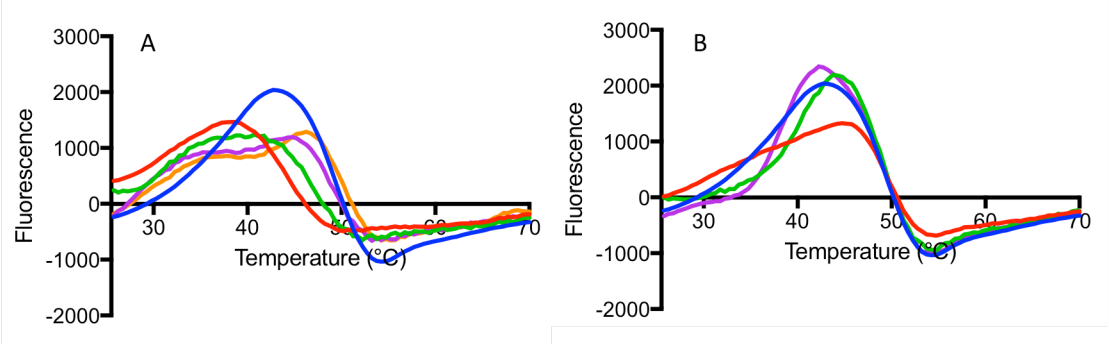

Figure 141: DSF of BACE1 with CMH2 in 50 mM sodium acetate buffer pH 4.0 **A**= (–) 3 µM native BACE1 with (–) 6.0 µM CMH2, (–) 3.0 µM CMH2, (–) 1.5 µM CMH2, (–) 0.75 µM CMH2. **B**= (–) 3 µM native BACE1 with (–) 0.38 µM CMH2, (–) 0.19 µM CMH2, (–) 0.09 µM CMH2, (–) 0.05 µM CMH2.

The large Tm shift and associated higher than native Tm seen in CMH1 experiments also occurs with other chemically modified heparins. CMH2 drops the Tm of native BACE1 at the highest concentration tested (6.0 µM) to 38.25°C, but not as significantly as CMH1 (Figure 140A). Decreasing concentrations of this chemically modified heparin gradually increase the native BACE1 Tm, but at 0.75 µM CMH2 the Tm increases to a melting temperature higher than the native BACE1 alone (Figure 141A). At 0.38 µM and 0.19 µM CMH1, the Tm of native BACE1 are higher than

BACE1 alone, but are gradually reducing to reach approximately the same as native BACE1 alone with 0.09 µM of the chemically modified heparin.

2-Desulphated CMH3 has a different effect on native BACE1, when compared to the actions of CMH1 and CMH2, as the higher concentrations of this modified heparin does not peturb the melting temperature of native BACE1 (43.07°C) but 3.0 µM, 1.5 µM, 0.75 µM (Figure 142A) and 0.38 µM (Figure 142B) increase the Tm up to a high of 46.09°C, suggesting a stabilisation effect. The two lowest concentrations of CMH3 have Tm similar to the native BACE1 control.

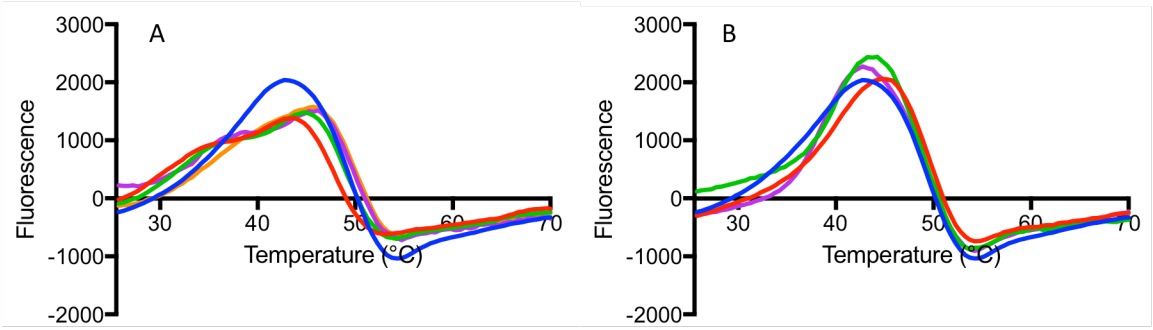

Figure 142: DSF of BACE1 with CMH3 in 50 mM sodium acetate buffer pH 4.0. **A**= (–) 3 µM native BACE1 with (–) 6.0 µM CMH3, (–) 3.0 µM CMH3, (–) 1.5 µM CMH3, (–) 0.75 µM CMH3. **B**= (–) 3 µM native BACE1 with (–) 0.38 µM CMH3, (–) 0.19 µM CMH3, (–) 0.09 µM CMH3, (–) 0.05 µM CMH3.

CMH4 at 6.0 µM reduces native BACE1 Tm to 38°C, with subsequent reduced concentrations increasing the Tm of the protein, until 0.75 µM CMH4 which has a Tm of 44.98°C (Figure 143A). The addition of 0.38 µM CMH4 increases the Tm to above native BACE1 melting (46.34°C), as with CMH1. Subsequently lower concentrations of CMH4 lead to a reducing Tm, at 0.09 µM this Tm is 43.43°C (Figure 143B).

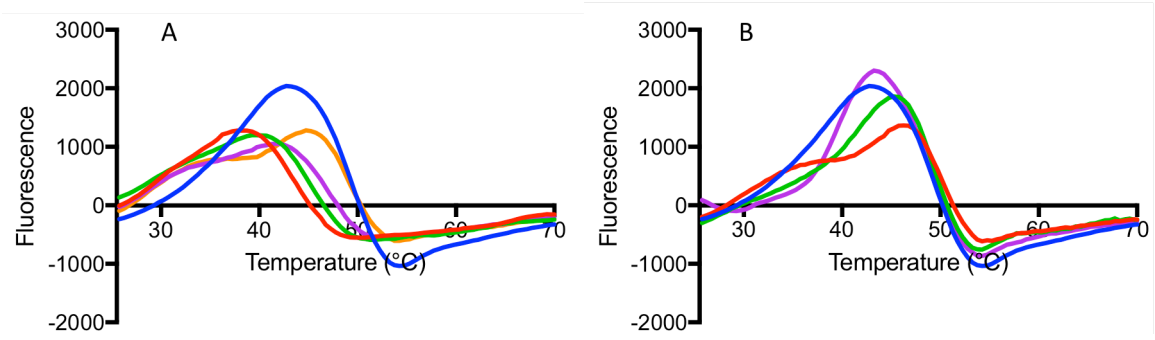

Figure 143: DSF of BACE1 with CMH4 in 50 mM sodium acetate buffer pH 4.0. **A**= (–) 3 µM native BACE1 with (–) 6.0 µM CMH4, (–) 3.0 µM CMH4, (–) 1.5 µM CMH4, (–) 0.75 µM CMH4. **B**= (–) 3 µM native BACE1 with (–) 0.38 µM CMH4, (–) 0.19 µM CMH4, (–) 0.09 µM CMH4, (–) 0.05 µM CMH4.

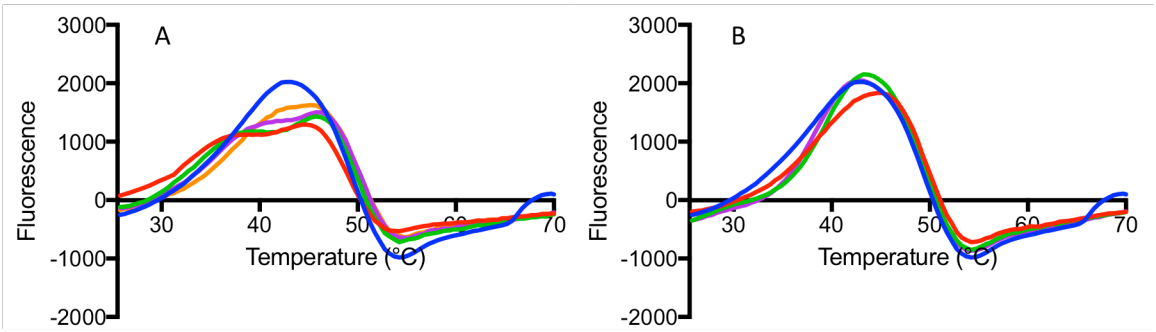

Figure 144: DSF of BACE1 with CMH5 in 50 mM sodium acetate buffer pH 4.0. **A**= (–) 3 µM native BACE1 with (–) 6.0 µM CMH5, (–) 3.0 µM CMH5, (–) 1.5 µM CMH5, (–) 0.75 µM CMH5. **B**= (–) 3 µM native BACE1 with (–) 0.38 µM CMH5, (–) 0.19 µM CMH5, (–) 0.09 µM CMH5, (–) 0.05 µM CMH5.

CMH5 has a different effect on the Tm of native BACE1 than the other compounds discussed thus far. 6.0 µM has a Tm of 44.28°C, which is above the Tm of native BACE1 alone (42.99 ± 0.087°C). This Tm increases further with the addition of lower concentrations of CMH5 (3.0 µM and 1.5 µM) but then moves to gradually decrease from the maxima Tm of 46.13°C, to temperatures similar to the Tm of native BACE1 alone (0.09 µM Tm of 42.71°C). This compound seems to stabilise native BACE1 at most concentrations tested.

At 6.0 µM 6-desulphated, N-acetylated heparin (CMH6), the Tm of BACE1 is increased to 45.46°C, with the Tm decreasing with reducing concentrations of CMH6 (Figure 145A&B). However at 6.0 µM and 3.0 µM of CMH6 the 1st derivative curve in

Figure 145A demonstrates a broad peak, with a minor peak at the lower temperature of 38.10°C; this suggests a population of native BACE1 is more susceptible to temperature linked denaturation; with some less stable than native BACE1 and some more stable. The Tm of BACE1 decreases with decreasing concentrations of CMH6, with the lowest concentration (0.09 µM) producing a 42.78°C Tm (Figure 145B).

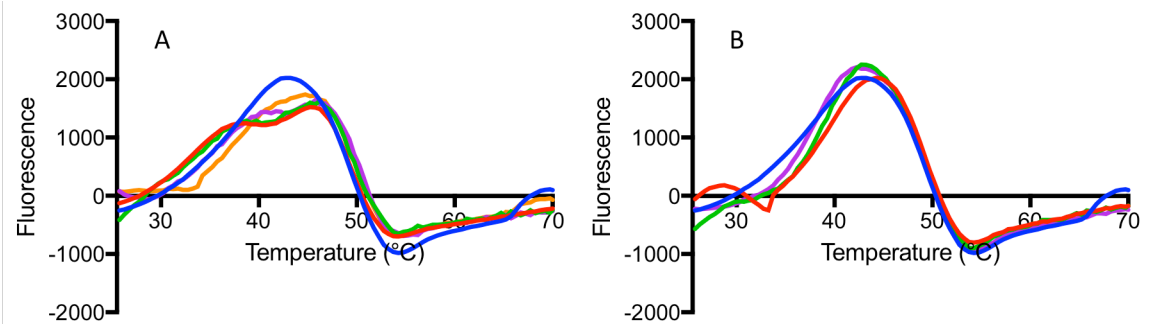

Figure 145: DSF of BACE1 with CMH6 in 50 mM sodium acetate buffer pH 4.0. **A**= (–) 3 µM native BACE1 with (–) 6.0 µM CMH6, (–) 3.0 µM CMH6, (–) 1.5 µM CMH6, (–) 0.75 µM CMH6. **B**= (–) 3 µM native BACE1 with (–) 0.38 µM CMH6, (–) 0.19 µM CMH6, (–) 0.09 µM CMH6, (–) 0.05 µM CMH6.

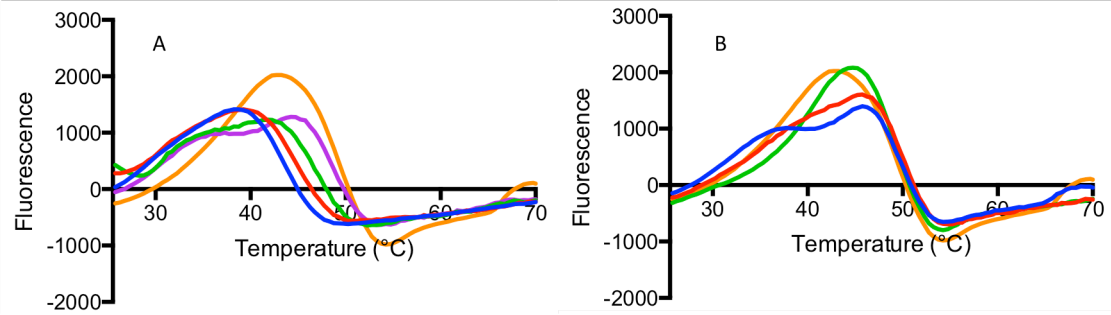

Figure 146: DSF of BACE1 with CMH7 in 50 mM sodium acetate buffer pH 4.0. **A**= (–) 3 µM native BACE1 with (–) 6.0 µM CMH7, (–) 3.0 µM CMH7, (–) 1.5 µM CMH7, (–) 0.75 µM CMH7. **B**= (–) 3 µM native BACE1 with (–) 0.38 µM CMH7, (–) 0.19 µM CMH7, (–) 0.09 µM CMH7, (–) 0.05 µM CMH7.

CMH7 at 6.0 µM reduces the Tm of native BACE1 by 4.6°C, to 38.38°C (Figure 146A). Both 3.0 µM and 1.5 µM have Tm values, which increase toward the native BACE1 only Tm. At 0.75 µM however, the Tm increases to 44.53°C, with the first derivative melt curve showing a shoulder curve, with a flat peak region occurring at the lower temperature of 36.34°C (Figure 146A). The Tm with the lowest concentration of

CMH7 tested (0.09 µM) is still greater than the Tm of native BACE1 alone (42.99 ± 0.087°C), suggesting some stability increases at this concentration.

Unsulphated heparin, CMH8 demonstrated a maximum change in Tm of 0.5°C. with the addition of 6.0 µM shifting the Tm of native BACE1 to 42.52°C (Figure 147A). Unsulphated heparin has the no effect on the Tm of native BACE1, displaying no difference across the modified heparin concentration gradient tested.

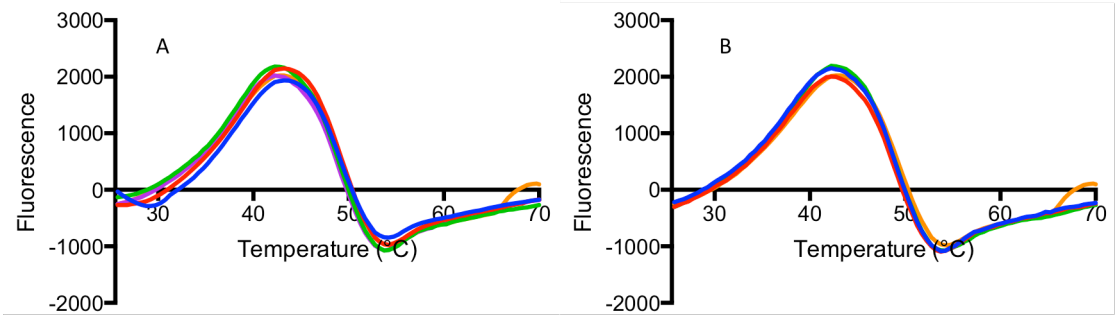

Figure 147: DSF of BACE1 with CMH8 in 50 mM sodium acetate buffer pH 4.0 **A**= (–) 3 µM native BACE1 with (–) 6.0 µM CMH8, (–) 3.0 µM CMH8, (–) 1.5 µM CMH8, (–) 0.75 µM CMH8. **B**= (–) 3 µM native BACE1 with (–) 0.38 µM CMH8, (–) 0.19 µM CMH8, (–) 0.09 µM CMH8, (–) 0.05 µM CMH8.

Conversley, the greatest change in Tm displayed occurs with the addition of per-sulphated heparin (CMH9). The first derivative melt curve of concentrations greater than 0.38 µM CMH9 with native BACE1 suggest the protein has undergone thermal destabilisation temperatures lower than the limit of this experiment (< 25.5°C). With concentrations of CMH9 0.38 µM and lower, the first derivative melt curve returns with Tm of 36.87°C at this concentration (Figure 148C). The Tm of BACE1 then increases to 46.98°C, with 0.19 µM CMH9, an increase of 10.11°C from the Tm at 0.38 µM (Figure 145B). The final concentration tested, 0.09 µM, displays a reducing Tm but remains higher than native BACE1 at 45.43°C (Figure 148B).

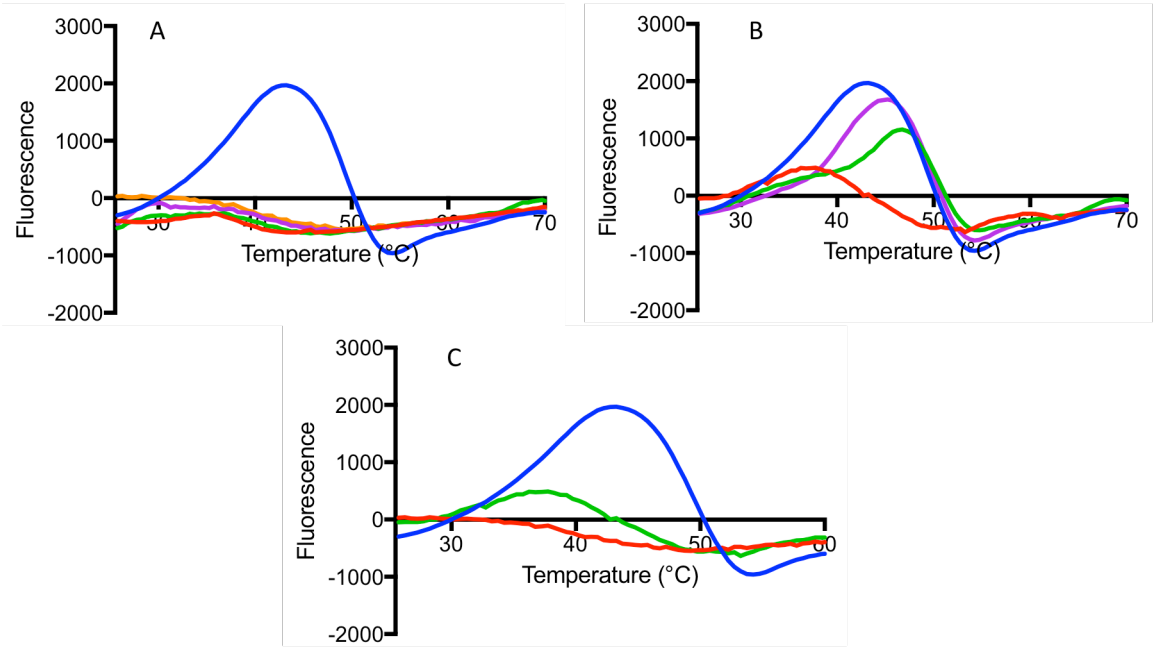

Figure 148: DSF of BACE1 with CMH9 in 50 mM sodium acetate buffer pH 4.0. A= (–) 3 µM native BACE1 with (–) 6.0 µM CMH9 (–) 3.0 µM CMH9 (–) 1.5 µM CMH9 (–) 0.75 µM CMH9. **B**= (–) 3 µM native BACE1 with (–) 0.38 µM CMH9 (–) 0.19 µM CMH9 (–) 0.09 µM CMH9 (–) 0.05 µM CMH9 **C**) (–) 3 µM native BACE1 with, (–) 0.75 µM CMH9 (–) 0.38 µM CMH9.

7.2.2 The comparison of BACE1 thermal stability and known BACE1 inhibition with the addition of chemically modified heparins

The research paper that initially identified chemically modified heparin as potential BACE1 regulating compounds worked to identify a modification which would allow for simultaneous BACE1 modulation and negated anti-coagulant activity (Patey et al., 2006). Table 14 is modified from the Patey *et al.,* 2006 publication.

Table 14: Experimental results from the BACE1 FRET inhibition experiments by Patey *et al.* (2006) The library of chemically modified heparin compounds was assayed for BACE1 inhibition with the half maximal inhibitory concentration (IC_{50}).

CMH	Compound	IC_{50} BACE1 FRET (µg/ml)	R_2 of IC_{50}
1	IdoA(2S)-GlcNS(6S)	0.028	0.998
2	IdoA(2S)-GlcNAc(6S)	0.031	0.995
3	IdoA-GlcNS(6S)	0.053	0.995
4	IdoA-GlcNAc(6S)	0.091	0.999
5	IdoA(2S)-GlcNS	0.100	0.996
6	IdoA(2S)-GlcNAc	0.410	0.995
7	IdoA-GlcNS	0.786	0.994
8	IdoA-GlcNAc	> 100	n/a
9	IdoA(2S,3S)-GlcNS(3S,6S)	0.053	0.998

There appears no correlation between FRET BACE1 inhibiton (data from Patey *et al*., 2006) and structural stability defined by Tm change upon addition of 6.0 µM any chemically modified heparin (p= 0.3734).

Patey *et al.,* 2006 found that replacement of N-sulphate with N-acetyl did not greatly reduce the BACE1 inhibitory properties of the modified heparin, but improved the anti-coagulant profile of the compounds. The melting point data show interchanging N-sulphate and N-acetyl can both destabilise BACE1, shown by reduced Tm at the high concentrations tested (6.0 µM). The destabilising BACE1 compounds are more frequently 6-sulphated, possibly suggesting a role for this modification (Table 15).

The average number of sulphates per disaccharide in the modified heparin compounds that demonstrate a destabilisation effect on BACE1 is 2.4, whereas the compounds that exhibit a stabilisation effect (CMH8, CMH5 and CMH6) have an average of 1 sulphate per disaccharide.

Table 15: Chemically modified heparan sulphate configuration at positions R1, R2, and R3 alongside the Tm of BACE1 with CMH in DSF. Differential scanning fluorimetry in 50 mM sodium acetate buffer pH 4.0 with 3 µM native BACE1. Tm of native BACE1 with 6.0 µM of each heparin type recorded.

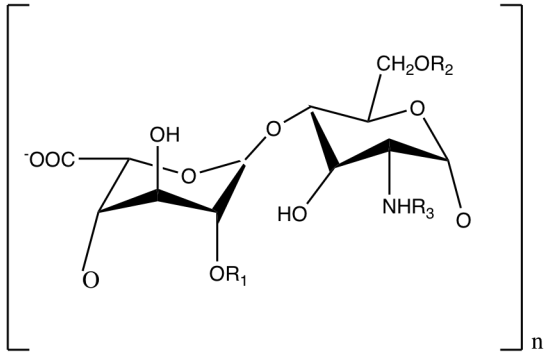

R_1 = SO^{3-}/H, R_2= SO^{3-}/H, R_3= SO^{3-}/H/$COCH^3$

CMH	Compound	R_1	R_2	R_3	Number of SO_3^- per disaccharide	Tm at 6.0 µM
9	IdoA(2S,3S)-GlcNS(3S,6S)	SO_3^-	SO_3^-	SO_3^-	5	<25.50 °C
1	IdoA(2S)-GlcNS(6S)	SO_3^-	SO_3^-	SO_3^-	3	35.96 °C
4	IdoA-GlcNAc(6S)	H	SO_3^-	$COCH_3$	1	38.00 °C
2	IdoA(2S)-GlcNAc(6S)	SO_3-	SO_3^-	$COCH_3$	2	38.25 °C
7	IdoA-GlcNS	H	H	SO_3^-	1	38.38 °C
3	IdoA-GlcNS(6S)	H	SO_3^-	SO_3^-	2	43.07 °C
8	IdoA-GlcNAc	H	H	$COCH_3$	0	43.52 °C
5	IdoA(2S)-GlcNS	SO_3^-	H	SO_3^-	2	44.28 °C
6	IdoA(2S)-GlcNAc	SO_3^-	H	$COCH_3$	1	45.46 °C

CMH3 is quoted as having a BACE1 inhibitory IC_{50} of 53 ng/ml, the same as the per-sulphated heparin CMH9, however the DSF thermal stability data suggest these two modified heparins have a different effect on the stability of BACE1 during thermal denaturation. CMH3 improves BACE1 thermal stability at some concentrations (most efficiently at 0.75 μM), but CMH9 causes destabilisation and melting under the 25.5 °C DSF starting temperature.

The Pearson correlation between the number of sulphates per disaccharide and the Tm with 6.0 μM of chemically modified heparin; the outcome of which suggests a significant correlation, Pearson correlation coefficient (n = 9) r = -0.81 (P < 0.01 95 % CI -0.96 to -0.30). This significance suggests rejection of the null hypothesis that there is no causal link between the number of sulphates present on the disaccharide of the chemically modified heparin and the action of the aforementioned heparin in BACE1 destabilisation as measured a change in Tm in DSF. A relationship therefore may exist in this data to show broadly, that the increasing number of sulphate moieties present in the chemically modified heparin allows for increasing BACE1 destabilisation and reducing Tm.

If the persulphated heparin (CMH9 is removed as a outlier, the correlation coefficient changes to r = -0.42 but with a P = 0.32 suggesting a relationship cannot be shown between the Tm of the chemically sulphated heparin in BACE1 melting and the number of sulphate moieties present on the heparin disaccharide. However, the number of sulphate moieties per disaccharide alone is not an accurate predictor of the effect of modified heparin on the thermal stability of BACE1.

The PCA of BACE1 1st derivative DSF data with the chemically modified heparin library suggests a link between the spread of principle component 1 data and the IC50 inhibitory concentration of the CMH. The more potent BACE1 inhibiting CMH1 and

CMH9 have a concentration dependant effect on the 1st derivative DSF data, with these variances displayed as a larger range PC1 dataset (Figure 149).

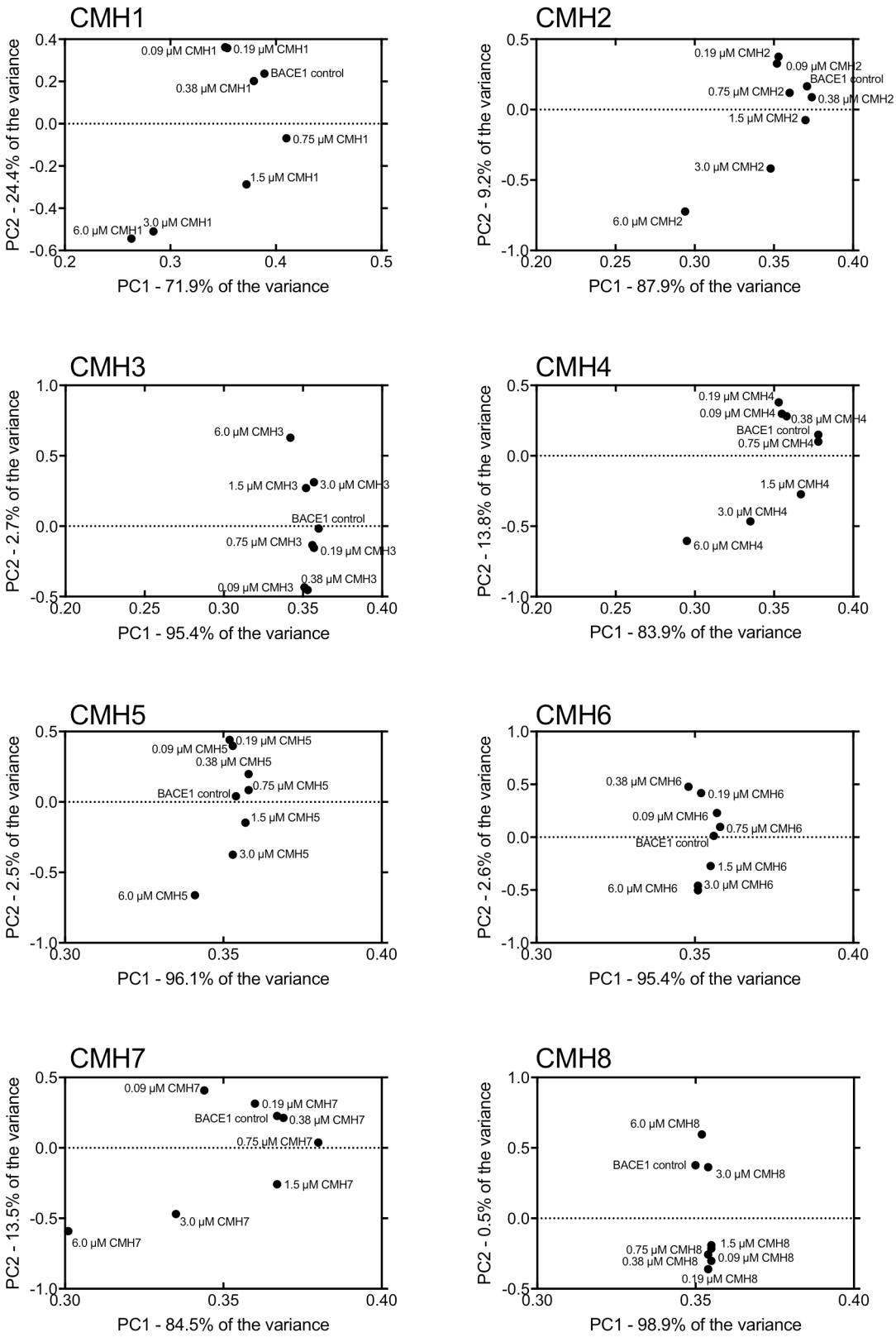

Figure 149: PCA of 1st derivative DSF data of BACE1 with CMH1-8.

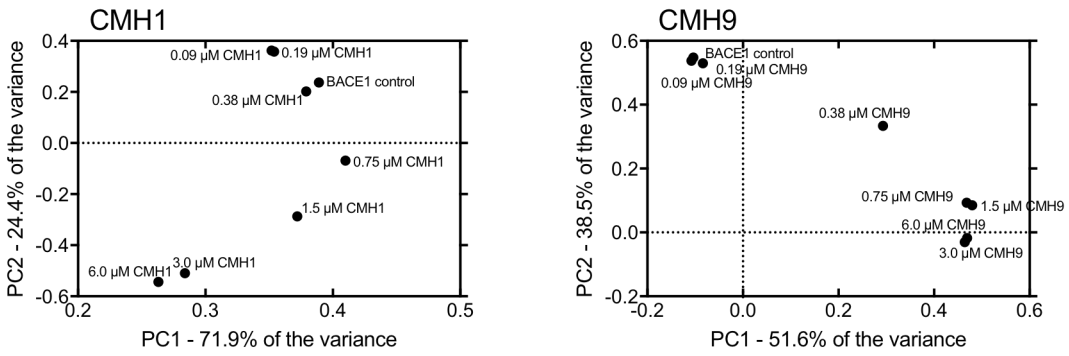

Figure 150: PCA of 1st derivative DSF data of BACE1 with CMH1 and CMH9.

7.2.3 Far-UV circular dichroism studies of BACE1 and chemically modified heparins

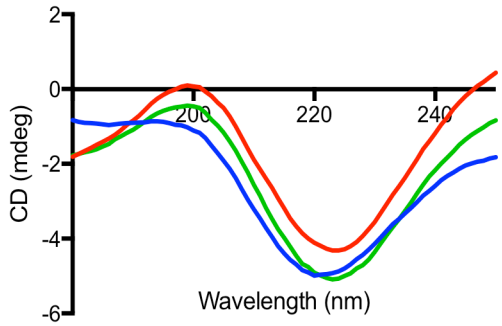

Figure 151: Far-UV CD of human BACE1 with CMH1 and CMH8 in 50 mM sodium acetate pH 4.0, (–) 3 µM native BACE1 with (–) CMH1 (–) CMH8.

The CD spectra of BACE1 alone is shown in the Figure 151. The native BACE1 enzyme in 50 mM sodium acetate buffer pH 4.0 has a trough at λ = 220.5 nm (Figure 151). This feature shifts to a higher λ = 224.1 nm with CMH1 and to λ = 223.7 with CMH8.

Table 16 is a summation of the spectral changes seen at the λ = 220 nm region. CMH8 and the 2-O-sulphated cousin, CMH6, have the same spectral features in this region with the ellipticity of -5.22 mdeg at λ = 233.72 nm. This suggests the 2-O-sulphate

moiety of the chemically modified heparin does not modify the secondary structure of native BACE1 at this concentration.

Table 16: Far-UV CD of BACE1 with CMH in 50 mM sodium acetate pH 4.0.

CMH	Wavelength (nm)	CD (mdeg)
None	220.56	-5.07
CMH6	223.72	-5.22
CMH8	223.72	-5.22
CMH2	223.93	-4.69
CMH9	223.98	-4.66
CMH1	224.13	-4.38
CMH7	224.43	-3.59
CMH4	224.86	-3.96
CMH5	226.04	-4.97
CMH3	228.44	-1.14

CMH2 and the more heavily sulphated CMH9 also have a similar spectra in this region with the ellipticity maxima at λ = 223.9 nm (-4.6 mdeg). This may mean either the additional 3-O-sulphates and N-sulphates on persulphated heparin do not change the secondary structure of BACE1 when compared to CMH2, or the structural change triggers, on average, the same degree of secondary structural modification.

CMH3 is an outlier of this data, with this chemically modified heparin producing an ellipticity maximum (-1.14 mdeg) at λ = 228.44. The shape of the spectra in this area is more flat when compared to the other modified heparins (Figure 152).

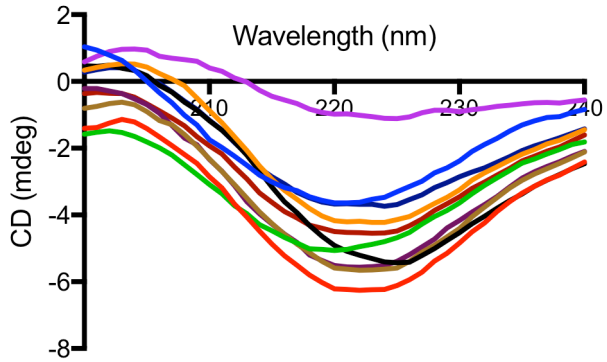

Figure 152: Far-UV CD of human BACE1 with CMH in 50 mM sodium acetate pH 4.0 (–) BACE1 with (–) CMH1, (–) CMH2, (–) CMH3, (–) CMH4, (–) CMH5, (–) CMH6, (–) CMH7, (–) CMH8, (–) CMH9.

No simple correlation between number of sulphates per disaccharide and perturbation of the CD spectra in this area is apparent, with both low and highly sulphated modifications present across this spectral region (Figure 152).

7.2.4 The effect of cation form on the ability of heparin to perturb the thermal stability of BACE1

Table 17: DSF Tm of BACE1 with a library of defined cation forms of heparin in 50 mM sodium acetate buffer pH 4.0 with 3.0 μM native BACE1 and 6.0 μM heparin.

Heparin preparation	Melting temperature (°C)	Atomic radii (pm)	Valency
Purchased sodium heparin (Celsus)	34.7	-	-
Sodium	38.8	190	1+
Potassium	38.8	243	1+
Barium	40.2	253	2+
Copper	40.9	145	2+
Ammonium	41.2	175	4+
Manganese	41.3	161	2+
Calcium	41.7	194	2+
Lithium	42.1	167	1+
Iron (II)	42.3	156	2+
Magnesium	43.0	145	2+
Zinc	43.6	142	2+
Silver	43.7	165	1+
Iron (III)	43.9	156	3+

The aim of these experiments was to determine whether the type of cation paired to highly electronegative heparin would modify the structure or functional properties of the molecule sufficiently when bound to BACE1 to change the melting temperature of this protein. To this end, a range of valancies, atomic sizes, and a polyatomic ion was employed.

BACE1 alone in DSF data posesses a Tm of 42.99 ± 0.087°C. Unmodified sodium heparin supplied from Celsus Laboratories with BACE1 in DSF reduced the melting point by 8.2°C to 34.7°C (Table 17). Using the same Celsus heparin source and batch, the cations were exchanged to sodium, which reduced the magnitude of Tm shift seen with

the unmodified heparin and BACE1. Sodium and potassium cation forms gave the same Tm when added to BACE1 with a Tm of 38.8°C, a Tm shift of 4.1°C.

Using a correlation matrix, strong correlation (Pearson correlation r = -0.69 (P < 0.01 95% CI -0.90 to -0.23, n = 13) was identified between the Tm of BACE1 with cation heparin in the DSF termal stability assay and the atomic radius of the cation used. Valency did not show a correlation to Tm.

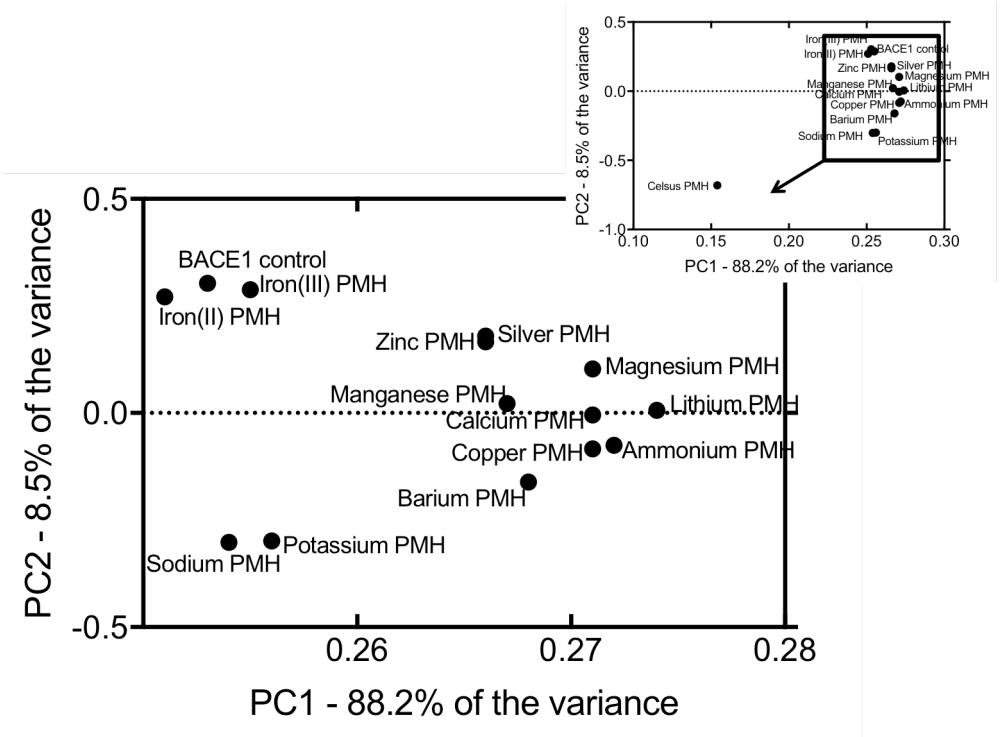

Figure 153: PCA of 1st derivative DSF of BACE1 with defined cation forms of heparin in 50 mM sodium acetate buffer pH 4.0.

Heparin preparations for pharmaceutical use are supplied in sodium, potassium, lithium, and ammonium forms. In this data, the sodium and potassium forms of heparin perturb the melting temperature to a greater degree (38.8°C) than ammonium (41.2°C) and lithium (42.1°C). The unmodified sodium Celsus heparin shifts the Tm of BACE1 to 34.7°C, which is closer to the result seen with chemically modified CMH1 seen in section 7.2.1 (35.96°C). The method for production of the cation heparins therefore could

modify the action of these compounds in DSF as the two sodium heparins differ in effect of Tm by 4.1°C (Table 17).

PCA of the thermal denaturation curves from DSF of human BACE1 with cation forms of heparin at a single screening concentration is shown in Figure 153. Potassium and sodium form of heparin are grouped together with a similar principle component 1 (PC1) and the same PC2. Magnesium, calcium and copper PMH exhibit the same PC1, and differing PC2. Zinc and silver PMH have the same PC1 and PC2 values, suggesting these cation forms have the same effect on thermal denaturation BACE1 in DSF. The two iron oxidation states tested demonstrate the smallest effect on BACE1, migrating in the same group as BACE1 control. Interestingly, the cation forms which demonstrate the lowest thermal destabilisation of BACE1 in DSF (Figure 153) are the closest in the PC2 to the BACE1 control in PCA. The forms of heparin with the greatest effect on Tm, sodium, potassium and barium are the furthest from the BACE1 control in PC2.

7.3 Discussion

Grouping the effects of the chemically modified heparin library allows identification of four main effects on native BACE1 in 50 mM sodium acetate pH 4.0, in DSF. Using the first derivative melt curve, the Tm of each BACE1:modified heparin ratio was determined.

The first group, the destabilisers, act at the high concentrations tested (≥ 0.75 μM), to destabilise the structure of native BACE1 as shown in a reduction in Tm. At low concentrations (≤ 0.38 μM), these chemically modified heparins have the opposite effect, stabilising the native BACE1 and increasing the Tm. 6.0 μM CMH1 destabilises native BACE1 to reduce the Tm from 42.99°C to 35.96°C. This maximum thermal destabilisation reduces with decreasing CMH1 concentration, at 0.38 μM the effect is reversed, with a more stable Tm of 46.53°C. Concentrations lower than this reduce the Tm to close to the native BACE1 Tm. CMH2 follows a similar pattern, with the Tm shift with 6.0 μM is 38.27°C and the stabilisation effect occurring at 0.75 μM CMH2, suggesting a less potent destabiliser than CMH1. CMH4 reduces the Tm to 38.00°C with 6.0 μM with 0.75 μM causing a stabilisation (44.98°C), but with 0.38 μM causing a more stable comformation with Tm of 46.34°C. CMH7 has an effect on BACE1 most similar to CMH2 with 0.75 μM CMH7 causing a wide Tm peak with two Tm values, one at a lower Tm of 37.56°C the other at 44.53°C, suggesting an intermediate with two populations of BACE1.

The second group, the stabilisers, act to improve the thermal stability of native BACE1 in DSF. CMH3 at the highest concentration tested (6.0 μM) does not have a stabilising effect, but at lower concentrations, the Tm of native BACE1 increases to a maximum of 46.09°C. CMH5 has a similar effect, with the high Tm of 46.13 °C caused by 1.5 μM of CMH3. CMH6 has a stabilising effect at all concentrations tested, with the

highest Tm of 45.46°C. The high concentration peaks have a peak shape in the 38°C region however, suggesting a population of BACE1 with a lower melting point.

The third group of one, CMH8, has a minimal effect on the thermal stability of native BACE1, with no concentration dependence. This lack of concentration dependence suggests this chemically modified heparin may not bind to native BACE1 under these conditions. The work done by Patey *et al.* (2006) described the activity of this unsulphated heparin derivative as 'almost abolished' (Patey et al., 2006); this would align with the thermal stability data shown here.

The fourth group of one, CMH9 caused the most dramatic change in the thermal stability of native BACE1, with high concentrations tested of 6.0 μM to 1.5 μM causing the absence of a melt curve. This indicates native BACE1 denatured at room temperature prior to the initial 25.5°C starting experimental temperature. At 0.19 μM and 0.09 μM, CMH9 still retains the ability to stabilise BACE1 causing an increase in Tm to a maximum of 46.98°C. The inhibitory activity of persulphated heparin is described by Patey *et al*. (2006) (Patey et al., 2006) and demonstrates activity similar to CMH3 but these two compounds have very different effects in on the thermal stability of BACE1. This suggests that the heparin-BACE1 binding interaction is different for these two compounds, but the effect the compounds have on the activity of the enzyme is similar.

Klaver *et al.* 2010 suggests a relationship between heparin concentration, the binding between BACE1 to heparin, and the activity of BACE1 (Klaver et al., 2010). Heparin high affinity binding, occurring at low heparin concentrations allows enzyme activation, whereas low affinity binding occurring at high heparin concentrations causes BACE1 enzyme inhibition (*idem*). This suggests a balance to regulate the activity of the enzyme through variable binding roles for heparin (*idem*). Here, the chemically modified heparins that act to stabilise BACE1 at low concentrations; this may suggest

binding with high affinity at low concentrations. Chemically modified heparins that act to destabilize at high PMH concentrations, may be binding with low affinity. The BACE1 inhibitory activity of the chemically modified heparins identified in the work by Patey *et al.* (2006) does not directly align with the changes seen in the Tm and therefore stability of BACE1 in these DSF experiments. However, the action of unsulphated CMH8 suggests some crossover between the activity and structural studies.

Future repetition of the DSF thermal stability experiments with CMH with BACE1 including the APP peptide will demonstrate if the destabilisation changes occur and if the activity of BACE1 is modified.

Far-UV CD identifies changes to the secondary structure of BACE1 at physiological pH (4.0) with the addition of heparin and chemically modified heparins. The peak at λ = 220 nm in native BACE1 alone demonstrated the greatest change with the addition of CMH3, which does not follow the trend spectral shape, also causing a decrease in ellipticity at this wavelength, as seen by other chemically modified heparins.

CMH8 and CMH6 display the same spectral features at the λ = 223 nm peak suggesting the 2-O-sulphate on this disaccharide repeat unit does not cause a change in the glycosaminoglycan chain able to generate a secondary structural change to BACE1 upon binding. Instead, CMH7 and CMH5 display a 1.6 nm peak difference, suggesting some aspect of the 2-O-sulphate addition to this heparin form causes some BACE1 structural modification.

In the analysis of the CD spectra using the BeStSel analysis software, the proportion of secondary structure elements of BACE1 remains consistant with the addition of the chemically modified heparin library. The changes to BACE1 secondary structure occurred through the reduction in antiparallel (right-twisted) β-sheet present in the protein, becoming disordered. Considering per-sulphated heparin an outlier, the

next most potent Tm reducing chemically modified heparin is CMH1, which also causes the greatest loss of ordered antiparallel (right-twisted) β-sheet in BACE1. This suggests a possible causal relationship between the reduced β-sheet, the increase in BACE1 structural disorder and the resulting decrease in thermal stability seen in DSF in the presence of a polymer of the most common disaccharide in heparin, the most potent inhibitor of the BACE1 enzyme (Scholefield et al., 2003), IdoA(2S)-GlcNS(6S).

However, across the whole chemically modified heparin library the relationship between the proportion of BACE1 antiparallel (right-twisted) β-sheet loss due to chemically modified heparin and the melting point of BACE1 with the same modified heparin shows no correlation (Pearson correlation coefficient (n = 9) r = -0.16 (P > 0.01 95 % CI -0.74 to -0.57)).

The sodium form of Celsus PMH used as received, caused a reduction in Tm of native BACE1 double that of the sodium cation form of PMH created for these experiments. The process in which the specific cation forms are made could have modified a property of the PMH, thereby changing the binding capabilities or destabilisation effect of the treated PMH form. Conversley, unmodified Celsus PMH could contain an assortment of cations that give rise to an effect greater than for any single homogeneous cation change. Removal and replacement of this 'Celsus type' positively charged mixture and replacement with pure sodium cations reduces the destabilisation effect of PMH. At low pH, Na^{+}, Ca^{2+}, and Mg^{2+} interact with heparin in a delocalized way, in anionic sites across the molecule, at neutral pH Ca^{2+} binds forming chelate bonds in specific regions of the heparin polymer; no preferred binding site was detected for Na^{+} and Mg^{2+} (Karpukhin, Feofanova, Nikolaeva, Mamontov, & Dobrynina, 2006). Calcium binding at neutral pH alters the proportion of conformation states, from 60:40 ratio of $^{1}C_{4}$:$^{2}S_{0}$, to 80:20, stiffening the molecule (*idem*).

Potassium ions had the same effect as replacement with known sodium ions, demonstrating the same level of destabilisation of BACE1 to a Tm of 38.8°C. The other 1^+ valency cations, lithium and silver have a less pronounced effect on PMH destabilisation of BACE1. Some cation forms negate the large destabilising effect seen with full-length heparin, and the effects seen with cation forms such as sodium and potassium heparin. Iron (II) and magnesium forms halt the Tm reduction and BACE1 thermal destabilisation seen with the addition of PMH. This suggests a structural change to the heparin molecule, such as the stiffening seen with calcium binding, which either halts binding to BACE1, or binds without modification to the structure of BACE1 thereby not altering the Tm in DSF. Experiments to determine if there is binding and consequently a concentration dependant effect to this interaction would shed light on this question.

Zinc, silver and iron (III) all demonstrate small stabilising effects on BACE1 melting. The increase in BACE1 Tm in the presence of these cation heparins is <1°C over the Tm of BACE1 alone (42.99 ± 0.087°C), so the significance of this increase in stability is undetermined.

The substitution pattern and cation form of the heparin/HS disaccharide constituents of the glycopolymer are known to have subtle and complex effects on the conformation of the iduronate ring (Ferro et al., 1986) and the glycosidic linkage geometries (Yates et al., 2000). Here, these changes have demonstrated a differing effect on the thermal stability and secondary structure of the target protein, BACE1.

Chapter 8: Investigating glycosaminoglycan structural mimetics as potential inhibitors of BACE1

8.1 Introduction

8.1.1 The requirement for heparin and HS mimetics

Heparan sulphate and its highly sulphated analogue heparin can interact with proteins or peptides utilising a chain specific binding fragment, or in a charge-dependant, monosaccharide non-specific manner (Krylov, Ustyuzhanina, & Nifantiev, 2011). Specific chain structural requirements include the pentasaccharide binding sequence in the AT interaction and fibroblast growth factor FGF-FGFR binding interactions, requiring a minimum trisaccharide fragment (*idem*). Conversley, charge-based, non-specific binding occurs through the spatial organisation of charged groups creating favourable binding pockets or regions within the polysaccharide 3D structure and usually occurs over a greater area than that of chain-specific binding (*idem*).

The diverse variety of physiological and pathological actions in which heparin and HS are involved, places substantial restraints on the use of these drugs, with effects of heparin administration including haemorrhagia and thrombocytopenia (Gollub & Ulin, 1962). The anticoagulant activity of heparin and heparin-derived polysaccharides precludes their therapeutic application as anti-inflammatory, anti-tumour and anti-viral agents. Identification of specific sequence requirements (akin to the AT interaction) may negate the anticoagulant efficacy through more targeted pharmacology, and lead to alternative treatments for disease targets (Geerts et al., 2008). Due to the complex nature of heparin and HS electrostatic binding interactions, this may not be possible, rather, the selection of heparin/HS mimetics that have mitigated anti-coagulant action with minimum saccharide size, no off-target effects and a defined structure, would offer a attractive alternative to polysaccharides such as heparin. Due to the difficulty in obtaining pure GAGs from animal extractions, the unavoidable contamination risk and

high financial burden of using animal derived tissue, chemical synthesis of HS/heparin mimicking GAG saccharides has been investigated (Schworer et al., 2013) (Miura, Fukuda, Seto, & Hoshino, 2016).

Another method for the identification of heparin mimetics is the isolation of GAG mimicking compounds from plant and animal sources, which can be chemically modified using routine and scalable chemistry, to produce active heparin mimetics. This method may be more feasible than full synthesis as the high availability of the starting material and good yield would allow for scalable production. The source of starting material can also be highly tractable ensuring high purity and low risk. The cost of chemical modification would be low when compared with full synthesis of GAG based saccharides, due to the equipment, reagents, environment, and synthetic steps required for the production, with each step reducing the final product yield. Heparin mimetics have been demonstrated to have activity in many biochemical interactions commonly involving heparin or HS, some of which are discussed below.

8.1.2 Examples of heparin mimetics

The attachment and entry of *Flavivirus* to host cells occurs through endogenous GAG binding (Baba, Snoeck, Pauwels, & Declercq, 1988). Heparin mimetics can compete for these viral high-affinity GAG binding regions through competitive inhibition, halting the infectivity of the invading virus (*idem*). Dengue fever infection of Vero cells (*in vitro*) can be inhibited by the heparin analogue suramin (Chen et al., 1997) as well as with a series of polyanionic compounds that probed requirements for molecular size and sulphation levels (Marks et al., 2001). Sulphated polysaccharides κ/ι/ν carrageenan G3d and the D/L-galactan hybrid C2S-3 derived from red seaweeds *Gymnogongrus griffithsiae* and *Cryptonemia crenulata,* showed 50% inhibition against dengue serotype 2 (1 μg/ml) (Talarico et al., 2005). Activity was seen against serotype 1 in hepatoma

HepG2 cells, foreskin fibroblast cells and Vero cells, but showed no activity in mosquito C6/36 HT cells (*Aedes albopictus),* suggesting a differing route of cell entry (*idem*).

Galactomannans isolated from *Mimosa scabrella* and *Leucaena leucocephala* seeds were chemically sulphated by Ono *et al*. (2003) and tested as anti-viral agents against dengue and yellow fever virus (Ono et al., 2003). When testing against intraperitoneal yellow fever infections of young mice, with a dose of 49 mg/kg, the galactomannan from *M. scabrella* showed an 87.7% protection against death while galactomannan from *L. leucocephala* gave 96.5% protection (*idem*). Inoculation simultaneously with yellow fever virus (37.5 LD_{50}) afforded even more protection with 93.3% and 100% resistance respectively (*idem*).

Many sulphated polysaccharides have been demonstrated to inhibit the viral invasion of human immunodeficiency virus (HIV) including carrageenans (Nakashima, Kido, et al., 1987), heparin (T. Ito & Tsumoto, 2013), dextran sulphate ((1-6)−α-glucan) (Nakashima, Yoshida, et al., 1987), fucoidan (Baba, Snoeck, et al., 1988), pentosan polysulphate (Baba, Nakajima, et al., 1988), polysulphated polyxylan (Biesert et al., 1988) and mannan sulphate (M. Ito et al., 1989) *in vitro*, however the anti-coagulant capabilities of these compounds were a barrier to their therapeutic use in HIV.

Semi-synthetic sulphated polysaccharides with attenuated anti-coagulant capabilities such as lentinan sulphate (branched (1-3)-β-glucan) (Yoshida et al., 1988) and curdlan sulphate ((1-3)-β-glucan) have been shown to retain potent anti-viral (Kaneko et al., 1990) and anti-parasite action (Kyriacou et al., 2007).

Sulphated glycosides derived from kelp (*Laminaria spp.)* were synthesised by Katsuraya *et al.* (1999) from tetraose, pentaose and hexaose saccharides and tested for the effects seen with changing alkyl chain length and number of glucose residues as anti-HIV agents (Katsuraya, Nakashima, Yamamoto, & Uryu, 1999). The anti-HIV activity of

both the dodecyl laminara-pentaosides and hexaosides increased with increasing sulphate level with the fully sulphated pentaoside showing highest activity (*idem*).

Infection of the *Anopheles* mosquito by *Plasmodium* spp. occurs post blood meal when the parasite ookinete invades midgut epithelial cells through micronemal proteins, with the essential involvement of CS on the luminal surface and HS on the basal surface (Sinnis et al., 2007). Knockdown of essential CS and HS biosynthetic enzymes in the mosquito vector showed limited infection by *plasmodium* spp. illustrating CSA and chondroitin sulphate E (CSE) are essential for some micronemal invasion (F. W. Li et al., 2004). Mathias *et al.* (2013) designed small CS mimics capable of competitive inhibition, blocking the ookinete-GAG interactions required through PfWARP (von Willebrand factor A domain-related protein) and PfCTRP (circumsporozoite protein and thrombospondin-related anonymous protein-related protein) binding for entry into mosquito microneme (Mathias et al., 2013). The synthetic polysulfonated polymer blocked oocyst development by up to 99% ($P < 0.0001$) in *P. falciparum* and *P. berghei* infected mosquitos (*idem*). The CS mimicking compound was found to bind the GAG binding PfCTRP blocking the transmission to the mosquito and therefore ookinete to oocyst parasite progression (*idem*).

Most GFs and cytokines involved in cellular growth and repair are found in the extracellular matrix and stored via specific interactions with GAGs (Tillman, Ullm, & Madihally, 2006). The use of GAG mimetics such as fucoidan, pentosan polysulphate and dextran sulphate in wound healing have been demonstrated to stimulate tissue repair similarly to endogenous GAGs, with others improving on the efficacy seen with these native GAGs (Ikeda et al., 2011). These GAG mimetics act to replace endogenous GAGs degraded by matrix endoglycosidases, improving the tissue scaffold and potentiating the effects of heparin-binding GF (Rouet et al., 2006), heparin binding proteins such as

thrombin, and chemokines RANTES (Regulated on Activation, Normal T Expressed and Secreted/CCL5) (Sutton et al., 2007) and SDF1 (stromal cell-derived factor-1) (Friand et al., 2009). Ikeda *et al.* (2011) determined topical application of a heparin mimetic d.p.12 oligosaccharide named HM4120, promoted the healing of skin ulcers as well as the polymeric control material but had preferable attenuated effects in coagulation (Ikeda et al., 2011). Garcia-Filipe *et al*. (2007) also identified a heparan sulphate mimetic dubbed RGTA OTR4120 synthesised from T40 dextran, as a potent post-burn, tissue regenerating treatment (Garcia-Filipe et al., 2007).

Interferon-γ (IFN-γ) along with a number of cytokines and GF, interact with HS with high affinity (IFN-γ = 10^{-9} M), acting as a molecular sink, providing increased local concentrations of the cytokines and GFs (Lortat-Jacob, Turnbull, & Grimaud, 1995). HS moderates IFN-γ C-terminal proteolytic cleavage through binding proximity, providing an increase or decrease in biological activity of this cytokine (*idem*). Other GAGs tested such as CS and DS do not bind IFN-γ suggesting a more specific binding requirement than a polyanionic nature (*idem*). The IFN-γ binding domain of HS was identified as two small N-sulphated hexa- to octa- saccharides flanking a N-acetylated region, rich in GlcA residues of approximately 7 kDa in length (*idem*). Synthetic production of this region may permit modulation of IFN-γ levels useful for immune stabilisation.

The complex growth factor family of FGFs and FGFRs are involved with many processes in growth and development, and require HS to create binding complexes between ligand and receptor in order for signalling to occur (Ornitz, 2000). HS synthesis alters over the course of development and the substitution along the polysaccharide chain is also both tissue and cell dependent (Allen & Rapraeger, 2003). Changes to HS therefore, may regulate morphogen signalling and effect the growth and development of an organism (*idem*). In HS-FGF complex binding, polysaccharide sequence specificity is

absent, but there is a degree of structural requirement for FGF complex signalling (Rudd et al., 2010). Charge density alone does not account for the HS/FGF/FGFR signalling capabilities as shown by Yates *et al.* 2004 (Yates et al., 2004). Rudd *et al.* (2010) hypothesised that an effective FGF/FGFR binding complex required a polysaccharide not with a specific primary sequence, but rather with conformation and charge characteristics specific for the binding complex activation (Rudd et al., 2010). This research proposed any polysaccharide could have the potential to fulfil the FGF complex requirements irrespective of the primary chain sequence, as factors such as hydration and pH affect the molecular structure (*idem*). In addition to 9 modified heparin polysaccharides (Yates et al., 2000; Yates et al., 1996), 39 alternative chemically sulphated polysaccharides, including tylose, gums such as xanthan gum, pectin, ι-carrageenan and glycogen were tested for the ability to promote FGF/FGFR signalling using differential scanning fluorimetry (DSF), synchrotron radiation circular dichrosim (SRCD) and a BaF signalling assay (Rudd et al., 2010). The stability and signalling ability of FGF-1 was reached by chemically sulphated xanthan gum and ι-carrageenan (*idem*). FGF2 was stabilised and active with chemically sulphated tylose and locust bean gum with lower levels of activity seen with the other sulphated polysaccharides, through differences between FGF1 and FGF2 structural and charge requirements (*idem*). Chemical sulphation is one of the most exploited approaches to heparin mimetic production (Papy-Garcia 2005).

8.1.3 Experimental aims

The aim of this study is to identify and quantify a small group of polysaccharide heparin analogues with potent BACE1 inhibition activity and attenuated action in the coagulation cascade, to take forward for future therapeutic development.

8.1.4 Composition of the polysaccharide scouting library

The examples of non-heparin GAG analogues acting as mimetics for heparin or HS in biological systems lends support to the thesis that these more easily accessible, cheaper and safer polysaccharides can be investigated with potential in all heparin/HS biological systems, including as modulators of the heparin/HS binding aspartyl protease BACE1. The creation of a chemically sulphated polysaccharide library of heparin mimetics employed as a screening resource has enabled identification of hit BACE1 inhibitors, with potential for future combinatorial chemistry to produce an effective BACE1 inhibitor.

The members of this polysaccharide library were selected based on criteria including cost, tractability, scalability, purity, required purification, and composition. Table 18 is a summary of the compounds selected. The qualitative yield upon chemical sulphation is included to identify potential hits alongside brief information on the compound composition.

Table 18: GAG mimetic library composed of tractable, scalable and economically selected polysaccharide members.

Precursor compound	Chemical sulphation yield	Precursor compound information
Tylose (MH300)	++++	Methyl 2-hydroxyethyl cellulose ethers
Gum Accroides	++	Or Yacca gum. Derived from *Podocarpus coriaceus* and *Podocarpus purdicanus*. Unknown composition.
(Hydroxypropyl)methyl cellulose	+++	9% hydroxypropyl cellulose
Alginic acid	++++	A straight-chain, polyuronic acid composed primarily of anhydro-β-D-mannuronic acid residues with 1→4 linkage. (Also glucuronic acid present)
Locust Bean Gum	+++	Galactomannan with a backbone of (1-4) b-D-mannopyranosyl units having branches of (1-6)-linked a-D-galactopyranosyl units. However, Locust bean gum has substantially fewer side chains than guar gum and these are clustered in blocks leaving longer regions of unsubstituted mannosyl regions.
Starch	++	From maize. Glucopyranose units alpha-linked. 15-20% amylose and 80-85% amylopectin (branched D-glucose linked α-D-(1-4) linkages and α-D-(1-6) linkages at branch points)
Gum Mastic	+	From *Pistacia lentiscus*. Unknown composition.
Inulin	+++	Composed of b-(1-2)-linked fructopyranoside units with up to 60 fructose residues per chain
i-carrageenan	+++	Strictly alternating masked repeating unit of (1-3) linked α-D-galactose and (1-4) linked β-D-galactose. The α-linked galactose occurs as a 3,6-anhydro-2-sulphate unit and the β-linked sugar occurs as the 3-sulphate.
Guar	+++	The structure of the polysaccharide consists of a main chain of (1-4)-linked β-D-mannopyranosyl units with single α-D-galactopyranosyl units linked (1-6) on average to every second main chain unit.
Gum Ghatti	+++	The polysaccharide has a backbone chain of (1-6)-linked b-D-galactopyranosyl units with some (1-4)-D-glucopyranosyluronic acid units, some joining (1-2)-D-mannopyranosyl units, and some L-arabinofuranose units.
Ethyl cellulose	+	46.5% ethyl vs. OH
Gellan Gum	++++	The molecular structure of gellan gum is a linear chain based on repeating glucose, rhamnose and glucuronic acid units. In its native, or high acyl form, two acyl substituents - acetate and glycerate - are present. Both substituents are located on the same glucose residue, and on average, there is one glycerate per repeat and one acetate per every two repeats
Xanthan Gum	+++	Xanthan gum is an anionic polysaccharide composed of a ß-(1→4)-D-glucopyranose glucan backbone with side chains of (1→3)-α-D-mannopyranose-(2→1)-ß-D-glucuronic acid-(4→1)-ß-D-mannopyranose on alternating residues. Approximately half of the terminal mannose residues are 4,6-pyruvated while most of the inner mannose residues are 6-acetylated
Gum Arabic	++++	The polysaccharide is branched with a main chain of (1-3) linked β -D-galactopyranosyl units with side chains of (1-3) β -D-galactopyranosyl units joined to it by (1-6) links. The side chains are 2-5 units in length. Both the main chain and the side chains have attached units of α-L-arabinofuranosyl, α-L-rhamnopyranosyl, β-D-glucuronopyranosyl and 4-O-methyl-β-D-glucuronopyranosyl units.
Styrax	++	From from *Liquidambar* spp. Unknown composition.
Pectin	+++	Poly-D-galacturonic acid methyl ester
Pottasium Pectate	++	Esterified pectin.

Table 18 continued.

Precursor compound	Chemical sulphation yield	Precursor compound information
Carboxymethyl cellulose	++	Cellulose with carboxymethyl groups of the glucopyranose residues.
Karaya Gum	+++	Believed to be a partially acetylated polymer of galactose, rhamnose, and glucuronic acid with a M.W. of approx. 9,500,000.
Arabic acid	+	Component of gum arabic containing D-arabinose and hexoses
Hypromellose	++	Hydroxypropyl methyl cellulose
Pullulan	++	The chemical structure is essentially repeating units of maltotriose joined by α-D-(1-6) linkages.
Paramylon	+	β1-3-glucan synthesised by *Euglena glacilis.*
K-carrageenan	++	The structure of all carrageenans consists of a strictly alternating masked repeating unit of (1-3) linked α-D-galactose and (1-4) linked β-D-galactose. The α-linked galactose occurs as a 3,6-anhydro unit and the β-linked sugar occurs as the 3-sulphate.
Chitosan	+	Made from cristacean shell treatment with sodium hydroxide. β-(1-4)-linked D-glucosamine (deacetylated unit) and N-acetyl-D-glucosamine(acetylated unit).
Welan	+++	The structure is similar to Gellan based on repeating glucose, rhamnose and glucuronic acid units but with a single side chain of either an α-L-rhamnopyranosyl or an α-Lmannopyranosyl unit linked (1-3) to the 4-O-substituted β-D-glucopyranosyl unit in the backbone.
Propylene glycol Alginate	+	Derived from kelp. Ester of alginic acid, with some of the carboxyl groups esterified with propylene glycol. Produced by reacting alginic acid with propylene oxide.
Tara gum	+	From *Caesalpinia spinosa*. Unknown composition.
Amylose	++	Helical polymer made of α-D-glucose units with α-D-(1-4) linkages
Glycogen Type II	++	Structure similar to amylopectin but more highly branched and compact.
Levan	++	β-(2-6)-fructose polymer
Fucogalactan	+	The polysaccharide is a sulphated galactose containing fucan which can be supplied in a range of molecular weights namely (a) 2,000,000, (b) 100,000, (c) 50.000 and (d) 25,000.
lambda-carrageenan	+++	The structure of all carrageenans consists of a strictly alternating masked repeating unit of (1-3) linked α-D-galactose and (1-4) linked β-D-galactose. λ-Carrageenan has the α-linked unit 2-6 disulphated and the β-linked unit 2 sulphated.
Konjac glucomannan	++	Acetylated (1-4)-β-D-glucomannan
Psyllium Seed Gum	+++	The proposed structure is of a backbone of D-xylopyranosyl units linked (1-4) and (1-3) with the 4-linked units bearing side chains. The side chains consist of α-L-arabinofuranosyl units linked (1-3) and (1-2) and β-D-xylopyranosyl units linked (1-3) and (1-2) and the α-D-Galap-(1-2)-α-L-Rhap aldobiuronic acid units linked (1-2) to the main chain.
Sodium Alginate	++	Sodium salt of alginic acid, extracted from brown algae. A linear polymer constructed of blocks of (1-4)-linked β-D-mannuronate and its epimer, α-L-guluronate.
Tamarind gum	+++	Galactoxyloglucan isolated from seed kernel of *Tamarindus indica.*
Agarose	+++	Supercoiled structure formed from repeating disaccharides of D-galactose and 3,6-anhydro-L-galactopyranose (L-galactose with an anhydro bridge between positions 3 and 6) with some residues being methlyated, pyruvated or sulphated.

8.1.5 Background of methods used

8.1.5.1 Fluorescent resonant energy transfer (FRET)

Förster coupling is the transfer of energy from one atom to a closely linked second atom through the transfer of a virtual photon (exhibiting the same characteristics of photon transfer but only acting for a limited time) in a non-radiative manner when maintaining proximity (Forster, 1959). The Förster radius is the distance through which half the emission energy is transferred to the acceptor (3-6 nm), but the transfer can occur over larger distances of up to 10 nm with a weaker effect (Sekar & Periasamy, 2003). Förster coupling is used experimentally to examine if two chromophores are close to each other and has been described as a 'molecular ruler' (Stryer, 1978).

Förster (fluorescence) resonance energy transfer (FRET) utilises the energy transfer between a donor and acceptor, with the donor or the donor and acceptor being light sensitive molecules (Clegg, 2009). Bound to a peptide, receptor or other target, the donor and acceptor identify real-time changes to the proximity of these two molecules. Figure 154 illustrates this interaction.

Figure 154: Schematic of fluorescence resonance energy transfer reaction with BACE1 cleaving APP_{SW} FRET peptide, excitation at λ_{ex}= 320 nm. Inhibition of BACE1 halts APP_{SW} cleavage, therefore quenching the emission at λ_{em}= 405 nm.

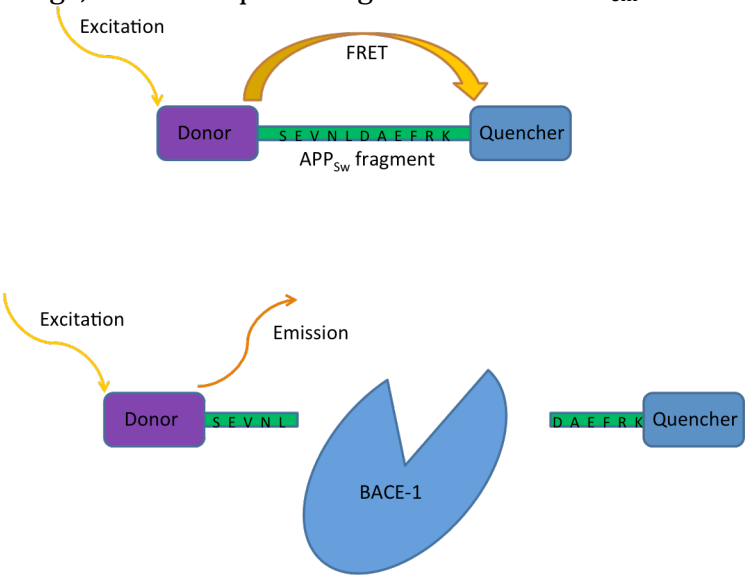

FRET allows for the real time analysis of biological interactions at a distance far beyond that of the diffraction limit for optical microscopy (Clegg, 2009). The donor fluorescence lifetime is extended due to the method of energy transfer and deactivation, leading to slower photobleaching kinetics (*idem*). If both the donor and acceptor molecules are light sensitive, the fluorescence of the acceptor can be directly measured, allowing a real-time and direct measurement of the proximity of the fluorophores; this is called sensitised emission (*idem*).

The decoupling of donor or acceptor molecule from the peptide, ligand or receptor can lead to a false positive assay result. This is more important in complex systems such receptor studies and microscopy than in a three constituent biochemical assay, where controls can account for any unpredicted changes in fluorescence.

The FRET method to screen for BACE1 inhibitors was modified from Yokosawa *et al.,* (1983) using Swedish mutation APP fragment (SEVNLDAEFRK replacing KM, lysine methionine for NL asparagine leucine) bound to the donor molecule 7-amino-4-methylcoumarin (MCA) on the N-terminus and acceptor molecule 2,4-dinitrophenol (DNP) on the C-terminus (Yokosawa, Ito, Murata, & Ishii, 1983). This MCA-APP_{SW}-DNP substrate is cleaved by BACE1 to form a MCA-containing fragment that excites at λ_{ex} = 320 nm fluoresces at λ_{em} = 405 nm. Inhibition of BACE1 diminishes the fluorescence seen at λ_{em} = 405 nm. Proteolytic cleavage of the APP_{SW} by BACE1 between asparagine and leucine residues releases the fluorophores, energy quenching of DNP no longer occurs, allowing the excitation and emission of MCA. Scholefield *et al.* (2003) employed this FRET assay to identify heparin as a physiological regulator of BACE1 and other work further utilised the method for identifying the structural requirements for BACE1 modulation and improving the hit heparin derivatives (Patey et al., 2006; Scholefield et al., 2003) (Patey et al., 2006) (Beckman et al., 2006) (Patey et al., 2008).

8.1.5.2. Coagulation assays

The action of each semi-synthetic sulphated polysaccharide in the intrinsic pathway was determined through the activated partial thromboplastin time (aPTT) assay, which assesses the contact activation or intrinsic pathway and the factors XII, XI, IX and the common pathway factors X and II, forming a clot upon activation of fibrin (factor I).

The prothrombin time (PT) assay was used to identify sulphated polysaccharides that perturb the activation of the tissue factor (trauma) pathway, or extrinsic pathway that utilises factor VII, and common pathway factors X and II, forming a clot upon activation of fibrin.

The aPTT and PT results are presented as half maximal effective concentration (EC_{50}) as a maximum clotting time cut off of 120 seconds was used. Unfractionated heparin inhibits the activation of factor X, thrombin (factor II), factors VIII, IX, XI and XII directly or through the specific interaction with serpin inhibitor, antithrombin. LMWH interact more specifically with factor X to minimise the off target effects seen with unfractionated heparin such as heparin induced thrombocytopenia (HIT).

Sulphated polysaccharide candidates demonstrating intrinsic pathway results 100 times less active than PMH may be considered a possible hit as the anti-coagulant capacity of these hits will be negated and therefore limit the off-target effects as potential therapeutics.

Clinical data suggest measurement of aPTT does not adequately correlate with blood heparin levels or patients anti-thrombotic activity (Baker, Adelman, Smith, & Osborn, 1997). Baker and colleagues suggest the differences in the heparin requirements for each patient, alongside the pharmacokinetic and pharmacodynamics variations in heparin dosing, leads to the aPTT being an unreliable test method for

assessing patient heparin therapy (*idem*), however the assay will demonstrate interaction with other factors not just AT, factor IIa and factor Xa. This work found there was no causal relationship between aPTT results and more specific screening to determine the anti-factor Xa activity of the heparin from a blood sample, in a significant number of cases (*idem*). The aPTT and PT assays screen compound activity through the coagulation pathway, using human serum, allowing for indications of anti-coagulation effect. Specific anticoagulation factor screening provides a more accurate picture of the effects of the hit compound. The aPTT therapeutic range corresponding to a heparin concentration that gives 0.35 to 0.7 anti-factor Xa heparin units per millilitre has been suggested to be a more reliable metric for heparin monitoring (Hirsh & Raschke, 2004).

The interaction between heparin and antithrombin during inhibition of factor Xa occurs through a specific pentasaccharide sequence (Vanboeckel & Petitou, 1993). The more non-specific binding of heparin saccharides >18 mer in length is required when acting as a scaffold for AT/thrombin (factor IIa) interactions, leading to the inhibition of factor II (Olson, Halvorson, & Bjork, 1991). Almost all heparin chains are of sufficient length (>18 mer) to mediate the AT/factor IIa interaction leading to the equal action of UF heparin in factor IIa inhibition and the more specific sequence requirement anti-factor Xa, with a ratio of 1:1 factor IIa to factor Xa inhibition (Bates & Weitz, 2005).

8.1.5.3 Level of sulphation

In order to quantify the level of sulphation for each chemically modified hit polysaccharide, a biochemical colorimetric assay was employed, with calibration obtained with dextran sulphate due to its independently ascertained sulphation level. The level of sulphate, and therefore the charge of the polysaccharide is important when designing therapeutics, as the least charged molecules are less likely to interact strongly with the myriad of other possible binding targets within the body.

The assay employed was modified for a multiwall format from the work by Terho and Hartiala in 1971 and utilises the reduction of barium chloride by the liberated sulphate ion, which in turn results in the colour change of the reporter dye, rhodizonic acid to a rhodizonate anion (Terho & Hartiala, 1971).

8.1.5.4 Determining Molecular weight

Size exclusion chromatography (SEC) separates molecules on the basis of hydrodynamic volume; the effective hydrated radius in solution, or Stokes radius. This radius depends on the molecular shape and the arrangement of water molecules surrounding the molecule. The result of these factors when moving through a viscous liquid causes drag.

$$R_H = \frac{k_B T}{6\pi\eta D}$$

Where R_H is the hydrodynamic volume, k_B is the Boltzmann constant, T is the temperature, η is the liquid viscosity and D is the diffusion constant.

The diffusion constant (D) is effected by the mobility constant (μ) and the electrical charge (q).

$$D = \frac{\mu k_B T}{q}$$

The mobility constant takes into account the ionic charge of the molecule (ze) and the drag through the mobile phase (f).

$$\mu = \frac{ze}{f}$$

Solutes of R_H larger than the column matrix pores are too large to penetrate the beads, therefore pass through the mobile phase of the column only, and are eluted first. Molecules with a R_H less than the matrix pore size pass through the bead pores, and are therefore eluted at a later time; fractionating the sample by molecular size. The HPLC

profile demonstrated the size distribution of the molecules within the sample, and is defined as the molecular weight distribution of the sample.

Gel permeation chromatography utilises samples with known molecular weight to calibrate each column, to allow for calculation of unknown sample weight average molecular weight (Mw), number average molecular weight (Mn) and polydispersity index (PDI). PDI of a polymer is the distribution of molecular mass and is calculated by:

$$PDI = \frac{M_w}{M_n}$$

8.1.5.5 ^{1}H Nuclear magnetic resonance spectroscopy

Proton nuclear magnetic resonance spectroscopy (^{1}H-NMR) occurs through the absorption and resonant frequency of the proton in the sample, relative to the strength of the magnetic field acting on the sample (Bloembergen, Purcell, & Pound, 1947). The spin of the protons align either with (α orientation) or opposing (β orientation) the magnetic field (*idem*). Electromagnetic energy is used to switch orientation of more protons into the β orientation (*idem*). Upon cessation of energy input, the nuclei 'relax' back into the lower energy α orientation, causing a fluctuating local magnetic field; this is the resonance of the proton and is displayed as a NMR peak (*idem*).

The number of peaks indicates the number of different protons present in the molecule, with the integral of each peak indicating the number of protons experiencing the same environments, allowing deduction of the chemical structure of organic molecules (*idem*). Splitting of the peaks indicates the near environment to each proton in the molecule, with neighboring hydrogen atoms affecting the split (*idem*). The electronic environment the proton experiences in the molecule alters the resonance within the applied magnetic field, therefore indicating the amount shielding the proton experiences through electronegativity (*idem*).

1H-NMR was utilised in this work to identify changes to proton environments upon chemical sulphation of the hit polysaccharides.

8.1.5.6 Fourier transform infra-red spectroscopy

Fourier transform infrared spectroscopy (FTIR) involves the absorption or transmittance of infrared radiation through a sample (B.C.Smith, 2011). Intra-molecular bonds absorb IR radiation at different frequencies, depending on the functional groups present (*idem*). Bonds absorb light of different wavelengths depending on the environment, including the atoms present, their conformation and the local environment functional groups (*idem*). These environmental influences modify bond vibrations including stretching, rocking, scissoring, wagging and twisting, which change the frequency of the radiation being absorbed, therefore shifting the resulting IR peaks (*idem*).

The interferogram of a sample is collected through the use of a broadband light source that is modulated through interference to produce a spectrum with each wavelength of light periodically blocked, until a full spectrum has been measured (*idem*). Fast fourier transform of the interferogram gives light absorbtion or transmittance for each wavelength (*idem*). FTIR was employed to identify changes to the structure of hit polysaccharides when they have been chemically sulphated.

8.2 Results

8.2.1 Fluorescent resonance energy transfer (FRET) for the screening of BACE1 inhibitors

An initial test of FRET activity using previously assayed heparins, to determine the reproducibility and comparability to published literature was done to ensure validity of this technique and assess the assay post method transfer.

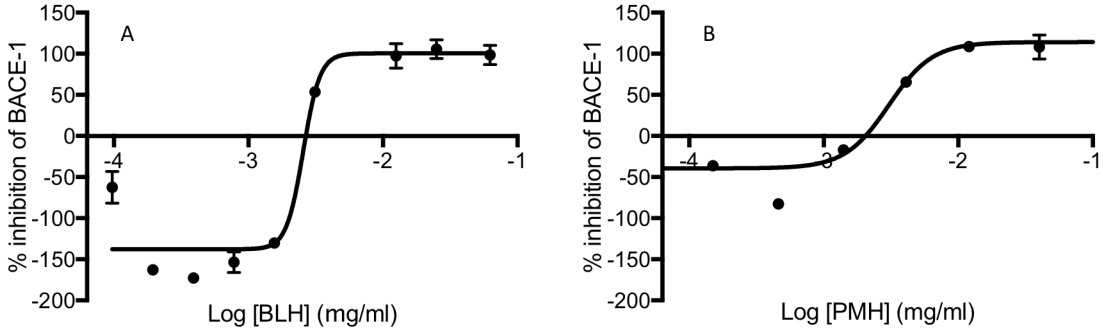

Figure 155: Dose response curve of BACE1 FRET utilised to determine the affect of human BACE1 (FLAG-tag) detecting the cleavage of FRET peptide derived from the APP_{SW} (Mca-SEVNLDAEFRK(Dnp)RR-NH2 Fluorogenic Peptide Substrate) λ_{ex}= 320 nm λ_{em}= 405 nm, in 50 mM sodium acetate pH 4.0, over 1.5 hours. A) BLH IC_{50} = 2.554 µg/ml R^2= 0.9303 and B) PMH IC_{50}= 2.943 µg/ml R^2= 0.8949

Bovine lung heparin (BLH) and porcine mucosal heparin (PMH) were assayed in triplicate. Figure 155 demonstrates the dose-response curves obtained once both no enzyme control and full reaction control were taken into account, with the resulting fluorescence represented as a percentage of BACE1 inhibition. The inhibition activity seen by Scholefield *et al*. (2003) with BLH gave an IC_{50} of 1-2 µg/ml in the FRET BACE1 inhibition assay, with PMH IC_{50} of 5 µg/ml (Scholefield et al., 2003). Later, Patey *et al.* (2006) noted a significantly reduced IC_{50}, with PMH IC_{50} of 28.0 ng/ml, however BLH was not tested (Patey et al., 2008). Neither publication noted a promotive effect at lower concentrations of heparin (< 1 µg/ml), but this effect was noted in the Beckman *et al.* (2006) publication, with inhibitory concentrations of heparin >10 µg/ml and promotive

concentrations <1 μg/ml in rBACE1 (Beckman et al., 2006). The results in Figure 155A demonstrate BLH in BACE1 FRET had an IC_{50} of 2.554 μg/ml (R^2= 0.9303) with 12.5 μg/ml and above giving ≈ 100% inhibition of BACE1 processing of the APP_{SW} FRET peptide, relative to the no enzyme control. The control containing no enzyme was used as a 100% inhibition control to allow for the native fluorescence levels of the FRET peptide. BLH at 3.13 μg/ml showed a 54% inhibition of BACE1, with concentrations of BLH lower than this (1.56 μg/ml and lower) demonstrating the ability to improve the fluorescence signal beyond levels seen in the full reaction control. BLH at 1.56 μg/ml exhibits a 130% increase in fluorescence over the uninhibited FRET fluorescence. At 0.78 μg/ml, 0.39 μg/ml and 0.20 μg/ml the level of fluorescence promotion is ≈ 150%, with this level reducing to 62% at 0.097 μg/ml.

Figure 155B shows the comparable FRET dose response of PMH yielding an IC_{50} of 3.045 μg/ml (R^2= 0.9303) with concentrations over 12 μg/ml exhibiting inhibition of FRET peptide cleavage of ≈ 100%. PMH at 4.1 μg/ml yields 65% inhibition and concentrations lower than this show some stimulating activities but this action is not as pronounced as BLH.

The data show BLH and PMH have similar potency as BACE1 inhibitors as evidenced by their IC_{50} values, but as described by Beckman *et al.,* (2006) at lower concentrations, in this data < 1.4 μg/ml in PMH and < 1.56 μg/ml in BLH, heparin acts to promote the fluorescence as measured at λ_{em}= 405nm. The reasons for this increased fluorescence were investigated to determine whether the effect was due to actual BACE1 inhibition or an effect of fluorophore uncoupling, energy donation or alike. Heparins were assayed with APP_{SW} FRET peptide alone to detect any increase in fluorescence due to MCA/DNP uncoupling or energy donation but no change fluorescence above baseline was seen (data not shown) leading to the conclusion BLH and to a lesser extent PMH

can, at lower concentrations (< 1.4 μg/ml), stimulate the activity of this BACE1 in an *in vitro* FRET cleavage assay.

Even though BLH is the more potent BACE1 inhibitor when compared to PMH, BLH is currently more difficult and expensive to obtain. This form is not utilised aas a pharmaceutic due to concerns with prion contaminants. With the availability of PMH at the required quantities for comparison throughout the following investigations, this heparin source will be utilised in the following experiments.

8.2.2 FRET screening of semi-synthetic chemically sulphated polysaccharide library

A library of 39 polysaccharides from various different sources were chemically sulphated using adaptation to the method of Yoshida et al. (Yoshida et al., 1988). The resulting library was screened using FRET for BACE1 inhibitory activity at 1 μg/ml to ensure screening ruled out polysaccharides with the ability to stimulate BACE1 in a similar way to BLH/PMH. Screening occurred with BACE1 alongside control readings including sulphated polysaccharide and FRET substrate alone, to ensure no fluorophore:substrate decoupling. The results in Figure 133 show the percentage inhibition of BACE1 by each chemically sulphated polysaccharide in the library, alongside the known BACE1 inhibitor OM99-2 (100 nM) and PMH (1 μg/ml) for reference.

Both sulphated gum arabic and per-sulphated ι-carrageenan exhibited the strongest capacity for BACE1 inhibition with over 100% inhibition of fluorescence. The reduction in fluorescence was assayed without BACE1 enzyme to determine the effect of sulphated polysaccharide alone to ensure the test polysaccharides did not directly quench fluorescence at λ_{em}= 405nm or decouple the fluorophors. Gum arabic derivative arabic acid is a purified polysaccharide but exhibits lower but still significant BACE1 inhibitory activity (76.5%). This may be explained by the molecular complexity of the

gum including other polysaccharides that further improve its inhibitory activity beyond the action of the more pure arabic acid. Both gum arabic and ι-carrageenan are comprised of galactopyranosyl residues, in the case of ι-carrageenan, these take the form of a repeating disaccharide of (1-3) linked α-D-galactose and (1-4) linked β-D-galactose and in arabic acid this (1-3) linked β-D-galactose chain is branched with (1-3) β-D-galactose chains linked (1-6) to the main chain. All carrageenans contain the same strictly alternating disaccharide sequence with the α-linked galactose occurring as a 3,6-anhydro unit and the β-linked sugar occurring as the 3-sulphate. The ability of the three carrageenans tested to inhibit BACE1 are different, with ι-carrageenan the best carrageenan inhibitor, with λ-carrageenan inhibition by 62% and κ-carrageenan by 47%. The differences between the carrageenan structures include modifications to the native sulphation level and the presence of the 3,6-anhydro unit replacing the α-D-galactose as shown in Figure 156.

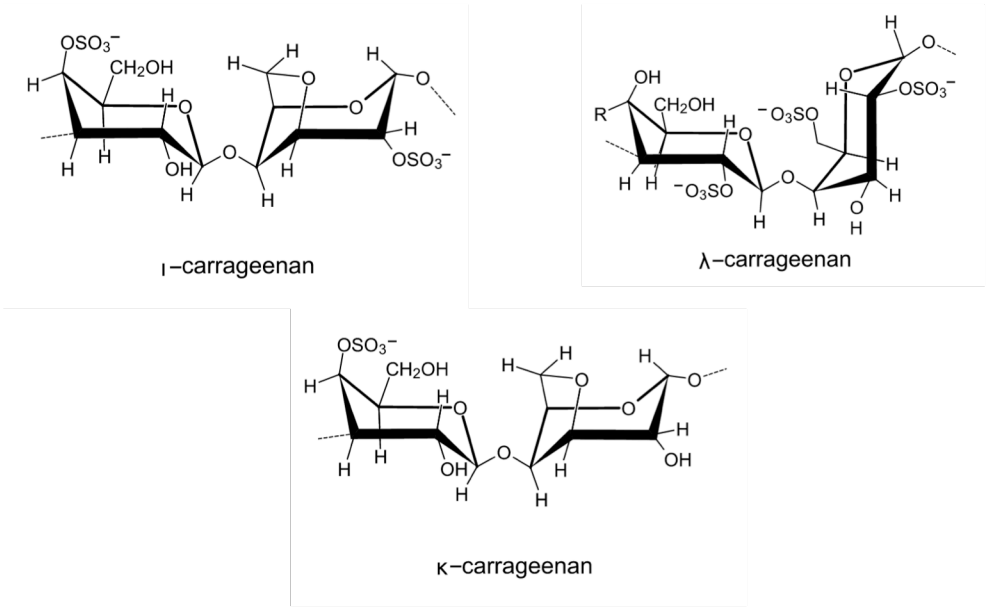

Figure 156: Haworth projections of the ι, λ and κ carrageenans displaying the differences in structure.

Sulphated gum mastic, ethyl cellulose and agarose demonstrated BACE1 inhibition of 98.5%, 94.2% and 91.4% respectively. Other cellulose derivatives did not

show similar efficacy, with tylose the most active at 47.37% and then carboxymethyl cellulose (21.79%), hypromellose (3.97%) and (hydroxypropyl)methyl cellulose (-15.39%). (Hydroxypropyl)methyl cellulose caused increased fluorescence measured at λ_{em}= 405 nm by 15% above the non-inhibited control. Locust bean gum and paramylon produced increased fluorescence as calculated as normalised percentage inhibition (NPI), with sulphated locust bean gum giving a 12.36% fluorescence increase and sulphated paramylon displaying the highest promotive effect at 41.59%. These sulphated compounds did not increase the fluorescence in the no-enzyme controls, suggesting they act to promote BACE1 activity beyond *in vitro* 100% activity.

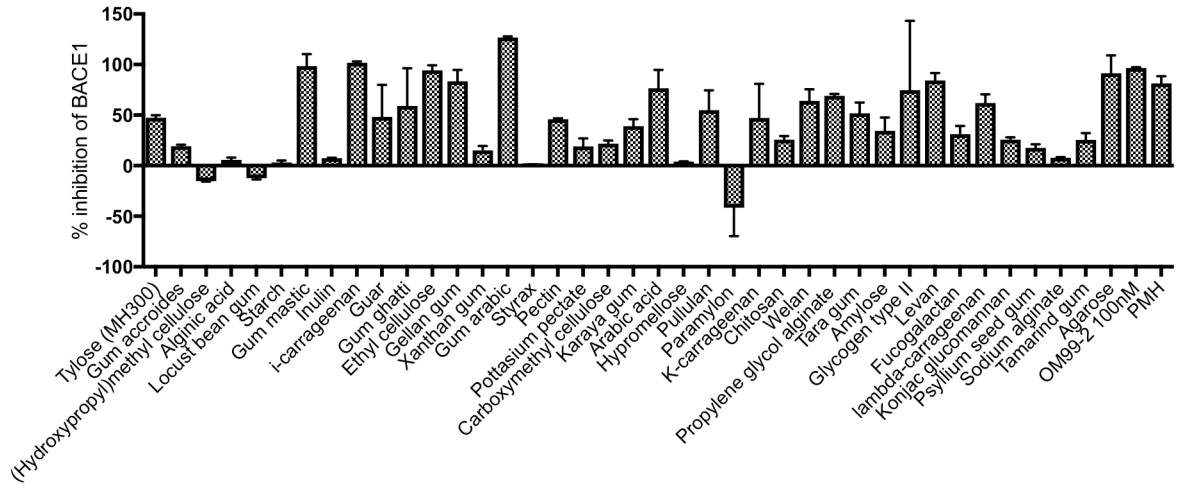

Figure 157: Dose response curve of BACE1 FRET utilised to determine the affect of human BACE1 (FLAG-tag) detecting the cleavage of FRET peptide derived from the APP_{SW} (Mca-SEVNLDAEFRK(Dnp)RR-NH2 Fluorogenic Peptide Substrate) λ_{ex}= 320 nm λ_{em}= 405 nm, in 50 mM sodium acetate pH 4.0, over 1.5 hours. Initial screen of chemically sulphated polysaccharide library at 1 µg/ml in FRET with BACE1 and APP_{SW} FRET peptide (n=3). Known BACE1 inhibitor OM99-2 was assayed at 100 nM and PMH (1 µg/ml) included for reference.

Sulphated levan and gellan gum inhibited BACE1 by 84.3% and 83.5% respectively. Glycogen type II (74.71%) inhibited BACE1 to a similar degree of arabic acid (76.51%), but the standard deviation shows disparity between the two screening well results, suggesting an error that could have originated in pipetting or alike. Glycogen type II will be taken as a hit compound for further testing to determine the activity to a more precise degree.

Sulphated compounds that showed negligible efficacy in BACE1 inhibition as determined by FRET include hypromellose (3.97%), starch (2.46%) and styrax (0.86%). Starch contains 80-80% amylopectin which is composed of branched D-glucose α-D-(1-4) linkaged and α-D-(1-6) linkaged at branch points and gives a negligable BACE1 inhibition of 3.97%, whereas the structurally related glycogen type II contains a more highly branched and compact amylopectin structure inhibits by 74.71%.

8.2.3 Coagulation screening of chemically sulphated polysaccharide library

The screening of the sulphated polysaccharide candidate library for their perturbation of the extrinsic and intrinsic coagulation pathway was carried out to identify unfavourable anti-coagulant activity, potentially mimicking the action of heparin and its low molecular weight counterparts in coagulation.

8.2.3.1 Activated partial thromboplastin time

The activated partial thromboplastin time (aPTT) assay was used to identify compounds that have unfavourable activity in the contact activation (intrinsic) coagulation pathway.

The PMH is more active in the intrinsic aPTT assay, leading to a reduced $EC_{50.}$ This is due to the multiple points for inhibition by heparin alongside the common

pathway factors, whereas heparin can only effect ATIII binding to factor VII in the extrinsic pathway so the inhibitory effect is reduced.

Table 19: Activated partial thromboplastin (aPTT) of chemically sulphated polysaccharides using 50 µl Seimens Pathromtin SL reagent, 50 µl normal human citrated plasma, 25 µl test sample and 25 µl 50 mM calcium chloride, maximum time for clot formation 120 seconds. Half maximal effective concentration (EC_{50}) of sulphated library screening including R^2 and PMH control. EC_{50} is quoted as x fold higher than PMH.

Chemically sulphated polysaccharide	EC_{50} (µg/ml) aPTT	R^2	aPTT x Fold higher than PMH
PMH	0.274	0.9990	1.00
Gellan Gum	2.189	0.9980	7.99
Gum Mastic	2.302	0.9991	8.40
Agarose	2.344	0.9999	8.55
Pullulan	2.597	0.9996	9.47
Psyllium Seed Gum	2.644	0.9993	9.65
Welan	2.806	0.9990	10.24
Arabic acid	2.920	0.9998	10.65
Amylose	3.140	0.9998	11.46
K-carrageenan	3.289	0.9992	12.00
lambda-carrageenan	4.125	0.9989	15.05
Ethyl cellulose	4.377	0.9986	15.97
Propylene glycol Alginate	6.289	0.9983	22.94
Tamarind gum	7.006	0.9989	25.56
Fucogalactan	7.212	0.9988	26.31
i-carrageenan	7.555	0.9924	27.56
Xanthan Gum	8.221	0.9951	29.99
Tara gum	14.350	0.9938	52.35
Gum Ghatti	15.880	0.9997	57.94
Gum Accroides	22.870	0.9999	83.44
Gum Arabic	23.200	0.9900	84.64
Pottasium Pectate	23.970	0.9994	87.45
Pectin	30.260	0.9963	110.40
Karaya Gum	33.660	0.9989	122.80
Chitosan	44.050	0.9984	160.71
Tylose (MH300)	58.820	0.9900	214.59
Guar	65.830	0.9965	240.17
Starch	138.300	0.9996	504.56
Glycogen Type II	213.700	0.9997	779.64
Alginic acid	235.300	0.9991	858.45
Sodium Alginate	323.900	0.9983	1181.69
Styrax	760.600	0.9970	2774.90
Carboxymethyl cellulose	921.700	0.9999	3362.64
Konjac glucomannan	956.800	0.9997	3490.70
Inulin	1151.000	0.9874	4199.20
Paramylon	1162.000	0.9996	4239.33
Levan	1671.000	0.9984	6096.32
(Hydroxypropyl)methyl cellulose	7922.000	0.9994	28901.86
Hypromellose	52341.000	0.9999	190955.86
Locust Bean Gum	78801.000	0.9999	287489.97

Candidates showing intrinsic pathway results greater than 10 fold that of PMH may be considered a possible hit as the anti-coagulant capacity of these hits will be negated and therefore limit the off-target effects as potential therapeutics as shown in Table 19.

All tested sulphated compounds exhibit an attenuated anticoagulant capacity suggesting no compound mimics the precise polyanionic sulphated arrangement required for anti-thrombin binding or direct serpin interactions of the intrinsic and common pathway. Sulphated gellan gum shows the highest potency of the library compounds at inhibiting clotting in the contact activation pathway (aPTT assay), with an EC_{50} of 2.18 μg/ml, a nearly 8 fold lower activity as compared to PMH EC_{50} of 0.27 μg/ml. Gum mastic, agarose, pullulan and psyllium seed gum also have EC_{50} values within 10 fold of PMH.

κ and λ carrageenan have similar potency in the aPTT assay with EC_{50} of 3.28 and 4.12 μg/ml respectively. ι-carrageenan has an EC_{50} approximately double the related carrageenans, at 7.55 μg/ml. Tara gum and gum ghatti have similar activities, with EC_{50} of 14.35 and 15.88 μg/ml respectively. A similar relationship is seen between the gums accroides and gum arabic with EC_{50} of 22.87 and 23.20 μg/ml respectively. Sulphated pectin and its esterified cousin potassium pectate have similar activities in which potassium pectate is the more potent with EC_{50} of 23.97 μg/ml and pectin 30.26 μg/ml. These related compounds however are 100 fold less potent than PMH. Sulphated compounds with higher EC_{50} than pectin will be considered to have no remarkable anti-coagulant capabilities.

The main constituent of starch, amylopectin, has similar potency as the more branched amylopectin cousin, glycogen type II, with starch 500 fold less potent than PMH at inhibiting the contact activation pathway, and glycogen 780 fold less potent.

Progressing to alginic acid and sodium alginate, these structurally related compounds have similar potency at 235.3 and 323.9 μg/ml EC_{50}. The related compound propylene glycol alginate displays approximately 40 times higher activity in aPTT (EC_{50} of 6.28 μg/ml).

Fructose polymers, sulphated inulin and levan have similar influence in aPTT, with inulin EC_{50} of 1151 μg/ml and levan EC_{50} of 1671 μg/ml. Similarly, related compounds (hydroxypropyl)methyl cellulose and hypromellose, differing in their quantity of hydroxypropyl constituent, show no anti-coagulant activity.

Locust bean gum returns an interrupted result for the R^2 value due to Prism 6 software working to a maximal number of iterations to analyse for non-linear regression. If the software cannot reach a result within a dozen iterations, a interrupted result is returned in order to not consume processing power.

8.2.3.2 Prothrombin time

Sulphated agarose is the most potent anti-coagulant screened in the PT assay measuring the perturbation of the extrinsic with a 8.1 fold reduced EC_{50} from PMH, with PMH EC_{50} of 5.19 μg/ml and agarose EC_{50} of 42.10 μg/ml. Sulphated agarose is similarly 8 fold reduced in the aPTT assay relative to PMH.

Levan has an EC_{50} of 42.65 μg/ml in PT, which is 8.2 fold less potent than PMH at perturbing clotting through tha extrinsic pathway, but relative to its effects in the aPTT assay, where this compound shows limited effects (EC_{50} of 1671 μg/ml); 6000 fold less potent than PMH. Sulphated welan and inulin are structurally related fructose polymers, but their activities in the PT assay are distinctive as compared to the similarity in potency seen in the aPTT assay.

Table 20: Prothrombin time (PT) of chemically sulphated polysaccharides using 50 µl Seimens Thromborel S reagent, 50 µl normal human citrated plasma, 50 µl test sample, maximum time for clot formation 120 seconds. Half maximal effective concentration (EC_{50}) of sulphated library screening including R^2 and PMH control. EC_{50} is quoted as x fold higher than PMH.

Chemically sulphated polysaccharide	EC_{50} (µg/ml) PT	R^2	PT x Fold higher than PMH
PMH	5.196	1.0000	1.00
Agarose	42.1	0.9990	8.10
Propylene glycol alginate	42.19	1.0000	8.12
Levan	42.65	1.0000	8.21
Welan	43.51	1.0000	8.37
Tara gum	43.72	1.0000	8.41
Tamarind gum	44.05	1.0000	8.48
κ-carrageenan	44.07	1.0000	8.48
Guar	44.2	1.0000	8.51
Pottasium pectate	45.25	1.0000	8.71
Pectin	45.34	1.0000	8.73
Gellan gum	46.27	0.9990	8.90
Gum mastic	46.35	0.9999	8.92
Gum ghatti	46.6	1.0000	8.97
λ-carrageenan	47.05	1.0000	9.06
Pullulan	47.48	1.0000	9.14
Ethyl cellulose	47.51	1.0000	9.14
Psyllium seed gum	50.46	1.0000	9.71
ι-carrageenan	50.95	0.9999	9.81
Amylose	51.18	0.9990	9.85
Fucogalactan	53.12	0.9999	10.22
Arabic acid	53.2	1.0000	10.24
Xanthan gum	105.4	1.0000	20.28
Sodium alginate	105.4	0.2177	20.28
Gum accroides	443.9	0.9990	85.43
Karaya gum	456.1	1.0000	87.78
Chitosan	459.8	1.0000	88.49
Locust bean gum	466.3	1.0000	89.74
Gum arabic	467.1	1.0000	89.90
Konjac glucomannan	467.5	1.0000	89.97
Alginic acid	472.1	1.0000	90.86
(Hydroxypropyl)methyl cellulose	490.3	1.0000	94.36
Tylose (MH300)	491.9	1.0000	94.67
Glycogen type II	604	0.9999	116.24
Hypromellose	1545	1.0000	297.34
Inulin	2093	0.9996	402.81
Paramylon	2096	0.9799	403.39
Starch	2361	0.9983	454.39
Carboxymethyl cellulose	2697	0.9646	519.05
Styrax	2952	0.7634	568.13

Welan occupies similar anticoagulant activities in both the PT and aPTT assays with 8.3 fold attenuated action in the extrinsic pathway, and 10.2 fold attenuation in the aPTT assay. A group of gums occupy a similar potency in the PT assay between 44 and 46 fold reduced anti-coagulant activity. These compounds include sulphated tara, tamarind, guar, gellan, mastic and ghatti gums with decreasing action in the PT.

Sulphated xanthan gum and sodium alginate have the same EC_{50} of 105.4 μg/ml in the PT assay; with a 20 fold reduced potency than PMH. After which the next compounds are another group of gums with 85 to 90 fold attenuated PT activity including gum accroides, karaya gum, locust bean gum and gum arabic. Compounds occupying the least potent anti-coagulant positions in the PT assay correspondingly in the aPTT are hypromellose, inulin and paramylon.

The carrageenans tested, ι, κ and λ show similar activity in the PT assay, with κ carrageenan the most potent anti-coagulant with an EC_{50} of 44.07 μg/ml, with λ carrageenan EC_{50} of 47.05 μg/ml and finally ι carrageenan EC_{50} of 50.95 μg/ml, varing from 8.48 to 9.81 fold less activity than PMH.

Cellulose based sulphated compounds are also spread through the compounds tested, with varying EC_{50} values. The most potent anticoagulant of the cellulose compounds tested is ethyl cellulose with an EC_{50} of 47.51 μg/ml. (Hydroxypropyl)methyl cellulose and tylose (MH300) have very similar EC_{50} of 490.3 μg/ml and 491.9 μg/ml respectively. The potency of hypromellose in the PT assay is further reduced with an EC_{50} of 1545 μg/ml followed by carboxymethyl cellulose with an EC_{50} of 2697 μg/ml (500 fold less activity than PMH).

Structurally related alginate compounds, alginic acid propylene glycol alginate and sodium alginate show no related activity in the PT assay, with anti-coagulant potency ranging from EC_{50} of 42.19 μg/ml in propylene glycol anginate, to 105.4 μg/ml

in sodium alginate and of 472.1 μg/ml in alginic acid (8.12, 20.38 and 94.36 fold less than PMH respectively).

8.2.4 Sulphated library: hit selection

A strategy for hit selection of the library of chemically sulphated polysaccharides from various sources was chosen to identify compounds for further experimentation. Screening anti-coagulant activity versus the highly active anti-coagulant unfractionated PMH. This metric allows selection of compounds with attenuated potency in intrinsic, extrinsic and common coagulation pathways to ensure a primary requirement for limiting off target effects of these complex anionic polysaccharides. The anti-coagulant activity of the sulphated library of polysaccharides was combined into a 'coagulation factor' determined by multiplying the EC_{50} values in μg/ml of aPTT and PT assays. The following hit selection criteria:

1- Inhibition of BACE1 in FRET assay at one concentration (1 μg/ml) demonstrating greater than 50% BACE1 inhibition.

2- Screening anti-coagulant activity versus the highly active anti-coagulant unfractionated PMH. The selection of compounds based on this anti-coagulation metric required hit to have activity 100 fold less than that of unfractionated PMH to limit off-target effects.

3- The yield of the chemical sulphation method is required to be greater than 40% as shown in table 4 (greater than +), which will allow for an economically viable and scalable product.

Table 21 identifies the 6 top compounds identified from the initial screening following assessment derived from the above-mentioned metrics. The hit compounds are gum arabic, ι-carrageenan, glycogen type II, levan, λ-carrageenan, gum ghatti and

guar. Five other sulphated compounds passed the metrics outlined above, apart from the yield requirements. These include tara gum, ethyl cellulose, propylene glycol alginate, welan, and arabic acid. However, these compounds could be listed in phase 2 investigations if no hits can be brought forward after further analysis with a view to improving the yield of the sulphation reaction.

Table 21: Hit selection Table to demonstrate sulphated polysaccharide library members in two required metrics, % inhibition of BACE1 in FRET required 50% inhibition, and coagulation factor (aPTT (µg/ml) *PT (µg/ml)) required 100 fold less potent anti-coagulant activity relative to unfractionated PMH.

Compound:	Coagulation factor aPTT*PT. Hit requirement >100 fold that of PMH	% Inhibition of BACE-1 in FRET at 1 µg/ml. Hit requirement >50% inhibition of BACE1
PMH	1.4	103.38
Gum arabic	10836.7	126.80
ι-carrageenan	384.9	101.78
Glycogen type II	1282.2	74.71
Levan	71268.2	84.31
λ-carrageenan	194.1	62.04
Gum ghatti	740.0	59.10
Guar	2909.7	50.17
Tara gum	627.4	51.84
Ethyl cellulose	208.0	94.27
Propylene glycol alginate	265.3	69.04
Arabic acid	155.3	76.51
Welan	122.1	64.07
Tylose (MH300)	28933.6	47.37
Pectin	1372.0	45.93
Agarose	98.7	91.43
Gum mastic	106.7	98.52
Pullulan	123.3	54.96
κ-carrageenan	144.9	47.25
Gellan gum	101.3	83.52
Karaya gum	15352.3	39.07
Amylose	98.7	34.56
Fucogalactan	383.1	31.21
Konjac glucomannan	447304.0	25.82
Chitosan	20254.2	25.71
Tamarind gum	308.6	25.60
Carboxymethyl cellulose	2485824.9	21.79
Gum accroides	10152.0	19.22
Pottasium pectate	1084.6	19.04
Psyllium seed gum	133.4	17.51
Xanthan gum	866.5	15.18
Sodium alginate	34139.1	7.78
Inulin	2409043.0	7.49
Alginic acid	111085.1	5.78
Hypromellose	80866845.0	3.97
Starch	326526.3	2.46
Styrax	2245291.2	0.86
Locust bean gum	36744906.3	-12.36
(Hydroxypropyl)methyl cellulose	3884156.6	-15.39
Paramylon	2435552.0	-41.59

Interestingly, ι -carrageenan, λ-carrageenan and gum arabic contain 1-3 linked D-galactopyranose residues, differing as the carrageenans are α-1-3 rather than the gum arabic being β-1-3 and the carrageenans include alternating 1-4 linked β-D-galactose residues. Gum arabic contains side chains limited to 2 - 5 residues in length and is constructed with α-L-arabinofuranosyl, α-L-rhamnopyranosyl, β-D-glucuronopyranosyl and 4-O-methyl-β-D-glucuronopyranosyl units. The carrageenans have differing sulphate patterns, with λ-carrageenan containing the α-linked unit 2-6 disulphated and the β-linked unit 2 sulphated, and ι-carrageenan containing an α-linked galactose occurring as a 3,6-anhydro-2-sulphate unit and the β-linked sugar occurring as the 3-sulphate unit.

Guar has a main chain of (1-4)-linked β-D-mannopyranosyl units with single α-D-galactopyranosyl units linked (1-6) on average to every second main chain unit, whereas gum ghatti has backbone chain of (1-6)-linked β-D-galactopyranosyl units with some (1-4)-D-glucopyranosyluronic acid units, some joining (1-2)-D-mannopyranosyl units, and some L-arabinofuranose units.

8.2.5 BACE1 FRET hit dose response

The seven hit compounds were tested for their potency in BACE1 FRET inhibition using a dose response assay. The results of which are found in Figure 158 and Table 22.

The most potent inhibitor of the tested hit compounds was sulphated levan with an IC_{50} of 0.822 μg/ml (R^2 0.9893) which is ~3 times more potent than that of BLH (2.554 μg/ml) in the FRET BACE1 inhibition experiment. At lower concentrations, each sulphated carbohydrate promoted the activity of BACE1 in the FRET assay, apart from sulphated gum ghatti, which at the lowest concentration tested (10 ng/ml) still showed BACE1 inhibition of ~20% (Figure 19). Sulphated gum arabic, λ-carrageenan and ι–

carrageenan all exhibit more potent BACE1 activity than BLH and PMH, with IC_{50} of 1.034 µg/ml, 1.194 µg/ml and 1.481 µg/ml respectively. Guar and glycogen type II have similar IC_{50} values of 9.904 µg/ml and 10.030 µg/ml respectively, which are ~3.5 times less potent than heparin, but as selected concurrently with their anti-coagulant potency, are more favourable BACE1 inhibitors than both BLH and PMH.

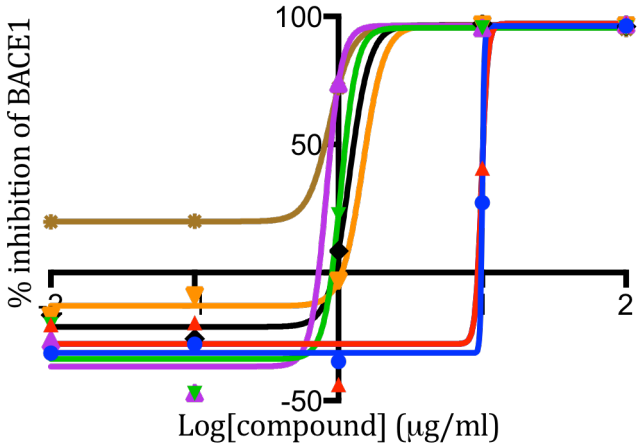

Figure 158: Dose response curve of BACE1 FRET utilised to determine the affect of human BACE1 (FLAG-tag) detecting the cleavage of FRET peptide derived from the APP_{SW} (Mca-SEVNLDAEFRK(Dnp)RR-NH2 Fluorogenic Peptide Substrate) λ_{ex}= 320 nm λ_{em}= 405 nm, in 50 mM sodium acetate pH 4.0, over 1.5 hours. Chemically sulphated (–) glycogen, (–) guar, (–) gum arabic, (–) levan, (–) ι-carrageenan, (–) λ-carrageenan, (–) gum ghatti.

In addition to testing the seven sulphated hit compounds, the unmodified parent compounds were tested to assess for BACE1 inhibition activity. Unmodified gum ghatti and guar would not solubilise at the required concentration so were not included in this screening. The Figure 159 illustrates the percentage inhibition of BACE1 in FRET assay.

Table 22: Dose response curve of BACE1 FRET utilised to determine the affect of human BACE1 (FLAG-tag) detecting the cleavage of FRET peptide derived from the APP_{SW} (Mca-SEVNLDAEFRK(Dnp)RR-NH2 Fluorogenic Peptide Substrate) λ_{ex}= 320 nm λ_{em}= 405 nm, in 50 mM sodium acetate pH 4.0, over 1.5 hours. Half maximal inhibitory concentration (IC_{50}) of BACE1 in the FRET assay.

Compound:	IC_{50} (µg/ml)	R^2
Levan	0.822	0.9893
Gum ghatti	0.871	0.9994
Gum arabic	1.034	0.9790
λ carrageenan	1.194	0.9970
ι carrageenan	1.481	0.9978
Guar	9.904	0.9715
Glycogen type II	10.030	0.9983

The BACE1 inhibition of chemically sulphated guar and glycogen type II is lower at 1 μg/ml in the FRET dose response experiments (Figure 158) than in the initial one concentration screen (Figure 157). This disparity could be due to the polydisperse nature of the polysaccharides, with one sample containing a mixture of more potent inhibitory polysaccharide.

PMH at 1.0 μg/ml inhibits ~100% of BACE1, with this effect mirrored in both ι- and λ- carrageenans tested. These saccharides have native levels of sulphation, and this may be the reason the unmodified compounds maintain BACE1 inhibition activity akin to PMH when tested in FRET experiments (Figure 159). Unmodified glycogen type II and levan gave similar results with 16% and 12% promotion of BACE1 respectively while unmodified gum arabic promoted BACE1 action in the FRET by 71%, suggesting that chemical sulphation dramatically changes the activity of this compound upon interaction with BACE1.

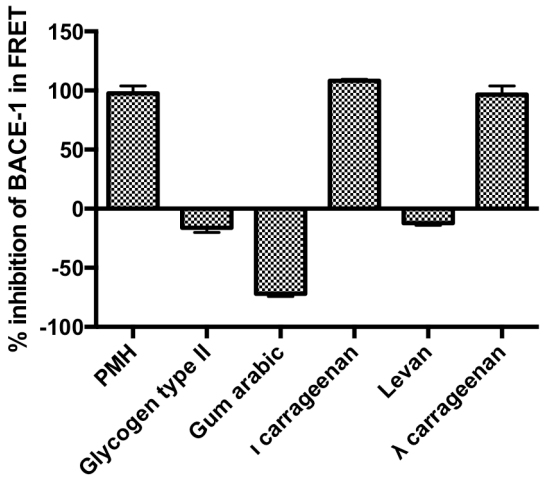

Figure 159: BACE1 FRET utilised to determine the affect of human BACE1 (FLAG-tag) detecting the cleavage of FRET peptide derived from the APP_{SW} (Mca-SEVNLDAEFRK(Dnp)RR-NH2 Fluorogenic Peptide Substrate) λ_{ex}= 320 nm λ_{em}= 405 nm, in 50 mM sodium acetate pH 4.0, over 1.5 hours. Original, unmodified compounds tested at 1.0 μg/ml.

Further investigations into the effectiveness of unmodified ι- and λ- carrageenans were completed to analyse the potency of BACE1 inhibition. Figure 160 demonstrates that while for λ-carrageenan a dose response curve was obtained with an IC_{50} of 2.347 μg/ml, no similar dose response curve could be obtained through Prism 6 software.

The position of data points, when comparing both carrageenans, show similarity but Prism 6 software has been unable to plot a curve to the non-linear regression analysis for ι-carrageenan. With the position of the data points being similar in both instances however, an IC_{50} of ~2.5 μg/ml could be extrapolated.

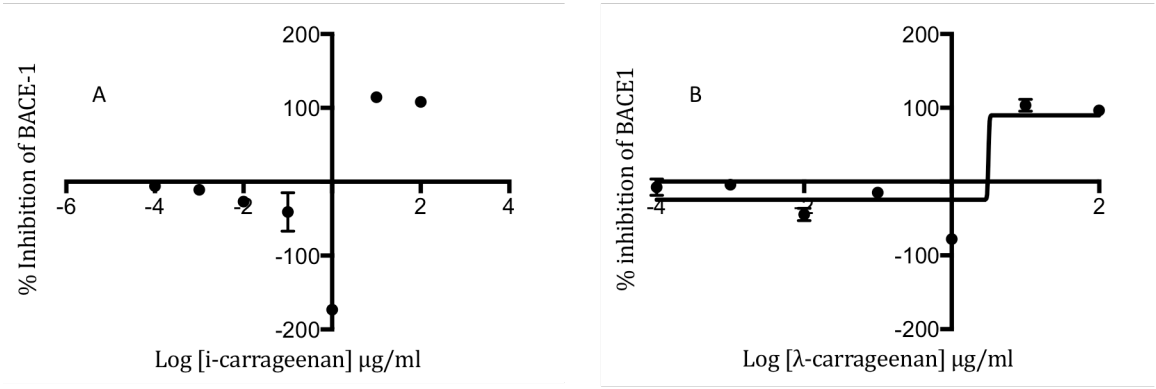

Figure 160: Dose response curve of unmodified compounds, BACE1 FRET utilised to determine the affect of human BACE1 (FLAG-tag) detecting the cleavage of FRET peptide derived from the APP_{SW} (Mca-SEVNLDAEFRK(Dnp)RR-NH2 Fluorogenic Peptide Substrate) λ_{ex}= 320 nm λ_{em}= 405 nm, in 50 mM sodium acetate pH 4.0, over 1.5 hours. A) ι-carrageenan, no dose response B) λ-carrageenan IC_{50}= 2.347 μg/ml.

8.2.6 Anti-factor Xa and IIa activity

PMH and the hit sulphated compounds were tested in colorimetric assays to determine their effectiveness at inhibiting factor Xa and factor IIa (thrombin) through the binding and promotion of anti-thrombin. Unfractionated PMH reported an IC_{50} of 13 ng/ml (R^2 0.9778) in the anti-factor Xa assay, and 19 ng/ml (R^2 0.9837) in the anti-factor IIa, representing similarly 1:1 ratio in activity in anti-factor IIa to anti-factor Xa.

Table 23: Results of colorimetric assays for anti-factor Xa and anti-factor IIa activity of unfractionated PMH along with the chemically sulphated hit polysaccharides. Results reported as IC_{50} values indicating inhibition to half maximal enzymatic activity and R^2 values.

Factor Xa			Factor IIa		
Compound	IC_{50} (µg/ml)	R^2	Compound	IC_{50} (µg/ml)	R^2
PMH	0.013	0.9778	ι carrageenan	0.008	0.9980
Levan	0.790	0.9615	PMH	0.019	0.9837
λ carrageenan	1.100	0.9354	λ carrageenan	0.075	0.9895
Guar	1.170	0.9513	Levan	0.330	0.9950
Gum ghatti	10.110	0.9141	Guar	2.500	0.9677
Gum arabic	29.700	0.7790	Gum ghatti	7.000	0.9867
Glycogen type II	730.400	0.9648	Gum arabic	10.550	0.9375
ι carrageenan	No dose response	-	Glycogen type II	100.900	0.9053

In the anti-factor Xa assay, the most potent inhibitor after PMH was sulphated levan, with an IC_{50} of 790 ng/ml (R^2 = 0.9615), ~60 fold less than PMH (Table 23). Both sulphated λ-carrageenan and guar had similar potency, with IC_{50} of 1.100 µg/ml (R^2 = 0.9354) and IC_{50} of 1.170 µg/ml (R^2 = 0.9513), 85 and 90 times less activity to anti-factor Xa than PMH respectively. As a specific pentasaccharide structural sequence is required for the binding to anti-thrombin and subsequent inhibition of factor-Xa, the sulphated structure of levan and possibly λ-carrageenan and guar may include correctly orientated functional groups to mimic the pentasaccharide including the required and rare 3-0-sulphate, or the chemically sulphated polysaccharides include sequence or structural features which promote in a different way, but achieve similar results in this *in vitro* colorimetric assay.

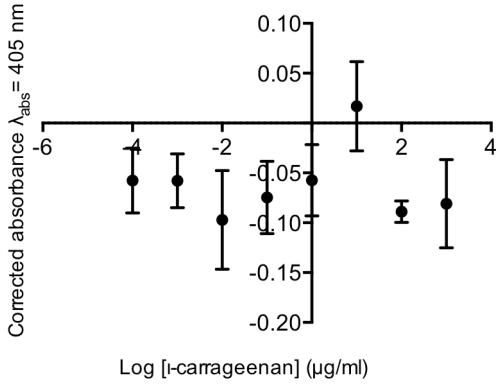

Figure 161: Dose response of chemically sulphated ι-carrageenan in anti-factor Xa inhibition assay. Promotive action of ι-carrageenan measured through anti-thrombin binding and subsequent inhibition of the serpin factor X activation. Colour change measured at λ_{abs}= 405 nm, with inhibition leading to an increase in absorbance at this wavelength.

Chemically sulphated polysaccharides gum ghatti, gum arabic, and glycogen type II have the most favourable anti-factor Xa profiles, with each reporting an IC_{50} >500 fold that of PMH. Gum arabic (IC_{50} of 29.7 μg/ml) correlation coefficient is significantly lower suggesting the IC_{50} determined from this experimental set is not as representative of the raw data, when compared to the other polysaccharides tested. ι-carrageenan shows no dose response relationship and no anti-factor Xa activity (Figure 161).

The anti-factor IIa action of PMH and hit polysaccharides is also shown in Table 23. In this activity assay, ι-carrageenan is a more potent activator of AT than that of unfractionated PMH, with IC_{50} of 8.0 ng/ml (R^2 0.9980) and 19.0 ng/ml (R^2 0.9837) respectively. This high level of activity is entirely different from the same compounds action in AT/factor Xa interactions suggesting no specific sequence simulating the heparin pentasaccharide, but the saccharide size required to mimic the >18 saccharides required for the less specific AT/thrombin promotion.

λ-carrageenan has approximately 4 times less activity than PMH in the anti-factor II assay, with IC_{50} of 75.0 ng/ml (R^2 0.9895), followed by levan with ~18 times less activity than PMH. The three chemically sulphated polysaccharides that show >300 fold reduced activity with anti-thrombin in factor II activation are gum ghatti, gum arabic and glycogen type II, with IC_{50} of 7.0 μg/ml, 10.6 μg/ml and 100.9 μg/ml respectively.

With ι-carrageenan displaying higher activity in the anti-factor IIa assay than PMH, this polysaccharide is not favourable even considering its complete inactivity in the anti-factor Xa assay. The three hit compounds displaying favourable characteristics from these specific serpin activation assays are gum ghatti, gum arabic and glycogen type II.

There is no significant correlation (Pearson correlation coefficient) between the actions of sulphated hit polysaccharides in factor Xa and factor IIa experiments and the Mw or degree of sulphation of these compounds (data not shown).

8.2.7 Sulphate level determination

Table 24: Sulphate level determination completed with hydrolysed sulphated compound, λ_{abs}= 520 nm reading. Calibration with dextran sulphate, the sulphate levels of 7 hit polysaccharides and PMH, in nmoles of sulphate per µg of compound.

Compound	SO_4^{2-} per µg compound
Glycogen type II	6.6 to 8.0 nmoles
Gum ghatti	4.6 to 6.5 nmoles
Levan	4.5 to 4.7 nmoles
ι-carrageenan	2.8 to 3.4 nmoles
PMH	2.3 to 3.0 nmoles
λ-carrageenan	2.1 to 3.2 nmoles
Gum arabic	1.7 to 2.3 nmoles
Guar	0.45 nmoles

A modified version of the assay by Terho and Hartiala (1971) was used for sulphate level determination. Barium chloride and rhodizonic acid calorimetric assay was used to determine the level of sulphation for each compound. Dextran sulphate contains approximately 17% sulphur, which equates to 2.3 sulphate groups per glycosyl residue, with the molecular weight calculated as 438.04 Da. Calibration of the assay by dextran sulphate allowed deduction of moles of sulphate per microgram of material. Unfractionated PMH has 2.3 to 3.0 nmoles of sulphate per microgram of PMH (Table 24) and was used as a control as the average sulphate level has been determined as 2.3 sulphates per disaccharide (Sarrazin et al., 2011) or 2.7 sulphate groups per disaccharide (Toida et al., 1997).

Glycogen type II is the most sulphated of the hit compounds, with between 6.6 and 8.0 nmoles of sulphate groups per microgram of polysaccharide (Table 24). The

most variation in sulphate level estimates comes from gum ghatti, which contains between 4.6 and 6.5 nmoles of sulphate per microgram of polysaccharide (Table 24). The range is quoted due to the linear range of the assay giving multiple absorbance readings applicable for conversion into moles/μg. The sulphation level of levan crosses into the broad range determined for gum ghatti, with levels estimated between 4.5 and 4.7 nmoles/μg giving a more specific value when compared with the range of 1.9 nmoles/μg in gum ghatti (Table 24).

Chemically sulphated ι-carrageenan is more highly sulphated than λ-carrageenan with both carrageenans spanning the sulphate range of PMH. ι-carrageenan has between 2.8 and 3.4 nmoles of sulphate per microgram of polysaccharide, whereas λ-carrageenan has the lower number of 2.1 to 3.2 nmoles/μg. λ-carrageenan has a wider sulphate range than that of heparin, but spans the whole sulphate level range of unfractionated PMH measured in this assay (Table 24).

Gum arabic has a reduced level of sulphation compared with PMH, with levels between 1.7 and 2.3 nmoles per microgram of polysaccharide. Chemically sulphated guar has sulphate levels of 0.45 nmoles per microgram, which is the lowest sulphation level of the hit compounds tested (Table 24).

8.2.8 Molecular weight determination

Gel permeation chromatography using two 1.6 x 70 cm columns packed with different media, sephacryl S100 and S500 matrix, was used with isocratic 250 mM ammonium chloride to separate a range of molecular weights from 1×10^3 Da to 2×10^7 Da. Molecular weight markers were used to calibrate the system, before sulphated hit compounds were tested. Number average molecular weight (Mn) is a measure of the mean molecular weight of the molecules in the polysaccharide, expressed as the sum of

weights molecules divided by the number (n) of molecules in the sample. The weight average molecular weight accounts for larger molecules containing more of the total mass compared to smaller molecules of the polysaccharide, therefore the Mw is always larger than Mn. Polydispersity index (PDI) is a measure of the spread of molecular weights in the sample illustrating the heterogeneity of polymer molecular weights. The gel permeation chromatography (GPC) peak was analysed to calculate the above values, disregarding the zero intensity regions.

Number average molecular weight was calculated as follows:

Normalised intensity I = Intensity – minimum intensity

Elution time at intensity I: ET (min)= (time (s)/sampling rate (Hz))/60

Elution volume EV (ml)= ET/flow rate (ml/min)

Fraction of column volume FCV (ml)= EV/total column volume (ml)

Mass at intensity I- Input FCV into line equation from SEC calibration (example as follows)

$$x = 10\text{^}(-(85.821\times FCV^3) + (191.93\times FCV^2) - (147.61\times FCV) + 42.862)$$

Mn= ($\Sigma\, x$)/ (Σ I)

To calculate Mw:

Weight fraction W= (x I)/($\Sigma\, x$ I)

Total mass at time point WM = W x

Mw= Σ (W x)

To calculate PDI:

PDI = Mw/ ($\Sigma\, x$ I)

The example SEC HPLC spectrum in Figure 162 has been annotated to show Mn, Mw, and peak molecular weight (Mp).

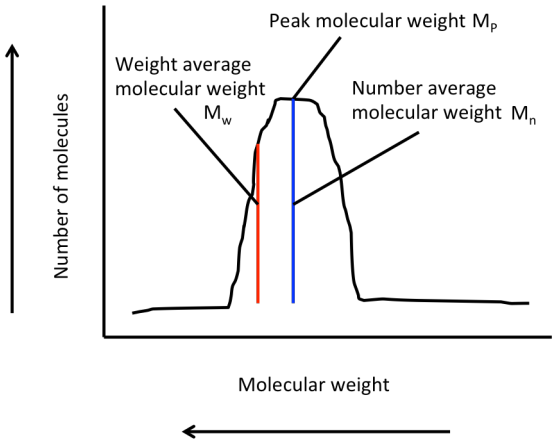

Figure 162: Schematic of a GPC chromatogram annotated to demonstrate Mw, Mn, and Mp values of a single peak elution.

Table 25 demonstrates the chemically sulphated compound with the largest molecular weight is gum arabic (4.5×10^{13} Da), followed by λ-carrageenan (1.25×10^{13} Da). These compounds also have the largest polydispersity index of the hit library tested, as expected with glycopolymers of this size. The larger the molecular weight of the polymer, the more possibilities for different size glycopolymer chains due to random chain depolmerisation. ι-carrageenan and glycogen type II have similar molecular weights of 7900 Da and 8100 Da respectively, but glycogen type II chains demonstrate a larger size range (PDI = 2.1). Average molecular weight of tinzaparin is 6500 Da, therefore ι-carrageenan is most representative of these pharmaceutically important LMWH.

Chemically sulphated gum ghatti has a larger polydispersity than chemically sulphated guar, but a molecular weight 10^4 lower than this hit compound. Whether the PDI of gum ghatti is large for the molecular weight of this glycopolymer, or the PDI for guar is low for this larger Mw is unknown. However, the large PDI of gum ghatti suggests

fractionation, without further depolmerisation, of this chemically sulphated hit compound could yield lower molecular weight glycopolymer, preferential in therapeutic development, for a BACE1 inhibitor.

Table 25: GPC results of hit sulphated polysaccharides, Cecil HPLC system and two C16/70 columns, with sephacryl S100 and S500 media. Isocratic 250 mM ammonium chloride was used to separate at 0.5 ml/min with a sampling rate of 2.63 Hz using Analogue devices AD 7194 data collection software on a Cecil CE1200 wavelength monitor at λ_{abs}= 210 nm, with a run time of 9.38 hours.

Chemically sulphated polysaccharide	Molecular weight (Mw)	Number weight (Mn)	Polydispersity Index (PDI)
ι-carrageenan	7.9E+03	7.3E+03	1.08
Glycogen type II	8.1E+03	3.9E+03	2.10
Levan	2.6E+04	1.5E+04	1.73
Gum ghatti	9.8E+07	2.1E+06	47.78
Guar	6.5E+11	2.7E+10	24.46
λ-carrageenan	1.2E+13	7.0E+10	164.97
Gum arabic	4.5E+13	1.7E+11	261.21

8.2.9 Spectroscopic analysis of sulphation

Structural analysis with H^+ nuclear magnetic resonance (NMR) and Fourier transform infra-red spectroscopy (FTIR) was employed to detect changes of the molecular structure from the original source material upon chemical sulphation.

Introduction or increase of the absorption bands related to levels of sulphate in FTIR have been identified near 1250 cm^{-1}, representing asymmetrical S=0 stretching vibration and near 820 cm^{-1} for symmetrical stretching of the C-O-S in the C-O-SO_3 group (J. K. Yan, Wang, Ma, & Wu, 2013). The associated reduction of absorption bands at 2940 cm^{-1} and 1020 cm^{-1} relating to the C-H and C-O-H respectively, are reduced due to the increasing addition of sulphate moieties (J. K. Yan et al., 2013).

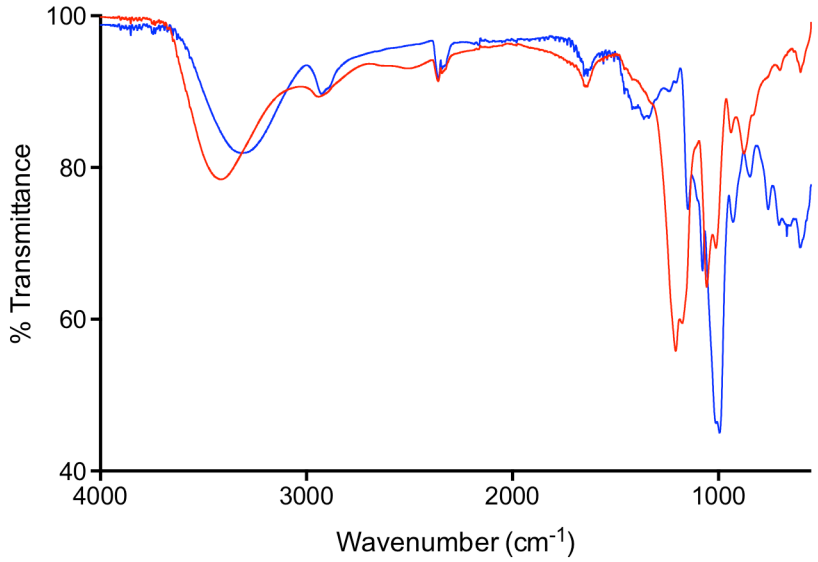

Figure 163: FTIR spectra of glycogen type II and chemically sulphated glycogen type II. Thermo Scientific Nicolet iS5 Spectrometer, analysed with OMNIC series software. Spectra from 550 cm^{-1} – 4000 cm^{-1}. Average of five independent measurements with 128 scans at a resolution of 2 cm^{-1}. (–) Chemically sulphated glycogen, (–) unmodified glycogen.

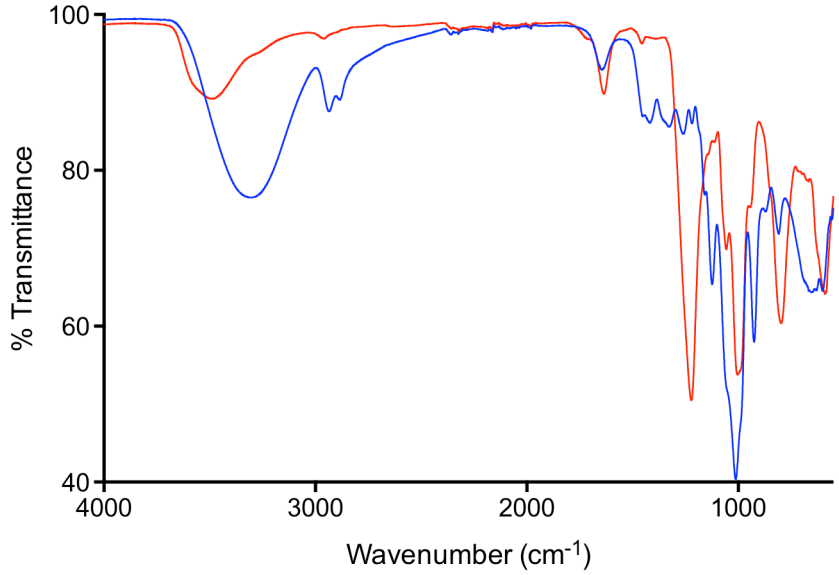

Figure 164: FTIR spectra of levan and chemically sulphated levan. Thermo Scientific Nicolet iS5 Spectrometer, analysed with OMNIC series software. Spectra from 550 cm^{-1} – 4000 cm^{-1}. Average of five independent measurements with 128 scans at a resolution of 2 cm^{-1}. (–) Chemically sulphated levan, (–) unmodified levan.

Figure 163 shows the FTIR spectra of glycogen type II, comparing absorption bands between unmodified material and chemically sulphated compound. In sulphated

glycogen, a strong absorption peak around 1250 cm^{-1} appears alongside a smaller increase in intensity near 820 cm^{-1} suggesting an increase in S=O asymmetrical stretch (1250 cm^{-1}) and C-O-S symmetrical stretching (820 cm^{-1}). Concurrent reduction in the peak intensity near 1020 cm^{-1} illustrates reduction in the C-O-H intensity and a less defined, flatter region near 2940 cm^{-1} may imply a decrease in C-H. A peak shift from unmodified glycogen at 3300 cm^{-1} to 3450 cm^{-1} seen in sulphated glycogen is also observed and could be due to a change in R-O-H. Non-hydrogen bonded hydroxyl groups absorb strongly between 3700-3584 cm^{-1}, with intermolecular hydrogen bonding occurring at lower 3550-3200 cm^{-1}, at the expense of the free hydroxyl peak.

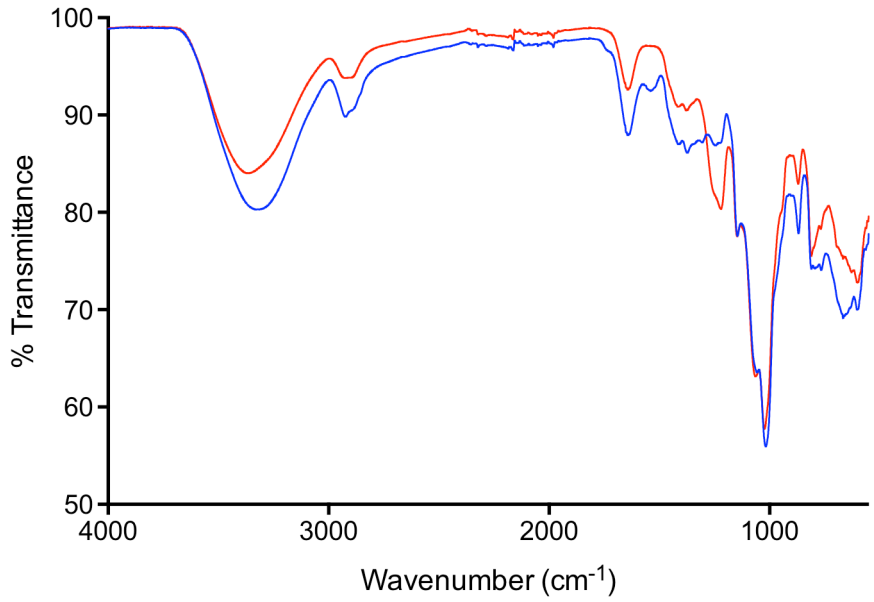

Figure 165: FTIR spectra of guar and chemically sulphated guar. Thermo Scientific Nicolet iS5 Spectrometer, analysed with OMNIC series software. Spectra from 550 cm^{-1} – 4000 cm^{-1}. Average of five independent measurements with 128 scans at a resolution of 2 cm^{-1}. (–) Chemically sulphated guar, (–) unmodified guar.

Similar spectral changes are seen in levan as shown in Figure 164. With a more pronounced reduction in peak intensities near 2940 cm^{-1} and 820 cm^{-1}. The FTIR spectra of levan contains a more pronounced change in peak wavenumber and intensity

between 3300 cm^{-1} to 3500 cm^{-1}, however the intensity is greater in unmodified levan and reduced dramatically in sulphated levan.

Sulphated guar has a peak at around 1250 cm^{-1} when compared to unmodified guar, but does not exhibit a similar change in peak structure around 820 cm^{-1} (Figure 165). Near 810 cm^{-1} and 890 cm^{-1}, both the sulphated and unmodified guar have the similar peak shapes, which Li *et al.* (2005) attribute to the two carbohydrate moieties of α-D-galactopyranosyl and β-D-mannopyranosyl units respectively (Li, He, Chen, & Ni, 2005). The hydrolysis of guar during the acidic environment of the sulphation reaction did not change the frequencies in the FTIR spectra and showed no selectivity between the pyranose units, according to Li and colleagues (*idem*).

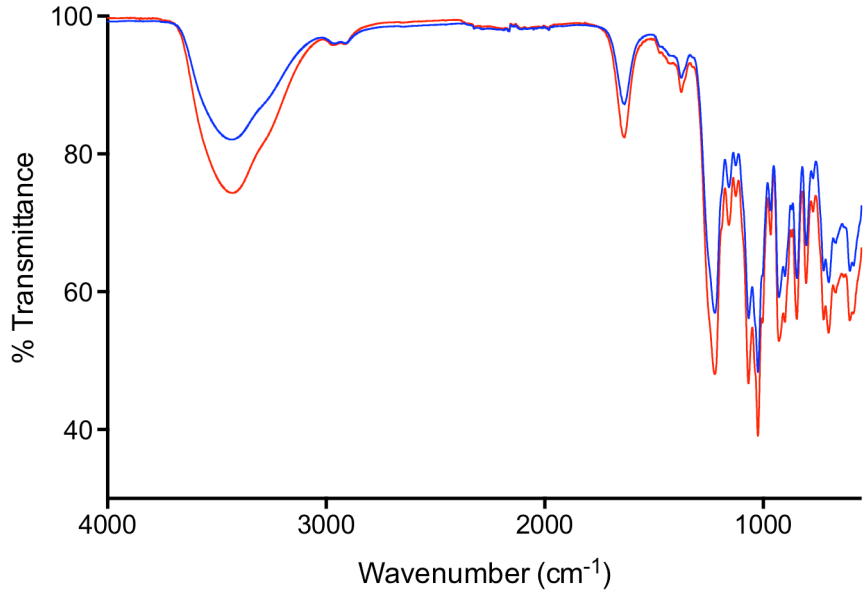

Figure 166: FTIR spectra of ι-carrageenan, and chemically sulphated ι-carrageenan. Thermo Scientific Nicolet iS5 Spectrometer, analysed with OMNIC series software. Spectra from 550 cm^{-1} – 4000 cm^{-1}. Average of five independent measurements with 128 scans at a resolution of 2 cm^{-1}. (–) Chemically sulphated ι-carrageenan, (–) unmodified ι-carrageenan.

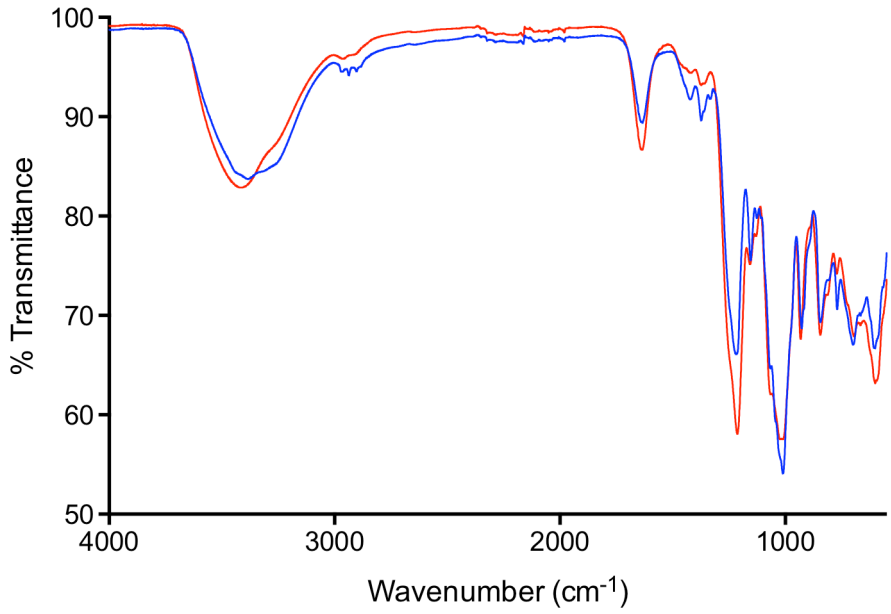

Figure 167: FTIR spectra of λ-carrageenan and chemically sulphated λ-carrageenan. Thermo Scientific Nicolet iS5 Spectrometer, analysed with OMNIC series software. Spectra from 550 cm^{-1} – 4000 cm^{-1}. Average of five independent measurements with 128 scans at a resolution of 2 cm^{-1}. (–) Chemically sulphated λ-carrageenan, (–) unmodified λ-carrageenan.

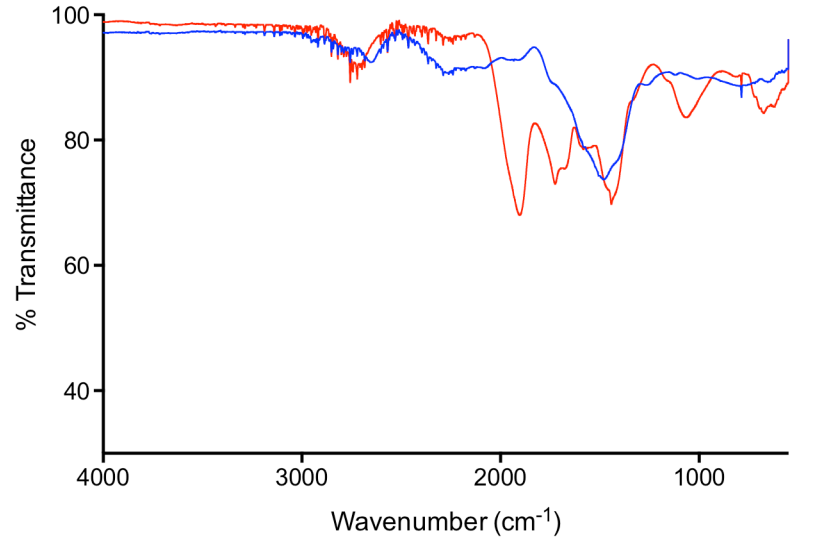

Figure 168: FTIR spectra of gum ghatti and chemically sulphated gum ghatti. Thermo Scientific Nicolet iS5 Spectrometer, analysed with OMNIC series software. Spectra from 550 cm^{-1} – 4000 cm^{-1}. Average of five independent measurements with 128 scans at a resolution of 2 cm^{-1}. (–) Chemically sulphated gum ghatti, (–) unmodified gum ghatti.

The carrageenans tested have native sulphation, shown in Figures 166 and 167 are very similar in structure between chemically modified and native compound. The intensity of peaks around 1250 cm^{-1} and 820 cm^{-1} is increased in both chemically sulphated carrageenans, but little else of the spectra is changed.

The FTIR spectra of gum ghatti and chemically sulphated gum ghatti show differences at 659 cm^{-1}, 1080 cm^{-1}, 1730 cm^{-1}, and 1920 cm^{-1} (Figure 168). These peaks appear with the chemical sulphation of the glycopolymer. The peak at 1510 cm^{-1} in unsulphated gum ghatti is shifted to a lower wavenumber (1440 cm^{-1}) with chemical sulphation, suggesting the bond seen here is still present but has been modified with the sulphation process.

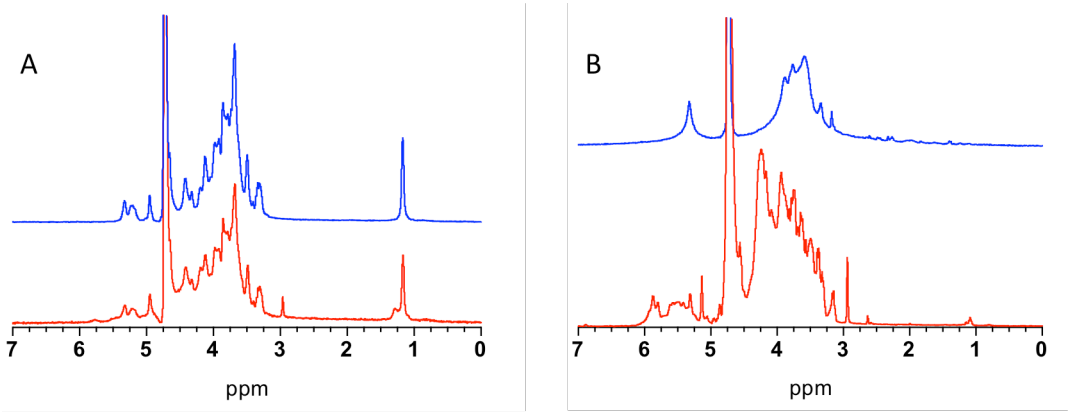

Figure 169: ^{1}H NMR spectra (400 MHz) of (–) chemically sulphated and (–) unmodified (A) gum arabic (B) glycogen type II.

A similar result is seen in the H+ NMR spectra of gum arabic, with both sulphated and unsulphated compound showing little discernable difference in structure (Figure 169A), aside from the appearance of a peak at 3 p.p.m in chemically sulphated gum arabic.

The spectra of glycogen type II is more complex post-sulphation, with the number and intensity increasing between 3 and 6 p.p.m. Introduction of a defined peak at 3 p.p.m is similar to that of gum arabic and is also seen in the spectra of sulphated levan. A wide and undefined peak increases from unmodified glycogen between 3 and 4 p.p.m, to between 3 and 4.5 p.p.m, before the defined water peak. The loss of the single post-water peak in unmodified glycogen is replaced with a peak around 5.1 p.p.m, with other peaks visible to 6 p.p.m as seen in Figure 169B.

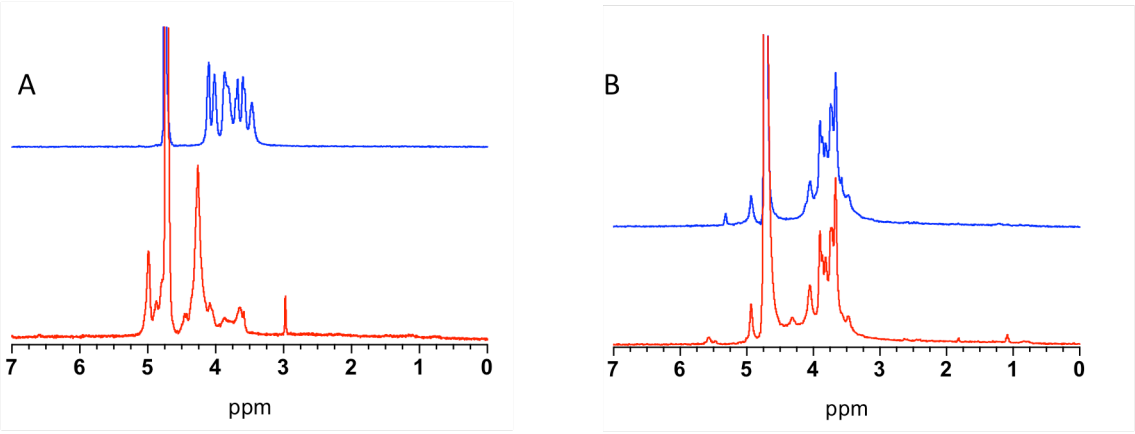

Figure 170: ^{1}H NMR spectra (400 MHz) of (–) chemically sulphated and (–) unmodified (A) levan (B) guar.

Aside from the peak seen at 3 p.p.m in the sulphated levan, structural changes from the unmodified compound are seen between 3.6 and 4.5 p.p.m. Smaller peaks seen clustered in unmodified levan in this range resolve into a defined peak at approximately 4.2 p.p.m. A less defined and a lower intensity peak is seen at at 3.7 p.p.m (Figure 170A). Levan, along with gum arabic and guar share a peak at 5 p.p.m. The 5 p.p.m peak in guar is present in both the unmodified and chemically sulphated compound to a similar degree of relative intensity. The NMR spectra for guar mirrors the FTIR spectra, with minimal changes seen upon chemical sulphation.

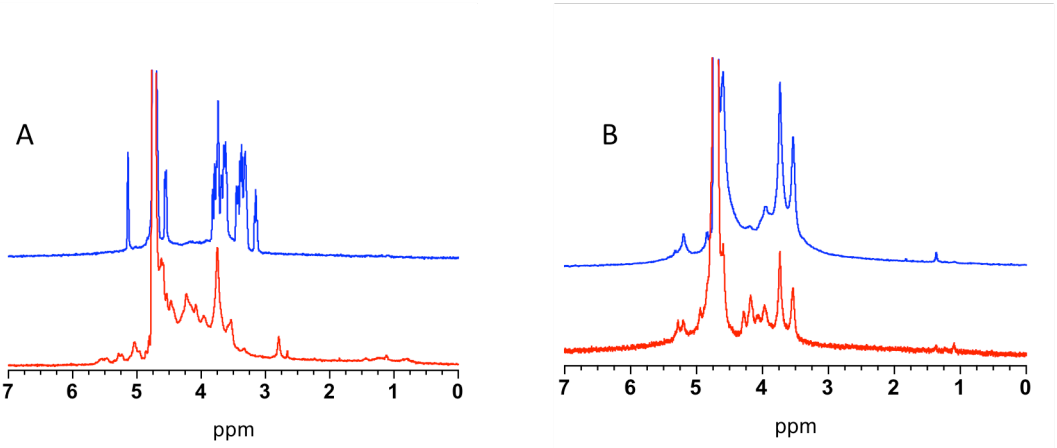

Figure 171: ^{1}H NMR spectra (400 MHz) of (–) chemically sulphated and (–) unmodified (A) λ carrageenan (B) ι carrageenan.

λ carrageenan spectra changes with chemical sulphation are shown in peak changes at 2.8 and 5.2 p.p.m, with the appearance of peaks, peak loss is seen at 3.2, 3.4 and 5.0 p.p.m. In ι carrageenan, less structural change is seen with chemical sulphation, small peaks seen between 4.0-4.3 p.p.m the only apparent change (Figure 147).

8.2.10: Interaction studies: Circular dichroism (CD) analysis of hit compounds with BACE1

The evidence of specific structural changes in BACE1 due to the binding of the chemically sulphated hit compounds was analysed with the known BACE1 binding control PMH, shown in Chapter 7. Each hit compound tested changes the structure of BACE1, when compared to BACE1 alone, and each has a similar effect to the changes seen between BACE1 and PMH.

The far-UV CD spectra of BACE1 including UF PMH causes a change in the angle of polarisation leading to an increased amplitude into the negative range between λ = 200 and λ = 250 nm, with a trough at approximately λ = 215 nm that could be attributed to increased β-sheet formation.

Table 26: Far UV-CD peak maxima to identify β-sheet structure of native BACE1. Reaction buffer 50 mM sodium acetate pH 4.0, data captured by Spectral Manager and processed with Prism 7 data analysis software.

Chemically sulphated polysaccharide	Trough maxima λ (nm)	CD (mdeg)
PMH	218	-12
Glycogen type II	218	-12
Levan	218	-14
Gum ghatti	219	-8.5
λ carrageenan	219	-7
Guar	219	-8
Gum arabic	220	-6
ι carrageenan	221	-3

A similar increase in ellipticity is displayed upon addition of each hit sulphated GAG analogue. Addition of the carbohydrate leads to an increased negative signal between λ = 215 and λ = 225 nm. Hit compounds also demonstrate spectral changes in the region lower than λ = 200 nm.

Peak wavelength position alters upon addition of the hit compounds (Table 26). As the peak amplitude in the negative region of the CD spectrum increases in wavelength, the CD intensity has exhibits an inverse trend. The amplitude of the peak reduces as the peak maxima shifts toward a higher wavelength.

High tension (HT) voltage increases in each sample tested at wavelengths lower than 200 nm suggesting a increase in detector saturation possibly due to the high concentration of BACE1 used in these experiments. The theoretical cut off for HT voltage affecting the spectra is > 500 V: no compound tested increases over 400 V.

8.2.11 Interaction studies: differential scanning fluorimetry (DSF) analysis of hit compounds with BACE1

8.2.11.1 Differential scanning fluorimetry with porcine mucosal heparin

Figure 172 is the thermal denaturation of native BACE1 with differing concentrations of UF PMH, displayed as the first derivative of the data, averages smoothed across 12 neighbours. Quantities of heparin above 12.5 μg/ml shift the stability of BACE1 to an unstable configuration with a reduced Tm, while heparin concentrations below this increase the Tm of BACE1 suggesting a stabilising effect. This change is more effectively illustrated in Figure 172, where the Tm values are displayed relative to their stability of BACE1, including the standard deviation across three readings to show accuracy and reproducibility. The change in Tm occurring between 12.5 μg/ml and 6.25 μg/ml UF PMH is 5.3 °C and spans the Tm of BACE1 alone,

suggesting a shift between these PMH concentrations from more unstable, to a more stable configuration. The lowest concentration of PMH tested affords the stability most like that of BACE1 alone, taking standard deviation of the readings into account, could be considered the same Tm.

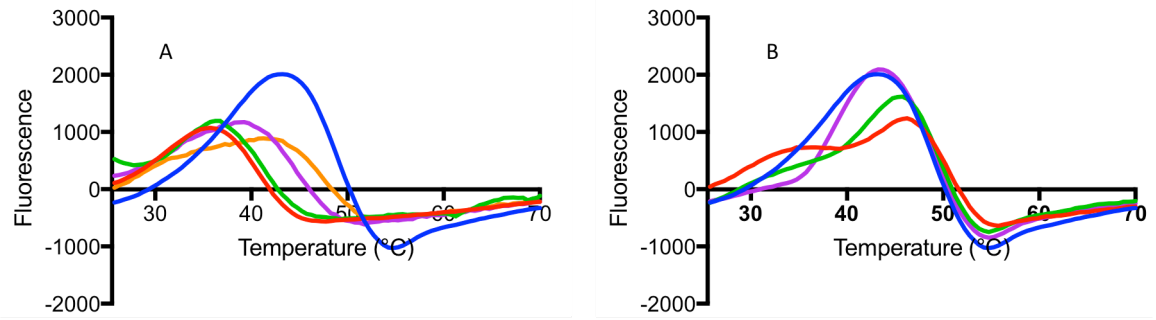

Figure 172: 1st derivative DSF of BACE1 with UF PMH in 50 mM sodium acetate buffer with 3 µM native human BACE1. **A**= (–) 3 µM native BACE1 with (–) 100 µg/ml UF PMH, (–) 50 µg/ml UF PMH, (–) 25 µg/ml UF PMH (–) 12.5 µg/ml UF PMH **B**= (–) 3 µM native BACE1 with (–) 6.25 µg/ml UF PMH (–) 3.125 µg/ml UF PMH (–) 1.56 µg/ml UF PMH.

At 100 µg/ml UF PMH into a solution containing 3.0 µM of native BACE1, the Tm of BACE1 becomes more unstable, from 43.06 °C ± 0.19 °C to a destabilised Tm of 35.53 °C ± 0.41 °C (Figures 172 and 173).

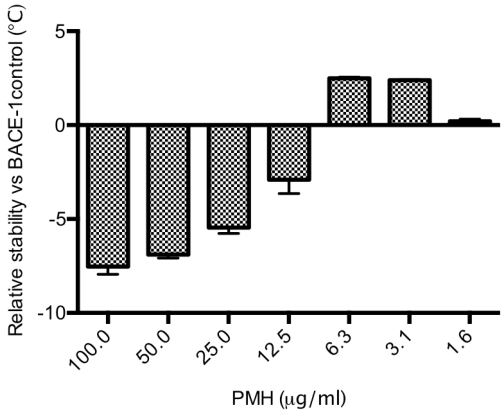

Figure 173: Change in Tm of native BACE1 with UF PMH relative to native BACE1 (alone) as expressed in DSF from the results in Figure 172 including the standard deviation of n=3 repeats. Zero value equates to BACE1 alone, no PMH added.

Analysing the relationship between PMH and BACE1 in DSF studies alongside the initial experiments into the activity relationship between PMH and BACE1 seen in

section 3.2.1, there is a relationship between the stability of BACE1 with PMH and the activity of the enzyme in FRET. When comparing the relative ratios of enzyme and PMH ligand, to negate the differences in required concentrations, the highest concentration of PMH in DSF (100 µg/ml) exhibits inhibition in the BACE1 FRET assay. The smallest shift in Tm seen with 12.5 µg/ml of PMH in DSF in the equivalent FRET assay shows the least change from the control in the BACE1 activity. When BACE1 is most unstable with PMH, PMH is most inhibitory in FRET, and when PMH has the least effect on BACE1 activity it is the most similar in stability to unchallenged BACE1.

A simple relationship between stability and effect on activity is not clear as PMH activities as a BACE1 promotor do not align with the region of more stable than normal Tm, therefore a Pearson correlation test will be conducted to determine whether a correlation is present and to what significance.

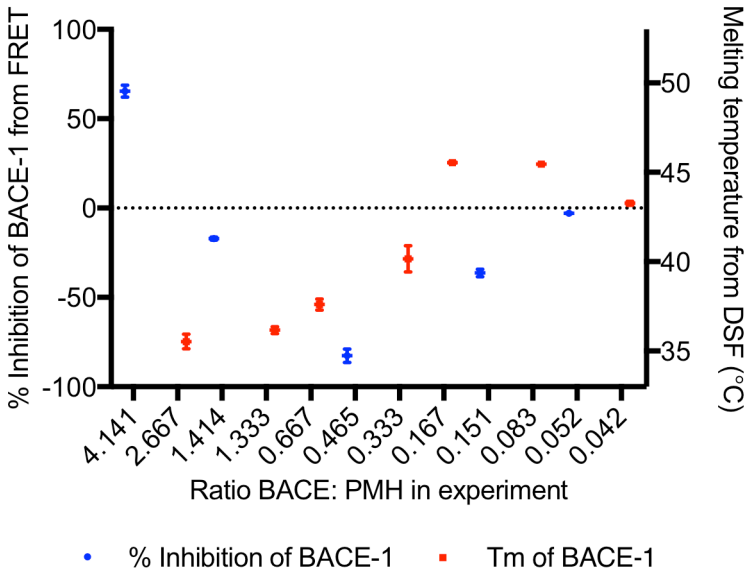

Figure 174: Combined results from DSF and FRET, showing Tm and activity of BACE1 with PMH presented as a ratio of BACE:PMH to allow for comparison between assays. Grid line on LHS showing native BACE1 activity with no PMH and on RHS the melting point of native BACE1 with no PMH. (43.06 °C).

PMH has a concentration dependant effect on BACE1 in DSF and this range was utilised in further experiments to screen the hit sulphated analogue compounds. The

unknown molarity of the hit compounds and the unidentified binding ratio of protein and compound prompted the use of the same w/v ratios as PMH (µg/ml) (Uniewicz et al., 2010).

8.2.11.2 Differential scanning fluorimetry with hit sulphated compounds

The hit sulphated carbohydrates were screened in differential scanning fluorimetry to identify the effects on BACE1 denaturation. Each compound changed BACE1 Tm in a concentration dependent manner to differing degrees. Table 27 shows the changing Tm with the addition of the hit compounds and PMH, and includes the Tm of BACE1 alone in each experiment.

Table 27: Melting temperatures of BACE1 in DSF with differing concentrations of hit compounds and PMH for comparison. Differential scanning fluorimetry in 50 mM sodium acetate buffer pH 4.0 with 3 µM native BACE1. StepOnePlus PCR machine, temperature ramping 25.5 °C - 99 °C, 0.5 °C increments, every 30 seconds, with 30 second plate read time. Sypro Orange reporter dye. Read with TAMRA filter λ_{exc}= 546 nm λ_{em}= 579 nm

Compound:	Guar	Gum ghatti	Gum arabic	ι carrageenan	Levan	Glycogen type II	λ carrageenan	PMH
Concentration (µg/ml):	T_m ± SD	T_m ± SD	T_m ± SD	T_m ± SD	T_m ± SD	T_m ± SD	T_m ± SD	T_m ± SD
100.0	44.53 ± 0.35	None	33.74 ± 0.37	None	34.61 ± 0.28	43.82 ± 0.73	None	35.53 ± 0.41
50.0	45.01 ± 0.24	None	35.53 ± 0.24	None	34.42 ± 0.19	45.55 ± 0.04	None	36.17 ± 0.19
25.0	43.72 ± 0.11	None	39.44 ± 1.07	None	35.35 ± 1.56	45.42 ± 0.23	None	37.60 ± 0.31
12.5	42.10 ± 1.56	46.12 ± 0.21	39.71 ± 0.43	34.43 ± 0.12	36.72 ± 0.12	44.59 ± 0.14	33.36 ± 0.44	40.16 ± 0.74
6.3	42.72 ± 0.56	44.33 ± 1.70	45.02 ± 0.55	37.99 ± 0.66	44.36 ± 0.80	43.85 ± 0.09	37.99 ± 0.39	45.55 ± 0.06
3.1	43.17 ± 0.20	43.63 ± 0.27	45.18 ± 0.07	45.32 ± 0.06	45.64 ± 0.02	43.16 ± 0.03	45.77 ± 0.45	45.46 ± 0.02
1.6	43.12 ± 0.12	43.17 ± 0.19	44.20 ± 0.42	44.51 ± 0.03	45.55 ± 1.93	43.25 ± 0.10	45.30 ± 0.31	43.27 ± 0.11
None	42.56 ± 0.26	42.56 ± 0.26	42.56 ± 0.26	42.56 ± 0.26	43.06 ± 0.19	43.06 ± 0.19	43.06 ± 0.19	43.06 ± 0.19

Both gum ghatti and ι carrageenan at 100, 50 and 25 µg/ml show no first derivative peak structure within the tested temperature range of 25 °C to 99 °C. This slow reduction in fluorescence from between 52-61 kFU to 45-47 kFU over the 25 °C to 99 °C cycle may suggest BACE1 has denatured at room temperature and is further aggregating over the experimental course, excluding the Sypro dye. This is shown in ι-carrageenan in DSF with BACE1 in Figure 175.

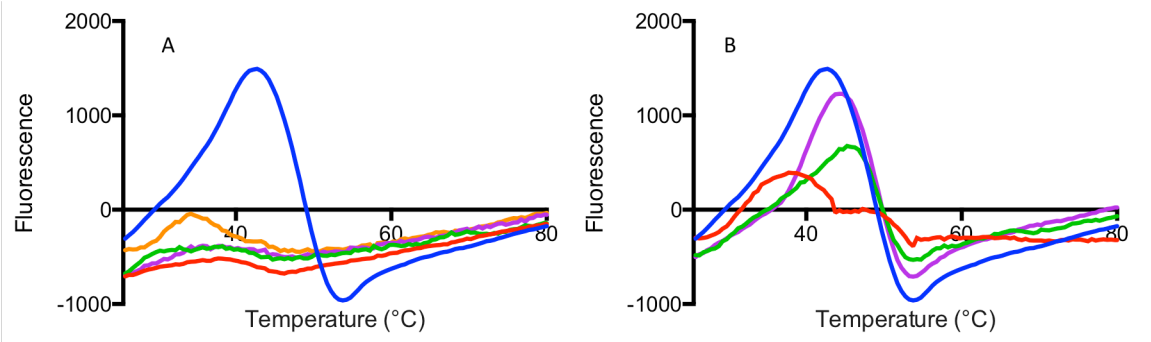

Figure 175: 1st derivative DSF of BACE1 with ι-carrageenan in 50 mM sodium acetate buffer pH 4.0 with 3 µM native human BACE1 **A**= (–) 3 µM native BACE1 with (–) 100 µg/ml ι carrageenan, (–) 50 µg/ml ι-carrageenan, (–) 25 µg/ml ι-carrageenan (–) 12.5 µg/ml ι-carrageenan **B**= (–) 3 µM native BACE1 with (–) 6.25 µg/ml ι-carrageenan (–) 3.125 µg/ml ι-carrageenan (–) 1.56 µg/ml ι-carrageenan.

ι Carrageenan at 12.5 µg/ml reduces the Tm of BACE1 to 34.43°C; approximately 1°C lower than 100 µg/ml PMH in the same experiment. The Tm increases with reducing ι carrageenan concentration, with 6.25 µg/ml Tm of 37.99°C, and subsequent lower concentrations tested giving Tm of BACE1 higher than BACE1 alone, implying a stabilising effect similar to that seen with PMH at 6.25 and 3.125 µg/ml (Table 27).

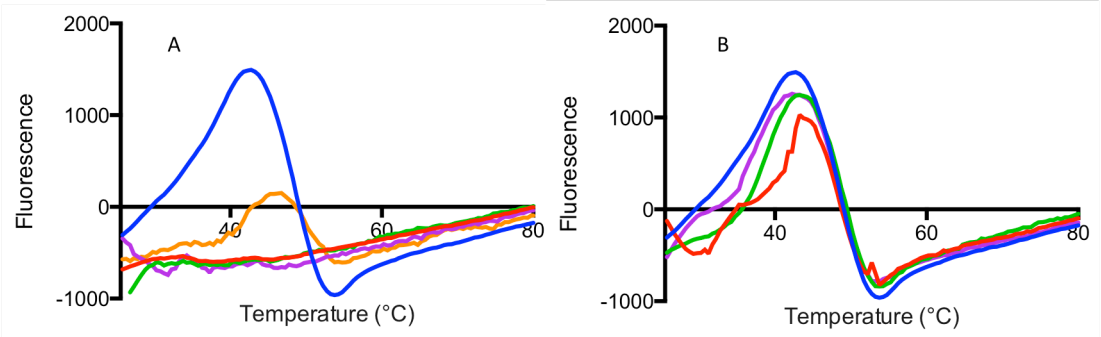

Figure 176: 1st derivative DSF of BACE1 with gum ghatti in 50 mM sodium acetate buffer pH 4.0 with 3 µM native BACE1. **A**= (–) 3 µM native BACE1 with (–) 100 µg/ml gum ghatti, (–) 50 µg/ml gum ghatti, (–) 25 µg/ml gum ghatti (–) 12.5 µg/ml gum ghatti **B**= (–) 3 µM native BACE1 with (–) 6.25 µg/ml gum ghatti (–) 3.125 µg/ml gum ghatti (–) 1.56 µg/ml gum ghatti.

Addition of gum ghatti at 12.5 µg/ml gives a Tm peak with BACE1 at a temperature higher than that of BACE1 alone, suggesting this ratio of gum ghatti to

BACE1 stabilises the enzyme structure (Figure 176). At double the concentration of gum ghatti (25 µg/ml), BACE1 shows no melt curve as mentioned above (Figure 176). The higher Tm seen may suggest a stabilising effect, which is gradually lessened upon titration of gum ghatti to the lowest concentration tested of 1.56 µg/ml, which a similar Tm of BACE1 alone (Table 27).

The melting curve of λ carrageenan has a similar structure to ι carrageenan and gum ghatti at 100, 50 and 25 µg/ml sulphated compound, but below 30°C there is greater change in the spectra (Figure 177), suggesting the room temperature denaturation prior to the experimental ramping was occurring prior to the first fluorescence reading at 25.5°C. The curve flattening post 30°C suggests aggregation and exclusion of Sypro dye (Figure 153).

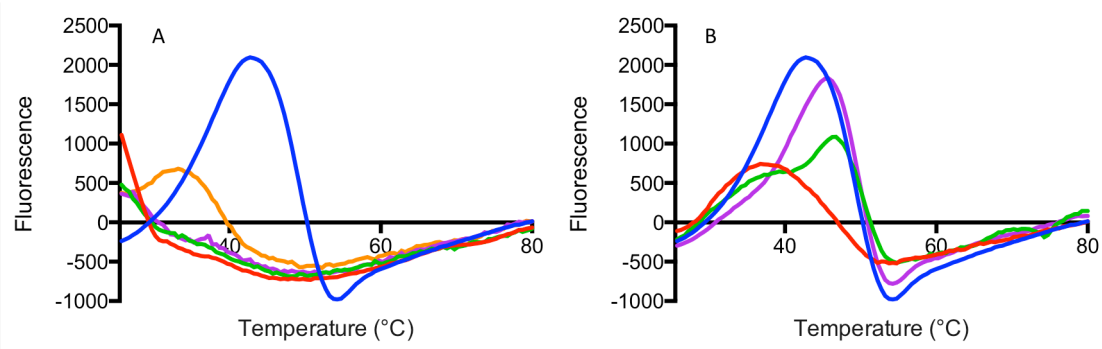

Figure 177: 1st derivative DSF of λ carrageenan in 50 mM sodium acetate buffer pH 4.0 with 3 µM native BACE1. **A**= (–) 3 µM native BACE1 with (–) 100 µg/ml λ carrageenan, (–) 50 µg/ml λ carrageenan, (–) 25 µg/ml λ carrageenan (–) 12.5 µg/ml λ carrageenan **B**= (–) 3 µM native BACE1 with (–) 6.25 µg/ml λ carrageenan (–) 3.125 µg/ml λ carrageenan (–) 1.56 µg/ml λ carrageenan.

With 12.5 and 6.3 µg/ml of λ carrageenan, BACE1 has an unstable structure with the Tm shifting from the native form at 42.5°C to 33.36°C and 37.99°C respectively. Concentrations of λ carrageenan lower than this have an increased Tm exhibiting some stabilising capabilities (Table 27).

Chemically sulphated glycogen type II and guar both have similar effects in the DSF experiments with BACE1. Guar increases BACE1 Tm at 100, 50 and 25 µg/ml concentrations, at 12.5 µg/ml and 6.25 µg/ml the Tm shifts to within the expected Tm of BACE1 alone suggesting the presence of guar at these concentration has no structural effect on the enzyme. Concentrations of guar below this have a negligible stabilising effect when compared to the unchallenged BACE1 (Table 27). Chemically sulphated Glycogen type II stabilises BACE1 at 12.5 µg/ml (Tm 44.59°C ± 0.14°C) and to a lesser extent at 6.25 µg/ml (Tm 43.85°C ± 0.09°C), but this effect is absent at the lower concentrations tested (Table 27).

The hit compounds chemically sulphated levan and gum arabic have similar effects to PMH in BACE1 DSF; both compounds destabilise BACE1 at high concentrations. Between 12.5 µg/ml and 6.3 µg/ml the Tm changes from 39.71°C ± 0.43°C to 45.02°C ± 0.55°C, a difference of 5.3°C, a greater change than PMH at the same v/w concentration (Figure 178). Sulphated levan shows a similar trend at these concentrations, with the difference between the destabilising 12.5 µg/ml to the stabilising 6.25 µg/ml 7.6°C (Table 27).

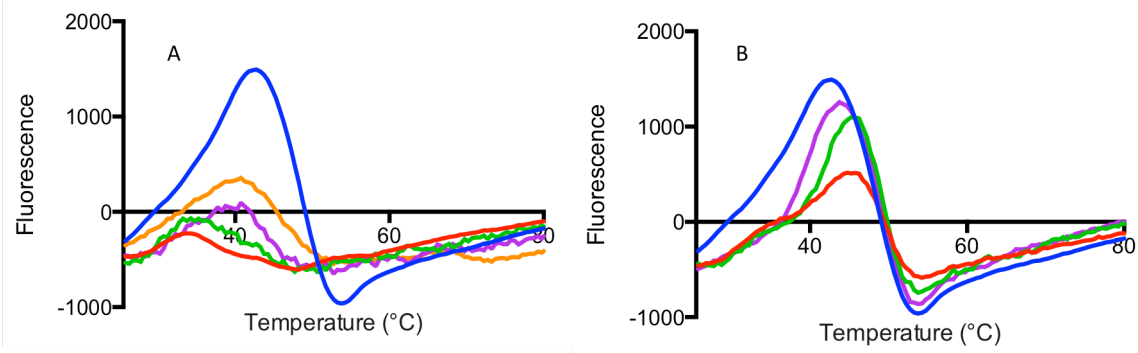

Figure 178: 1st derivative DSF data of BACE1 with gum arabic in 50 mM sodium acetate buffer pH 4.0 with 3 µM native BACE1. **A**= (–) 3 µM native BACE1 with (–) 100 µg/ml gum arabic, (–) 50 µg/ml gum arabic, (–) 25 µg/ml gum arabic (–) 12.5 µg/ml gum arabic **B**= (–) 3 µM native BACE1 with (–) 6.25 µg/ml gum arabic (–) 3.125 µg/ml gum arabic (–) 1.56 µg/ml gum arabic.

The trends associated with DSF have revealed groupings according to the effects of the hit chemically sulphated compounds on BACE1 in the thermal stability assay DSF. One group consists of guar and glycogen type II, which show the least effect on BACE1 at all concentrations tested, another group comprising of ι carrageenan and λ carrageenan have a significant effect on BACE1 structure at the higher concentrations tested, and offer a measure of stability at the lower concentrations. A group containing gum arabic and levan mimic the trend seen when PMH is used in the same w/v concentrations in the DSF experiments. The last group comprises of gum ghatti, which has a similarly destabilising effect on BACE1 at the higher concentrations tested as the carrageenans, but subsequent concentrations tested lend an immediate stabilising effect to BACE1 with 12.5 μg/ml giving a 3.5°C improvement in stability.

8.2.12 Correlation anaysis

Correlation analysis was performed to identify any relationship between the activity of chemically sulphated hit compound in BACE1 inhibition in FRET and structural and activity characteristics of the hit compounds. This was done using a 2-tailed Pearson correlation coefficient analysis (95% confidence interval) with Prism 6 software. Data were compared to the BACE1 IC_{50} to ascertain relationships between experimental results. The following Table 28 shows the correlation coefficient (r) and significance.

This data show there is no significant correlation between sulphated hit compound Mw, Mn, PDI, anti-factor Xa activity, anti-factor IIa activity, sulphate level and shift in CD peak maxima. However there is significant correlation ($P < 0.05$) between BACE1 inhibition in FRET and the effect of 100 μg/ml of hit sulphated compound on the Tm of BACE1 as measured in DSF. The +0.8645 correlation in this relationship may

show reduced potency in BACE1 inhibition is linked to a higher Tm and a more stabilising effect in DSF, with a more potent BACE1 inhibitor having a more destabilising effect on BACE1 in DSF.

Table 28: Pearson correlation matrix between the BACE1 FRET IC_{50} concentrations of the chemically sulphated heparin mimetics and the Mw, Mn, PDI, anti-factor Xa activity, anti-factor IIa activity, sulphate level, change in CD λ from 220 nm, and perturbation of Tm. Significant correlation identified between the FRET IC_{50} results and DSF change in Tm of the modified compound library.

Correlation	r	95% confidence interval	R squared	P (two-tailed)	Significant? (alpha = 0.05)	Number of XY Pairs
BACE µg/ml vs. Mw	-0.3209	-0.8650 to 0.5698	0.103	0.4828	No	7
BACE µg/ml vs. Mn	-0.2664	-0.8491 to 0.6088	0.07097	0.5636	No	7
BACE µg/ml vs. PDI	-0.3948	-0.8848 to 0.5098	0.1559	0.3807	No	7
BACE µg/ml vs. anti-factor Xa µg/ml	0.6288	-0.3732 to 0.9537	0.3954	0.1811	No	6
BACE µg/ml vs. anti-factor Iia µg/ml	0.6368	-0.2234 to 0.9394	0.4055	0.1241	No	7
BACE µg/ml vs. SO_3^{2-} nmoles/ug	0.08111	-0.7157 to 0.7862	0.006579	0.8627	No	7
BACE µg/ml vs. CD mdeg (PMH -12 mdeg)	-0.2687	-0.8498 to 0.6073	0.07218	0.5602	No	7
BACE µg/ml vs. Tm 100ug/ml (PMH 35.5)	0.8645	0.3195 to 0.9797	0.7474	0.012	Yes	7

No correlation between BACE1 inhibition and Mw of hit sulphated compound rules out the simple relationship between number of molecules and activity. The smaller Mw hit compounds such as ι-carrageenan and glycogen type II have no correlation with high potency in BACE1 inhibition due to the increased molarity only.

8.3 Discussion

8.3.1 Heparin activity with BACE1

BACE1 was inhibited by PMH and BLH, with BLH a more effective inhibitor (IC_{50} 2.554 μg/ml, R^2 = 0.9303) than PMH (IC_{50} 2.943 μg/ml, R^2 = 0.8949). Scholefield *et al.* (2003) concluded the inhibition of BACE1 with BLH had an IC_{50} of 1-2 μg/ml with a maximum inhibition level of 50-60%, however this research saw inhibition with BLH at 100% (Scholefield et al., 2003). PMH was a similarly slightly less potent inhibitor of BACE1, but also displayed BACE1 inhibition levels up to 100%. BLH at 12.5 μg/ml gave 100% inhibition, with levels of PMH greater than 12.5 μg/ml exhibiting the same potency for complete BACE1 inhibition.

At concentrations of BLH lower than 1.56 μg/ml, the fluorescence of FRET substrate exceeded that of the standard uninhibited reaction, suggesting some promotion activity. At concentrations of PMH lower than 4.1 μg/ml this promotion of fluorescence was also seen. More promotion activity was seen in BLH, with 130% increased fluorescence with 1.56 μg/ml BLH. PMH had less of a promotionary effect, as at 4.1 μg/ml the increased fluorescence is 54% over the uninhibited control.

No change in fluorescence was seen with the substrate and heparin alone, suggesting no heparin induced decoupling of the FRET pair, or changes to the FRET action with the additional ligand. This suggests the increase in fluorescence is an effect of heparin on the BACE1 enzyme directly linked to the activity in cleaving the FRET peptide.

Beckman *et al*. (2006) surmised this dual modulatory effect may be caused by the existence of a large potential GAG binding region present on the BACE1 surface, which is located near the pro-domain and loop regions (Beckman et al., 2006). The ability of pro-

BACE1 to be inhibited by low concentrations of heparin is thought to be due to the positively charged GAG binding region, which can conceivably bind heparin chains in a variety of different conformations, some at high affinity and some with lower affinity (*idem*). The concentration of the heparin in solution, therefore, effects which affinity binding can occur, with high concentrations of heparin allowing for both high and low affinity binding and low concentrations experiencing high affinity binding only. The difference in GAG orientation within this region may act to modulate BACE1 activity.

Klaver *et al*. (2010) show pro BACE1 is strongly activated by low concentrations of heparin due to the increase in positively charged binding sites on the pro domain (Klaver et al., 2010). This may suggest the BACE1 used in these experiments was rich in pro-BACE1 and therefore experienced activation at the lower concentrations of heparin tested. The level of stimulation of BACE1 activity was shown to be dependant on the overall structure and charge of heparin, with more highly sulphated heparin having more of a stimulating effect on BACE1 cleavage of the FRET peptide (Klaver et al., 2010). BLH is more highly sulphated than PMH suggesting a reason for the increased activity of this heparin source over the PMH.

The source of FLAG-BACE1 used in these FRET experiments may include a higher level of pro-BACE1 than Scholefield *et al.* (2003) using HEK293T expressed as an Fc fusion protein, possibly explaining why their results do not exhibit any heparin induced activation of BACE1. Sucessive work by Patey *et al.* (2006) used C-terminal FLAG tagged BACE1 from HEK293 from Sigma; no mention of BACE1 promotion is mentioned in this or subsequent work (Patey et al., 2006, 2008). Post-assay transfer, the FRET assay is calibrated with outcomes expected from published data.

8.3.2 Sulphated compound library screening

A total of 39 chemically sulphated polysaccharides were screened in the calibrated BACE1 FRET activity assay, with seven compounds identified exhibiting over 80% inhibition of BACE1 when tested at 1 μg/ml and acceptable yield. These compounds were chemically sulphated gum arabic, levan, ethyl cellulose, agarose, ι carrageenan, gum mastic and gellan gum, the most potent of which are chemically sulphated gum arabic and ι carrageenan. Compounds which display between 60 and 80% BACE1 inhibition at 1 μg/ml are chemically sulphated glycogen type II, λ carrageenan, propylene glycol alginate, arabic acid and welan. Compounds which exhibit BACE1 FRET inhibition of between 50 and 60% are chemically sulphated gum ghatti, guar, tara gum and pullulan. Chemically sulphated members of the polysaccharide library that show little to no effect in BACE1 FRET (<5% inhibition) are hypromellose, starch and styrax. In a similar way to BLH and PMH tested previously, activators of BACE1 were identified among the chemically sulphated library, including locust bean gum, (hydroxypropyl)methyl cellulose and paramylon.

Fluorescence level assays were completed with each compound to show no polysaccharide:FRET substrate interactions to artificially supress or improve the fluorescence reading.

The activated partial thromboplasin time (aPTT) measures the intrinsic and common pathways of coagulation. This assay has many coagulation factors involved, when compared to the simpler extrinsic pathway. This complexity engenders more binding sites for the interaction with ATIII and heparin, therefore lower concentrations of heparin have a greater effect in aPTT. This is demonstrated by the reduced EC_{50} of PMH in this assay (0.274 μg/ml). aPTT experiments demonstrated all sulphated polysaccharide library members were five fold or more less active than PMH.

Compounds that are within 10 fold the activity of PMH are chemically sulphated gellan gum, gum mastic, agarose, pullulan and psyllium seed gum. Compounds within 20 fold of the activity of PMH in aPTT are chemically sulphated welan, arabic acid, amylose, κ carrageenan, λ carrageenan and ethyl cellulose.

The prothrombin time (PT) assay measures the time for clotting through the extrinsic and common pathways initially stimulated by the production of tissue fluid from damaged cells. The EC_{50} control of PMH in the PT assay was 5.196 μg/ml; no chemically sulphated polysaccharides achieved within 5 fold the activity of heparin, however 19 polysaccharides displayed EC_{50} within 10 fold of heparin activity.

Chemically sulphated agarose has anticoagulant activity within 10 fold the activity of PMH (PT EC_{50} of 42.1 μg/ml, APTT EC_{50} of 2.344 μg/ml). The anti-coagulant activity of chemically sulphated agarose has been published by Matsuhiro *et al.* (2014) with data suggesting similar results at low concentrations of polysaccharide (Matsuhiro, Barahona, Encinas, Mansilla, & Ortiz, 2014). Matsuhiro *et al.* (2014) employed a SO_3 pyridine-complex method of sulphation differing from the method stated above by the use of formamide and sulfur trioxide pyridine complex (Vogl, Paper, & Franz, 2000) as opposed to the chlorosulphonic acid method (Matsuhiro et al., 2014). Agarose was sulphated at positions C-6 of the β-galactopyranosyl residue and C-2 of the α-3,6-anhydrogalactopyranosyl residue and partially sulfated at position C-2 of the β residue (idem). The similarity in anti-coagulation activity of chemically sulphated agarose from Matsuhiro *et al.* (2014) and this data could indicate a similar pattern of polysaccharide sulphation.

Chemically sulphated levan exhibited much higher activity in the PT assay (8.2 fold of PMH), than the aPTT assay (6000 fold less than PMH) when compared to PMH,

which may suggest a more specific interaction between particular coagulation factors and this polysaccharide.

Chemically sulphated welan displays similar activities in both PT and aPTT (PT 8.3 fold APTT 10.2 fold), which may suggest a non-specific interaction across all coagulation factors, or a more specific role in the common pathway to both aPTT and PT coagulation.

The identification of lead compounds from the BACE1 FRET activity assay (>50% inhibition) and attenuated effects in the coagulation assays are chemically sulphated gum arabic, ι carrageenan, glycogen type II, levan, λ carrageenan, gum ghatti, guar gum, tara gum, ethyl cellulose, propylene glycol alginate and arabic acid. Reasonable requirement for the yield of sulphated polysaccharide to be over 40% after chemical sulphation identifies a lead compound library including 7 polysaccharides: gum arabic, ι carrageenan, λ carrageenan, glycogen type II, levan, gum ghatti and guar gum.

Sulphated glycosaminoglycans have been evidenced to act as heparin/HS mimics in many instances. The 7 lead compounds have been investigated to varying degrees in other research as heparin/HS mimetics as outlined below. Some of this research has included toxicity screening of library members, adding favourable evidence to the hit compound as a potential therapeutic.

Heparin and HS are structural analogues of *C. trachomatis* LGV biovar attachment ligand used to attach and enter epithelium at mucosal surfaces (Stephens et al., 2000). Heparin and HS can completely inhibit the cell invasion by *C. trachomatis.* (idem). In HELA229 cells, arabic gum and sulphated glycogen can inhibit the binding and epithelial invasion by *C. trachomatis* and was attributed to both the charge and structure of the polysaccharides (Petronio et al., 1997). The similar activity of carrageenans was shown in ME180 human cervical cell line (Zaretzky, Pearcepratt, & Phillips, 1995).

Glycogen type II can inhibit rubella virus multiplication by 20% with no toxicity reported at 1 mg/ml; the method of virus replication is thought to be blocking of viral invasion (Mastromarino et al., 1997).

Carrageenans are extensively shown in the literature to inhibit viral adherence and invasion. This viral inhibition activity occurs in dengue virus (Talarico et al., 2005), HIV (Pirrone, Wigdahl, & Krebs, 2011), Herpes (Carlucci 1997), mumps virus, influenza B (Gerber, Dutcher, Adams, & Sherman, 1958), and murine CMV (Hamasuna, Eizuru, Shishime, & Minamishima, 1993).

The anti-herpes activity of carrageenans is directly related to the amount of a-D-galactose 2,6-disulphate residues present in the polysaccharide chain, suggesting a degree of structural specificity for the polysaccharide to inhibit invasion (Carlucci et al., 1997). No toxicity was seen in the λ carrageenans and the partially cyclized υ/ν carrageenan derived from red seaweed *Gigartina skottsbergii* (idem).

Heparin and HS bind lipopolysaccharide receptor protein on murine lymphocytes; this action is mimicked by λ carrageenan along with other polysaccharides (Dziarski & Gupta, 1994).

Sulphated levan from *Halomonas smyrnensis* has anti-coagulant activity in intrinsic pathway like heparin (Erginer 2016). The action in coagulation of levan is shown to proceed by thrombin inhibition, with decreasing factor Xa activity with increasing concentration. Sulphated levan was a better inhibitor of factor X than heparin (Erginer 2016). This potent anti-coaguation activity was not seen in this work, however the source of levan is different (*Zymomonas mobilis*), resulting in levan of differing chain length and could be the cause for the dissimilarity.

Chemically sulphated guar gum from *Cyamopsis tetragonolobus* has a 1,4-β-linked-D-mannopyranosyl main chain with α-D-galactopyranosyl units attached by (1 -

6) linkages (Li et al., 2005). Unsulphated guar gum had no activity in the intrinsic pathway of coagulation, but a 3.4 x 10^4 Da (DS of 0.85) fraction of sulphated guar had the high anticoagulant activity in the aPTT assay (idem).

Sulphated polysaccharides and unmodified carrageenans have activity in other heparin/HS mimicking processes. However, the lead compounds show little structural similarity within the group, suggesting the screening has not identified an easily identifiable structural requirement for BACE inhibition while limiting the anticoagulation effects of these compounds.

8.3.3 Lead compound analysis

The IC_{50} of the lead compound library splits the polysaccharides into a group of 5 chemically sulphated polysaccharides including levan, gum ghatti, gum arabic, λ-carrageenan, and ι-carrageenan with IC_{50} range of 0.8-1.5 μg/ml, exceeding the BACE1 inhibition activity seen with full length PMH and BLH. The second group has approximately 10 fold less activity and contains chemically sulphated guar and glycogen type II with IC_{50} of 9.9-10 μg/ml.

The two carrageenans selected differ as λ carrageenan has an alpha linked 2,6 disulphated subunit and β-linked 2-sulphated subunit (3 sulphates per disaccharide). ι carrageenan has alpha linked 3,6 anhydro-2-sulphated unit and β linked 3-sulphated subunit (2 sulphates per disaccharide) (Knutsen, Myslabodski, Larsen, & Usov, 1994), however in chemically sulphated carrageenan this discrete sulphate structure may not be present as every available position on the disaccharide may be sulphated. ι and κ carrageenan can self assemble into helical structures in solution, while λ carrageenan does not form a helical structure (idem). The similarities in activity of ι and λ

carrageenans in BACE-1 FRET indicate these structural differences do not differentially affect these compounds in inhibition screening.

The inhibition activity of the carrageenans follows the native (unmodified) sulphate level of the disaccharides, with λ carrageenan the most active carrageenan BACE1 inhibitior (3 sulphates per disaccharide), ι carrageenan second most active (2 sulphates per disaccharide) and κ carrageenan the least active carrageenan tested (1 sulphate per disaccharide). However, chemical sulphation of these compounds increasing the number of sulphates per disaccharide will have subsequently modified this DS number, with the sulphate level of chemically sulphated ι carrageenan (2.8 – 3.4 nmoles sulphate/μg compound) higher than that of chemically sulphated λ carrageenan (2.1 – 3.2 nmoles sulphate/μg compound).

Gum ghatti and gum arabic are both constructed of β-D galactopyranosyl units, differentially linked, with gum ghatti 1-6 linked and gum arabic 1-3 linked. Gum arabic includes 1-2 D-mannopyranosyl units in the core structure. Both compounds have a branched structure. Gum ghatti has a complex array of branching neutral sugar units including galactopyranose, arabinofuranose and arabinopyranose units (Deshmukh, Setty, Badiger, & Muralikrishna, 2012). Gum arabic side chains are 1-6 linked to the main chain and consist of 1-3 β-D galactopyranosyl units, averaging 2-5 units long. This structure is further modified with neutral sugars arabinofuranosyl, rhamnopyranosyl, glucuronopyranosyl and 4-O-methyl-β-D-glucuronopyranosyl units. Chemically sulphated gum ghatti (IC_{50} 0.871 μg/ml) is marginally more potent BACE1 inhibitor than gum arabic (IC_{50} 1.034 μg/ml).

Levan is composed of β-(2,6) linked D-fructo-furanosyl core with β-(2,1) linked D-fructo-furanosyl branches with a D-glucosyl residue at the end of the chain (R. Srikanth et al., 2015). Chemically sulphated levan has the most favourable IC_{50} in the

FRET BACE1 inhibition experiment (IC_{50} 0.822 μg/ml). Levan is the only hit compound utilising a furan disaccharide repeat unit, with gum ghatti and gum arabic also containing a furan but not as the staple repeat unit of the saccharide. The presence of this chemically sulphated furan could be involved with the increased potency of these three compounds in comparison to the pyran-based other hit polysaccharides.

Chemically sulphated guar (IC_{50} 9.904 μg/ml) and type II glycogen (IC_{50} 10.030 μg/ml) are hit compounds that give BACE1 FRET IC_{50} results ten-fold less potent than the other identified hit polysaccharides. Guar gum is constructed of β-D-mannopyranosyl residues with 1-6 linked branches of alpha-D-galactopyranosyl units on average every 2 core units (Wang, Zhao, Wang, Yao, & Zhang, 2012). Glycogen is constructed of α 1,4 linked glucose with α 1-6 glucose branching.

Unmodified (native) carrageenans have activity in BACE FRET inhibition, while naturally unsulphated parent compounds such as levan show levels of BACE1 promotion, suggesting a possible charge requirement for inhibitory activity. λ carrageenan for example has IC_{50} of 1.194 μg/ml when chemically sulphated, and an IC_{50} of 2.347 μg/ml when unmodified. The chemical sulphation has modified the compound to increase the anti-BACE1 activity. This could be caused by the increase in sulphate levels in the compound, or the depolymerisation of the compound caused by the vigorous sulphation reaction. Unmodified glycogen, gum arabic and guar promote the activity of BACE1 at 1 μg/ml, by up to 65% in the case of gum arabic. Gum ghatti and guar are insoluble at 1 mg/ml when unmodified so cannot be tested for BACE1 activity.

Hit compound sulphated levan had the most potent action in the antithrombin: factor Xa interaction (60 fold less than PMH). Erginera *et al.* (2016) showed chemically sulphated levan from *Halomonas smyrnensis* displayed activity through the intrinsic pathway of coagulation, similar to the action of heparin (Erginer et al., 2016). Sulphated

levan from *H. smyrnensis* was found to be a poor inhibitor of the extrinsic pathway, like heparin. In the investigation by Erginera *et al.,* all sulphated levans tested were shown to bind to the pentasaccharide binding site of antithrombin (Arg 47, Lys 114, Lys 125 and Arg 129), mimicking the heparin interaction (idem). Some sulphated levan derivatives also bind factor II (thrombin) via direct inhibition (Hsd 57, Asp 102 and Ser 195), unlike heparin, with the most sulphated levan (Fru*f* 1S-β(2-6)-Fru*f* 1S) also bound in a similar way to heparin at Exosite II (Arg 93, Lys 126, Lys 236 and Lys 240) (idem). Chemically sulphated levan from *Zymomonas mobilis* appears to retain the pentasaccharide binding capabilities associated with Erinera *et al.* 2016 and exhibited less potent anti-factor II activity (approximately 40 fold less potent than PMH) suggesting this compound is different in structure, Mw and/or DS than the (Fru*f* 1S-β(2-6)-Fru*f* 1S)$_9$ from Erginera et al (2016) (Muro, Rodriguez, Abate, & Sineriz, 2000).

The anticoagulation activity of the carrageenans is thought to act through more than one mechanism, with direct and indirect inhibition of thrombin and the activation of AT and heparin co-factor II (Pereira, Mulloy, & Mourao, 1999). Some fucans have been demonstrated to have anti-factor Xa activity (Church, Meade, Treanor, & Whinna, 1989), whereas others do not (Colliec et al., 1991). The action of fucoidan on heparin cofactor II and AT occurs in most cases, with action on thrombin, factor X and factor II more variable (Pereira et al., 1999). Factors that have been demonstrated to affect the anti-coagulation activity of carrageenans include core composition, molecular weight, degree of sulphation and sulphate position (Jiao, Yu, Zhang, & Ewart, 2011). High fucose, sulphate level (Nishino & Nagumo, 1992) and higher molecular weight carrageenans displayed greater anti-coagulant activity (Nishino, Aizu, & Nagumo, 1991).

ι carrageenan has been determined to have higher average sulphate level (2.8-3.4 nmoles sulphate/ug compound), and significantly smaller Mw (7.9 kDa) and PDI (1.08)

than λ carrageenan (2.1 -3.2 nmoles sulphate/ug compound). λ carrageenan is marginally active in anti-factor Xa (approximately 64 fold less potent than PMH), but shows potency in anti-factor II assay with approximatley 9 fold less potency than PMH. ι carrageenan has no dose dependent effect in anti-factor Xa, but is more potent than PMH in anti-factor II experiments. This could be due to a direct effect on factor IIa, or a improved ATIII:factor IIa interaction, not beneficial for factor Xa dependent anti-coagulation. Chemically sulphated ι carrageenan and glycogen share the same order of magnitude molecular weight, but have opposing effects in anti-factor Xa (no dose response vs IC_{50} 730 μg/ml respectivley) and anti-factor IIa (most potent anti-factor IIa vs least potent respectively) suggesting molecular weight alone does not account for anti-coagulant success.

Chemically sulphated gum ghatti, gum arabic and glycogen type II have favourable attenuated anti-factor Xa and factor-IIa activities; there is no correlation between compound size (Mw) and degree of sulphation.

There is no correlation between the activity of the hit chemically sulphated compounds in BACE1 inhibition and anti-factor Xa activity ($P = 0.18$) or anti-factor IIa activity ($P = 0.12$) as shown from a two-tailed Pearson correlation coefficient analysis. This suggests some selectivity or differing requirements rather than an 'active molecule' versus an 'inactive molecule'. A strong correlation between these anti-coagulation results and BACE1 inhibitor results would add more complexity to the search for a specifically targeting BACE1 inhibitor with no off-target activity.

The degree of sulphation of the hit compounds does not account for the potency in FRET BACE1 inhibition. Chemically sulphated glycogen has the highest measured level of sulphate (6.6-8.0 nmoles/ug compound) but is 12 times less potent than the best BACE1 inhibitor, Levan.

Chemically sulphated levan and gum ghatti are the most potent of the hit compounds in the BACE1 FRET assay, and share a similar degree of sulphation (levan 4.5-4.7 nmoles/ug compound and gum ghatti 4.6-6.5 nmoles/ug compound). Gum ghatti more broad sulphate range may be due to the wider PDI demonstrating greater variation in Mw of molecules of the compound.

The larger PDI of gum ghatti and wider range estimated for the degree of sulphation may lead to a reduction in active molecules capable of BACE1 inhibition; size fractionation to purify the chemically sulphated gum ghatti may yield a fraction with high levels of BACE1 potency, a more specific DS, and lower molecular weight, which is more suitable for advancement.

Structure of native λ carrageenan may protect the compound from depolyerisation effects caused by the strongly acidic and increased temperatures associated with the sulphation reaction. λ carrageenan retains a high molecular weight and a wide range of PDI, whereas ι carrageenan has a considerable lower molecular weight and the smallest range of PDI of the hit compounds tested. The native forms of both these carrageenans have similar molecular weights and PDI due to the similarities in origin and method of extraction.

FTIR spectra show little change upon chemical sulphation to the natively sulphated ι and λ carrageenans and to guar gum. This is corroborated by the sulphate level determination data, which identifies chemically sulphated guar to have a low sulphate level of 0.45 nmoles sulphate/μg compound. The carrageenan FTIR spectra show little change as these compounds have native sulphation. ι carrageenan sulphate peaks in FTIR have a lower % transmittance, suggesting more 'bonds' and therefore molecules at this wavenumber. Lower transmittance and therefore higher absorbance at

1250 cm^{-1} and 820 cm^{-1} suggest chemical sulphation has added to the sulphate peaks at these wavenumbers.

Appearance of sulphate peaks and the reduction of C-H and C-O-H peaks in chemically sulphated glycogen, levan, guar and gum ghatti illustrates the chemical modification of additional sulphate and quantifies the results of the barium chloride and rhodizonic acid calorimetric assay to determine sulphate levels.

It may be that FTIR is not high resolution enough to identify sulphate position, rather acting as a basic detector of modified compound, caused by the sulphation reaction and resulting structural changes.

Structural changes as a result of chemical sulphation are mirrored in H^+ NMR spectroscopy. With chemical sulphation largely leading to more complex spectra with the appearance of novel peaks. The number, chemical shift and intensity of the peaks are indicative of large structural change from the parent material, including an increase in peak number and intensity at the high chemical shift region. This suggests more H deshielding in the molecule due to the addition of electronegative sulphate groups. An average chemical shift reduction (main broad peak shifting left) suggests the addition of electronegative functional groups due to sulphation.

The greatest change seen in H^+ NMR is with chemical sulphation of glycogen type II, which was determined to have the highest sulphate level of the hit compounds in the colourmetric assay.

Gum arabic, with the quanitified sulphate level of 1.7-2.3 nmoles sulphate/μg compound exhibits much less structural change upon chemical sulphation than glycogen in ^1H NMR.

Peaks in the ^{1}H NMR of levan upon chemical sulphation are reduced, with peaks appearing at between 3.6 and 4.5 ppm, with a new defined peak at 4.2 ppm and 5 ppm; both with higher intensity. This suggests the deshielding of H^{+} due to sulphate additions. Sulphated levan sulphate levels are 4.5-4.7 nmoles/µg, whereas guar sulphate levels are 10 fold lower at 0.45 nmoles sulphate/µg compound. The H^{+} NMR spectra of these chemically sulphated compounds mirrors this, with sizeable changes in sulphate levan spectra, and minimal changes to chemical shift, and peak intensity in sulphated guar. A small peak at 5.5 ppm in sulphated guar, from a more shielded 5.3 ppm is the only clear indication of additional sulphate integration.

The average chemical shift moves downfield in both carrageenans upon chemical sulphation, but the clear peak at 5.2-5.5 ppm is reduced in λ carrageenan and the same as the parent compound in ι carrageenan.

More variation in peak location and intensity is seen in λ carrageenan than ι carrageenan; this may be due to the large molecular weight spread PDI (164.97) in this polymer, with molecular polydispersity leading to increased spectral complexity.

Far UV circular dichroism experiments with PMH and hit chemically sulphated compounds with BACE1 in 50 mM sodium acetate buffer at pH 4.0, show secondary structure changes with the addition of each polysaccharide. The buffer conditions were chosen to mirror the activity effects seen in the BACE1 FRET activity assay. The addition of PMH at the same molar ratio as the BACE1 FRET experiments causes a peak at 218 nm (-12 mdeg), which is not evident with BACE1 alone and could be representative of the increase of β sheet motif in BACE1. This additional β sheet structure could modify the structure of BACE1 active site or flap region leading to enzymic inhibition.

The change in the angle of light polarisation due to BACE1 secondary structure modification is mirrored with the addition of each chemically sulphated hit compound

suggesting a similar mode of interaction between sulphated polysaccharide and BACE1. Levan causes the greatest change in absorbance, with glycogen displaying the second highest absorbance.

Differential scanning fluorimetry of BACE1 with PMH illustrates destabilisation of BACE1 with the addition of concentrations of PMH greater than 12.5 μg/ml and a more stable configuration with a greater melting point at concentrations of PMH less than 12.5 μg/ml. This data may suggest the presence of high concentrations of PMH bind in low affinity sites or both high and low affinity sites causing inhibition of proteolysis as suggested by Beckman *et al.,* 2006 (Beckman et al., 2006). The lower concentrations of PMH binding only to high affinity sites on BACE1 could cause alternate conformational modifications which increase enzyme stability and therefore the promote BACE1 proteolysis of the APP ligand (idem).

The highest concentrations of hit polysaccharides λ carrageenan and ι carrageenan tested in DSF have a more pronounced effect than that of PMH, which indicates potein denaturation at room temperature or in the first 10 °C of experimentation. Glycogen type II and guar both show Tm increases with the highest polysaccharide concentrations tested, suggesting a stabilising effect mirroring activity and CD structural data previously described. Levan and gum arabic show a similar effect as the same concentrations of PMH in DSF, possibly indicating similar binding regions or pattern. Gum ghatti follows a similar denaturation pattern as the carrageenans at high concentrations but at 12.5 μg/ml, this sulphated polysaccharide lends stabilising activity to BACE1, increasing the Tm. This concentration may indicate a 'sweet spot' of number of binding interaction in low affinity regions, leading to a very stable form of BACE1.

Pearson correlation analysis of BACE1 activity in the FRET inhibition experiment with each chemically sulphated polysaccharide was analysed againist the other results

inclusing molecular weight of sulphated polysaccharide, coagulation effects, sulphate level and perturbation of CD spectra. The correlation between BACE1 inhibition activity in the FRET and perturbation of BACE1 melting point as measured in the DSF experiment was $P < 0.05$. This suggests a link between the binding of the sulphated polysaccharides in low and high affinity sites, depending on the concentration, modifies BACE1 structure to effect the action of BACE1 proteolysis of APP. The correlation analysis of the CD, measuring the secondary structure changes associated with sulphated polysaccharide binding, does not show the same relationship, possibly indicating a more subtle structural change than this far UV CD experiment has realised.

The conformation change associated with binding of these sulphated polysaccharides could be further investigated using other techniques such as more specialised NMR to determine changes in rotational correlation time, small angle x-ray (SAXS) or neutron scattering (SANS) experiments (Seeliger & de Groot, 2010).

The aim of this investigation was to identify sulphated polysaccharide compounds with analogous activity to PMH in the inhibition of BACE1, while lacking other PMH characteristics such as anti-coagulant activity, high charge and molecular weight.

Chemically sulphated levan is the best BACE1 inhibitor identified, has 58 times lower factor X activity and 17 times lower factor II activity. The factor X activity of sulphated levan however, is the highest of the 7 hit compounds identified in this research, therefore is not the most ideal candidate when looking only at this performance metric. Sulphate determination results suggest this polysaccharide is more highly sulphated than PMH, but has a relatively low molecular weight when compared to the other polysaccharides tested. The far UV CD spectra show BACE1 secondary structural change associated with saccharide binding is similar to that of PMH binding

and melting point when challenged with 100 μg/ml sulphated levan the most similar to the effects of PMH (34.5 °C with PMH melting point of 35.5 °C).

Chemically sulphated gum ghatti also has a BACE1 activity in the nanogram range, without detrimental anti-coagulant activity. The estimated range of sulphate level for this polysaccharide is the widest of the hit compounds tested, which may indicate varying degrees of sulphation of the saccharide chains. The molecular weight is significantly greater than levan, with a wider dispersibility index, suggesting the range of sulphate detected could be due to a wider range of molecular size. Structural changes associated with the binding of chemically sulphated gum ghatti differ in DSF, with the thermal stability suggesting a denaturation effect with the highest concentrations tested. CD data shows structurally similar changes to PMH but absorbance reduced. This hit compound has desireable characteristics for further analysis including depolymerisation and size fractionation to isolate active fragments with lower molecular weight and sulphation level, and investigation into the structural effects associated with BACE1 binding.

Chemically sulphated gum arabic has low microgram activity in BACE1 inhibition and favourable anti-coagulation activity, alied with one of the lowest charge sulphation levels. However, this compound has been identified as having the highest molecular weight of all hit compounds tested, with the greatest PDI ranges. Further work to depolymerise, separate and characterise the resulting fractions may allow for isolation of a more size and charge specific fraction, possibly emphasising a more potent BACE1 inhibitior. Structural analysis of this polysaccharide suggests similar action as PMH in DSF experiments with CD results giving a similar structural change but with reduced absorbance.

Chemically sulphated carrageenan hit compounds, λ and ι, have low microgram BACE1 inhibition values, but are potent anti-factor II inhibitors. The anti-thrombin (factor II) activity of chemically sulphated ι carrageenan is greater than PMH, but this chemically sulphated polysaccharide does not show a concentration dependant interaction with factor X. This suggests ι carrageenan may alternatively be a candidate for further investigations as a direct thrombin inhibitor, if other off-target interactions are attenuated.

Chemically sulphated guar and glycogen type II have similar BACE1 inhibition potency and have produced a similar DSF thermal stability profile. These two candidates however, do not have similar anti-coagulant profiles, molecular weight characteristics or sulphate levels. The similarity in their BACE1 activity and melt profile therefore, is not due to similarities in the molecular structure, size or charge. Chemically sulphated guar gum is the candidate with the lowest charge, while glycogen II has both the highest sulphation levels and the most attenuated factor II and X activity.

Chemically sulphated levan and gum ghatti are the two candidate hits to progress to structural analysis, production refinement, BACE1 binding characterisation, combinatorial chemistry, scalability and tractability studies. Chemically sulphated gum arabic has a favourable BACE1 inhibiton profile, but retains a large molecular weight and PDI. Production refinement, depolymerisation, fractionation, fraction re-testing and characterisation of the active fractions are the next step for this hit compound.

Chapter 9: Discussion and future direction

This study has established the heparin binding activity of an antibody, at acid pH. The three main antibody fragments Fc, Fab, and F(ab')2 demonstrated heparin binding between pH 4.0 and 5.0. To ensure the presence of heparin binding region/s of immunoglobulins, whole immunoglobulins were selected, and also demonstrated heparin binding at these pH. Antibodies raised to a range of antigen were utilised to ensure the traditional antibody-antigen binding was not occurring, masking the studied heparin-antibody interaction.

The demonstration of heparin binding on both the Fc region, consisting of only heavy chain immunoglobulin domains, and the Fab/F(ab')2 regions, constructed of both heavy and light chain domains, suggests a feature common to all of these domain regions being the cause of heparin affinity. Also, the cross species nature (human and mouse Ig used) suggests a feature present in both species immunoglobulin.

No heparin binding was seen at pH > 5.0, suggesting the acidic nature of the buffer system created the binding capacity. This could occur through the protonation of positively charged residues, creating a de novo heparin binding site/s on the immunoglobulin. Also, relatively neutral immunoglobulin pI (IgG ≈ 7.4 and IgM ≈ 6.5) suggests a level of unfolding possible at this pH. However, the antibodies do not demonstrate denaturation at this pH, as demonstrated by differential scanning flurometry and far-UV CD experiments. This may suggest the initial stages of intra-immunoglobulin domain unfolding, which would occur on each antibody and fragment tested. This initial unfolding could expose or create a de novo heparin-binding region, not accessible or constructed at physiological pH.

The use of structurally defined heparins to initially screen the immunoglobulin binding requirements isolated no disaccharide specific structural requirements (i.e preference for 2-O-desulphated or 6-O-desulphated heparin), but did suggests a

preference for macroscopic structural trends, for example, completely desulphated CMH8 had a reduced effect on the structural changes associated with heparin binding (demonstrated by UF PMH).

The chemically modified heparin used in these studies was screened for binding activity in the structural stability assay, differential scanning fluorimetry, to detect a shift in thermal denaturation due to ligand binding, and in far-UV CD spectroscopy to determine secondary structural changes associated with binding. To improve on these methods, surface plasmon resonance (Liedberg, Nylander, & Lundstrom, 1983) will quantify the strength of binding to each form of chemically modified heparin. Also, to screen a larger, more specifically structured heparin library, a glycan microarray (Heimburg-Molinaro, Song, Smith, & Cummings, 2011; Otto et al., 2011) could be used to isolate specific structural residues required for binding, if they exist.

To identify the protein sites of heparin binding, site-directed mutagenesis (Flavell, Sabo, Bandle, & Weissmann, 1974; Ho, Hunt, Horton, Pullen, & Pease, 1989) of the heparin binding site could be used. This method would insert point mutation in the gene sequence, that when expressed, may alter or remove the heparin binding site. This level of specific residue mutation allows for the determination of both the antibody region for heparin binding, and also the arrangement of amino acids, critical for the binding. This method commonly allows elucidation into the type of binding and sequence specific requirements for the interaction.

Later, CRISPR/Cas technology (Cong et al., 2013; Jinek et al., 2012) could modify the heparin binding regions *in vivo*, to determine any phenotype alterations. However, as the heparin-immunoglobulin interaction occurs under acidic conditions *in vitro*, this may not result in a modified phenotype.

The investigation into biochemical tags and the influence these peptide sequences can have on the structure of BACE1 was investigated. The branch of therapeutic discovery based on the ability of heparin to inhibit BACE1 requires the screening of highly polyanionic glycosaminoglycans. These molecules are unlike conventional small molecular inhibitors selected by pharmaceutical companies for scouting libraries in both molecular weight and charge. Glycosaminoglycans are more likely to interact with charged amino acids and with regions of positive charge in a protein, having concequences for the type of biochemical tag suitable for this BACE1 inhibitor screening. This work found the FLAG-BACE1 is most similar to the structure of native, untagged BACE1. This is not unexpected, as the molecular weight of this tag is the smallest of the three tested, but the charge of the additional DYKDDDDK motif seems to have a negligable effect on BACE1 secondary structure and thermal stability. Native BACE1 is still the gold standard choice for all BACE1 studies, however, the additional cost of this form of protein requires a suitable proxy and therefore FLAG-BACE1 is recommended.

Unfractionated heparin inhibition of BACE1 was assessed in a fluorescent resonant energy transfer (FRET) assay to determine the activity of UF BLH and PMH. Currently available literature is conflicted with regards to the action of heparin. Some groups identify heparin solely as a BACE1 inhibitor (Patey et al., 2006, 2008; Scholefield et al., 2003), while others have determined both inhibitory and promotionary activity (Beckman et al., 2006; Klaver et al., 2010). This work identified both heparin inhibition and activation of BACE1, with high concentrations of PMH/BLH > 12.5 μg/ml demonstrating BACE1 inhibition of 100 %, while concentrations < 1.56 μg/ml of BLH and <4.1 μg/ml of PMH displaying potent stimulation of BACE1 APP proteolysis.

This existence of two forms of heparin binding regions, one with high affinity, one with low affinity for heparin could explain the modulatory effect of heparin *in vitro*. High concentrations of heparin bind both the high and low affinity regions on BACE1 causing inhibiton of activity. Low concentrations of heparin bind only the high affinity regions, preferentially; therefore stimulation of BACE1 activity occurs.

This dual action may be a result of the non-physiologic system used to monitor BACE1 action *in vitro*, as the concentrations of heparan sulphate *in vivo* are unlikely to reach these proportions. However, the intricacies of this interaction cannot be measured in this FRET assay. Molecular elucidation of the BACE1- heparin/HS interaction would be required to ascertain the exact mechanism for this interplay. X-ray crystallography could establish the structure of heparin bound BACE1. The presence of multiple heparin chains bound in different regions, or a single region populated by one or more chains could be determined.

The 39 member chemically sulphated polysaccharide library was screened for BACE1 inhibiton and anti-coagulant activity, to identify selected polysaccharides for further analysis. More specific anti-coagulant activity was assessed through anti-factor Xa and IIa activity, the glycopolymer size was determined with SEC GPC, molecular charge to identify sulphate levels was completed, structural studies with BACE1 was completed using far-UV CD, DSF, NMR, and FTIR. FRET using FLAG-BACE1 was done to determine the hit compound IC_{50} and this data was processed to correlate activity to the other assayed metrics.

The reduction in Tm seen with the binding of GAGs to BACE1 occurs at high concentrations of all the GAG and GAG analogues tested. The Tm reduction from DSF correlated with the FRET IC_{50} in the hit sulphated compound library. This suggests DSF

to measure the Tm perturbation may offer an alternative to the expensive and time-consuming FRET experiments, to isolate hit compounds for BACE1 inhibition.

From the 7 chemically sulphated hit compounds forming the 'hit' library, chemically sulphated levan and gum ghatti have been determined as the two compounds to take forward to the next stage of inhibitor studies. Depolymerisation and fractionation of these two chemically sulphated glycopolymers would yield a new library of lower molecular weight compounds. Further BACE1 activity experiments will identify the active fractions of the two primary hit compounds. Structural characterisation will be possible on the smaller glycopolymers, with possible combinatorial chemistry potential in the future.

Chapter 10: References

Akerstrom, B., & Bjorck, L. (1986). A PHYSICOCHEMICAL STUDY OF PROTEIN-G, A MOLECULE WITH UNIQUE IMMUNOGLOBULIN-G-BINDING PROPERTIES. *Journal of Biological Chemistry, 261*(22), 240-247.

Akerstrom, B., Brodin, T., Reis, K., & Bjorck, L. (1985). PROTEIN-G - A POWERFUL TOOL FOR BINDING AND DETECTION OF MONOCLONAL AND POLYCLONAL ANTIBODIES. *Journal of Immunology, 135*(4), 2589-2592.

Akhouri, R. R., Bhattacharyya, A., Pattnaik, P., Malhotra, P., & Sharma, A. (2004). Structural and functional dissection of the adhesive domains of Plasmodium falciparum thrombospondin-related anonymous protein (TRAP). *Biochemical Journal, 379*, 815-822. doi:10.1042/bj20031500

Akilesh, S., Christianson, G. J., Roopenian, D. C., & Shaw, A. S. (2007). Neonatal FcR expression in bone marrow-derived cells functions to protect serum IgG from catabolism. *Journal of Immunology, 179*(7), 4580-4588.

Allen, B. L., & Rapraeger, A. C. (2003). Spatial and temporal expression of heparan sulfate in mouse development regulates FGF and FGF receptor assembly. *Journal of Cell Biology, 163*(3), 637-648. doi:10.1083/jcb.200307053

Arya, S., Chen, F., Spycher, S., Isenman, D. E., Shulman, M. J., & Painter, R. H. (1994). MAPPING OF AMINO-ACID-RESIDUES IN THE C-MU-3 DOMAIN OF MOUSE IGM IMPORTANT IN MACROMOLECULAR ASSEMBLY AND COMPLEMENT-DEPENDENT CYTOLYSIS. *Journal of Immunology, 152*(3), 1206-1212.

Ashikari, S., Habuchi, H., & Kimata, K. (1995). CHARACTERIZATION OF HEPARAN-SULFATE OLIGOSACCHARIDES THAT BIND TO HEPATOCYTE GROWTH-FACTOR. *Journal of Biological Chemistry, 270*(49), 29586-29593.

Ashikari- Hada, S., Habuchi, H., Kariya, Y., & Kimata, K. (2005). Heparin regulates vascular endothelial growth factor(165)-dependent mitogenic activity, tube formation, and its receptor phosphorylation of human endothelial cells - Comparison of the effects of heparin and modified heparins. *Journal of Biological Chemistry, 280*(36), 31508-31515. doi:10.1074/jbc.M414581200

B.C.Smith. (2011). *Fundamentals of Fourier transform infrared spectroscopy* (2nd ed.). FL, USA: CRC Press Inc.

Baba, M., Nakajima, M., Schols, D., Pauwels, R., Balzarini, J., & Declercq, E. (1988). PENTOSAN POLYSULFATE, A SULFATED OLIGOSACCHARIDE, IS A POTENT AND SELECTIVE ANTI-HIV AGENT INVITRO. *Antiviral Research, 9*(6), 335-343. doi:10.1016/0166-3542(88)90035-6

Baba, M., Snoeck, R., Pauwels, R., & Declercq, E. (1988). SULFATED POLYSACCHARIDES ARE POTENT AND SELECTIVE INHIBITORS OF VARIOUS ENVELOPED VIRUSES, INCLUDING HERPES-SIMPLEX VIRUS, CYTOMEGALO-VIRUS, VESICULAR STOMATITIS-VIRUS, AND HUMAN IMMUNODEFICIENCY VIRUS. *Antimicrobial Agents and Chemotherapy, 32*(11), 1742-1745.

Backstrom, G., Hook, M., Lindahl, U., Feingold, D. S., Malmstrom, A., Roden, L., & Jacobsson, I. (1979). Biosynthesis of heparin. Assay and properties of the microsomal uronosyl C-5 epimerase. *The Journal of biological chemistry, 254*(8), 2975-2982.

Baker, B. A., Adelman, M. D., Smith, P. A., & Osborn, J. C. (1997). Inability of the activated partial thromboplastin time to predict heparin levels - Time to reassess guidelines for heparin assays. *Archives of Internal Medicine, 157*(21), 2475-2479. doi:10.1001/archinte.157.21.2475

Ballard, C., Gauthier, S., Corbett, A., Brayne, C., Aarsland, D., & Jones, E. (2011). Alzheimer's disease. *Lancet, 377*(9770), 1019-1031. doi:10.1016/s0140-6736(10)61349-9

Bame, K. J., Danda, J., Hassall, A., & Tumova, S. (1997). A beta(1-40) prevents heparanase-catalyzed degradation of heparan sulfate glycosaminoglycans and proteoglycans in vitro - A role for heparan sulfate proteoglycan turnover in Alzheimer's disease. *Journal of Biological Chemistry, 272*(27), 17005-17011. doi:10.1074/jbc.272.27.17005

Barragan, A., Fernandez, V., Chen, Q. J., von Euler, A., Wahlgren, M., & Spillmann, D. (2000). The Duffy-binding-like domain 1 of Plasmodium falciparum erythrocyte membrane protein 1 (PfEMP1) is a heparan sulfate ligand that requires 12 mers for binding. *Blood, 95*(11), 3594-3599.

Basi, G., Frigon, N., Barbour, R., Doan, T., Gordon, G., McConlogue, L., Zeller, M. (2003). Antagonistic effects of beta-site amyloid precursor protein-cleaving enzymes 1 and 2 on beta-amyloid peptide production in cells. *Journal of Biological Chemistry, 278*(34), 31512-31520. doi:10.1074/jbc.M300169200

Basu, A., Kanda, T., Beyene, A., Saito, K., Meyer, K., & Ray, R. (2007). Sulfated homologues of heparin inhibit hepatitis C virus entry into mammalian cells. *Journal of Virology, 81*(8), 3933-3941. doi:10.1128/jvi.02622-06

Bates, S. M., & Weitz, J. I. (2005). Coagulation assays. *Circulation, 112*(4), E53-E60. doi:10.1161/circulationaha.104.478222

Beckman, M., Holsinger, R. M. D., & Small, D. H. (2006). Heparin activates beta-secretase (BACE1) of Alzheimer's disease and increases autocatalysis of the enzyme. *Biochemistry, 45*(21), 6703-6714. doi:10.1021/bi052498t

Benjannet, S., Elagoz, A., Wickham, L., Mamarbachi, M., Munzer, J. S., Basak, A., Seidah, N. G. (2001). Post-translational processing of beta-secretase (beta-amyloid-converting enzyme) and its ectodomain shedding - The pro- and transmembrane/cytosolic domains affect its cellular activity and amyloid-beta production. *Journal of Biological Chemistry, 276*(14), 10879-10887. doi:10.1074/jbc.M009899200

Berg, J. M., Tymoczko, J.L, Stryer, L. (2002). The Immunoglobulin Fold Consists of a Beta-Sandwich Framework with Hypervariable Loops *Biochemistry* (5th ed.). NY, USA: W H Freeman.

Bergamaschini, L., Rossi, E., Vergani, C., & De Simoni, M. G. (2009). Alzheimer's disease: another target for heparin therapy. *ScientificWorldJournal, 9*, 891-908. doi:10.1100/tsw.2009.100

Bernfield, M., Gotte, M., Park, P. W., Reizes, O., Fitzgerald, M. L., Lincecum, J., & Zako, M. (1999). Functions of cell surface heparan sulfate proteoglycans. *Annual Review of Biochemistry, 68*, 729-777. doi:10.1146/annurev.biochem.68.1.729

Biesert, L., Suhartono, H., Winkler, I., Meichsner, C., Helsberg, M., Hewlett, G., . Rubsamenwaigmann, H. (1988). INHIBITION OF HIV AND VIRUS-REPLICATION BY POLYSULFATED POLYXYLAN - HOE/BAY 946, A NEW ANTIVIRAL COMPOUND. *Aids, 2*(6), 449-457.

Bisio, A., Urso, E., Guerrini, M., de Wit, P., Torri, G., & Naggi, A. (2017). Structural Characterization of the Low-Molecular-Weight Heparin Dalteparin by Combining Different Analytical Strategies. *Molecules (Basel, Switzerland), 22*(7). doi:10.3390/molecules22071051

Bjorck, L., & Kronvall, G. (1984). PURIFICATION AND SOME PROPERTIES OF STREPTOCOCCAL PROTEIN-G, PROTEIN-A NOVEL IGG-BINDING REAGENT. *Journal of Immunology, 133*(2), 969-974.

Bjork, I., & Lindahl, U. (1982). MECHANISM OF THE ANTICOAGULANT ACTION OF HEPARIN. *Molecular and Cellular Biochemistry, 48*(3), 161-182. doi:10.1007/bf00421226

Blennow, K., de Leon, M. J., & Zetterberg, H. (2006). Alzheimer's disease. *Lancet, 368*(9533), 387-403. doi:10.1016/s0140-6736(06)69113-7

Block, H., Maertens, B., Spriestersbach, A., Brinker, N., Kubicek, J., Fabis, R., Schafer, F. (2009). IMMOBILIZED-METAL AFFINITY CHROMATOGRAPHY (IMAC): A REVIEW. In R. R. Burgess & M. P. Deutscher (Eds.), *Guide to Protein Purification, Second Edition* (Vol. 463, pp. 439-473).

Bloembergen, N., Purcell, E. M., & Pound, R. V. (1947). Nuclear magnetic relaxation. *Nature, 160*(4066), 475. doi:10.1038/160475a0

Boltz, M. (2011). *Evidence-Based Geriatric Nursing Protocols for Best Practice: Fourth Edition*: Springer Publishing Company.

Boneu, B., & de Moerloose, P. (2001). How and when to monitor a patient treated with low molecular weight heparin. *Seminars in Thrombosis and Hemostasis, 27*(5), 519-522. doi:10.1055/s-2001-17961

Bork, P., Holm, L., & Sander, C. (1994). THE IMMUNOGLOBULIN FOLD - STRUCTURAL CLASSIFICATION, SEQUENCE PATTERNS AND COMMON CORE. *Journal of Molecular Biology, 242*(4), 309-320. doi:10.1016/s0022-2836(84)71582-8

Born, J., Jann, K., Assmann, K. J., Lindahl, U., & Berden, J. H. (1996). N-Acetylated domains in heparan sulfates revealed by a monoclonal antibody against the Escherichia coli K5 capsular polysaccharide. Distribution of the cognate epitope in normal

human kidney and transplant kidney with chronic vascular rejection. *The Journal of biological chemistry, 271*(37), 22802-22809.

Braak, H., Braak, E., Bohl, J., & Reintjes, R. (1996). Age, neurofibrillary changes, A beta-amyloid and the onset of Alzheimer's disease. *Neuroscience Letters, 210*(2), 87-90. doi:10.1016/0304-3940(96)12668-9

Brack, C., Hirama, M., Lenhardschuller, R., & Tonegawa, S. (1978). COMPLETE IMMUNOGLOBULIN GENE IS CREATED BY SOMATIC RECOMBINATION. *Cell, 15*(1), 1-14. doi:10.1016/0092-8674(78)90078-8

Brady, S. F., Singh, S., Crouthamel, M. C., Holloway, M. K., Coburn, C. A., Garsky, V. M., Lai, M. T. (2004). Rational design and synthesis of selective BACE-1 inhibitors. *Bioorganic & Medicinal Chemistry Letters, 14*(3), 601-604. doi:10.1016/j.bmcl.2003.11.061

Brik, A., & Wong, C. H. (2003). HIV-1 protease: mechanism and drug discovery. *Organic & Biomolecular Chemistry, 1*(1), 5-14. doi:10.1039/b208248a

Brown, W. R., Newcomb, R. W., & Ishizaka, K. (1970). PROTEOLYTIC DEGRADATION OF EXOCRINE AND SERUM IMMUNOGLOBULINS. *Journal of Clinical Investigation, 49*(7), 1374-&. doi:10.1172/jci106354

Brunden, K. R., Richtercook, N. J., Chaturvedi, N., & Frederickson, R. C. A. (1993). PH-DEPENDENT BINDING OF SYNTHETIC BETA-AMYLOID PEPTIDES TO GLYCOSAMINOGLYCANS. *Journal of Neurochemistry, 61*(6), 2147-2154. doi:10.1111/j.1471-4159.1993.tb07453.x

Buddecke, E. (2009). Proteoglycans. In G. H.J (Ed.), *The Sugar Code* (1 ed., pp. 199-216). Germany: Wiley-VCH.

Burton, D. R., & Woof, J. M. (1992). HUMAN-ANTIBODY EFFECTOR FUNCTION. *Advances in immunology, 51*, 1-+. doi:10.1016/s0065-2776(08)60486-1

Caglic, D., Pungercar, J. R., Pejler, G., Turk, V., & Turk, B. (2007). Glycosaminoglycans facilitate procathepsin B activation through disruption of propeptide-mature enzyme interactions. *J Biol Chem, 282*(45), 33076-33085. doi:10.1074/jbc.M705761200

Cai, H. B., Wang, Y. S., McCarthy, D., Wen, H. J., Borchelt, D. R., Price, D. L., & Wong, P. C. (2001). BACE1 is the major beta-secretase for generation of A beta peptides by neurons. *Nature Neuroscience, 4*(3), 233-234. doi:10.1038/85064

Cai, X. D., Golde, T. E., & Younkin, S. G. (1993). RELEASE OF EXCESS AMYLOID BETA-PROTEIN FROM A MUTANT AMYLOID BETA-PROTEIN PRECURSOR. *Science, 259*(5094), 514-516. doi:10.1126/science.8424174

Capon, D. J., Chamow, S. M., Mordenti, J., Marsters, S. A., Gregory, T., Mitsuya, H., Smith, D. H. (1989). DESIGNING CD4 IMMUNOADHESINS FOR AIDS THERAPY. *Nature, 337*(6207), 525-531. doi:10.1038/337525a0

Capra, J. K. (1971). HYPERVARIABLE REGION OF HUMAN IMMUNOGLOBULIN HEAVY CHAINS. *Nature-New Biology, 230*(10), 61-&.

Carlson, J., Ekre, H. P., Helmby, H., Gysin, J., Greenwood, B. M., & Wahlgren, M. (1992). DISRUPTION OF PLASMODIUM-FALCIPARUM ERYTHROCYTE ROSETTES BY STANDARD HEPARIN AND HEPARIN DEVOID OF ANTICOAGULANT ACTIVITY. *American Journal of Tropical Medicine and Hygiene, 46*(5), 595-602.

Carlucci, M. J., Pujol, C. A., Ciancia, M., Noseda, M. D., Matulewicz, M. C., Damonte, E. B., & Cerezo, A. S. (1997). Antiherpetic and anticoagulant properties of carrageenans from the red seaweed Gigartina skottsbergii and their cyclized derivatives: Correlation between structure and biological activity. *International Journal of Biological Macromolecules, 20*(2), 97-105. doi:10.1016/s0141-8130(96)01145-2

Carter, P. J. (2011). Introduction to current and future protein therapeutics: A protein engineering perspective. *Experimental Cell Research, 317*(9), 1261-1269. doi:10.1016/j.yexcr.2011.02.013

Castillo, G. M., Ngo, C., Cummings, J., Wight, T. N., & Snow, A. D. (1997). Perlecan binds to the beta-amyloid proteins (A beta) of Alzheimer's disease, accelerates A beta fibril formation, and maintains A beta fibril stability. *Journal of Neurochemistry, 69*(6), 2452-2465.

Casu, B. (2005). Structure and Active Domains of Heparin. In R. J. L. a. C. A. H. Hari G. Garg (Ed.), *Chemistry and Biology of Heparin and Heparan Sulfate* (1 ed., pp. 1-28). USA: Elsevier.

Casu, B., & Lindahl, U. (2001). Structure and biological interactions of heparin and heparan sulfate. In D. Horton (Ed.), *Advances in Carbohydrate Chemistry and Biochemistry, Vol 57* (Vol. 57, pp. 159-206). San Diego: Elsevier Academic Press Inc.

Casu, B., Oreste, P., Torri, G., Zoppetti, G., Choay, J., Lormeau, J. C., Sinay, P. (1981). THE STRUCTURE OF HEPARIN OLIGOSACCHARIDE FRAGMENTS WITH HIGH ANTI-(FACTOR-XA) ACTIVITY CONTAINING THE MINIMAL ANTITHROMBIN-III-BINDING SEQUENCE - CHEMICAL AND C-13 NMR-STUDIES. *Biochemical Journal, 197*(3), 599-609.

Caughey, G. H. (2011). MAST CELL PROTEASES AS PROTECTIVE AND INFLAMMATORY MEDIATORS. *Mast Cell Biology: Contemporary and Emerging Topics, 716*, 212-234.

Celej, M. S., Montich, C. G., & Fidelio, G. D. (2003). Protein stability induced by ligand binding correlates with changes in protein flexibility. *Protein Science, 12*(7), 1496-1506. doi:10.1110/ps.0240003

Chang, W. P., Koelsch, G., Wong, S., Downs, D., Da, H., Weerasena, V., Tang, J. (2004). In vivo inhibition of Abeta production by memapsin 2 (beta-secretase) inhibitors. *J Neurochem, 89*(6), 1409-1416. doi:10.1111/j.1471-4159.2004.02452.x

Chen, Y. P., Maguire, T., Hileman, R. E., Fromm, J. R., Esko, J. D., Linhardt, R. J., & Marks, R. M. (1997). Dengue virus infectivity depends on envelope protein binding to

target cell heparan sulfate. *Nature Medicine, 3*(8), 866-871. doi:10.1038/nm0897-866

Chevalier, F., Angulo, J., Lucas, R., Nieto, P. M., & Martin-Lomas, M. (2002). The heparin-Ca(2+) interaction: Structure of the Ca(2+) binding site. *European Journal of Organic Chemistry*(14), 2367-2376.

Church, F. C., Meade, J. B., Treanor, R. E., & Whinna, H. C. (1989). ANTITHROMBIN ACTIVITY OF FUCOIDAN - THE INTERACTION OF FUCOIDAN WITH HEPARIN COFACTOR-II, ANTITHROMBIN-III, AND THROMBIN. *Journal of Biological Chemistry, 264*(6), 3618-3623.

Cimmperman, P., Baranauskiene, L., Jachimoviciute, S., Jachno, J., Torresan, J., Michailoviene, V., Matulis, D. (2008). A quantitative model of thermal stabilization and destabilization of proteins by ligands. *Biophysical Journal, 95*(7), 3222-3231. doi:10.1529/biophysj.108.134973

Cines, D. B., Yasothan, U., & Kirkpatrick, P. (2008). Romiplostim. *Nature Reviews Drug Discovery, 7*(11), 887-888. doi:10.1038/nrd2741

Clegg, R. M. (2009). Forster resonance energy transfer-FRET what is it, why do it, and how it's done. In T. W. J. Gadella (Ed.), *Fret and Flim Techniques* (Vol. 33, pp. 1-57). Amsterdam: Elsevier Science Bv.

Cohen, T., Gitaygoren, H., Sharon, R., Shibuya, M., Halaban, R., Levi, B. Z., & Neufeld, G. (1995). VEGF(121), A VASCULAR ENDOTHELIAL GROWTH-FACTOR (VEGF) ISOFORM LACKING HEPARIN-BINDING ABILITY, REQUIRES CELL-SURFACE HEPARAN SULFATES FOR EFFICIENT BINDING TO THE VEGF RECEPTORS OF HUMAN-MELANOMA CELLS. *Journal of Biological Chemistry, 270*(19), 11322-11326. doi:10.1074/jbc.270.19.11322

Cohlberg, J. A., Li, J., Uversky, V. N., & Fink, A. L. (2002). Heparin and other glycosaminoglycans stimulate the formation of amyloid fibrils from alpha-synuclein in vitro. *Biochemistry, 41*(5), 1502-1511. doi:10.1021/bi011711s

Cole, S. L., & Vassar, R. (2007). The basic biology of BACE1: A key therapeutic target for Alzheimer's disease. *Current Genomics, 8*(8), 509-530.

Colliec, S., Fischer, A. M., Taponbretaudiere, J., Boisson, C., Durand, P., & Jozefonvicz, J. (1991). ANTICOAGULANT PROPERTIES OF A FUCOIDAN FRACTION. *Thrombosis Research, 64*(2), 143-154. doi:10.1016/0049-3848(91)90114-c

Cong, L., Ran, F. A., Cox, D., Lin, S. L., Barretto, R., Habib, N., Zhang, F. (2013). Multiplex Genome Engineering Using CRISPR/Cas Systems. *Science, 339*(6121), 819-823. doi:10.1126/science.1231143

Congy-Jolivetab, N., Probst, A., Watier, H., & Thibaulta, G. (2007). Recombinant therapeutic monoclonal antibodies: Mechanisms of action in relation to structural and functional duality. *Critical Reviews in Oncology Hematology, 64*(3), 226-233. doi:10.1016/j.critrevonc.2007.06.013

Cook, P. W., Ashton, N. M., Karkaria, C. E., Siess, D. C., & Shipley, G. D. (1995). DIFFERENTIAL-EFFECTS OF A HEPARIN ANTAGONIST (HEXADIMETHRINE) OR CHLORATE ON AMPHIREGULIN, BASIC FIBROBLAST GROWTH-FACTOR, AND HEPARIN-BINDING EGF-LIKE GROWTH-FACTOR ACTIVITY. *Journal of Cellular Physiology, 163*(2), 418-429. doi:10.1002/jcp.1041630222

Corder, E. H., Saunders, A. M., Strittmatter, W. J., Schmechel, D. E., Gaskell, P. C., Small, G. W., . . . Pericakvance, M. A. (1993). GENE DOSE OF APOLIPOPROTEIN-E TYPE-4 ALLELE AND THE RISK OF ALZHEIMERS-DISEASE IN LATE-ONSET FAMILIES. *Science, 261*(5123), 921-923. doi:10.1126/science.8346443

Cosconati, S., Marinelli, L., Di Leva, F. S., La Pietra, V., De Simone, A., Mancini, F., Olson, A. J. (2012). Protein Flexibility in Virtual Screening: The BACE-1 Case Study. *Journal of Chemical Information and Modeling, 52*(10), 2697-2704. doi:10.1021/ci300390h

Crowther, R. A. (1991). STRAIGHT AND PAIRED HELICAL FILAMENTS IN ALZHEIMER-DISEASE HAVE A COMMON STRUCTURAL UNIT. *Proceedings of the National Academy of Sciences of the United States of America, 88*(6), 2288-2292. doi:10.1073/pnas.88.6.2288

Crowther, R. A., & Wischik, C. M. (1985). IMAGE-RECONSTRUCTION OF THE ALZHEIMER PAIRED HELICAL FILAMENT. *Embo Journal, 4*(13B), 3661-3665.

Czajkowsky, D. M., Hu, J., Shao, Z. F., & Pleass, R. J. (2012). Fc-fusion proteins: new developments and future perspectives. *Embo Molecular Medicine, 4*(10), 1015-1028. doi:10.1002/emmm.201201379

Daeron, M., Malbec, O., Latour, S., Arock, M., & Fridman, W. H. (1995). REGULATION OF HIGH-AFFINITY IGE RECEPTOR-MEDIATED MAST-CELL ACTIVATION BY MURINE LOW-AFFINITY IGG RECEPTORS. *Journal of Clinical Investigation, 95*(2), 577-585. doi:10.1172/jci117701

Damus, P. S., Hicks, M., & Rosenber.Rd. (1973). ANTICOAGULANT ACTION OF HEPARIN. *Nature, 246*(5432), 355-357. doi:10.1038/246355a0

Das, S. K., Mallet, J. M., Esnault, J., Driguez, P. A., Duchaussoy, P., Sizun, P., Sinay, P. (2001). Synthesis of conformationally locked L-iduronic acid derivatives: Direct evidence for a critical role of the skew-boat (2)S(0) conformer in the activation of antithrombin by heparin. *Chemistry-a European Journal, 7*(22), 4821-4834.

Dawes, J., & Pepper, D. S. (1979). CATABOLISM OF LOW-DOSE HEPARIN IN MAN. *Thrombosis Research, 14*(6), 845-860. doi:10.1016/0049-3848(79)90004-5

Deitcher, S. R., & Carman, T. L. (2001). Heparin-induced thrombocytopenia: natural history, diagnosis, and management. *Vascular Medicine, 6*(2), 113-119. doi:10.1177/1358836x0100600208

DeMattos, R. B., Bales, K. R., Cummins, D. J., Dodart, J. C., Paul, S. M., & Holtzman, D. M. (2001). Peripheral anti-A beta antibody alters CNS and plasma A beta clearance and decreases brain A beta burden in a mouse model of Alzheimer's disease.

Proceedings of the National Academy of Sciences of the United States of America, 98(15), 8850-8855. doi:10.1073/pnas.151261398

Deshmukh, A. S., Setty, C. M., Badiger, A. M., & Muralikrishna, K. S. (2012). Gum ghatti: A promising polysaccharide for pharmaceutical applications. *Carbohydrate Polymers, 87*(2), 980-986. doi:10.1016/j.carbpol.2011.08.099

Diakun, G. P., Edwards, H. E., Wedlock, D. J., Allen, J. C., & Phillips, G. O. (1978). RELATIONSHIP BETWEEN COUNTERION ACTIVITY-COEFFICIENTS AND ANTICOAGULANT ACTIVITY OF HEPARIN. *Macromolecules, 11*(6), 1110-1114. doi:10.1021/ma60066a009

Dickler, H. B. (1976). Lymphocyte receptors for immunoglobulin. *Advances in immunology, 24*, 167-214. doi:10.1016/s0065-2776(08)60330-2

Dikov, M. M., Reich, M. B., Dworkin, L., Thomas, J. W., & Miller, G. G. (1998). A functional fibroblast growth factor-1 immunoglobulin fusion protein. *Journal of Biological Chemistry, 273*(25), 15811-15817. doi:10.1074/jbc.273.25.15811

Dodart, J. C., Bales, K. R., Gannon, K. S., Greene, S. J., DeMattos, R. B., Mathis, C., Paul, S. M. (2002). Immunization reverses memory deficits without reducing brain A beta burden in Alzheimer's disease model. *Nature Neuroscience, 5*(5), 452-457. doi:10.1038/nn842

Doody, R. S., Thomas, R. G., Farlow, M., Iwatsubo, T., Vellas, B., Joffe, S., Solanezumab Study, G. (2014). Phase 3 Trials of Solanezumab for Mild-to-Moderate Alzheimer's Disease. *New England Journal of Medicine, 370*(4), 311-321. doi:10.1056/NEJMoa1312889

Douaiher, J., Succar, J., Lancerotto, L., Gurish, M. F., Orgill, D. P., Hamilton, M. J., Stevens, R. L. (2014). Development of Mast Cells and Importance of Their Tryptase and Chymase Serine Proteases in Inflammation and Wound Healing. In F. W. Alt (Ed.), *Advances in Immunology, Vol 122* (Vol. 122, pp. 211-252). San Diego: Elsevier Academic Press Inc.

Drechsel, D. N., Hyman, A. A., Cobb, M. H., & Kirschner, M. W. (1992). MODULATION OF THE DYNAMIC INSTABILITY OF TUBULIN ASSEMBLY BY THE MICROTUBULE-ASSOCIATED PROTEIN TAU. *Molecular Biology of the Cell, 3*(10), 1141-1154.

Duncan, A. R., & Winter, G. (1988). THE BINDING-SITE FOR CLQ ON IGG. *Nature, 332*(6166), 738-740. doi:10.1038/332738a0

Dziarski, R., & Gupta, D. (1994). HEPARIN, SULFATED HEPARINOIDS, AND LIPOTEICHOIC ACIDS BIND TO THE 70-KDA PEPTIDOGLYCAN LIPOPOLYSACCHARIDE RECEPTOR PROTEIN ON LYMPHOCYTES. *Journal of Biological Chemistry, 269*(3), 2100-2110.

Economides, A. N., Carpenter, L. R., Rudge, J. S., Wong, V., Koehler-Stec, E. M., Hartnett, C., . . . Stahl, N. (2003). Cytokine traps: multi-component, high-affinity blockers of cytokine action. *Nature Medicine, 9*(1), 47-52. doi:10.1038/nm811

Edbauer, D., Winkler, E., Regula, J. T., Pesold, B., Steiner, H., & Haass, C. (2003). Reconstitution of gamma-secretase activity. *Nature Cell Biology, 5*(5), 486-488. doi:10.1038/ncb960

Eggert, S., Paliga, K., Soba, P., Evin, G., Masters, C. L., Weidemann, A., & Beyreuther, K. (2004). The proteolytic processing of the amyloid precursor protein gene family members APLP-1 and APLP-2 involves alpha-, beta-, gamma-, and epsilon-like cleavages - Modulation of APLP-1 processing by N-glycosylation. *Journal of Biological Chemistry, 279*(18), 18146-18156. doi:10.1074/jbc.M311601200

Egleton, R. D., & Davis, T. P. (1997). Bioavailability and transport of peptides and peptide drugs into the brain. *Peptides, 18*(9), 1431-1439. doi:10.1016/s0196-9781(97)00242-8

Ehehalt, R., Keller, P., Haass, C., Thiele, C., & Simons, K. (2003). Amyloidogenic processing of the Alzheimer beta-amyloid precursor protein depends on lipid rafts. *Journal of Cell Biology, 160*(1), 113-123. doi:10.1083/jcb.200207113

Ehehalt, R., Michel, B., Tonelli, D. D., Zacchetti, D., Simons, K., & Keller, P. (2002). Splice variants of the beta-site APP-cleaving enzyme BACE1 in human brain and pancreas. *Biochemical and Biophysical Research Communications, 293*(1), 30-37. doi:10.1016/s0006-291x(02)00169-9

Ejima, D., Tsumoto, K., Fukada, H., Yumioka, R., Nagase, K., Arakawa, T., & Philo, J. S. (2007). Effects of acid exposure on the conformation, stability, and aggregation of monoclonal antibodies. *Proteins-Structure Function and Bioinformatics, 66*(4), 954-962. doi:10.1002/prot.21243

Erginer, M., Akcay, A., Coskunkan, B., Morova, T., Rende, D., Bucak, S., Oner, E. T. (2016). Sulfated levan from Halomonas smyrnensis as a bioactive, heparin-mimetic glycan for cardiac tissue engineering applications. *Carbohydrate Polymers, 149*, 289-296. doi:10.1016/j.carbpol.2016.04.092

Esko JD, K. K., Lindahl U. (2009). Essentials of Glycobiology. In C. R. Varki A, Esko JD, Freeze HH, Stanley P, Bertozzi CR, Hart GW, Etzler ME (Ed.), (2nd edition ed.). NY: Cold Spring Harbor Laboratory Press.

Esko, J. D., & Lindahl, U. (2001). Molecular diversity of heparan sulfate. *Journal of Clinical Investigation, 108*(2), 169-173. doi:10.1172/jci13530

Evan, G. I., Lewis, G. K., Ramsay, G., & Bishop, J. M. (1985). ISOLATION OF MONOCLONAL-ANTIBODIES SPECIFIC FOR HUMAN C-MYC PROTO-ONCOGENE PRODUCT. *Molecular and Cellular Biology, 5*(12), 3610-3616.

Ey, P. L., Prowse, S. J., & Jenkin, C. R. (1978). ISOLATION OF PURE IGG1, IGG2A AND IGG2B IMMUNOGLOBULINS FROM MOUSE SERUM USING PROTEIN A-SEPHAROSE. *Immunochemistry, 15*(7), 429-436. doi:10.1016/0161-5890(78)90070-6

Faghihi, M. A., Modarresi, F., Khalil, A. M., Wood, D. E., Sahagan, B. G., Morgan, T. E., Wahlestedt, C. (2008). Expression of a noncoding RNA is elevated in Alzheimer's

disease and drives rapid feed-forward regulation of beta-secretase. *Nature Medicine, 14*(7), 723-730. doi:10.1038/nm1784

Ferro, D. R., Provasoli, A., Ragazzi, M., Torri, G., Casu, B., Gatti, G., Choay, J. (1986). EVIDENCE FOR CONFORMATIONAL EQUILIBRIUM OF THE SULFATED L-IDURONATE RESIDUE IN HEPARIN AND IN SYNTHETIC HEPARIN MONOSACCHARIDES AND OLIGOSACCHARIDES - NMR AND FORCE-FIELD STUDIES. *Journal of the American Chemical Society, 108*(21), 6773-6778. doi:10.1021/ja00281a052

Filmus, J., & Selleck, S. B. (2001). Glypicans: proteoglycans with a surprise. *Journal of Clinical Investigation, 108*(4), 497-501. doi:10.1172/jci13712

Flanagan, M. L., Arias, R. S., Hu, P., Khawli, L. A., & Epstein, A. L. (2007). Soluble Fc Fusion Proteins for Biomedical Research. In M. Albitar (Ed.), *Monoclonal Antibodies: Methods and Protocols* (pp. 33-52). Totowa, NJ: Humana Press.

Flavell, R. A., Sabo, D. L., Bandle, E. F., & Weissmann, C. (1974). SITE-DIRECTED MUTAGENESIS - GENERATION OF AN EXTRACISTRONIC MUTATION IN BACTERIOPHAGE Q-BETA-RNA. *Journal of Molecular Biology, 89*(2), 255-+. doi:10.1016/0022-2836(74)90517-8

Forster, T. (1959). 10TH SPIERS MEMORIAL LECTURE - TRANSFER MECHANISMS OF ELECTRONIC EXCITATION. *Discussions of the Faraday Society*(27), 7-17.

Friand, V., Haddad, O., Papy-Garcia, D., Hlawaty, H., Vassy, R., Hamma-Kourbali, Y., Charnaux, N. (2009). Glycosaminoglycan mimetics inhibit SDF-1/CXCL12-mediated migration and invasion of human hepatoma cells. *Glycobiology, 19*(12), 1511-1524. doi:10.1093/glycob/cwp130

Frizelle, S., Schwarz, J., Huber, S. A., & Leslie, K. (1992). EVALUATION OF THE EFFECTS OF LOW-MOLECULAR-WEIGHT HEPARIN ON INFLAMMATION AND COLLAGEN DEPOSITION IN CHRONIC COXSACKIEVIRUS B3-INDUCED MYOCARDITIS IN A/J MICE. *American Journal of Pathology, 141*(1), 203-209.

Fu, H. J., Liu, B., Frost, J. L., & Lemere, C. A. (2010). Amyloid-beta Immunotherapy for Alzheimer's Disease. *Cns & Neurological Disorders-Drug Targets, 9*(2), 197-206.

Fukumoto, H., Cheung, B. S., Hyman, B. T., & Irizarry, M. C. (2002). beta-secretase protein and activity are increased in the neocortex in Alzheimer disease. *Archives of Neurology, 59*(9), 1381-1389. doi:10.1001/archneur.59.9.1381

Gallagher, J. T., & Walker, A. (1985). MOLECULAR DISTINCTIONS BETWEEN HEPARAN-SULFATE AND HEPARIN - ANALYSIS OF SULFATION PATTERNS INDICATES THAT HEPARAN-SULFATE AND HEPARIN ARE SEPARATE FAMILIES OF N-SULFATED POLYSACCHARIDES. *Biochemical Journal, 230*(3), 665-674.

Garcia-Filipe, S., Barbier-Chassefiere, V., Alexakis, C., Huetl, E., Ledoux, D., Kerros, M. E., Kern, P. (2007). RGTA OTR4120, a heparan sulfate mimetic, is a possible long-term active agent to heal burned skin. *Journal of Biomedical Materials Research Part A, 80A*(1), 75-84. doi:10.1002/jbm.a.30874

Garratt, A. N., Britsch, S., & Birchmeier, C. (2000). Neuregulin, a factor with many functions in the life of a Schwann cell. *Bioessays, 22*(11), 987-996. doi:10.1002/1521-1878(200011)22:11<987::aid-bies5>3.0.co;2-5

Geerts, W. H., Bergqvist, D., Pineo, G. F., Heit, J. A., Samama, C. M., Lassen, M. R., & Colwell, C. W. (2008). Prevention of venous thromboembolism. *Chest, 133*(6), 381S-453S. doi:10.1378/chest.08-0656

Gerber, P., Dutcher, J. D., Adams, E. V., & Sherman, J. H. (1958). PROTECTIVE EFFECT OF SEAWEED EXTRACTS FOR CHICKEN EMBRYOS INFECTED WITH INFLUENZA-B OR MUMPS VIRUS. *Proceedings of the Society for Experimental Biology and Medicine, 99*(3), 590-593.

Germi, R., Crance, J. M., Garin, D., Guimet, J., Lortat-Jacob, H., Ruigrok, R. W. H., Drouet, E. (2002). Heparan sulfate-mediated binding of infectious dengue virus type 2 and yellow fever virus. *Virology, 292*(1), 162-168. doi:10.1006/viro.2001.1232

Ghetie, V., & Ward, E. S. (2000). Multiple roles for the major histocompatibility complex class I-related receptor FcRn. *Annual Review of Immunology, 18*, 739-766. doi:10.1146/annurev.immunol.18.1.739

Ghezzi, S., Cooper, L., Rubio, A., Pagani, I., Capobianchi, M. R., Ippolito, G., Vicenzi, E. (2017). Heparin prevents Zika virus induced-cytopathic effects in human neural progenitor cells. *Antiviral Research, 140*, 13-17. doi:10.1016/j.antiviral.2016.12.023

Ghosh, A. K., Kumaragurubaran, N., & Tang, J. (2005). Recent developments of structure based beta-secretase inhibitors for Alzheimer's disease. *Current Topics in Medicinal Chemistry, 5*(16), 1609-1622. doi:10.2174/156802605775009711

Ghosh, A. K., Kumaragurubarana, N., Hong, L., Kulkarni, S., Xu, X. M., Miller, H. B., Tang, J. (2008). Potent memapsin 2 (beta-secretase) inhibitors: Design, synthesis, protein-ligand X-ray structure, and in vivo evaluation. *Bioorganic & Medicinal Chemistry Letters, 18*(3), 1031-1036. doi:10.1016/j.bmcl.2007.12.028

Ghosh, A. K., Rao, K. V., Yadav, N. D., Anderson, D. D., Gavande, N., Huang, X. P., Tang, J. (2012). Structure-Based Design of Highly Selective beta-Secretase Inhibitors: Synthesis, Biological Evaluation, and Protein-Ligand X-ray Crystal Structure. *Journal of Medicinal Chemistry, 55*(21), 9195-9207. doi:10.1021/jm3008823

Ghosh, A. K., Reddy, B. S., Yen, Y. C., Cardenas, E. L., Rao, K. V., Downs, D., Mesecarabc, A. D. (2016). Design of potent and highly selective inhibitors for human beta-secretase 2 (memapsin 1), a target for type 2 diabetes. *Chemical Science, 7*(5), 3117-3122. doi:10.1039/c5sc03718b

Ghosh, A. K., Shin, D. W., Downs, D., Koelsch, G., Lin, X. L., Ermolieff, J., & Tang, J. (2000). Design of potent inhibitors for human brain memapsin 2 (beta-secretase). *Journal of the American Chemical Society, 122*(14), 3522-3523. doi:10.1021/ja000300g

Goedert, M., Spillantini, M. G., Jakes, R., Rutherford, D., & Crowther, R. A. (1989). MULTIPLE ISOFORMS OF HUMAN MICROTUBULE-ASSOCIATED PROTEIN-TAU -

SEQUENCES AND LOCALIZATION IN NEUROFIBRILLARY TANGLES OF ALZHEIMERS-DISEASE. *Neuron, 3*(4), 519-526. doi:10.1016/0896-6273(89)90210-9

Goldsby.R.A, K., .T.J and Osborne.B.A. (2000). Immunoglobulins *Kuby Immunology* (4th ed., pp. 83-113). USA: W.H.Freeman and Co.

Gollub, S., & Ulin, A. W. (1962). HEPARIN-INDUCED THROMBOCYTOPENIA IN MAN. *Journal of Laboratory and Clinical Medicine, 59*(3), 430-&.

Gonzalez-Iglesias, R., Pajares, M. A., Ocal, C., Espinosa, J. C., Oesch, B., & Gasset, M. (2002). Prion protein interaction with glycosaminoglycan occurs with the formation of oligomeric complexes stabilized by Cu(II) bridges. *Journal of Molecular Biology, 319*(2), 527-540. doi:10.1016/s0022-2836(02)00341-8

Gorfe, A. A., & Caflisch, A. (2005). Functional plasticity in the substrate binding site of beta-secretase. *Structure, 13*(10), 1487-1498. doi:10.1016/j.str.2005.06.015

Gray, E., Mulloy, B., & Barrowcliffel, T. W. (2008). Heparin and low-molecular-weight heparin. *Thrombosis and Haemostasis, 99*(5), 807-818. doi:10.1160/th08-01-0032

Greenfield, N., Davidson, B., & Fasman, G. D. (1967). The use of computed optical rotatory dispersion curves for the evaluation of protein conformation. *Biochemistry, 6*(6), 1630-1637. doi:10.1021/bi00858a009

Greenwood, J., Clark, M., & Waldmann, H. (1993). STRUCTURAL MOTIFS INVOLVED IN HUMAN-IGG ANTIBODY EFFECTOR FUNCTIONS. *European Journal of Immunology, 23*(5), 1098-1104. doi:10.1002/eji.1830230518

Haas, C. (2012). Strategies, Development, and Pitfalls of Therapeutic Options for Alzheimer's Disease. *Journal of Alzheimers Disease, 28*(2), 241-281. doi:10.3233/jad-2011-110986

Haass, C., Lemere, C. A., Capell, A., Citron, M., Seubert, P., Schenk, D., Selkoe, D. J. (1995). THE SWEDISH MUTATION CAUSES EARLY-ONSET ALZHEIMERS-DISEASE BY BETA-SECRETASE CLEAVAGE WITHIN THE SECRETORY PATHWAY. *Nature Medicine, 1*(12), 1291-1296. doi:10.1038/nm1295-1291

Haass, C., & Selkoe, D. J. (2007). Soluble protein oligomers in neurodegeneration: lessons from the Alzheimer's amyloid beta-peptide. *Nature Reviews Molecular Cell Biology, 8*(2), 101-112. doi:10.1038/nrm2101

Habuchi, H., Habuchi, O., & Kimata, K. (1995). PURIFICATION AND CHARACTERIZATION OF HEPARAN-SULFATE 6-SULFOTRANSFERASE FROM THE CULTURE-MEDIUM OF CHINESE-HAMSTER OVARY CELLS. *Journal of Biological Chemistry, 270*(8), 4172-4179.

Hage.D.S, K. H. S. (2005). Immobilization methods for affinity chromatography. In J. C. David S. Hage (Ed.), *Handbook of Affinity Chromatography* (2nd ed., pp. 36-68). Lincoln, NE, USA.: Taylor & Francis.

Hagner-McWhirter, A., Li, J. P., Oscarson, S., & Lindahl, U. (2004). Irreversible glucuronyl C5-epimerization in the biosynthesis of heparan sulfate. *Journal of Biological Chemistry, 279*(15), 14631-14638. doi:10.1074/jbc.M313760200

Hagner-McWhirter, A., Lindahl, U., & Li, J. P. (2000). Biosynthesis of heparin/heparan sulphate: mechanism of epimerization of glucuronyl C-5. *Biochemical Journal, 347*, 69-75. doi:10.1042/0264-6021:3470069

Hamasuna, R., Eizuru, Y., Shishime, Y., & Minamishima, Y. (1993). PROTECTIVE EFFECT OF CARRAGEENAN AGAINST MURINE CYTOMEGALOVIRUS-INFECTION IN MICE. *Antiviral Chemistry & Chemotherapy, 4*(6), 353-360.

Haniu, M., Denis, P., Young, Y., Mendiaz, E. A., Fuller, J., Hui, J. O., Citron, M. (2000). Characterization of Alzheimer's beta-secretase protein BACE - A pepsin family member with unusual properties. *Journal of Biological Chemistry, 275*(28), 21099-21106. doi:10.1074/jbc.M002095200

Hari, S. B., Lau, H., Razinkov, V. I., Chen, S. A., & Latypov, R. F. (2010). Acid-Induced Aggregation of Human Monoclonal IgG1 and IgG2: Molecular Mechanism and the Effect of Solution Composition. *Biochemistry, 49*(43), 9328-9338.

Harrison, S. M., Harper, A. J., Hawkins, J., Duddy, G., Grau, E., Pugh, P. L., . . . Dingwall, C. (2003). BACE1 (beta-secretase) transgenic neurochernical deficits ind knockout mice: identification of and behavioral changes. *Molecular and Cellular Neuroscience, 24*(3), 646-655. doi:10.1016/s1044-7431(03)00227-4

Hayley, M., Perspicace, S., Schulthess, T., & Seelig, J. (2009). Calcium enhances the proteolytic activity of BACE1: An in vitro biophysical and biochemical characterization of the BACE1-calcium interaction. *Biochimica Et Biophysica Acta-Biomembranes, 1788*(9), 1933-1938. doi:10.1016/j.bbamem.2009.05.015

Heidarieh, M., Maragheh, M. G., Shamami, M. A., Behgar, M., Ziaei, F., & Akbari, Z. (2013). Evaluate of heavy metal concentration in shrimp (Penaeus semisulcatus) and crab (Portunus pelagicus) with INAA method. *Springerplus, 2*. doi:10.1186/2193-1801-2-72

Heimburg-Molinaro, J., Song, X., Smith, D. F., & Cummings, R. D. (2011). Preparation and analysis of glycan microarrays. *Current protocols in protein science, Chapter 12*, Unit12.10. doi:10.1002/0471140864.ps1210s64

Heinegard, D. (2009). Proteoglycans and more - from molecules to biology. *International Journal of Experimental Pathology, 90*(6), 575-586. doi:10.1111/j.1365-2613.2009.00695.x

Heinegard, D., Larsson, T., Sommarin, Y., Franzen, A., Paulsson, M., & Hedbom, E. (1986). 2 NOVEL MATRIX PROTEINS ISOLATED FROM ARTICULAR-CARTILAGE SHOW WIDE DISTRIBUTIONS AMONG CONNECTIVE TISSUES. *Journal of Biological Chemistry, 261*(29), 3866-3872.

Henry, S. P., Takanosu, M., Boyd, T. C., Mayne, P. M., Eberspaecher, H., Zhou, W., Mayne, R. (2001). Expression pattern and gene characterization of asporin - A newly

discovered member of the leucine-rich repeat protein family. *Journal of Biological Chemistry, 276*(15), 12212-12221. doi:10.1074/jbc.M011290200

Hirsh, J., & Fuster, V. (1994). GUIDE TO ANTICOAGULANT-THERAPY .1. HEPARIN. *Circulation, 89*(3), 1449-1468.

Hirsh, J., & Raschke, R. (2004). Heparin and low-molecular-weight heparin - The Seventh ACCP Conference on Antithrombotic and Thrombolytic Therapy. *Chest, 126*(3), 188S-203S. doi:10.1378/chest.126.3_suppl.188S

Hirsh, J., Warkentin, T. E., Raschke, R., Granger, C., Ohman, E. M., & Dalen, J. E. (1998). Heparin and low-molecular-weight heparin - Mechanisms of action, pharmacokinetics, dosing considerations, monitoring, efficacy, and safety. *Chest, 114*(5), 489S-510S. doi:10.1378/chest.114.5_Supplement.489S

Ho, S. N., Hunt, H. D., Horton, R. M., Pullen, J. K., & Pease, L. R. (1989). SITE-DIRECTED MUTAGENESIS BY OVERLAP EXTENSION USING THE POLYMERASE CHAIN-REACTION. *Gene, 77*(1), 51-59. doi:10.1016/0378-1119(89)90358-2

Holm, I., Ollo, R., Panthier, J. J., & Rougeon, F. (1984). EVOLUTION OF ASPARTYL PROTEASES BY GENE DUPLICATION - THE MOUSE RENIN GENE IS ORGANIZED IN 2 HOMOLOGOUS CLUSTERS OF 4 EXONS. *Embo Journal, 3*(3), 557-562.

Holmes, B. B., Devos, S. L., Kfoury, N., Li, M., Jacks, R., Yanamandra, K., Diamond, M. I. (2013). Heparan sulfate proteoglycans mediate internalization and propagation of specific proteopathic seeds. *Proceedings of the National Academy of Sciences of the United States of America, 110*(33), E3138-E3147. doi:10.1073/pnas.1301440110

Holmes, C., Boche, D., Wilkinson, D., Yadegarfar, G., Hopkins, V., Bayer, A., Nicoll, J. A. R. (2008). Long-term effects of A beta(42) immunisation in Alzheimer's disease: follow-up of a randomised, placebo-controlled phase I trial. *Lancet, 372*(9634), 216-223. doi:10.1016/s0140-6736(08)61075-2

Hong, L., Koelsch, G., Lin, X. L., Wu, S. L., Terzyan, S., Ghosh, A. K., Tang, J. (2000). Structure of the protease domain of memapsin 2 (beta-secretase) complexed with inhibitor. *Science, 290*(5489), 150-153. doi:10.1126/science.290.5489.150

Hong, L., & Tang, J. (2004). Flap position of free memapsin 2 (beta-secretase), a model for flap opening in aspartic protease catalysis. *Biochemistry, 43*(16), 4689-4695. doi:10.1021/bi0498252

Hong, L., Turner, R. T., Koelsch, G., Shin, D. G., Ghosh, A. K., & Tang, J. (2002). Crystal structure of memapsin 2 (beta-secretase) in complex with an inhibitor OM00-3. *Biochemistry, 41*(36), 10963-10967. doi:10.1021/bi026232n

Hossler, P., Khattak, S. F., & Li, Z. J. (2009). Optimal and consistent protein glycosylation in mammalian cell culture. *Glycobiology, 19*(9), 936-949. doi:10.1093/glycob/cwp079

Hu, X. Y., Hicks, C. W., He, W. X., Wong, P., Macklin, W. B., Trapp, B. D., & Yan, R. Q. (2006). Bace1 modulates myelination in the central and peripheral nervous system. *Nature Neuroscience, 9*(12), 1520-1525. doi:10.1038/nn1797

Hughes, J. (2011). Assessing pain in dementia: One little study but one big concept. *International Psychogeriatrics, 23*, S27-S28.

Hull, R. D., Raskob, G. E., Hirsh, J., Jay, R. M., Leclerc, J. R., Geerts, W. H., Gent, M. (1986). CONTINUOUS INTRAVENOUS HEPARIN COMPARED WITH INTERMITTENT SUBCUTANEOUS HEPARIN IN THE INITIAL TREATMENT OF PROXIMAL-VEIN THROMBOSIS. *New England Journal of Medicine, 315*(18), 1109-1114. doi:10.1056/nejm198610303151801

Humphries, D. E., Wong, G. W., Friend, D. S., Gurish, M. F., Qiu, W. T., Huang, C. F., Stevens, R. L. (1999). Heparin is essential for the storage of specific granule proteases in mast cells. *Nature, 400*(6746), 769-772. doi:10.1038/23481

Hunt, C. E., & Turner, A. J. (2009). Cell biology, regulation and inhibition of beta-secretase (BACE-1). *Febs Journal, 276*(7), 1845-1859. doi:10.1111/j.1742-4658.2009.06929.x

Huntington, J. A. (2005). Heparin activation of serpins. In H. G. Garg, R. J. Linhardt, & C. A. Hales (Eds.), *Chemistry and biology of heparin and heparan sulfate* (1 ed., pp. 367-398). Oxford UK: Elsevier Ltd.

Ikeda, Y., Charef, S., Ouidja, M. O., Barbier-Chassefiere, V., Sineriz, F., Duchesnay, A., . . . Papy-Garcia, D. (2011). Synthesis and biological activities of a library of glycosaminoglycans mimetic oligosaccharides. *Biomaterials, 32*(3), 769-776. doi:10.1016/j.biomaterials.2010.09.043

Ionescu, R. M., Vlasak, J., Price, C., & Kirchmeier, M. (2008). Contribution of variable domains to the stability of humanized IgG1 monoclonal antibodies. *Journal of Pharmaceutical Sciences, 97*(4), 1414-1426. doi:10.1002/jps.21104

Iozzo, R. V. (1997). The family of the small leucine-rich proteoglycans: Key regulators of matrix assembly and cellular growth. *Critical Reviews in Biochemistry and Molecular Biology, 32*(2), 141-174. doi:10.3109/10409239709108551

Iozzo, R. V., & Schaefer, L. (2015). Proteoglycan form and function: A comprehensive nomenclature of proteoglycans. *Matrix Biol, 42*, 11-55. doi:10.1016/j.matbio.2015.02.003

Ito, M., Baba, M., Hirabayashi, K., Matsumoto, T., Suzuki, M., Suzuki, S., Declercq, E. (1989). INVITRO ACTIVITY OF MANNAN SULFATE, A NOVEL SULFATED POLYSACCHARIDE, AGAINST HUMAN IMMUNODEFICIENCY VIRUS TYPE-1 AND OTHER ENVELOPED VIRUSES. *European Journal of Clinical Microbiology & Infectious Diseases, 8*(2), 171-173. doi:10.1007/bf01963907

Ito, M., Baba, M., Sato, A., Pauwels, R., Declercq, E., & Shigeta, S. (1987). INHIBITORY EFFECT OF DEXTRAN SULFATE AND HEPARIN ON THE REPLICATION OF

HUMAN-IMMUNODEFICIENCY-VIRUS (HIV) INVITRO. *Antiviral Research, 7*(6), 361-367. doi:10.1016/0166-3542(87)90018-0

Ito, T., & Tsumoto, K. (2013). Effects of subclass change on the structural stability of chimeric, humanized, and human antibodies under thermal stress. *Protein Sci, 22*(11), 1542-1551. doi:10.1002/pro.2340

Iverius, P. H. (1971). COUPLING OF GLYCOSAMINOGLYCANS TO AGAROSE BEADS (SEPHAROSE 4B). *Biochemical Journal, 124*(4), 677-&.

Iwatsubo, T., Saido, T. C., Mann, D. M. A., Lee, V. M. Y., & Trojanowski, J. Q. (1996). Full-length amyloid-beta(1-42(43)) and amino-terminally modified and truncated amyloid-beta 42(43) deposit in diffuse plaques. *American Journal of Pathology, 149*(6), 1823-1830.

Jacobsson, I., Lindahl, U., Jensen, J. W., Roden, L., Prihar, H., & Feingold, D. S. (1984). BIOSYNTHESIS OF HEPARIN - SUBSTRATE-SPECIFICITY OF HEPAROSAN N-SULFATE D-GLUCURONOSYL 5-EPIMERASE. *Journal of Biological Chemistry, 259*(2), 1056-1063.

Jaikaran, E., & Clark, A. (2001). Islet amyloid and type 2 diabetes: from molecular misfolding to islet pathophysiology. *Biochimica Et Biophysica Acta-Molecular Basis of Disease, 1537*(3), 179-203. doi:10.1016/s0925-4439(01)00078-3

Janeway C.A , T. P., Walport. M, and Shlomchik, M.J. (2001) *Immunobiology* (5th ed.). NY: Garland Science.

Jazayeri, J. A., & Carroll, G. F. (2008). Fc-based cytokines - Prospects for engineering superior therapeutics. *Biodrugs, 22*(1), 11-26.

Jiao, G. L., Yu, G. L., Zhang, J. Z., & Ewart, H. S. (2011). Chemical Structures and Bioactivities of Sulfated Polysaccharides from Marine Algae. *Marine Drugs, 9*(2), 196-223. doi:10.3390/md9020196

Jin, L., Abrahams, J. P., Skinner, R., Petitou, M., Pike, R. N., & Carrell, R. W. (1997). The anticoagulant activation of antithrombin by heparin. *Proceedings of the National Academy of Sciences of the United States of America, 94*(26), 14683-14688. doi:10.1073/pnas.94.26.14683

Jinek, M., Chylinski, K., Fonfara, I., Hauer, M., Doudna, J. A., & Charpentier, E. (2012). A Programmable Dual-RNA-Guided DNA Endonuclease in Adaptive Bacterial Immunity. *Science, 337*(6096), 816-821. doi:10.1126/science.1225829

Johnson, H. J., Rosenberg, L., Choi, H. U., Garza, S., Hook, M., & Neame, P. J. (1997). Characterization of epiphycan, a small proteoglycan with a leucine-rich repeat core protein. *Journal of Biological Chemistry, 272*(30), 18709-18717. doi:10.1074/jbc.272.30.18709

Johnson, R. G., Carty, S. E., Fingerhood, B. J., & Scarpa, A. (1980). THE INTERNAL PH OF MAST-CELL GRANULES. *Febs Letters, 120*(1), 75-79. doi:10.1016/0014-5793(80)81050-7

Johnson, W. C. (1988). SECONDARY STRUCTURE OF PROTEINS THROUGH CIRCULAR-DICHROISM SPECTROSCOPY. *Annual Review of Biophysics and Biophysical Chemistry, 17*, 145-166.

Jonquieres, R., Pizarro-Cerda, J., & Cossart, P. (2001). Synergy between the N- and C-terminal domains of InIB for efficient invasion of non-phagocytic cells by Listeria monocytogenes. *Molecular Microbiology, 42*(4), 955-965. doi:10.1046/j.1365-2958.2001.02704.x

Kaneko, Y., Yoshida, O., Nakagawa, R., Yoshida, T., Date, M., Ogihara, S., . . . Yamamoto, N. (1990). INHIBITION OF HIV-1 INFECTIVITY WITH CURDLAN SULFATE INVITRO. *Biochemical Pharmacology, 39*(4), 793-797.

Karpukhin, L. E., Feofanova, M. A., Nikolaeva, L. S., Mamontov, M. N., & Dobrynina, N. A. (2006). Complexation of magnesium and calcium ions with heparin. *Russian Journal of Inorganic Chemistry, 51*(6), 908-914. doi:10.1134/s0036023606060106

Karsten, C. M., & Kohl, J. (2012). The immunoglobulin, IgG Fc receptor and complement triangle in autoimmune diseases. *Immunobiology, 217*(11), 1067-1079. doi:10.1016/j.imbio.2012.07.015

Katsuraya, K., Nakashima, H., Yamamoto, N., & Uryu, T. (1999). Synthesis of sulfated oligosaccharide glycosides having high anti-HIV activity and the relationship between activity and chemical structure. *Carbohydrate Research, 315*(3-4), 234-242. doi:10.1016/s0008-6215(98)00315-2

Kayed, R., Head, E., Thompson, J. L., McIntire, T. M., Milton, S. C., Cotman, C. W., & Glabe, C. G. (2003). Common structure of soluble amyloid oligomers implies common mechanism of pathogenesis. *Science, 300*(5618), 486-489. doi:10.1126/science.1079469

Kearney, B. P., & Aweeka, F. T. (1999). The penetration of anti-infectives into the central nervous system. *Neurologic Clinics, 17*(4), 883-+. doi:10.1016/s0733-8619(05)70171-7

Kenig, M., Gaberc-Porekar, V., Fonda, I., & Menart, V. (2008). Identification of the heparin-binding domain of TNF-alpha and its use for efficient TNF-alpha purification by heparin-Sepharose affinity chromatography. *Journal of Chromatography B-Analytical Technologies in the Biomedical and Life Sciences, 867*(1), 119-125. doi:10.1016/j.jchromb.2008.03.023

Kim, D. Y., Ingano, L. A. M., Carey, B. W., Pettingell, W. H., & Kovacs, D. M. (2005). Presenilin/gamma-secretase-mediated cleavage of the voltage-gated sodium channel beta 2-subunit regulates cell adhesion and migration. *Journal of Biological Chemistry, 280*(24), 23251-23261. doi:10.1074/jbc.M412938200

Kim, J. K., Tsen, M. F., Ghetie, V., & Ward, E. S. (1994). LOCALIZATION OF THE SITE OF THE MURINE IGG1 MOLECULE THAT IS INVOLVED IN BINDING TO THE MURINE INTESTINAL FC RECEPTOR. *European Journal of Immunology, 24*(10), 2429-2434. doi:10.1002/eji.1830241025

Kim, J. K., Tsen, M. F., Ghetie, V., & Ward, E. S. (1995). EVIDENCE THAT THE HINGE REGION PLAYS A ROLE IN MAINTAINING SERUM LEVELS OF THE MURINE IGG1 MOLECULE. *Molecular Immunology, 32*(7), 467-475. doi:10.1016/0161-5890(95)00019-b

Kimberly, W. T., LaVoie, M. J., Ostaszewski, B. L., Ye, W. J., Wolfe, M. S., & Selkoe, D. J. (2003). gamma-secretase is a membrane protein complex comprised of presenilin, nicastrin, aph-1, and pen-2. *Proceedings of the National Academy of Sciences of the United States of America, 100*(11), 6382-6387. doi:10.1073/pnas.1037392100

Kimberly, W. T., & Wolfe, M. S. (2003). Identity and function of gamma-secretase. *Journal of Neuroscience Research, 74*(3), 353-360. doi:10.1002/jnr.10736

Kisilevsky, R., Lemieux, L. J., Fraser, P. E., Kong, X. Q., Hultin, P. G., & Szarek, W. A. (1995). ARRESTING AMYLOIDOSIS IN-VIVO USING SMALL-MOLECULE ANIONIC SULFONATES OR SULFATES - IMPLICATIONS FOR ALZHEIMERS-DISEASE. *Nature Medicine, 1*(2), 143-148. doi:10.1038/nm0295-143

Kitazume, S., Tachida, Y., Oka, R., Shirotani, K., Saido, T. C., & Hashimoto, Y. (2001). Alzheimer's beta-secretase, beta-site amyloid precursor protein-cleaving enzyme, is responsible for cleavage secretion of a Golgi-resident sialyltransferase. *Proceedings of the National Academy of Sciences of the United States of America, 98*(24), 13554-13559. doi:10.1073/pnas.241509198

Kivipelto, M., Helkala, E. L., Laakso, M. P., Hanninen, T., Hallikainen, M., Alhainen, K., Nissien, A. (2001). Midlife vascular risk factors and Alzheimer's disease in later life: longitudinal, population based study. *British Medical Journal, 322*(7300), 1447-1451. doi:10.1136/bmj.322.7300.1447

Kjellen, L., & Lindahl, U. (1991). PROTEOGLYCANS - STRUCTURES AND INTERACTIONS. *Annual Review of Biochemistry, 60*, 443-475. doi:10.1146/annurev.biochem.60.1.443

Klaver, D. W., Wilce, M. C., Gasperini, R., Freeman, C., Juliano, J. P., Parish, C., Small, D. H. (2010). Glycosaminoglycan-induced activation of the beta-secretase (BACE1) of Alzheimer's disease. *J Neurochem, 112*(6), 1552-1561. doi:10.1111/j.1471-4159.2010.06571.x

Knutsen, S. H., Myslabodski, D. E., Larsen, B., & Usov, A. I. (1994). A MODIFIED SYSTEM OF NOMENCLATURE FOR RED ALGAL GALACTANS. *Botanica Marina, 37*(2), 163-169. doi:10.1515/botm.1994.37.2.163

Koenig, A., Norgard-Sumnicht, K., Linhardt, R., & Varki, A. (1998). Differential interactions of heparin and heparan sulfate glycosaminoglycans with the selectins - Implications for the use of unfractionated and low molecular weight heparins as therapeutic agents. *Journal of Clinical Investigation, 101*(4), 877-889. doi:10.1172/jci1509

Koike, M., Nakanishi, H., Saftig, P., Ezaki, J., Isahara, K., Ohsawa, Y., Uchiyama, Y. (2000). Cathepsin D deficiency induces lysosomal storage with ceroid lipofuscin in mouse CNS neurons. *Journal of Neuroscience, 20*(18), 6898-6906.

Kontermann, R. E. (2011). Strategies for extended serum half-life of protein therapeutics. *Current Opinion in Biotechnology, 22*(6), 868-876. doi:10.1016/j.copbio.2011.06.012

Koo, E. H., & Squazzo, S. L. (1994). EVIDENCE THAT PRODUCTION AND RELEASE OF AMYLOID BETA-PROTEIN INVOLVES THE ENDOCYTIC PATHWAY. *Journal of Biological Chemistry, 269*(26), 17386-17389.

Krumdieck, R., Hook, M., Rosenberg, L. C., & Volanakis, J. E. (1992). THE PROTEOGLYCAN DECORIN BINDS C1Q AND INHIBITS THE ACTIVITY OF THE C1 COMPLEX. *Journal of Immunology, 149*(11), 3695-3701.

Krylov, V. B., Ustyuzhanina, N. E., & Nifantiev, N. E. (2011). Synthesis of low-molecular-weight carbohydrate mimetics of heparin. *Russian Journal of Bioorganic Chemistry, 37*(6), 672-706. doi:10.1134/s1068162011060100

Kuschert, G. S. V., Coulin, F., Power, C. A., Proudfoot, A. E. I., Hubbard, R. E., Hoogewerf, A. J., & Wells, T. N. C. (1999). Glycosaminoglycans interact selectively with chemokines and modulate receptor binding and cellular responses. *Biochemistry, 38*(39), 12959-12968. doi:10.1021/bi990711d

Kyriacou, H. M., Steen, K. E., Raza, A., Arman, M., Warimwe, G., Bull, P. C., . . . Rowe, J. A. (2007). In vitro inhibition of Plasmodium falciparum Rosette formation by curdlan sulfate. *Antimicrobial Agents and Chemotherapy, 51*(4), 1321-1326. doi:10.1128/aac.01216-06

Landt, M., Hortin, G. L., Smith, C. H., McClellan, A., & Scott, M. G. (1994). INTERFERENCE IN IONIZED CALCIUM MEASUREMENTS BY HEPARIN SALTS. *Clinical Chemistry, 40*(4), 565-570.

Langone, J. J. (1978). I125 PROTEIN-A - TRACER FOR GENERAL USE IN IMMUNOASSAY. *Journal of Immunological Methods, 24*(3-4), 269-285. doi:10.1016/0022-1759(78)90131-x

Latypov, R. F., Hogan, S., Lau, H., Gadgil, H., & Liu, D. J. (2012). Elucidation of Acid-induced Unfolding and Aggregation of Human Immunoglobulin IgG1 and IgG2 Fc. *Journal of Biological Chemistry, 287*(2), 1381-1396. doi:10.1074/jbc.M111.297697

Laurent, T. C., & Fraser, J. R. E. (1992). HYALURONAN. *Faseb Journal, 6*(7), 2397-2404.

Lazarov, O., Lee, M., Peterson, D. A., & Sisodia, S. S. (2002). Evidence that synaptically released beta-amyloid accumulates as extracellular deposits in the hippocampus of transgenic mice. *Journal of Neuroscience, 22*(22), 9785-9793.

Lee, V. M. Y., Goedert, M., & Trojanowski, J. Q. (2001). Neurodegenerative tauopathies. *Annual Review of Neuroscience, 24*, 1121-1159. doi:10.1146/annurev.neuro.24.1.1121

Lesne, S., Koh, M. T., Kotilinek, L., Kayed, R., Glabe, C. G., Yang, A., Ashe, K. H. (2006). A specific amyloid-beta protein assembly in the brain impairs memory. *Nature, 440*(7082), 352-357. doi:10.1038/nature04533

Lever, R., & Page, C. P. (2002). Novel drug development opportunities for heparin. *Nat Rev Drug Discov, 1*(2), 140-148. doi:10.1038/nrd724

Leveugle, B., Ding, W., Durkin, J. T., Mistretta, S., Eisle, J., Matic, M., Fillit, H. M. (1997). Heparin promotes beta-secretase cleavage of the Alzheimer's amyloid precursor protein. *Neurochemistry International, 30*(6), 543-548. doi:10.1016/s0197-0186(96)00103-9

Leveugle, B., Ding, W. H., Laurence, F., Dehouck, M. P., Scanameo, A., Cecchelli, R., & Fillit, H. (1998). Heparin oligosaccharides that pass the blood-brain barrier inhibit beta-amyloid precursor protein secretion and heparin binding to beta-amyloid peptide. *Journal of Neurochemistry, 70*(2), 736-744.

Li, F. W., Templeton, T. J., Popov, V., Comer, J. E., Tsuboi, T., Torii, M., & Vinetz, J. M. (2004). Plasmodium ookinete-secreted proteins secreted through a common micronemal pathway are targets of blocking malaria transmission. *Journal of Biological Chemistry, 279*(25), 26635-26644. doi:10.1074/jbc.M401385200

Li, Q., He, D. B., Chen, W., & Ni, L. H. (2005). Preparation, characterization and anticoagulant activity of guar gum sulphate. *Journal of Macromolecular Science-Pure and Applied Chemistry, A42*(8), 1085-1094. doi:10.1081/ma-200065936

Li, R., Lindholm, K., Yang, L. B., Yue, X., Citron, M., Yao, R. Q., Shen, Y. (2004). Amyloid beta peptide load is correlated with increased beta-secretase activity in sporadic Alzheimer's disease patients. *Proceedings of the National Academy of Sciences of the United States of America, 101*(10), 3632-3637. doi:10.1073/pnas.0205689101

Lichtenthaler, S. F., Dominguez, D., Westmeyer, G. G., Reiss, K., Haass, C., Saftig, P., Seed, B. (2003). The cell adhesion protein P-selectin glycoprotein ligand-1 is a substrate for the aspartyl protease BACE1. *Journal of Biological Chemistry, 278*(49), 48713-48719. doi:10.1074/jbc.M303861200

Liedberg, B., Nylander, C., & Lundstrom, I. (1983). SURFACE-PLASMON RESONANCE FOR GAS-DETECTION AND BIOSENSING. *Sensors and Actuators, 4*(2), 299-304. doi:10.1016/0250-6874(83)85036-7

Lin, X. L., Koelsch, C., Wu, S. L., Downs, D., Dashti, A., & Tang, J. (2000). Human aspartic protease memapsin 2 cleaves the beta-secretase site of beta-amyloid precursor protein. *Proceedings of the National Academy of Sciences of the United States of America, 97*(4), 1456-1460. doi:10.1073/pnas.97.4.1456

Lin, Y. L., Leib, H. Y., Lin, Y. S., Yeh, T. M., Chen, S. H., & Liu, H. S. (2002). Heparin inhibits dengue-2 virus infection of five human liver cell lines. *Antiviral Research, 56*(1), 93-96. doi:10.1016/s0166-3542(02)00095-5

Lindahl, U. (1989). Heparin: Chemical and Biological Properties, Clinical Applications. In D. A. L. Lane, U. (Ed.), *Heparin: Chemical and Biological Properties, Clinical Applications* (pp. 159). FL, USA: CRC Press Inc.

Lindahl, U., Backstrom, G., Thunberg, L., & Leder, I. G. (1980). EVIDENCE FOR A 3-O-SULFATED D-GLUCOSAMINE RESIDUE IN THE ANTITHROMBIN-BINDING SEQUENCE OF HEPARIN. *Proceedings of the National Academy of Sciences of the United States of America-Biological Sciences, 77*(11), 6551-6555. doi:10.1073/pnas.77.11.6551

Lindahl, U., Feingold, D. S., & Roden, L. (1986). BIOSYNTHESIS OF HEPARIN. *Trends in Biochemical Sciences, 11*(5), 221-225. doi:10.1016/0968-0004(86)90011-3

Linhardt, R. J., & Gunay, N. S. (1999). Production and chemical processing of low molecular weight heparins. *Seminars in Thrombosis and Hemostasis, 25*, 5-16.

Liu, J., Shworak, N. W., Fritze, L. M. S., Edelberg, J. M., & Rosenberg, R. D. (1996). Purification of heparan sulfate D-glucosaminyl 3-O-sulfotransferase. *Journal of Biological Chemistry, 271*(43), 27072-27082.

Lortat-Jacob, H., Turnbull, J. E., & Grimaud, J. A. (1995). MOLECULAR-ORGANIZATION OF THE INTERFERON GAMMA-BINDING DOMAIN IN HEPARAN-SULFATE. *Biochemical Journal, 310*, 497-505.

Love, D. C., Esko, J. D., & Mosser, D. M. (1993). A HEPARIN-BINDING ACTIVITY ON LEISHMANIA AMASTIGOTES WHICH MEDIATES ADHESION TO CELLULAR PROTEOGLYCANS. *Journal of Cell Biology, 123*(3), 759-766. doi:10.1083/jcb.123.3.759

Luo, X. Y., & Yan, R. Q. (2010). Inhibition of BACE1 for therapeutic use in Alzheimer's disease. *International Journal of Clinical and Experimental Pathology, 3*(6), 618-628.

Luo, Y., Bolon, B., Kahn, S., Bennett, B. D., Babu-Khan, S., Denis, P., Vassar, R. (2001). Mice deficient in BACE1, the Alzheimer's beta-secretase, have normal phenotype and abolished beta-amyloid generation. *Nature Neuroscience, 4*(3), 231-232. doi:10.1038/85059

Ma, Q., Dudas, B., Hejna, M., Cornelli, U., Lee, J. M., Lorens, S., Fareed, J. (2002). The blood-brain barrier accessibility of a heparin-derived oligosaccharides C3. *Thrombosis Research, 105*(5), 447-453. doi:10.1016/s0049-3848(02)00050-6

Malo, N., Hanley, J. A., Cerquozzi, S., Pelletier, J., & Nadon, R. (2006). Statistical practice in high-throughput screening data analysis. *Nat Biotechnol, 24*(2), 167-175. doi:10.1038/nbt1186

Marks, R. M., Lu, H., Sundaresan, R., Toida, T., Suzuki, A., Imanari, T., Linhardt, R. J. (2001). Probing the interaction of dengue virus envelope protein with heparin: Assessment of glycosaminoglycan-derived inhibitors. *Journal of Medicinal Chemistry, 44*(13), 2178-2187. doi:10.1021/jm000412i

Mascotti, D. P., & Lohman, T. M. (1995). THERMODYNAMICS OF CHARGED OLIGOPEPTIDE HEPARIN INTERACTIONS. *Biochemistry, 34*(9), 2908-2915. doi:10.1021/bi00009a022

Mastromarino, P., Petruzziello, R., Macchia, S., Rieti, S., Nicoletti, R., & Orsi, N. (1997). Antiviral activity of natural and semisynthetic polysaccharides on the early steps of rubella virus infection. *Journal of Antimicrobial Chemotherapy, 39*(3), 339-345. doi:10.1093/jac/39.3.339

Mathias, D. K., Pastrana-Mena, R., Ranucci, E., Tao, D. Y., Ferruti, P., Ortega, C., Dinglasan, R. R. (2013). A Small Molecule Glycosaminoglycan Mimetic Blocks Plasmodium Invasion of the Mosquito Midgut. *Plos Pathogens, 9*(11), 14. doi:10.1371/journal.ppat.1003757

Matsuhiro, B., Barahona, T., Encinas, M. V., Mansilla, A., & Ortiz, J. A. (2014). Sulfation of agarose from subantarctic Ahnfeltia plicata (Ahnfeltiales, Rhodophyta): studies of its antioxidant and anticoagulant properties in vitro and its copolymerization with acrylamide. *Journal of Applied Phycology, 26*(5), 2011-2019. doi:10.1007/s10811-014-0297-3

Matsumoto, A., Matsumoto, R., Enomoto, T., & Baba, H. (1996). Human brain beta-secretase contains heparan sulfate glycoconjugates. *Neuroscience Letters, 211*(2), 105-108. doi:10.1016/0304-3940(96)12723-3

Matulis, D., Kranz, J. K., Salemme, F. R., & Todd, M. J. (2005). Thermodynamic stability of carbonic anhydrase: Measurements of binding affinity and stoichiometry using ThermoFluor. *Biochemistry, 44*(13), 5258-5266. doi:10.1021/bi048135v

Maurel, P., Rauch, U., Flad, M., Margolis, R. K., & Margolis, R. U. (1994). PHOSPHACAN, A CHONDROITIN SULFATE PROTEOGLYCAN OF BRAIN THAT INTERACTS WITH NEURONS AND NEURAL CELL-ADHESION MOLECULES, IS AN EXTRACELLULAR VARIANT OF A RECEPTOR-TYPE PROTEIN-TYROSINE-PHOSPHATASE. *Proceedings of the National Academy of Sciences of the United States of America, 91*(7), 2512-2516. doi:10.1073/pnas.91.7.2512

McGaughey, G. B., & Holloway, M. K. (2007). Structure-guided design of beta-secretase (BACE-1) inhibitors. *Expert Opinion on Drug Discovery, 2*(8), 1129-1138. doi:10.1517/17460441.2.8.1129

McLaurin, J., Franklin, T., Kuhns, W. J., & Fraser, P. E. (1999). A sulfated proteoglycan aggregation factor mediates amyloid-β peptide fibril formation and neurotoxicity. *Amyloid, 6*(4), 233-243. doi:10.3109/13506129909007334

Medesan, C., Radu, C., Kim, J. K., Ghetie, V., & Ward, E. S. (1996). Localization of the site of the IgG molecule that regulates maternofetal transmission in mice. *European Journal of Immunology, 26*(10), 2533-2536. doi:10.1002/eji.1830261038

Medina, M., & Avila, J. (2014). New perspectives on the role of tau in Alzheimer's disease. Implications for therapy. *Biochemical Pharmacology, 88*(4), 540-547. doi:10.1016/j.bcp.2014.01.013

Meneghetti, M. C. Z., Hughes, A. J., Rudd, T. R., Nader, H. B., Powell, A. K., Yates, E. A., & Lima, M. A. (2015). Heparan sulfate and heparin interactions with proteins. *Journal of the Royal Society Interface, 12*(110), 13. doi:10.1098/rsif.2015.0589

Metcalfe, D. D., Lewis, R. A., Silbert, J. E., Rosenberg, R. D., Wasserman, S. I., & Austen, K. F. (1979). ISOLATION AND CHARACTERIZATION OF HEPARIN FROM HUMAN-LUNG. *Journal of Clinical Investigation, 64*(6), 1537-1543. doi:10.1172/jci109613

Micsonai, A., Wien, F., Kernya, L., Lee, Y. H., Goto, Y., Refregiers, M., & Kardos, J. (2015). Accurate secondary structure prediction and fold recognition for circular dichroism spectroscopy. *Proceedings of the National Academy of Sciences of the United States of America, 112*(24), E3095-E3103. doi:10.1073/pnas.1500851112

Miura, Y., Fukuda, T., Seto, H., & Hoshino, Y. (2016). Development of glycosaminoglycan mimetics using glycopolymers. *Polymer Journal, 48*(3), 229-237. doi:10.1038/pj.2015.110

Morgan, D. (2011). Immunotherapy for Alzheimer's disease. *Journal of Internal Medicine, 269*(1), 54-63. doi:10.1111/j.1365-2796.2010.02315.x

Moses, J., Oldberg, A., Cheng, F., & Fransson, L. A. (1997). Biosynthesis of the proteoglycan decorin - Transient 2-phosphorylation of xylose during formation of the trisaccharide linkage region. *European Journal of Biochemistry, 248*(2), 521-526. doi:10.1111/j.1432-1033.1997.00521.x

Mowrer, K. R., & Wolfe, M. S. (2008). Promotion of BACE1 mRNA alternative splicing reduces amyloid beta-peptide production. *Journal of Biological Chemistry, 283*(27), 18694-18701. doi:10.1074/jbc.M801322200

Mrak, R. E., & Griffin, W. S. T. (2004). Trisomy 21 and the brain. *Journal of Neuropathology and Experimental Neurology, 63*(7), 679-685.

Mulloy, B. (2012). Structure and physicochemical characterisation of heparin. *Handbook of experimental pharmacology*(207), 77-98. doi:10.1007/978-3-642-23056-1_5

Mulloy, B., Forster, M. J., Jones, C., & Davies, D. B. (1993). NMR AND MOLECULAR-MODELING STUDIES OF THE SOLUTION CONFORMATION OF HEPARIN. *Biochemical Journal, 293*, 849-858.

Multhaup, G. (1994). IDENTIFICATION AND REGULATION OF THE HIGH-AFFINITY BINDING-SITE OF THE ALZHEIMERS-DISEASE AMYLOID PROTEIN-PRECURSOR (APP) TO GLYCOSAMINOGLYCANS. *Biochimie, 76*(3-4), 304-311. doi:10.1016/0300-9084(94)90163-5

Muro, A. C., Rodriguez, E., Abate, C. M., & Sineriz, F. (2000). Levan production using mutant strains of Zymomonas mobilis in different culture conditions. *Biotechnology Letters, 22*(20), 1639-1642. doi:10.1023/a:1005623911287

Nahmias, A. J., & Kibrick, S. (1964). INHIBITORY EFFECT OF HEPARIN ON HERPES SIMPLEX VIRUS. *Journal of Bacteriology, 87*(5), 1060-&.

Nakashima, H., Kido, Y., Kobayashi, N., Motoki, Y., Neushul, M., & Yamamoto, N. (1987). PURIFICATION AND CHARACTERIZATION OF AN AVIAN-MYELOBLASTOSIS AND HUMAN-IMMUNODEFICIENCY-VIRUS REVERSE-TRANSCRIPTASE INHIBITOR, SULFATED POLYSACCHARIDES EXTRACTED FROM SEA ALGAE. *Antimicrobial Agents and Chemotherapy, 31*(10), 1524-1528.

Nakashima, H., Yoshida, O., Tochikura, T. S., Yoshida, T., Mimura, T., Kido, Y., Yamamoto, N. (1987). SULFATION OF POLYSACCHARIDES GENERATES POTENT AND SELECTIVE INHIBITORS OF HUMAN IMMUNODEFICIENCY VIRUS-INFECTION AND REPLICATION INVITRO. *Japanese Journal of Cancer Research, 78*(11), 1164-1168.

Neve, R. L., Harris, P., Kosik, K. S., Kurnit, D. M., & Donlon, T. A. (1986). IDENTIFICATION OF CDNA CLONES FOR THE HUMAN MICROTUBULE-ASSOCIATED PROTEIN TAU AND CHROMOSOMAL LOCALIZATION OF THE GENES FOR TAU AND MICROTUBULE-ASSOCIATED PROTEIN-2. *Molecular Brain Research, 1*(3), 271-280. doi:10.1016/0169-328x(86)90033-1

NICE. (2011). *Donepezil, galantamine, rivastigmine and memantine for the treatment of Alzheimer's disease*.

Niesen, F. H., Berglund, H., & Vedadi, M. (2007). The use of differential scanning fluorimetry to detect ligand interactions that promote protein stability. *Nat Protoc, 2*(9), 2212-2221. doi:10.1038/nprot.2007.321

Nilsson, B., Abrahmsen, L., & Uhlen, M. (1985). IMMOBILIZATION AND PURIFICATION OF ENZYMES WITH STAPHYLOCOCCAL PROTEIN-A GENE FUSION VECTORS. *Embo Journal, 4*(4), 1075-1080.

Nimmerjahn, F., & Ravetch, J. V. (2008). Fc gamma receptors as regulators of immune responses. *Nature Reviews Immunology, 8*(1), 34-47. doi:10.1038/nri2206

Nishimura, K., Shima, K., Asakura, M., Ohnishi, Y., & Yamasaki, S. (2005). Effects of heparin administration on Trypanosoma brucei gambiense infection in rats. *Journal of Parasitology, 91*(1), 219-222. doi:10.1645/ge-328r

Nishino, T., Aizu, Y., & Nagumo, T. (1991). THE INFLUENCE OF SULFATE CONTENT AND MOLECULAR-WEIGHT OF A FUCAN SULFATE FROM THE BROWN SEAWEED ECKLONIA-KUROME ON ITS ANTITHROMBIN ACTIVITY. *Thrombosis Research, 64*(6), 723-731. doi:10.1016/0049-3848(91)90072-5

Nishino, T., & Nagumo, T. (1992). ANTICOAGULANT AND ANTITHROMBIN ACTIVITIES OF OVERSULFATED FUCANS. *Carbohydrate Research, 229*(2), 355-362. doi:10.1016/s0008-6215(00)90581-0

Norderhaug, L., Brekke, O. H., Bremnes, B., Sandin, R., Aase, A., Michaelsen, T. E., & Sandlie, I. (1991). CHIMERIC MOUSE HUMAN IGG3 ANTIBODIES WITH AN IGG4-LIKE HINGE REGION INDUCE COMPLEMENT-MEDIATED LYSIS MORE

EFFICIENTLY THAN IGG3 WITH NORMAL HINGE. *European Journal of Immunology, 21*(10), 2379-2384. doi:10.1002/eji.1830211013

Nossal, G. J. V., & Lederberg, J. (1958). ANTIBODY PRODUCTION BY SINGLE CELLS. *Nature, 181*(4620), 1419-1420. doi:10.1038/1811419a0

Noti, C., & Seeberger, P. H. (2005). Synthetic approach to define structure-activity relationship of heparin and heparan sulphate. In H. G. Garg, R. J. Linhardt, & C. A. Hales (Eds.), *Chemistry and biology of heparin and heparan sulphate* (1 ed., Vol. 1, pp. 79-142). Oxford UK: Elseview Ltd.

Nyland, H., & Nilsen, R. (1982). LOCALIZATION OF FC-GAMMA RECEPTORS IN THE HUMAN CENTRAL NERVOUS-SYSTEM. *Acta Pathologica Microbiologica Et Immunologica Scandinavica Section C-Immunology, 90*(4), 217-221.

O'Connor, T., Sadleir, K. R., Maus, E., Velliquette, R. A., Zhao, J., Cole, S. L., Vassar, R. (2008). Phosphorylation of the Translation Initiation Factor eIF2 alpha Increases BACE1 Levels and Promotes Amyloidogenesis. *Neuron, 60*(6), 988-1009. doi:10.1016/j.neuron.2008.10.047

Ohno, M., Sametsky, E. A., Younkin, L. H., Oakley, H., Younkin, S. G., Citron, M., Disterhoft, J. F. (2004). BACE1 deficiency rescues memory deficits and cholinergic dysfunction in a mouse model of Alzheimer's disease. *Neuron, 41*(1), 27-33. doi:10.1016/s0896-6273(03)00810-9

Olfe, J., Domanska, G., Schuett, C., & Kiank, C. (2010). Different stress-related phenotypes of BALB/c mice from in-house or vendor: alterations of the sympathetic and HPA axis responsiveness. *BMC Physiology, 10*, 2. doi:10.1186/1472-6793-10-2

Olson, S. T., & Bjork, I. (1994). REGULATION OF THROMBIN ACTIVITY BY ANTITHROMBIN AND HEPARIN. *Seminars in Thrombosis and Hemostasis, 20*(4), 373-409. doi:10.1055/s-2007-1001928

Olson, S. T., Halvorson, H. R., & Bjork, I. (1991). QUANTITATIVE CHARACTERIZATION OF THE THROMBIN-HEPARIN INTERACTION DISCRIMINATION BETWEEN SPECIFIC AND NONSPECIFIC-BINDING MODELS. *Journal of Biological Chemistry, 266*(10), 6342-6352.

Olsson, P., Lagergren, H., & Ek, S. (1963). ELIMINATION FROM PLASMA OF INTRAVENOUS HEPARIN - AN EXPERIMENTAL STUDY ON DOGS AND HUMANS. *Acta Medica Scandinavica, 173*(5), 619-+.

Ono, L., Wollinger, W., Rocco, I. M., Coimbra, T. L. M., Gorin, P. A. J., & Sierakowski, M. R. (2003). In vitro and in vivo antiviral properties of sulfated galactomannans against yellow fever virus (BeH111 strain) and dengue 1 virus (Hawaii strain). *Antiviral Research, 60*(3), 201-208. doi:10.1016/s0166-3542(03)00175-x

Orgogozo, J. M., Gilman, S., Dartigues, J. F., Laurent, B., Puel, M., Kirby, L. C., Hock, C. (2003). Subacute meningoencephalitis in a subset of patients with AD after A beta 42 immunization. *Neurology, 61*(1), 46-54.

Ornitz, D. M. (2000). FGFs, heparan sulfate and FGFRs: complex interactions essential for development. *Bioessays, 22*(2), 108-112. doi:10.1002/(sici)1521-1878(200002)22:2<108::aid-bies2>3.0.co;2-m

Otto, D. M. E., Campanero-Rhodes, M. A., Karamanska, R., Powell, A. K., Bovin, N., Turnbull, J. E., Crocker, P. R. (2011). An expression system for screening of proteins for glycan and protein interactions. *Analytical Biochemistry, 411*(2), 261-270. doi:10.1016/j.ab.2010.12.036

Pantoliano, M. W., Petrella, E. C., Kwasnoski, J. D., Lobanov, V. S., Myslik, J., Graf, E., Salemme, F. R. (2001). High-density miniaturized thermal shift assays as a general strategy for drug discovery. *Journal of Biomolecular Screening, 6*(6), 429-440. doi:10.1089/108705701753364922

Para, M. F., Baucke, R. B., & Spear, P. G. (1980). IMMUNOGLOBULIN G(FC)-BINDING RECEPTORS ON VIRIONS OF HERPES-SIMPLEX VIRUS TYPE-1 AND TRANSFER OF THESE RECEPTORS TO THE CELL-SURFACE BY INFECTION. *Journal of Virology, 34*(2), 512-520.

Parham, P. (2015). In P. Parham (Ed.), *The Immune System* (4th ed., pp. 81-111). NY, USA: Garland Science, Taylor & Francis Group, LLC.

Park, J. E., Keller, G. A., & Ferrara, N. (1993). VASCULAR ENDOTHELIAL GROWTH-FACTOR (VEGF) ISOFORMS - DIFFERENTIAL DEPOSITION INTO THE SUBEPITHELIAL EXTRACELLULAR-MATRIX AND BIOACTIVITY OF EXTRACELLULAR MATRIX-BOUND VEGF. *Molecular Biology of the Cell, 4*(12), 1317-1326.

Patel, N., Hoang, D., Miller, N., Ansaloni, S., Huang, Q. H., Rogers, J. T., Saunders, A. J. (2008). MicroRNAs can regulate human APP levels. *Molecular Neurodegeneration, 3*, 6. doi:10.1186/1750-1326-3-10

Patey, S. J., Edwards, E. A., Yates, E. A., & Turnbull, J. E. (2006). Heparin derivatives as inhibitors of BACE-1, the Alzheimer's beta-secretase, with reduced activity against factor Xa and other proteases. *Journal of Medicinal Chemistry, 49*(20), 6129-6132. doi:10.1021/jm051221o

Patey, S. J., Edwards, E. A., Yates, E. A., & Turnbull, J. E. (2008). Engineered heparins: novel beta-secretase inhibitors as potential Alzheimer's disease therapeutics. *Neurodegener Dis, 5*(3-4), 197-199. doi:10.1159/000113701

Pereira, M. S., Mulloy, B., & Mourao, P. A. S. (1999). Structure and anticoagulant activity of sulfated fucans - Comparison between the regular, repetitive, and linear fucans from echinoderms with the more heterogeneous and branched polymers from brown algae. *Journal of Biological Chemistry, 274*(12), 7656-7667. doi:10.1074/jbc.274.12.7656

Perlmutter, L. S., Chui, H. C., Saperia, D., & Athanikar, J. (1990). MICROANGIOPATHY AND THE COLOCALIZATION OF HEPARAN-SULFATE PROTEOGLYCAN WITH AMYLOID IN SENILE PLAQUES OF ALZHEIMERS-DISEASE. *Brain Research, 508*(1), 13-19. doi:10.1016/0006-8993(90)91111-s

Peterson, P. A., Berggard, I., Edelman, G. M., & Cunningham, B. A. (1972). BETA2-MICROGLOBULIN - FREE IMMUNOGLOBULIN DOMAIN. *Proceedings of the National Academy of Sciences of the United States of America, 69*(7), 1697-+. doi:10.1073/pnas.69.7.1697

Petronio, M. G., Mansi, A., Gallinelli, C., Pisani, S., Seganti, L., & Chiarini, F. (1997). In vitro effect of natural and semi-synthetic carbohydrate polymers on Chlamydia trachomatis infection. *Chemotherapy, 43*(3), 211-217.

Pirrone, V., Wigdahl, B., & Krebs, F. C. (2011). The rise and fall of polyanionic inhibitors of the human immunodeficiency virus type 1. *Antiviral Research, 90*(3), 168-182. doi:10.1016/j.antiviral.2011.03.176

Polgar, L. (1987). THE MECHANISM OF ACTION OF ASPARTIC PROTEASES INVOLVES PUSH-PULL CATALYSIS. *Febs Letters, 219*(1), 1-4. doi:10.1016/0014-5793(87)81179-1

Porath, J., Carlsson, J., Olsson, I., & Belfrage, G. (1975). METAL CHELATE AFFINITY CHROMATOGRAPHY, A NEW APPROACH TO PROTEIN FRACTIONATION. *Nature, 258*(5536), 598-599. doi:10.1038/258598a0

Price, M. A., Wanshura, L. E. C., Yang, J. B., Carlson, J., Xiang, B., Li, G. Y., McCarthy, J. B. (2011). CSPG4, a potential therapeutic target, facilitates malignant progression of melanoma. *Pigment Cell & Melanoma Research, 24*(6), 1148-1157. doi:10.1111/j.1755-148X.2011.00929.x

Probst, G., & Xu, Y. Z. (2012). Small-molecule BACE1 inhibitors: a patent literature review (2006-2011). *Expert Opinion on Therapeutic Patents, 22*(5), 511-540. doi:10.1517/13543776.2012.681302

Pyzik, M., Rath, T., Lencer, W. I., Baker, K., & Blumberg, R. S. (2015). FcRn: The Architect Behind the Immune and Nonimmune Functions of IgG and Albumin. *Journal of Immunology, 194*(10), 4595-4603. doi:10.4049/jimmunol.1403014

Quader, M. A., Stump, L. S., & Sumpio, B. E. (1998). Low molecular weight heparins: Current use and indications. *Journal of the American College of Surgeons, 187*(6), 641-658. doi:10.1016/s1072-7515(98)00255-5

Querfurth, H. W., & LaFerla, F. M. (2010). MECHANISMS OF DISEASE Alzheimer's Disease. *New England Journal of Medicine, 362*(4), 329-344. doi:10.1056/NEJMra0909142

Rabenstein, D. L. (2002). Heparin and heparan sulfate: structure and function. *Natural Product Reports, 19*(3), 312-331. doi:10.1039/b100916h

Racke, M. M., Boone, L. I., Hepburn, D. L., Parsadainian, M., Bryan, M. T., Ness, D. K., . DeMattos, R. B. (2005). Exacerbation of cerebral amyloid angiopathy-associated microhemorrhage in amyloid precursor proteintransgenic mice by immunotherapy is dependent on antibody recognition of deposited forms of amyloid beta. *Journal of Neuroscience, 25*(3), 629-636. doi:10.1523/jneurosci.4337-04.2005

Raghavan, M., Bonagura, V. R., Morrison, S. L., & Bjorkman, P. J. (1995). ANALYSIS OF THE PH-DEPENDENCE OF THE NEONATAL FC RECEPTOR IMMUNOGLOBULIN-G INTERACTION USING ANTIBODY AND RECEPTOR VARIANT. *Biochemistry, 34*(45), 14649-14657. doi:10.1021/bi00045a005

Ramasamy, R., Vannucci, S. J., Yan, S. S. D., Herold, K., Yan, S. F., & Schmidt, A. M. (2005). Advanced glycation end products and RAGE: a common thread in aging, diabetes, neurodegeneration, and inflammation. *Glycobiology, 15*(7), 16R-28R. doi:10.1093/glycob/cwi053

Ravetch, J. V., & Kinet, J. P. (1991). FC-RECEPTORS. *Annual Review of Immunology, 9*, 457-492.

Rehn, M., Hintikka, E., & Pihlajaniemi, T. (1994). PRIMARY STRUCTURE OF THE ALPHA-1 CHAIN OF MOUSE TYPE-XVIII COLLAGEN, PARTIAL STRUCTURE OF THE CORRESPONDING GENE, AND COMPARISON OF THE ALPHA-1(XVIII) CHAIN WITH ITS HOMOLOG, THE ALPHA-1(XV) COLLAGEN CHAIN. *Journal of Biological Chemistry, 269*(19), 13929-13935.

Rich, D. H., Sun, E. T. O., & Ulm, E. (1980). SYNTHESIS OF ANALOGS OF THE CARBOXYL PROTEASE INHIBITOR PEPSTATIN - EFFECT OF STRUCTURE ON INHIBITION OF PEPSIN AND RENIN. *Journal of Medicinal Chemistry, 23*(1), 27-33. doi:10.1021/jm00175a006

Riesenfeld, J., Thunberg, L., Hook, M., & Lindahl, U. (1981). THE ANTITHROMBIN-BINDING SEQUENCE OF HEPARIN - LOCATION OF ESSENTIAL N-SULFATE GROUPS. *Journal of Biological Chemistry, 256*(5), 2389-2394.

Roberds, S. L., Anderson, J., Basi, G., Bienkowski, M. J., Branstetter, D. G., Chen, K. S., McConlogue, L. (2001). BACE knockout mice are healthy despite lacking the primary beta-secretase activity in brain: implications for Alzheimer's disease therapeutics. *Human Molecular Genetics, 10*(12), 1317-1324. doi:10.1093/hmg/10.12.1317

Robertson, A. D., & Murphy, K. P. (1997). Protein structure and the energetics of protein stability. *Chemical Reviews, 97*(5), 1251-1267. doi:10.1021/cr960383c

Robinson, H. C., Horner, A. A., Hook, M., Ogren, S., & Lindahl, U. (1978). PROTEOGLYCAN FORM OF HEPARIN AND ITS DEGRADATION TO SINGLE-CHAIN MOLECULES. *Journal of Biological Chemistry, 253*(19), 6687-6693.

Rodewald, R., & Kraehenbuhl, J. P. (1984). RECEPTOR-MEDIATED TRANSPORT OF IGG. *Journal of Cell Biology, 99*(1), S159-S164. doi:10.1083/jcb.99.1.159s

Rodriguez-Lebron, E., Gouvion, C. M., Moore, S. A., Davidson, B. L., & Paulson, H. L. (2009). Allele-specific RNAi Mitigates Phenotypic Progression in a Transgenic Model of Alzheimer's Disease. *Molecular Therapy, 17*(9), 1563-1573. doi:10.1038/mt.2009.123

Rong, J. H., Habuchi, H., Kimata, K., Lindahl, U., & Kusche-Gullberg, M. (2001). Substrate specificity of the heparan sulfate hexuronic acid 2-O-sulfotransferase. *Biochemistry, 40*(18), 5548-5555. doi:10.1021/bi002926p

Rossjohn, J., Cappai, R., Feil, S. C., Henry, A., McKinstry, W. J., Galatis, D., Parker, M. W. (1999). Crystal structure of the N-terminal, growth factor-like domain of Alzheimer amyloid precursor protein. *Nature Structural Biology, 6*(4), 327-331.

Rouet, V., Meddahi-Pelle, A., Miao, H. Q., Vlodavsky, I., Caruelle, J. P., & Barritault, D. (2006). Heparin-like synthetic polymers, named RGTAs, mimic biological effects of heparin in vitro. *Journal of Biomedical Materials Research Part A, 78A*(4), 792-797. doi:10.1002/jbm.a.30723

Rudd, T. R., Guimond, S. E., Skidmore, M. A., Duchesne, L., Guerrini, M., Torri, G., Yates, E. A. (2007). Influence of substitution pattern and cation binding on conformation and activity in heparin derivatives. *Glycobiology, 17*(9), 983-993. doi:10.1093/glyco/cwm062

Rudd, T. R., Uniewicz, K. A., Ori, A., Guimond, S. E., Skidmore, M. A., Gaudesi, D., Yates, E. A. (2010). Comparable stabilisation, structural changes and activities can be induced in FGF by a variety of HS and non-GAG analogues: implications for sequence-activity relationships. *Org Biomol Chem, 8*(23), 5390-5397. doi:10.1039/c0ob00246a

Sakano, H., Huppi, K., Heinrich, G., & Tonegawa, S. (1979). SEQUENCES AT THE SOMATIC RECOMBINATION SITES OF IMMUNOGLOBULIN LIGHT-CHAIN GENES. *Nature, 280*(5720), 288-294. doi:10.1038/280288a0

Sakano, H., Maki, R., Kurosawa, Y., Roeder, W., & Tonegawa, S. (1980). 2 TYPES OF SOMATIC RECOMBINATION ARE NECESSARY FOR THE GENERATION OF COMPLETE IMMUNOGLOBULIN HEAVY-CHAIN GENES. *Nature, 286*(5774), 676-683. doi:10.1038/286676a0

Salloway, S., Gur, T., Berzin, T., Zipser, B., Correia, S., Hovanesian, V., Stopa, E. (2002). Effect of APOE genotype on microvascular basement membrane in Alzheimer's disease. *Journal of the Neurological Sciences, 203*, 183-187. doi:10.1016/s0022-510x(02)00288-5

Salloway, S., Sperling, R., Gilman, S., Fox, N. C., Blennow, K., Raskind, M., Bapineuzumab 201 Clin Trial, I. (2009). A phase 2 multiple ascending dose trial of bapineuzumab in mild to moderate Alzheimer disease. *Neurology, 73*(24), 2061-2070. doi:10.1212/WNL.0b013e3181c67808

Sankaranarayanan, S., Price, E. A., Wu, G. X., Crouthamel, M. C., Shi, X. P., Tugusheva, K., . Simon, A. J. (2008). In vivo beta-Secretase 1 inhibition leads to brain A beta lowering and increased alpha-secretase processing of amyloid precursor protein without effect on neuregulin-1. *Journal of Pharmacology and Experimental Therapeutics, 324*(3), 957-969. doi:10.1124/jpet.107.130039

Sarrazin, S., Lamanna, W. C., & Esko, J. D. (2011). Heparan Sulfate Proteoglycans. *Cold Spring Harbor Perspectives in Biology, 3*(7), 33. doi:10.1101/cshperspect.a004952

Sasaki, M., Namioka, Y., Ito, T., Izumiyama, N., Fukui, S., Watanabe, A., Miura, M. (2001). Role of ICAM-1 in the aggregation and adhesion of human alveolar macrophages in response to TNF-alpha and INF-gamma. *Mediators of Inflammation, 10*(6), 309-313.

Sassenfeld, H. M., & Brewer, S. J. (1984). A POLYPEPTIDE FUSION DESIGNED FOR THE PURIFICATION OF RECOMBINANT PROTEINS. *Bio-Technology, 2*(1), 76-81. doi:10.1038/nbt0184-76

Sathya, M., Premkumar, P., Karthick, C., Moorthi, P., Jayachandran, K. S., & Anusuyadevi, M. (2012). BACE1 in Alzheimer's disease. *Clinica Chimica Acta, 414*, 171-178. doi:10.1016/j.cca.2012.08.013

Scallon, B., Cai, A., Solowski, N., Rosenberg, A., Song, X. Y., Shealy, D., & Wagner, C. (2002). Binding and functional comparisons of two types of tumor necrosis factor antagonists. *Journal of Pharmacology and Experimental Therapeutics, 301*(2), 418-426. doi:10.1124/jpet.301.2.418

Schechte.I, & Berger, A. (1967). ON SIZE OF ACTIVE SITE IN PROTEASES .I. PAPAIN. *Biochemical and Biophysical Research Communications, 27*(2), 157-&. doi:10.1016/s0006-291x(67)80055-x

Schedin-Weiss, S., Arocas, V., Bock, S. C., Olson, S. T., & Bjork, I. (2002). Specificity of the basic side chains of Lys114, Lys125, and Arg129 of antithrombin in heparin binding. *Biochemistry, 41*(41), 12369-12376. doi:10.1021/bi020406j

Scholefield, Z., Yates, E. A., Wayne, G., Amour, A., McDowell, W., & Turnbull, J. E. (2003). Heparan sulfate regulates amyloid precursor protein processing by BACE1, the Alzheimer's beta-secretase. *J Cell Biol, 163*(1), 97-107. doi:10.1083/jcb.200303059

Schroeder, H. W., & Cavacini, L. (2010). Structure and function of immunoglobulins. *Journal of Allergy and Clinical Immunology, 125*(2), S41-S52. doi:10.1016/j.jaci.2009.09.046

Schulze, A., Gripon, P., & Urban, S. (2007). Hepatitis B virus infection initiates with a large surface protein-dependent binding to heparan sulfate proteoglycans. *Hepatology, 46*(6), 1759-1768. doi:10.1002/hep.21896

Schur, P. H., & Christian, G. D. (1964). ROLE OF DISULFIDE BONDS IN COMPLEMENT-FIXING + PRECIPITATING PROPERTIES OF 7S RABBIT + SHEEP ANTIBODIES. *Journal of Experimental Medicine, 120*(4), 531-&. doi:10.1084/jem.120.4.531

Schworer, R., Zubkova, O. V., Turnbull, J. E., & Tyler, P. C. (2013). Synthesis of a targeted library of heparan sulfate hexa- to dodecasaccharides as inhibitors of beta-secretase: potential therapeutics for Alzheimer's disease. *Chemistry, 19*(21), 6817-6823. doi:10.1002/chem.201204519

Seeliger, D., & de Groot, B. L. (2010). Conformational Transitions upon Ligand Binding: Holo-Structure Prediction from Apo Conformations. *Plos Computational Biology, 6*(1). doi:10.1371/journal.pcbi.1000634

Sekar, R. B., & Periasamy, A. (2003). Fluorescence resonance energy transfer (FRET) microscopy imaging of live cell protein localizations. *Journal of Cell Biology, 160*(5), 629-633. doi:10.1083/jcb.200210140

Selkoe, D. J. (1991). THE MOLECULAR PATHOLOGY OF ALZHEIMERS-DISEASE. *Neuron, 6*(4), 487-498. doi:10.1016/0896-6273(91)90052-2

Selkoe, D. J. (2011). Resolving controversies on the path to Alzheimer's therapeutics. *Nature Medicine, 17*(9), 1060-1065. doi:10.1038/nm.2460

Semisotnov, G. V., Rodionova, N. A., Razgulyaev, O. I., Uversky, V. N., Gripas, A. F., & Gilmanshin, R. I. (1991). STUDY OF THE MOLTEN GLOBULE INTERMEDIATE STATE IN PROTEIN FOLDING BY A HYDROPHOBIC FLUORESCENT-PROBE. *Biopolymers, 31*(1), 119-128. doi:10.1002/bip.360310111

Shen, J., Bronson, R. T., Chen, D. F., Xia, W. M., Selkoe, D. J., & Tonegawa, S. (1997). Skeletal and CNS defects in Presenilin-1-deficient mice. *Cell, 89*(4), 629-639. doi:10.1016/s0092-8674(00)80244-5

Shimizu, H., Tosaki, A., Kaneko, K., Hisano, T., Sakurai, T., & Nukina, N. (2008). Crystal structure of an active form of BACE1, an enzyme responsible for amyloid beta protein production. *Molecular and Cellular Biology, 28*(11), 3663-3671. doi:10.1128/mcb.02185-07

Shinomura, T., Nishida, Y., Ito, K., & Kimata, K. (1993). CDNA CLONING OF PG-M, A LARGE CHONDROITIN SULFATE PROTEOGLYCAN EXPRESSED DURING CHONDROGENESIS IN CHICK LIMB BUDS - ALTERNATIVE SPLICED MULTIFORMS OF PG-M AND THEIR RELATIONSHIPS TO VERSICAN. *Journal of Biological Chemistry, 268*(19), 14461-14469.

Shriver, Z., Capila, I., Venkataraman, G., & Sasisekharan, R. (2012). Heparin and heparan sulfate: analyzing structure and microheterogeneity. *Handbook of experimental pharmacology*(207), 159-176. doi:10.1007/978-3-642-23056-1_8

Siemers, E. R., Sundell, K. L., Carlson, C., Case, M., Sethuraman, G., Liu-Seifert, H., . . . Demattos, R. (2016). Phase 3 solanezumab trials: Secondary outcomes in mild Alzheimer's disease patients. *Alzheimers & Dementia, 12*(2), 110-120. doi:10.1016/j.jalz.2015.06.1893

Sinha, S., Anderson, J. P., Barbour, R., Basi, G. S., Caccavello, R., Davis, D., John, V. (1999). Purification and cloning of amyloid precursor protein beta-secretase from human brain. *Nature, 402*(6761), 537-540. doi:10.1038/990114

Sinnis, P., Coppi, A., Toida, T., Toyoda, H., Kinoshita-Toyoda, A., Xie, J., Linhardt, R. J. (2007). Mosquito heparan sulfate and its potential role in malaria infection and transmission. *Journal of Biological Chemistry, 282*(35), 25376-25384. doi:10.1074/jbc.M704698200

Skidmore, M. A., Kajaste-Rudnitski, A., Wells, N. M., Guimond, S. E., Rudd, T. R., Yates, E. A., & Vicenzi, E. (2015). Inhibition of influenza H5N1 invasion by modified heparin derivatives. *Medchemcomm, 6*(4), 640-646. doi:10.1039/c4md00516c

Small, D. H., Nurcombe, V., Reed, G., Clarris, H., Moir, R., Beyreuther, K., & Masters, C. L. (1994). A HEPARIN-BINDING DOMAIN IN THE AMYLOID PROTEIN-PRECURSOR OF ALZHEIMERS-DISEASE IS INVOLVED IN THE REGULATION OF NEURITE OUTGROWTH. *Journal of Neuroscience, 14*(4), 2117-2127.

Snow, A. D., Sekiguchi, R. T., Nochlin, D., Kalaria, R. N., & Kimata, K. (1994). HEPARAN-SULFATE PROTEOGLYCAN IN DIFFUSE PLAQUES OF HIPPOCAMPUS BUT NOT OF CEREBELLUM IN ALZHEIMERS-DISEASE BRAIN. *American Journal of Pathology, 144*(2), 337-347.

Snow, A. D., & Wight, T. N. (1989). PROTEOGLYCANS IN THE PATHOGENESIS OF ALZHEIMERS-DISEASE AND OTHER AMYLOIDOSES. *Neurobiology of Aging, 10*(5), 481-497. doi:10.1016/0197-4580(89)90108-5

Snow, A. D., Wight, T. N., Nochlin, D., Koike, Y., Kimata, K., Dearmond, S. J., & Prusiner, S. B. (1990). IMMUNOLOCALIZATION OF HEPARAN-SULFATE PROTEOGLYCANS TO THE PRION PROTEIN AMYLOID PLAQUES OF GERSTMANN-STRAUSSLER SYNDROME, CREUTZFELDT-JAKOB DISEASE AND SCRAPIE. *Laboratory Investigation, 63*(5), 601-611.

Srikanth, R., Siddartha, G., Reddy, C., Harish, B. S., Ramaiah, M. J., & Uppuluri, K. B. (2015). Antioxidant and anti-inflammatory levan produced from Acetobacter xylinum NCIM2526 and its statistical optimization. *Carbohydrate Polymers, 123*, 8-16. doi:10.1016/j.carbpol.2014.12.079

Srikanth, V., Maczurek, A., Phan, T., Steele, M., Westcott, B., Juskiw, D., & Munch, G. (2011). Advanced glycation endproducts and their receptor RAGE in Alzheimer's disease. *Neurobiology of Aging, 32*(5), 763-777. doi:10.1016/j.neurobiolaging.2009.04.016

Stachel, S. J., Coburn, C. A., Steele, T. G., Jones, K. G., Loutzenhiser, E. F., Gregro, A. R., . . . Vacca, J. P. (2004). Structure-based design of potent and selective cell-permeable inhibitors of human beta-secretase (BACE-1). *Journal of Medicinal Chemistry, 47*(26), 6447-6450. doi:10.1021/jm049379g

Stadlmann, J., Pabst, M., Kolarich, D., Kunert, R., & Altmann, F. (2008). Analysis of immunoglobulin glycosylation by LC-ESI-MS of glycopeptides and oligosaccharides. *Proteomics, 8*(14), 2858-2871. doi:10.1002/pmic.200700968

Stanga, S., Lanni, C., Govoni, S., Uberti, D., D'Orazi, G., & Racchi, M. (2010). Unfolded p53 in the pathogenesis of Alzheimer's disease: is HIPK2 the link? *Aging-Us, 2*(9), 545-554.

Stephens, R. S., Fawaz, F. S., Kennedy, K. A., Koshiyama, K., Nichols, B., van Ooij, C., & Engel, J. N. (2000). Eukaryotic cell uptake of heparin-coated microspheres: a model of host cell invasion by Chlamydia trachomatis. *Infection and Immunity, 68*(3), 1080-1085. doi:10.1128/iai.68.3.1080-1085.2000

Stryer, L. (1978). FLUORESCENCE ENERGY-TRANSFER AS A SPECTROSCOPIC RULER. *Annual Review of Biochemistry, 47*, 819-846. doi:10.1146/annurev.bi.47.070178.004131

Sugahara, K., & Kitagawa, H. (2000). Recent advances in the study of the biosynthesis and functions of sulfated glycosaminoglycans. *Current Opinion in Structural Biology, 10*(5), 518-527. doi:10.1016/s0959-440x(00)00125-1

Sugahara, K., Ohi, Y., Harada, T., Dewaard, P., & Vliegenthart, J. F. G. (1992). STRUCTURAL STUDIES ON SULFATED OLIGOSACCHARIDES DERIVED FROM THE CARBOHYDRATE-PROTEIN LINKAGE REGION OF CHONDROITIN-6-SULFATE PROTEOGLYCANS OF SHARK CARTILAGE .1. 6 COMPOUNDS CONTAINING 0 OR 1 SULFATE AND OR PHOSPHATE RESIDUE. *Journal of Biological Chemistry, 267*(9), 6027-6035.

Suguna, K., Padlan, E. A., Smith, C. W., Carlson, W. D., & Davies, D. R. (1987). BINDING OF A REDUCED PEPTIDE INHIBITOR TO THE ASPARTIC PROTEINASE FROM RHIZOPUS-CHINENSIS - IMPLICATIONS FOR A MECHANISM OF ACTION. *Proceedings of the National Academy of Sciences of the United States of America, 84*(20), 7009-7013. doi:10.1073/pnas.84.20.7009

Sutton, A., Friand, V., Papy-Garcia, D., Dagouassat, M., Martin, L., Vassy, R., Charnaux, N. (2007). Glycosaminoglycans and their synthetic mimetics inhibit RANTES-induced migration and invasion of human hepatoma cells. *Molecular Cancer Therapeutics, 6*(11), 2948-2958. doi:10.1158/1535-7163.mct-07-0114

Svensson, L., Narlid, I., & Oldberg, A. (2000). Fibromodulin and lumican bind to the same region on collagen type I fibrils. *Febs Letters, 470*(2), 178-182. doi:10.1016/s0014-5793(00)01314-4

Talarico, L. B., Pujol, C. A., Zibetti, R. G. M., Faria, P. C. S., Noseda, M. D., Duarte, M. E. R., & Damonte, E. B. (2005). The antiviral activity of sulfated polysaccharides against dengue virus is dependent on virus serotype and host cell. *Antiviral Research, 66*(2-3), 103-110. doi:10.1016/j.antiviral.2005.02.001

Tan, L. K., Shopes, R. J., Oi, V. T., & Morrison, S. L. (1990). INFLUENCE OF THE HINGE REGION ON COMPLEMENT ACTIVATION, C1Q BINDING, AND SEGMENTAL FLEXIBILITY IN CHIMERIC HUMAN-IMMUNOGLOBULINS. *Proceedings of the National Academy of Sciences of the United States of America, 87*(1), 162-166. doi:10.1073/pnas.87.1.162

Tao, M. H., Smith, R. I. F., & Morrison, S. L. (1993). STRUCTURAL FEATURES OF HUMAN IMMUNOGLOBULIN-G THAT DETERMINE ISOTYPE-SPECIFIC DIFFERENCES IN COMPLEMENT ACTIVATION. *Journal of Experimental Medicine, 178*(2), 661-667. doi:10.1084/jem.178.2.661

Terho, T. T., & Hartiala, K. (1971). METHOD FOR DETERMINATION OF SULFATE CONTENT OF GLYCOSAMINOGLYCANS. *Analytical Biochemistry, 41*(2), 471-&. doi:10.1016/0003-2697(71)90167-9

Terpe, K. (2003). Overview of tag protein fusions: from molecular and biochemical fundamentals to commercial systems. *Applied Microbiology and Biotechnology, 60*(5), 523-533. doi:10.1007/s00253-002-1158-6

Tillman, J., Ullm, A., & Madihally, S. V. (2006). Three-dimensional cell colonization in a sulfate rich environment. *Biomaterials, 27*(32), 5618-5626. doi:10.1016/j.biomaterials.2006.07.006

Tischenko, V. M., Abramov, V. M., & Zav'yalov, V. P. (1998). Investigation of the cooperative structure of Fc fragments from myeloma immunoglobulin G. *Biochemistry, 37*(16), 5576-5581. doi:10.1021/bi972647a

Tischenko, V. M., Zavyalov, V. P., Medgyesi, G. A., Potekhin, S. A., & Privalov, P. L. (1982). A THERMODYNAMIC STUDY OF COOPERATIVE STRUCTURES IN RABBIT IMMUNOGLOBULIN-G. *European Journal of Biochemistry, 126*(3), 517-521. doi:10.1111/j.1432-1033.1982.tb06811.x

Tiwari, V., Clement, C., Xu, D., Valyi-Nagy, T., Yue, B., Liu, J., & Shukla, D. (2006). Role for 3-O-sulfated heparan sulfate as the receptor for herpes simplex virus type 1 entry into primary human corneal fibroblasts. *Journal of Virology, 80*(18), 8970-8980. doi:10.1128/jvi.00296-06

Toida, T., Yoshida, H., Toyoda, H., Koshishi, I., Imanari, T., Hileman, R. E., . . . Linhardt, R. J. (1997). Structural differences and the presence of unsubstituted amino groups in heparan sulphates from different tissues and species. *Biochemical Journal, 322*, 499-506.

Tsien, R. Y. (1998). The green fluorescent protein. *Annual Review of Biochemistry, 67*, 509-544. doi:10.1146/annurev.biochem.67.1.509

Turnbull, J., Powell, A., & Guimond, S. (2001). Heparan sulfate: decoding a dynamic multifunctional cell regulator. *Trends in Cell Biology, 11*(2), 75-82. doi:10.1016/s0962-8924(00)01897-3

Turner, R. T., Hong, L., Koelsch, G., Ghosh, A. K., & Tang, J. (2005). Structural locations and functional roles of new subsites S-5, S-6, and S-7 in memapsin 2 (beta-secretase). *Biochemistry, 44*(1), 105-112. doi:10.1021/bi048106k

Turner, R. T., Loy, J. A., Nguyen, C., Devasamudram, T., Ghosh, A. K., Koelsch, G., & Tang, J. (2002). Specificity of memapsin 1 and its implications on the design of memapsin 2 (beta-secretase) inhibitor selectivity. *Biochemistry, 41*(27), 8742-8746. doi:10.1021/bi025926t

Uhlen, M., Nilsson, B., Guss, B., Lindberg, M., Gatenbeck, S., & Philipson, L. (1983). GENE FUSION VECTORS BASED ON THE GENE FOR STAPHYLOCOCCAL PROTEIN-A. *Gene, 23*(3), 369-378. doi:10.1016/0378-1119(83)90025-2

Umezawa, H., Aoyagi, T., Morishim.H, Matsuzak.M, Hamada, M., & Takeuchi, T. (1970). PEPSTATIN, A NEW PEPSIN INHIBITOR PRODUCED BY ACTINOMYCETES. *Journal of Antibiotics, 23*(5), 259-&.

Uniewicz, K. A., Ori, A., Ahmed, Y. A., Yates, E. A., & Fernig, D. G. (2014). Characterisation of the interaction of neuropilin-1 with heparin and a heparan sulfate mimetic library of heparin-derived sugars. *PeerJ, 2*, e461. doi:10.7717/peerj.461

Uniewicz, K. A., Ori, A., Xu, R. Y., Ahmed, Y., Wilkinson, M. C., Fernig, D. G., & Yates, E. A. (2010). Differential Scanning Fluorimetry Measurement of Protein Stability Changes upon Binding to Glycosaminoglycans: A Screening Test for Binding Specificity. *Analytical Chemistry, 82*(9), 3796-3802. doi:10.1021/ac100188x

Unkeless, J. C., Scigliano, E., & Freedman, V. H. (1988). STRUCTURE AND FUNCTION OF HUMAN AND MURINE RECEPTORS FOR IGG. *Annual Review of Immunology, 6*, 251-281.

Utsumi, S., Okada, M., Udaka, K., & Amano, T. (1985). PREPARATION AND BIOLOGIC CHARACTERIZATION OF FRAGMENTS CONTAINING DIMERIC AND MONOMERIC C-GAMMA-2 DOMAIN OF RABBIT IGG. *Molecular Immunology, 22*(7), 811-819. doi:10.1016/0161-5890(85)90147-6

van Marum, R. J. (2008). Current and future therapy in Alzheimer's disease. *Fundamental & Clinical Pharmacology, 22*(3), 265-274. doi:10.1111/j.1472-8206.2008.00578.x

Vanboeckel, C. A. A., & Petitou, M. (1993). THE UNIQUE ANTITHROMBIN-III BINDING DOMAIN OF HEPARIN - A LEAD TO NEW SYNTHETIC ANTITHROMBOTICS. *Angewandte Chemie-International Edition in English, 32*(12), 1671-1690. doi:10.1002/anie.199316713

Vassar, R., Bennett, B. D., Babu-Khan, S., Kahn, S., Mendiaz, E. A., Denis, P., . . . Citron, M. (1999). beta-secretase cleavage of Alzheimer's amyloid precursor protein by the transmembrane aspartic protease BACE. *Science, 286*(5440), 735-741. doi:10.1126/science.286.5440.735

Vassar, R., Kovacs, D. M., Yan, R., & Wong, P. C. (2009). The beta-secretase enzyme BACE in health and Alzheimer's disease: regulation, cell biology, function, and therapeutic potential. *J Neurosci, 29*(41), 12787-12794. doi:10.1523/JNEUROSCI.3657-09.2009

Vedadi, M., Niesen, F. H., Allali-Hassani, A., Fedorov, O. Y., Finerty, P. J., Wasney, G. A., . . . Edwards, A. M. (2006). Chemical screening methods to identify ligands that promote protein stability, protein crystallization, and structure determination. *Proceedings of the National Academy of Sciences of the United States of America, 103*(43), 15835-15840. doi:10.1073/pnas.0605224103

Velliquette, R. A., O'Connor, T., & Vassar, R. (2005). Energy inhibition elevates beta-secretase levels and activity and is potentially amyloidogenic in APP transgenic mice: Possible early events in Alzheimer's disease pathogenesis. *Journal of Neuroscience, 25*(47), 10874-10883. doi:10.1523/jneurosci.2350-05.2005

Vemuri, P., & Jack, C. R. (2010). Role of structural MRI in Alzheimer's disease. *Alzheimers Research & Therapy, 2*(4). doi:10.1186/alzrt47

Venugopal, C., Demos, C. M., Rao, K. S. J., Pappolla, M. A., & Sambamurti, K. (2008). Beta-Secretase: Structure, Function, and Evolution. *Cns & Neurological Disorders-Drug Targets, 7*(3), 278-294. doi:10.2174/187152708784936626

Verbeek, M. M., Otte-Holler, I., Veerhuis, R., Ruiter, D. J., & De Waal, R. M. W. (1998). Distribution of A beta-associated proteins in cerebrovascular amyloid of Alzheimer's disease. *Acta Neuropathologica, 96*(6), 628-636.

Vermeer, A. W. P., & Norde, W. (2000). The thermal stability of immunoglobulin: Unfolding and aggregation of a multi-domain protein. *Biophysical Journal, 78*(1), 394-404.

Vieira, T., Cordeiro, Y., Caughey, B., & Silva, J. L. (2014). Heparin binding confers prion stability and impairs its aggregation. *Faseb Journal, 28*(6), 2667-2676. doi:10.1096/fj.13-246777

Visentin, G. P., Ford, S. E., Scott, J. P., & Aster, R. H. (1994). ANTIBODIES FROM PATIENTS WITH HEPARIN-INDUCED THROMBOCYTOPENIA/THROMBOSIS ARE SPECIFIC FOR PLATELET FACTOR-4 COMPLEXED WITH HEPARIN OR BOUND TO ENDOTHELIAL-CELLS. *Journal of Clinical Investigation, 93*(1), 81-88. doi:10.1172/jci116987

Vives, R. R., Imberty, A., Sattentau, Q. J., & Lortat-Jacob, H. (2005). Heparan sulfate targets the HIV-1 envelope glycoprotein gp120 coreceptor binding site. *Journal of Biological Chemistry, 280*(22), 21353-21357. doi:10.1074/jbc.M500911200

Vlasov, A. P., Kravchuk, Z. I., & Martsev, S. P. (1996). Non-native conformational states of immunoglobulins: Thermodynamic and functional studies of rabbit IgG. *Biochemistry-Moscow, 61*(2), 155-171.

Vogl, H., Paper, D. H., & Franz, G. (2000). Preparation of a sulfated linear (1 -> 4)-beta-D-galactan with variable degrees of sulfation. *Carbohydrate Polymers, 41*(2), 185-190. doi:10.1016/s0144-8617(99)00076-4

von Arnim, C. A. F., Kinoshita, A., Peltan, I. D., Tangredi, M. M., Herl, L., Lee, B. M., . . . Hyman, B. T. (2005). The low density lipoprotein receptor-related protein (LRP) is a novel beta-secretase (BACE1) substrate. *Journal of Biological Chemistry, 280*(18), 17777-17785. doi:10.1074/jbc.M414248200

Wang, J. L., Zhao, B. T., Wang, X. F., Yao, J., & Zhang, J. (2012). Structure and antioxidant activities of sulfated guar gum: Homogeneous reaction using DMAP/DCC catalyst. *International Journal of Biological Macromolecules, 50*(5), 1201-1206. doi:10.1016/j.ijbiomac.2012.03.009

Wangsell, F., Gustafsson, K., Kvarnstrom, I., Borkakoti, N., Edlund, M., Jansson, K., . . . Samuelsson, B. (2010). Synthesis of potent BACE-1 inhibitors incorporating a hydroxyethylene isostere as central core. *European Journal of Medicinal Chemistry, 45*(3), 870-882. doi:10.1016/j.ejmech.2009.11.013

Wardrop, D., & Keeling, D. (2008). The story of the discovery of heparin and warfarin. *British Journal of Haematology, 141*(6), 757-763. doi:10.1111/j.1365-2141.2008.07119.x

Watson, D. J., Lander, A. D., & Selkoe, D. J. (1997). Heparin-binding properties of the amyloidogenic peptides A beta and amylin - Dependence on aggregation state

and inhibition by Congo red. *Journal of Biological Chemistry, 272*(50), 31617-31624. doi:10.1074/jbc.272.50.31617

West, D. C., Rees, C. G., Duchesne, L., Patey, S. J., Terry, C. J., Turnbull, J. E., . . . Fernig, D. G. (2005). Interactions of multiple heparin binding growth factors with neuropilin-1 and potentiation of the activity of fibroblast growth factor-2. *Journal of Biological Chemistry, 280*(14), 13457-13464. doi:10.1074/jbc.M410924200

Westmeyer, G. G., Willem, M., Lichtenthaler, S. F., Lurman, G., Multhaup, G., Assafalg-Machleidt, I., . . . Haass, C. (2004). Dimerization of beta-site beta-amyloid precursor protein-cleaving enzyme. *Journal of Biological Chemistry, 279*(51), 53205-53212. doi:10.1074/jbc.M410378200

WHO. (2012). *Dementia: A public health priority*. (978 92 4 156445 8). Geneva, Switzerland: WHO Retrieved from http://apps.who.int/iris/bitstream/10665/75263/1/9789241564458_eng.pdf?ua=1.

Willem, M., Garratt, A. N., Novak, B., Citron, M., Kaufmann, S., Rittger, A., . . . Haass, C. (2006). Control of peripheral nerve myelination by the beta-secretase BACE1. *Science, 314*(5799), 664-666. doi:10.1126/science.1132341

Willem, M., Lammich, S., & Haass, C. (2009). Function, regulation and therapeutic properties of beta-secretase (BACE1). *Seminars in Cell & Developmental Biology, 20*(2), 175-182. doi:10.1016/j.semcdb.2009.01.003

Williams, A. F., & Barclay, A. N. (1988). THE IMMUNOGLOBULIN SUPERFAMILY - DOMAINS FOR CELL-SURFACE RECOGNITION. *Annual Review of Immunology, 6*, 381-405. doi:10.1146/annurev.iy.06.040188.002121

Xiao, L. H., Yang, C. F., Patterson, P. S., Udhayakumar, V., & Lal, A. A. (1996). Sulfated polyanions inhibit invasion of erythrocytes by plasmodial merozoites and cytoadherence of endothelial cells to parasitized erythrocytes. *Infection and Immunity, 64*(4), 1373-1378.

Yamada, K., Yabuki, C., Seubert, P., Schenk, D., Hori, Y., Ohtsuki, S., . . . Iwatsubo, T. (2009). A beta Immunotherapy: Intracerebral Sequestration of A beta by an Anti-A beta Monoclonal Antibody 266 with High Affinity to Soluble A beta. *Journal of Neuroscience, 29*(36), 11393-11398. doi:10.1523/jneurosci.2021-09.2009

Yan, D., & Lin, X. H. (2009). Shaping Morphogen Gradients by Proteoglycans. *Cold Spring Harbor Perspectives in Biology, 1*(3), 16. doi:10.1101/cshperspect.a002493

Yan, J. K., Wang, W. Q., Ma, H. L., & Wu, J. Y. (2013). Sulfation and Enhanced Antioxidant Capacity of an Exopolysaccharide Produced by the Medicinal Fungus Cordyceps sinensis. *Molecules, 18*(1), 167-177. doi:10.3390/molecules18010167

Yates, E. A., Guimond, S. E., & Turnbull, J. E. (2004). Highly diverse heparan sulfate analogue libraries: Providing access to expanded areas of sequence space for bioactivity screening. *Journal of Medicinal Chemistry, 47*(1), 277-280. doi:10.1021/jm0309755

Yates, E. A., Santini, F., De Cristofano, B., Payre, N., Cosentino, C., Guerrini, M., . . . Hricovini, M. (2000). Effect of substitution pattern on H-1, C-13 NMR chemical shifts and (1)J(CH) coupling constants in heparin derivatives. *Carbohydrate Research, 329*(1), 239-247. doi:10.1016/s0008-6215(00)00144-0

Yates, E. A., Santini, F., Guerrini, M., Naggi, A., Torri, G., & Casu, B. (1996). H-1 and C-13 NMR spectral assignments of the major sequences of twelve systematically modified heparin derivatives. *Carbohydrate Research, 294*, 15-27.

Yayon, A., Klagsbrun, M., Esko, J. D., Leder, P., & Ornitz, D. M. (1991). CELL-SURFACE, HEPARIN-LIKE MOLECULES ARE REQUIRED FOR BINDING OF BASIC FIBROBLAST GROWTH-FACTOR TO ITS HIGH-AFFINITY RECEPTOR. *Cell, 64*(4), 841-848. doi:10.1016/0092-8674(91)90512-w

Yokosawa, H., Ito, H., Murata, S., & Ishii, S. (1983). PURIFICATION AND FLUOROMETRIC ASSAY OF PROTEINASE A FROM YEAST. *Analytical Biochemistry, 134*(1), 210-215. doi:10.1016/0003-2697(83)90286-5

Yoshida, O., Nakashima, H., Yoshida, T., Kaneko, Y., Yamamoto, I., Matsuzaki, K., . . . Yamamoto, N. (1988). SULFATION OF THE IMMUNOMODULATING POLYSACCHARIDE LENTINAN - A NOVEL STRATEGY FOR ANTIVIRALS TO HUMAN IMMUNODEFICIENCY VIRUS (HIV). *Biochemical Pharmacology, 37*(15), 2887-2981. doi:10.1016/0006-2952(88)90272-9

Young, E., Prins, M., Levine, M. N., & Hirsh, J. (1992). HEPARIN BINDING TO PLASMA-PROTEINS, AN IMPORTANT MECHANISM FOR HEPARIN RESISTANCE. *Thrombosis and Haemostasis, 67*(6), 639-643.

Zaretzky, F. R., Pearcepratt, R., & Phillips, D. M. (1995). SULFATED POLYANIONS BLOCK CHLAMYDIA-TRACHOMATIS INFECTION OF CERVIX-DERIVED HUMAN EPITHELIA. *Infection and Immunity, 63*(9), 3520-3526.

Zavodszky, M., Chen, C. W., Huang, J. K., Zolkiewski, M., Wen, L., & Krishnamoorthi, R. (2001). Disulfide bond effects on protein stability: Designed variants of Cucurbita maxima trypsin inhibitor-V. *Protein Science, 10*(1), 149-160. doi:10.1110/ps.26801

Zhang, K. J., & Filbin, M. T. (1994). FORMATION OF A DISULFIDE BOND IN THE IMMUNOGLOBULIN DOMAIN OF THE MYELIN P-0 PROTEIN IS ESSENTIAL FOR ITS ADHESION. *Journal of Neurochemistry, 63*(1), 367-370.

Zhang, L. J., & Esko, J. D. (1994). AMINO-ACID DETERMINANTS THAT DRIVE HEPARAN-SULFATE ASSEMBLY IN A PROTEOGLYCAN. *Journal of Biological Chemistry, 269*(30), 19295-19299.

Zhang-van Enk, J., Mason, B. D., Yu, L., Zhang, L., Hamouda, W., Huang, G., . . . Zhang, J. (2013). Perturbation of thermal unfolding and aggregation of human IgG1 Fc fragment by Hofmeister anions. *Mol Pharm, 10*(2), 619-630. doi:10.1021/mp300378y

Zhao, H. (2016). Protein stabilization and enzyme activation in ionic liquids: specific ion effects. *Journal of Chemical Technology and Biotechnology, 91*(1), 25-50. doi:10.1002/jctb.4837

Zimmermann, D. R., & Ruoslahti, E. (1989). MULTIPLE DOMAINS OF THE LARGE FIBROBLAST PROTEOGLYCAN, VERSICAN. *Embo Journal, 8*(10), 2975-2981.

Zuckier, L. S., Chang, C. J., Scharff, M. D., & Morrison, S. L. (1998). Chimeric human-mouse IgG antibodies with shuffled constant region exons demonstrate that multiple domains contribute to in vivo half-life. *Cancer Research, 58*(17), 3905-3908.

Appendix

11.1 Native BACE1 amino acid sequence

The amino acid sequence of native recombinant BACE1 is as follows:

tqhgirlplrsglggaplglrlpretdeepeepgrrgsfvemvdnlrgksgqgyyvemtvgsppqtlnilvdtgssnfavga
aphpflhryyqrqlsstyrdlrkgvyvpytqgkwegelgtdlvsiphgpnvtvraniaaitesdkffingsnwegilglaya
eiarpddslepffdslvkqthvpnlfslqlcgagfplnqsevlasvggsmiiggidhslytgslwytpirrewyyeviivrvei
ngqdlkmdckeynydksivdsgttnlrlpkkvfeaavksikaasstekfpdgfwlgeqlvcwqagttpwnifpvislylm
gevtnqsfritilpqqylrpvedvatsqddcykfaisqsstgtvmgavimegfyvvfdrarkrigfavsachvhdefrtaav
egpfvtldmedcgynipqtdestlmt-ddddk